These reasons persuaded us of the need for developing adequate models of pyrotechnic deflagration, and we began to organize the knowledge and to attempt a model development. Our initial choice was to develop a solid state reaction model for a "ceramic" delay mix since it provided ease of experimental verification and initial [illegible]

II. SYSTEM FORMULATION

A. Equation Definition

The attempts to form an analytical solution have utilized the heat diffusion equation with additional terms to encompass the heat generation. The initial one-dimensional equation is:

$$\rho C \frac{\partial T(x,t)}{\partial t} = K \frac{\partial^2 T(x,t)}{\partial x^2} + \rho'(x,t)\, Q Z e^{-E/RT(x,t)}$$

Parameters:

- ρ = density
- C = heat capacity
- Z = frequency factor
- T(x,t) = absolute temperature
- K = thermal conductivity
- E = activation energy
- $\rho'(x,t)$ = reactant density
- Q = heat of reaction
- R = gas constant

The term, $\rho C \frac{\partial T(x,t)}{\partial t}$, is rate of heat increase per unit volume. The term, $K \frac{\partial^2 T(x,t)}{\partial x^2}$, is the net rate of heat flow into the volume and $\rho'(x,t)\, Q Z e^{-E/RT(x,t)}$ is the rate of heat generation in the volume by the reaction.

An analytical solution for the equation is not known. Other methods must be sought. Initial analysis of the equation form suggested that finite difference equations, (using a computer to solve them) would allow a first attack, which could then then be expanded.

B. Pyrotechnic System Selection

Since there was no available system for which we knew all the parameters with good accuracy, we chose a model pyrotechnic which had properties similar to the boron/molybdenum trioxide system, except we assumed no gaseous products at the reaction temperature. Assuming the stoichiometric reaction is:

$$2B + MoO_3 \rightarrow B_2O_3 + Mo$$

where the stoichiometric percentages are

B = 13.0 %, MoO_3 = 87.0%

The selected values of the parameters are shown in Table I.

TABLE I

PARAMETER	VALUE
Thermal Conductivity	.001 cal °K cm sec
Heat of Reaction	725 cal/gram
Frequency Factor	1×10^{16} collision/sec
Heat Capacity*	0.50 cal/gram °K
Activation Energy	40,000 cal/mole
Density of Material	2.0 gram/cm^3
Reaction Temperature	2520°K

* Later put in as f(T) using $C_p = aT + bT^2 - A$ from handbook for components.

III. DEVELOPMENT OF MATH MODEL

A. Initial Assumptions

The model is based on several simplifying assumptions which are highly idealized to allow a start to be made in the study without facing the horrible complexities of real life. It takes a good deal of faith to accept that these assumptions will not obscure the whole problem, but accept our word that this is so. Gradually the most absurd of the assumptions can be removed to approach the desired reality. The assumptions include:

- The mixture is a homogeneous solid extending as a half space from the "ignition plane".
- All of the properties of the system are independent of temperature and can be represented by "average" values.
- Properties of the reactants and the products are identical except for heat of formation.
- When the reactants are heated, the resultant heat release can be represented by an Arrhenius type expression.

Using these assumptions, one can formulate a model of the burning phenomenon by dividing the half space up into infinitesimal cells, all initially at room temperature, and considering what happens if all the cells in the Y-Z plane (i.e., the "ignition plane") are instantaneously raised to some high temperature.

1. Because of the uniform high temperature in the cells in the Y-Z plane, the heat will flow in the X direction only.
2. Because of the high temperature, the reactants will begin to combine chemically releasing further heat to supplement the initial heat added.

One may generalize the resulting temperature history for any cell by writing the differential equation:

$$\rho C \frac{\partial T(x,t)}{\partial t} = K \frac{\partial^2 T(x,t)}{\partial x^2} + \rho'(x,t) Q e^{-E/RT(x,t)},$$

The calculated variable is the temperature distribution across the slab as a function of time. The burn rate is obtained from the rate of progress of the peak temperature from one infinitesimal cell to another.

This phenomenon can be observed in the following illustration.

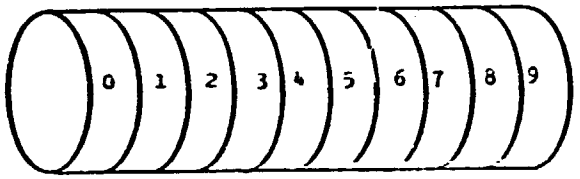

I—— Heat Flow Illustration 1
Heat Flow through Cells in a Semi-infinite Slab

As the temperature in the cells of the semi-infinite slab is increased (by some unspecified process), the heat will flow in the X direction only. When sufficient energy is conducted into a cell so that its ignition temperature is reached (say in cell zero), the reactants will begin to combine chemically. This reaction causes additional heat to be conducted in the X direction (into unreacted material). At some point in time, sufficient energy will be conducted into cell 1 to cause ignition here. The process of conducting energy and obtaining additional heat from the reaction will continue as the flame front proceeds through the slab. The calculated variable in the differential equation, the temperature as a function of time, is recorded during this reaction process. The computed burn rate is simply calculated from the distance the reaction temperature travelled in a known time.

B. Equation Programming and Initial Computer Run

The original work was performed by Professor Herbert Peckham of Gavilan College, Gilroy, California. Mr. Peckham was responsible for setting up the differential equations and programming them into a computer language.

The values selected for the parameters, listed in Table I, were programmed into the model. For this initial computer run, the time and space steps were one on relatively large (Δx = .01 cm, Δt=.002 sec) to permit rapid scanning. The temperature profile from the initial computer run is shown in Table II.

TABLE II

TEMPERATURE PROFILE FOR THERMAL CONDUCTION RUN

TIME SEC	Cell (Width = .01 cm) 1	2	3	4	5
0	1000	600	300	300	300
.002	2520	2520	306	300	300
.004	2520	2476	350	300	300
.006	2518	2434	392	301	300
.008	2515	2395	431	303	300
.010	2510	2358	467	305	300
.012	2503	2323	502	306	300
.014	2497	2290	547	312	300
.016	2488	2260	892	317	301
.018	2479	2237	2520	328	301

Cell 1 at zero time was an assigned temperature of 1000°K, assumed to be equal to or above the ignition temperature. Cell 2 was assigned a temperature of 600°K. In the next time iteration, (.002 seconds later), Cell 1 and 2 show maximum temperature, 2520°K. Cell 3 now is at 306°K, up from the starting ambient temperature of 300°K. As the time period increases, Cell 3 temperature slowly rises until the fixed maximum peak is reached at 0.018 second. If the computations had continued, Cell 4 would show in general the same temperature profile as Cell 3. From the data presented, the calculated burn rate from Cells 2 and 3 would be .01 cm (distance)/ .016 sec (time) = 0.62 cm/sec (.25 in/sec).

Several conclusions were drawn from this run:

a) Once the ignition temperature is exceeded, the reaction proceeds extremely rapidly to completion within a cell before the end of that time step. The cell is then assigned the temperature present at completion of reaction as though it had occurred at the end of that time step. Thus, it is essential that both the cell distance and computer time step are greatly reduced.

b) The cell array should be changed to start cell 1 at the reaction temperature, 2520°K and have all remaining cells at 300°K (room temperature). This would provide a more accurate profile by assuring the reaction had started at point zero and then watch the reaction temperature advance through the cells from there.

c) Burning rate can be estimated from the time for the reaction temperature to progress from one cell to the next.

C. Model Response to Reduce Computer Time Step and Cell Width

The computer time step was reduced from .002 sec to 2×10^{-5} seconds; the cell width was now .0004 cm instead of .01 cm. These changes should help in tracking the progress of the flame front across the slab.

The same input parameter values listed in Table I were employed for this trial run. The resultant temperature vs time profiles for two adjoining cells are shown in Figure 2.

Initially, the cell temperature increases due to heat conduction from the previous hot cell. Once ignition point is reached, the reaction temperature rises to adiabatic reaction temperature rapidly. After burn out, the cell temperature begins a slow decline. This slow decline results from the semi-infinite heat condition in which there is no heat loss except that conducted to the material ahead. The computed burn rate of 19 in/sec is substantially higher than the original computed rate of 0.25 in/sec. This may be accounted for by reduction in cell space and computer time step. Since the cell is much smaller in size, the thermal conductivity and specific heat parameters would have greater influence on the heat transfer to the next cell. The preheating affect would cause the ignition temperature to be reached in less time and, consequently, result in faster burn rates. (The burn rate is calculated indirectly from the time required to reach the peak temperature from one cell to another.)

D. Computer Calculation of Maximum Reaction Temperature

The normal procedure for calculating the reaction temperature of a given stoichiometric mixture is from the empirical heat capacity equations of the products and the heat of reaction value integrated over the range of temperatures with room temperature taken as the reference temperature. A numerical figure for the reaction temperature is consequently estimated. If this description were applied to a material in a given cell, the reaction temperature would be defined as that temperature to which a known quantity of products would rise when heated by a precise quantity of energy released by a pre-determined mass of reactants.

However, the total energy of a cell includes the heat required to raise the reactants to the ignition temperature, plus its known heat of reaction. This combined energy is transferred to the products and produces the true maximum temperature, which is higher than that calculated from only the heat of reaction. This is a fact that is usually overlooked when one is estimating the maximum temperature achieved by a reaction.

During the computer run, the maximum peak temperature for all the cells (except cell 1 which was started at 2820°K) were obtained by using the total heat content determined to be in that cell. The resultant maximum peak temperatures were found to be slightly greater than 3000°K. The temperature profile for two adjoining cells can be seen in Figure 2. The increase in burn rate to 25 in/sec from 19 in/sec is principally due to higher reaction temperature, more heat flow and, thus, faster burn rates.

B. Incorporation of Specific Heat as a Function of Temperature and the Programming for Phase Changes of Materials

The specific heat parameter was assigned a fixed value in previous runs in order to simplify the ease of operations. The necessity to relate the specific heat value as a function of temperature is an obvious fact. The programming was altered so that now the model computes a new specific value for the reactants at each temperature from the general formula: $C_p = aT + bT^2 - A$. The specific heat is updated after the new cell temperature is calculated. A fixed average value is still assigned for the product, however, since the temperature drop during the cooling cycle is relatively small.

The physical change of state of the materials in the cell also has to be considered. The energy required for these transitions will effect the reaction front and consequently the computed burn rate. The initial attempt was to input the energy required to melt the reactant molybdenum trioxide. Difficulties were encountered during the programming on execution of this task. The problem was that this physical change (MoO_3 at 1068°K, MoO_3) occurs shortly after ignition (around 0.5 sec) from which the reaction temperature rises to peak value very rapidly. The sequence of events had to be slowed to allow for the absorption of energy needed to melt the ever decreasing amounts of molybdenum trioxide. The computing time step was reduced to permit the physical change, although the overall time sequence was controlled in order to calculate the burn rate.

The temperature/time profiles for adjoining cells A and B of a computer run are shown in Figure 3. The effect of molybdenum trioxide melting phase change is seen in the expanded time scale insertion. The reaction temperature rise is so rapid that the curve plotted to the pre-selected computer speed shows no change in its slope. However, a slope change is evident when the iteration interval is reduced. The reaction temperature remains constant during the period required for the molybdenum trioxide to absorb the necessary energy to complete the melting transition. Once this physical change is complete, the reaction temperature resumes its upward climb.

The computed burn rate for this run is 51 inches per second. The reason for this increase from the previous computation of 25 inches per second is that the heat capacity is re-calculated as the temperature rises and is not (as before) an average value for the reactants. This upgrading actually decreases the cell's heat capacity at the lower temperatures; thus, the heat flow to adjacent cell will be greater. This means the next cell will have a shorter preheating time to ignition temperature, and consequently reach peak temperature faster than was computed in the previous version.

This burn rate result of 51 inches per second is markedly different than the 2 inches per second observed in the real system we are trying to simulate. A small part of the difference can be explained by the semi-infinite approximation. However, it is very possible that there are significant errors in the assumed values of the other parameters (Z for instance is only a guess) to explain much of the discrepancy.

IV. SUMMARY OF THE PROGRAM TO DATE

The heat diffusion equation for an Arrhenius Type reaction is the basis for the deflagration theory. Although this equation applies to all computation involving reaction rates, the usual application is for an analytical solution. This approach proved unsatisfactory for the mathematical description had to be generalized and simplified to the point where the model became too removed from reality.

An alternative approach was chosen, in which a numerical solution could be obtained from a properly programmed model, using a digital computer. The model was refined from one using parameters related to only general conditions, to one sophisticated enough to incorporate melting phase changes in a semi-infinite system.

The numerical solution of the model depends on the values of the pertinent parameters. It is apparent that several critical parameters, such as thermal conductivity and frequency factory, will have to be accurately determined before any real significance can be placed in the absolute burn rate values obtained. However, the model has produced qualitative results in the realm of scientific reason in a semi-infinite slab condition.

The premise of the model is one of a homogenuous semi-infinite slab, computing differential equations on a "gasless" mix. The present model will allow computation of the effects of various parameter changes such as thermal conductivity, ambient temperature, and the effect of diluents on the burning rate. The eventual final model will have to be one that can handle a hetrogeneous system of a "gassy" mix. This will allow calculation of the effect of particle size, pore size, and non-homogeneities on the burning rate. But, before one can reach this idealistic goal, the old and familiar path of research and development will have to be followed. The direction is two fold: 1) one of actual computer model development and 2) critical parameter data investigation. The marriage of the two paths is a hoped for partnership that will result in a useful research and design tool for pyrotechnic systems.

V. ACKNOWLEDGEMENTS

The authors express their deepest appreciation to Dr. D. B. Davenport, who worked on the original equation formulation with Professor H. Peckham and whose guiding hand kept us along the straight and narrow scientific path; to Mr. M. Farrand for his many critique comments; to Mr. D. Lee for his literary expertness and lastly to Mr. P. Jewhurst who helped convert the program into computer language and ran the machines.

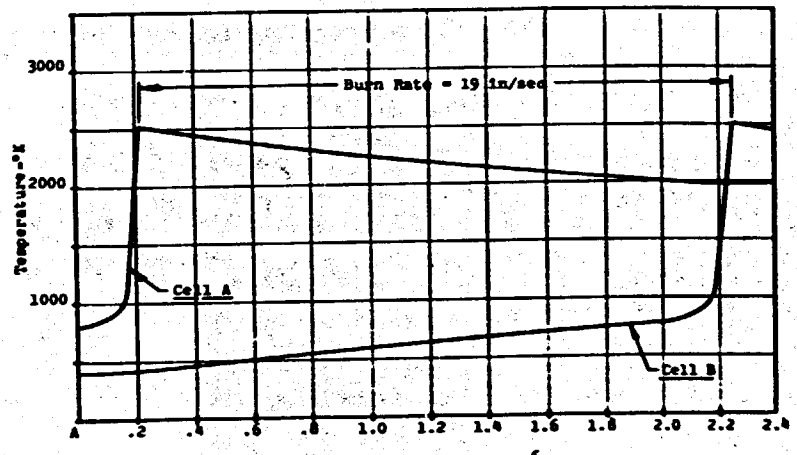

TEMPERATURE VS TIME FOR TWO ADJOINING CELLS USING INITIAL INPUT PARAMETER VALUES

FIGURE 1

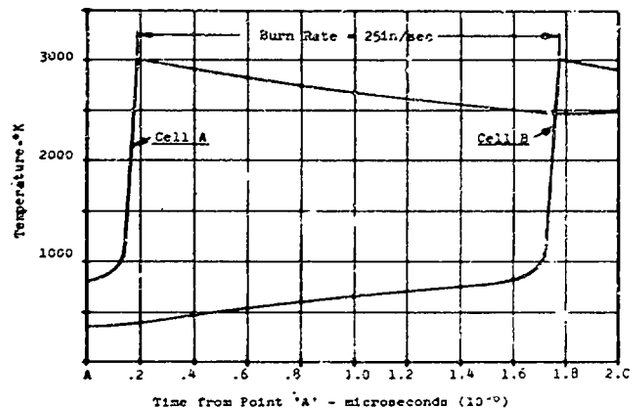

TEMPERATURE VS TIME PROFILE FOR TWO ADJOINING CELLS IN WHICH MAXIMUM PEAK TEMPERATURE WAS CALCULATED BY COMPUTER

FIGURE 2

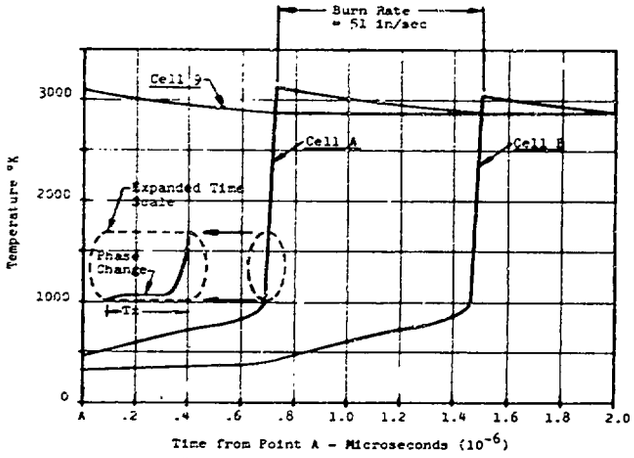

$T_x = 3 \times 10^{-9}$ sec

TEMPERATURE VS TIME FOR CELLS A AND B IN WHICH THE MELTING PHASE OF MOLYBDENUM TRIOXIDE WAS INCORPORATED

FIGURE 3

I-4. Recent Developments in Modeling the Hotwire Igniter

by

John T. Petrick and Robert L. Montgomery

of the Naval Weapons Laboratory, Dahlgren, Virginia

INTRODUCTION

For over 10 years the government and the explosives industry have been seeking a means to take the "art" out of building igniters and to provide the design engineer with a simple igniter model. Modeling attempts by Davenport and Reynolds, (1) Montgomery, (2) and Massey (3) have primarily been concerned with determining the heat transfer coefficient (H) for a fine wire embedded in an essentially unreactive explosive. Now it is possible to proceed with the model by including measured values of H and the heat generated by the explosive's chemical reaction. Inclusion of an empirical H and the chemical reaction will complete the igniter model and provide the engineer with accurate guidelines for igniter design.

The Heat Transfer Equation:

Carslaw and Jaeger (4) gives the basic heat transfer equation for a current carrying wire References (1), (2), and (3) use the basic heat transfer equation as shown in figure 1.

If a long thin wire is used, the Laplacian term in equation 1 can be neglected due to the absence of significant temperature gradient variations. Thus equation 1 simplifies to equation 2 shown in figure 2.

The work of Levitsky and Schaffer (5) permits modification of equation 2 to allow heat generation due to an exothermic first order chemical reaction Equation 2 is modified as shown in equation 3 (of figure 3). Equation 3 describes the development of average temperature in a long, thin bridgewire surrounded by explosive. Solution of this equation shall be the first modeling goal.

There are, however, several parameters in equation 3 which must be measured or theoretically derived. Three parameters which cause the greatest difficulty are the bead temperature (T_B), the heat transfer coefficient (H), and the pre-exponential factor (C'). As will be shown later, the term containing the pre-exponential factor is significant only near the no-fire level. Since we have not yet investigated no-fire characteristics we have not needed C' and will not discuss the methods of measuring C' in this paper.

Measurement of T_B is essentially impossible without significantly disturbing the bridgewire-explosive system, thus one of the following assumptions must be made. Assume either the wire heating rate to be sufficiently large that T_B remains constant at ambient temperature, or assume any contributions to the term containing T_B which are due to changes in T_B will be seen only in H, when H is experimentally determined.

Thus H becomes the single remaining unknown parameter. Davenport (1) has theoretically derived H and is able to match his model to firing data in the regions of rather long functioning times. Using the bridgewire as a thermometer we have been able to experimentally determine H thereby extending the model to the shorter functioning times.

Experimental Determination of H:

For moderate temperature changes (0-100°C), bridgewire resistance is related to average wire temperature by:

4) $$R' = R_o (1 + \alpha T)$$

Application of a constant current to the wire produces a voltage which is related to average wire temperature as follows:

5) $$V = IR' = IR_o (1 + \alpha T)$$

Letting $IR_o = V_o$ and $V - V_o = \Delta V$ the average wire temperature can be found by measuring the voltage change, ΔV, and either R_o or V_o.

Temperature is thus:

6) $$T = \frac{\Delta V}{\alpha V_o} = \frac{\Delta V}{IR_o \alpha}$$

ΔV is recorded by an oscilloscope and camera, and a polynomial equation is fit to the data by the least squares method. Neglecting the chemical reaction term, thereby reverting to equation 2, allows an explicit determination of H. Let T be the temperature rise above ambient, then H is given as equation 7 shown in figure 5.

Temperature will probably never exceed a second order polynomial, thus:

8) $$T = at^2 + b\,t + c \text{ and}$$

9) $$\frac{\partial T}{\partial t} = 2\,at + b$$

From experimental data of T vs t we can easily compute H at any time or temperature. Before examining the results of such experiments and computations a closer look at the effects of the chemical reaction will be made.

The Chemical Reaction:

Ignition in an igniter can be broken up into three fairly distinct events. These are:

- Heating by the bridgewire
- Chemical self heating of the explosive, and
- Autoignition

Present theory, substantiated by our experiments, is that the wire heats a film of surrounding explosive until the exothermic decomposition begins, then wire temperature rises as the sum of the wire and chemical heating increase. When the temperature at the wire-explosive interface reaches the explosive's autoignition temperature, ignition occurs.

The experimental results supporting this theory are the temperature vs. time curves near and above no-fire, some of which are schematically shown in figures 6, 7, and 8. Near no-fire, as in figure 6 and 7, the beginning of the chemical reaction is clearly defined and chemical heating is seen to raise the wire temperature above what would normally be a smooth curve. A variation in heating rate produced by raising the current increases the interface temperature so rapidly that no chemical heating is seen, as shown in figure 8, yet the explosive ignites at about the same temperature. This temperature is near the published value of autoignition temperature.

Further support of this theory is obtained by calculating the magnitude of the chemical reaction term in equation 3. Clearly for short functioning times this term rapidly becomes negligible in accordance with experiment. Also our model accounts for the fact that no reaction occurs unless an energy equal to the activation energy(E) has been furnished to the explosive. Thus no reaction occurs until sufficient energy causes the decomposition temperature to be reached as is clearly seen near no-fire levels.

The Experimental Arrangement:

Equipment used in the experiments included a storage oscilloscope and camera, a 36 volt lead-acid storage battery, a variable resistor network, a firing control panel, an ammeter, and a Kelvin bridge. The storage oscilloscope contains a differential amplifier with an accurately presettable voltage offset which facilitates the measurements. By calculating $V_o = IR_o$ and presetting V_o as an offset we see only ΔV on the screen.

The ammeter, 36 volt battery, variable resistors, firing control panel, and the explosive device form a series circuit as shown in figure 8a. Current was set to desired values by short circuiting the device under test, closing the circuit at the firing panel and varying the resistors until the desired values of current are attained.

Compensation should be made for the added resistance of the igniter during firing, however, in the experiments conducted thus far no compensation was made. The error incurred by not compensating for device resistance depends on the ratio of device resistance to circuit resistance. This error was small for the platinum wires thus the results of the experiments described herein were not affected.

Another serious source of error is the length of leads to connect the oscilloscope to the igniter. These leads should never exceed a few inches in length as their resistance adds to R_o but does not vary during the experiment. Short leads require location of the igniter near expensive equipment thus special firing techniques must be employed to ensure equipment safety.

Initial experiments used a 2.0 mil platinum bridgewire, .10 inch long, coated with nitrocellulose. R_o was not measured by the Kelvin bridge because V_o could be measured directly from the oscilloscope trace.

The second set of experiments used a 2.0 mil platinum bridgewire, .10 inch long, coated with normal lead styphnate. V_o was again measured from the oscilloscope trace.

Data were reduced to a set of temperatures vs time for each device and a second degree polynomial was fitted to the data by the least squares method. To avoid difficulties with the effects of the chemical reaction, only the beginning portion of the temperature curves was used to determine H.

Figure 9 shows H vs t for I = 2.0 amp as obtained from equation 7 and experimental T vs t data.

A comparison of our H and Davenport's theoretical curve for H at I = 1.15 amp is shown in figure 10. Davenport's curve fits firing data only in the region shown, however our results provide the additional heat transfer needed to better fit Davenport's firing data as given in reference (1).

Test Results:

The polynomial curve fits of temperature vs time for three igniters at three currents are shown in figures 11(a, b, and c). The corresponding H vs T curves as computed from equation 7 are shown in figures 12 (a, b, and c).

Conclusion:

The process of ignition in a hotwire igniter is accomplished by:

- Heating by the bridgewire,
- Explosive self heating, and
- Autoignition.

Using the bridgewire as a thermometer allows H to be measured for classes of devices and thus permits formulation of an igniter model. Inclusion of the explosive's chemical reaction will permit no-fire predictions possibly with predictable confidence levels.

Experiments are underway to determine how H varies with igniter parameters such as wire composition, explosive material, current, wire size, etc. Later plans include a determination of C' and formulation of methods to predict no-fire levels.

SYMBOLS USED

H - Heat Transfer Coefficient

T - Bridgewire Temperature

C' - Pre-exponential Factor

T_B - Explosive Bead Temperature near the Bridgewire

R - Total Bridgewire Resistance

C - Bridgewire Specific Heat

p - Bridgewire Perimeter

W - Bridgewire Cross Sectional Area

ρ - Bridgewire Density

H - Volumetric Heat of Reaction

K - Wire Thermal Conductivity

t - Time

E - Activation Energy

σ - Wire Electrical Conductivity

R - Universal Gas Constant

j - Conversion Factor from Joules to Calories

I - Current

α - Thermal Coefficient of Resistivity

∇^2 - Laplacian Operator

R_o - Total Bridgewire Resistance at a Reference Temperature

ΔV - Voltage Change

V_o - Voltage Across Igniter at Ambient Wire Temperature

a, b, c, - Constants in Polynomial

REFERENCES

(1) Davenport, L. E. and Reynolds, H., "Quantitative Predictions of EED Firing Characteristics," Proceedings of the 6th Symposium on Electro-explosive Devices, The Franklin Institute, Philadelphia, Pennsylvania, July 1969.

(2) Montgomery, R. L., "An Investigation of the Steady State Equation of the Hotwire Initiator," U.S. Naval Weapons Laboratory, Dahlgren Virginia, Technical Memorandum No. T-10164, 1964.

(3) Massey, J. A., Jr., "A Heat Transfer Model Study of the Hotwire Initiator", Naval Weapons Laboratory, Dahlgren, Virginia, Technical Report No. 1917, 1964.

(4) Carslaw, H. S. and Jaeger, J. C., Conduction of Heat in Solids, Oxford University Press, London 1959.

(5) Levitsky, M. and Shaffer, B.W., "Transient Temperature Distribution During an Exothermic Chemical Reaction", New York University, 1970.

FIGURE 1

WIRE EQUATION-1

$$\frac{\partial T}{\partial t} = \frac{K}{\rho C}\nabla^2 T - \frac{H\rho}{\rho C\omega}(T - T_0) + j\frac{I^2(1+\alpha T)}{\rho C\omega^2\sigma_e}$$

FIGURE 2

WIRE EQUATION-2

$$\frac{\partial T}{\partial t} = \frac{-H\rho}{\rho C\omega}(T - T_0) + j\frac{I^2(1+\alpha T)}{\rho C\omega^2\sigma_e}$$

FIGURE 3

HEAT GENERATION EQUATION

$$\frac{\partial Q}{\partial t} = C\exp\left[\frac{-E}{RT} - \frac{C}{H}\int_0^t e^{\frac{-E}{RT}}dt'\right]$$

FROM "TRANSIENT TEMPERATURE DISTRIBUTION DURING AN EXOTHERMIC CHEMICAL REACTION," M. LEVITSKY AND B W SHAFFER, NYU, 1970

FIGURE 4

WIRE EQUATION-3

$$\frac{\partial T}{\partial t} = \frac{-H\rho}{\rho C\omega}(T - T_0) + j\frac{I^2(1+\alpha T)}{\rho C\omega^2\sigma_e} + \frac{C'}{\rho C_w}\exp\left[\frac{-E}{RT} - \frac{C'}{H'}\int_0^t e^{\frac{-E}{RT}}dt'\right]$$

FIGURE 5

HEAT TRANSFER COEFFICIENT (H)

$$H = \frac{\rho C\omega}{\rho T}\left[j\frac{I^2(1+\alpha T)}{\rho C\omega^2\sigma_e} - \frac{\partial T}{\partial t}\right]$$

Pt WIRE–NITROCELLULOSE

FIGURE 6

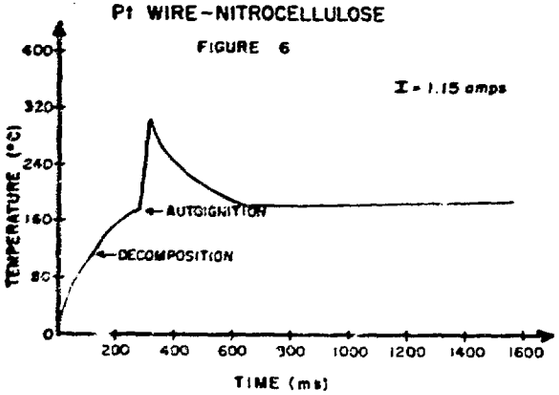

Pt WIRE–LEAD STYPHNATE

FIGURE 7

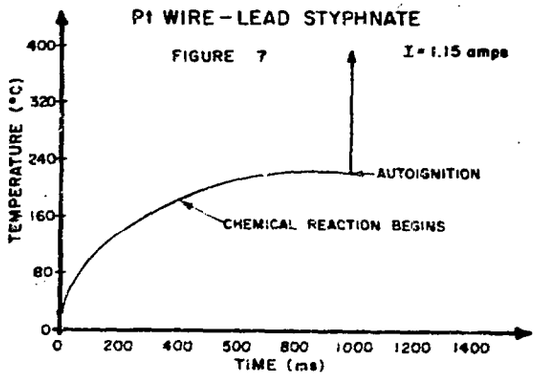

Pt - LEAD STYPHNATE

FIGURE 8

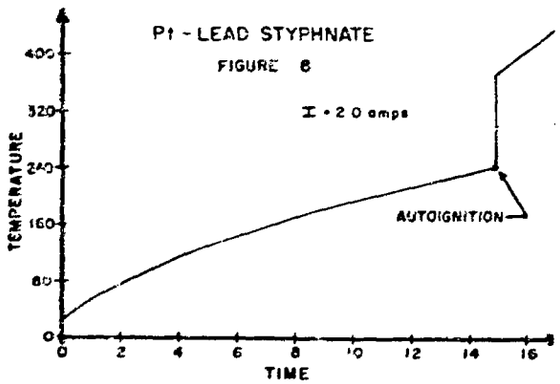

FIRING CIRCUIT

FIGURE 8a

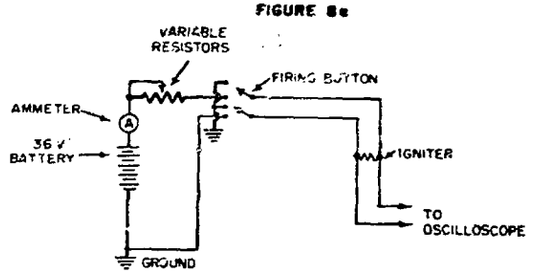

Pt-LEAD STYPHNATE

FIGURE 9

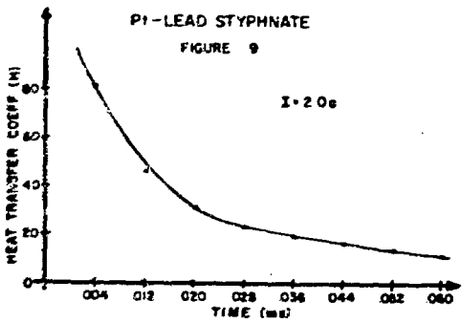

FIGURE 10

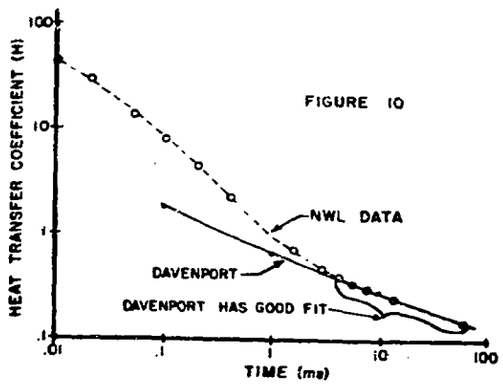

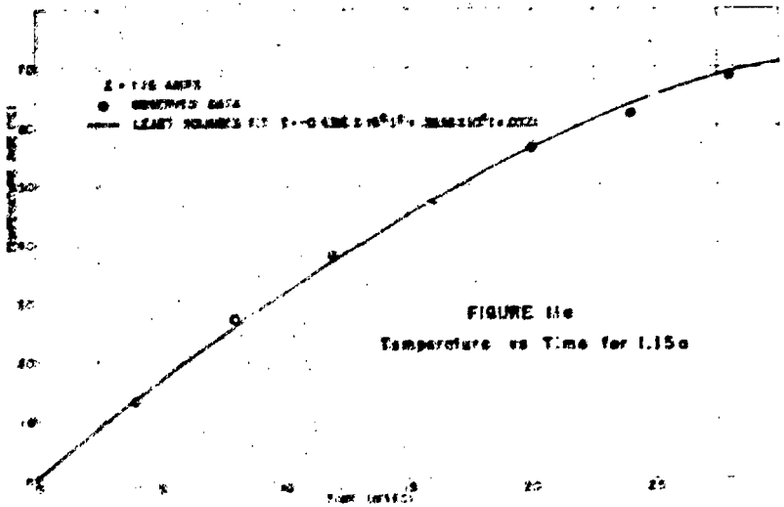

FIGURE 11a
Temperature vs Time for 1.15a

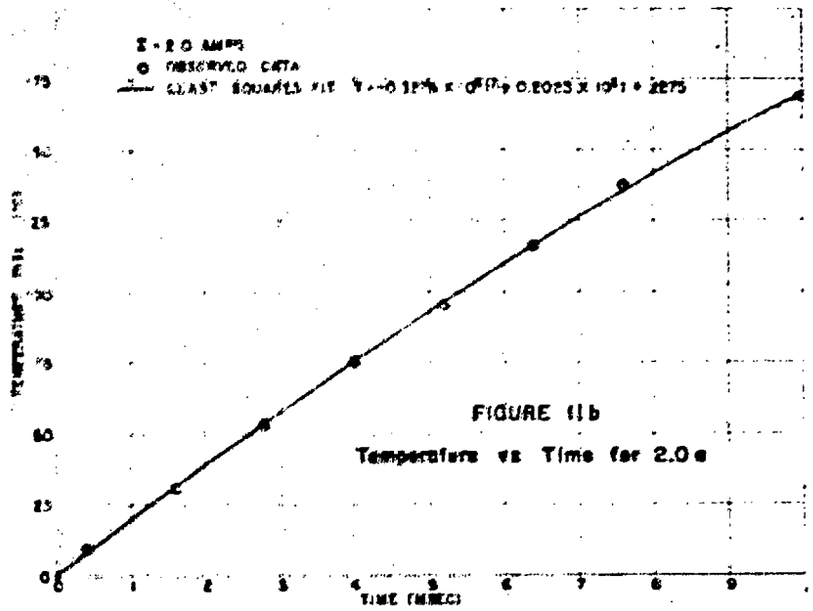

FIGURE 11b
Temperature vs Time for 2.0a

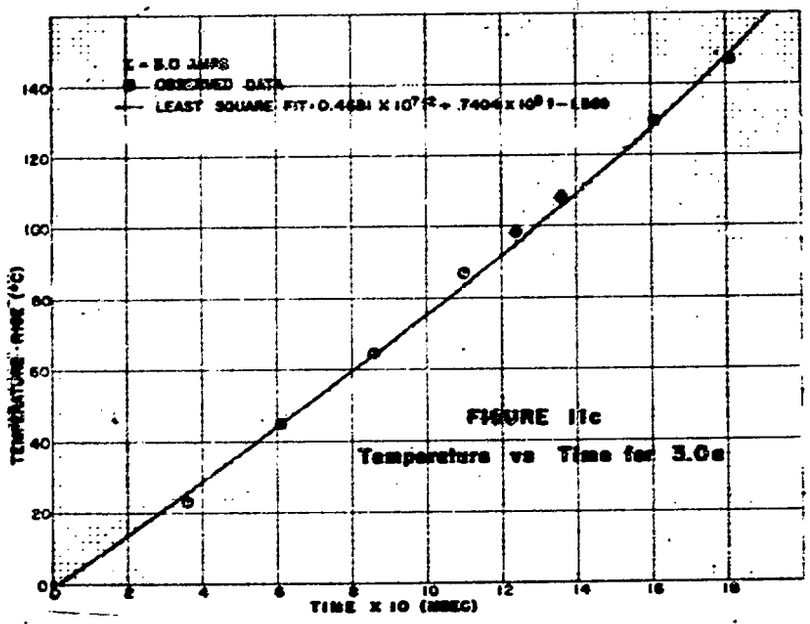

FIGURE 11c
Temperature vs Time for 3.0a

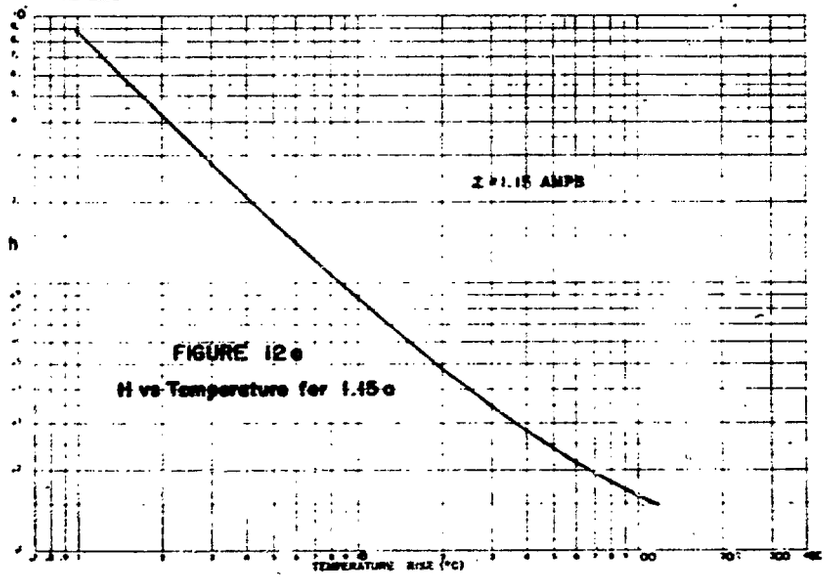

FIGURE 12a
H vs Temperature for 1.15a

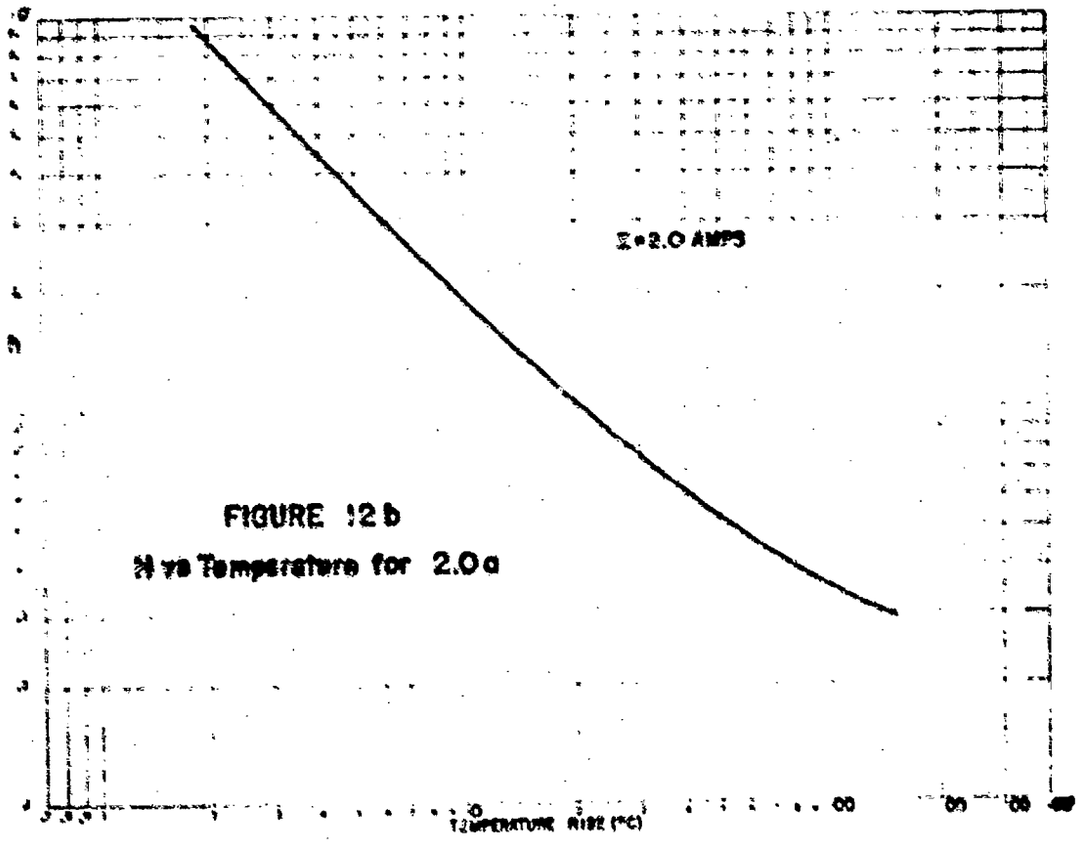

FIGURE 12b

H vs Temperature for 2.0a

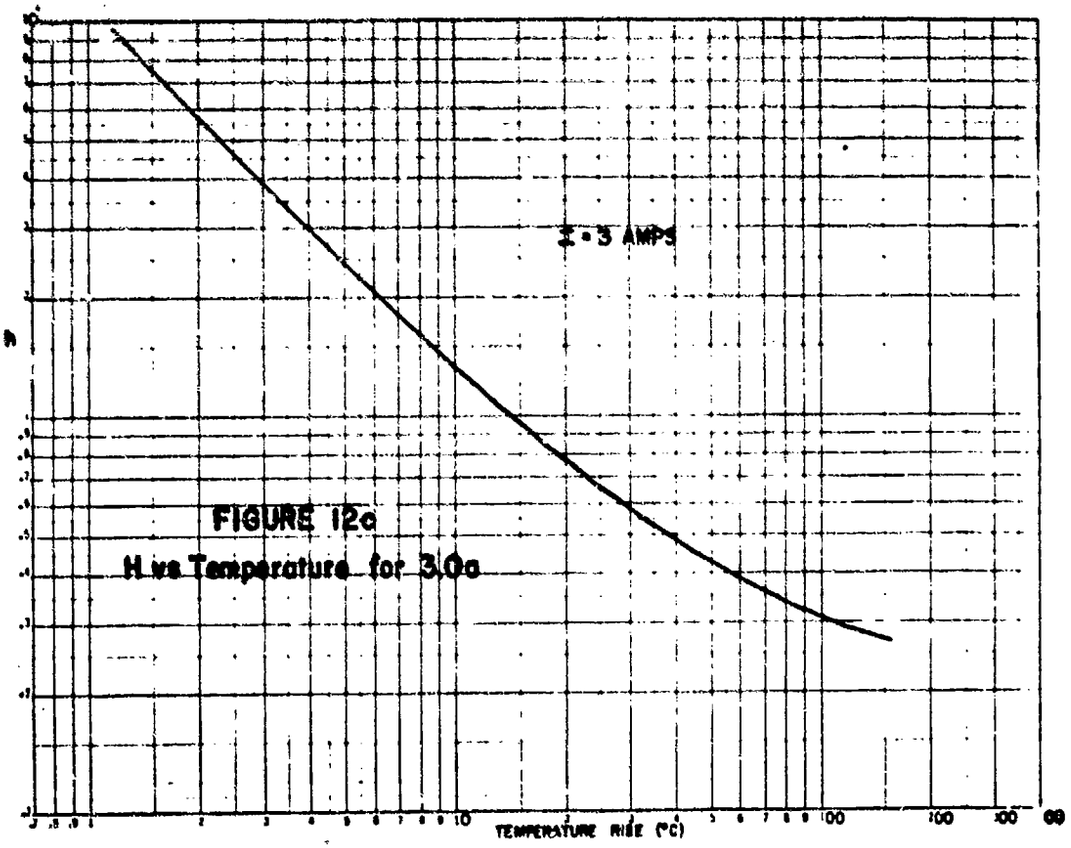

FIGURE 12c

H vs Temperature for 3.0a

I-5. THE THERMAL DECOMPOSITION OF β-HMX

by
F. E. Sinclair and W. Roessler
Naval Postgraduate School
Monterey, California - 93940

1. Introduction

Tetramethylene tetranitramine HMX has four polymorphs, α, β, γ, and δ. These are stable at different temperature ranges and have different impact sensitivities. The most stable form at normal room temperature is the β polymorph and it has been reported that near its melting point, β-HMX obeys a first-order rate law but at lower temperatures it obeys the sigmoid preconversion relationship displayed by solids undergoing autocatalysis.[2] For β-HMX activation energies obtained in this report, Fig. 5 and other similar data were:

Temperature °K	Activation Energy Kcal/mole
483°-506°	44.30
506°-512°	63.73
Above 515°	52.65

Suryanarayana and Graybeal also reported[2] a variation in composition as a function of temperature from a mass spectrometric analysis of the decomposition products.

2. Reaction Kinetics in Differential Thermal Analysis[3]

DTA is the measurement of changes in heat content and other thermal properties of a material. These changes are indicated by a deflection or peak on the plot. If the reaction rate is proportional to temperature, the position of the peak is also a function of temperature. This peak temperature variation can be used to calculate the energy of activation with the temperature of maximum deflection being the temperature at which the reaction rate is greatest.

Solid → Solid + gas reactions can be described by

$$\frac{dx}{dt} = A(1-x)^{n} e^{-Ea/RT} \qquad (1)$$

If the temperature rises during the reaction, the reaction rate dx/dt will rise to a maximum and return to zero when the reactant is expended. The maximum rate is at $\frac{d}{dt}\left[\frac{dx}{dt}\right] = 0$. If the temperature rises at a constant rate $\frac{dT}{dt}$, differentiation of (1) gives

$$\frac{d}{dt}\left[\frac{dx}{dt}\right] = \frac{dx}{dt}\left[\frac{Ea\left(\frac{dT}{dt}\right)}{RT^2} - An(1-x)^{n-1} e^{-Ea/RT}\right] = 0 \qquad (2)$$

If the temperature at which the maximum rate occurs is labeled Tm, Eqn (2) can be rearranged to give:

$$\frac{Ea\left[\frac{dT}{dt}\right]}{RTm^2} = An(1-x)_m^{n-1} e^{-Ea/RTm} \qquad (3)$$

The temperature, Tm, is the sample temperature at which the peak DTA deflection occurs and comparing it to information in Ref 3 is is found to follow the first-order rate law, and we obtain

$$\frac{dT}{dt} = \frac{A\ P\ Tm^2}{Ea} e^{-Ea/RTm} \qquad (4)$$

when n = 1.

Taking the $\ln\left(\frac{dT/dt}{Tm^2}\right)$ and differentiating on both sides,

$$\frac{d\ \ln\left(\frac{dT/dt}{Tm^2}\right)}{d(1/Tm)} = -\frac{Ea}{R} \qquad (5)$$

The plot of $\ln\left(\frac{dT/dt}{Tm^2}\right)$ versus 1/Tm should give a straight line which has a slope $-Ea/R$ and an intercept of $\ln(AR/Ea)$.

3. EXPERIMENTAL

3.1 Material. The commercial HMX salt was purified by recrystallization from an acetone solution using water precipitation. This was repeated until no trace of RDX was detectable by thin layer chromatography techniques which use diphenylamine exposed to ultraviolet light as the indicators[4].

3.2 Apparatus. The apparatus used to study thermal decomposition of β-HMX was a "du Pont 900 Differential Thermal Analyzer" capable of measuring exotherms or endotherms as a function of sample temperature with variable starting temperatures and heating rates.

In the DTA measurements the sample of 0.4 mg of β-HMX and also the reference glass beads were loaded in a capillary tube 2 mm in diameter. The reaction then proceeds in 1 atmosphere of air with the heating temperature of 200°C using chromel-alumel thermocouples.

4. RESULTS

In Fig. 1, the sample β-HMX has been "analyzed" in 1 atmosphere of air with a heating rate of 2°C/min. The most significant features are the endothermic and exothermic process at 192°C and 276°C respectively. The endothermic is the crystal phase change β-δ transformation of the β-polymorph[5] and it is an irreversible transformation[8].

Examination of the DTA trace shows that the decomposition of δ-HMX is very exothermic. These thermal decomposition exotherms also exhibit very small endotherms which is due to the formation of a liquid phase during thermal decomposition and at the phase change β-δ it also exhibits the very small endotherms. This phenomenon of the formation of a liquid phase during solid state decomposition has been observed in the other organic solids[5].

Fig. 2 shows that the Tm values increase with increase in heating rate.

According to the various theories of DTA, the peak area should be directly proportional to the fractional decomposition of the sample. Since thermogravimetry is used as a complementary technique to aid in the interpretation of DTA curve peaks, many attempts have been made to correlate TGA weight-loss temperatures with the DTA peaks' maximum temperatures. Generally, little agreement exists between the two types of experimental curves because of the different conditions of pyrolysis[6].

In Figs. 3-4, curves are shown plotting the temperature of β-HMX in °K versus time-in-seconds for the heating rates of 0.5° and 4.5°C/min. Intermediate ranges were also plotted but are not included in this paper. From these plots, three separate slopes can be seen. These are at the temperature ranges of 473°-506°K, 506°-514°K, and above 514°K.

In Fig. 5 is shown the curve of $\ln\left(\frac{dT/dt}{Tm^2}\right)$ versus 1000/Tm, °K for Figs. 3-4, the first portion of 473°-506°K from which is obtained Ea = 44.20 Kcal/mole.

Fig. 6 shows the data from Figs. 3 & 4, the second portion of 506°-514°K from which is obtained Ea = 63.23 Kcal/mole.

$$\frac{dx}{dt} = 10^{22.89}(1-x)\, e^{-Ea/RT}$$

$$\frac{dT}{dt} = 10^{22.89}\, \frac{R}{Ea} \cdot Tm^2 \cdot e^{-Ea/RTm}$$

Fig. 7 shows the data from Figs. 3-4, the result of the third portion of the temperature above 514°K from which is obtained Ea = 52.65 Kcal/mole.

Comparing the data from Ref 2 with our values is difficult but the general range is good and our values of 44.20 Kcal/mole in the range of 473°-506°K agrees with the authors' value of 45 Kcal/mole in the range of 499°-518°K.

5. DISCUSSION

Ref 2 states: "Several causes for the acceleration of the decomposition of β-HMX to a constant rate have, therefore, to be considered:

1. Progressive melting as a result of lowered melting point by the products.
2. Self-heating
3. Autocatalysis by products, both solid and gaseous
4. Acceleration due to structural factors such as an increase in the number of nuclei or in the surface area analogous to the inorganic solids.

Either 1 or 3 can account for the increasing rate which would compensate for the fall in rate as the material is consumed."

The results of activation energy in the temperature above 514°K of 52.65 Kcal/mole agrees with A. J. B. Robertson[8].

All calculations were carried out on a WANG 700A using its n^{th} order regression to obtain intercepts and slopes for Figs. 3-7 and the equation T = f(t) for Figs. 3-4 . When the time is known this equation can be used to predict the temperature for a known heating rate.

While the decomposition of β-HMX is accelerated, the DTA plots show three separate peaks indicating a change of reaction mechanism. This is also indicated by the activation energy plots which contain three different activation energies.

6. ACKNOWLEDGEMENTS

We are grateful for the helpful assistance of Mr. Robert Smith as Electronics Technician and Mr. Robert C. Scheile as glassblower. This project has been sponsored by the Naval Air Systems Command.

7. REFERENCES

1 H. H. Cady, A. C. Larson, and D. T. Cromer, ACTA Crystallographica, 16, 617 (1963).

2 B. Suryanarayana and R. J. Graybush, Industrie Chimique Belge, Brussels, Vol 32 (spec. no. Pt. 3) 1967.

3 H. E. Kissinger, Anal. Chem., 29, 1702 (1957).

4 J. E. Sinclair, Explosivstoffe Nr, 11/12/69, Pg. 259.

5 W. E. Garner, Ed. Chemistry of the Solid States, Pg. 254, Butterworth's Scientific Publication, London (1955).

6 Chemical Analysis, Vol. 19, Thermal Method of Analysis, Wendlandt, W. M., 1964, Interscience Publishers, Pg. 132.

7 A. J. B. Robertson, Trans Faraday Soc., 45, 85 (1949).

8 J. N. Maycock, et at, Explosivstoffe, Nr 1, (1969), Pg. 6.

TABLE OF SYMBOLS

$\frac{dx}{dt}$ = The rate of reaction

x = Fraction of reacted material

n = The empirical order of reaction

T = Temperature in °K

R = Gas constant = 1.987 cal/mole-°K

Ea = Activation energy in calories/mole

DTA = Differential Thermal Analysis

Tm = The sample temperature at which the peak differential thermal analysis deflection occurs

$\frac{dT}{dt}$ = Heating rate of sample explosive °K/sec.

A = Constant

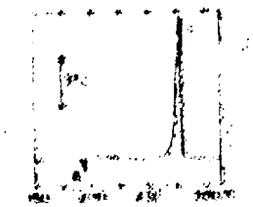

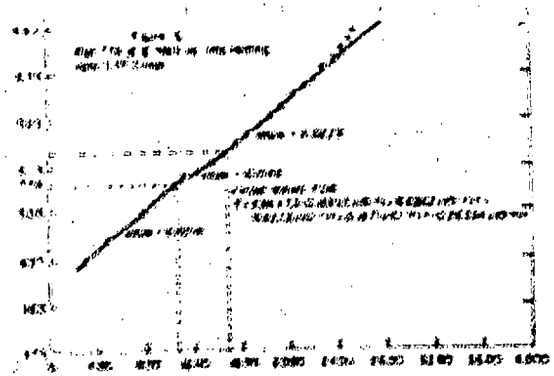

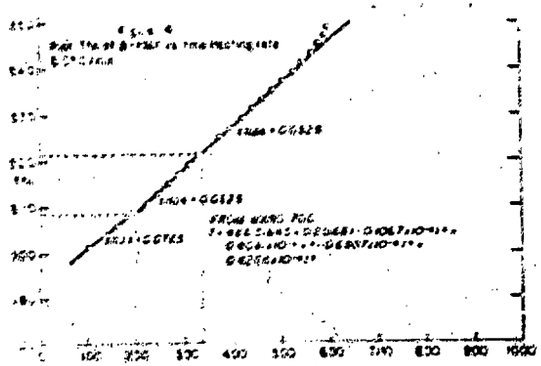

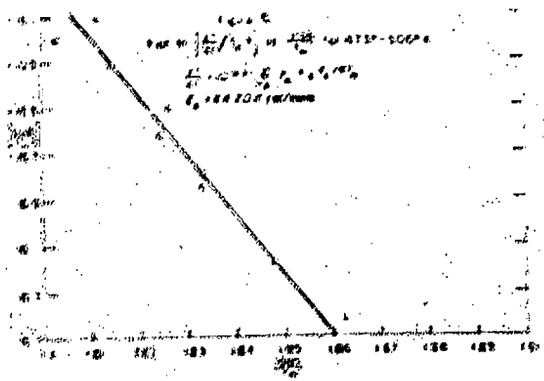

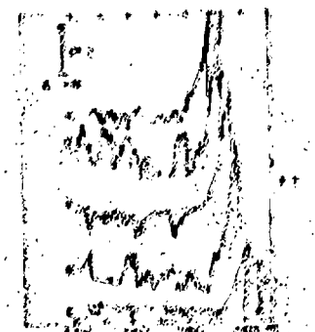

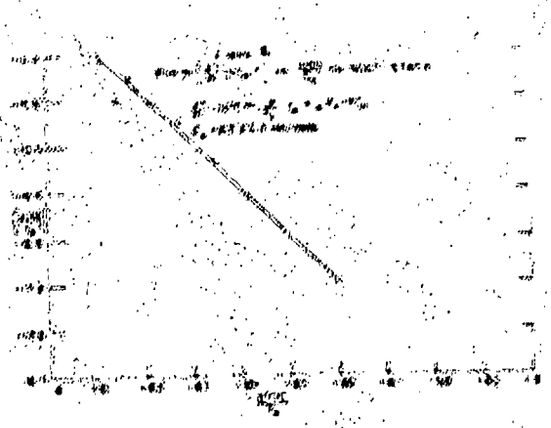

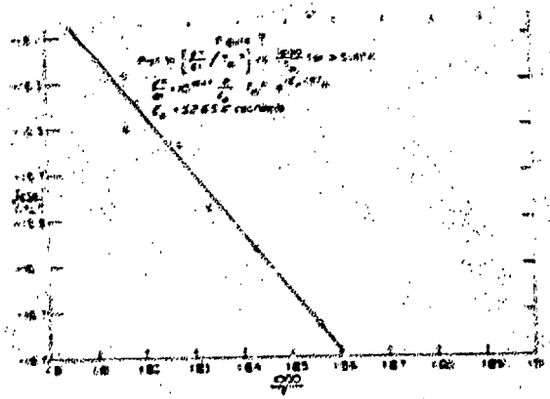

6-6. THERMODYNAMIC STUDY OF THE IGNITION AND PRE-IGNITION REACTIONS IN THE ZIRCONIUM-MOLYBDENUM TRIOXIDE DELAY SYSTEM

By

A. D. Kirshenbaum, C. Campbell and A. J. Beardsell
Pyrotechnics Laboratory, Picatinny Arsenal, Dover, New Jersey

INTRODUCTION

The delay composition M-143 is an element in the experimental delay train XM204E1 and consists of 70% Zr, 25% MoO_3, 10% Cr_2O_3 and 1% organic binder (Vinyl Alcohol-Acetate Resin, VAAR). The component concentrations are dictated by the requirement of a specific burning rate to provide a precise time interval (~ 40 ms). The main reaction is between Zr and MoO_3, according to the equation

$$3Zr + 2MoO_3 \longrightarrow 3ZrO_2 + 2Mo \qquad (1)$$
$$\Delta H = -441 \text{ Kcal}$$

Since the Zr is an excess, it may also undergo reaction with the chromium sesquioxide according to the equation

$$3Zr + 2Cr_2O_3 \longrightarrow 3ZrO_2 + 4Cr \qquad (2)$$
$$\Delta H = -218 \text{ Kcal}$$

Although reactions (1) and (2) are completed in the combustion of M-143, only 44% of the Zr is consumed. However, the original intent in the use of Cr_2O_3 was to lower the burning rate to the desired level, that is, to act as a diluent. The primary purpose of the organic resin is to bind the solid mixture to prevent it from crumbling.

A DTA curve on the M-143 composition is shown in Figure 1. There is no thermal activity up to 1200° at which point a strong exotherm begins to develop. This exothermic reaction is sufficient heat to ignite the mixture. In actuality, this curve only gives some idea of the minimum ignition temperature and further studies on the mechanisms of the system are required to identify the underlying processes.

Therefore, the purpose of the work reported here is to investigate the pre-ignition reactions responsible for the ignition of M-143. To our knowledge, there is no reported literature in this area of this system. The main method of investigation was the method of differential thermal analysis coupled with x-ray analysis of the reactants and products.

EXPERIMENTAL PROCEDURES

The differential thermal analysis was performed using a Du Pont 900 instrument. A 40 mg sample was placed in a glass vial which was inserted into the DTA block. Aluminum oxide was used as the reference material with a heating rate of 10°/min. The sample was protected from air oxidation by using an argon atmosphere at a constant flow rate. The simultaneous DTA-TGA runs were made using a Mettler thermoanalyzer. A 20 mg sample was placed in a platinum cup for these experiments, using the conditions described above.

The x-ray diffraction analyses of the products were made using a Siemans Crystalloflex II.

MATERIALS

The Zirconium used in most of this study was obtained from Foote Mineral Co. A typical analysis of the Foote Mineral zirconium is as follows:

Zr (total)	= 95.5%
Fe	= 0.02
Al	= 0.10
H_2	= 0.13
Acid soluble calcium	= 0.07
Gain on Ignition	= 31.0

which indicates that 6.5% of the zirconium was present as the oxide and 5.5% as the hydride. In addition to the Foote Mineral zirconium, the following zirconium samples were used in the studies on the effect of particle size:

Alfa Inorganics	99.9% Zr
Carborundum Metals Co.	Grade 93-1-6
Space Metal Corp	Lot SM-2-2μ 117-67

The MoO_3 was obtained from Fisher Scientific. It has an average particle size of 4 μ, was 99.5% pure and was used as received.

The Cr_2O_3 used in these studies was technical grade material obtained from the Fisher Scientific Company.

RESULTS

Zr-MoO_3 Reaction

The DTA curves for mixtures of 70% Zr-30% MoO_3 (the same ratio used in M-143) are shown in Figure 2. The significant feature of these curves is the presence of two exotherms, which appeared as two distinct

peaks or as a shoulder and a peak depending upon the zirconium batch used. The first exotherm peaks at 550°C and the second at 650°C. Zirconium of various particle sizes was also used in these studies. The major effect of particle size is to raise the temperature at which the two exotherms peak, as the particle size increases as shown in Table I. This correspondence can be explained by a decrease in the rate of oxidation of the zirconium as the particle size increases.

TABLE I

Effect of Zr Particle Size on the DTA Curves of Zr-MoO_3 Mixture

Average Particle Size, μ	Start of Reaction, °C	Temperature, °C: First Exothermic Peak	Temperature, °C: Second Exothermic Peak
2	485	Ignited	-
3	470	545	590
10	495	580	695
44	485	670	710
57	490	720	785
44-177 (mixture)	490	>> 700	-

The interpretation of the two stage reaction was derived from x-ray diffraction analysis of the products of the complete reaction as shown in Figure 3, Curve a, by separating the two exotherms. The first exotherm was isolated by running the temperature up to 580°C after which it was held constant for 15 minutes, before further heating to 700°C, as shown in Figure 3, Curve a. The results of the x-ray diffraction analysis are shown in Table II.

TABLE II

X-Ray Diffraction Results of Reaction Products From Zr-MoO_3 Reaction

Maximum Reaction Temperature (°C): 580°	700°
Zr	Zr
ZrO_2	ZrO_2
Mo_2O_3	Mo
MoO_2	Mo_2O_3

On the basis of these results it appears that the reaction responsible for the first exotherm is

$$Zr + 2MoO_3 \longrightarrow ZrO_2 + 2MoO_2 \qquad (3)$$
$$\Delta H = -163.5 \text{ Kcal}$$

And the second exotherm is due to

$$Zr + 4MoO_2 \longrightarrow ZrO_2 + 2Mo_2O_3 \qquad (4)$$

$$3Zr + 2Mo_2O_3 \longrightarrow 3ZrO_2 + 4Mo \qquad (5)$$

There is some question about the existence of Mo_2O_3[1]. It is contended that the substance is a solid solution of Mo in MoO_2. However, the x-ray analysis corresponds to that reported for Mo_2O_3[2]. It is quite possible that the MoO_2 is reduced to Mo, which is retained in the crystal lattice of the dioxide. In that case reactions (4) and (5) would be

$$Zr + MoO_2 \longrightarrow ZrO_2 + Mo \qquad (6)$$
$$\Delta H = -30 \text{ Kcal}$$

To confirm this, a DTA experiment was run on a Zr-MoO_2 mixture with the result shown in Figure 3, Curve c, the exotherm begins at 545°C and peaks at 625°C and corresponds closely with the second exotherm derived from the Zr-MoO_3 reaction.

The presence of Mo was more clearly established when the Zr-MoO_3 was ignited and burned to completion in a helium atmosphere. The products were scraped from the wall of the reaction vessel (a glass bulb) and subjected to x-ray analysis. The analysis revealed the presence of Mo, Zr, ZrO_2, $ZrMo_2$.

A residual pressure in the reaction bulb prompted an investigation of the gases. The excess gas pressure was found to be due mainly to hydrogen, which is believed to be produced in the decomposition of zirconium hydride, an impurity in the zirconium powder (about 5.5%).

The effect of zirconium hydride on the reaction of Zr/MoO_3 is shown in Figure 4. The hydride decomposes upon heating from 410°C to 720°C in several endothermic steps (Curve a). The effect of this endothermic decomposition is seen in Curve b when a 35% ZrH_2, 35% Zr and 30% MoO_3 mixture is heated. This is shown by a decrease in the heights of the 2 exotherms observed when Zr/MoO_3 are heated and by the endotherm at 710°C. Thus the hydride reduces the exothermicity of the Zr/MoO_3 reaction.

Effect of Chromium Sesquioxide

Chromium sesquioxide is added to the SI-143 composition to lower the burning rate of the mixture. It therefore acts as a diluent although it can still enter into reaction with zirconium.

A DTA curve of the Zr-Cr_2O_3 mixture, shown in Figure 5, Curve d exhibits an exotherm which begins at about 650°C. However, the Cr_2O_3 appears to have only a minor effect on the Zr-MoO_3 interaction. The temperature at which the reaction of both the binary mixture of Zr-MoO_3 and the tertiary of Zr-MoO_3-Cr_2O_3 initiates is 480–490°C. However, the Cr_2O_3 appears to influence only the Zr-MoO_3 second stage reaction exotherm, the energy output appearing to be somewhat lower as shown by the smaller exotherm (Figure 5, Curves a & b). This observation indicates that the heat output of the second stage process controls the propagating reaction since the overall effect of Cr_2O_3 is to lower the burning rate.

Effect of Organic Binder

The organic resin, vinyl alcohol acetate resin (VAAR) is added to the delay to impart cohesion characteristics to the pressed blend. The DTA on VAAR itself, shown in Figure 6, Curve a, displays a small endotherm at about 300°C where it also begins to pyrolyze forming a carbon ash with the evolution of the gases CO, CO_2 and CH_4. The DTA on a mixture of Zr-MoO_3-VAAR (Figure 6, Curve b) shows a slight exotherm at 450°C, the beginning of a strong exotherm at 480°C and ignition at about 550°C. Thus, it appears that the resin promotes the ignition of the fuel-oxidant system. Its dominant effect is to aid in the ignition reaction which leads to propagation.

To further investigate the effect of VAAR on the ignition reaction, a Zr-MoO_3 mixture containing the carbon ash formed from the degradation of VAAR was prepared and a DTA for the mixture was obtained. As shown in Figure 6, c, the mixture initiates at 555°C; similar behavior was observed when activated charcoal was used instead of the VAAR pyrolysis residue.

Shown in Figure 7 is a simultaneous DTA-TGA of this mixture. The DTA displays an exotherm at 490°C and an endotherm at 775°C which begins to deepen at 530°C. The TGA shows a two-step weight loss at temperatures corresponding to these exotherms and verifies data reported by Hegedus and Neugebauer[3]. In addition, the DTA-TGA of a MoO_2-C mixture give the same endothermic peaks and weight loss as the MoO_3 mixture. The reactions, therefore, appear to be

$$2MoO_3 + C \longrightarrow 2MoO_2 + CO_2 \qquad (7)$$
$$\Delta H = -14 \text{ Kcal}$$

$$MoO_2 + 2C \longrightarrow Mo + 2CO \qquad (8)$$
$$\Delta H = +77 \text{ Kcal}$$

and
$$MoO_2 + C \longrightarrow Mo + CO_2 \qquad (9)$$
$$\Delta H = +37 \text{ Kcal}$$

Reaction (7) is exothermic by 14 Kcal and occurs at about the same temperature at which the Zr-MoO_3 reaction begins (485–490°C). It therefore appears that the VAAR initially degrades to a carbon ash which in turn reacts with the MoO_3 releasing sufficient heat to produce ignition.

DISCUSSION

The correlation of DTA data with the features of the reaction that lead to ignition and propagation of the SI-143 composition appear quite clear. The main reaction is between zirconium and molybdenum trioxide which react exothermically in a two stage process according to equations (3) and (6).

The two stage reaction found for the Zr/MoO_3 system appears to be of a general nature. Thus, the metals Ti, W, and Ge and the non-metals such as C[3] and H_2[5,6] react with MoO_3 in a two or more stage process. Shown in Figure 8 are DTA curves of Ti/MoO_3 where three exothermic peaks are observed and W/MoO_3 in which four appear. In considering the first stage process it should be noted that the temperature at which the fuel powder and the MoO_3 begin to interact appears to be practically independent of the nature of the fuel powder, varying over a narrow range of 450 to 550°, this indicates that the energy requirements to initiate the first stage are the same for the different fuel powders and therefore involves the activation of MoO_3. Schwalb[4] contends that this activation process is

$$MoO_3 \longrightarrow MoO_2 + 2O_2$$

with oxygen diffusing through product layers to react with the metal.

It is highly probable that the exothermicity of the reaction $MoO_2 \longrightarrow Mo$ is required to promote the self propagation of the metal - MoO_3 reaction. For fuel powders such as carbon or germanium, the second stage reaction is endothermic and therefore these mixtures will not ignite and sustain combustion, as was observed in attempts to ignite pressed pellets of C-MoO_3 and Ge-MoO_3 in this Laboratory. The DTA results on the effect of organic binder (VAAR) and Cr_2O_3 on the Zr-MoO_3 reaction indicate that they affect the second stage process. The Cr_2O_3 appears to act as a heat sink in that it absorbs heat from the second stage process and consequently lowers the propagation rate. The heat liberated in the first stage process is distributed between the Cr_2O_3 and reaction products. In addition as the first stage reaction takes place, at least initially, the metal and fuel are in close contact, thus allowing the reaction to proceed at an unimpeded rate. However, for the Zr to react further, active oxygen must diffuse through a ZrO_2 layer, thus slowing down the reaction. The heat liberated in the process can then be absorbed by the Cr_2O_3 as well.

As previously stated, the organic binder appears to aid in the ignition of the Zr-MoO_3 system by providing heat from the exothermic reaction (-14 Kcal) between C and MoO_3. This reaction proceeds at a high rate at about 480°C and is close to the minimum ignition temperature of the Zr-MoO_3 reaction of about 490°C. It was originally conjectured that the CO formed during the decomposition of VAAR might react according to

$$CO + MoO_3 \longrightarrow MoO_2 + CO_2$$
$$\Delta H = -26 \text{ Kcal}$$

While this reaction is exothermic it may occur to a certain extent but it is believed to be insignificant because the carbon ash, which is completely decomposed, produces the same effect as the VAAR.

REFERENCES

1. H. Remy, "Treatise on Inorganic Chemistry", Elsevier Publishing Co. (1956) p. 166.

2. J. D. Hanawalt, H. W. Rinn & L. K. Frevel, Industrial & Engineering Chemistry, Analytical Edition, 10, 457 (1938).

3. A. J. Hegedus & J. Neugebauer, Z. Anorg. Allg. Chem. 305 216 (1960)

4. G. M. Schwab & J. Gerlach, Z. Physik, Chimie Neu Folge. 56, 121 (1967).

5. H. Kay & B. G. Langston, J. Metals 16, 877 (1966).

6. C. Vasseleo, T. Nikolov & M. Chimbulev, Inst. Mining & Met. (London), Trans. Sect. C, 77, C36 (1968).

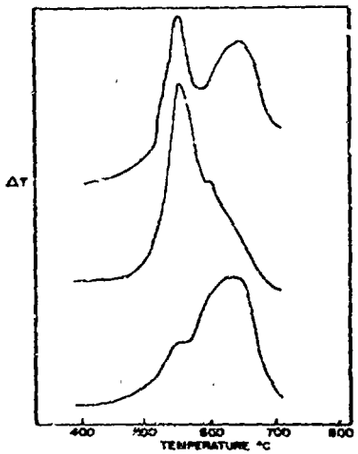

FIGURE 2: THERMOGRAMS OF 70% Zr - 30% MoO_3 MIXTURES USING THREE DIFFERENT BATCHES OF ZIRCONIUM (AVERAGE PARTICLE SIZE 3μ)

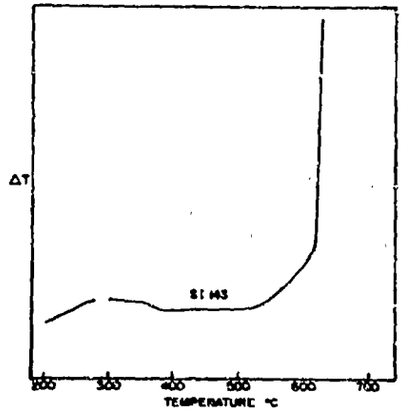

FIGURE 1: THERMOGRAM OF DELAY COMPOSITION SI 143

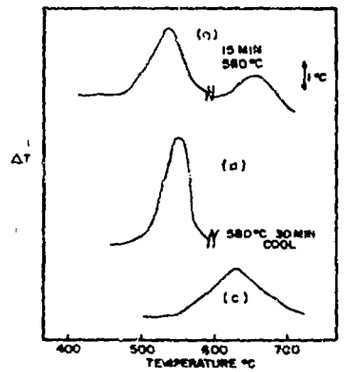

FIGURE 3: THERMOGRAM OF 70% Zr - 30% MoO_3 WITH PARTIAL ISOTHERMAL HEATING UNDER CONDITIONS (a) HEATING RATE 10°C / MIN TO 580°C, ISOTHERMAL AT 580°C FOR 15 MINUTES FOLLOWED BY CONTINUED HEATING (b) HEATING RATE 10°C/MIN TO 580°C, ISOTHERMAL AT 580°C FOR 30 MINUTES FOLLOWED BY COOLING AND (c) THERMOGRAM OF Zr - MoO_2

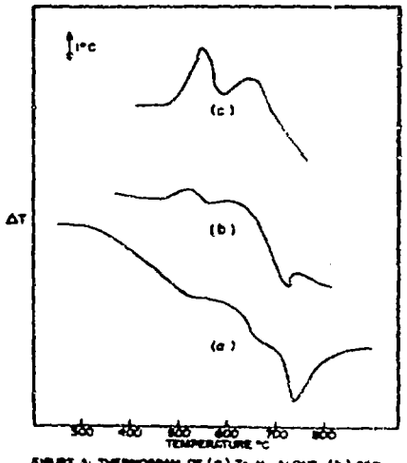

FIGURE 4: THERMOGRAM OF (a) Zr H_2 ALONE, (b) 35% Zr H_2, 35% Zr, 30% MoO_3 AND (c) 70% Zr, 30% MoO_3

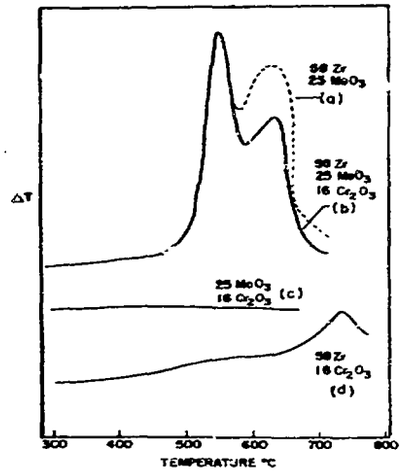

FIGURE 5 THERMOGRAM OF Zr–MoO_3 MIXTURE WITH ADDED Cr_2O_3

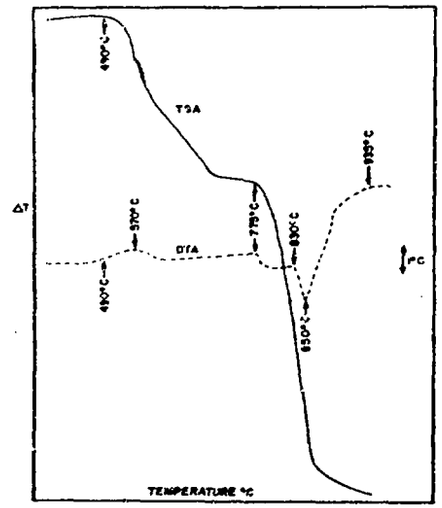

FIGURE 7 THERMOGRAM OF CARBON–MoO_3 MIXTURE

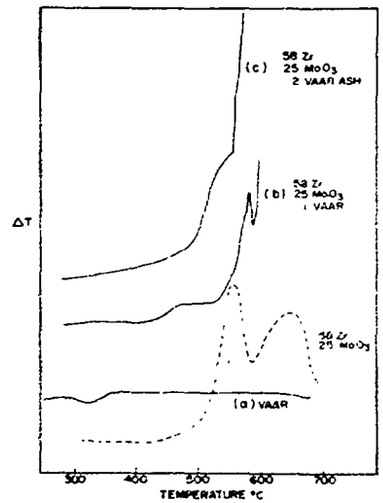

FIGURE 6 THERMOGRAM OF VINYL ALCOHOL ACETATE RESIN (VAAR) (a) ALONE (b) ADDED TO Zr–MoO_3 AND (c) VAAR ASH MIXED WITH Zr–MoO_3

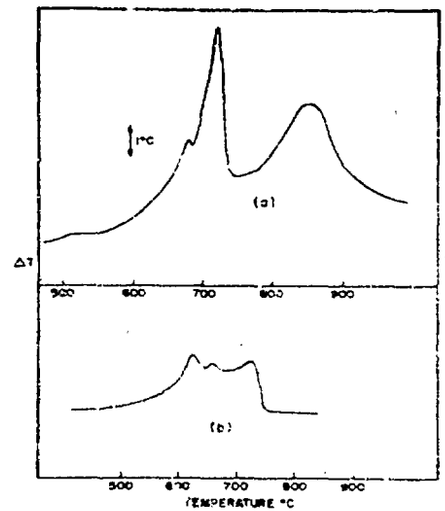

FIGURE 8. THERMOGRAM OF (a) Ti–MoO_3 (b) W–MoO_3

I-7. ADAPTATION OF FAULT TREE TO THE SAFETY ANALYSIS OF PYROTECHNIC DEVICES

by R. E. McClay and M. M. Hoobchaak, Naval Ordnance Station

INTRODUCTION

There is a current recognition of the concept where the total effectiveness of weapons systems is expressed not only in terms of raw performance capabilities but also in terms of reliability, safety, ability to be successfully operated, maintained, and to survive hostile action. Now involved in the weapons RDT&E process with the technologist are new groups of specialists whose function it is to review and enchance these special qualities of systems effectiveness. These groups are comprised of safety and reliability engineers, maintainability and survivability or systems hardening specialists together with human factors engineers, training experts, psychologists, and other behavioral scientists concerned with the man-machine interface.

In conjunction with this evolution, new systems analysis and predictive techniques are being devised to augment the existing methodologies in each of these rapidly specializing areas. Criteria, standards, and minimum system requirements are evolving and are being included in stated system performance goals. Planning is, or soon will be, required to insure that safety, reliability, maintainability, operability, and survivability are designed into all new weapons systems and that test programs are structured for verification of these special attributes.

Military Standard 882 sets forth the general requirements for System Safety Programs and identifies Preliminary Hazard Analysis, System/Subsystem Hazard Analysis and Operating Hazard Analysis as methods appropriate for the identification and control of weapon system hazards. Most weapons systems development agencies soon will have System Safety Manuals in print to set forth specific analytical procedures and requirements for the performance of these analyses within the system life cycle. The day is approaching when no pyrotechnic system, regardless of its simplicity, will be developed by the military without some sort of system safety analysis.

The pyrotechnic system designer in most cases will be the focal point for these system safety analyses. If they are not performed under his direction, they certainly will not be completed without his direct input. The designer also will be involved in system changes necessitated by the outcome of these analyses. System trade-offs probably will be required to eliminate certain failure modes or to minimize others. The purpose of this paper is to discuss the application and elementary mechanics of the Fault Tree Analysis (FTA), one of the more common and complex forms of System Hazard Analysis as defined by Military Standard 882.

The historical development of this technique goes back only to the early 1960's. It was in this time-frame that the U.S. Air Force contracted with Bell Telephone Laboratories for the development of an analytical technique which could probabilistically identify and relate factors which might contribute to an unacceptable failure of the Minuteman ICBM Launch System.[1] The Fault Tree Technique came out of this work and resulted in:

(1) The development of a tree-like logic block diagram portraying each and every factor contributing to a hazardous or unacceptable event (such as an inadvertant launch).

(2) An algebraic formulation of logic equations which expressed the relationship of these fault-producing events to each other.

(3) The application of probabilistic mathematics to provide an estimate of an undesirable event occuring and a means of predicting those contributing factors most likely to cause it.

BASICS OF FAULT TREE ANALYSIS

Before delving into the mechanics of the analytical technique, it would be well to note what information the resulting analysis can be expected to provide.

(1) The analysis will show the number of ways that an undesirable event can occur. Even without absolute probability information, the pyrotechnic system designer might be forewarned by this and attempt to eliminate possible failure causes. A choice between designs can be aided where one design has significantly fewer failure modes than the others.

(2) Those system failures which require no or few contributing conditions will be illustrated. These are inherently more hazardous than those failures which require coexisting conditions or simultaneous occurences and will be isolated for control or elimination. For example, fuel exhaustion in aircraft is inherently a greater hazard than mechanical failure because it requires fewer contributing conditions in order to cause an undesired event such as a crash landing.

(3) The presentation of all failure causes and contributing events in an FTA can point out areas where additional test data might be desirable.

(4) Where complete failure rate data is available, the FTA permits a calculation of the overall probability of the undesired event. The most probable failure mode is also made apparent.

As in any system analysis, the initial step is to define the system under consideration. Interfaces with other systems should be carefully reviewed to insure that all subsystems in these areas are included. For example, one would be sure to include the ejection subsystem consisting of cartridges and their actuating mechanism in any analysis of an aircraft parachute flare system. While not an integral part of the flare, the ejection subsystem can directly contribute to system failure thus affecting both reliability and safety.

A question can arise as to whether operating personnel should be included in the analysis as part of a pyrotechnic system. Where the system is complex or where the interest is only in material failures, this may not be necessary. However, since many incidents involve some sort of personnel error, significant information can be gained if operating errors are included as system failures. It may therefore be advisable to repeat the analysis including operating personnel as part of the system.

It also is important to define the life stage in which the analysis is being made. A separate analysis may be required for the test, shipment, storage, operational use, and disposal stages of a pyrotechnic system. The environmental conditions, failure modes, and hazards can be considerably different in each of these life stages.

The next step in the analysis is to single out and define the undesirable end event which is the statement placed at the top of the fault tree. If this event is stated too broadly, the fault tree will

to large, unwieldy, and will contain failure modes unrelated to system safety. If a too-narrow definition of the end event is given, the analysis may prove to be incomplete and misleading. For example, in an operational shoulder-fired parachute flare system the undesired end event could be stated as follows:

[redacted] OF SYSTEM

This end event will produce a very large fault tree and will include malfunctions such as non-ignition of flare and failure of flare-chute to deploy. From a reliability stand point these are important, however, they might not be unsafe failures and probably are extraneous to a system safety analysis of this system.

The undesired event also could be stated thusly:

[redacted] INITIATION OF FLARE

A more manageable tree develops from this statement, however, omitted are hazardous failures associated with the intentional functioning of the device such as the possible jamming of the round in its launcher.

To summarize this point, the following considerations apply:

(1) When the FTA is being performed as a System Safety Analysis, the end event should be stated so as to restrict the analysis to unsafe failures.

(2) It must be clear to the analyst what information is desired from a particular FTA, ie, detailed information on a specific failure (such as inadvertant missile launch) or general information on all possible system failures.

(3) Computation time for a quantitative FTA will place some limitation upon the number of failure events which can be considered. Limited computation time will therefore favor a narrow statement of the final undesired event.

Once the final undesired event is properly defined, the system is then analyzed and all the logical combinations of fault events which can cause the end event are determined. This development is continued until all input fault events on the tree are expressed in terms of basic identifiable faults which can be assigned probability values.

Some of the various kinds of events used in fault trees are represented by the following symbols:[2]

A. The RECTANGLE identifies an event that results from a combination of fault events.

B. The CIRCLE identifies a basic failure of a component.

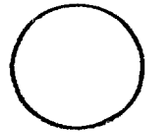

C. The HOUSE identifies a basic event which is normal for the system.

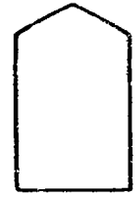

D. The DIAMOND identifies a failure which has not been fully developed due to lack of information or significance.

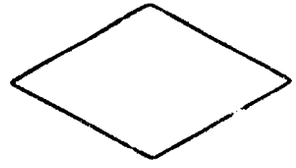

E. The SQUARE is used here to indicate a human error.

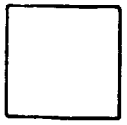

The logic operators required to develop the fault trees have been symbolized as follows:

A. The AND GATE describes the logical operation which requires the coexistence of all inputs to cause output.

B. The PRIORITY AND GATE performs the same function as the AND GATE except that the inputs must occur in the sequence stipulated.

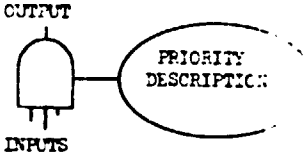

C. The OR GATE describes the logical operation whereby the output is caused by the occurrence of any of the inputs.

D. The EXCLUSIVE OR GATE performs the same function as the OR GATE except that specified inputs cannot coexist.

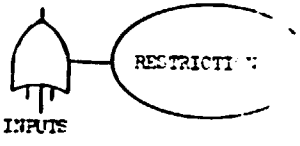

E. The INHIBIT GATE describes a situation in which a certain condition of the system must exist before one failure produces another. The inhibit condition may be either normal to the system or be the result of equipment failures.

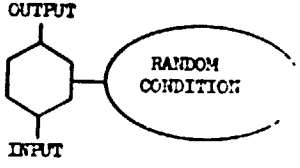

Special symbols are used in order to simplify the graphic representation of fault tree construction. An example of these special symbols is shown below:

The TRANSFER symbol is used to show continuity between two parts of the tree. A line into the side of the triangle transfers everything below to another area identified by the triangle with a line drawn from the apex.

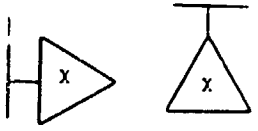

An oversimplified example of a domestic hot-water system is shown in Figure 1,[3] to illustrate the symbolic combinations of fault events. The fault tree as it is constructed here shows that if event B, C, or D should occur, heat will be applied continuously to the water tank. If this happens and event A also occurs, the pressure will not be relieved and the final undesirable event, tank rupture, will occur.

In this example, events A, B, C, and D represent identifiable and unrelated component failures; these are known as primary failures and in terms of analysis complexity, comprise the first order of magnitude. Where the analysis goes beyond the primary to include secondary failures, the level of graphic and mathematical complexity increases by another order of magnitude. Secondary failures include the effects of a component failure on the failure probability of the other components in the system. In secondary failure analysis, the

inhibit gates such as the conditional, priority, and restricted gates come into use to define the circumstances under which these failures occur.[4]

The logic equations relating the failure events are developed and simplified according to the propositions of Boolean Algebra.[5,6] Though this realm of mathematics may not seem familiar to most ordnance engineers and scientists, it is relatively straightforward and will not receive detailed treatment in this paper. For illustration however, we will work out the equation for the example given above.

The Boolean AND Statement is simply that the probability of two events occurring together is the product of the probabilities that each will occur.

$A \text{ (AND) } B = A \cap B = A \cdot B = AB$

Similarly the OR statement defines the probability that at least one of several events will occur, as equal to the sum of the probabilities that each will occur.

$B \text{ (OR) } C = B \cup C = B + C$

$B \text{ (OR) } C \text{ (OR) } D = B \cup C \cup D = B + C + D$

The Distributive Law of Boolean Algebra then indicates that in the Hot-Water System Example, the probability (F) of the occurrence of the undesired event can be calculated by the equation:

$F = A \cap (B \cup C \cup D) = A \cdot (B + C + D)$

For very large systems such as Minuteman or Manned Orbital Laboratory, with many levels of subsystem and component failure events, the fault tree becomes enormous and must be drawn with the aid of computers. Needless to say, the computation of failure probabilities in these cases would be impossible without computers. Because of the complexity, these analyses are almost always quantitative with their usefulness limited by the accuracy of the failure rate data.

Since most pyrotechnic systems have a limited number of subsystems and components, the FTAs can be used to provide qualitative as well as quantitative information based on documented failure rates. Two examples will be given here to show how this can be done.

Functional and descriptive information about the M. 111 Hand Fired Signal is given on the next few pages to aid in following the FTA on this device. This FTA has been developed here for illustration only and was not expanded in its full detail.

Since the system is not inordinately complex, it was possible to use a rather general statement as the undesired end event. The objective here was to view all possible unsafe failures in the operational phase rather than to concentrate on any particular failure mode. It also was possible to single out a branch for the analysis of unsafe operational procedures (Event No. 2). Human error thus can be viewed and assessed by the system designer as a real restraint to the system safety aspects of design.

The system safety analyst looks first at the FTA for failures which lead to the end event through chains of unrestricted OR gates. In Figure 2, events No.'s 111, 112, 1211,1221, 1231, 122321, 1222, 122311, and 211 are all of this type. They are important in a qualitative sense because they theoretically require no contributing events in order to cause the undesired end event. Unless other information is available, they should be considered to be more probable than events falling below INHIBIT or AND gates since these require coexisting circumstances.

FUNCTIONAL DESCRIPTION OF MK 111 MOD 0

HAND-FIRED SIGNAL

The Mk 111 Mod 0 Signal is made-up of an aluminum body containing a pyrotechnic candle and a M42G percussion primer. The signal has a screw thread connector with which it is attached to the Mk 31 Mod 0 projector. The primer ignites a black powder expelling charge which drives off cloth spacers and a sealing cap and propels the flare upward to a height above 250 ft. The signals are carried in groups of seven packaged in bandoleers which have protective tabs covering the percussion caps to guard against accidental initiation.

The Mk 31 projector is hand held and uses a spring actuated firing pin to initiate the primer. The device is cocked by sliding the trigger screw down a slot compressing the spring which is then locked until the signal can be seated. To launch the flare, the projector is held over the head and the trigger screw pressed sideways to release the firing pin.

The operating sequence can be illustrated as follows:

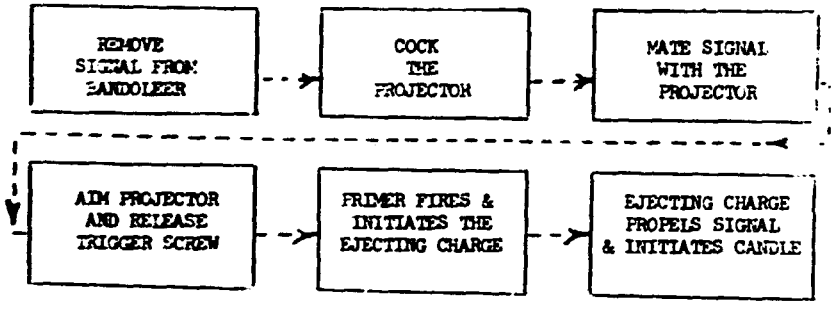

In the example the designer would note that events No.'s 111, 112, 1211, 1221, and 1231 identify subsystem or component defects which directly affect system safety. These areas thus can be singled out for greater inspection and quality control. Redundancies might also be indicated. Similarly, events No.'s 1222, 122311, and 211 seem to be the most serious possible occurrences of human error. These might indicate areas for redesign, special training, printed precautions, and warnings.

The analyst also will review the conditional failures falling below AND or INHIBIT gates. Testing may be desirable to show in a more absolute way how probable these failures are. Failures leading to events No.'s 22, 222, 33, and 321 in the example should be so reviewed.

The FTA of the Mk 48 Decoy Flare is more precise in its specification of those conditions contributing to a fleet accident involving a Navy pyrotechnic system. Shipboard fire damage, oxygen depletion, smoke, or toxic gases in the ships' interior spaces, or ordnance/personnel in close proximity to a malfunction are all conditions which, if satisfied, will lead to a serious unsafe situation. Again in Figure 5 there are long chains of events, unrestricted by AND GATES and leading directly to the first echelon of system failure. Event 211220 is situated so that if electrolyte finds its way into the salt water battery of the Mk 48, an unsafe failure can occur through events 211 or 212 (via the transfer point at event 212211) contingent upon events 1, 2, or 3.

FUNCTIONAL DESCRIPTION OF MK 48 MOD 0 DECOY FLARE

The Mk 48 Mod 0 Decoy Flare is a system deployed either by hand or by launcher which burns while floating on the surface of the water.

The flare assembly consists of an aluminum outer tube which encases a styrofoam spacer, a fiberglass-melamine heat shield, and the flare grain candle. The ignition system consists of a Mk 72 Salt-Water-Actuated Battery, which is mounted within the flare base, and a Mk 1 Squib. The battery is protected from water contact by two base plugs and a base cover. The base plugs are fitted into holes on opposite sides of the assembly. The base cover is recessed in the flare base end and held in place by a retainer ring. In addition to functioning as an enclosure, the cover serves as part of the arming device. It may be rotated in the flare to render the flare either SAFE or ARMED by aligning the arrow with either the word "SAFE" or "ARMED" on the flare base. The candle is ignited by an electric squib for which power is supplied by the salt-water-activated battery. The device is functioned by pushing the base plugs into the base cavity; sea water then enters the battery cavity through the base plug holes. The battery provides current to fire the Mk 1 Squib. The squib ignites the candle and the resulting pressure build-up ruptures a burst disc diaphragm at the forward end of the flare. This action allows the flame and gases to be emitted.

The operational sequence is a follows:

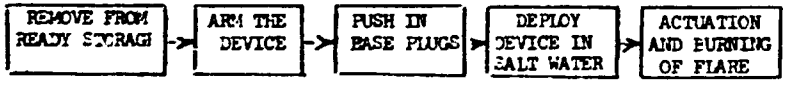

One of the basic limitations to FTA is that there is difficulty in comparing the severity of the outcome from several failures. In the Mk 48 example, there is no way to determine without further analysis if events 1, 2, or 3 would be most catastrophic in the event of an unsafe failure of the Decoy Flare. Until a data bank is established to accumulate failure rate data on pyrotechnic components and sub-systems, these FTAs will have only qualitative value. Since this analysis can be quickly performed on most pyrotechnic systems and since it provides a systematic method of evaluating the inherent safety in an overall system, the pyrotechnic system designer can find FTA a most useful tool even with the limitations above.

To summarize then, the development of complex weapons systems has led to the use of special methodology to evaluate the adequacy of systems reliability, safety, operability, maintainability and survivability. System safety analysis techniques such as FTA tend to pinpoint hazardous conditions and failure modes thus alerting design agencies to situations where corrective action should be taken. Even on systems of lesser complexity such as those involving pyrotechnics, the Fault Tree Analysis offers a more comprehensive and detailed view of systems safety than can be obtained with more intuitive approaches.

REFERENCES

1. P. A. Hilty: "The Fundamentals of Fault Tree Analyses" North American Aviation Inc., March 1963 (AD - 485377 --- Defense Documentation Center)

2. T. A. Waldeck: "System Safety Engineering Analyses Techniques" Boeing Inc., March 22, 1967 (AD - 809302L --- Defense Documentation Center)

REFERENCES (cont'd)

3. C. R. Eckberg: "WS-1338 Fault Tree Analysis Program Plan"
Boeing Inc., March 16, 1965
(Report No. D2 - 30207-1)

4. D. F. Haasl: "Advanced Concepts in Fault Tree Analyses"
Presented at System Safety Symposium June 8-9, 1965
Seattle, Washington

5. J. E. Whitesett: "Boolean Algebra and its Applications"
Addison-Wesley Publishing Co., 1961
London, England

6. F. E. Hahn: "Applied Boolean Algebra"
The Macmillan Co., 1966
New York, N.Y.

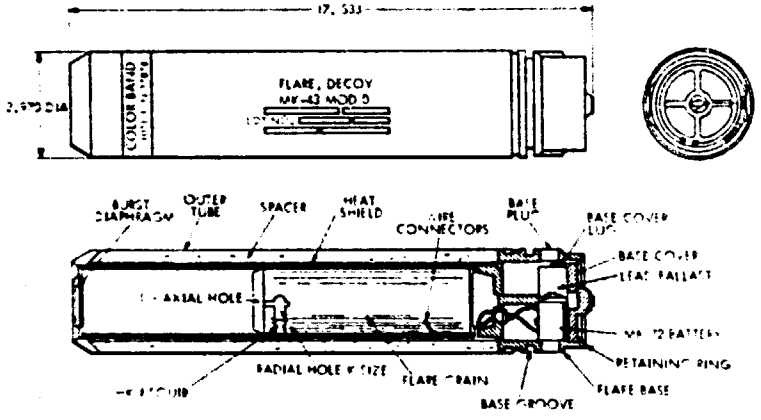

FIG 4. MK 48 MOD 0 DECOY FLARE

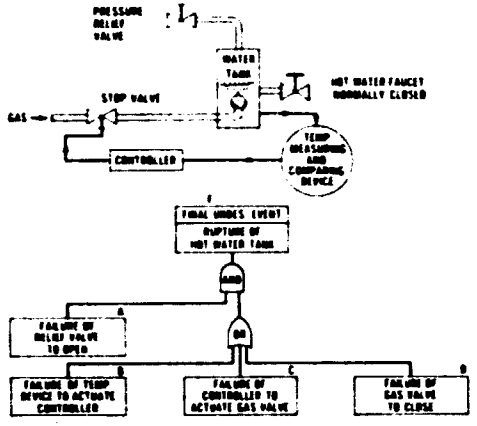

FIGURE 1 ILLUSTRATIVE EXAMPLE OF FAULT TREE DIAGRAM DOMESTIC HOT WATER SYSTEM

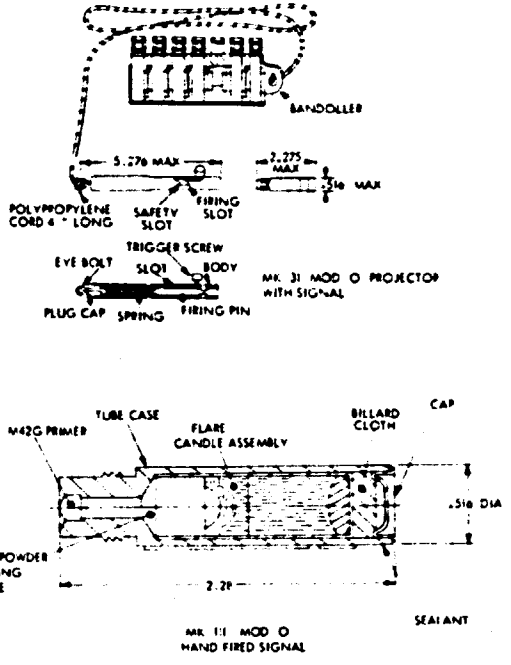

FIG 2. MK 111 MOD 0 HAND FIRED SIGNAL AND MK 31 MOD 0 PROJECTOR

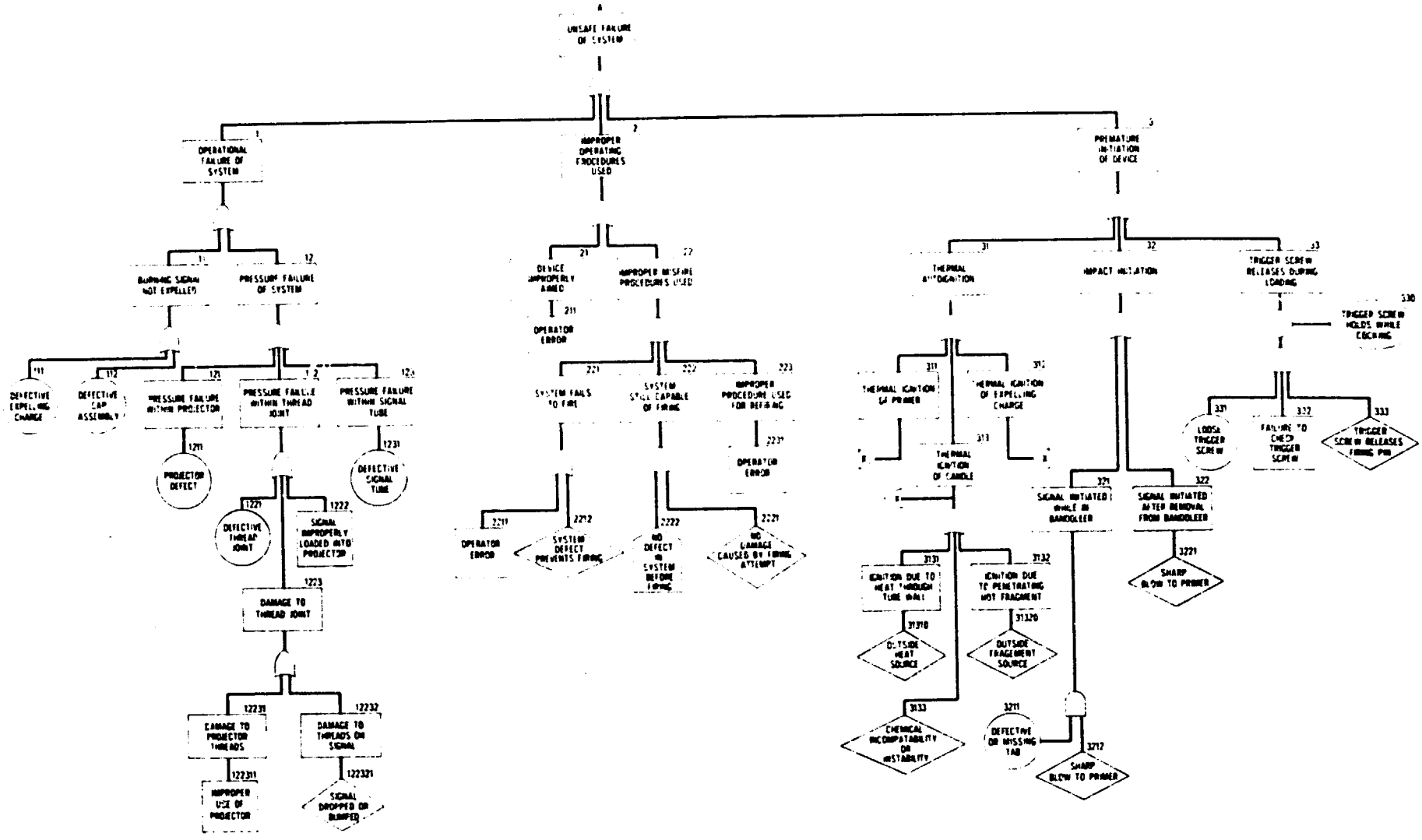

FIGURE 3. SYSTEM SAFETY ANALYSIS FAULT TREE MK 111 MOD 0 HAND FIRED SIGNAL OPERATIONAL PHASE

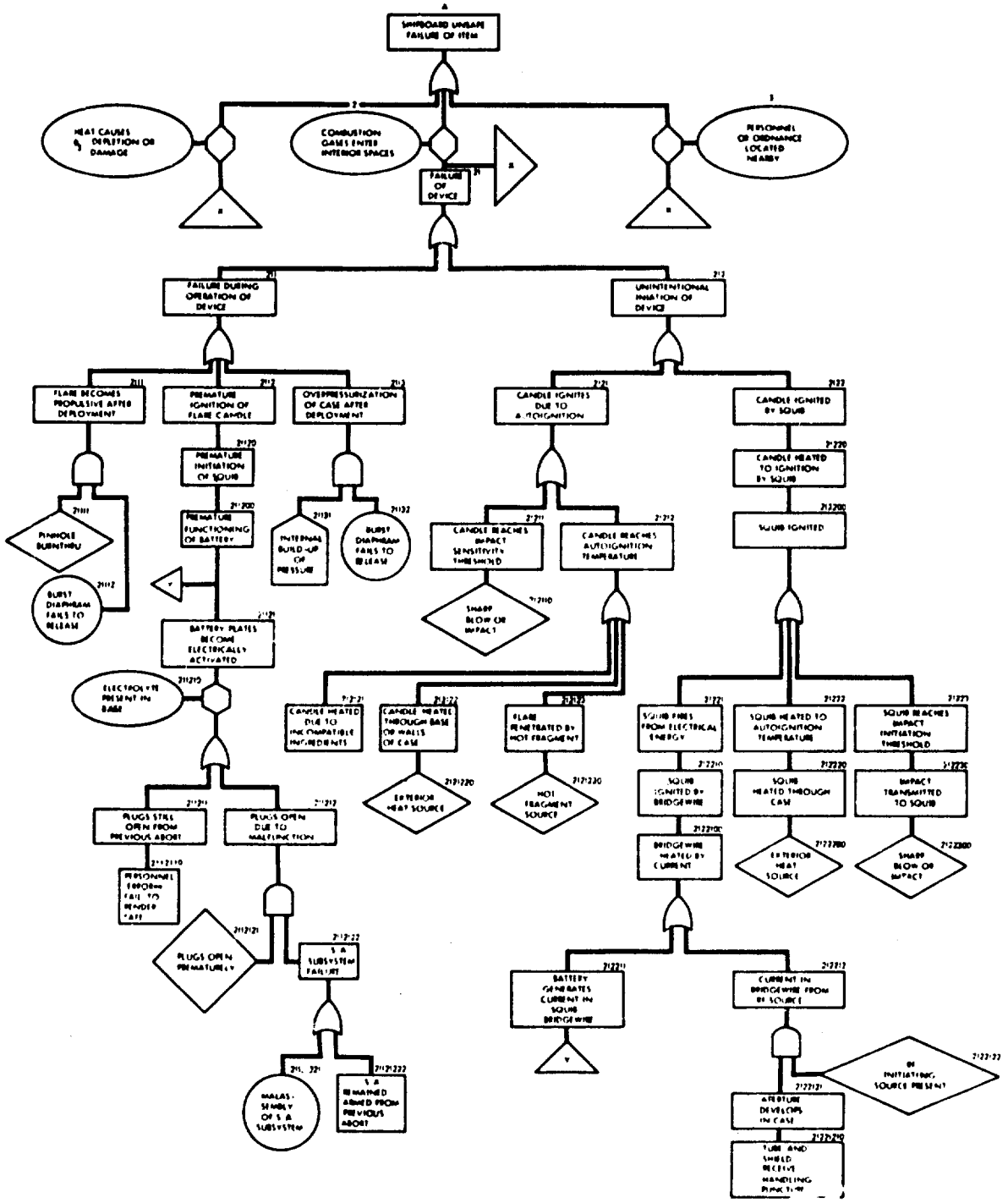

FIGURE 5 SYSTEM SAFETY ANALYSIS - FAULT TREE MK 48 MOD 0 DECOY FLARE OPERATIONAL PHASE

I-8. REMOTE INITIATION WITH NON-COHERENT LIGHT

FRANCIS H. BRATTON
APRAND, INC.
AVON, CONN.

Summary and Conclusions

Research carried out for Bickford Research Laboratories of Ensign Bickford Co. showed that non-coherent light from pyrotechnic, electric and explosive sources could produce ignition of materials through up to tens of feet of fiber optics. The lights used ranged from milliseconds to nanoseconds in duration.

These methods of utilization of radiant energy present different mechanisms for construction of pyrotechnic and explosive delay and ignition signal transfer devices.

The success obtained with pyrotechnic and primary explosive materials, in combination with theoretical considerations point to potential for extension to remote initiation over much greater distances and to remote initiation of less sensitive target materials.

Experimental Findings

On the basis of reported laser initiation (1) and after several exploratory experiments confirmed that the "light"* from small incandescent sources and from pyrotechnic compositions contained in photographic flash bulbs was capable of producing ignition of some primer materials when collected by techniques similar to those used in arc-image studies the effort was shifted to the use of fiber optics and other light conduits. A great deal of the later work was done using small targets of a boron - red lead delay material (B - Pb_3O_4) containing about a 15 to 85 ratio of the ingredients.

As intense light similar in nature to that generated by flash bulbs was of greatest interest at the outset, methods to improve their use were sought, and means for channeling light through tubes, fiber optics and coated rods were explored. Generally the best results were obtained

1. When bulbs with high (caloric) energy per unit of surface area were used.
2. When fiber optics of glass were highly polished and placed near the bulb surface.
3. When the bulb was suitably protected from rupture.
4. When the target was placed near the end of the fiber optic.
5. When the fiber optic was drawn to provide some concentration of energy.
6. When fiber optics with more fibers, and hence larger cross-sectional areas, were used.

A summary of results obtained in this investigation is presented in Table 1. From those data it can be seen that the light from a flash bulb, properly arranged with polished glass fiber optics, produced ignition through up to 15 feet. With acrylic fiber optics (Crofon* 1610) positive results ranged up to about 3 feet with these long duration light sources. Without

*The term "light" is used to include infrared and ultraviolet as well as the visible wave lengths.

*Trade Mark, E. I. duPont de Nemours

Table 1

MAXIMUM DISTANCES OF REMOTE INITIATION OF BORON - RED LEAD TARGETS WITH NON-COHERENT LIGHT

Light Source	Light Conduit	Maximum length for Ignition (Inches)	Approx. Duration of Light Pulse (Seconds)
Flash Bulb	Glass Fiber Optic Corning 5013	180	40×10^{-5}
"	Acrylic Fiber Optic Crofon* 1610	28	"
"	Acrylic Rod 1/8th in. - Bare	2	"
"	Acrylic Rod 1/8th in. - Al wrap	10	"
Ultrablitz Electronic Flash	Acrylic Fiber Optic Crofon 1610	18	1×10^{-3}
80 gr. RDX-63 mm Argon	Glass Fiber Optic Corning 5010	14	8×10^{-6}
"	Acrylic Fiber Optic Crofon 1610	7	"
80 gr. RDX Butted	Glass Fiber Optic Corning 5010	60	50×10^{-9}
Boron - Red Lead	Acrylic Fiber Optic Crofon 1610	2	ca 3×10^{-3}

*Trade Mark, E. I. duPont de Nemours

elaborate study ignitions from a small electronic flash unit were produced through 1.5' of acrylic fiber optics. With light from detonating explosive ignitions were obtained through 5 feet of small diameter glass fiber optics, in this case Corning Glass 5010 material. For the intense light from a shock wave acting on an inert gas in a small assembly the maximum length of glass fiber optics was about 1.3 feet. Generally ignition transfer distances through acrylic fiber optics were less than half those obtained with glass optics, and fiber optics with more fibers (greater transmission area) were more effective than those with fewer fibers.

A few experiments with dextrinated lead azide targets gave positive results through very short (3 - 6 mm) lengths of acrylic fiber optics only when a small amount of graphite was lightly wiped on the surface. More extensive studies were not carried out as the systems then of greatest interest involved pyrotechnic delay elements as well as primary explosive.

In considering the successes it must be pointed out that failure to channel, direct and control the important radiation will result in initiation failures. This can be seen from the listing of barriers to (light) ignition in Table 2.

Relays, Boosters, Delays

As the program of experimental work progressed it was realized that remote initiation effects might be combined to provide a series of units capable of producing "pyrotechnic - radiant energy - pyrotechnic" delay systems operating on mechanisms

Table 2

BARRIERS TO REMOTE INITIATION OF BORON - RED LEAD TARGETS FROM BURNING BORON - RED LEAD

Light Source	Barrier
.040" Boron - Red Lead in lead	More than 2 - 3 inches Crofon* 1610 Acrylic Fiber optics
"	Less than .001 inch Aluminum Foil
"	Less than .007 inch Filter Paper
"	Less than .002 inch Lead Foil
"	Less than .010 inch Clear Poly Olefin
"	Less than .0075 inch Mylar* (Polyethylene terephthalate)
"	Much less than 1/8 inch glass, or quartz

different from any in common use. Such devices were made in standard sizes of brass tubing from alternated cut lengths of close fitting commercially available acrylic fiber optics and the proper diameter of boron - red lead, lead jacketed Timeline* delay. By varying the ratio of length of delay material to the length of fiber optic in a given housing the delay time of the device could be varied. Exploratory study of these delay devices showed them to be reliable and to possess some potential for good reproducibility. They did not offer marked improvement in any area however and further product development studies were not pursued.

The above segmented delays for use in systems isolated from the environment required for their operation on their "light in - light out" principle that the output light be sufficiently great to jump a gap in the fiber optic system. To ensure that the output would go from one piece of fiber optic to another the needed booster was provided by incorporating a small amount of more energetic light producing mixture (e.g. Zr, Ti, - $KClO_4$) next to the output fiber optic and were shown to be operable.

Some Theoretical Considerations

It has appeared throughout the investigations carried out on this subject that initiation must occur through attainment of a given minimum temperature in at least a very small portion of a target material. Energy must, therefore, be received at a rate sufficiently great to ensure that the temperature is achieved despite losses due to conduction and radiation. Similar situations have been treated in the case of electrical detonator systems and as an example the work of Davenport (2) sets forth the basic

parameters. It is known that the ignition temperature of the boron - red lead mixes is near 450°C (2). It appears that the choice of boron - red lead was a fortuitous one as it apparently absorbs "light" very effectively, but conducts heat rather slowly. In the present system the 450°C must be realized at the end of a fiber optic bundle from the .02 to .04 calorie measured to be present in that .003 square inch area. This is a calculated heat flux of about 50 calories per square centimeter per second from a flash bulb of 30 x 10^{-3} second duration.

For such a system the part of the output of energy from a flash bulb available for ignition may be visualized as the area under the bell-shaped intensity vs. time curve to the point of ignition. Due to losses at roughly a logarithmic rate with distance in the fiber optics, increasingly greater amounts of energy (and time) are required for increasing lengths of fiber optics. If ignition does not occur at about the time the peak output energy is reached, the target is losing energy at such a rate that ignition will probably never be reached. While a similar intensity reached in a shorter time might lead to ignition, most shorter duration light sources have had greater intensities.

Demonstration that ignition from light from shock wave interaction with inert gas occurs indicates that times of a few microseconds or less only need be involved. Ignition must result from rapid absorption of energy in a very thin layer of target material. Experiments with argon filled tubes excited by detonating 80 grain per foot RDX Primacord* indicated the maximum length through which ignition occurs passes through two maxima - one at a chamber length of about 63 mm or 2.5 inches and the second at a very short length of 3 mm or 1/8 inch or less. Finally, the elimination of the chamber entirely led to ignition through even longer lengths of fiber optics with the indication that the extremely short bursts of detonation light could also cause ignition.

By similarity of these experiments to the work of others it appears that the duration of the shock wave - argon source is about 10 microseconds for the 63 mm chamber. For the other small chamber the light is tens of nanoseconds in duration. This would be inferred from the work of Liddiard, Jacobs and Kabik (4) who reported a 30 nanosecond light for photography from a 0.25 mm confined air gap between explosive and a glass plate. The duration of detonation light, arising in particulate solid explosives, is reported by Blackburn and Seely (5) to be of the same order - tens of nanoseconds.

Several theoretical approaches provide interpretation for the observed ignition phenomena. Blanchard (6) and Boddington (7) point to the importance of intense bursts of light for initiation of explosives. Concerning the critical energy Boddington indicates its value "could be extremely low for a well designed light pulse - - in the neighborhood of the fundamental absorption edge the absorption coefficient may be as great as $10^{J}\,cm^{-1}$ so that the critical energy density for the corresponding radiation is about 10^{-2} joule cm^{-2}, if the flash duration is less than 0.1 microseconds."

In essentially all of the quite extensive literature relating

*Trade Mark, Ensign Bickford Co.

light initiation of explosives extreme importance is given to the thermal regime.

Sensitivity of Target Materials

In some studies with different target materials an organic material which would vigorously propagate burning was mixed with a little carbon black and used as a target. Its ignition as a loose powder with light from a flash bulb was possible through up to 30 feet of Corning 5013 fiber optics. This occurred even though no improvement with usual target material as loose powder was noted. This may indicate that the sensitivity to impact, heat, static electricity, etc., will not be directly related to "light" sensitivity. Properties of the target materials are shown below.

	Boron - Red Lead in Lead (Compacted)	Black Organic Self Oxidizer (Loose Powder)
Maximum Leagth of Fiber Optic Ignition	15 feet	30 feet
Approx. Ignition Temperature	450°C	160°C+
SENSITIVITY		
Vertical Impact	100 cm	105 cm
Sliding Impact		
Phenolic Block	4 in	13 in
Steel	3 in	7 in

The experimental work on this subject and the evidence that sensitivity to light initiation is not necessarily related to other forms of sensitivity combined with theoretical considerations make the author believe that fiber optic ignition systems with non-coherent light that operate through hundreds of feet rather than tens of feet will be possible.

Acknowledgements

The work reported here was carried out largely for Bickford Research Laboratories of the Ensign Bickford Co. Some further development work resulted in Remote Initiation Kit No.1 which was offered for a time by Aprand, Inc. and was carried out under license from Ensign Bickford of a patent application, RADIANT ENERGY SIGNAL TRANSMISSION SYSTEMS, authored by Francis H. Bratton and John M. Smith.

REFERENCES

(1) Pay, Rex, Lasers, Fiber Bundles Yield RFI - Immune Explosive Initiator, Technology Week, November 4, 1966

(2) Davenport, D. E., Temperature Coefficient of Resistivity Effects on 1A/1W No-Fire Initiators, Paper 3-1, 5th EED June 1967

(3) Ensign Bickford Co., Private Communication, 1967

(4) Liddiard, T. P., Jr., Jacobs, S. J., and Kabik, I., An Explosive Light Source of Low Energy for 30-Nanosec Schieren or Shadowgram Photography, Journal of the SMPTE, Volume 74, pp90-94.

(5) Blackburn, J. H., and Seely, L. B., Detonation Light in Granular Explosives, Trans. Faraday Society 61, (507) pp 537-45 (1965)

(6) Blanchard, Mme Raymonde, Physique des Explosifs - Initiation thermique des explosifs au moyen d'eclairs lumineux. Etude thoerique, Academie des Sciences, Seance du Mars 18, 1963 pp 2550-3

(7) Boddington, T., Theory of Initiation of Explosion in Solids by an Intense Light Flash, DDC AD 619,542, 11 November 1963

I-9. SECONDARY EXPLOSIVE SPARK DETONATORS*

T. J. Tucker, J. E. Kennedy, and D. L. Allensworth

Sandia Laboratories, Albuquerque, N. M. 87115

ABSTRACT

In this work several aspects of the design and performance of spark detonators are considered. The requirements for spark initiation of two granular secondary explosives are studied. Two approaches for designing detonators with improved thermal stability are demonstrated, and the effects of variations of ambient pressure on firing characteristics are determined. Experimental firings were done using a low-inductance firing circuit so that electrical energy could be delivered to the detonator very rapidly. Using this circuit, detonators loaded with either ZPCP or PETN have been fired with stored energies of less than 20 millijoules. The history of energy deposition in the spark is viewed as the electrical parameter which directly determines whether spark initiation of a given secondary explosive will be achieved. For firings near the initiation threshold, measured current waveforms were analyzed to determine the history of energy deposition in the spark.

I. INTRODUCTION

Electrical requirements for direct spark initiation of PETN were discussed in a safety context in a previous paper.[1] That study showed that within practical limits, electrostatic charges developed on the bodies of personnel handling PETN cannot initiate detonation of the explosive. In the present work we apply the results of that study to the development of practical detonators based on spark initiation of secondary explosives.

In addition to the handling safety factor cited above, we perceive a number of advantages for these detonators over other types. Among these are simplicity of manufacture and firing energy requirements which are very low for a detonator containing only secondary explosives. The low firing energy also permits use of a firing circuit which is smaller, simpler, cheaper, and much less of an electrical shock hazard to personnel than the firing circuit required for a comparable exploding bridgewire (EBW) detonator.

Although spark detonator studies have been reported by several authors,[2,3] little attention has been directed toward understanding the spark detonator firing requirements. In this paper dynamic characteristics of spark breakdown of two granular explosives, PETN and ZPCP,* and fundamental requirements for a spark initiation of their detonation are discussed. The stability of spark detonators loaded with these two explosives is also evaluated under two types of environments, thermal cycling and reduced ambient pressure.

Because severe requirements for thermal stability are often imposed on detonators, we have paid special attention to this aspect of the design problem. Finally, because the details of electrical breakdown (spark formation) in air are highly dependent on ambient pressure, we have studied spark detonator performance at pressures simulating high-altitude firing.

1.1 Background

In Ref. 1 it was shown that the spark initiation of PETN resembled exploding bridgewire (EBW) initiation[4] in that the explosive's sensitivity was dependent upon both the magnitude and the rate of increase of current. It was postulated that spark initiation of PETN occurred only when the power input into some small region of the explosive was of sufficient magnitude to produce

*This work was supported by the U. S. Atomic Energy Commission

*ZPCP is azidopentaammine-cobalt (III) perchlorate.

a very high energy density.[1,4] These observations provide a basis for the formulation of initiation criteria suggested in this paper.

Thermal cycling tends to shrink the explosive away from the header surface within a detonator, thereby decoupling the powder from the source of energy deposition and increasing the energy required to fire the detonator. One approach devised to improve the thermal stability of spark detonators was to elevate the electrodes into the PETN powder. Alternatively, because ZPCP has better thermal stability than PETN, it was believed that the thermal stability of a ZPCP-loaded detonator would be greater than that of one loaded with PETN. Both approaches were pursued. For each explosive, variation in the specific surface area of the powder was included as a part of the test program because this parameter is known to strongly affect the firing energy threshold.

1.2 Organization of this Paper

This paper first describes our spark detonator designs and the firing set and its switching mode. Current measurements made during a shot, and the method of analysis of these data are then discussed. The separate plans employed in conducting initiation threshold tests and environmental tests on ZPCP and PETN detonators are presented. Experimental data are presented in graphical and tabular form in the following section. Next, initiation criteria are presented in the form of spark energy histories required to initiate reactions which can grow to detonation. This permits comparison of the spark sensitivities of ZPCP and PETN powders of various specific surface areas. An adaptation of Paschen's law is then suggested to explain apparently contradictory effects of environments on breakdown voltage behavior. Finally, drawing upon experimental results of this as well as previous spark and EEW initiation studies, the requirements for spark initiation of granular secondary explosives are summarized.

2. DETONATOR AND FIRING CIRCUIT DESIGN FEATURES

2.1 Detonators

Design details of two models of spark detonators utilized in this study are shown in Fig. 1. Because of the requirement that electrical energy from the capacitor be delivered rapidly to the spark gap, we have employed a conventional header* of almost completely coaxial design. Two electrode configurations were tested, a simple flush gap configuration and a more complicated raised gap configuration in which the spark breakdown would occur in the interior of the explosive pressing rather than at its surface.

PETN was obtained from the Mound Laboratory of Monsanto Research Corporation and ZPCP was prepared in our own laboratories by H. E. Brown. The PETN was obtained in three specific surface areas, S_0^p, ranging from 3700 cm^2/g (coarse) to 10,500 cm^2/g (fine), and was loaded in the detonators as compacts of various densities in the range 0.80 to 1.10 g/cm^3. The ZPCP was obtained in four specific surface areas ranging from 2,800 cm^2/g (coarse) to 33,000 cm^2/g (ultra-fine), and was loaded as compacts of density 0.95 g/cm^3. In each material the compacts were of approximately 50% crystal density, and were formed by pressing a specified explosive mass into a controlled volume in the detonator.

Electrode gap spacing and configuration were controlled as follows: for ZPCP, flush headers with a 20-mil gap were used for all tests; for PETN, the header electrodes were either flush or raised, with gaps ranging from 10 to 40 mils.

2.2 Self-Breakdown Firing Mode

Voltage breakdown of the powder pressing was used as the switching mode of the firing circuit for two primary reasons: (1) Introduction of any type of

*Type SE1-31, fabricated by Reynolds Industries, Marina del Rey, California.

external switch would add both inductance and resistance to the circuit, thereby degrading performance and, (2) Presence of these uncertain circuit impedances would make it more difficult to evaluate the actual energy deposition into the gap. From the standpoints both of device design and of technical understanding of the spark initiation process, then, it was undesirable to add a switch.

Switching through voltage breakdown of the powder (denoted as the "self-breakdown" mode) introduces certain problems, however. The breakdown voltage of a pressed explosive bed has some variability from shot to shot, so the stored electrical energy cannot be accurately predetermined for a given shot. Both thermal and altitude environments can also influence the breakdown voltage of a pressing. Electrode spacing will affect the breakdown voltage; this introduces some additional variability, but can also be used as a design parameter to control the approximate breakdown voltage. Thus, when a system is operated in this self-breakdown mode, knowledge of the effects of several parameters on the breakdown voltage behavior is as pertinent to solution of the design problem as knowledge concerning the initiation threshold.

2.3 Firing Circuit

Construction details of a typical firing set utilized for the experiments reported here are also shown in Fig. 1. As shown in Fig. 2, the circuit is equivalent to a simple LRC circuit, thus both circuit resistance and inductance need to be minimized in order to provide the high current and power levels required for explosive initiation at reasonable values of voltage and capacitance. As can be seen in Fig. 1, this minimization was accomplished by very tight physical coupling of the ceramic firing capacitor to the detonator with lead lengths as short as possible.

In some ZPCP tests, the ceramic capacitors were replaced by Mylar capacitors of lower inductance and resistance. Circuit inductances as low as 40 nanohenries were obtained. As will be shown, these Mylar capacitors permitted threshold firing at a lower stored energy than that required with ceramic capacitors.

3. TEST PLANS AND EXPERIMENTAL PROCEDURES

For each explosive preliminary test firing experiments were performed to determine the most favorable detonator loading and construction parameters. Detonators loaded at these optimum conditions were then subjected to certain environments to determine whether their firing performance was degraded.

Detonator loading conditions were sought for which the breakdown voltage was sufficiently high to achieve initiation, but not so high as to demand excessive operating voltages. Breakdown voltages between 3 kV and 5 kV were desired.

3.1 Experimental Measurements

In a typical test the voltage across the detonator sparkgap was slowly increased until breakdown occurred. Breakdown resulted in a sudden drop in the reading observed on a digital voltmeter connected across the gap. The maximum reading of the voltmeter was recorded. The response of the explosive to the spark breakdown, i.e., detonation or no detonation, was also recorded. Other quantities monitored were the discharge current waveform, as measured by the low-inductance current-viewing resistor,* and the explosive function time from voltage breakdown to closure of an ionization pin switch at the terminal end of the explosive column.

*Type WM CVR, .05 Ω; T & M Research Products, Albuquerque, New Mexico

3.2 PETN Screening Tests

For PETN, four detonator loading parameters -- PETN density and specific surface area, and electrode configuration and gap length -- were varied over wide ranges, as described in Section 2. Several firing trials were performed at each selected set of conditions. Thus the firing performance for many combinations of detonator loading conditions were surveyed prior to selecting conditions suitable for environmental testing.

The firing source capacitance was fixed at 8100 pF for nearly all tests. For a given source capacitance, the breakdown voltage governs the firing source energy, which is a critical parameter in determining whether the powder will be initiated. As a result, initiation threshold conditions were found for PETN detonators only when they fell within the range of breakdown voltages experienced for a given loading configuration.

As will be shown in Section 6, experimental results indicate that the specific surface area of the powder influences a detonator's performance much more strongly than do the other three loading parameters.

3.3 ZPCP Threshold Tests

Because the powder's specific surface area had been found to be the most important parameter in PETN tests, we chose to employ four powders of different specific surface area in conducting the ZPCP threshold tests, and to fix the other detonator loading parameters. The powder density was held at 0.95 g/cm^3 in detonators with 20-mil gap flush headers.

The capacitance of the firing set was treated as a variable in the ZPCP tests. Since the breakdown voltage of a detonator is a function of the powder specific surface, but not of the firing set capacitance, it was possible to find threshold conditions for initiation of each powder by varying the capacitance. One particular ZPCP powder was then chosen for study of the effects of thermal and altitude environments on detonator performance.

3.4 Thermal and Altitude Environments

Environmental testing to study low temperature effects was done at -65°F with both the detonator and the firing set at low temperature. Heating of the detonators for 30 hours at 190°F, henceforth denoted as 30-190 treatment or thermal cycling, was arbitrarily selected as an accelerated measure of long term storage effects.

High altitude environments were also of concern because the reduced interstitial air pressure within the detonator was expected to alter the breakdown voltage. Reduced pressure levels corresponding to various altitudes up to 100,000 ft. were selected. To avoid connector breakdown problems, low pressure firing was performed with only the detonator inside the altitude chamber, as shown in Fig. 3.

4. CIRCUIT ANALYSIS

Typical current waveforms as monitored by the current viewing resistor are shown in Fig. 4. The heavily damped LRC character of the waveforms is clearly evident. Peak current was typically attained within 20 to 40 nsec.

4.1 Time-Resolved Circuit Analysis

Determination of the resistance history of the powder-filled gap during spark passage requires solution of the LRC circuit equation.

$$L \frac{dI(t)}{dt} + I(t) \left[R_g(t) + R_{ckt} \right] - V_c(t) = 0 \quad , \tag{1}$$

and L is the circuit inductance, I(t) the instantaneous current, $R_g(t)$ the instantaneous spark resistance, R_{ckt} the circuit resistance, and $V_c(t)$ the voltage remaining on the capacitor.

The amount of charge removed from the capacitor at any time t may be calculated by integration of the current waveform to that time, thus the capacitor voltage may be computed as

$$V_c(t) = V_0 - \frac{1}{C}\int_0^t I(\tau)\, d\tau \quad , \tag{2}$$

where V_0 is the breakdown voltage of the gap and C is the capacitance. L and R_{ckt} are assumed to remain constant at known values. By differentiation of the current trace, $\frac{dI}{dt}$ can be evaluated at any given value of time. Spark resistance can then be explicitly evaluated by solution of Eqs. (1) and (2).

The spark power deposition history, P(t), and accumulated spark energy, E(t), can be evaluated by use of the spark resistance history and the current history.

$$P(t) = [I(t)]^2 R(t) \quad , \tag{3}$$

and

$$E(t) = \int_0^t P(t)\, dt \quad . \tag{4}$$

These parameters will be used in the analysis of detonator responses in Sections 5 and 6.

4.2 Critically Damped Circuit Analysis

The time-resolved nature of the foregoing analysis is helpful in providing insight into electrical requirements in the spark initiation process, but it is difficult to digest or even to tabulate the results obtained from a large number of tests. To simplify the comparison of responses under various detonator loading conditions, we have found it useful also to perform a "lumped parameter" analysis of the data. In this method the circuit was assumed to be critically damped and the value of a constant "effective spark resistance" R* required to produce the observed maximum current was calculated as follows:

$$R^* = [2V_C/(I^* e)] - R_{ckt} \quad , \tag{5}$$

where I* is the maximum current and e = 2.718...is the natural logarithm base. Estimates of instantaneous power P* and energy E* delivered at the time of peak current can also be derived for a critically damped circuit with the results:

$$P^* = 4V_C^2/R^* e^2 \tag{6}$$

$$E^* = E_0(1 - 5e^{-2}) = .3233\, E_0 \quad , \tag{7}$$

where E_0 (equal to $CV_0^2/2$) is the initially stored energy.

4.3 Definition of Threshold Initiation Conditions

In comparing the performances of detonators, we shall be concerned with the electrical requirements to achieve threshold conditions, i.e., conditions at which the firing probability is near 50%. The best estimate of threshold conditions for a given detonator loading condition was reached by selecting from the sample that test having the largest stored energy for a no-detonation response and that test having the smallest stored energy for a detonation response, then averaging the values of a given parameter. For example, the best estimate of the threshold stored energy denoted

$$E_{0,th} = [\text{largest } E_0(\text{no detonation}) + \text{smallest } E_0(\text{detonation})]/2 \quad . \tag{8}$$

Using results of the same two tests selected for the computation of $E_{0,th}$, best estimate values were computed similarly for several other threshold quantities which are defined below: I^*_{th} = threshold peak current, R^*_{th} = effective spark resistance at threshold, P^*_{th} = threshold peak power into the spark, and E^*_{th} = threshold energy into the spark to the time of peak current.

5. EXPERIMENTAL RESULTS

Firing threshold data and the results of environmental tests on ZPCP and PETN detonators are tabulated in Tables 1 and 2, respectively. The results are based on 15 trials with each ZPCP powder; the number of PETN trials performed at each condition varied between 5 and 15, and is quoted in Table 2.

5.1 Detonator Breakdown Voltage

In Tables 1 and 2, $\bar{V}_0$ denotes the mean breakdown voltage and $S(V_0)$ is an estimate of the standard deviation about the mean breakdown voltage. For both PETN and ZPCP, breakdown voltage increased as the powder specific surface area increased. This relationship was nearly linear for ZPCP powders,[5] except for the finest powder (33,000 cm^2/g), which was observed to have a different crystal shape than the others.

In the PETN trials, the detonator breakdown voltage was found to increase with increasing PETN density or electrode gap length as well as with the specific surface area. A change from the flush-gap to the raised-gap electrode configuration affected the breakdown voltage very little.

5.2 ZPCP Detonator Firing Threshold

Although breakdown voltage increased with specific surface, the capacitance required for initiation decreased in such a way that the threshold value of the initial source energy, $E_{0,th}$, was very nearly constant at 20 mJ. Although the measured peak current, I^*_{th}, and the calculated effective spark resistance, R^*_{th}, varied widely, the peak power varied only from 1/3 to 2/3 MW and the spark energy to the time of peak current was nearly constant at 5 mJ.

The explosive function time was grossly affected by specific surface. The time observed for the low specific surface sample was, in fact, so long that the establishment of stable detonation was in doubt. For the other samples, a limiting value of about 2 μsec was approached. Since the column length of the pressing was 0.250 in., this led to a first estimate of 3 mm/μsec for ZPCP detonation velocity within the detonator.

5.3 ZPCP Detonator Environmental Stability

As indicated in Table 1, the 7500 cm^2/g powder was selected for study of the effects of thermal and altitude environments on ZPCP spark detonator performance. The firing source for these environmental tests was a Mylar capacitor of lower impedance than the ceramic capacitors used in the firing threshold tests, so it was possible to deliver the stored energy at a faster rate. As a consequence, a "control" lot of detonators fired with the Mylar capacitors at ambient conditions received a higher peak current and fired at about half the stored energy required in the ceramic capacitors.

The faster delivery of energy by the Mylar capacitor is illustrated by comparison of Figs. 5(a) and 5(b), which result from analyses of current waveforms measured in Shots 5Z and 7. The initial voltages for these two shots differed only slightly and although the capacitance and the initially stored energy was much greater in Shot 7, the steeper early slope of the power curve in Shot 5Z maintained a higher cumulative energy into the spark for a period of 30 nsec. In the study of spark resistance histories for many experiments, it has been observed that higher currents (whether due to higher initial voltage or lower inductance) are associated with lower spark resistances; this relationship also holds true between Shots 7 and 5Z at early times in the spark.

The mean breakdown voltage $\bar{V}_0$ of ZPCP detonators was elevated significantly under reduced interstitial air pressure and at low temperature. This effect will be discussed in Section 7.

Thermal cycling alone did not change the mean breakdown voltage. It might be expected then that thermally cycled units fired at low temperature would

exhibit an increase in breakdown voltage; no voltage increase was observed, but the threshold firing energy tripled. These points suggest that the ZPCP powder may agglomerate under thermal cycling, then may pull away from the flush header slightly due to powder contraction at low temperature.

5.4 PETN Detonator Firing Threshold

On the basis of their firing energy thresholds and mean breakdown voltages, three favorable sets of loading conditions were selected for study under environmental treatments. These loading conditions and PETN detonator performance under ambient conditions and under thermal or altitude environments are listed in Table 2.

Type 1 loading conditions represent the best overall raised-gap PETN detonator configuration tested. The threshold firing source energy was about 60 mJ. This configuration appears to be in the midst of a favorable operating region in the dimensions of PETN density, PETN specific surface, and gap length, such that small changes in any of these loading parameters should not bring about unreliable operation.

Type 2 detonator loading conditions were identical to those for Type 1 except that the header was flush for Type 2, rather than raised. The mean breakdown voltage and threshold firing source energy for Type 2 detonators were also nearly identical to those for Type 1. Subjection of Type 2 detonators to environmental tests therefore offered an opportunity for direct evaluation of the effectiveness of the raised electrodes in improving environmental stability (see Section 5.5 for results).

Type 3 conditions exhibited the lowest threshold firing source energy for a PETN spark detonator, and were included in the environmental effects experimental program for this reason. It was expected that this configuration would be susceptible to degradation under thermal cycling both because of the flush header and because of the fine particle size of the powder.

From the data collected in these PETN spark detonator screening tests, we conclude that coarse PETN (2800 cm^2/g) is substantially less sensitive than medium (5700 cm^2/g) or fine (10,500 cm^2/g) PETN. Initiation of coarse PETN required a stored energy and delivered power level at least twice that needed for initiation of the finer PETN powders. No clear conclusion could be reached regarding the trend in sensitivity with PETN density or electrode configurations.

Fig. 5(c) shows the time-resolved behavior of electrical parameters pertaining to the raised gap in a Type 1 PETN detonator fired at a voltage near threshold. The spark resistance, power, and energy curves for shots at similar voltage for a given loading condition were remarkably consistent both for PETN and ZPCP, regardless of whether the detonator response was "go" or "no go." This implies that the current waveforms were consistent for a given firing condition.

There was, however, a great deal of difference between characteristic curve shapes for different loading conditions. For example, for loading conditions where one might suspect the presence of an "air gap" path between electrodes (such as medium surface powder at low density, or coarse powder at low or moderate density), the spark's electrical characteristics often resembled those of an air gap for 10 to 20 nsec; little energy was deposited in the spark. Even very strong power surges after such a delay were usually insufficient to initiate detonation. In favorably performing regions of loading conditions, such as those from which our Types 1, 2, and 3 PETN detonators were chosen, the spark resistance curve dropped sharply with increasing time, but remained finite, and the power-time curve was convex upward.

5.5 PETN Detonator Environmental Stability

Detonators of all three selected types were first subjected to experiments

in which interstitial air pressure was reduced to simulate high altitude operation of the detonator (see Table 2). As pressure was reduced, the detonator breakdown voltage in general rose significantly. The flush header units (Types 2 and 3) fired at all altitudes to 100,000 ft. The Type 1 detonator experienced a failure regime, however, from 35,000 to 50,000 ft., then firing resumed at 75,000 ft. following a large increase in breakdown voltage. A hypothesis concerning the cause of these failures is offered in Section 6.

The Type 1 detonator, with raised electrodes, survived 30-190 thermal cycling well, although the mean breakdown voltage increased and the threshold firing source energy was 50% higher then for detonators not subjected to the 30-190 treatment.

Both types of detonators employing the flush header failed entirely after subjection to a 30-190 thermal cycle. For the Type 3 detonator, loaded with fine powder, it was clear that the powder indeed pulled away from the header, because the breakdown voltage was extremely low. Since the breakdown voltage for the Type 2 detonator did not increase as had been seen for the same powder in Type 1 units, it is believed that pull-away occurred between the header and the pressing in Type 2 detonators also.

Type 1 units were then subjected to -65°F firings both with and without prior 30-190 thermal cycle treatment. They functioned satisfactorily, although with a further increase in the threshold firing source energy. The breakdown voltages for the thermally cycled units fired at low temperature were high, indicating no pull-away of powder from the electrode tips.

6. SPARK ENERGY REQUIREMENTS FOR INITIATION

6.1 Theory

We view the initiation of granular secondary explosives either by an electrical spark or an exploding bridgewire (EBW) as a shock process.[4] In EBW operation, the wire may be considered to represent a current shunt which allows the current to increase to a high level before the vaporizing wire becomes so highly resistive that spark breakdown occurs in the space surrounding the wire. The principal shock is driven by this spark. Hence the secondary initiation processes in EBW detonators and in spark detonators are considered to be closely related.

A shock wave is driven by a spark as a result of the very high density of electrical energy deposited at early times into the spark channel. As the shock front expands radially, the energy density in the shocked zone decreases, because the rate of continuing deposition of energy will normally not increase as fast as the rate of increase in volume of the shocked zone.

The electrical initiation of detonation in a granular secondary explosive is brought about by the elevation of some volume of the explosive pressing to a sufficiently high energy density. It is postulated that, as the included volume of the explosive pressing increases, the energy density required for initiation decreases but the total energy increases. Energy introduced early in the shock expansion would then be more effective toward achieving the required energy density than the same amount of energy would be if it were introduced later.

Analysis of current waveforms to yield spark energy histories, as illustrated in Fig. 5, permits consideration of the existence of a correlation between spark energy histories and initiation thresholds of spark detonators. The question of whether a given spark energy history is sufficient to initiate detonation of an explosive is fundamental and is independent of the operating voltage and firing circuit which produced that spark energy history.

6.2 ZPCP and PETN Detonators

Fig. 6 and Table 3 present spark energy histories for ZPCP and PETN detonators at threshold initiation conditions and other conditions of interest. Each of these curves in Fig. 6 describes a particular experiment which is representative for the noted conditions, since the spark energy history was found to be quite reproducible at a given loading condition and firing voltage, regardless of whether detonation was initiated. In comparing these curves for different loading or firing conditions, note that as a first approximation the energy density in the shocked zone at any time will be proportional to the energy deposited in the spark up to that time.

Table 3 was prepared on the basis of Fig. 6 by approximating each spark energy curve as a ramp function from zero time to a time at which the energy curve became essentially horizontal. Based on this simplification, the average spark power level and duration required to produce threshold initiation are tabulated, together with the resulting spark energy.

Spark energy histories for threshold initiation by ceramic capacitors of three ZPCP powders of different specific surface fall quite close together on Fig. 6(a), indicating that the spark sensitivity of ZPCP is not markedly affected by specific surface over that range. The effect of reducing the firing circuit inductance by switching to Mylar capacitors is also evident; energy was delivered into the spark earlier, and the 7500 cm^2/g ZPCP powder was initiated with about one-third less spark energy.

Spark energy histories in PETN detonators are shown in Fig. 6(b). It is clear from this figure and Table 3 that PETN spark sensitivity is strongly affected by the specific surface area of the powder. Initiation of the fine PETN (10,500 cm^2/g) required about the same spark energy as ZPCP and much less spark energy than required to initiate detonation in medium or coarse PETN.

The threshold curves for medium PETN are rather tightly clustered although they represent various combinations of powder densities, electrode configurations and gap lengths; the powder surface area thus appears to be a more controlling factor than these other parameters. The lowest curve at late times among the medium PETN group represents a failure where the initial input energy rate was highest, but the total spark energy was low. This indicates that, at least for the medium powder, energy entering the spark channel even after 40 msec can be effective in contributing toward initiation.

Coarse PETN required a much larger stored energy and spark power level for threshold initiation than medium PETN. The spark energy history for threshold initiation of coarse powder shown in Fig. 6(b) indicates very little energy deposition for 20 msec, followed by an extremely high spark power level. The poor coupling of electrical energy into the spark at early times is believed to be due to the presence of relatively large air gaps between explosive particles, which can carry large currents with low power deposition.

6.3 Altitude Effects on Spark Energy Requirements

Low interstitial air pressure had a desensitizing effect on both PETN and ZPCP spark detonators. Threshold initiation of 7500 cm^2/g ZPCP by a Mylar capacitor required about 60% more spark energy at 50,000 ft. altitude than at 5,000 ft. altitude, as illustrated in Fig. 6(a). A spark energy curve is given in Fig. 6(b) which represents the failure regime observed at 50,000 ft. altitude for medium PETN in the Type 1 detonator. This curve shows that an energy input rate more than twice the threshold value for a 5,000 ft. altitude was insufficient to initiate detonation at a 50,000 ft. altitude.

Reduced air pressure will not decrease the shock strength at the front of a diverging air shock driven by a given amount of energy, but it will reduce the duration of the positive pressure behind the front.[7] Experiments by Gittings[8] and Trott and Jung[9] have shown that, when the duration of shock

loading on a secondary explosive is decreased, a higher shock front amplitude is needed to initiate detonation. The reduced duration of shock loading associated with reduced air pressure is believed to be responsible for the increased spark energy requirements found in high altitude firings of spark detonators.

7. INTERPREDATION OF ENVIRONMENTAL EFFECTS ON BREAKDOWN VOLTAGE

It is apparent from the data in Tables 1 and 2 that changes in either the explosive's physical properties or the environment produce significant effects upon the self-breakdown voltages of powder-filled spark gaps. A survey of available literature yielded little information regarding electrical breakdown in granular powder beds. To explain the effects of various parameters on breakdown voltage, a model based upon an extension of breakdown processes in air is proposed.

7.1 Breakdown Model

The potential difference imposed between the detonator electrodes will be assumed to be partitioned among the various grains of explosive and the interstitial air pockets along any path between the electrodes. Since our explosive pressings were at about one-half crystal density, we may assume that the length of a given path between electrodes was divided equally between air pockets and explosive particles. The potential difference between two faces of an (air or explosive) element of dielectric constant ϵ which are separated by distances d_1 and d_2 from a charge q will be

$$V_2 - V_1 = \frac{q}{\epsilon}\left(\frac{1}{d_2} - \frac{1}{d_1}\right) \quad . \tag{9}$$

because the dielectric constant of air is several times smaller than that of solid explosive, an estimated 80% or more of the total voltage drop will occur across the air pockets present in any path of interest.

Let us now consider the division of voltage among several air pockets of different lengths which may comprise a breakdown path. This assemblage may be viewed as a set of capacitors in series. The capacitance C_j of air pocket j is inversely proportional to its length, d_j:

$$C_j \propto \frac{\epsilon_j}{d_j} \quad . \tag{10}$$

Since the same charge q is impressed across each of the series capacitors, the voltage across the j^{th} air pocket is inversely proportional to its capacitance, and thus is directly proportional to its length:

$$q = C_j V_j \quad . \tag{11}$$

hence

$$V_j \propto \frac{1}{C_j} \propto d_j \quad . \tag{12}$$

In order for spark breakdown to occur, it is necessary that the voltage imposed on each air pocket along some path be greater than that air pocket can withstand. The Paschen law[6] states that the breakdown voltage of an individual air gap is a function, V(pd), of the product of air density and gap length. At a constant temperature, air pressure is directly proportional to density, so the Paschen law can be expressed as V(Pd), as has been done in Fig. 7. Thus, given the Paschen curve for air at 72°F, application of the perfect gas law permits calculation of the Paschen curve for air at -65°F, which is also shown in Fig. 7. Note that each of the Paschen curves exhibits a minimum.

The capacitive voltage division among the air pockets will not correspond

to the distribution of breakdown voltages of the pockets; as the total voltage is increased, some pockets will reach their breakdown voltages, and will break down accordingly, before others. After an air pocket breaks down it can be considered to be equivalent to a conductor; the interelectrode voltage is then redistributed among the remaining air pockets, with the result that an increased voltage is impressed on each of them.

In every case there will be one key air pocket whose breakdown leads to total spark breakdown. That pocket may be standing off essentially all the interelectrode voltage at the time of its breakdown, or merely a small fraction of the total voltage.

To investigate the effect that environments may have upon the breakdown voltage of spark detonators, let us consider a hypothetical breakdown path composed of three air pockets, one long, one short, and one very short. Since the interelectrode spacing was about 0.05 cm, we assign lengths of 0.05, 0.01, and 0.001 cm to these pockets. Table 3 demonstrates the roles of air pockets of such quite different lengths under three environments of interest.

Capacitive division of the interelectrode voltage occurs in proportion to the relative lengths of the separate air pockets, as indicated in Eq. (12), and applies without regard to the environment which might be imposed on the detonator. The indicated division of voltage applies until one or more of the individual air pockets suffers voltage breakdown.

For each of the given environments, we have tabulated the breakdown voltage V(Pd) expected for each air pocket as derived from the Paschen curve for air at the appropriate temperature. To determine the voltages across each pocket at breakdown, the total voltage V_0 is raised (and partitioned among the three pockets) to a level at which (a) one of the pockets will break down and, (b) the resulting redistributed voltage will cause successive breakdown of the remaining pockets.

Note that the longest air pocket controls the breakdown process at a pressure of 625 mm Hg, but control shifts to the shortest pocket when the pressure is dropped to 87 mm Hg.

The long air pockets control the 625 mm Hg experiments because they are well up along the right branch of the Paschen curve. A second consequence of being on the right branch is that a decrease in air temperature may be expected to result in an increase in breakdown voltage, i.e., Point A of Fig. 7 as compared to Point P.

Low air pressures lead to high breakdown voltages across very short gaps, as indicated on the left branch of the Paschen curve. If all available breakdown paths contain at least one very short air pocket, the breakdown voltage for detonators would be expected to increase sharply with increasing altitude.

7.3 Comparison with Experimental Data

The trends in our experimental data on detonator breakdown voltage behavior with environments correspond with the conclusions we have drawn on the basis of the simple hypothetical model described above. For both explosives, the high-pressure shots (625 mm Hg) exhibited decreasing breakdown voltage with increasing temperature (see Tables 1 and 2), indicating that the controlling air pockets were of large enough dimensions to be on the right branch of the Paschen curve at that pressure. As atmospheric pressure was decreased, detonator breakdown voltage increased at an ever-increasing rate, suggesting that at these conditions the controlling air pockets represented operation on the left branch of the Paschen curve; this requires that the controlling gaps must be very small in size.

On the basis of both the analysis of the hypothetical model and study of the the experimental data, then, it appears that the long air pockets in a breakdown path dominate the voltage breakdown process at about one atmosphere,

but that very short air pockets dominate breakdown behavior at substantially reduced air pressure.

7.4 Specific Surface Effects on Voltage Breakdown

For both ZPCP and PETN of a given pressing density, an increase in breakdown voltage resulted from the use of a finer powder (e.g., see Table 1). Inspection of the test results in which S_0^p was varied suggests that at least for ZPCP the functional dependence of the mean breakdown voltage upon specific surface was of the form

$$\bar{V}_0 = 0.182\ (S_0^p)^{1/3} \quad . \tag{13}$$

It is conjectured that the increase in breakdown voltage associated with finer powders is due to the creation of a much larger number of air pockets of small dimensions, in series arrangements along the possible breakdown paths.

8. SUMMARY

Secondary explosive spark detonators appear to be good candidates for commercial application because they can be made inexpensively, and both the detonators and the firing sets are safe. The firing set must be closely coupled to the detonator if minimum firing energies are to be realized; spark detonators loaded with ZPCP or PETN can be fired with stored energies ranging from 10 to 60 mJ if the firing circuit is capable of delivering most of its energy in a sufficiently short period of time. Both explosives have been initiated with as little as 10 mJ total energy deposited in the spark gap within the first 30 nsec of the spark's lifetime.

Analysis of measured current waveforms has yielded the spark energy history in each experiment. It is clear that energy entering the spark at early times is more effective in contributing toward explosive initiation than energy entering the spark at later times. Whereas the spark energy history required for initiation of ZPCP appears to be independent of the powder's specific surface over a wide range, the energy requirement for initiation of PETN is quite dependent upon its specific surface.

Spark initiation of secondary explosives has been shown to depend upon both the amount and the rate of energy deposited in the spark gap. Results of these experiments with ZPCP and PETN support this point, but the present data do not cover a sufficiently wide range of spark energy history profiles to permit us to quantitatively define in a general form the spark energy history requirements for initiation.

The following criteria pertain for firing spark detonators loaded with granular secondary explosives:

(1) The operating voltage of the firing set must equal or exceed the breakdown voltage of the powder-filled spark gap.

(2) The spark energy must exceed some minimum value which is dependent on the explosive properties. This value is estimated to be 10 mJ for ZPCP and for PETN of fine particle size, and to be ~ 30 mJ for PETN of medium particle size.

(3) The stored energy must exceed the minimum spark energy by some quantity which is firing system dependent. The minimum amount of excess energy which must be stored will decrease toward zero as the time of energy delivery decreases. This may be accomplished by reducing the circuit inductance and circuit resistance.

An explanation of the effects of low temperature and low interstitial air pressure upon breakdown voltage has been suggested through application of the Paschen law for the voltage breakdown of air.

The two approaches taken in this study to improve the environmental stability of spark detonators have both shown merit. First, replacement of PETN

by ZPCP, a more thermally stable explosive, in a flush-gap detonator has resulted in better performance after thermal cycling. Secondly, elevation of electrodes into the powder in PETN detonators also improved performance after thermal cycling. It appears that ZPCP loaded into a raised-gap detonator might provide even better environmental performance.

ACKNOWLEDGMENTS

The authors are indebted to Mr. R. J. Martiss and Mr. T. G. Trucano for assistance in data reduction. They also wish to thank Dr. L. W. Davison and Mr. E. C. Chare for many helpful suggestions concerning the manuscript.

REFERENCES

1. Tucker, T. J., "Spark Initiation Requirements of a Secondary Explosive," Annals. N. Y. Acad. Sci. 152, 643-653, Oct. 28, 1968.
2. Leopold, H., "Initiation of High Explosive Conductive-Powder Mixes by Electric Sparks," Proc. of the Electric Initiator Symp., Paper 15, Phila., Pa., 1960.
3. Liddiard, T. P., Jr. and Drimmer, B. E., "The Electric-Spark Initiation of Mixtures of High Explosives and Powdered Electrical Conductors," Proc. of the Electric Initiator Symp., Paper 16, Phila., Pa., 1960.
4. Tucker, T. J., "Exploding Wire Detonators: Threshold Burst Current Dependence Upon Detonator and Environmental Parameters," Exploding Wires, Vol. 4, 211-232, edited by W. G. Chace and H. K. Moore, Plenum Press, 1968.
5. Tucker, T. J., Allensworth, D. L., and Kennedy, J. E., "A Study of ZPCP Spark Detonators," SC-RR-70-825, Sept. 1970.
6. Meek, J. M. and Craggs, J. D., Electrical Breakdown in Gases, p. 84, Oxford Press, 1953.
7. Lin, S-C., "Cylindrical Shock Waves Produced by Instantaneous Energy Release," J. Appl. Phys. 25, 54, 1954.
8. Gittings, E. F., "Initiation of a Solid Explosive by a Short-Duration Shock," Fourth Symp. (Intl.) on Detonation, 373-380, O.N.R. ACR-126, Oct. 12-15, 1965.
9. Trott, B. D. and Jung, R. G., "Effect of Pulse Duration on the Impact Sensitivity of Solid Explosives," Preprints, Fifth Symp. (Intl.) on Detonation, Pasadena, Calif., Aug., 1970.

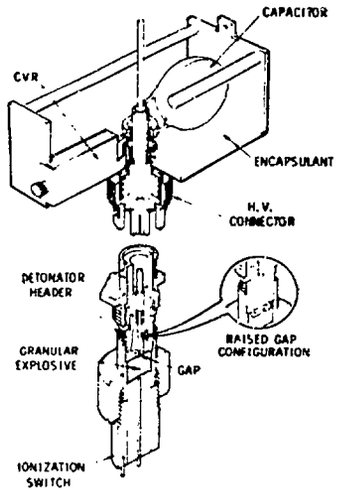

FIGURE 1

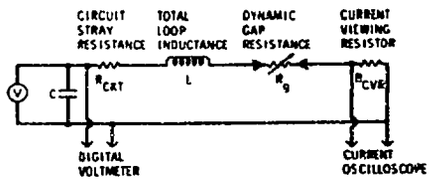

FIGURE 2

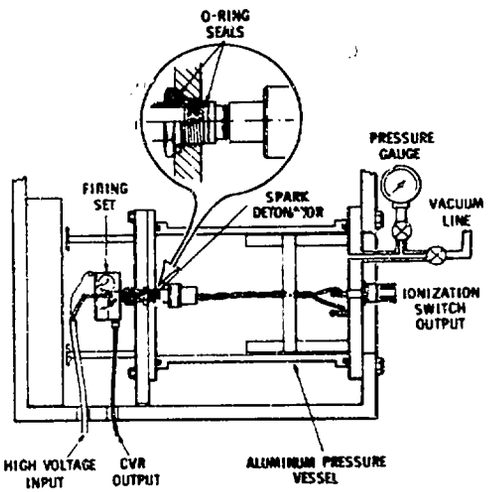

FIG. 3 FIRING CHAMBER FOR HIGH-ALTITUDE SIMULATION

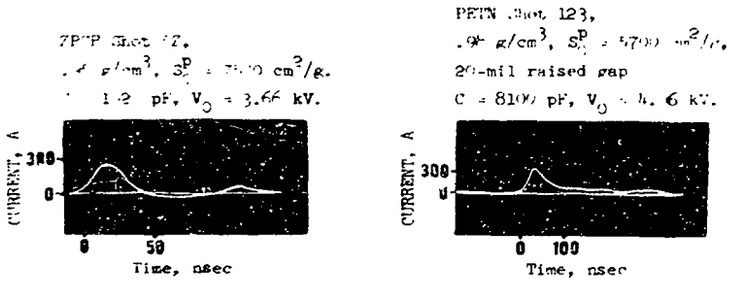

FIG. 4 TYPICAL CURRENT WAVEFORMS

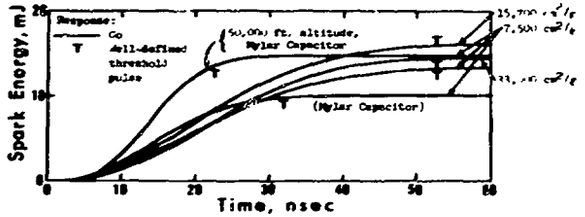

(a) ZPCP Detonators. Ceramic capacitors were used except where indicated.

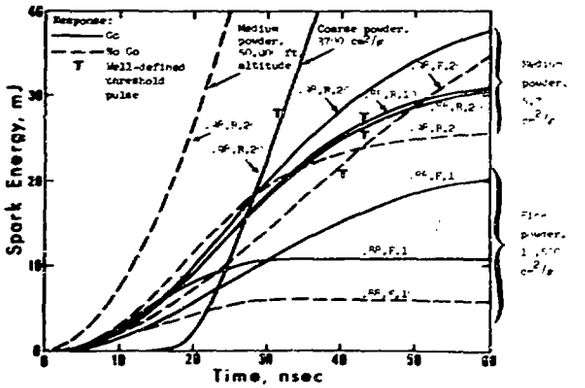

(b) PETN detonators, fired with ceramic capacitors. Loading conditions marked along each curve denote PETN density (g/cm3), gap geometry (raised, R, or flush, F), and gap length (mils), respectively.

FIG. 6 SPARK ENERGY HISTORIES IN DETONATORS

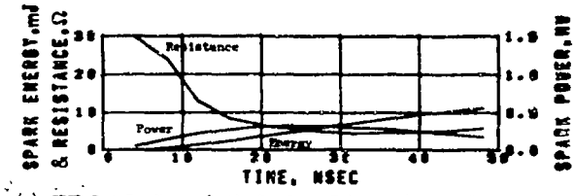

(a) ZPCP Shot 7: V = 3.64 kV, C = 244 pF (ceramic), E = 18.0 mJ. 72 cm²/g powder at .7 g/cm³. Response: Threshold "Go."

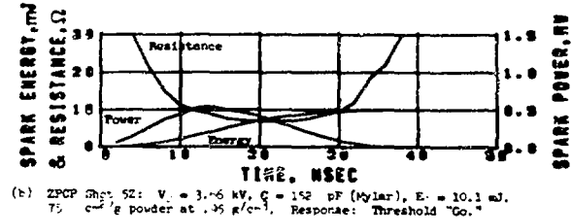

(b) ZPCP Shot 52: V = 3.66 kV, C = 152 pF (Mylar), E = 10.1 mJ. 72 cm²/g powder at .95 g/cm³. Response: Threshold "Go."

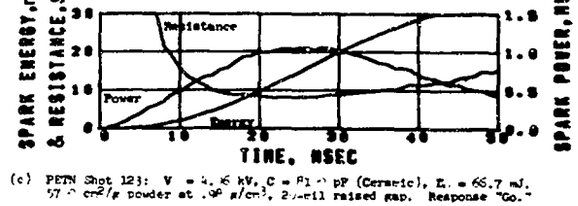

(c) PETN Shot 123: V = 4.46 kV, C = 81[illegible] pF (Ceramic), E = 66.7 mJ. 57[illegible] cm²/g powder at .9[illegible] g/cm³, 20-mil raised gap. Response "Go."

FIG. 5 DYNAMIC ELECTRICAL PARAMETERS OF SPARK DETONATORS

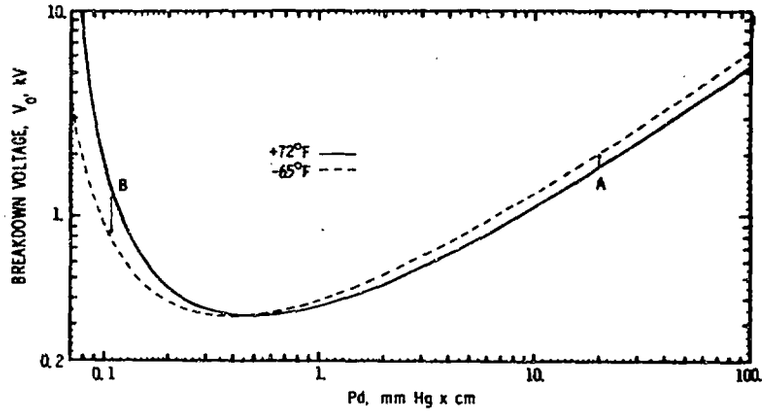

FIG. 7 PASCHEN BREAKDOWN CURVES FOR AIR

TABLE 1: SUMMARY OF ZPCP TEST RESULTS*

S^P cm^2/g	TEMP. °F	PRESSURE[d] mm Hg	TREATMENT	$\bar{V}_0$ kV	$\sigma(V_0)$ kV	$E_{0,th}$ mJ	I^*_{th} A	$t^c_{e,th}$ μsec	R^*_{th} Ω	P^*_{th} MW	E^*_{th} mJ
2,800	72	625		2.56[a]	.16	20.0	259	10.	5.1	.340	4.35
7,500	72	625		3.61[a]	.24	19.0	167	2.7	14.4	.397	5.23
15,700	72	625		5.55[a]	.58	20.0	130	1.97	35.3	.495	6.05
33,000	72	625		5.62[a]	.68	16.3	192	1.99	17.8	.640	4.62
7,500	72	625		3.91[b]	.26	10.9	282	3.00	9.5	.750	3.37
7,500	72	349		3.86[b]	.80	12.9	311	3.10	8.6	.840	3.98
7,500	72	87		4.81[b]	1.09	15.8	422	2.75	9.3	1.653	4.90
7,500	72	625	30-190	4.07[b]	.55	15.5	160	2.99	18.4	.395	4.89
7,500	-65	625		4.96[b]	.57	23.2	241	3.24	14.3	.831	7.30
7,500	-65	625	30-190	4.18[b]	.40	65.6	452	2.81	6.7	1.382	19.99

* All detonators were 20-mil flush gap type SEI-31 units loaded to a density of 0.95 g/cm^3.

a Ceramic capacitor; R_{ckt} = 2.5 Ω and L = 80 nH

b Mylar capacitor; R_{ckt} = 0.4 Ω and L = 40 nH

c Typical function time observed in tests fired at threshold input levels.

d Altitude effects were simulated by atmospheric pressure reduction with following correspondence:

625 mm Hg ≈ 5,000 ft. 349 mm Hg ≈ 20,000 ft. 87 mm Hg ≈ 50,000 ft.

TABLE 2: SUMMARY OF PETN ENVIRONMENTAL TEST RESULTS[a]

DETONATOR DESCRIPTION	TEMP. °F	PRESSURE[b] mm Hg	TREATMENT	FIRING ATTEMPTS	$\bar{V}_0$ kV	$\sigma(V_0)$ kV	$E_{0,th}$ mJ	I^*_{th} A	$t^c_{e,th}$ μsec	R^*_{th} Ω	P^*_{th} MW	E^*_{th} mJ
Type 1	72	625		14/15	4.0	.70	50	<20	1.97	7.2	0.74	1[illegible]
PETN: 0.98 g/cm^3,	72	179		2/5	4.2	.30	[illegible]	<40	1.91	4.2	1.01	22
5,700 cm^2/g	72	87		0/5	5.3	.57	>130	[illegible]	----	5.1	2.14	[illegible]
Gap: 20-mil,	72	8		5/5	8.0	1.44	<155	<[illegible]	1.90	3.1	[illegible]	[illegible]
raised	72	625	30-190	12/15	5.3	.54	[illegible]	[illegible]	c	5.9	1.[illegible]	[illegible]
	-65	625		14/15	5.3	.44	[illegible]	[illegible]	c	11.0	1.09	[illegible]
	-65	625	30-190	8/15	6.2	.90	18	10[illegible]	c	2.5	2.[illegible]	[illegible]
Type 2	72	625		6/12	4.9	.25	6[illegible]	[illegible]	1.99	4.0	0.50	1[illegible]
PETN: 0.98 g/cm^3,	72	179		5/5	4.4	.38	<[illegible]	[illegible]	1.92	5.4	1.06	1[illegible]
5,700 cm^2/g	72	87		5/5	5.3	.52	<[illegible]	<[illegible]	1.[illegible]	5.9	1.2[illegible]	22
Gap: 20-mil,	72	8		5/5	7.2	2.72	<[illegible]	<[illegible]	1.91	5.1	1.28	20
flush	72	625	30-190	0/15	3.8	.40	<1[illegible]	>[illegible]	----	4.2	1.[illegible]	25
Type 3	72	625		6/6	4.0	.90	<31	<425	1.60	[illegible]	.[illegible]0	[illegible]
PETN: 0.88 g/cm^3,	72	179		5/5	4.8	.90	<[illegible]	<[illegible]	1.62	[illegible]	1.0[illegible]	12
10,500 cm^2/g	72	87		5/5	4.0	.49	<[illegible]	<520	1.[illegible]	[illegible]	.[illegible]	10
Gap: 10-mil,	72	8		5/5	6.4	2.24	<[illegible]	<[illegible]	1.[illegible]	[illegible]	1.[illegible]	19
flush	72	625	30-190	0/15	1.8	.15	>1[illegible]	>[illegible]	----	1.0	.[illegible]	2

Notes: a Firing capacitor was 8100 pF, ceramic, for all shots.

b Altitude effects were simulated by atmospheric pressure reduction with following correspondence:

625 mm Hg ≈ 5,000 ft. 87 mm Hg ≈ 50,000 ft.
179 mm Hg ≈ 35,000 ft. 8 mm Hg ≈ 100,000 ft.

c $t_{e,th}$ denotes function time near threshold initiation. This was not measured in thermal environmental tests.

TABLE 3: SPARK ENERGY REQUIREMENTS FOR THRESHOLD INITIATION

Explosive	S_o^p, cm^2/g	ρ, g/cm^3	Pressure, mm Hg	Threshold spark power, MW	Duration, nsec	Threshold spark energy, mJ
ZRCP	7,500	0.95	625	0.30	40	12
ZRCP	7,500	0.95	625	0.36	25	9
ZRCP	7,500	0.95	87	0.60	24	14
PETN	10,500	0.88	625	0.33	30	10
PETN	5,700	0.98	625	0.60	50	30
PETN	3,700	0.98	625	1.1	36	40
PETN	5,700	0.98	87	1.6	25	40

TABLE 4: ENVIRONMENTAL EFFECTS ON BREAKDOWN OF A HYPOTHETICAL SERIES ARRANGEMENT OF AIR POCKETS

Pockets in Series		Long pocket	Short Pocket	Very Short Pocket
Pocket length, x, cm		0.150	0.010	0.001
Hypothetical division of voltage, ΣV		0.62	0.17	0.21
Environment:				
P = 625 mm Hg, T = 72°F	Pd, mm Hg x cm	31.	6.2	0.62
	V(Pd), kV	2..	1.4	0.3
	V_b, kV	2..*	.9	0.1
	$V_t = \Sigma V_b$ = 2. kV			
P = 625 mm Hg, T = 95°F	Pd, mm Hg x cm	31.	6.2	0.62
	V(Pd), kV	2.9	1.0	0.3
	V_b, kV	2.0**	0.6	0.1
	$V_t = \Sigma V_b$ = 2.5 kV			
P = 87 mm Hg, T = 72°F	Pd, mm Hg x cm	4.4	0.87	0.087
	V(Pd), kV	.7	0.4	4..
	V_b, kV	. **	0.0**	4.1*
	$V_t = \Sigma V_b$ = 4.1 kV			

*Key air pocket, whose breakdown leads to total spark breakdown.

**Broken down and conducting.

Notes:
1. V(Pd) denotes voltage required to break down air pocket per Paschen curve (Fig. 7) for appropriate temperature.
2. V_b denotes voltage on individual pocket at instant of breakdown.
3. V_t denotes total voltage required between detonator electrodes to cause breakdown.

1-10. LONG-LIFE AEROSPACE EXPLOSIVE COMPONENTS

Sidney A. Moses

Development Engineering
McDonnell Douglas Astronautics Company
Huntington Beach, California

ABSTRACT

The expected shelf life of explosive components is discussed. Possible mechanisms which may cause material degradation are categorized and examined. The mechanisms relating to changed chemical activity within sealed components include the effects of (1) temperature changes, (2) pressure changes, (3) inhalation or diffusion of moisture laden air, (4) moisture introduced during manufacture, (5) reactions between explosives and polymers, (6) mutually incompatible explosives, (7) nucleating effects of impurities, (8) catalytic effects, and (9) reactions with contaminating residues.

Based on these mechanisms, guidelines are presented to assist a manufacturer in meeting a 10-year shelf life requirement.

INTRODUCTION

Like other companies engaged in the aerospace business, McDonnell Douglas Astronautics Company (MDAC) has experienced its share of problems with a small percentage of explosive components which degrade in storage. These problems have resulted in excessive component testing, in rush orders for additional components, in launch date slippages, and in the loss of at least one missile.

As a result, the Ordnance Development Branch at MDAC has under consideration a policy that new designs for aerospace explosive components shall be satisfactory for use after 10 years of normal storage. This policy will demand a little something extra from the manufacturers but is still well within the capability of modern explosive technology.

This paper categorizes and discusses the various types of chemical reactions that may cause degradation of explosive components. Guidelines are presented for designing components to meet the projected MDAC policy. These guidelines present no new or startling concepts – just good engineering practices.

AEROSPACE EXPLOSIVE COMPONENTS

For the purpose of this discussion, aerospace explosive components are defined as "components on aircraft, missiles or space vehicles (excluding armament and the main propulsive units) which contain detonating or deflagrating explosives." Although this definition covers a wide variety of devices, these devices may be categorized by their explosive output as (1) *gas producers*, in which this gas is used to generate power or to operate a mechanical device, (2) *hot and [illegible] materials*, in which these products are used to initiate a larger explosive device, such as an igniter or rocket motor, or (3) *shock producers*, in which the output is used to initiate or transfer detonations, or to fracture material.

These components are used in a wide variety of applications, however, they are similar in that each component contains one or more explosive materials, and the explosive materials are incorporated within a sealed container which is designed to prevent atmospheric contamination.

Because of this, an aerospace explosive component may be considered as a little universe containing a complex variety of chemically reactive materials (Figure 1). In addition to one or more explosives, it frequently includes organic or polymeric bonding, structural, or sealing compounds. It will, to some extent, contain a number of contaminates including minute percentages of chemical impurities, moisture, and residues of materials introduced during the course of manufacturing.

This little universe is tightly sealed to prevent the ingress of moisture. However, it may be affected by heat, cold, mechanical abuse (vibration, shock, etc.) and possibly, high frequency electromagnetic radiation (EMR). The discussion contained herein will be confined to those effects which may be expected due to cyclic heating and cooling during long-term storage.

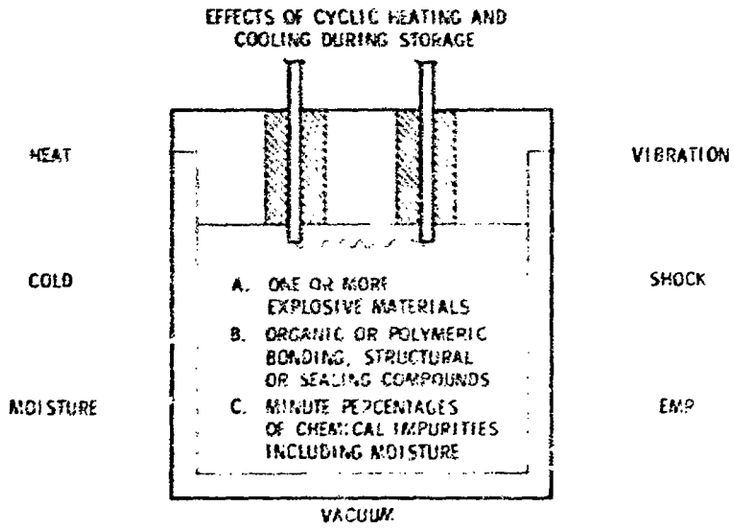

Figure 1. Aerospace Explosive Component – A Tightly Sealed Universe

Most of the changes which occur during the cooling cycles are related to the physical, rather than the chemical makeup of the explosive components. For example, at extremely cold temperatures the materials may become brittle and crack, or the differential shrinkage of mating parts may weaken bonds or otherwise affect the component. The chemical reaction rates are slowed during the cooling cycles.

Although some of the adverse effects of heating are related to the physical properties of the materials, the greatest effects are due to increased chemical reactivity resulting from increased molecular activity.

As indicated in Reference 1, military explosives have a satisfactory long storage life. Considering this fact, one may reasonably ask, "Why do some few explosive components degrade in storage?" The possible degradation mechanisms are largely related to the increased activity of the chemicals involved. Although it is unrealistic to attempt to consider the actual chemical reactions, these appear to be influenced by one or more of the following:

A. Increased Chemical Reactivity with an Increase in Temperature Occurring Either During Manufacture or During Shipment and Storage* – Although an old rule-of-thumb indicates that the rate of a chemical reaction doubles for every 10°C (18°F) rise in temperature, it is probable that this is conservative. For example, the decomposition rate of nitrocellulose increases 3.7 times for each 10°C temperature rise (Reference 1). If this is the case, components containing nitrocellulose will age an equivalent of three months at 68°F for every day they are exposed to a temperature of 130°F. During storage, periods of higher temperature are usually counterbalanced by periods of lower temperature. In fact, the average annual temperature is 70°F or less in all parts of the United States except the southern-most tip of Florida (Reference 2). Considering the above, along with the excellent storage record of individual explosive materials, it appears that if the components degrade in storage, they do so because of reactions between materials rather than degradation of a single material. This possibility will be discussed later.

B. Increased Reactivity with an Increase of Pressure Within Sealed Components Due in Turn, to an Increase in Temperature – Looking at the case in which the temperature increases from 68° to 130°F, the gas pressure inside the closed container increases from 760 mm to 850 mm or approximately 12 percent. This increase of gas pressure, in itself, does not appear sufficient to cause a major increase in chemical activity. However, the vapor pressure of some materials increases drastically with an increase in temperature and, in a closed container, may certainly affect the reaction rate.

*If component may be required to function after exposure to an elevated temperature for a specified time period, however, this is beyond the scope of this discussion.

For example, the vapor pressure of nitroglycerin (a component of double-base propellant) increases by a factor of 40 over the range from 68° to 130°F or by a factor of over 900 if the temperature is increased to 194°F (Reference 3). Although it is unlikely that temperatures of this magnitude are encountered during storage, there have been instances in which components, as a subassembly of a larger system, were accidentally exposed to even higher temperatures during manufacturing.

C. Inhalation or Diffusion of Moisture-Laden Air into Supposedly Sealed Containers, Brought About by Temperature Changes During Storage - As previously stated, aerospace explosive components are sealed to prevent the entrance of moisture. Unfortunately, some components which meet strict leak-rate requirements at the time of manufacture, do not remain leak-tight after numerous cycles of heating and cooling, or after being subject to vibration during transportation.

If the seal is imperfect, moisture-laden air can be drawn into the component because of temperature changes. This moisture, once inside the container, may be absorbed or adsorbed by the material so that the percentage of moisture will tend to increase over many such temperature cycles.

Moisture can affect the explosive components in a variety of ways. At low temperature, the formation of ice crystals may result in undesirable movement of parts. With electroexplosive devices, ice forming around the bridgewire may result in initiation failures. At any temperature, the moisture acts as a diluent and in sufficient quantities will cause failures.

At elevated temperatures, moisture may enter into combination with other materials and seriously degrade the output characteristics. For example, one type of pressure cartridge was stored at a constant temperature of 200°F. Samples pulled from storage at monthly intervals were fired in a pressure chamber. Degradation (as indicated by a significant decrease in the peak pressure) did not occur until the thirty-second month. Additional samples from the same lot were cycled between 200° and 70°F on a daily basis. Degradation was noticed at the end of only four months of this treatment. It was concluded that airborne moisture, leaking through the seal during the cyclic changes, was the major cause of this rapid degradation.*

D. Moisture Introduced During the Manufacture of the Explosive Component - Finely ground explosives will absorb or adsorb moisture from the air at the time the components are being loaded. During this operation, it is common practice to maintain the loading area at a high humidity for safety reasons. If the components are not dried after loading, or if the dried components are left uncovered in a humid atmosphere before sealing, undesirable moisture can be sealed into the components.

E. Reactions Between Explosives and Polymers - Picatinny Arsenal has established information on the compatibility of several hundred combinations of explosives and polymers (adhesives, potting agents, elastomers, etc.) as given in Reference 4. Although the program was not specifically directed at investigating aerospace explosive components, some generalized statements can be made regarding the compatibility problem:

1. Polymers appear to be compatible with black powder and metal-oxidizer mixes.

2. Double-base propellants, especially high-energy propellants, are incompatible with many polymers.

*Obtained by personal communication with the development engineer.

3. Primary explosives are compatible with polymers from a limited number of tests.

4. The high explosive, RDX, is incompatible with many polymers.

5. Uncured polymers, especially those which use amines as the curing agent, are extremely reactive with many classes of explosive materials.

F. Mutually Incompatible Explosives - MDAC has recent experience with a small gas generator which contained three explosive materials (1) an electric match, (2) a powdered metal-oxidizer ignition charge, and (3) a machined grain of a high-energy, double-base propellant. Although each of these explosive materials is quite stable by itself, even short exposure to high temperature caused the nitroglycerin from the double-base to degrade the match to the point that subsequent initiation failures were observed.

The high-energy, double-base propellants are more likely to be incompatible with other explosive materials than any other combinations in common use in aerospace components. Nevertheless, unless the materials are known to be compatible, it appears reasonable to separate all the explosive materials within the component by inert barriers.

G. Nucleating Effect of Impurities - Assuming that heat is the major contributing cause of the degradation of explosive components, what types of heat-activated reactions may be expected? In addition to the reactions with moisture or vapors previously mentioned, there are also solid reactions which result in gaseous products. A typical reaction is: A solid + B solid + C gas, although frequently, more than one solid is involved.

With increasing molecular activity due to heating, this type of reaction begins at nuclei within the crystals. The actual source may be due to either crystal imperfections or contaminating molecules. Beginning at these nuclei, the reaction grows with the rate of growth being related to the temperature, the original number of nuclei and other conditions.

Little is known concerning the effect of small percentages of contaminating materials on the degradation of explosives. It may be that these contaminates supply sufficient nucleating molecules to accelerate the degradation process at elevated temperatures. Many explosive materials contain relatively large percentages of impurities when these are compared to chemically pure substances. For example, explosive delay materials are considered pure if the amount of the various constituents are measured to ±0.1 percent, or 1,000 parts per million (Reference 5). This is, of course, far different than the purity of reagent chemicals in which certain specified impurities are measured to as low as 0.0002 percent or 2 parts per million.

For comparative purposes, the density of Los Angeles smog is well known, although the highest reading of ozone ever recorded in Los Angeles County was only 0.90 parts per million parts of air (Reference 6). Yet no one would hesitate to say that smog has a deleterious effect on many substances.

H. Catalytic Effects - A catalyst is a substance which accelerates the rate of a chemical reaction while remaining chemically unchanged. A small quantity of catalyst is often sufficient to bring about a considerable amount of reaction. Although this desirable effect of catalytic action is used in a wide variety of chemical processes, the undesirable effects of shortening the useful life of explosive components has received little attention.

Many of the heavy metals and metal-oxides used in pyrotechnic mixes may act as catalysts with organic materials. Thus, these pyrotechnics may affect the stability of both propellants and high explosives. In

addition, they may affect organic binders and adhesives and the products may further act on the explosive materials.

I. Reactions Between Explosives and Contaminating Residues Left from Manufacturing Operations – Improperly cleaned components may contain small traces of grease or cutting oils that have a deleterious effect on organic explosives. With those electroexplosive devices in which the bridgewire is soldered to the lead-in pins, traces of solder flux may react with the explosives. Touching the bridgewire with bare hands as the wire is being applied will leave traces of oil or acids which may react with the explosives. These and other manufacturing operations may deposit undesirable contaminates within the components.

The nine degradation mechanisms described may affect the shelf life of components in different ways and at different rates. It may be that one of these mechanisms is predominant over one given temperature range while another is predominant over a different range. Despite these differences, each of the mechanisms may be accelerated by either (1) increased temperature, or (2) temperature cycling with high humidity. These two factors provide a basis for an accelerated life test to be mentioned later.

DESIGN AND MANUFACTURING REQUIREMENTS

Based upon the nine degradation mechanisms, it is apparent that aerospace explosive components can be designed for a 10-year minimum shelf life. This 10-year shelf life may be a requirement for future designs originating within MDAC. The following criteria will serve as guidelines to design components that will meet the requirement.

A. The components shall have a leak rate of 10^{-6} cc/sec or less at 1 atmosphere differential when tested by a helium leak tester or equivalent. All components shall be so tested on a 100 percent basis. Note that a helium test will not provide reliable information on the leak rate for some component seal areas. For example, at the interface between confined detonating fuse and a metal sleeve there will be leakage through the outer braid material. With components of this nature, the seal shall satisfactorily pass an adequate temperature-humidity test.

B. The explosive components shall be hermetically sealed. Preferred methods include welding, glass-to-metal seals, and ceramic-to-metal seals. For some components (e.g., the joint between detonating fuse and a metal sleeve), these seals are impractical. With components of this nature, the seal shall satisfactorily pass an adequate temperature-humidity test.

C. The seal shall not be degraded by changes in pressure brought about by changes in temperature or altitude. Both of these conditions may be simulated by a temperature-humidity test. When applicable, the helium leak shall be repeated following the temperature-humidity cycling.

D. The explosive materials shall conform to the applicable material specifications concerning the minimum percentages of moisture and impurities.

1. When material specifications are not available, the manufacturer shall prepare such a specification. As a guide, the percent of moisture shall not exceed 0.05 percent and the total impurities (including moisture) shall not exceed 0.10 percent.

2. As indicated previously, finely-ground explosives will absorb or adsorb moisture from the air at the time the components are loaded. During this operation, it is common practice to maintain the loading area at a high humidity for safety reasons. When this condition exists, the loaded explosive components shall be dried for a minimum of 24 hours at a minimum of 120°F prior to hermetic sealing. Components shall be kept in covered containers between the time they are removed from the drier and the time they are sealed.

E. No polymers (adhesives, potting agents, elastomers, etc.) shall be used in intimate contact with explosive materials unless it is determined that they are nonreactive with the materials in question. Reference 4 gives information on the compatibility of several hundred combinations of explosives and polymers. The test methods used to determine these data also are given.

F. The components shall be completely clean before loading. It is common practice to clean all metal components in a vapor degreaser just prior to loading. When the components contain a soldered bridgewire, excessive solder flux shall be removed with a suitable cleaner which leaves no residue.

G. High energy, double-base propellants shall be separated from other explosive materials by a leak-proof metal barrier.

1. The nitroglycerin in these propellants has a great affinity for many other organic materials (including polymers and explosives). This may cause the nitroglycerin to leach out of the propellant degrading one or both materials. These reactions may be catalyzed by the presence of heavy metals which are frequently used in pyrotechnic mixtures.

2. The rocket propellants (N-5, N-9, N-12, etc.) and the mortar propellants (M8 and M9) appear to be the most reactive of the double-base propellants. These materials, if separated from other explosives, are sufficiently stable to meet the 10-year shelf life requirement.

3. Double-base, small arms propellants may be separated from other explosives by plastic film or tape providing the plastic meets the requirements of Item E.

H. When the explosive components contain pyrotechnic delay trains, the pyrotechnic material shall be pretreated to prevent degradation.

1. Generally speaking, pyrotechnic delay powders are combinations of finely ground metals and metal-oxides which are then compacted at high pressure. Under these conditions the surface of the powdered metal may oxidize during storage resulting in increased delay times. Some manufacturers prevent this by inducing an oxidized surface on the powdered metal, prior to compounding with the metal oxide.

2. Explosive components having pyrotechnic delays in which the delay is less than one second and in which the tolerance is 10 percent or less shall be subjected to surveillance tests on a yearly basis to determine possible out-of-tolerance conditions.

I. All explosive component designs shall be subjected to an accelerated life test. This test is described in Reference 7.

The above criteria demand careful attention to details in design and manufacturing. However, a manufacturer should have no difficulty in meeting the 10-year criterion providing his procedures are closely controlled as demanded for quality products.

REFERENCES

1. Military Explosive. Department of the Army and the Air Force, TM9-1910, TO 11A-1-34, April 1955.
2. The Weather Handbook. Conway Publications, Inc., Atlanta, Ga.
3. Properties of Explosives of Military Interest. Section 1, ORDP20-177, Ordnance Corps Pamphlet, May 1960.
4. N. E. Beach et al. Compatibility of Explosives with Polymers (II); Addendum to Picatinny Arsenal Technical Report 2595. AD 672-01 Plastics Technical Evaluation Center, Picatinny Arsenal, Dover, N. J.
5. MIL-P-22264. Powders, Ignition, Gasless. 30 March 1962.
6. The Alert System. Air Pollution Control District, County of Los Angeles.
7. S. A. Moses. Accelerated Life Test for Aerospace Explosive Components. McDonnell Douglas Astronautics Company Paper WD 1657, July 1971.

ABSTRACTS - SESSION II EVALUATION AND TESTING TECHNIQUES

II-1 Monitoring of Explosive/Pyrotechnic Performance

Laurence J. Bement

In the application of explosive and pyrotechnic devices to aerospace or commercial systems, it is necessary to utilize performance monitoring techniques for acceptance, lot qualification, and comparison testing, as well as providing engineering guidelines for system design. Test techniques and apparatus have been developed at the Langley Research Center to evaluate the performance of squibs, initiators, gas generating cartridges, detonators and linear explosives for aerospace applications. A variety of devices has been tested in each of these apparatuses, including the Apollo Standard Initiator, the Apollo End Detonating Cartridge, and mild detonating fuse and flexible linear shaped charge. These performance monitoring test techniques and apparatus have exhibited a high degree of simplicity, accuracy, and reproducibility; each could be used as a performance monitoring standard.

II-2 Fast-Rise High-Current Constant Current Firing Circuit for Electroexplosive Devices

James L. Austing
Arthur L. Usher

The design and operation of a constant current firing circuit for evaluating the no-fire and all-fire characteristics of electroexplosive devices is described. The circuit is triggered into forward conduction by a silicon controlled rectifier, and is designed to provide a current of 3.5 to 25 amp with a rise time of 20 to 30 μsec. Flat two-conductor transmission line is utilized throughout the circuit to minimize inherent inductance. Typical oscillographs are presented showing the current rise and stability that is obtained. The use of the circuit to evaluate the performance of an electroexplosive device under all-fire conditions is described in detail.

II-3 Accelerated Life Test for Aerospace Explosive Components

Sidney A. Moses

An analysis was made of the stability tests used for explosive materials. It was determined that although these are satisfactory for bulk materials, they have serious limitations when applied to hermetically sealed explosive components. A test method is proposed for predicting the expected shelf or storage life of aerospace explosive components. This method, which is based on a modification of the Arrhenius reaction rate equation, includes the following tests: (1) short-period, high-temperature, (2) temperature-cycling (combined with high humidity), (3) long-period, constant-temperature, and (4) performance comparison. The proposed method is compared with tests from typical military specifications which are sometimes used as a basis for predicting the shelf life of explosive cartridges.

II-4 Response of Electroexplosive Devices to Impulsive Waveforms

Louis A. Rosenthal
Vincent J. Menichelli

The firing characteristics of insensitive electroexplosive devices to certain impulsive waveforms has been investigated. For these waveforms, energy is delivered in a time short compared to the thermal time constant and therefore cooling plays a negligible role. One waveform is a terminated capacitor discharge wherein the regular discharge of a capacitor is terminated at a preset point. Another is a half-sine wave pulse. Good agreement is obtained with the well established capacitor discharge mode of firing and certain conveniences and advantages may be offered. The theory, design, and application of both impulsive waveform generators are presented together with certain limited experimental observa-

II-5 Interrelationship of Nondestructive Testing to Fault Determination

Vincent J. Menichelli
Louis A. Rosenthal

Several nondestructive test techniques have been developed for electroexplosive devices. The device will respond, when pulsed with a safe level current, by generating a characteristic heating curve. The response is indicative of the electrothermal behavior of the bridgewire-explosive interface. Devices which deviate from the characteristic heating curve have been dissected and examined to determine the cause for the abnormality. Deliberate faults have been fabricated into squibs and the resulting abnormalities observed. The relationship of the specific abnormality and the fault associated with it are discussed.

II-6 Short Pulse Testing

R.H. Thompson
Victor Goldie

The gross sensitivity of several EED's to a short damped burst of RF energy was determined. Both pin-to-pin and pin-to-case firing data were obtained. It is calculated that 85% of the stimulus energy is delivered to the EED in one half the period of the frequency of the burst. Frequencies ranged from five to forty-five megahertz.

II-7 Repeatable Hermetic Seal Quality Determinations by the Helium Bombardment Technique

W.P. Garton

Hermetic properties of seals in small aerospace ordnance devices are frequently verified by the helium bombardment leak testing technique. The standard test procedures are relatively simple and inexpensive, but yield inherently ambiguous results. A common complaint is that repeated tests of a unit lead to widely varying estimates of seal quality. A modification of the normal test procedure is described which permits estimates of seal quality to be based on the decay of measured lead rate with time following bombardment. For many parts such estimates are found to be both precise and highly repeatable in successive tests. The advantages and limitations of the new technique are discussed.

II-8 Minuteman HERO Testing — Leonard Doellner

This paper delineates methods used by The Boeing Company in implementing HERO (Hazards of Electromagnetic Radiation to Ordnance) missile preflight checkout procedures on the Minuteman Weapon System. The work started on the first Minuteman I System in the early 1960's and is continuing for all new configurations of Minuteman. Early HERO instrumentation consisted of simple voltage monitoring techniques. Present instrumentation systems are capable of measuring the effects of low level transient energy (50 microjoules) and high frequency (to 10 gigahertz) steady state or transient phenomena. An EMP level ordnance monitoring system employing fiber optic data links is described.

II-9 The Colt's PotAct and PyrAcc — C.R. Olsen

Two pyrotechnic devices have been developed: The RotAct, provides a direct curvilinear output in a fully sealed system. The device consists of a twisted, fluted tube, which untwists when pressurized. Sizes tested range from 1/10" diameter to 3-3/8" in diameter with torque outputs ranging from 1 to 72 hundred inch lbs. of torque. Graphs showing the relationship of pressure, wall thickness and initial twist to torque output and degrees of total untwisting are presented. The PyrAcc is a non-contaminating fluid dispenser or accumulator which utilizes a fluted, metal liner as an expansion bellows. The PyrAcc is being evaluated for automotive crash safety applications as well as a one shot fluid power source for aerospace and commercial applications.

II-10 Pyrotechnic Hazard Classification — Joseph H. McLain

The purpose of classification of explosive substances is to afford reasonable protection to personnel and property in the event of an accidental explosion. In the past it has been the practice to include pyrotechnics with high explosives and propellants. This practice is based upon false assumptions both as to degree of protection afforded and frequency of accidents. The concept of providing a separate hazard classification for pyrotechnics is explored, explained and proposed.

II-11 Doping Explosive Materials for Neutron Radiographic Enhancement — K.G. Golliher

Doping of organic and inorganic simulated explosive materials, to improve neutron radiographic imaging, has been successfully demonstrated. Materials, with doping concentrations ranging from 10 ppm to 10^4 ppm, were neutron radiographed with thermal neutrons using the activation transfer and the direct neutron detection techniques. Neutron radiography of electroexplosives devices (EED's) has been successfully used during the past 4 years as a nondestructive technique to examine the explosive material contained in a metallic housing. This method of examination has been highly successful with explosive materials containing hydrogen or boron.

II-12 Confusion Concerning Booster and Lead Explosives — R.H. Stresau

Since World War II the number of booster explosives in use permitted by official documents or being actively considered for use in leads or boosters of fuzes for the U. S. Armed Services has increased from one or two to 40 or 50. Data whereby these explosives can be compared with respect to their advantages in any given application are fragmentary and scattered. Conflicting requirements of the various Services and their agencies preclude interchangeability. In some cases arbitrary restrictions combine with design considerations to limit the choice to expensive and strategic materials. A cooperative effort of all concerned is suggested to alleviate the present chaotic situation.

II-1. MONITORING OF EXPLOSIVE/PYROTECHNIC PERFORMANCE

by
Laurence J. Bement
National Aeronautics and Space Administration
Langley Research Center, Hampton, Virginia

INTRODUCTION

Users of explosive/pyrotechnic systems have a need for accurate performance monitoring techniques to meet a variety of requirements, such as the comparison of explosive functional characteristics, lot acceptance tests, system qualification, determining the effects of environments and demonstrating performance margins. Individual organizations have developed specialized test apparatuses which often do not measure the most informative performance parameters, or have sufficient accuracies to allow detailed comparisons. Comparison of test information between organizations is seriously hampered by the lack of standardized test hardware.

This report describes techniques and test apparatus for monitoring the performance of the primary energy sources for explosive/pyrotechnic devices, including squibs, initiators and gas generators, detonators, and linear explosives. These techniques have been developed and evaluated at the Langley Research Center, have been demonstrated to be accurate and reproducible, and the simplicity of their design supports the use of these techniques and test apparatus as standards. These techniques are applicable primarily as comparison tests, and should be utilized only as general guidelines for final applications. The performance of explosive/pyrotechnic materials are strongly affected by the volume in which combustion takes place, the rigidity of structure, and the actual structural loading and required force levels of the system.

DESCRIPTION OF APPARATUS AND RESULTS

The description of the test techniques and apparatus has been divided into three sections based on the output characteristics of the particular item to be characterized. These sections are: 1) squibs, initiators, and gas generating cartridges, 2) detonators, and 3) linear explosives. The important performance parameters for these devices will be listed with a description of the accepted standard performance monitoring techniques. This will be followed by a description of the Langley recommendations for the monitoring apparatus, the techniques that have been developed and representative results from the demonstration tests.

Squibs, Initiators, and Gas Generating Cartridges

The important performance parameters are:

Electrical ignition characteristics - current (constant current, or capacitor) versus function time, and bridgewire heating.

Output - pressure, time to peak pressure, and energy through heat, or mechanical work.

Accepted standards. - A typical closed bomb setup which is presently used to monitor the output of pressure-producing devices is shown in Figure 1. The most commonly-used recording instruments are oscilloscopes with polaroid cameras to achieve a permanent record, rather than using a magnetic tape recorder with playback into a recording oscillograph to obtain a higher degree of resolution. The performance measured by the closed bomb is strongly influenced by the actual volume of the bomb, its

shape, the bomb materials and their mass (as related to thermal transfer characteristics), the location and mounting of the pressure transducers and the frequency response of the transducers and recording apparatus. The frequency response and absolute pressure values provided by the commonly used piezoelectric pressure transducers are often impaired by dirty connectors, cables with insufficiently high electrical impedance, or damaged cables.

Recommended techniques. - A "Dynamic Test Device" was originated by Martin Marietta to provide information on mechanical energy delivered and combustion dynamics in configurations representative of an actual application. This is to help overcome the weakness of the data produced by the closed bomb systems. The NASA-Langley Research Center has taken the Dynamic Test Device shown in Figure 2 and developed an apparatus to monitor the velocity of the one-pound piston, as shown in Figure 3. The internal volume of the Dynamic Test Device is pressurized by the firing of a gas generating device, causing the piston to accelerate through a one-inch stroke. The velocity is monitored by determining the time intervals between five contact switches, spaced 0.25 inch apart. The electrically-grounded needle mounted to the face of the one-pound piston contacts each of five electrically charged foil switches. This discharges their respective capacitor circuits, producing electrical signals which are recorded with the functional characteristics, (ignition, pressure) on a magnetic tape recorder. A second velocity measurement is obtained by using the McDonnell-Douglas developed energy sensor shown in cross section in Figure 4 (See Reference 1). The displacement produced in the honeycomb of known uniform crush strength by the impact of the piston provides an energy measurements in inch-pounds. The original velocity of the piston can be calculated from this value. The data produced in each firing are: the firing energy, the pressure produced, four time intervals between the foil switches, producing a final velocity measurement, and a honeycomb-crush energy measurement as a final velocity verification.

The pressure performance of two supposedly identical initiators, the Single Bridgewire Apollo Standard Initiator (SBASI) and the Hi Shear PC S1-003 initiator, are shown in Figures 5 and 6. The higher burn rate of the SBASI produced higher peak pressures within a shorter period of time, and delivered less velocity to the one-pound piston; the SBASI produced an average velocity of 37.2 feet per second with a standard deviation of 1.27, while the PC 81-003 produced 50.1 feet per second with a standard deviation of 3.4. The energy sensor-calculated velocity value was 60% of the actual velocity, due to impact and friction losses.

Other important considerations for monitoring explosive and pyrotechnic performance are the following:

A magnetic tape recorder coupled with play-back through a recording oscillograph provides a much higher degree of flexibility over an oscilloscope in a time frame as low as 0.1 milliseconds. This approach to recording data eliminates the need for trigger circuits and offers excellent accuracy and resolution over long recording time periods. The shapes of closed bomb internal volumes should be symmetrical, avoiding large surface areas/unit volume. Pressure transducers are generally recessed in minimum volume cavities especially designed to minimize resonance effects. Also, the tranducers are normally installed

perpendicular to the output of the gas source to avoid pressure and thermal shocks, as well as erosive burning. The pressure transducer electrical impendance problems can be eliminated within a narrow temperature range around laboratory ambient by using impedance matching electronics that are built in or closely coupled to the transducer. The overall frequency response of the monitoring system should be at least 20 kHz.

It is important to test the electrical ignition characteristics of devices over the total possible range of current and voltage, as compared to existing practices of Bruceton tests at the 50% firing energy and subsequent tests at the statistical "recommended firing current." The value of off-limits tests has been demonstrated by the many devices that have performed abnormally, or have malfunctioned at higher energy levels. A convenient way to display function time data (the times from energy application to bridgewire break and the first indication of pressure) for reproducibility comparisons is shown in Figure 7.

An improvement over the existing closed bomb systems would be to provide the capability to simultaneously measure the caloric output, as well as the previously described data. The design and demonstration of a system of this type to an accuracy of ± 5 calories is presently being performed under contract to the NASA-Langley Research Center.

Detonators

The important performance parameters are:

Electrical ignition characteristics - current versus function time, bridgewire heating

Output - pressure as monitored by energy delivery and dents, high velocity fragments, and fragment patterns

The transfer of detonation across hermetically sealed interfaces, such as from detonator to linear explosive columns, is probably the least understood mechanism in the explosive and pyrotechnic field. A study of these mechanisms under contract to NASA-Langley Research Center (See Reference 2) has revealed that the energy delivered by explosive donors consists of at best 30% pressure-delivered energy and the remainder delivered by high velocity fragments created by the explosive breakup of the donor's end closure, or housing material. This study, when complete, is intended to provide a quantitative description of the effect of the following variables:

(1) Explosive materials - energy delivery and sensitivity to ignition.

(2) Density and quantity of explosive.

(3) Inert housing materials

(4) Energy delivery versus explosive separation distances and thickness of end closures.

Accepted standards. - The existing efforts to cope with this detonation transfer problem have been through dent block output tests of donors under MIL STD 316 which makes no allowances for measuring the energy delivered by the end closure fragments, and through "50% gap tests" in which the two explosives are separated to the point where propagation no longer occurs. However, failures to propagate have occurred within the statistically established recommended margin and at zero separation, due to poor designs and the inhibiting of high velocity fragment generation.

Recommended techniques. - The fixtures developed at Langley Research Center for the evaluation of detonators are shown in Figures 8 and 9. The fixture shown in Figure 8 monitors the fragment velocity through the use of parallel foil switches separated by one inch. Each switch has two foils; one electrically grounded and the other attached to a capacitor circuit. The arrival of the fragments at each switch short circuits the foils, producing two electrical pulses which can be monitored electronically. The fragment patterns are observed on witness plates at a distance of three inches from the detonator. The fixture in Figure 9 monitors the energy delivered by the explosive pressure. The dent block provides the standard dent, transfers the energy to the honeycomb energy sensor described earlier, and protects the energy sensor, as well as providing a smooth interface to the detonator for each test. The screw assembly provides a method of rigidizing the components of the apparatus with the only moving element being the energy sensor piston.

An example of typical data obtained with this apparatus is the results of test programs with 55 Apollo End Detonating Cartridges (27 were used for fragment velocity and patterns and 28 were used for energy output and dent tests), and eight inexpensive Dupont Model E-106 blasting caps. The Apollo End Detonating Cartridge produced fragment velocities ranging from 8,013 to 12,626 feet per second, delivered 128 to 254 inch pounds of energy, and each firing produced dents of 0.023 inch. The Dupont Model E-106 blasting cap produced velocities ranging from 12,438 to 12,821 and delivered from 330 to 390 inch pounds with dents of 0.021 to 0.025 inch. Although the Apollo End Detonating Cartridge had a wide range of performance, as compared to the Dupont blasting cap, (the only consistency was in the dent which is of questionable value) its system reliability was achieved through a large overdesign.

Linear Explosives

Mild Detonating Fuse or Flexible Linear Shaped Charge

The important performance parameters are:

- Energy output
- Velocity of detonation propagation
- Cutting or rupturing ability

Accepted Standards. - The existing linear explosive monitoring techniques rely heavily on the consistency of the velocity of detonation propagation, and difficult to measure dents or cuts in flat witness plates produced by the explosive output.

Recommended techniques. - A sketch of the test fixture developed at NASA-Langley Research Center to measure the three performance parameters simultaneously is shown in Figure 10. (See Reference 3) The specimen holder is a 17-4 P.H. steel bar with a groove machined on each side to conform to the linear explosive test specimen. The witness plate is 2024-T4 aluminum, tapering from 0.200 to 0.010 inch. The steel hold-down plate, utilized only for MDF firings, produces a rigid backup and confinement for the tapered plate by providing an 0.125 inch bearing surface on each side of the explosive. The hold-down plate is bolted rigidly to the test stand. No hold-down plate is necessary for the FLSC firings, due to the directionality of its output.

Timing of the detonation propagation velocity is accomplished by a capacitive circuit and timing wires which are placed across the explosive at each end of the tapered plate. Upon arrival of the detonation an

electrical short circuit is produced, which discharges their respective capacitors. The resultant pulses are monitored by an electronic timer gating circuit.

The explosive column is ignited by a detonator. An initial two-inch length is provided to assure stable detonation before any measurements are made. The next two-inch length provides an impulse to the energy sensor. The first timing wire is short-circuited to ground by the explosion which starts the timer. The explosive specimen then cuts the tapered plate to its maximum capability, and finally short circuits the second timing wire which stops the timer. The energy output is computed by multiplying the displacement of the honeycomb by its crush strength. The cutting ability is established by measuring the thickness of the plate at the point where complete rupturing occurs for MDF or where cracking ends for FLSC.

The results of three simultaneous performance evaluations on ten samples each of six different explosives in MDF and FLSC configurations are shown in Figure 11 - Energy output comparison, Figure 12 - Velocity of propagation comparison, and Figure 13 - Cutting ability comparison. Each bar in the figures is labled with the explosive and the sheath materials. The explosives tested were: PETN (pentaerythritoltetranitrate) RDX (cyclotrimethylenetrinitramine); HMX (cyclotetramethylenetetranitramine) HNDS (hexanitrodiphenylsulfone); HNS-II (hexanitrostilbene) and DIPAM (dipicramid). The maximum, average, and minimum value are indicated by horizontal lines, and the standard deviation for each group is a number at the top of the bar. The average energy outputs of the test groups ranged from 159 to 330 inch-pounds with the largest standard deviation being 9.5% of its respective group average. The average velocity of propagation values ranged from 20,380 to 26,265 feet per second with the largest standard deviation being 2.3%. The range of average cutting ability was 0.097 to 0.140 inch with the largest standard deviation of 14%. Do not expect these measurements to directly apply to any particular system requirements. Explosives are extremely sensitive to their immediate confining media. For example, the smallest change in the energy sensor interface to the explosive can halve the energy delivered. These performance parameters should be used only for comparison and should provide only general design guidelines and relative orders of magnitude in considering different explosive applications.

SUMMARY AND RECOMMENDATIONS

This report describes test techniques and apparatus developed at the NASA-Langley Research Center for the monitoring of squibs, initiators, and gas generators; detonators; and linear explosives. These techniques have demonstrated an accuracy and reproducibility that appear to be superior to the currently-accepted standards as well as providing additional, more informative test data on the most influential performance perameters. It is believed that these techniques could provide the basis for approaches to standardized explosive and pyrotechnic monitoring equipment.

Based on the use of these techniques, the following tolerances on the output measurements have been established at the NASA Langley Research Center:

For squibs, initiators and gas generators:

(1) The pressure performance should have a largest standard deviation of 10% or less of its respective mean value.

(2) The ignition performance should fall on each unit's characteristic function time curve within ± 10%.

(3) The velocity output in the Dynamic Test Device should have a standard deviation of less than 5% of its mean value.

For detonators:

(1) Proper designs should produce fragment velocities with standard deviations less than 5% of its mean value.

(2) The energy output should have standard deviations less than 15% of its mean value.

For linear explosives:

(1) The energy output should have a largest standard deviation of less than 10% of its mean value.

(2) The velocity of detonation propagation should have a largest standard deviation of less than 2% of its mean value.

(3) The cutting ability should have a largest standard deviation of less than 15% of its mean value.

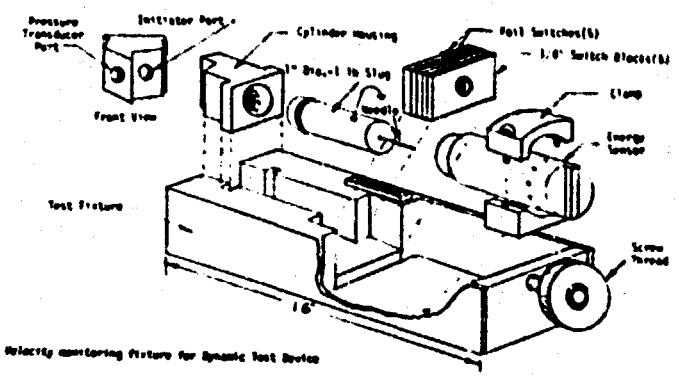

Figure 1. Velocity monitoring fixture for Dynamic Test Device

REFERENCES

1. Schimmel, M. L.; and Drexelius, V. W.: Measurement of Explosive Output. Proceedings of the Fifth Symposium on Electroexplosive Devices, June 1967.

2. Shimmel, M. L.: Quantitative Understanding of Explosive Stimulus Transfer. Contract NAS1-9903, and Extension of Experimental Program for Quantitative Understanding of Explosive Stimulus Transfer. Contract NAS1-10762.

3. Bement, L. J.: Application of Temperature-Resistant Explosives to NASA Missions. Presented at the Symposium on Thermally Stable Explosives, June 1970.

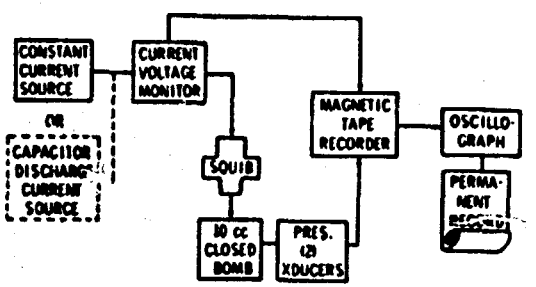

Figure 1 - Closed bomb firing and monitoring system.

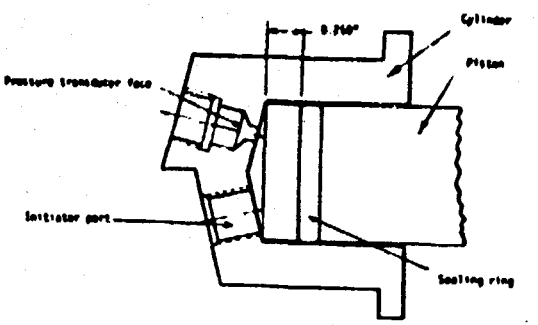

Figure 2. Cross section of NASA-LaRC Dynamic Test Device

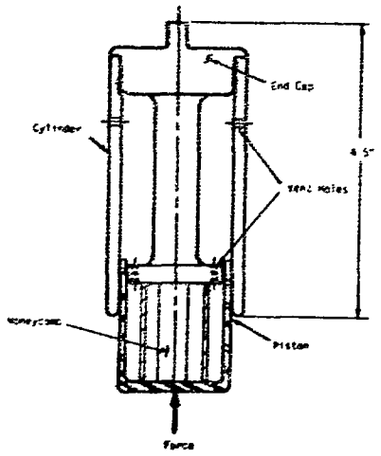

Figure 4. - Energy sensor cross section

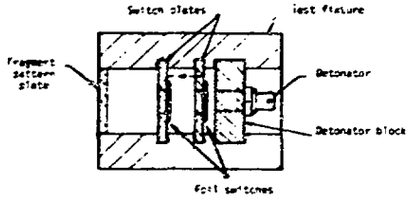

Figure 8. - Fragment velocity test fixture

Figure 9 - Energy output test fixture

Figure 5. - Typical SBASI pressure traces.

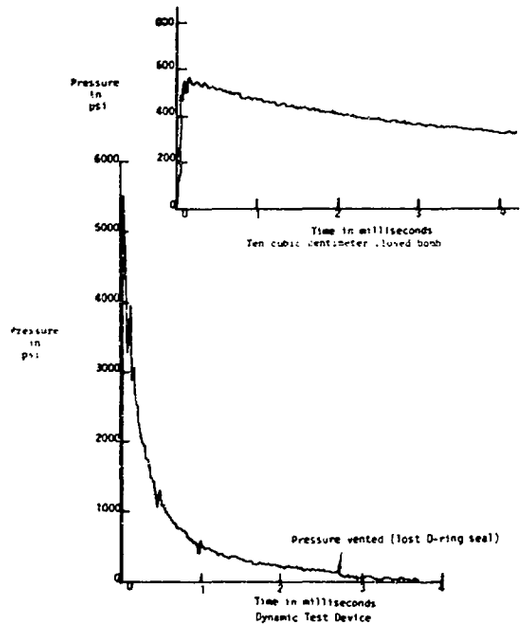

Figure 6. - Typical PCBI-003 pressure traces

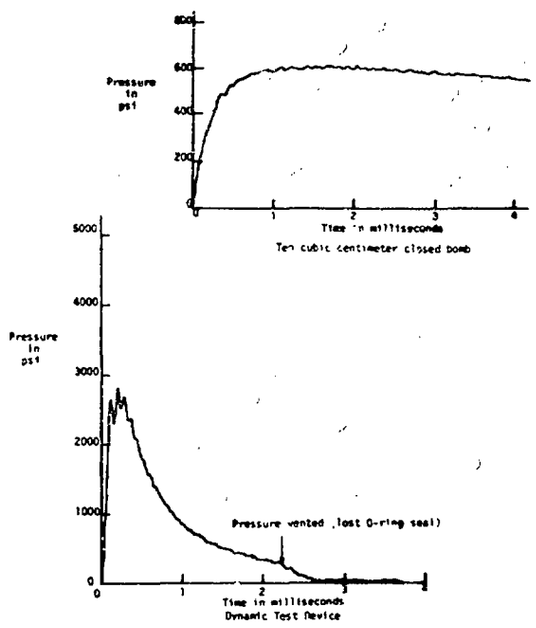

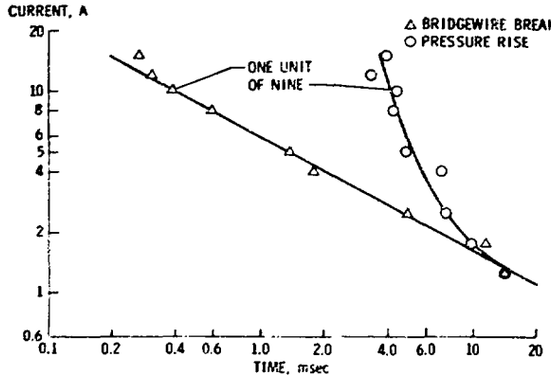

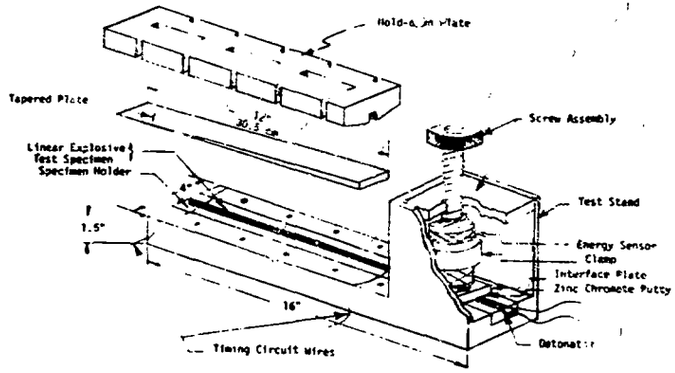

Figure 10- Linear explosive test fixture.

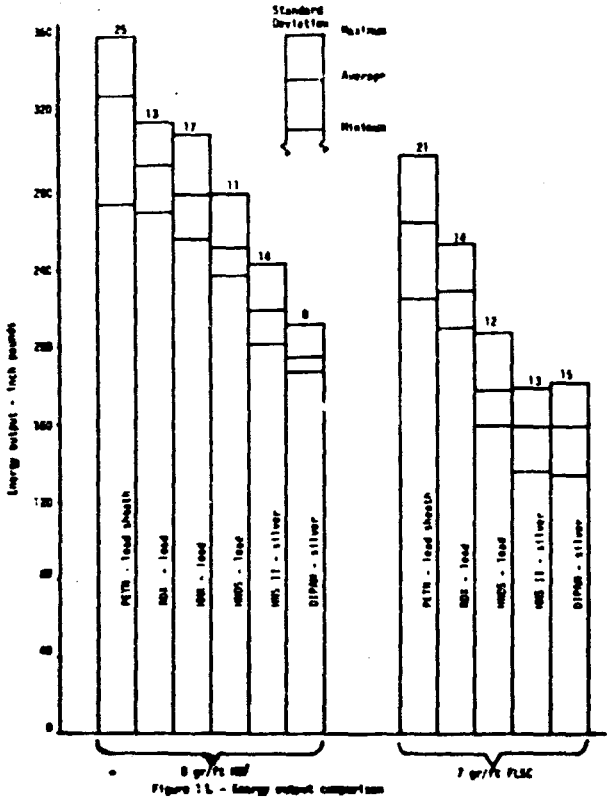

Figure 11. - Energy output comparison

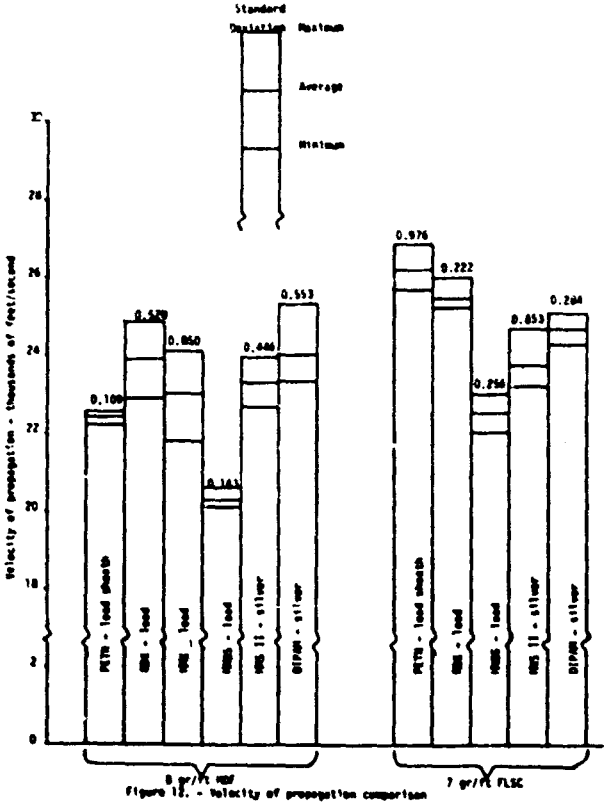

Figure 12. - Velocity of propagation comparison

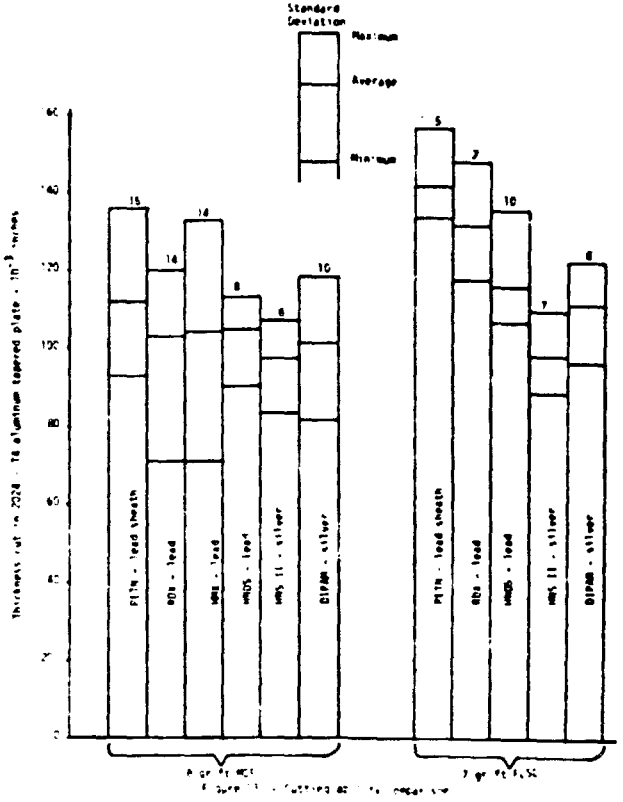

II-2. FAST-RISE HIGH-CURRENT CONSTANT CURRENT FIRING CIRCUIT FOR ELECTROEXPLOSIVE DEVICES*

James L. Austing
Arthur L. Usher**
IIT Research Institute
Chicago, Illinois 60616

The design and operation of a constant current firing circuit for evaluating the no-fire and all-fire characteristics of electroexplosive devices is described. The circuit is triggered into forward conduction by a silicon controlled rectifier, and is designed to provide a current of 3.5 to 25 amp with a rise time of 20 to 30 μsec. Flat two-conductor transmission line is utilized throughout the circuit to minimize inherent inductance. Typical oscillographs are presented showing the current rise and stability that is obtained. The use of the circuit to evaluate the performance of an electroexplosive device under all-fire conditions is described in detail.

Research and development activities in the area of electroexplosive devices (EED's) over the last decade have been directed towards improving the safety of these devices, while maintaining their high reliability. Specifications have been drawn up which require that EED's dissipate without functioning, input no-fire currents and powers of 1-amp, 1-watt for 5 minutes or 5-amp, 5-watts for 15 minutes; on the other hand, such devices must function reliably upon the receipt of an all-fire current of 5 amp or 15 amp, respectively. This paper describes the construction and operation of a constant current firing circuit for evaluating the no-fire and all-fire characteristics of electroexplosive devices. This circuit provides a current in the range 3.5 to 25.0 amp with a rise time of 20 to 30 μsec.

A schematic diagram of the constant current firing circuit is depicted in Figure 1. The 36-v power supply consists of three 12-v lead-acid storage batteries connected in series, although any other type of battery from which high currents can be drawn could have been utilized. The design of the circuit, which consists of a silicon controlled rectifier (SCR) triggered by a unijunction transistor (UJT), was suggested in the SCR Manual.[1] The portion of the circuit containing the UJT is basically a simple relaxation oscillator, and operates in the following manner. When the "Fire" push button switch (PBSW) is closed, the 0.05-μf capacitor is charged through the 10-Kohm resistor until the emitter voltage of the UJT reaches the socalled peak point voltage; at this time the UJT turns on, discharges the capacitor through the 27-ohm resistor, and triggers the SCR into forward conduction in the DC latched mode at an anode current level dictated by the supply voltage and load resistance. The SCR remains in conduction until the battery on-off switch is opened or the EED is initiated, effecting commutation.

The procedure that is utilized in evaluating an EED is as follows. The calibrating resistor R_c is set equal to the sum of the EED resistance R_e plus 0.044 ohm, which is the value of the current viewing resistor (CVR). The circuit is triggered by pressing the PBSW, and the calibrating current I_c through R_c

*Work supported by IIT Research Institute.

**Present address: Federal Sign and Signal Corporation
Blue Island, Illinois 60406

is adjusted to the desired value by moving the rheostat. The battery on-off switch is opened momentarily to stop the current flow: the calibrate switch is opened, and the ready switch is closed. Again the circuit is triggered by pressing the PBSW, and the initial current through the EED is equal to the pre-selected value of I_c. The switching of the resistor R_s into the circuit permits higher currents at a given rheostat setting.

The current I_c is read with Singer-Metrics* Sensitive Research ammeters, which have an accuracy of 0.5% of full scale. The variable resistor R_c is constructed from 45-mil diameter Alchrome-D** resistance wire having a resistance of 0.0134 ohm/cm, and is suspended along a meter stick graduated to the nearest one-tenth of a centimeter: adjustment of the value of R_c is made by varying the effective length of Alchrome-D being used. The CVR is also constructed of a length of Alchrome-D of the same diameter as above. Alchrome-D was specifically utilized for these resistances because of its very low temperature coefficient of resistance (±0.00002/°C). The resistor R_s and the rheostat are wire-wound power resistors rated at 100 watts and 300 watts, respectively. All of the circuit components are conveniently mounted on a 24 by 21 by 11-inch desk type rack and chassis with bolt-in panels. The cables to the EED extend into a steel reinforced firing chamber, in which the EED is evaluated.

Of particular importance is proper cooling of the SCR to maintain its junction within the specified operating temperature range. The SCR is constructed such that its anode terminal provides a heat transfer path from the junction to a copper fin, which serves as a heat sink and which is secured to the SCR by means of a stud on the anode. The size of the fin, as suggested by The Semiconductor Data Book,[2] is 6 inches square by 0.0625 inch thick.

The very fast rise time, viz. 20-30 μsec, after SCR turn-on is achieved by using low-inducatance cable throughout the entire circuit. Stresau and Hillyer[3] showed that flat cable wherein the two conductors are separated by a thin insulating material has an extremely low inductance. The flat cable utilized in the present work and diagrammed in Figure 2 consists of two soft copper strips separated by Teflon tape. These three components are held together by a tight wrapping of Scotch No. 33 electrical tape. Conduit to switches and resistors are constructed in the same manner to minimize inductive loops. Probably the only remaining inherent inductance is in the wire-wound power resistor and rheostat. Figure 3 presents several records showing the current rise and stability that is obtained; these traces were recorded on a Tektronix type 555 oscilloscope equipped with type L plug-in units. The steady state voltage drop across the

---

*The Singer Manufacturing Company, Metrics Division, Bridgeport, Connecticut.

**Wilbor B. Driver Company, Newark, New Jersey.

CVR is 0.66 v. and hence the steady state current is 15 amp. It is seen that in 20 μsec the current has risen to 95% of the steady state value. An identical rise time is obtained across the entire range of currents that can be produced by the circuit.

The above-described circuit has been utilized to evaluate the constant current no-fire and all-fire characteristics of the EED depicted in Figure 4. When bridged with a 5-mil diameter Evanohm* wire, this EED has a 5-amp, 5-watt no-fire capability. For a particular all-fire test for example, one of these EED's having a resistance of 0.21 ohm was loaded with 4.0 mg of an aluminum-tungstic oxide[4] flash charge at a loading pressure of 10 300 psi; the height of the pressed flash charge column was 0.205 inch, and its density was 3.01 g/cc. Figure 5 shows the oscilloscope record from the firing of this EED at the all-fire current of 15 amp. This record was obtained on a Tektronix type 555 oscilloscope in which three channels were obtained by chopping the upper beam with a type CA plug-in unit; the lower beam was equipped with a type L plug-in unit. The current and applied voltage portions of the record correspond to those measurements indicated in Figure 1. The overall function time, defined as the time from initial flow of current to emergence of the reaction wave at the end of the flash charge column, was recorded on the lower beam of the oscilloscope; this measurement was accomplished by means of an ion probe, the circuitry of which is shown in Figure 6.

A number of important pieces of information about the performance of the EED can be deduced from Figure 5. Initially, the applied voltage decreases and the current flow increases slightly, indicating that the bridge resistance is decreasing. Then at approximately 6.1 msec the applied voltage trace becomes erratic, and this represents the time at which the flash charge is ignited.* The overall function time is 9.4 msec. The difference between the overall function time and ignition time is the burning time of the flash charge, which for this EED is 3.3 msec. Since the column height of the flash charge was 0.205 inch, the average burning rate is 0.062 inch/msec. It is seen that in the first milliseconds after the flash charge has completely burned (the last milliseconds of the record) the current does not return to zero, but maintains a slight trickle through the burned-out EED at approximately 0.5 amp due to the deposit of metallic tungsten from the reduction of tungstic oxide by aluminum. The resistance of the expended EED during this period is about 70 ohms.

*Wilbur B. Driver Company, Newark, New Jersey.

*This result was verified in a series of experiments in which the height of the flash charge column was decreased from one test to the next. The burning time, defined as the difference between overall function time and the assumed ignition time, was a linear function of column height and extrapolated to zero burning time at zero column height.

but for some applications a post-firing resistance of a magnitude this low would not be acceptable; this problem can be solved by using a flash charge that does not produce metallic products.

The constant current firing circuit described in this paper has been utilized extensively not only for all-fire tests of the type described above but also for 5-amp no-fire tests of 15-minute duration. No flaws have been detected in the performance of this circuit. It is obvious that the range of currents obtainable can be extended in either direction by utilizing a lower or higher supply voltage, a rheostat of different resistance, or a SCR having a higher current rating.

The authors are indebted to Dr. Morton J. Klein, Mr. Charles K. Hersh, and Mr. Robert F. Remaly, whose cooperation and direction made this work possible.

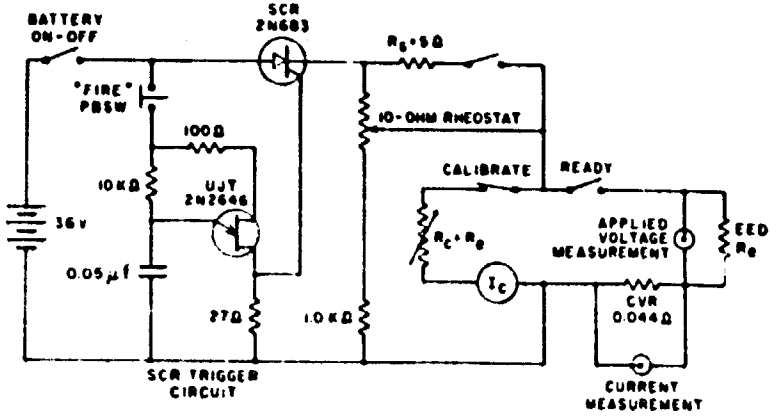

Figure 1

CONSTANT CURRENT FIRING CIRCUIT

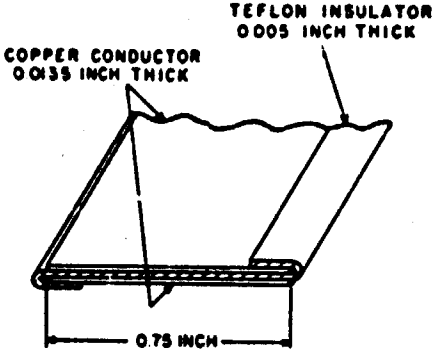

Figure 2

SCHEMATIC DRAWING OF FLAT CABLE UTILIZED IN CONSTANT CURRENT FIRING CIRCUIT OF FIGURE 1

References

1. F. W. Gutzwiller, Editor, General Electric Silicon Controlled Recitifier Manual, 4th Edition, 1967, pp. 70-78.

2. Motorola Semiconductor Data Book, 3rd Edition, 1968, p. 4-12.

3. R. H. Stresau and R. M. Hillyer, "Exploding Bridgewire Initiation of RDX with 50 Millijoules," Paper No. 5, Proceedings, Electric Initiator Symposium-1963, Picatinny Arsenal Report EIS-A2357.

4. J. L. Austing and R. F. Remaly, "Properties and Performance of Aluminum-Plated Pyrotechnics for Electroexplosive Device Applications," Paper No. III-6, This Symposium

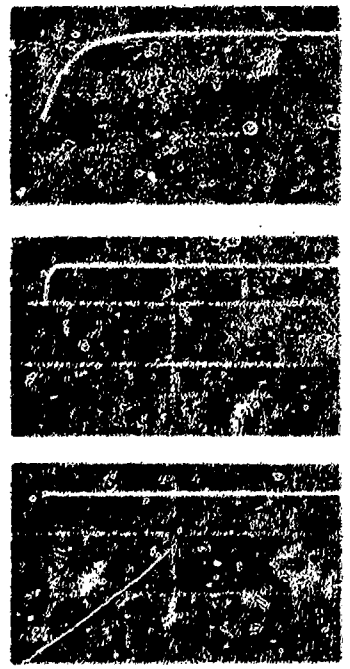

10.0 msec/cm

ZERO CURRENT BASE LINE

ZERO CURRENT BASE LINE

10.0 msec/cm

ZERO CURRENT BASE LINE

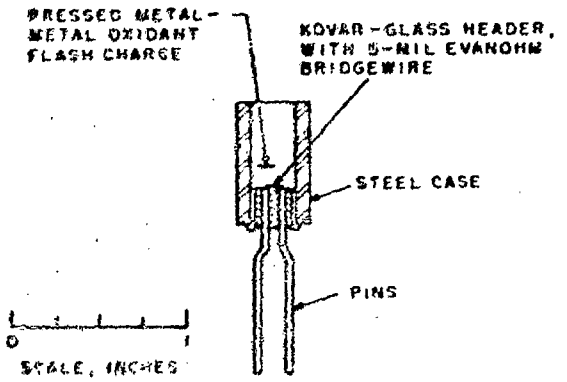

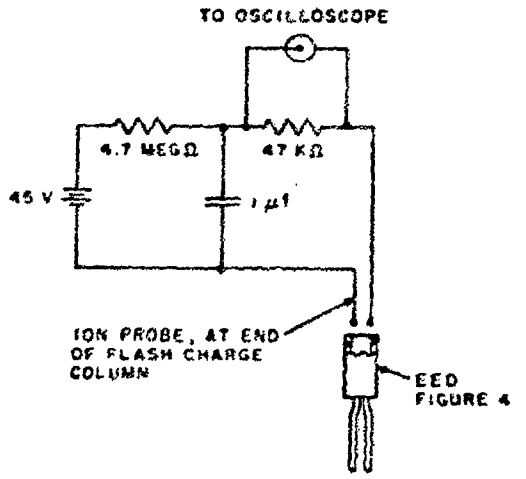

Figure 6

ION PROBE CIRCUITRY FOR MEASUREMENT OF OVERALL FUNCTION TIME OF EED

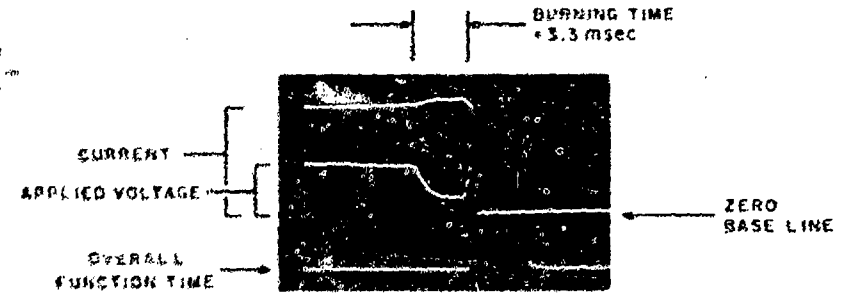

II-3. ACCELERATED LIFE TEST FOR AEROSPACE EXPLOSIVE COMPONENTS

Sidney A. Moses

Development Engineering
McDonnell Douglas Astronautics Company
Huntington Beach, California

ABSTRACT

The stability tests used for explosive materials are reviewed. Although these are satisfactory for bulk materials, they have serious limitations when applied to hermatically sealed explosive components.

A test method is proposed for predicting the expected shelf life or storage life of aerospace explosive components. In addition, the test may be used to extend the life of over-aged components. This method is based on a modification of the Arrhenius reaction rate equation.

The proposed method is compared with tests from typical military specifications which are sometimes used as a basis for predicting the shelf life of explosive cartridges.

INTRODUCTION

Degradation mechanisms for aerospace explosive components and suggested guidelines for designing these components to meet a 10-year shelf life requirement are categorized in Reference 1. One of these guidelines is to subject the components to an accelerated life test. An examination of the proposed accelerated life test is covered in greater detail herein.

An accelerated life test will serve the following purposes:

A. Identify those rare components which may quickly go bad in storage.

B. Prevent good components from being discarded at an excessive rate.

C. Reduce the unnecessary and expensive replacement of components in vehicles or missiles which must be in an "always ready" condition for long periods of time.

D. Provide, for components already in the field, a basis for extending the use of components beyond the shelf life date indicated at the time of manufacture.

E. Provide a firmer basis than the present "crystal ball" method for estimating the storage life.

STABILITY TESTS

Over the years, a number of stability tests (References 2, 3, and 4) have been developed for explosive materials. Without detailing, these tests include the following:

A. 75°C international test method.

B. 100°C heat test method.

C. 90°C, 100°C, and 120°C, vacuum stability tests.

D. Reactivity test (between explosives and other materials).

E. Heat test (120°C and 134.5°C).

F. Taliani test.

Of more recent origin are three testing methods which measure specific properties of the explosives. These include differential thermal analysis (DTA), thermal gravimetric analysis (TGA), and differential scanning calorimetry (DSC).

Although each of the above tests gives some indication of the stability of an explosive when subjected to a given temperature for a given period of time, no single test or combination of tests provides any real indication of the expected life of an explosive component. Following are a number of reasons for this.

A. Usually, the component contains not one, but a combination of materials all enclosed in a sealed container. Chemical reactions occurring under these conditions must take place at far different rates than in any of the tests outlined. This is especially true at elevated temperatures because of the increased pressure due to entrapped air or vapor pressure inside the sealed container. Preferably, for any accelerated life test, the component itself, rather than the individual materials, should be subjected to the test conditions.

B. Tests in which the rate of reactivity is measured (i.e., vacuum stability, Taliani, etc.) depend upon the formation of vapors from the heated materials. Ideally, for an accelerated life test, the reaction rate should be measured at a temperature which increases the reactivity of the chemical molecules without resulting in a change in state of the materials involved. Preferably, the test temperature should be less than any temperature at which exothermic or endothermic reactions occur (as measured by DTA, TGA, or DSC tests of the reactive materials).

C. Although many of the tests mentioned measure the amount of vapor given off from the materials, no attempt is made to determine the extent to which the explosive output is affected by this loss. Preferably, following the heating cycles, the components should be tested to give some measurement of the explosive output. Of course, this should be checked against some baseline measurement obtained from control samples. With the accelerated life test proposed in this paper, the above deficiencies are remedied as follows:

1. After preliminary tests of the various explosive materials, the components are subjected to the test conditions.

2. The maximum test temperature is less than that at which any exothermic or endothermic reactions occur.

3. Following exposure to the test temperature, the components are initiated and the output is compared with previous data.

TEST ASSUMPTIONS

The procedure outlined in the following paragraphs may be used to estimate the shelf life of explosive components. This test is based on an Arrhenius type reaction rate equation which is applicable for many chemical reactions.* With this equation, when the log of the reaction rate is plotted against the reciprocal of the absolute temperature the points fall on a straight line. The assumption is made that heating the components to a high temperature for a relatively short period of time is equivalent to storing them for a much longer time at a lower temperature. Likewise, it is assumed that if no degradation occurs during the high temperature, short exposure defined by the test, none will occur during a longer exposure period at a lower storage temperature.

---

*The Arrhenius equation usually takes one of two forms:

(1) $\log k = a - \frac{b}{T}$ where k is the reaction rate for a given absolute temperature (T) and a and b are constants.

(2) $k = Ae^{-E/RT}$ where A and E are constants; called the "frequency factor" and "energy of activation," respectively, and R is the gas constant.

Further, an assumption is made that the reaction rate increases by a factor of between 2 and 3 for each 10°C (18°F) rise in temperature. This is in line with experimental results for many chemical reactions. Stated in another way, this assumption indicates that the reaction time will double or triple with each 10°C drop in temperature. These factors are given for a general case in which the reaction rates are unknown. The actual rates, when known, may be substituted in the equations used in later paragraphs.

PRELIMINARY COMPONENT DATA REQUIREMENTS

Before performing this test, it is necessary to obtain statistical information on the performance characteristics of the components to be tested. With squibs, pressure cartridges, etc., this may include pressure-time and functioning time data. With high explosive devices, typical performance characteristics include detonation velocity (for detonating fuse), dent test data, or ballistic pendulum tests along with functioning time, if applicable. In addition, the leak rate of the sealed components should be determined using standard helium leak detector methods.

The performance data will be used as a baseline for comparative purposes following the accelerated shelf life test. For components that have been in storage for a considerable period of time, this information provides a reference point to determine if the life can be further extended.

TEST PURPOSES

This test may be used to estimate the useful life of explosive components for typical storage conditions (up to 10 years) when the components are to be stored in magazines or storage bunkers at an average temperature of between 70° and 90°F. These are the usual conditions for storage in temperate climates (Reference 6).

In addition, a modification of this test may be used to extend the life of components which are approaching the discard date.

TEST DESCRIPTION

The test method consists of subjecting sample components to different temperature versus time conditions. Following each conditioning period, the materials in some components are examined while the remaining components are fired. The results of these firing tests are compared with data previously collected on the components. A minimum of 13 components are recommended for each condition, 3 for examination and 10 for the firing tests.

The test conditions include:

A. A 24-hour constant temperature condition to provide a quick look to check for possible incompatibilities.

B. A 28-day temperature cycling test with high humidity to check the integrity of the environmental seal, an important factor for an extended shelf life.*

C. A 28-day constant temperature condition to extend the exposure period and establish confidence for meeting the required shelf life.

The highest temperature (for the 24-hour test) is selected by pretesting the individual explosive materials. A DTA or similar test is performed on each of these materials to provide information on the temperatures at which exothermic or endothermic reactions occur in the various materials.

The temperature for the 24-hour test should be less than that of the lowest temperature at which a reaction occurs as determined by the DTA tests. Until more information is gained, it is recommended that this temperature be between 160° and 250°F but at least 50°F below the lowest temperature at which a reaccion occurs with any of the explosive material involved. For example, with PETN which has a melting endotherm at 293°F, a temperature of 230°F is

*This period was selected to be compatible with other 28-day tests such as the temperature - humidity test specified in Reference 5.

recommended for the 24-hour test. It is desirable that this 24-hour test temperature be the maximum possible that will not result in a change of state of the materials involved.

One of the major assumptions concerning the accelerated life test is that the reaction time will double or triple with each 10°C drop in temperature. These limits are plotted on Figure 1 (solid lines). Starting from the 24-hour, 160°F point, these limits intersect the 70°F line at 768 and 5,832 hours (or less than one year). That is, applying the assumption, components exposed to a 24-hour, 160°F test without degradation, could only be guaranteed for the time indicated.

As the 24-hour test temperature is raised, the intersects on the 70°F line are increased. For example, if the temperature is 250°F, the limits are from 24,600 hours to over 10 years.* It is emphasized that a 24-hour test gives no more than a crude estimate of the expected life.

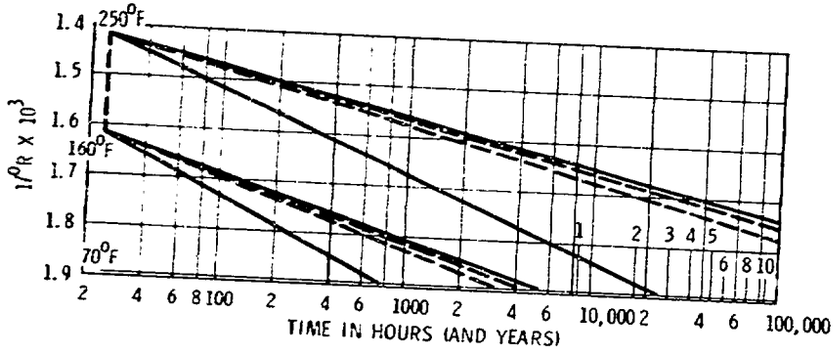

Figure 1. Effects of Test Temperatures and Reaction Rates

*It appears prudent to place an upper limit of 10 years on the life test described.

Actually, the limits indicated are far too broad to be of much value. A more reasonable approach is to make the assumption that the reaction time increases by a factor of between 3.00 and 3.25 for every 20°F decrease in temperature.* This is still conservative when compared with the known reaction rates of explosive materials. For example, the rate of decomposition of nitrocellulose increases 3.7 times for each 10°C rise in temperature according to Reference 7. Converting to Fahrenheit and restating, the reaction time increases by a factor of 4.1 for every 20°F decrease in temperature.

The 3.00 to 3.25 reaction rate limits are also plotted on Figure 1 (dotted lines). They intersect the 70°F line in a much tighter band within the previous limits. These intercept values may be determined from the formulas:

$$H_L = H_T\ 3.0^{\left(\frac{T_1-T_2}{20}\right)} \text{ and } H_U = H_T\ 3.25^{\left(\frac{T_1-T_2}{20}\right)}$$

where

H_L and H_U = the lower and upper points of intercept (hours)

H_T = the test time (hours)

T_1 = the test temperature (°F)

T_2 = the temperature of interest or average storage temperature (°F)

The major value of the 24-hour test is that it will provide a quick look at the components to determine possible incompatibilities between materials that may result in degraded performance. If incompatibilities occur, changes can be made before proceeding with the more time consuming 28-day tests.

*This represents a factor of between 2.7 and 2.9 for every 10°C temperature change.

Following exposure to each of the temperature time conditions indicated, the sample components are allowed to cool to ambient laboratory temperatures. All sealed components are checked for leaks with a helium leak tester. A portion of the sample components are opened and examined for possible degradation while others are subjected to performance tests. The results of these tests are then compared with previous tests of components which were not subjected to the accelerated storage tests.

TEMPERATURE – CYCLING TEST

During storage, moisture leaking through defective seals may be drawn into the components because of temperature changes. This moisture may seriously affect the useful storage life. To test the seal, a second set of components (again, a minimum of 13) is subjected to a modified 28-day test. For this, the temperature of the test chamber should be decreased or increased at 20-minute intervals to cycle the components between 50° and 90°F. A high relative humidity (90 percent or greater) should be maintained. This represents the cyclic temperature changes between nighttime cooling and daytime heating for a 10-year period. During this test, the hermetic seals are subjected to a series of cyclic pressure changes because of the changing temperatures. Following this test, the components are checked for leaks and subjected to performance tests.

28-DAY TEST

A third set of components are subjected to a constant-temperature 28-day test at an elevated temperature. Using the same formulas mentioned previously, intercepts are drawn from the 28-day temperature point to the storage temperature of interest. The intercept representing the shorter life span may be considered a high confidence limit (i.e., 90 percent) while that representing the longer life span may be considered a lower confidence limit (i.e., 80 percent). The region to the left and below the 90 percent confidence intercept may approach a 95 percent confidence level. Although these confidence values have no statistical significance, they do suggest that, as the storage life is extended over longer and longer periods, less reliance should be placed on the results of any accelerated test.

Values have been calculated for several 28-day temperature points for 70° and 90°F average storage temperatures as indicated in Table 1. Figure 2 shows these limits for three sets of temperature-time conditions.

Table 1

ESTIMATED LIFE AS RELATED TO 28-DAY TEST TEMPERATURE

28-Day Test Temperature	70°F Avg Storage Temp		90°F Avg Storage Temp	
	90%C	80%C	90%C	80%C
130°F	18,100 (2 to 3 years)	22,800 (Hr)	6,050 (less than 1 year)	7,100 (Hr)
140°F	31,600 (4 to 5 years)	41,600	11,300 (1 to 1-1/2 years)	12,800
150°F	54,400 (6 to 9 years)	75,300	18,100 (2 to 3 years)	22,800
160°F	94,000 (over 10 years)	134,000	31,600 (4 to 5 years)	41,600
170°F	163,000 (over 10 years)	242,000	54,400 (6 to 9 years)	75,000

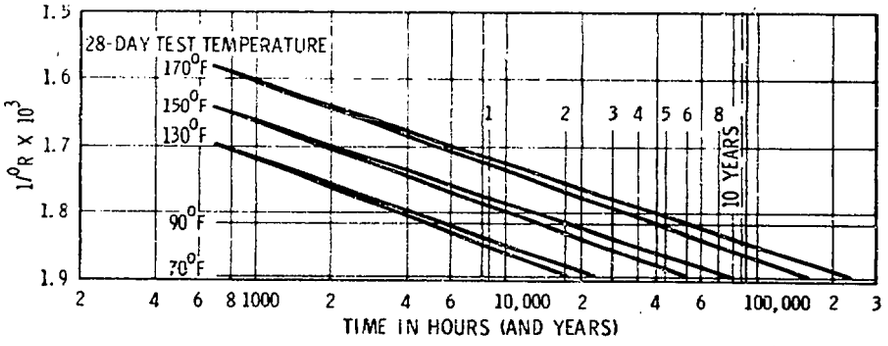

Figure 2. Estimated Life Based on 28-Day Test Temperature

COURSES OF ACTION FOLLOWING FAILURE

If any material degradation is noted, or if the test results indicate any change in performance, three courses of action are open (1) other materials may be substituted for those affected by the tests,* (2) the shelf life requirements may be lowered and the tests repeated at different temperature conditions, or (3) the components may be considered limited life items and subjected to periodic surveillance-type tests. On the other hand, if no degradation is found after 28 days, the expected useful life may be set with reasonable confidence.

TEST LIMITATIONS

This test is applicable to aerospace explosive components. Generally speaking, these may contain one or more explosives in the form of loose powder, pressed pellets or, on occasion, machined, cast, or extruded propellants. In rare cases, this propellant may be inhibited on one or more faces. For these inhibited grains, the bond strength between the propellant and inhibiting material may be affected adversely by the temperature conditioning proposed by these accelerated tests, and the test program outlined will not give a valid estimate of the expected life of the component. It is recommended that additional preliminary tests be performed to investigate the bond strength at elevated temperatures before subjecting components to the accelerated test program.

COMPARISON WITH OTHER TESTS

The concept of using high temperature and temperature-humidity tests to predict the life of explosive components is not new. However, former methods of utilizing these tests to determine the shelf life appear to be completely arbitrary.

A discussion of the accelerated life tests used by the military and a comparison of the proposed test follows. Data concerning the use of these older tests were gathered, in part, from various individuals during visits to military facilities. In addition to the tests to be described, both the Army and Navy depend upon large scale surveillance programs to further verify the life of components. Such surveillance is possible because of the extremely large quantities of components available; and it is necessary because of the widely varying conditions experienced during worldwide storage, or with actual installation in aircraft.

Frankford Arsenal indicates that newer cartridge actuated devices (CAD) for use with pilot escape systems have an indeterminately long shelf life. After installation in the aircraft, the CAD have an assigned service life of three years, although this is known to be conservative.

During design evaluation, cartridges are subjected to the various environmental tests specified in Reference 8. Included within the requirements of Reference 8 are a high temperature storage test (200°F for 50 hours) and a temperature cycling, humidity test in which the cartridges are exposed to cyclic periods at high humidity including exposure to 200°F for a period of 60 hours. These tests are usually rigorous as CAD are exposed to severe conditions after installation in the aircraft.

Using the formulas discussed previously, and with H_T = 60 hours and T_1 = 200°F the shelf life at 70°F may be calculated to be between 8.8 and 14.8 years. These limits appear compatible with the indeterminately long storage life indicated by Frankford Arsenal.

Cartridge actuated devices for Navy aircraft must meet the requirements of Reference 9.

After compliance with the specification requirements, the cartridges are deemed satisfactory for 2-1/2 years in storage plus an additional 2-1/2 years installed in the aircraft. Again, it is admitted that this is conservative and is partially an arbitrary decision based on a 30-month aircraft rework cycle.

*If degradation is noted, it is necessary to determine which material (or materials) are responsible. This will require a series of compatibility tests with materials from one of the standard methods previously mentioned.

The specification contains both humidity and high temperature storage tests. The former exposes the components to temperature cycling with 416 hours at 160°F while in the latter, the components are conditioned at 160°F for up to 24 days (576 hours).

Again, using the formulas given earlier, with t_T = 576 hours and T_1 = 160°F, the shelf life limits are calculated to be between 9.3 and 13.2 years at 70°F. Of course, once the cartridges are installed in aircraft, the average temperature may exceed the 70°F value, and the actual life should be based on both conditions.

Another accelerated aging procedure used by the Navy, referred to as a compressed-ambient cycle (Reference 10), is a 6 month storage test which is said to be roughly equivalent to 1 year of magazine storage.

For this test, components are held at 70°F for three weeks (representing the average spring temperature), 16 weeks at 100°F (summer), 3 weeks at 70°F (fall), and finally, 4 weeks at 40°F (winter). Notice that the compressed-ambient cycle does not test the component seal. However, using the 100°F, 4 week value is inserted into the formulas previously given the calculated shelf life at 70°F is between 1.6 and 1.8 years.

The examples presented indicate that the accelerated life test described in this paper is compatible with other tests now used by the military.

EXTENDING THE LIFE OF OVERAGED COMPONENTS

Apparently, there is no standard method for extending the life of over-aged components at the present time. Units returned from the field may be extensively tested and analyzed. At one military facility, cartridge actuated devices may require (1) visual inspection, (2) leak tests, (3) X-ray, (4) ballistic tests, (5) chemical analysis, if indicated by the results of the ballistic tests, and (6) statistical analysis of the ballistic tests.

The results of the ballistic tests are plotted and if a significant change is found, a projected time is calculated at which the cartridges will exceed the specification requirements (References 11 and 12). Unfortunately, no extension can be calculated until a change is noted, and at that time degradation has already affected the output.

A more reasonable approach would be to accelerate the degradation by a series of 28-day, constant temperature tests (i.e., 130°, 140°, and 150°F). Following ballistic tests, the projected life could be calculated with this extension based upon the highest temperature at which no degradation is noted.

Late in this study, it was learned that Picatinny Arsenal is using a somewhat similar technique to predict the safe life of propellants (Reference 13). For this work, it was found that the measurement of the residual stabilizer content of propellants offered the best means for establishing the stability potential of these materials.

The propellants are artificially aged at 10°C intervals between 60° and 90°C (for double-base) or between 60° and 100°C for single and triple-base materials. The percentage of stabilizer remaining after specific time intervals is then determined. Berthelot's law of deterioration phenomena is used to develop curves reflecting the variation of the rate of reaction with temperature.* The curves are then extrapolated to lower storage temperatures (and longer periods of storage).

Berthelot's and Arrhenius' laws are compared below.

	Formula	*Representation*	
		K	T
Berthelot:	*Log* $K = aT-b$	*Log scale*	*Linear scale*
Arrhenius:	*Log* $K = a-\frac{b}{T}$	*Log scale*	1/T, *Linear Scale*

In plotting the two, it is found that Berthelot is the more conservative. Reference 12 indicates that, "since it is not possible to determine exactly which of the two equations is more appropriate to describe the deterioration of propellants, the choice is left to the discretion of the investigator."

Good correlation has been obtained between the percentage of stabilizer predicted by these tests and the percentages remaining in four different propellants actually aged for periods as long as 33 years.

ADDITIONAL COMMENTS

The test method described in this paper was developed as the result of a Skills Retention Study supported by the McDonnell Douglas Astronautics Company. The method is expected to be included in component specifications at an early date.

REFERENCES

1. S. A. Moses. Long-Life Aerospace Explosive Components. McDonnell Douglas Astronautics Company Paper WD-1658, July 1971.

2. MIL-STD-286. Solid Propellants; Sampling, Inspection and Testing.

3. MIL-STD-650. Explosives, Sampling, Inspection and Testing.

4. MIL-STD-1234. Pyrotechnics; Sampling, Inspection and Testing.

5. MIL-STD-331. Fuze and Fuze Components, Environmental and Performance Tests for.

6. The Weather Handbook. Conway Publications, Inc., Atlanta, Ga.

7. Military Explosives. Department of the Army and the Air Force, TM9-1910, TO 11A-1-34, April 1955.

8. MIL-C-25918. Cartridge Actuated Devices, Aircraft Crew Emergency Escape, General Specification for.

9. MIL-D-21625. Design and Evaluation of Cartridges for Cartridge Actuated Devices.

10. Ordnance-Life Predictions. A Pamphlet of the Naval Ordnance Station, Indian Head, Maryland, July 1969.

11. Surveillance of Propellant Actuated Devices; M3A1 Initiator, Final Report. Frankford Arsenal, April 1969.

12. Statistical Treatments of Data for CAD/PAD Under the Air Force Surveillance Program. OREP-3000-1-68, Frankford Arsenal, November 1968.

13. J. P. Picard and N. S. Garman. Prediction of Safe Life of Propellants. Picatinny Arsenal, Dover, N. J., October 1969.

II-4. RESPONSE OF ELECTROEXPLOSIVE DEVICES TO IMPULSIVE WAVEFORMS*

L. A. Rosenthal**
Consultant to
Jet Propulsion Laboratory

V. J. Menichelli
California Institute of Technology
Jet Propulsion Laboratory
Pasadena, California 91103

ABSTRACT

The firing characteristics of insensitive electroexplosive devices to certain impulsive waveforms have been investigated. For these waveforms, energy is delivered in a time short compared to the thermal time constant and therefore cooling plays a negligible role. One waveform is a terminated capacitor discharge wherein the regular discharge of a capacitor is terminated at a preset point. Another is a half-sine wave pulse.

The theory, design, and application of both impulsive waveform generators are presented together with certain limited experimental observations.

*This paper presents the results of one phase of research carried out at the Jet Propulsion Laboratory, California Institute of Technology, under Contract No. NAS 7-100, sponsored by the National Aeronautics and Space Administration.

**Also Department of Electrical Engineering, Rutgers University, New Brunswick, New Jersey 08903.

INTRODUCTION

In impulsive firing of an electroexplosive device the energy is delivered in a time short compared to the thermal time constant. The firing current or voltage is delivered to the device bridgewire which heats in an adiabatic manner insensitive to the time dependent heat diffusion to the explosive mix and EED mechanical structure. As opposed to constant current firing wherein the thermal resistance between the bridgewire and EED enclosure determines the sensitivity, impulsive firing is primarly responsive to the bridgewire-explosive interface. The bridgewire and the immediate environment can be considered a lumped heat capacity (C_p) and the input energy results in a proportional temperature rise (θ) above ambient. This bridgewire-explosive interface is perhaps oversimplified by a lumped analysis treatment but the model proves meaningful for the normal fixed design system. It is the abnormal unit which violates this simple model and requires more detailed inspection. Impulsive firing based on the discharge of an energy storage capacitor is in practice a preferred mode of firing. Testing and specification based on the transfer of the stored capacitor energy ($CV^2/2$) via a high quality switch to an EED has been an accepted procedure. Ignoring switch and energy tranfer losses mollifies this classical testing procedure. When testing insensitive devices (i.e., 1 watt-1 amp), the higher currents and their time derivatives, and in general the higher energies switched, require a closer look at the test efficiency. Two impulsive waveforms and their application to insensitive EED testing are presented.

One system is based on the classical capacitor discharge technique with the additional capability of terminating the discharge at any preset time interval. Solid state switches and electrolytic capacitors as practical components are employed. A second system based on the generation of a half-sine wave firing current pulse provides an alternate technique.

The theory, apparatus, and experimental application of these two systems will be presented.

THEORETICAL CONSIDERATIONS

The energy delivered by an impulsive current, i(t), or voltage, v(t), waveform can be calculated based on a lumped electrothermal model for an EED (ref. 1). Practically the voltage across the device is observed, but the current through the device is of equal utility. The assumption that v(t) or i(t) are only time dependent ignores the reaction of the temperature sensitive EED on these waveforms due to impedance reflection to the generator.

Temperature rise (θ) and instantaneous power input are related according to

$$C_p \, d\theta/dt = v^2(t)/R_\theta \quad \text{or} \tag{1}$$

$$C_p \, d\theta/dt = i^2(t) \, R_\theta \tag{2}$$

The temperature coefficient of resistivity (TCR or α) of the bridgewire controls the temperature dependence of the bridgewire (R_θ) according to

$$R_\theta = R_o (1+\alpha\theta) \tag{3}$$

where R_o is the cold or initial resistance and θ is the temperature rise. With no thermal feedback $R_\theta = R_o$ a constant. Equations (1) and (2) become respectively when solved

$$\theta_m = \int_o^{t_w} v(t)^2 \, dt/C_p R_o \tag{1a}$$

and

$$\theta_m = R_o \int_o^{t_w} i(t)^2 \, dt/C_p \tag{2a}$$

In these equations θ_m is the temperature rise achieved at a time t_w, the termination of the pulse waveform. A basic or intrinsic energy (E_o) can be defined as

$$E_o = \int_o^{t_w} v^2(t) \, dt/R_o \quad \text{or} \tag{4}$$

$$E_o = R_o \int_o^{t_w} i^2(t) \, dt \tag{4a}$$

depending on the voltage or current waveform. This energy can be calculated from the observed waveform by analytically or graphically computing the integral of the square similar to an action integral.

It is meaningful to consider the effects of thermal feedback. With positive TCR bridgewires the resistance increases during the heating pulse. If the current waveform is observed, the actual energy delivered will be greater than E_o and if the voltage waveform is monitored, the true E_o will be less. For example solving equation (1) and with the appropriate expansion and approximation the maximum temperature is

$$\theta_m (1+\alpha\theta_m/2) = E_o/C_p \quad \text{or} \tag{5}$$

$$\theta_m = \frac{E_o}{C_p} \left[1 - \frac{1}{2} \frac{E_o \alpha}{C_p} \cdots \right] \tag{5a}$$

Since E_o/C_p is a temperature rise, a rough estimation of 500°C will establish the error involved. With a Tophet A bridgewire material α is 100×10^{-6}/°C and the second term shows that the temperature maximum is down by 2.5%. Without feedback the temperature rise from equations (1) and (2) would be E_o/C_p. Showing that the temperature rise in equation (5) is low by 2.5% is equivalent to saying that energy delivered according to a voltage observation would be low by 2.5%.

When a current waveform is observed equation (2) can be solved as

$$\ln (1 - \alpha \theta_m) = \alpha E_o/C_p \quad \text{or} \tag{6}$$

$$\alpha \theta_m = \exp (\alpha E_o/C_p) - 1 \tag{6a}$$

Since $\alpha E_o/C_p$ is a small quantity (i.e., 0.05), as in the previous example, an expansion and simplification results in

$$\theta_m = \frac{E_o}{C_p} \left[1 + \frac{E_o \alpha}{2C_p} \cdots \right] \tag{6b}$$

Now the temperature is higher due to thermal feedback by the same 2.5% for the figures cited previously. Measuring current will result in true energies delivered being higher than E_o.

Based on the above thermal feedback error calculations it appears wise to ignore such corrections and consider the simple energy E_o based on the cold resistance R_o and the integral of the waveform squared and related to the temperature maximum according to

$$\theta_m = E_o/C_p \tag{7}$$

Intrinsic energy calculations can be made for the terminated capacitor discharge and the half-sine wave pulse. Figure 1(a) shows a typical terminated capacitor waveform for several pulse widths. The termination time (t_w) is continuously adjustable and several traces are superimposed. Figure 2(b) is a half-sine waveform corresponding to a nominal current of 30 amperes peak at a width of 80 microseconds. Amplitude is continuously adjustable in this case at a predetermined pulse width.

For the terminated capacitor discharge waveform the initial current I_o, the final or termination current I_1, and pulse width t_w, can be obtained from an oscilloscope display. Although the discharge is an exponential with time constant τ, it will appear as a linear decay if t_w is small compared to τ. It can be shown that the energy transferred is

$$E_o = \left[\frac{I_o^2 - I_1^2}{\ln(I_o/I_1)} \right] \frac{R_\theta t_w}{2} \tag{8}$$

When the decay is linear, a simplified form results according to

$$E_o = I_o I_1 R_o t_w \tag{9}$$

In the case of the half-sine wave pulse, the maximum current I_m and the pulse width are observed from an oscilloscope display. The energy transferred can be shown to be

$$E_o = I_m^2 R_o t_w/2 \tag{10}$$

based on a reasonable circuit "Q" of 5 or more. This lower limit of "Q" insures a good symmetrical waveform.

APPARATUS

The apparatus employed to generate the required pulse waveforms will be superficially reviewed.

Figure 2 is the terminated capacitor discharge apparatus (ref. 2). The capacitor, voltage level, and discharge thyristor T_1 are similar to those

employed in a spacecraft firing system (ref. 3). The EED is in series with a ballast resistor of 1 ohm thus limiting the current to a maximum of 20 amperes (for a 1 ohm EED). Upon firing T_1, the voltage at the cathode of T_1 activates a constant current charging device (FET circuit T_2) for capacitor C_2. At a preset voltage across C_2, unijunction T_3 fires thyristor T4. The firing of T4, diverts the capacitor discharge from the EED and terminates the energy transfer. Timing is independent of the voltage level at the EED and controlled entirely by the resistor R3 in the range of 100 to 1300 microseconds. By increasing the ballast resistor, it is possible to preset the discharge current (I_o) to lower levels and other parameter variations are obvious. As shown in figure 1(a) there is a small time delay in the firing of T1 which conveniently provides a complete picture of the discharge. The termination is sufficiently rapid since energy follows the square of the current or voltage. The circuit loop inductance and resistance associated with T4 should be kept at a minimum.

Although the capacitor discharge waveform is basically impulsive in nature, there is an advantage in an adjustable termination. Most of the energy is delivered during the initial portion (i.e., in one time constant 86.5% of the capacitor stored energy is delivered) and the exponential tail is of trivial value. Pulse width control is a convenient parameter for firing sensitivity measurements. By abruptly terminating the energy, the growth of explosive reaction can be sensed at some time later in the cycle by bridgewire rupture or explosive output. By injecting a small positive current from an inductive loop circuit into the EED, bridgewire rupture can be observed as an inductive "kick" after the energy pulse has terminated.

Figure 3 is a circuit diagram of the half-sine wave pulser apparatus (ref. 4). With thyristor T1 off, the capacitor C, in series with inductor L, is charged to the preset but adjustable power supply voltage V (350 volts maximum). Upon firing T1, a half-sine wave current discharge is supplied to the EED in the cathode circuit of T1 (ref. 5). The pulse terminates itself due to the self commutation of the thyristor during the onset of the reversed swing of the second half cycle. Pulse width is preset according to

$$t_w = \pi \sqrt{LC} \tag{11}$$

and as a scaling factor, the peak current is

$$I_m = \frac{V}{\sqrt{L/C}} e^{-\pi/4Q} \tag{12}$$

where the circuit Q is $\sqrt{L/C}\ /R$ and R is the total discharge loop resistance. Conveniently the energy transferred follows the square of the voltage. For the L-C combination shown, the pulse width was 178 microseconds and at 300 volts (V) it is possible to deliver 50 millijoules to a one ohm device at a peak current (I_m) of 24 amperes. Decreasing L to obtain a narrow-pulse will result in higher peak currents and 125 amperes at 25 microseconds was provided for one series of tests. It can be shown that the energy delivered to the total load in this half-sine wave pulse circuit is

$$E_o = \frac{1}{2} CV^2 \left[1 - e^{-\pi/Q}\right] \tag{13}$$

Only a fraction of the energy stored on the capacitor (i.e., $1/2\ CV^2$) is delivered to the total circuit resistance. A high Q system produces the best waveform with the poorest energy transfer.

In comparing the two circuits described, they are equally capable of evaluating the impulsive firing behavior of EED's. The capacitor discharge circuit is more responsive to variations in the EED resistance and circuit resistance losses in the manner of a constant voltage driving source. The fast rise and fall times can be degraded by leads associated with the firing

chamber. The half-sine wave pulse has a controlled rise and fall time and is basically a constant current drive of internal impedance $\sqrt{L/C}$. Firing chamber leads providing resistance and inductance will not significantly disturb the current waveform. The latter circuit appears to offer the greatest convenience and versatility.

EXPERIMENTAL OBSERVATIONS

Some limited testing results will indicate the use of impulsive waveform testing. A basic application is in establishing the firing energy for various EED systems. For the insensitive items tested, the energy delivered is increased in small increments until firing takes place. It was previously established that as many as 30 prepulses at subfiring energy levels had negligible effect on the final observed firing energy. This may not be true for sensitive devices, or other explosive systems in which case Bruceton type testing procedures may be necessary. For items operating in the adiabatic mode the data should conform to

$$\theta_m = E_o/C_p \qquad (7)$$

Based on the explosive material, the item mechanical design, and simplified initiation concepts it would appear that the product $\theta_m C_p$ is a constant for a given EED. The data shown in figure 4 tabulates test results for the terminated capacitor discharge apparatus. Two different items were tested with nominal firing energies of 31 and 22 millijoules. Although the energy delivery rate varies over a range of 2.4 to 1 the firing energy E_o is constant.

Another way of presenting individual item data is shown as the plot of figure 5, again based on equation (7). The value of $I^2 t_w R$ should be a constant if the waveform is constant. In this case the half-sine wave pulse was employed and these preset pulse widths were chosen as 175, 110, and 75 seconds. Firing currents went from 1.7 to 2.6 amperes (I_m). An average firing energy based on 10 samples was 28.4 mj and this point is superimposed on the plot for comparison.

It was also observed through impulsive firing that bridgewire rupture is related to functioning time and occurs some time after the true firing energy has been delivered. Figure 1(b) shows the wire opening as a vestigial pulse after the half-sine wave energy has terminated. In cases of primary explosive mixes, the reaction rate can be sufficiently rapid to rupture the bridgewire during the energy transfer period.

As a conclusion it appears that the impulsive waveforms can provide an excellent evaluation and study mechanism and the described systems will provide the essential reliability, convenience, and interpretation.

REFERENCES

1. Rosenthal, L. A. "Electrothermal Measurements of Bridgewires Used in Electroexplosive Devices", IEEE Trans. Vol IM-12, June 1963.
2. Rosenthal, L. A. and Menichelli, V. J., "Terminated Capacitor Discharge Firing of Electroexplosive Devices", NASA Tech Report 32-1521, Feb. 15, 1971.
3. Earnest, J. E. Jr and Murphy, A. J., "Firing Squibs by Low Voltage Capacitor Discharge for Spacecraft Application", NASA Tech. Report 32-1230, Oct. 15, 1968.
4. Rosenthal, L. A., and Menichelli, V. J., "Half-Sine Wave Pulse Firing of Electroexplosive Devices", NASA Tech. Report 32-1534, July 15, 1971
5. Rosenthal, L. A., "Half-Sine Wave Generator using Shock-Excited Resonant Circuit Discharging through a Thyratron", U.S. Patent 3, 3,119,068 (issued to the U.S. Navy). U.S. Department of Commerce, Washington, D.C., Jan. 1, 1964.

Figure 1 a. The Terminated Capacitor Discharge Waveform For Several Pulse Widths is Shown.

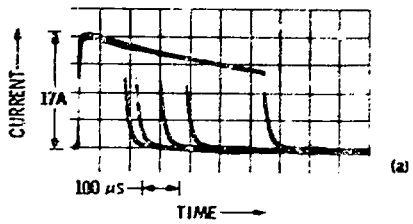

b. A Typical Half-Sine Wave Pulse is Shown With the Bridgewire burnout Appearing as a Secondary Pulse After Energy Delivery has Terminated.

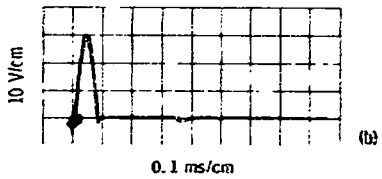

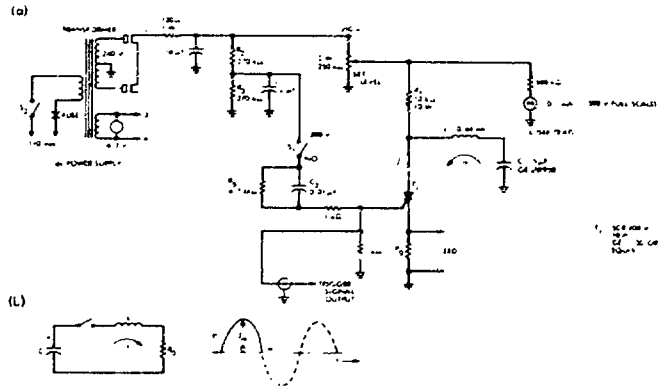

Figure 3 a. A Complete Circuit Diagram of the Half-Sine Wave Pulser is Shown. T1 is the Discharge Thyristor and the Energy Storage Component is the Capacitor C.

b. The Equivalent Discharge Loop for the First Half Cycle is Shown.

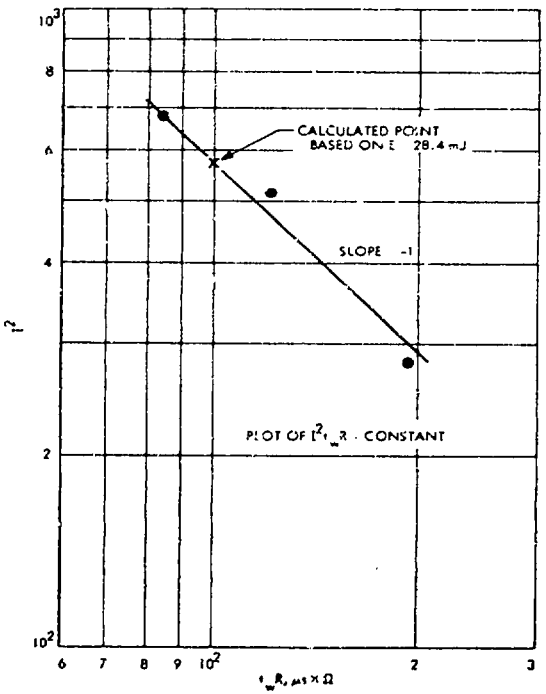

Figure 5. Energy for the Half-Sine Wave Firing Apparatus Can Be Presented for a Particular EED Design as the Plot Shown.

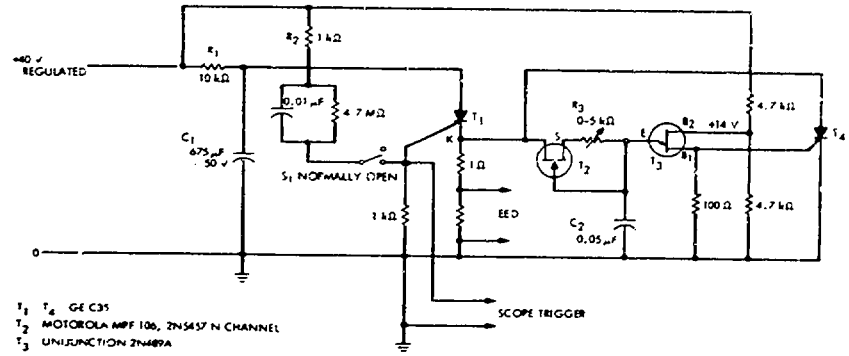

Figure 2. A Complete Circuit Diagram of the Terminated Capacitor Discharge Apparatus is Shown. T1 is the Discharge Thyristor and T4 is the Termination or by-Pass Device.

Group (samples)	I_f level, A	t_w, μs	W energy to fire, mJ
A-3	15.5	160	31.4
B-2	11.0	320	31.7
C-3	6.5	1050	31.6
D-1	12.4	155	23.5
E-1	18.5	74	23.0
F-1	8.2	400	31.7

Figure 4. A Tabulation of Firing Energies for Several Currents in the Terminated Capacitor Discharge Apparatus Characterizes Two Groups of EED's.

II-5. INTERRELATIONSHIP OF NONDESTRUCTIVE TESTING TO FAULT DETERMINATION*

Vincent J. Menichelli
California Institute of Technology
Jet Propulsion Laboratory
Pasadena, California 91103

Louis A. Rosenthal**
Consultant to
Jet Propulsion Laboratory

ABSTRACT

Several nondestructive test techniques have been developed for electroexplosive devices. The bridgewire will respond, when pulsed with a safe level current, by generating a characteristic heating curve. The response is indicative of the electrothermal behavior of the bridgewire-explosive interface. Bridgewires which deviate from the characteristic heating curve have been dissected and examined to determine the cause for the abnormality. Deliberate faults have been fabricated into squibs. The relationship of the specific abnormality and the fault associated with it are discussed.

*This paper presents the results of one phase of research carried out at the Jet Propulsion Laboratory, California Institute of Technology, under Contract No. NAS 7-100, sponsored by the National Aeronautics and Space Administration.

**Also Department of Electrical Engineering, Rutgers University, New Brunswick, New Jersey 08903.

INTRODUCTION

The evaluation of the reliability, quality, and behavior of an electroexplosive device (EED) is a formidable problem. Statistical methods, which require destruction of the EED, have been applied with some success. For example, predictions can be made as to the number and type of failure which can be expected to occur within a given lot of EED's. However, these methods do not predict which specific unit will fail or the failure mode. Although statistical methods are acceptable for some applications they practically do not meet the high reliability needs of the space industry. Special requirements of the space industry necessitate more detailed knowledge of the quality of each EED to be used. Failure of an EED during a space mission can result in partial or complete loss of the mission and perhaps life. Some space missions (i.e., Mars exploration) can last from six months to a year. Future space missions (i.e., the Grand Tour) can last as long as ten years during which time EED's will be called upon to function. To demonstrate by statistical methods the high reliability needed of EED's for these type space missions would require the firing of large quantities of EED's. Despite the predicted reliability value obtained some doubt about the particular EED's used will always remain. This paper will describe nondestructive techniques which yield data as to the quality and normal behavior of each EED without firing or degrading the unit. These techniques are limited to the bridgewire, explosive, header interface (Fig. 1) which is considered a critical link in the electroexplosive chain. Evaluation of this interface will contribute valuable information as to unit performance. The quality of the EED beyond this

interface can be evaluated to a certain degree by techniques such as weighing, X-ray, and neutron radiography.

INSTRUMENTATION AND TECHNIQUE

The nondestructive techniques are based on introducing a current waveform into the bridgewire. The current pulse is small enough to avoid firing or degradation of the EED yet large enough to provide a meaningful electrothermal response observed as a voltage developed at the bridgewire terminals. The bridgewire must have some temperature coefficient of resistivity and the signal developed can be related to the bridgewire temperature rise. Variations in the signal developed from unit to unit can be related but not limited to the following areas:

1. Bridgewire - resistance behavior responding to wire imperfections i.e., current crowding.
2. Welds - poor welds can produce certain nonohmic nonlinearities
3. Thermal transfer - intimacy of contact between bridgewire, header, and explosive mix.
4. Strain behavior of bridgewire - movement of the bridgewire upon heating resulting from coefficient of expansion.

Two types of apparatus have been used to observe the electrothermal response at the bridgewire terminals. Instrumentation referred to as "Transient Pulse Testing" and "Thermal Follow Display" are used to perform the tests in a rapid and efficient manner. For each instrument, the bridgewire becomes one arm of a Wheatstone Bridge. The "Transient Pulse" apparatus (ref. 1) applies a step current waveform (approximately 50 milliseconds on and then off) to the Wheatstone bridge circuit. As the bridgewire heats, the Wheatstone bridge unbalances and an error voltage is developed across the bridgewire terminals. Additional features of the instrumentation allows a measurement of the thermal conductance, the thermal time constant, and the cold resistance of the bridgewire. A lumped model analysis of the bridgewire system is the basis for derivation of the electrothermal equations (ref. 2). The apparatus furnishes quantitative results and provides for a visual oscilloscope display of the error voltage which can be related to the temperature rise in the bridgewire. Figure 2 shows a typical heating curve obtained from a normal healthy EED. The second apparatus, "Thermal Follow Display," employs a steady state 10 Hz, sinusoidal current to the Wheatstone-bridge circuit. A self-balancing feature of the Wheatstone-bridge takes the EED through a thermal cycle. The temperature excursion can be controlled and the bridgewire signal displayed on an oscilloscope. The display shows how bridgewire heating unbalances the Wheatstone-bridge in a cyclic manner producing a Lissajous display (ref. 3). This test is qualitative in nature and is best applied as a gross inspection tool. Figure 3 shows a typical Lissajous obtained from a normal healthy EED.

OBSERVED TRACES

Approximately one thousand bridgewires, in a variety of EED designs, have been examined with the "Transient Pulse" and "Thermal Follow" apparatus. Various abnormal responses have been observed. Figure 4 shows several abnormal heating curves resulting from the transient pulse test. Three types were selected to demonstrate different fault mechanisms. All thermally

induced nonlinearities require a time delay and never appear as trace discontinuities. Nonohmic nonlinearities occur instantaneously and will generally appear at the start of the heating curve. Curve (4a) is typical of a nonohmic nonlinear response attributed to defects in the bridgewire to pin weld. Curve (4b) starts out with a normal exponential rise but after reaching its peak temperature something happens to cool the bridgewire. This phenomenon is related to a phase change taking place in the explosive mixture. Curve (4c), at the onset, shows a nonohmic nonlinear response and then later in time thermally induced nonlinearities. The nonohmic response demonstrates weld defects while the thermal nonlinearities suggest poor thermal contact between the bridgewire and explosive mix. In all cases where an abnormal heating curve was observed with the transient pulse test a corresponding abnormal Lissajous was observed with the thermal follow test. Figure 5 compares a normal thermal follow display response from a healthy EED with a response from a defective EED. Identification of some faults or defects associated with a particular abnormal transient pulse response has been made. These have been verified through case histories and by purposely fabricating EED's with known defects and observing the electrothermal response.

INVESTIGATION AND DISCUSSION OF ABNORMAL RESPONSES

The responses observed with the transient pulse and thermal follow tests are directly related to the condition of the bridgewire, bridgewire weld, and header/bridgewire/explosive interface. To visually observe this interface a test fixture with a quartz header (Fig. 6) was designed. Microscopic observations were made while the bridgewire was subjected to the transient pulse test. Figure 7 is a photomicrograph (double exposure) of the bridgewire heating cycle in air. As the bridgewire heats, expansion and buckling of the wire occurs. This action strains the wire at the weld joints. Other observations were made with talc loaded on the bridgewire at 5K and 10K psi respectfully. Figure 8 shows the bridgewire before and after pulsing at each pressure. At 5K psi loading pressure some of the talc has managed to get between the bridgewire and header. When pulsed repeatedly the talc density is low enough to allow the bridgewire to buckle and move the powder away in the manner of a "Tunneling Effect". At 10K psi the tunneling effect is not apparent. These tests pointed out the importance of correct loading pressure to ensure that the explosive material is always in intimate contact with the bridgewire. The "Tunneling Effect" observed was a result of the transient pulse applied to the bridgewire, however, one can conceive of a similar effect resulting from external temperature cycling or vibration. Identification of an air gap between the bridgewire and explosive material can be determined by the transient pulse test and is demonstrated in figure 9. Here we see a rapid rise in the heating curve since the bridgewire is not in intimate contact with the explosive material, and heat loss is small. As the bridgewire expands and buckles, it makes contact with the explosive and the rate of temperature rise of the bridgewire decreases, creating a knee in the curve. This condition can lead to decreased reliability because of possible bridgewire burnout prior to the bridgewire contacting the explosive. As the loading pressure of the explosive is increased, the ability of the bridgewire to buckle when heated is minimized. However, the strain in the wire remains but is

now applied along the axis of the bridgewire terminating at the weld joints. Thus the confined bridgewire is under considerable strain. In the event a poor or defective weld exists a nonohmic nonlinear response will result and be observed when tested by the transient pulse or thermal follow technique.

Verification that poor welds lead to nonohmic nonlinear responses was made by actually building bridgewire systems purposely containing bad welds and also by dissecting EED's which demonstrated nonohmic nonlinear responses. Figure 10 shows two purposely fabricated bad bridgewire welds and the resulting heating curves observed by the transient pulse and thermal follow techniques. Actual EED's displaying nonohmic nonlinear responses were dissected and the explosive carefully removed from the bridgewire header surface exposing the welds. Figure 11 reveals the welds found in two cases. In the left picture corrosion has been at work while in the right picture the weld was improperly made and the bridgewire appears to be poorly fused to the pin.

Another area of considerable interest sensed by the transient pulse technique was the identification of phase changes taking place within the explosive mixture. Figure 12 shows two EED's which exhibited abnormal responses. Ignoring the nonohmic behavior, for the moment, at the start of the heating curve a peak temperature is reached and then cooling takes place. It was known that the explosive mixture pressed on the bridgewire contained a 5% Viton (R) binder. It was further learned that Viton binders for EED applications are usually dissolved in acetone or methyl ethyl ketone (MEK) and wet mixed with the explosive materials. The mixtures are then oven dried to drive off the solvent. In practice, driving out all of the solvent from Viton by heating is quite difficult (ref. 4). It is believed that the abnormal heating curves of figure 12 were a result of trapped acetone or MEK in the Viton which upon heating of the bridgewire changed the solvent from a liquid to a gaseous phase accounting for the cooling observed. Dissection of the faulty squibs found that the Viton had formed a thin skin (approx. 15 mils (0.48 mm) thick) about the inner walls of the ceramic cup and surface of the header. This may have occurred because the trapped solvent kept the Viton very plastic and when the explosive mixture was pressed into the cermic cup the pressure allowed the Viton to exude to the inner surfaces. Figure 13 shows photomicrographs of the explosive mixture removed from EED's emphasizing the exuded Viton. The examination showed that the explosive mixture was not homogeneous and that the bridgewire was not in intimate contact with the reactive ingredients of the explosive mixture. The implication of such conditions are obvious and certainly should be avoided. To further substantiate that the transient pulse technique was detecting a phase change heating curves were obtained for Viton, acetone, MEK, and a mixture (50/50) of acetone and Viton. Figure 14 shows these heating curves. Viton exhibits a normal heating curve while acetone, MEK, and acetone/Viton (50/50) definitely exhibit a phase change at bridgewire temperatures normally attained in the test.

It was stated earlier that the transient pulse technique allowed for the calculation of thermal conductance, thermal time constant, and cold bridgewire resistance. These parameters can be beneficial in further narrowing the sample selected for use. Recently a study was made of a single bridgewire squib supplied by the Manned Space Center, Houston. Two samples (50 each) each manufactured by different companies were subjected to the transient

pulse and thermal follow techniques. It was found that both samples displayed equivalent heating curves and no abnormalities were observed. One could stop at this point and randomly select units from either sample. However, on the basis of one or more of the thermal parameters, i.e., the thermal time constant, the distribution could be reviewed and the sample further narrowed by selecting units within a chosen bandwidth.

A number of faults have been detected and the cause determined by the transient pulse and thermal follow techniques. Not all faults have been detected but it is felt that those discussed in this paper are most likely to lead to failure. It was not the intent of JPL to determine all fault possibilities but rather to provide techniques and tools to nondestructively test each EED for quality and normality. Certainly different EED designs will generate variations of the responses discussed. The basic abnormalities have been discussed, any deviations from these must be attributed to the design of the EED under study. For those who must demonstrate very high reliabilities and confidences these techniques will provide a means to minimize the number of EED's that must be destructively tested. Total normality can be obtained by culling out abnormal or suspicious units (ref. 5). These techniques can be conveniently applied to in-process quality control. Specifically the transient pulse can be a total inspection and acceptance tool. In addition, designers of EED's will find the techniques useful in optimizing their designs and detecting hidden and subtle potential faults.

REFERENCES

1. Rosenthal, L. A., Merichelli, V. J., Technical Report 32-1344, "Nondestructive Testing of Insensitive Electroexplosive Devices by Transient Techniques", Jet Propulsion Laboratory, Pasadena, California, July 15, 1970.
2. Rosenthal, L. A., "Electro-Thermal Equations for Electroexplosive Devices", NAVORD Report 6684, U.S. Naval Ordnance Laboratory, Silver Spring, Maryland, Aug. 15, 1959. AD 230917.
3. Rosenthal, L. A., "Thermal Response of Bridgewires Used in Electroexplosive Devices", Rev. of Sci. Instr., Vol. 32, pp. 1035-1036, Sept. 1961.
4. Discussions with J. Sherman, Naval Weapons Center, China Lake, Calif.
5. Harwood, W. D., Steward, L. G., "Nondestructive Measurement of the Quality of Electroexplosive Interfaces," Materials Evaluation, Vol. XXVI, Dec. 1968.

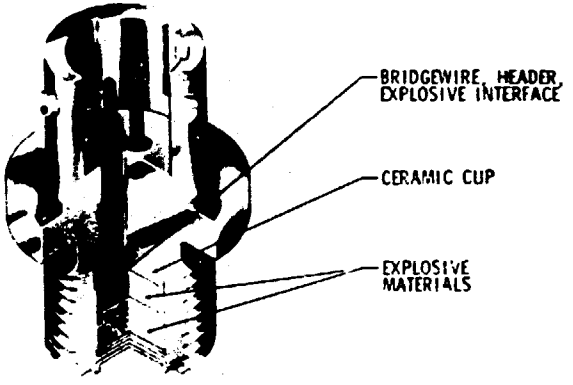

Figure 1. Typical Aerospace Electroexplosive Device

H - 10 msec/cm
V - 5 mV/cm

Figure 2. Typical Heating Curve Response from a Healthy, Normal EED as Sensed by the Voltage Drop at the Bridgewire

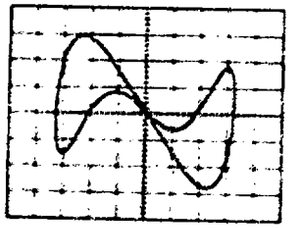

H - 2V/cm
V - 50 mV/cm

Figure 3. Typical Constant Response from a Healthy, Normal EED
H is Proportional to Time
V is Proportional to Bridgewire Drop Voltage

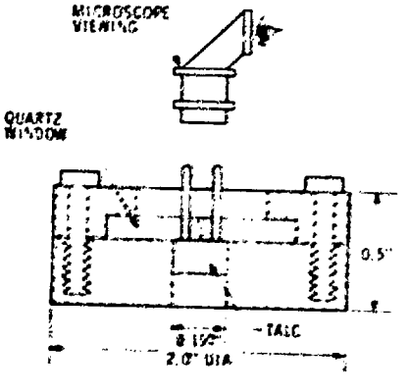

Figure 6. Test Fixture Used to Observe Bridgewire Behavior Subjected to Transient Pulse

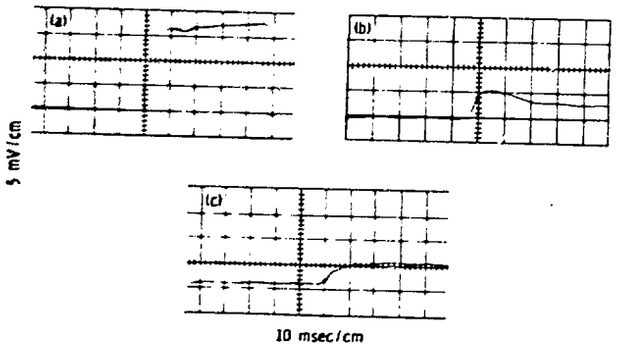

Figure 4. Several Abnormal Suspicious Heating Curves as a Result of Defects in the EED's

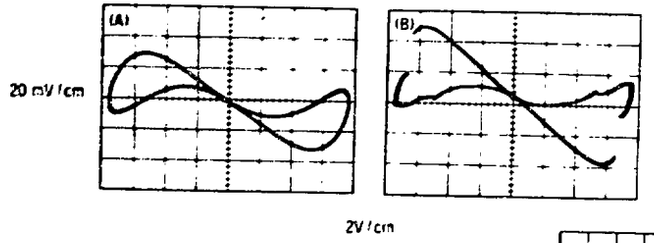

Figure 5. Comparison of a Normal "Thermal Follow" Response from a Healthy EED (A) with a Response from a Defective EED (B)

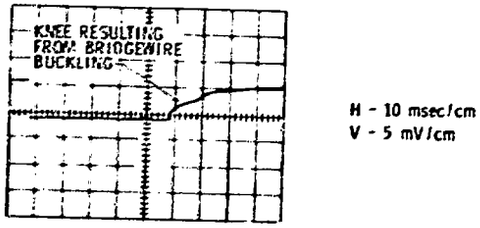

H - 10 msec/cm
V - 5 mV/cm

Figure 9. Heating Curve Resulting from Poor Contact Between Bridgewire and Explosive

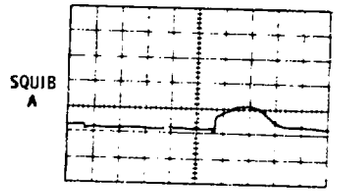

H - 10 msec/cm
V - 5 mV/cm

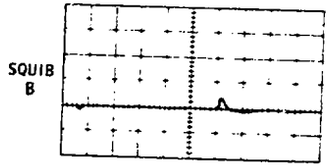

H - 10 msec/cm
V - 5 mV/cm

Figure 12. Heating Curves Resulting from an Apparent Phase Change Taking Place Within the Explosive Mixture

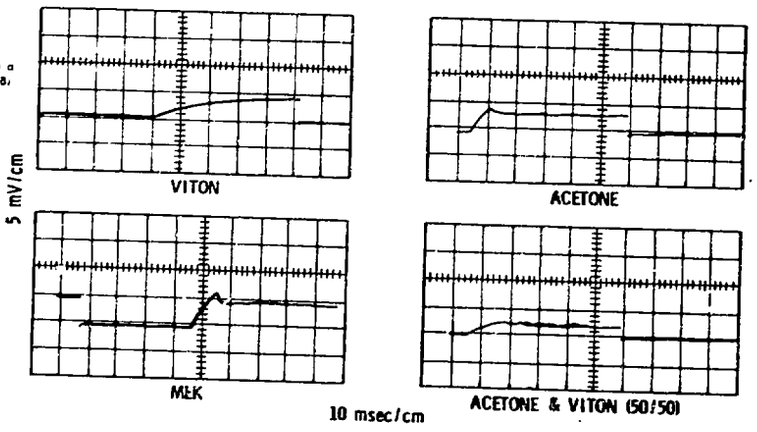

Figure 14. Heating Curves for Various Bridgewire Environments

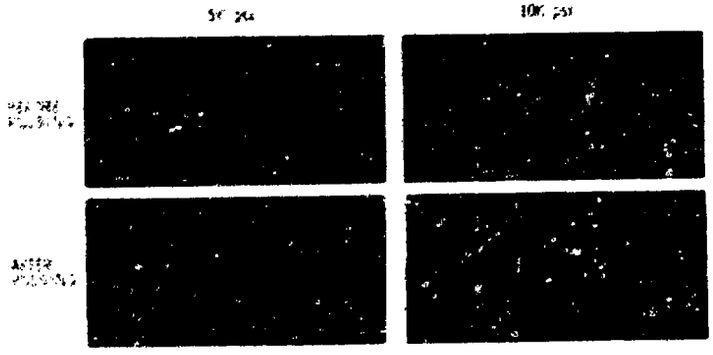

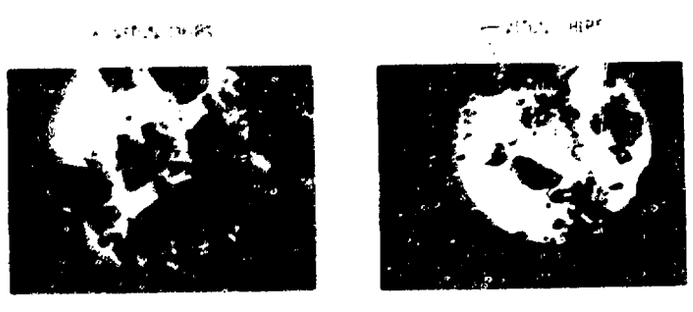

ERODED - OXIDIZED WELDS

40X 40X

H - 10 msec/cm
V - 5 mV/cm

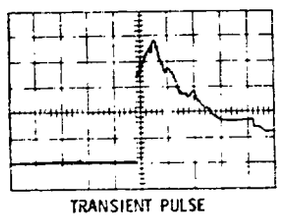

TRANSIENT PULSE

H - 2V/cm
V - 20 mV/cm

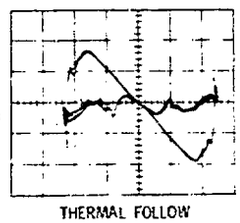

THERMAL FOLLOW

Figure 10. Heating Curves Resulting from Photographed Defective Welds

CORROSION

OXIDIZED, POOR FUSION

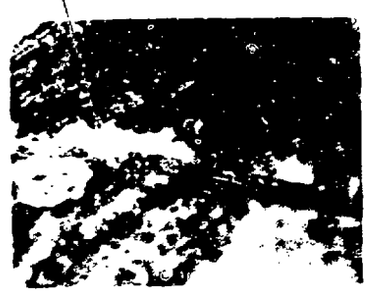

40X 40X

Figure 11. Bridgewire Welds of Dissected EED's that Demonstrate Nonohmic Nonlinear Responses to Transient Pulse and Thermal Follow Tests

II-6. SHORT PULSE TESTING

by

R. H. Thompson, The Franklin Institute Research Laboratories

V. Goldie, General Electric Co., Philadelphia, Penna.

1. INTRODUCTION

The overall objective of the work presented in this paper was the sensitivity of two typical Aerospace type electroexplosive devices (EEDs) to a relatively short, damped burst of RF energy.

We had previously performed continuous wave and pulsed RF susceptibility tests on a Hi-Shear pressure cartridge and an Atlantic Research FND Initiator. It was decided that the misfired items, of the RF tests, i.e., the items that had not fired when subjected to the continuous wave or pulsed RF stimulus, should be used to determine the sensitivity to a short damped RF burst. The decision was made on the basis that we would use, as far as possible, items that had previously been exposed to pin-to-pin (P-P) stimuli to determine pins-to-case (P-C) short, damped RF burst sensitivity and vice versa. Our previous experience with other EEDs indicates that this type of procedure yields, at least for CW and pulsed RF, relatively unbiased data. The main advantage of course is that fewer of the expensive EEDs are used in such a combined program.

As far as we can determine, no other tests for the short, damped RF sensitivity of EEDs have been performed; hence, we have no specific similar tests to guide us as to the applicability of the above procedure to the results obtained in this paper. The results must be interpreted with this in mind. Further tests on virgin items can, of course, be run to settle the matter.

The original approaches to obtaining the required stimuli were based on the application of quick risetime voltage and current square waves to series and parallel resonant circuits containing the EED P-P and P-C impedances. It was quickly discovered that the necessary risetimes could not be obtained with our equipment and the necessary circuits. We finally settled on a capacitor discharge approach that utilizes a vacuum switch.

2. THEORETICAL RESPONSE OF THE TEST CIRCUITS

The perfect switch models of the test circuits used in our evaluations are shown in Figure 2-1. Figure 2-2 shows a circuit completely equivalent to Figure 2-1a as far as i(t) and v(t) are concerned.

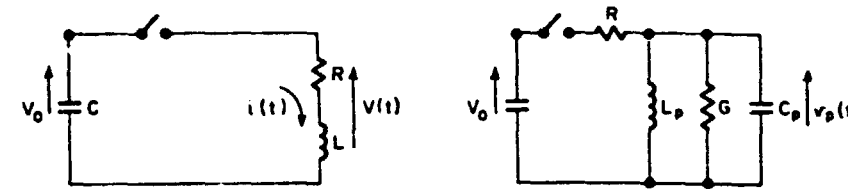

(a). Pin-to-Pin Test Circuit *(b). Pins-to-Case Test Circuit*

Fig. 2-1. Perfect Switch Model

The current source of Figure 2-2 is to be intrepreted as an impulse function ($S_o(t)$) occurring at t=0 of value CV_o, where V_o is the original voltage on C when the switch in Figure 2-1a is closed at t=0. Applying Laplace transform theory to the circuit of Figure 2-2 gives

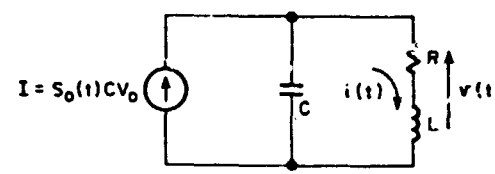

Fig. 2-2. Current Source Equivalent Circuit

$$i(t) = V_o \sqrt{\frac{C}{L}} \frac{\omega_o}{\omega_d} e^{-\alpha t} \sin(\omega_d t), \text{ and} \qquad (2\text{-}1)$$

$$v(t) = V_o \frac{\omega_o}{\omega_d} e^{-\alpha t} \sin\left(\omega_d t + \sin^{-1}\frac{\omega_d}{\omega_o}\right) , \qquad (2\text{-}2)$$

where

$$\omega_o = \sqrt{\frac{1}{LC}} ,$$

$$\alpha = \frac{R}{2L} \quad \text{and}$$

$$\omega_d = \sqrt{\frac{1}{LC} - \frac{R^2}{4L^2}} = \sqrt{\omega_o^2 - \alpha^2} = 2\pi f_d . \qquad (2\text{-}3)$$

If we wish the peak of some particular cycle to be d times ($d < 1$) the peak of a cycle that occurred n cycles previously then α must be such that

$$\alpha = \frac{f_d}{n} \ln\left(\frac{1}{d}\right) \qquad (2\text{-}4)$$

A convenient way of describing the damping of a waveshape described by Equations (2-1) or (2-2) is to define

$$\delta = \frac{f_d}{\alpha} = \frac{\omega_d}{2\pi\alpha} . \qquad (2\text{-}5)$$

The waveshapes in Figure 2-3 show the effect of various values of δ.

For δ equal to 2.0 the amplitude of the 5th peak is 13% of the first peak while for δ equal to 0.9 the amplitude decreases to 1% of the first. Our tests were run with δ approximately equal to one.

The total energy delivered to the total resistance is exactly that stored in the capacitor.

$$\text{Energy} = 1/2\ CV^2, \text{ joules} \qquad (2\text{-}6)$$

where

C = capacitance in farads

V = voltage in volts

The total energy delivered to the EED input depends, of course, on the EEDs input resistance and the resistance of the external circuit. Calculation of this energy for our tests is covered in Section 3.

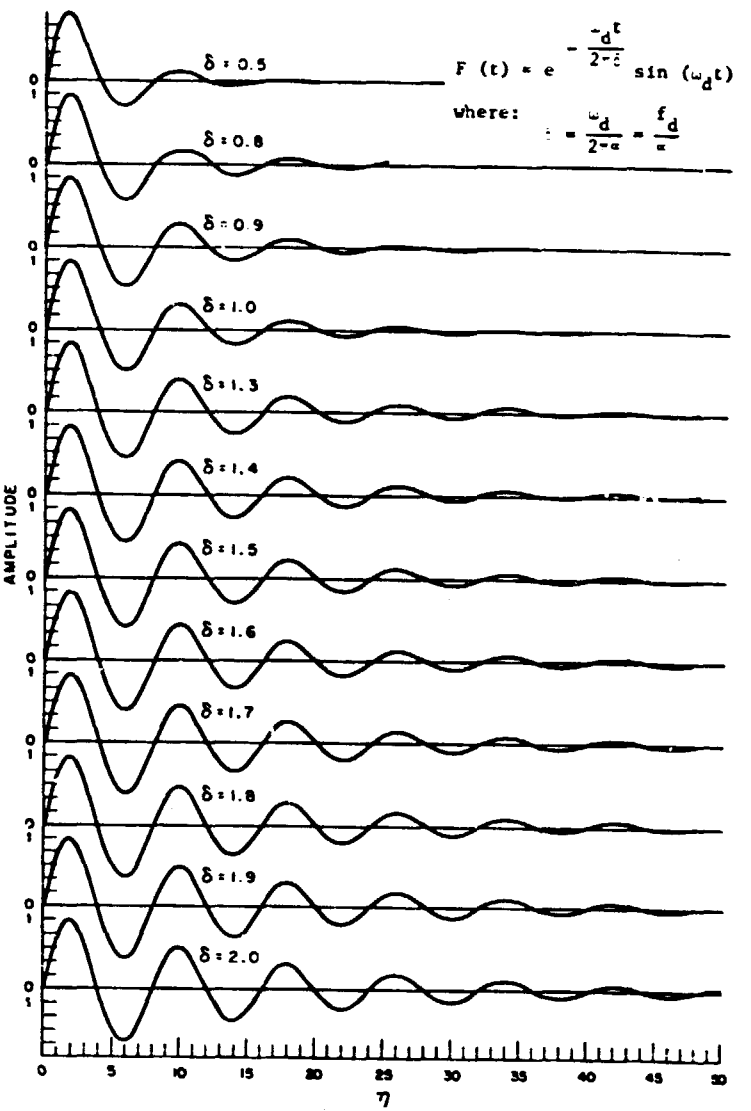

Fig. 2-3. Damped Waves for Various Values of $\delta = \frac{f_d}{\alpha}$

3. EXPERIMENTAL CONSIDERATIONS

3.1 Test Equipment

Figure 3-1 illustrates the basic system used to fire the Hi-Shear and the [illegible] EEDs in the pin-to-pin mode. The waveform is monitored with a Hewlett-Packard 456A current probe that uses an oscilloscope as an indicator. Insert (A) shows a 5.1 ohm resistor in series with the EED while insert (B) shows no resistor and the wire split into two parts such that the current probe measures one half the total current. Method (B) is preferred since it reduces the amplitude of the current monitored such that the initial peak can be recorded on the oscilloscope. However, the noise introduced due to stray capacitance and inductance distorts the waveform.

For our applications, the frequency of the damped sinewave is determined mainly by capacitor C_s and inductor L_1. The reactive part of the EED is also taken into consideration.

Figures 3-2 and 3-3 illustrate an actual test setup for firing the EED. In order to reduce the stray capacitance and inductance, the components are placed as close to the EED as possible.

For the pins-to-case and bridge-to-bridge tests the EED is placed in parallel with a monitoring resistor and a hand wound inductor is placed in parallel with the combination. Figure 3-4 illustrates how the EED is connected.

Most of the pin-to-pin tests required no actual inductors. The stray inductance of the circuit itself was adequate for our purposes.

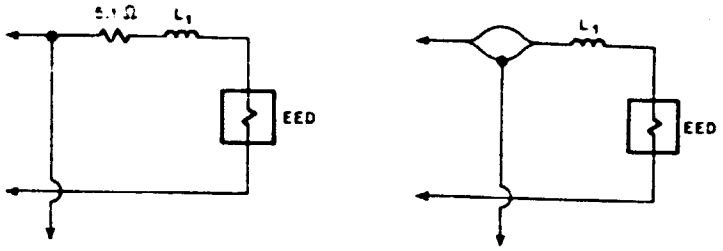

(a). Series Resistance (b). Current Split

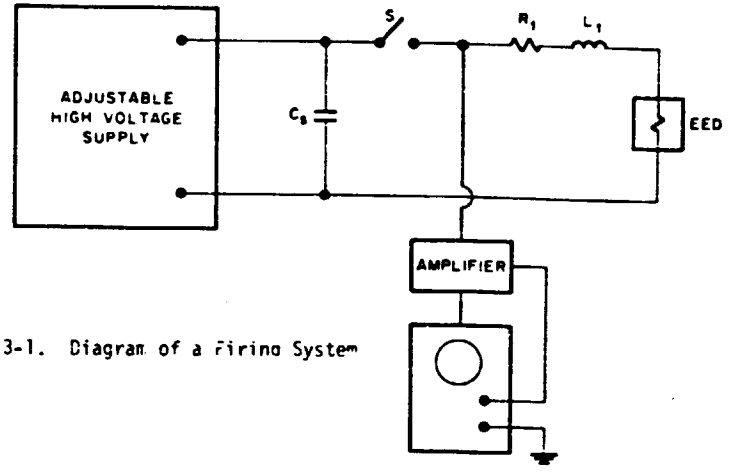

Fig. 3-1. Diagram of a Firing System

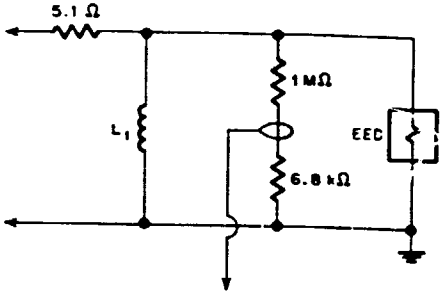

Fig. 3-4. EED Connection for Pins-to-Case and Bridge-to-Bridge Testing

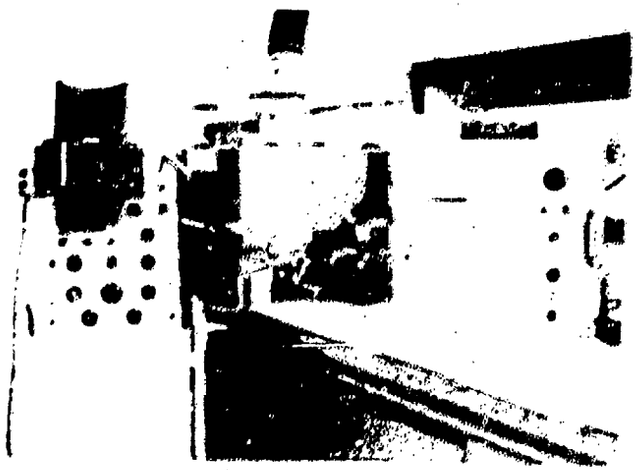

Fig. 3-2. Firing System and Current Monitoring

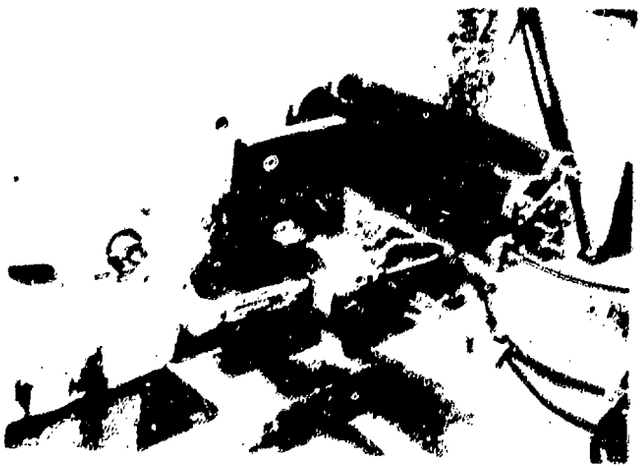

Fig. 3-3. Close Up of Firing System

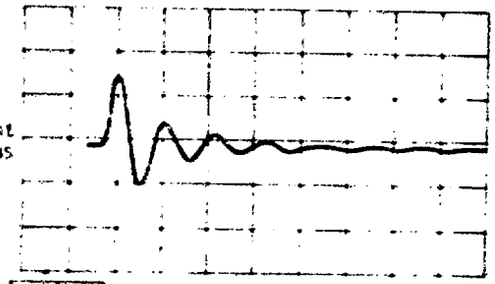

Fig. 3-5. Typical Low Current Pin-to-Pin Stimulus

Fig. 3-6. Typical Low Voltage Pin-to-Case Stimulus

Figure 3-5 is a retracing of a oscilloscope picture of a typical 10 MHz pulse applied to the pin-to-pin input of a PC-60, Hi-Shear item. This waveform was obtained with 1000 volts dc on a 900 μfarad capacitor. Sweep speed was 0.1 microseconds per division and the vertical deflection, including the probe response, had been calibrated as 38.4 peak amps per 1000 volts dc. Photos of actual firing pulses of hundreds of amps reveal only the last few cycles due to probe and vertical amplifier overdrive and the relatively slow writing rate of the scope.

Figure 3-6 is a retracing of a pins-to-case pulse photo. This photograph was obtained from the 5 MHz pins-to-case tests of the Hi-Shear item. The waveform was obtained from the bleeder resistance. Sweep speed was 0.2 microseconds per division. The source capacitor was 2000 μfarads charged to 1000 volts dc. The vertical deflection factor was 10 volts per division. Note the extremely rapid jump to the peak. This corresponds to the typical pins-to-case voltage behavior in our circuits showing that the pins-to-case applied waveform is approximately an exponentially damped cosine function.

The photographs of higher current and voltage stimuli are in general not as noise free as the two presented above.

3.2 Errors

The test equipment produces several effects that influence the test data and make the results somewhat uncertain. The stray capacity and inductance in the test set up contribute to the overall transfer function so that other damped frequencies are produced in addition to the primary frequency. Figure 3-7 shows the simplest circuit that can reasonably be drawn to account for this effect.

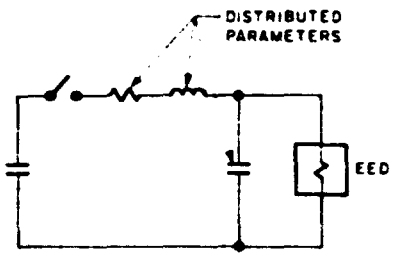

Fig. 3-7. Simple Circuit to Account for Distributed Parameter Effects

During the buildup of the test circuits the effect of the distributed components was clearly evident before we reduced all wiring to minimum length. The primary reason we cannot greatly reduce the effect further is the relatively large size of the firing switch we are using. We can reduce the firing capacitor sizes quite a bit by obtaining much smaller capacitors but there is a limit in this direction caused by the high voltage the capacitor must stand off without external breakdown.

The vacuum switch we are using was found to be superior to several others we tried. Its large size is a drawback, as explained above, but there is much less "hash" on the EED waveform when this switch is used than with any other switch tried. We speculate that the entire transient behavior is over before the contacts of the switch actually close. If we turn out the room lights we can observe a spark inside the vacuum switch even at very low voltages. If we assume that the sparks jump at 0.010 inch contact separation, and they probably start at much greater separations, then the contact must be moving about 850 ft/sec to actually touch within one microsecond of the spark start. Our whole transient behavior is over, even at the lowest frequency (5 MHz), within one microsecond.

The additional damped frequencies produced by the distributed parameters of the test equipment are probably present in all our tests. The fairly low bandwidth of our oscilloscope masks these higher frequency components of the stimuli. As long as these higher frequency components contain very small energies in relation to the fundamental component we do not believe that they will significantly influence our test results. We estimate that this is the case for the data reported herein.

Another possible source of error in our testing procedure is that due to the extrapolation of the current probe calibration to high currents. We calibrate the current probe with a fairly low current CW source. The frequency is that of the fundamental frequency of a given test. Next we observe the current waveform produced at the EED by low dc voltages on the discharge capacitor. We now relate dc voltage on the capacitor to the peak current of the damped stimuli. Tests are run by extrapolating this relationship between dc voltage on the capacitor to peak current of the stimuli to high dc voltages. Our scope pictures then show the third or fourth damped cycle of the stimuli. The procedure seems to be valid since the peaks of the observable (still on the screen of the oscilloscope) third or fourth cycles of the high dc voltage stimuli check with calculations based on the low voltage observed damping factors.

An observational error is also built into the experimental determination of ζ. We determine ζ by comparing the test waveshapes with the waveshapes of Figure 2-3. There is, therefore, some error in our assumption that the tests are all run with ζ equal to one.

3.3 Calibration

Our quoted peak currents for the pin-to-pin tests were computed for each damped frequency excitation by calibration of the current indicating system against an RF current of the same basic frequency. The current

probe was placed around the center conductor of a short specially built coaxial line feeding a 50 ohm calorimeter. The square of the line current was computed by dividing the calorimeter reading by the 50 ohm calorimeter impedance. A correction factor to be applied to the scope reading was then calculated. This method of calibration eliminates scope and current probe frequency responses from the calibration procedures. The change of calorimeter input impedance due to the probe and fixture insertion was measured and was quite small.

Our next step was to apply a known dc voltage to the source capacitor and observe the amplitude of the EED current. Then we could calculate an EED peak ampere/dc volt factor for the system.

A theoretical factor can also be derived. The peak current of Equation (2-1) occurs when

$$\sin(\omega_d t_p) = \frac{\omega_d}{\sqrt{\alpha^2 + \omega_d^2}} = \frac{\omega_d}{\omega_o} \qquad (3\text{-}1)$$

where t_p is the time at peak current.

For our applications $\omega_d \approx \omega_o$ so that

$$t_p \approx \frac{1}{4f_o} \qquad (3\text{-}2)$$

and the peak current is

$$i_p \approx V_o C \omega_o e^{-\frac{\alpha}{4f_o}} = V_o C \omega_o e^{-\frac{1}{4\tau}} \qquad (3\text{-}3)$$

For $\tau = 1$, which applies to our tests,

$$i_p \approx 4.9\, V_o C f_o \qquad (3\text{-}4)$$

where

i_p is the peak current in amps,

V_o is the dc voltage on the capacitor in volts,

C is the capacity of the capacitor in farads,

and f_o is the damped frequency in Hz.

Table 3-1 compares the theoretically calculated calibration factors with those determined by the RF continuous wave method. All our data are quoted using the RF continuous wave determined calibration factors.

Table 3-1

CALIBRATION FACTORS

(I_p/V (amps/1000 volts)

Frequency MHz	Capacity μf	Theoretically Calculated factors	From RF Continuous Wave Calibration
	Hi-Shear Item p to p		
5	2400	59	56
10	900	44	38.4
45	50	11	10
	FMD Item p to p		
5	2400	59	56
10	900	44	38.4
45	50	11	10

3.4 Energy Calculations

The total energy (E_{RS}) delivered to a resistor (R_S) that carries the current of Equation (2-1) is

$$E_{RS} = \frac{A^2}{4\alpha} \left(\frac{\omega_d}{\omega_o}\right)^2 R_S \qquad (3\text{-}5)$$

where

$$A = V_o \sqrt{\frac{C}{L}} \frac{\tau_o}{\omega_d} .$$

The peak current can be expressed for our conditions of $\zeta = 1$, as

$$i_p = A \frac{\omega_d}{\tau_o} e^{-\frac{1}{4\zeta}} . \qquad (3-6)$$

Using this expression to substitute for A in the energy expression,

$$E_{RS} = \frac{i_p^2 R_S}{4 \pi e^{-\frac{1}{2\zeta}}} \cong \frac{0.41\ i_p^2 R_S}{f_o} \qquad (3-7)$$

The above answer is in joules if i_p is in amps, R_S in ohms and f_o in Hertz.

$$E_{RS} \cong \frac{R_S\ i_p^2 \times 4.1}{f_{MHz}} \text{ ergs} \qquad (3-8)$$

if i_p is in amps, R_S in ohms and f_{MHz} is the damped frequency in megahertz. Table 3-2 gives the measured input impedances of the subject EEDs. The total energies delivered to the EEDs in the pin-to-pin tests can be approximated using the test currents, test frequencies and the real part of the input impedances given in Table 3-2.

Table 3-3 gives the energy supplied to the EEDs in our tests for 100 amps of peak current. If the current is ζ times 100 amps the energy is ζ^2 times that is given in Table 3-3.

Table 3-2

INPUT IMPEDANCE OF THE EEDs (ohms)
ROUNDED TO TWO SIGNIFICANT DIGITS

Freq. in MHz	Pin-to-Pin	Pins-to-Case
	Hi-Shear Item	
1.5	0.41 + j0	61 - j9000
3	0.37 + j1.0	29 - j4400
5	0.42 + j1.1	30 - j2800
10	0.51 + j1.3	31 - j1500
15	0.61 + j2.0	22 - j980
50	1.8 + j6.8	4 - j280
100	1.4 + j14	8 - j140

Freq. in MHz	Pin-to-Pin	Pins-to-Case	Bridge-to-Bridge
	END Item		
1.5	.73 + j0.33	61 - j6600	74 - j12 000
3.0	.80 + j0.33	21 - j3200	39 - j7000
5.0	.80 + j0.55	19 - j2000	40 - j4000
10.0	.80 + j1.1	17 - j1000	43 - j2000
15.0	.83 + j1.6	13 - j700	27 - j1400
30.0	.90 + j3.0	7.4 - j380	12 - j730
50.0	1.1 + j5.4	6.9 - j210	14 - j370
100.0	1.5 + j12	6.2 - j98	16 - j140

Table 3-3

ENERGY SUPPLIED TO THE EED p-p IMPEDANCE

f_{MHz}	ergs/100 amps	
	Hi-Shear Item	END Item
5	3450	6560
10	2100	3280
45	910	910

The determination of the stimuli applied to the pins-to-case impedance of the EEDs must consider several sources of error. Our instrumentation in this area was inferior to that in the pin-to-pin firing. Our observations and calculations lead us to believe, however, that the voltage across the pins-to-case impedances can be fairly well represented by

$$V_{pc} = V_{dc}\, e^{-\alpha t} \sin(\omega_d t + \pi/2) = V_{dc}\, e^{-\alpha t} \cos(\omega_d t) \qquad (3\text{-}9)$$

where $\zeta = \frac{f_d}{f}$ and is approximately equal to one for our experiments, and $\omega_d = 2\pi f_d$, the damped radial frequency.

The energy (E_T) delivered to the input conductance G of the individual EEDs during the tests is calculated as

$$E_T = \frac{V_{dc}^2\, G}{4 f_d} \qquad (3\text{-}10)$$

Equation (3-10) gives energy in joules if G is in mhos, V in volts and f_d in hertz. Table 3-4 gives the input Gs for our items at the frequencies nearest the test frequencies. The Gs are calculated from the pins-to-case and bridge-to-bridge impedances given in Table 3-2.

Table 3-4

INPUT CONDUCTANCE (G) FOR THE EEDs in MICROMHOS

Frequency MHz	Hi-Shear Item p to c	FND Item p to c	FND Item b to b
5	3.8	4.7	2.49
10	13.77	17.0	10.74
15	22.89	--	
30	--	51	22.51
50	107.		

4. TEST RESULTS

There were three types of tests performed: pin-to-pin, pins-to-case and (for the FND item) bridge-to-bridge. The test results are discussed in this order.

4.1 Pin-to-Pin Data

4.1.1 Hi-Shear Item

Summaries of the test data are recorded in Tables 4-1, 4-2, and 4-3. Since the amount of hardware was limited, it was necessary to reuse the items. The numbers recorded in the columns represents the order of exposure of the items. As an example, serial number 56184 in Table 4-1 shows 9 in the 200 A column and 16 in the 300 A column. This means that it was first tested at 200 A and then later at 300 A. The numbers with boxes around them designate firings.

At 5 MHz, one out of eight fired at 300 A, and two out of four at 400 A. With a damped wave of 10 MHz, one out of twelve fired at 400 A, one out of eight at 500 A and one out of four at 700 A. No firings were recorded with 75 A at 45 MHz.

4.1.2 FND Item

Tables 4-4, 4-5, and 4-6 record the pin-to-pin data for the FND item. At 5 MHz, one out of six fired at 400 A and ten out of ten at 500 A. With a damped wave of 10 MHz, one out of four fired at 600 A and three out of six at 700 A. No firings were recorded with 75 A at 45 MHz.

Table 4-1

FIRING SUMMARY OF THE HI-SHEAR ITEM
PIN-TO-PIN AT 5 MHz, DAMPED WAVE

Serial No.	Peak Current (Amperes) 200	300	400
56086		1	
56180		2	
56082		3	
56467		[4]	
56088			5
56289			6
56138			[7]
56446			[8]
56184	9	16	
56594	10	15	
56414	11	14	
56536	12	13	

Table 4-2

FIRING SUMMARY OF THE HI-SHEAR ITEM
PIN-TO-PIN AT 10 MHz, DAMPED WAVE

Serial No.	Peak Current (Amperes) 200	300	400	500	700
56538	1		25	26	[32]
56474	2		27	[28]	
56091	3		23	24	29
56524	4		21	22	30
56592			5		
56078			[6]		
56 08			7		
56682			8		
56187		9	19	20	31
56765		10	17	18	
56173		11	15	16	
56585		12	13	14	

Table 4-3

FIRING SUMMARY OF THE HI-SHEAR ITEM
PIN-TO-PIN AT 45 MHz, DAMPED WAVE

Serial No.	Peak Current (Amperes) 75
56175	1
56052	2
56673	3
56188	4
56036	5
56527	6
56650	7
56186	8
56531	9
56174	10
56185	11
56194	12

Table 4-4

FIRING SUMMARY OF THE FND ITEM
PIN-TO-PIN AT 5 MHz, DAMPED WAVE

Serial No.	Peak Current (Amperes) 300	400	500
QX 100	1		
289	2		[20]
153	3		
169	4		[21]
197	5		
192	6		
QW 282	25		
94598	24		[25]
QX 015		7	
068		[8]	
14		9	
216		10	
157		11	
QW 997		12	
QW 94577			[13]
590			[14]
966			[15]
QX 153			[16]
209			[17]
289			[18]
QW 995	23		
QX 271	22		[19]

Table 4-5

FIRING SUMMARY OF THE FND ITEM
PIN-TO-PIN AT 10 MHz, DAMPED WAVE

Serial No.	Peak Current (Amperes) 300	400	500	600	700
QW 94582	1		27		[28]
QX 17	2		21		[22]
QX 129	3		25		26
QW 94563	4		23		24
QX 211	5		19		20
QX 22	6		29		[30]
QW 94554		7			
QW 94559		8			
QW 94574		9			
QX 189		10			
QX 008		11			
QW 974		12			
QX 13			13		
QX 198			14		
QW 94588				[15]	
QW 996				16	
QW 94594				17	
QW 94596				18	

Table 4-10

FIRING SUMMARY OF THE FND ITEM
PINS-TO-CASE AT 5 MHz, DAMPED WAVE

Serial No.	Peak Voltage (Volts) 5000	28,500
QW 976	1	2
QW 980	3	4
QW 946	5	6

Table 4-6

FIRING SUMMARY OF THE FND ITEM
PIN-TO-PIN AT 45 MHz, DAMPED WAVE

Serial No.	Current (Amperes) 75
QW 992	1
QX 134	2
QX 131	3
QX 033	4
QX 014	5
QX 037	6
QX 002	7
QX 026	8
QW 977	9
QW 969	10
QX 261	11
QW 968	12
QX 154	13
QW 95499	14
QX 180	15
QX 218	16
QW 978	17

Table 4-7

FIRING SUMMARY OF THE HI-SHEAR
PINS-TO-CASE AT 5 MHz, DAMPED WAVE

Serial No.	Peak Voltage (Volts) 5000	28,500
56710		1
56350		2
56713		3
56352		4
56316		5
56317		6
56643		7
56595	8	9
56182	10	11

Table 4-8

FIRING SUMMARY OF THE HI-SHEAR
PINS-TO-CASE AT 10 MHz, DAMPED WAVE

Serial No.	Peak Voltage (Volts) 28,500
56417	1
56347	2
56464	3
56409	8
56007	9
56327	10
56687	4
56321	5
56353	6
56089	7

Table 4-9

FIRING SUMMARY OF THE HI-SHEAR
PINS-TO-CASE AT 33 MHz, DAMPED WAVE

Serial No.	Peak Voltage (Volts) 5000
56172	1
56533	2
56661	3
56662	4
56644	5
56652	6
56325	7
56139	8
56645	9
56261	10

4.2 Pins-to-Case Data

4.2.1 Hi-Shear Item

Summaries of the pins-to-case data for the Hi-Shear item are recorded in Tables 4-6 to 4-8. The maximum voltage available at 5 MHz and 10 MHz was 28,500 volts while the maximum at 33 MHz was 5000 volts. The limiting factor at 33 MHz is the voltage rating of the capacitor.

No initiation occurred at 5 MHz with 28,500 volts, but two out of ten initiated with a 10 MHz damped wave. Ten units were evaluated at 33 MHz with no fires at 5000 volts.

4.2.2 FND Item

The pins-to-case data for the FND item are listed in Tables 4-9 to 4-16. No initiation occurred at 5 MHz and 10 MHz with 28,500 volts at 33 MHz.

4.3 Bridgewire-to-Bridgewire Data

The FND item is a dual bridgewire device, therefore, it was necessary to conduct tests for bridgewire-to-bridgrewire sensitivity. No initiation occurred at 5 MHz and 10 MHz with 28,500 volts and with 5000 volts at 33 MHz.

Table 4-11

FIRING SUMMARY OF THE FND ITEM
PINS-TO-CASE AT 10 MHz, DAMPED WAVE

Serial No.	Peak Voltage (Volts) 5000	28,500
QX 005	1	2
QX 210	3	4
QW 94565		5
QX 240		6
QW 94954		7
QX 018		8

Table 4-12

FIRING SUMMARY OF THE FND ITEM
PINS-TO-CASE AT 33 MHz, DAMPED WAVE

Serial No.	Peak Voltage (Volts) 5000
QX 261	1
QX 218	2
QW 290	3
QW 978	4
QX 014	5
QX 1800	6
QW 98300	7

Table 4-13

FIRING SUMMARY OF THE FND ITEM
BRIDGE-TO-BRIDGE AT 5 MHz, DAMPED WAVE

Serial No.	Peak Voltage (Volts) 5000	28,500
QW 973	1	2
QX 284		3
QW 389		4
QW 420		6
QX [illegible]		7
QX [illegible]	8	9

Table 4-14

[illegible] FIRING SUMMARY OF THE FND ITEM
BRIDGE-TO-BRIDGE AT 10 MHz, DAMPED WAVE

Serial No.	Peak Voltage (Volts) 5000	28,500
QW [illegible]	1	2
QX [illegible]		3
[illegible]		4
QW [illegible]		5
QW 38		6
QW [illegible]		7

Table 4-15

FIRING SUMMARY OF THE FND ITEM
BRIDGE-TO-BRIDGE AT 33 MHz, DAMPED WAVE

Serial No.	Peak Voltage (Volts) 5000
QW 992	1
QW ?	2
QW 977	3
QX 002	4
QX 154	5
QX 037	6
QX 231	7

Table 4-16

LOWEST PIN-TO-PIN ENERGIES (ERGS)
FOR FUNCTIONING

f_{MHz}	Hi-Shear Item	FND Item
5	31,200	105,000
10	33,600	118,000
45	No Fires at 510 The Maximum Applied	No Fires at 510 The Maximum Applied

Table 4-17

CALCULATED PINS-TO-CASE AND BRIDGE-TO-BRIDGE ENERGIES SUPPLIED DURING THE TESTS (ERGS)

Test Frequency MHz	Hi-Shear Item p to c	FND Item p to c	FND Item b to b
5	1483	1830	970
10	2680	3310	2090
33	167	96.5	42.5

4.4 Pin-to-Pin Calculated Energies

The pin-to-pin energies supplied to the EEDs during the test can be calculated using the factors given in Table 3-3. Table 4-16 gives the lowest firing energies for the pin-to-pin tests. The accuracy of these energies can be questioned on the grounds that we are using the RF continuous wave resistance of the devices in the calculation whereas the actual phenomena is transient in nature. We feel that the error so introduced will be no more than that associated with the overall test instrumentation so that the calculated energies given in Table 4-16 are at least a good approximation.

4.5 Pins-to-Case and Bridge-to-Bridge Energies

Table 4-17 gives the pins-to-case and bridge-to-bridge energies supplied to the EEDs during the tests. The energies are calculated using equation 3-10 and the data given in Table 3-4. δ is assumed to be one. The same remarks concerning continuous wave impedance versus transient behavior as given in Section 4.3 apply.

Table 5-1

SUMMARY OF PIN-TO-PIN TEST RESULTS
Percentage Fired*

	Test Frequency (MHz)	Peak Current (Amperes) 75	200	300	400	500	600	700
Hi-Shear Item	5		$0^{(4)}$	$12.5^{(8)}$	$50^{(4)}$			
	10		$0^{(4)}$	$0^{(4)}$	$8.3^{(12)}$	$12.5^{(8)}$		$25^{(4)}$
	45	$0^{(12)}$						
FND Item	5			$0^{(16)}$	$16.6^{(6)}$	$100^{(10)}$		
	10			$0^{(6)}$	$0^{(6)}$	$0^{(8)}$	$25^{(4)}$	$50^{(6)}$
	45	$0^{(12)}$						

*The number in parentheses is the number of items exposed at a particular stimulus level.

5. SUMMARY AND COMMENT

Table 5-1 summarizes the results of the pin-to-pin tests in terms of the percentage of items fired at a given stimulus level. The percentage fired is computed by dividing the number of items fired at a given level by the number exposed. Table 5-2 summarizes the same type data for the pins-to-case and bridge-to-bridge tests.

Study of these tables emphasizes the lack of high stimuli level at 33 and 45 MHz. Any general trends are partially obscured by this lack; however, we can estimate that the Hi-Shear item begins to show sensitivity, to pin-to-pin current pulses of our type, at amplitudes around 200 amps for the overall frequency range (5 to 45 MHz) considered. The sensitivity seems to decrease with increasing frequency. The same remarks apply to the FND item except the sensitivity begins around 300 amps.

Little can be said about the pins-to-case and bridge-to-bridge results except that the FND item survived the 28,000 peak volt stimulus and the Hi-Shear item did not.

The similarity of the lowest energies for pin-to-pin firings of both the Hi-Shear item and FND item at 5 and 10 MHz (see Table 4-16) at least points to the fact that the EEDs are firing in a normal bridgewire mode.

More tests could easily verify this speculation.

In our opinion the presented work has served two useful functions. It has given us general levels for the EEDs sensitivity to very short, fast risetime pulses and has demonstrated the feasibility of such determinations. Accurate determinations of statistical levels for these sensitivities can be obtained by simply testing more samples in a Bruceton type evaluation.

We speculate that pulses of more complex form could also be used as stimuli by superposition of the basic pulse types used in this study.

Table 5-2

SUMMARY OF PINS-TO-CASE AND BRIDGE-TO-BRIDGE TEST RESULTS
Percentage Fired*

	Test Frequency MHz	D. C. Capacitor Voltage (Volts) 5000	28,500
Hi-Shear Item p-c	5	0(2)	0(9)
	10		20(10)
	33	0(10)	
FND Item p-c	5	0(3)	0(3)
	10	0(2)	0(6)
	33	0(7)	
FND Item B-B	5	0(5)	0(8)
	10	0(1)	0(6)
	33	0(7)	

*The number in parentheses is the number of items exposed at a particular stimulus level.

II-7. REPEATABLE HERMETIC SEAL QUALITY DETERMINATIONS BY THE HELIUM BOMBARDMENT TECHNIQUE

By

W. P. Garton

North American Rockwell Corporation
Space Division

INTRODUCTION

For many components, hermetic seals to prevent gaseous interchanges between the interior of the part and service environmental atmospheres are specified. If reliability requirements are high and function may be impaired by gaseous interchanges, individual seal quality verification may be justified. It then remains to choose a method of test and to specify an acceptance/rejection criterion.

Information is expensive. The test method employed should detect all items with faulty seals but usually need not provide a precise measure of seal quality for satisfactory parts. If large numbers of parts are involved, a simple GO/NO-GO test is desirable. Helium bombardment leak testing, as routinely practiced, is simple, inexpensive, and rapid. It has been widely used for seal verification of small aerospace ordnance devices. A common complaint, however, is that the test results are qualitative, only. Repeated tests of a part do not yield quantitatively identical results.

In theory, the rate of decay of measured leak rate following bombardment provides an accurate, repeatable index to a part hermetic seal quality parameter to be called A_L, if only non-viscous flows occur. Escape of contained gases by viscous flow during the time interval between two leak rate measurements will result in a conservative error in seal quality estimation.

In this paper, one method for determining the maximum permissible value of A_L for a particular sealed component is shown, together with a method for determining the bombardment time required for verification of seals of that quality by the leak rate decay method. Factors affecting the feasibility and practicability of leak rate decay seal verification are discussed, and the need for validation of any proposed test method is stressed.

BOMBARDMENT LEAK TESTING

Bombardment leak testing consists of three basic steps:

a) "Bombing" the components to be tested in a chamber filled with a tracer gas at a pressure P_E for a specified time t_E.

b) Removing the parts from the bombing atmosphere and, within a specified time, t_R, measuring the rate at which the tracer gas (forced into the parts during the bombing step) is leaking back out of each part.

c) Comparison of the leak rate measurement with an acceptance/rejection criterion value for the particular part.

While these three steps are always performed, variations in execution may include an initial "evacuation" step in which the parts are subjected to a high vacuum to remove some of the initially-contained gas prior to the bombardment, and a "parking" step in which bombed parts in excess of the number of leak measurements which may be performed in the time t_R are held in a chamber filled with the tracer gas at one atmosphere until leak rate measurement can be accomplished. The bombing pressure P_E is usually on the order

of two to ten atmospheres at ambient (room) temperature. Sometimes bombardment is conducted with a gaseous mixture (such as 10 percent helium, 90 percent nitrogen) rather than with a pure gas. The bombardment duration, t_E, is normally chosen to be from ten minutes to two hours or more. The maximum permissible delay time, t_R, between bombardment and leak rate measurement ranges from about 15 minutes to one hour. The leak rate measurement is ordinarily made with a mass spectrometer leak detector having a sensitivity of 5×10^{-10} atm-cc per second or better. Helium is commonly used as the tracer gas because it is inert, non-toxic, inexpensive, and the normal atmospheric concentration is only 5 parts per million.

PROBLEMS IN INTERPRETING TEST RESULTS

Several ambiguities or uncertainties are inherent in the bombardment/leak measurement technique as routinely employed. Some of these are:

a) Inability to determine flow mode

No single-measurement scheme is capable, over a wide range of observed leakage rates, of resolving the dominant flow regime (turbulent viscous, laminar viscous, choked, transition, molecular, diffusion, or permeation). This inability to resolve flow mode renders extrapolation from leak rate measurement to seal performance under service conditions a sporting proposition.

b) The "Gross Leaker" problem

If the sealed volume is tiny and the leak passage(s) large, it is possible that virtually all tracer gas will be drawn out of the part under test while pumping down to the high vacuum (50 to 100 microns) required for mass spectrometer leak rate measurement. A gross leaker may show an acceptably small tracer gas outflow by the time the measurement is made. For this reason, helium bombardment leak testing is frequently used as a fine leak test in conjunction with some less sensitive test to detect gross leakers. Parts which pass the fine leak test are subjected to the gross leak test. Unfortunately, parts with tiny net sealed volumes are not suited to bubble testing, one of the more common forms of gross leak testing.

c) "Cascade" effects

If manufacturing processes can produce porous structures or small partially-sealed cavities external to the main sealed chamber, leak rate measurements will be erroneously inflated, with consequent hazard of rejecting satisfactory parts.

d) Absorption and adsorption effects

If part materials can absorb the tracer gas or adsorb it on external surfaces during bombardment, leak rate measurements will be exaggerated. The error will decrease with time following bombardment, but prompt measurement is usually specified. Air-washing or nitrogen scrubbing is sometimes employed to speed the removal of adsorbed tracer gas. The effect of absorption/adsorption is to make more likely the rejection of satisfactory parts.

e) Variations in time of measurement

Ordinarily small parts are bombarded in batches, but leak rate measurements must be performed sequentially. The first part tested may have its leak rate measured within one or two minutes following bombardment, the last perhaps as much as an hour later. Identical parts cannot yield identical leak rate measurements when tested in this fashion.

f) Inaccuracy of the reference leak standard

Tracer gas reference leaks are not traceable to calibration sources maintained by the National Bureau of Standards. Overall agreement between leak standards in normal use is not better than ± 50 percent[1].

g) Failure to consider part internal free volume in specifying test conditions and leak rate criterion

To a first approximation, observed leak rate following a specified bombardment will be inversely proportional to part internal free volume. Unless seal quality requirement is known to increase as the sealed free volume shrinks, this means that a fixed leak rate rejection criterion discriminates against smaller parts.

A further complication arises in attempting to apply either the "Leak Conductance" or "Leak Size" concept to bombardment leak test results. This can be misleading because of the uncertainty concerning the dominant flow regime responsible for the observed leak rate. For the purposes of this discussion it is sufficient merely to characterize gaseous flows through solid barriers as viscous or non-viscous. Viscous flows are gross currents driven through leak passages by a difference in the total pressures upstream and downstream of the barrier. Tracer gases will be present in such flows in approximate proportion to their relative concentrations in the upstream gas mixture. Non-viscous flows are described as molecular, diffusion, or permeation, but all are driven, to a first approximation, by the difference in partial pressures of each gas species across the seal. For mixtures of gases the terms "upstream" and "downstream" have no meaning, or must be considered as uniquely determined for each gas species present, and net molecular and permeation flows of the different species may be proceeding in opposite directions, or from a region of low total pressure to one of high total pressure.

Tables I and II provide a gross characterization of viscous and non-viscous flows appropriate to the interpretation of bombardment leak testing results. In these tables, d represents the maximum cross-sectional dimension of a leak passage, and λ is the mean free path of the gas molecules.

TABLE I

VISCOUS FLOWS

Type	Leak Passage Dimension, d	Driving Force	Composition
Transition	$\lambda < d < 100\lambda$	$(P_1 - P_2)$	Approximately same as upstream mixture
Laminar	$100\lambda < d$ $(N_{Re} < 1200)$	$(P_1^2 - P_2^2)$	Same as upstream mixture
Turbulent	$100\lambda < d$ $(N_{Re} > 2100)$	$(P_1^2 - P_2^2)^{1/2}$	Same as upstream mixture
Choked (sonic	$100\lambda < d$ $(P_1/P_2 \geq r_c)$	P_1	Same as upstream mixture

(1) Leakage Testing Handbook, July 1969, NAS-38843

TABLE II

NON-VISCOUS FLOWS

Type	Leak Passage Dimension, d	Driving Force	Composition
Molecular	$d < \lambda$	$(P_1 - P_2)_i$	All flows of gas species "i" only
Diffusion	$\lambda < d$ $(P_1 = P_2)$	$(P_1 - P_2)_i$	
Permeation	undefined	$(P_1 - P_2)_i$	

Table III (adapted from data in the Leakage Testing Handbook) shows the difficulty in determining the mode of flow when it is known that only one physical leak passage exists, and a difference in total pressure of one atmosphere is assumed to be responsible for the observed leak rate. In bombardment leak testing, the total pressure differential during bombardment may be more or less than one atmosphere. During the leak rate measurement step the total pressure differential may again be either greater or less than one atmosphere; further, the concentration of tracer gas in the total leakage occurring during the measurement can be only crudely surmised. And more than one leak passage and flow mode are usually involved.

TABLE III

FLOW MODE vs LEAK RATE*
THROUGH ONE LEAK CHANNEL

Mode	Leak Rate, Q (atm-cc/sec)
Turbulent	$10^{-2} < Q$
Laminar	$10^{-6} < Q < 10^{-1}$
Transition	$10^{-7} < Q < 10^{-4}$
Molecular	$Q < 10^{-7}$

* Total Pressure Differential approximately one atmosphere

HERMETIC SEAL QUALITY REQUIREMENTS

The physical seals produced by any manufacturing process will vary in quality. In general, any seal having one or more leak passages large enough in cross-section to permit viscous flow will also contain finer leak passages capable of allowing gaseous transfer by permeation or molecular flow mechanisms. All real seals will permit non-viscous flow of one kind or another, and seals with pin-hole leaks large enough to permit viscous flows to develop will also permit gaseous diffusion exchanges when internal and external pressures are equalized. It seems, therefore, that non-viscous flows will take place during quiescent storage periods, bombardment, and leak rate measurement, but that viscous flows, if they occur at all, can take place only when the external pressure is varied, as in the bombardment and leak rate measurement steps of the leak test procedure.

Bombardment leak testing, as normally practiced, is oriented toward the detection of parts with seals exhibiting viscous leak characteristics. Acceptance criteria usually assure rejection of all parts with viscous leaks. For many parts such a criterion may not impose a high rejection rate while assuring that accepted parts have seals adequate for the anticipated service requirement. It is also possible that such a criterion may lead to the rejection of part with seals adequate for the service requirement, or that it may permit the acceptance of unsatisfactory parts.

Ordnance devices intended for use on aerospace launch vehicles normally have a brief service life following installation. Exposure to flight environments containing gas species injurious to the part, or to a hard vacuum, is brief.

The most stringent requirement for seals on such parts is to exclude moisture (in the form of water vapor) during extended periods of atmospheric storage prior to use. Inasmuch as daily atmospheric tidal excursions are very small, and barometric pressure changes associated with weather patterns rarely exceed ± 5 percent of one atmosphere, external total pressure variations are not sufficient to produce significant amounts of viscous flow through even large leak passages. In bunkers, daily and seasonal temperature cycles seldom exceed ± 1 percent and ± 5 percent, respectively. These figures may, perhaps, be doubled for open storage. Nevertheless, internal pressure variations caused by storage environment temperature changes cannot drive large viscous flows.

It follows, then, that the dominant mechanisms for moisture transport into parts during atmospheric storage will be non-viscous. And an appropriate measure of seal quality for this purpose (withstanding long-term atmospheric storage) will be one which estimates a seal's ability to limit non-viscous gaseous exchanges, in particular molecular and diffusion flows. Such a measure may be found in the concept of an "equivalent molecular leak area," to be called A_L, through which non-viscous flows of various gas species will pass in direct proportion to their differences in partial pressure. Equalization of the partial pressures of a particular gas species on the two sides of the barrier will then take place exponentially with time. The net non-viscous flow rates of the various gas species present also decay exponentially with time, unless absorption, reaction, permeation, or chemical reaction intervene to remove particles of the gas mixture on one or both sides of the barrier. Such a condition would exist for atmospheric water vapor entering an ordnance part by non-viscous flow, and then going into solution, or otherwise reacting chemically with the explosive, pyrogen, or other materials inside the part.

For ordnance parts which will be required to limit moisture ingress during extended periods of atmospheric storage, it becomes possible to estimate the maximum tolerable value of the effective molecular leak area parameter, A_L. This is accomplished as follows:

a) The maximum mass of water, m_w, in grams, which can be introduced into the sealed cavity without impairing functional capability is estimated or empirically determined.

b) Part storage conditions (temperature and water vapor pressure) for the designated maximum required storage life are averaged or conservatively estimated (100 percent relative humidity at 100 deg F overstates the mean water vapor pressure at Kennedy Space Center by a factor of two).

c) Assuming that each water molecule is absorbed or reacted with immediately upon entering the part, and hence that internal water vapor pressure remains zero throughout the storage period, the maximum tolerable uniform rate of water transport through the seal is found to be:

$$m_w = \frac{m_w}{t_s} \quad \text{(grams/sec)} \qquad (1)$$

where t_s is the storage period in seconds.

d) From the kinetic theory of gases the number of water molecules per second impacting the effective leak area A_L is estimated as

$$Z = 3.537 \times 10^{22} \frac{P_w A_L}{(M_w T)^{1/2}} \text{ (molecules/sec)} \qquad (2)$$

where P_w is the partial pressure of water vapor in the external atmosphere in mm Hg. M_w is the molecular weight of water (18.02 grams/mole). T is the absolute temperature (mean) in degrees Kelvin, and A_L is measured in square centimeters.

From equations (1) and (2) above, the maximum permissible leak area can be calculated:

$$A_{L\max} = \frac{4.02\ m_w\ (T^{1/2})}{t_s\ P_w} \ (\text{cm}^2) \qquad (3)$$

where, again m_w is the maximum mass of water which can safely be admitted during the storage period t_s. T is the mean temperature and P_w the mean water vapor pressure. For assumed environmental conditions of 100% relative humidity at 100 degrees F (311 K), (3) reduces to

$$A_{L\max} = 1.45 \frac{m_w}{t_s} \ , \ (\text{cm}^2) \qquad (3A)$$

DETERMINING THE VALUE OF A_L BY LEAK RATE DECAY

Having postulated that part serviceable life in the storage environment depends on a leak area parameter A_L, and found a way to estimate the maximum tolerable value of A_L, it remains to devise a test method for determining the A_L measure of a real part, or at least of verifying that this measure is less than $A_{L\max}$. Remembering that the A_L measure arose from considerations of non-viscous flow, for which exponential laws of partial pressure decay (or equalization) hold, it may be inferred that the partial pressure of a tracer gas, introduced into a sealed cavity during manufacture or bombardment, will decay exponentially with time during any period in which no viscous flows occur and the partial pressure of the tracer gas in the surrounding atmosphere is essentially zero. (Such conditions obtain if no physical leak passages exist for which $d > \lambda$, or if internal and external total pressures are equal). It may also be concluded that if internal partial pressure of the tracer gas is decaying exponentially, so also will the observed leak rate of the tracer gas when measured on a device such as the mass spectrometer leak detector. This exponential decay of the observed leak rate will hold true even if viscous flows take place during the leak rate measurements themselves, provided that essentially no viscous flow occurs between measurements. This is true because non-viscous flows (leak rates) are directly proportional to partial pressure, and viscous flows contain any tracer gas in a concentration directly proportional to its internal partial pressure. In stating these general conclusions about exponential decay of the observed leak rates, it is to be understood that constancy of the exponent of decay demands constant temperature and fixed viscosity at all tracer gas concentrations (if any viscous flow occurs during measurement). Normal variations in room temperature and viscosity ranges for mixtures of air or nitrogen and helium need be of no concern for practical application of the concept.

The physical law governing the decay of measured leak rate through non-viscous flow at constant temperature may be derived as follows:

Let N be the number of tracer gas molecules in the net sealed volume V_n at the time t, and let the temperature be constant at the value T. Then the

partial pressure of the tracer gas contained in V_n is:

$$P_a = \frac{N}{V_n} \times \frac{22414 \text{ cm}^3/\text{atm-mol} \times 760 \text{ mm Hg/atm}}{6.023 \times 10^{23} \text{ molecules/mol}} \times \left(\frac{T}{T_o}\right) \text{ (mm Hg)},$$

where V_n is given in cm^3, T is in degrees K, and T_o is 273 K. From which,

$$P_a = 1.035 \times 10^{-19} \left(\frac{NT}{V_n}\right) \text{ mm Hg.} \qquad (4)$$

Using equations (2) and (4), the change dN in N during the interval dt is:

$$dN = -Z\, A_L dt = \frac{-3.664 \times 10^3\, NTA_L\, dt}{V_n (M_a T)^{1/2}} \text{ (molecules)},$$

where M_a is the molecular weight of the tracer gas and dt is given in seconds.

Rearranging,

$$\frac{dN}{N} = -3.664 \left(\frac{T}{M_a}\right)^{1/2} \left(\frac{A_L}{V_n}\right) dt \text{ (dimensionless)} \qquad (5)$$

Equation (5) may be integrated from an initial number of molecules, N_1, at time t_1 to a lesser number of molecules, N_2, at time t_2:

$$\int_{N_1}^{N_2} \frac{dN}{N} = -3.664 \left(\frac{T}{M_a}\right)^{1/2} \left(\frac{A_L}{V_n}\right) \int_{t_1}^{t_2} dt \qquad (6)$$

From which,

$$\ln \left(\frac{N_2}{N_1}\right) = -3.664 \left(\frac{T}{M_a}\right)^{1/2} \left(\frac{A_L}{V_n}\right) (t_2 - t_1), \qquad (7)$$

where $(t_2 - t_1)$ is expressed in seconds. Since partial pressure of the tracer gas in V_n is, at constant temperature, directly proportional to N, and it has been deduced that, under the assumed conditions, observed leak rate is proportional to partial pressure, it must also be true that

$$\ln \left(\frac{Q_{m2}}{Q_{m1}}\right) = -3.664 \left(\frac{T}{M_a}\right)^{1/2} \left(\frac{A_L}{V_n}\right) (t_2 - t_1) \qquad (8)$$

where Q_{m1} and Q_{m2} are the observed leak rates at times t_1 and t_2 respectively, and are expressed in the same quantitative units, such as std atm-cc/sec or torr-liters/sec.

It is convenient to define a time interval, t^*, called the part characteristic time for the tracer gas "a" at the temperature T, such that t^* is the time interval required for the observed leak rate to decrease by one order of magnitude. Then:

$$\ln (0.1) = -2.303 = -3.664 \left(\frac{T}{M_a}\right)^{1/2} \left(\frac{A_L}{V_n}\right) t^*.$$

From which,

$$t^* = 6.285 \times 10^{-4} \left(\frac{M_a}{T}\right)^{1/2} \left(\frac{V_n}{A_L}\right) \text{ (seconds)}. \qquad (9)$$

Or,

$$t^* = 1.746 \times 10^{-7} \left(\frac{M_a}{T}\right)^{1/2} \left(\frac{V_n}{A_L}\right) \text{ (hours)}. \qquad (9A)$$

For helium ($M_a = 4.003$) at room temperature (75F = 297K), t^* is given by:

$$t^*_{He75} = \frac{2.027 \times 10^{-8}}{\left(\frac{A_L}{V_n}\right)} \text{ (hours)}. \qquad (9B)$$

It will be noted that the part characteristic time, t^*, is analogous to the half-life parameter of radioactive isotopes. Equation (9B) is plotted in Figure 1. for a small range of $\left(\frac{A_L}{V_n}\right)$ values. Assuming that only non-viscous flows occur at the temperature T, the time histories of tracer gas partial pressure in the sealed volume during bombardment and after are shown in Figure 2. as a function of elapsed time in t^* units. If internal tracer gas partial pressure following bombardment is sufficient to drive a measurable flow, Q_m, through

the seal, Q_m will be found to decay with time as shown on the semi-logarithmic or ratio plots of Figures 3A and 3B for the strictly non-viscous and mixed viscous/non-viscous cases, respectively. It will be noted that Q, the flow rate, and Q_m, the measured leak rate for the non-viscous case, are indistinguishable, because the tracer gas leak rate is not a function of the external total pressure (but only of external tracer gas partial pressure, which is taken to be essentially zero during either room atmospheric or leak measurement vacuum conditions). In the mixed viscous/non-viscous case, it is seen that the decay in Q with time is more rapid than exponential until internal and external total pressures are equalized; thereafter, Q decays at the exponential rate appropriate to the $\left(\frac{A_L}{V_n}\right)$ measure of the part. Q_m, the measured leak rate, presumably observed only intermittently during the time period depicted on the chart, is much larger in absolute value than Q, but, on the ratio scale, the decay of Q_m parallels that of Q (this is sufficiently exact if total leak rate measurement time is small in comparison to t^*, so that the momentarily high leakage rates during measurement may be ignored).

Observing the rate of leak decay after sufficient time has elapsed since bombardment to allow internal total pressure to equalize with room atmospheric and for the escape of the greater portion of externally adsorbed tracer gas permit the value of t^* to be estimated more accurately and, through equation 9A (or 9B for helium), the value of A_L to be estimated. The use of an acceptance/rejection chart such as Figure 4. is suggested. Two leak rate measurements taken at a suitable time interval following bombardment suffice to establish the exponential rate of leak decay, and hence of part t^* and A_L values (V_n being known or calculated with some degree of precision). The part acceptance criterion, t^*_{min}, is calculated with the aid of equation (6), using the maximum tolerable value of A_L, A_{Lmax}, and the minimum value of V_n anticipated from production tolerances in part dimensions and explosive loadings. If two leak rate measurements, Q_{m1} and Q_{m2} of a part are taken at times t_1 and t_2 following bombardment ($t_2 - t_1 = \Delta t_m$) and the ratios Q_{m2}/Q_{m1} plotted on the chart of Figure 4., it is immediately apparent that part A is acceptable and that part B is not.

DETERMINING THE REQUIRED BOMBARDMENT DURATION, t_E

Supposing that the maximum tolerable value of A_L, A_{Lmax}, for some part has been determined from equation (3), or by some other method, and that the existing leak detection equipment can clearly and repeatably measure some leak rate Q_o (Q_o is usually taken to be at least one order of magnitude greater than the minimum detectable leak rate), the minimum required bombardment duration for leak rate decay seal quality determination may be found in the following manner:

a) Choose a practicable bombardment pressure, P_E(mm Hg).

b) Using the partial pressure relationship of equation (2), we have:

$$\frac{Za}{2.69 \times 10^{19}} = \frac{1,314\ Pa}{(M_a\ T)^{1/2}} \times A_{Lmax} = Q_o \text{ atm-cc/sec} \qquad (10)$$

For helium at 75F, this may be written:

$$P_{He75} = \frac{Q_o}{38.1\ A_{Lmax}}, \text{ mm Hg,} \qquad (10A)$$

where p_{He75} is the partial pressure required to drive helium at the leak rate Q_o through a seal of quality A_{Lmax} by non-viscous modes of flow.

c) Form the ratios $\left(\frac{A_{Lmax}}{V_n}\right)$ and $\left(\frac{p_a}{P_E}\right)$ and use a chart similar to Figure 5. to determine the minimum bombardment duration required.

The procedure described above will yield a bombardment duration sufficient to assure the measurable flow rate, Q_o of tracer gas through the poorest acceptable seal immediately upon termination of bombardment. Ordinarily, however, the quality of production seals will be much better than the acceptance criterion, A_{Lmax}. As a rough rule of thumb, if only non-viscous flows take place, a part having an A_L measure one tenth of A_{Lmax} will need to be bombarded one hundred times as long if the same initial leak rate, Q_o, is to be observed. As part seal quality improves, therefore, bombardment times to produce measurable leak rates may become impractically long. To determine if it will be economically feasible to measure, by the leak rate decay method, the seal quality of all production parts, steps (b) and (c) above may be repeated, using $A_{Lmin\ prod}$ (the A_L measure of the "best" seal anticipated from the manufacturing process) instead of A_{Lmax}. If p_a/P_E is found to exceed unity, infinite bombardment times will fail to produce the measurable leak rate Q_o. If P_E cannot be safely increased, but seal quality measurements are still required, accumulation techniques may increase leak measurement sensitivity sufficiently to make leak rates much smaller than Q_o visible. For parts with very tiny internal volumes (0.01 cc or smaller), absence of measurable leak rates following bombardment may not rule out the possibility of gross viscous leaks. Immersion or bubble testing cannot be relied upon to detect gross leaks in such parts and again an accumulation technique may be employed. Mr. T. L. Altshuler has patented such a method.[2]

EXPERIMENTAL VERIFICATION

In October, 1970, an investigation into anomalous bombardment leak testing results on Saturn V CDF ordnance components was conducted under Change Order 1994 to NASA/MSFC Contract NAS7-200.[3] During the course of this investigation the theoretically-predicted exponential decays of measured leak rate with time during periods of non-viscous flow were observed. Test specimens included special non-viscous leak devices (AN unions with machined Teflon plugs), and small aircraft ordnance parts whose seals exhibited viscous flow capability. Repeatable seal quality determinations were made on both kinds of test parts. For the parts capable of viscous flow, repeatable determinations were obtained only when initial leak rate measurements were delayed until internal total pressures had decreased to near room ambient conditions.

The parts which had been of immediate concern in the investigation proved to have seals many orders of magnitude better than the service requirement. In terms of equation (10A), $\left(\frac{P_{He75}}{P_E}\right) \gg 1$, and bombardments of infinite duration at pressures capable of being withstood by the parts would not produce

(2) Reliable Method For Testing Gross Leaks in Semiconductor Component Packages, NASA Tech Brief 68-10562, and NASA Technology Utilization Division's Technical Support Package PB 180914

(3) North American Rockwell Corp., Space Division, "Final Report, Helium Leak Test Procedural Investigation", Dec 11, 1970, (Letter Report)

measurable leak rates. The leak rate decay method, therefore, could have been applied in verifying the seals of these parts only with the aid of an accumulation technique. It was embarrassing to note, however, that all three parts which had been rejected for excessive leak rate when inspected by the approved method had seals indistinguishable from those of three accepted parts - and all six parts had real leak rates below the threshold of detection following a 30-day bombardment.

PRACTICAL SIGNIFICANCE OF RESULTS

The results of this analysis and its experimental verification have certain aspects of practical significance.

a) It is meaningful to specify seal hermetic quality requirements of a part in terms of the parameter A_L.

b) Minimum bombardment duration for a part should be determined from equation (10A) and Figure 5. (Or a similar chart.)

c) Feasibility of leak rate decay method must be either calculated or empirically determined for the range of production seal qualities anticipated.

d) The proposed procedure must be validated on actual production hardware items to be sure that cascade or adsorption effects are not biasing results unfavorably.

e) While the leak rate decay method is based on the assumption of non-viscous flow, the results obtained are always conservative: if viscous flow occurs, it will cause an overestimate of the seal effective leak area, A_L.

f) Precise control of the bombardment duration and pressure are not required, as a large initial leak rate measurement is not an automatic cause for rejection. Overnight bombardments may prove convenient.

g) Precise control of the time interval, $\Delta t_{m,n}$, between leak rate measurements is not required (but the time should not be so short that no leak rate decay can be observed, nor so long that Q_{2m} is below the leak detector capability).

h) Lack of confidence in leak standard absolute accuracy, presence of a residual fill, or variation in bombardment parameters will not affect the ability of various testing stations to determine the same value of A_L for a part whose actual seal quality has not changed in the time interval between tests.

If it appears that production seal quality is so high that ordinary leak decay testing is impossible or impracticable, several alternatives may be considered. The choice among them should depend upon both seal quality and seal confidence (part reliability) requirements:

1) Employ individual seal verification by bombardment and accept viscous leak rejection criterion (existing technique, save for determination of bombardment duration).

2) Abandon individual seal verification and adopt some form of materials/process verification (a destructive sampling method, for instance).

3) Use (1) above in conjunction with a gross leak test (validate method for parts with tiny sealed volumes).

4) If sealed volumes are too tiny for conventional gross leak tests, yet part reliability considerations demand individual seal verification, some form of accumulation test must be devised, with or without leak rate decay techniques. In any event, such a test must be validated for each component.

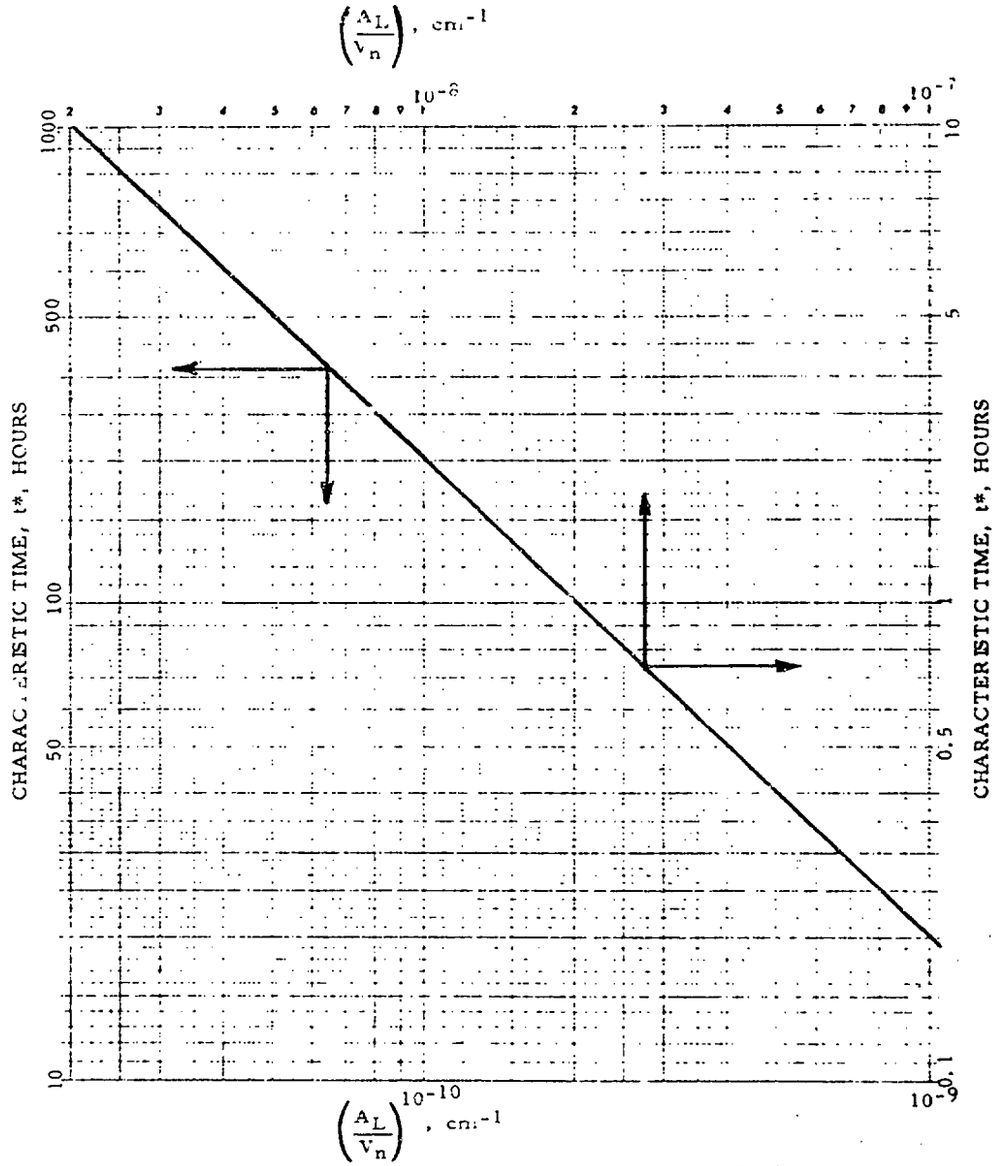

FIGURE 1. - PART CHARACTERISTIC TIME vs $\left(\frac{A_L}{V_n}\right)$ RATIO, TRACER GAS HELIUM AT 75F

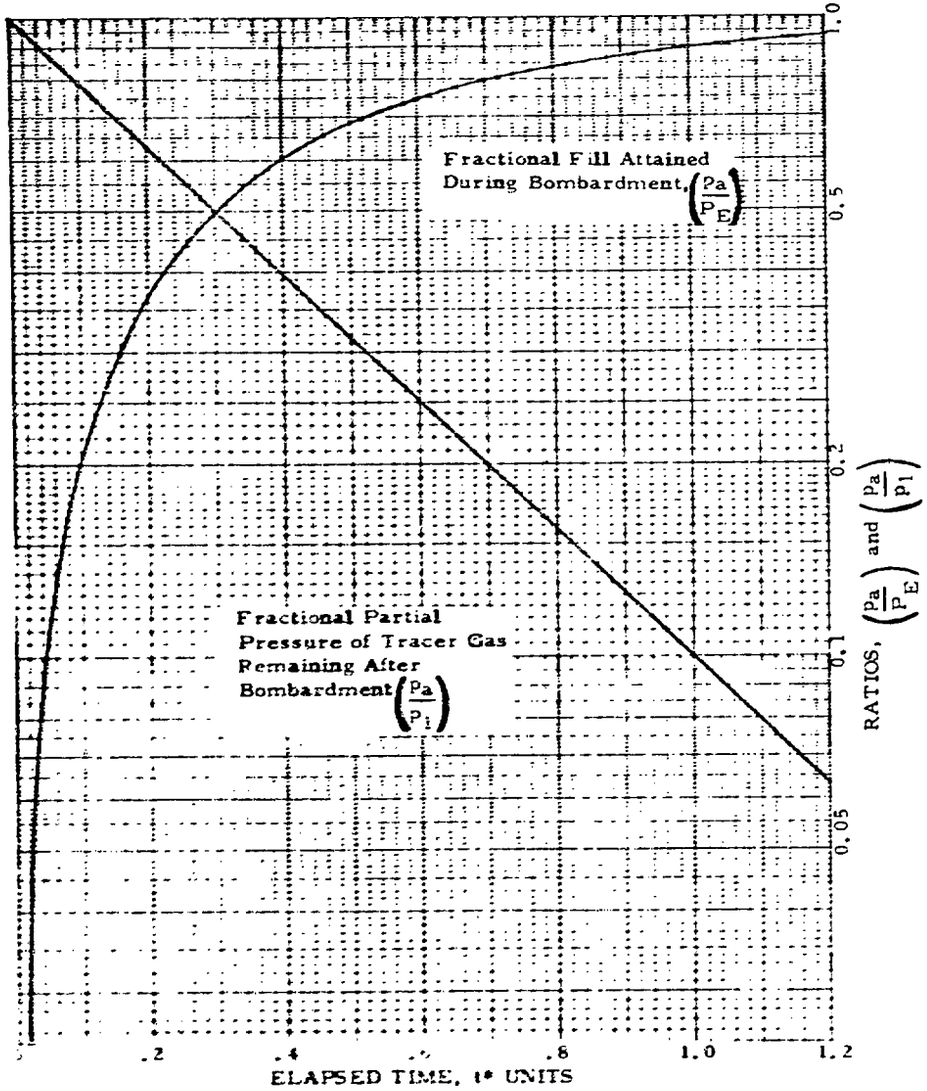

FIGURE 2. - TRACER GAS PARTIAL PRESSURE HISTORIES DURING & FOLLOWING BOMBARDMENT, NON-VISCOUS FLOW

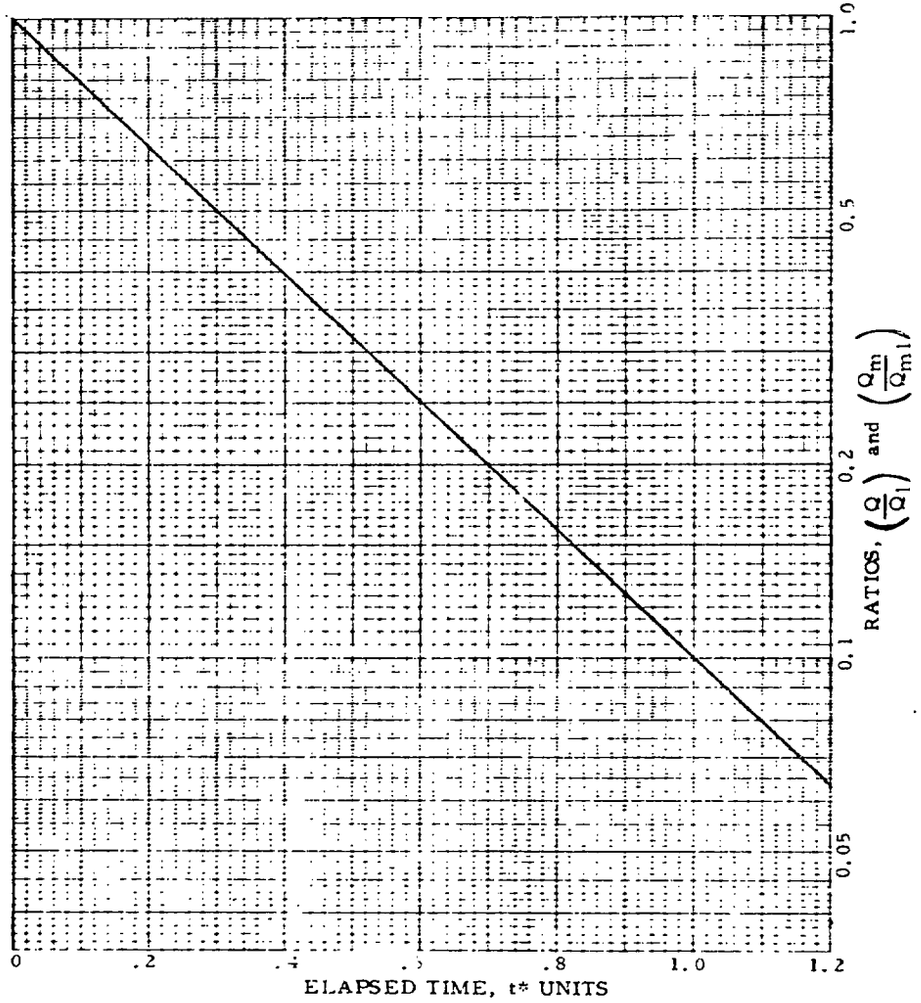

FIGURE 3A. - HISTORIES OF AMBIENT AND MEASURED LEAK RATES FOLLOWING BOMBARDMENT, NON-VISCOUS FLOW

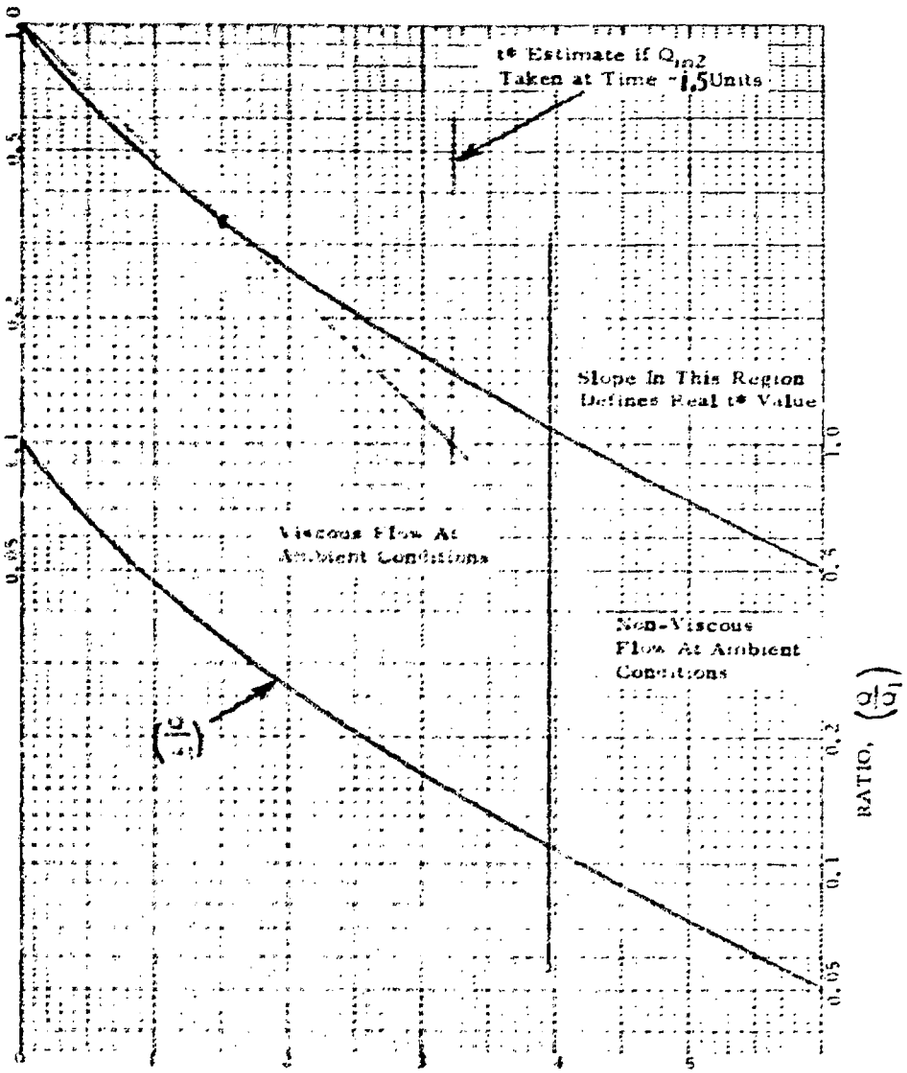

FIGURE 3B. - HISTORIES OF AMBIENT AND MEASURED LEAK RATES FOLLOWING BOMBARDMENT, VISCOUS AND NON-VISCOUS FLOW

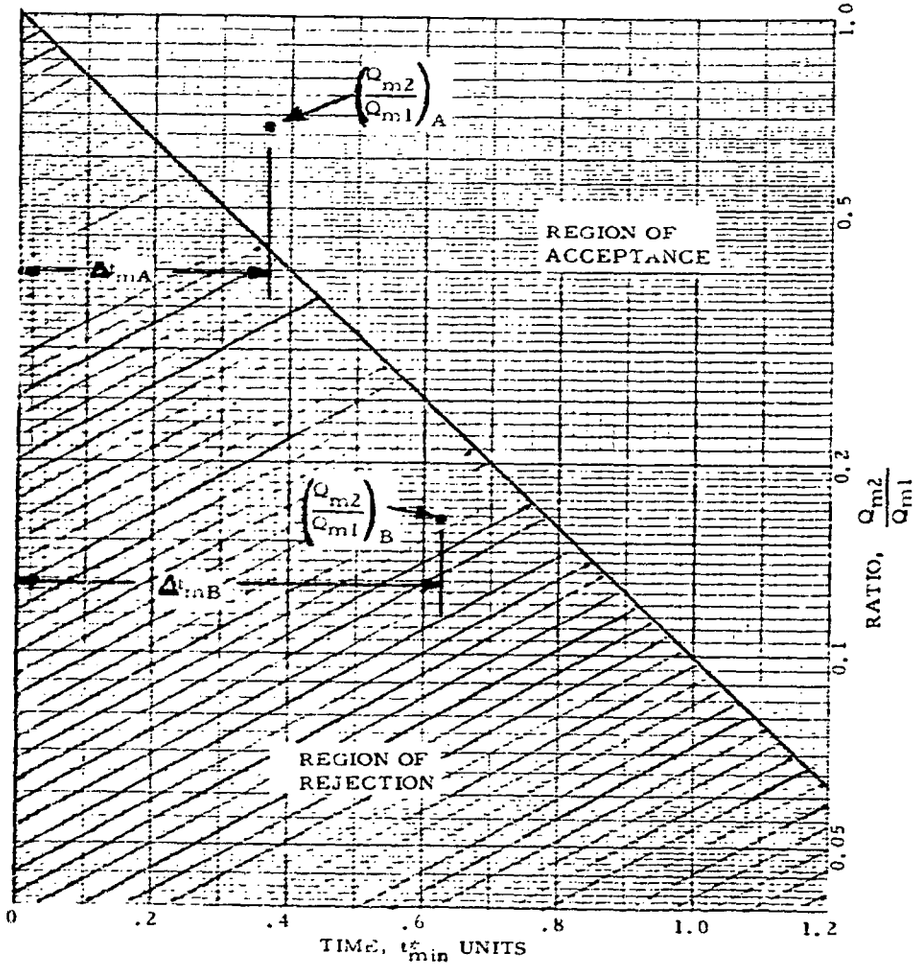

FIGURE 4. - LEAK RATE DECAY ACCEPTANCE/REJECTION CRITERION CHART

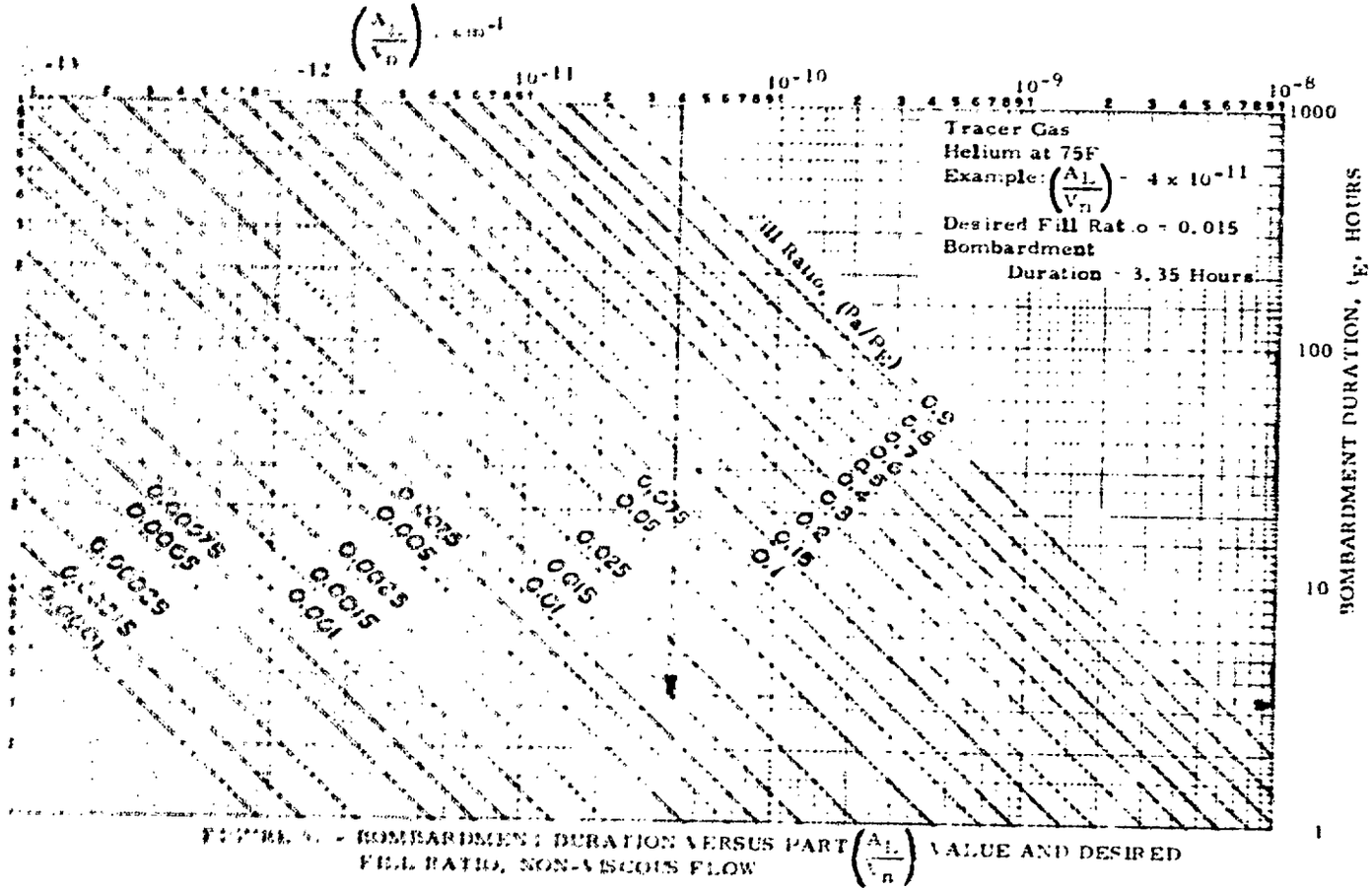

FIGURE 6 - BOMBARDMENT DURATION VERSUS PART $\left(\frac{A_L}{V_n}\right)$ VALUE AND DESIRED FILL RATIO, NON-VISCOUS FLOW

II-8. MINUTEMAN HERO TESTING

Leonard Doellner
The Boeing Company
Seattle, Washington

ABSTRACT

This paper delineates methods used by The Boeing Company in implementing HERO (Hazards of Electromagnetic Radiation to Ordnance) missile pre-flight checkout procedures on the Minuteman Weapon System. The work started on the first Minuteman I System in the early 1960's and is continuing for all new configurations of Minuteman. Early HERO instrumentation consisted of simple voltage monitoring techniques. Present instrumentation systems are capable of measuring the effects of low level transient energy (50 microjoules) and high frequency (to 10 gigahertz) steady state or transient phenomena. An EMP level ordnance monitoring system employing fiber optic data links is described.

INTRODUCTION

The Minuteman EED's (electro-explosive ordnance devices) are used for ejecting ground umbilical cables, recovering the launch facility cover, igniting rocket motors, separating expended stages, igniting generators used for roll control and thrust vector control functions, and to initiate various re-entry/control functions after main engine burn (Figure 1). The EED's used are rated one ampere no fire. Analytical RF susceptibility evaluations of the Minuteman ordnance systems have been made by The Franklin Institute (References 1 and 2).

HERO TESTING

The first Minuteman HERO test consisted of monitoring the spurious signals present on the simulated bridgewires of the ordnance devices in the Minuteman system. In concept this represents the basic approach to HERO monitoring. The frequency response limitations of the instrumentation used for these early measurements led to improved instrumentation systems described below.

Vacuum Thermoelements

The second Minuteman HERO test employed vacuum thermoelement* EED simulators. An EED bridgewire of 0.2 ohm, as an example, may be simulated by a vacuum thermoelement with a heater resistance of 0.2 ohm for any frequency of interest up to 10 megahertz. (The pin-to-pin impedance of a nichrome bridgewire remains essentially the same as its DC resistance to approximately 10 megahertz). For a weapon system where interference sources are limited to switching transients whose energy falls below 10 megahertz, thermoelement devices may be used as acceptable EED simulators, with the thermocouple accurately monitoring interference thermal effects for the bridgewire pin-to-pin mode.

---

* A vacuum thermoelement is a bi-metallic thermocouple element enclosed with a heater (bridgewire) element in an evacuated glass envelope. The bi-metallic portion is separated physically from the bridgewire by material which exhibits simultaneously a high thermal conductivity and a high electrical impedance.

Thin Film Thermocouples

Increased interest in higher frequencies (above 10 megahertz) led to the employing of thermocouples in the actual EED structures to retain the RF impedance characteristics of the EED. For good transient response and minimal bridgewire impedance perturbation, an extremely low mass thermal sensor was required. Denver Research Institute developed vacuum deposited thin film thermocouples for application within inert EED structures (References 3 and 4) which satisfied the low mass requirement. Laboratory tests proved the electrical impedance of the bridgewire section of these devices to be the same as that of the corresponding weapon system EED for all frequencies up to ten gigahertz. With these characteristics, thin film thermocouple/bridgewire (within the EED structure) devices are considered accurate for spurious signal measurements from DC to ten gigahertz.

Incorporating these devices into an instrumentation system was accomplished without the use of amplifiers (to avoid amplifier susceptibility problems) using the approach shown in Figure 2. Although upon superficial examination the system appears unorthodox (slow galvanometers, ultra-simplicity) this system meets or exceeds the design objectives for the Minuteman HERO tests. This instrumentation system was tested by exposing it to a high level of electromagnetic energy (over 100 watts/m^2) throughout its usable frequency range (low frequency to 10 gigahertz) and was insusceptible to these levels (to effects other than bridgewire heating). The steady state and transient responses of the system are considered representative of the actual EED thermal pin-to-pin response, broadband or CW. Despite the slow frequency response characteristics of the galvanometers used, in actual use the thin film EED simulators (as used in Figure 2) can detect the effects of transient levels as small as 50 microjoules of energy. Whether a pulse is of high amplitude and short duration or of low amplitude and long duration is irrelevant as far as oscillograph deflection is concerned provided that the pulse duration is short relative to the time constant of the nichrome bridgewire in the EED simulator. The time constants of typical EED's run around 5 milliseconds. As a rule of thumb, for any transient shorter than one millisecond, (regardless of waveform shape), oscillograph deflections may be equated to the deflections found with known amounts of energy injected into the bridgewires. A one-microsecond, 7.06 ampere pulse will give essentially the same galvanometer deflection as a one millisecond 224 milliampere pulse because both contain 50 microjoules of energy (I^2Rt for a one-ohm bridgewire). For a complex waveform high frequency transient perturbance (shorter than 1 millisecond), the nichrome bridgewire appears exactly as it would in a live EED and since the thin film thermocouple/galvanometer instrumentation system has been designed to look at and integrate this energy, oscillograph deflection may be equated to the deflections found by injecting known amounts of energy into the nichrome bridgewire.

As an example, the above system can be calibrated at 100 milliamperes DC. If a 1/2 inch galvanometer deflection corresponds to 100 milliamperes DC then a corresponding deflection caused by an RF source indicates the same thermal heating as that which is caused by 100 milliamperes. For transient phenomena a pulse generator is used to inject known amounts of energy into the EED simulator. For these pulsed energy calibrations the equipment is set up as shown in Figure 3. The following basic formula is used:

$$\text{Energy (joules)} = I^2Rt$$

where I = amplitude of current pulse in amperes

R = "cold" resistance of the EED bridgewire in ohms

t = time duration of pulse in seconds (t short relative to bridgewire time constant)

The above formula, for all practical purposes, is a good representation of the energy being injected into the EED simulator. The corresponding oscillograph deflections for each energy level injected are measured and recorded. Since most spurious phenomena occurring in typical weapon systems are either of a continuous nature (e.g., telemetry radiation) or of a short transient nature (e.g., nozzle motor switching on and off) the instrumentation lends itself well to HERO testing. During actual testing, the oscillographs may be operated at speeds as slow as 0.16 inch per second and, other than possibly time correlation, nothing is gained by running the oscillographs faster. Data is regarded as either of a st y state or transient nature and is analyzed accordingly. The data readouts are directly correlatable to the current and energy criteria derived from applicable weapon system criteria.

All possible weapon system modes are monitored during the HEPO tests. A Ground Test Missile is used and all the EED's are replaced with thin film EED simulators (typical installation for a Minuteman III configuration is shown in Figure 4). During some portions of these tests, ordnance current discretes as high as 10 amperes are sent to the individual EED's sequentially, exactly as in an actual missile launch operation. To prevent destruction of the thin film EED simulators, current limiting is required to limit the 10 ampere discretes to levels non-destructive to these EED monitor units. Current limiting resistors placed adjacent to the current activation switch (Figure 5) do not alter the energy pickup characteristics of the EED circuits and provide the required protection.

Firing Circuit Electromagnetic Interference Generation

Figure 6 shows a typical time domain waveform of the current firing first stage ignition for an actual flight test missile. Although the instrumentation used to monitor this current had limited frequency capability (1 kilohertz) it is evident that the waveform following the breakage of the bridgewire is most erratic and continues for a good 10 to 15 milliseconds. This phenomenon is apparently caused by a 28 volt "source voltage" arc discharge (Reference 5) pin-to-pin (on some initiations it occurs pin-to-case) through an ion cloud in the combustion chamber of the motor stage. On some firing currents, low resistance shorting (pin-to-pin and/or pin-to-case) has been observed during this arc discharge period. The erratic waveform (500 watts peak) is obviously a high-level electromagnetic interference generator. Speculating that this interference source could possibly cause some system anomalies, an attempt was made to create a more severe environment on some of the later HERO tests by firing live ordnance. Adjacently routed ordnance functions were monitored for coupled energy. The results of this investigation was that no energy was found to be induced differentially greater than the 50 microjoules threshold susceptibility of the instrumentation.

Silicon Cartide Sensor

The first of two unique HERO sensor/instrumentation systems built and tested at The Boeing Company (initially developed under contract to Rome Air Development Center, Reference 6) is shown in Figure 7. This system employed a silicon carbide whisker as a thermistor sensor and was experimentally used on one of the HERO tests. The advantage of this thermistor over thermal sensors previously employed, is that it has very low mass, tremendous strength (approaching theoretical limit for crystalline structure), and a short time constant. Time constants less than a millisecond are possible depending on sensitivity requirements. The big potential application of the silicon carbide whisker thermistor, is that it is believed that the sensor could be employed in live EED's with the pyrotechnic material intact and used for monitoring during actual flight (data would be obtained via telemetry).

Optically Linked Ordnance Monitoring System

Due to changing and more stringent requirements imposed by a rapidly advancing technology, The Boeing Company has developed a proven ordnance monitoring system employing fiber optic data links (Figures 8, 9 and 10). The system employs a thermal sensor (thermocouple or silicon carbide whisker) integrated into an EED with the output conditioned to drive a light emitting diode. The optical output of the diode is transmitted through a 40 or 50 foot length of fiber optics to a photoreceiver (data readout unit) located in a shielded area. The fiber optic data link and the completely shielded phototransmitter, which may be powered pneumatically or by batteries (on line or pneumatically switched), will allow this ordnance monitoring system to provide accurate measurements in areas of very high-level electromagnetic environment. In addition, the data link routing is not limited or affected by any concern of interaction with the environment. Therefore, this system is ideally suited for testing applications in high-level environments such as EMP or ECM transmitters.

CONCLUSIONS

A high level of confidence has been established that the Minuteman ordnance systems are safe from a dudding or inadvertent ignition standpoint for the day to day environment of the Minuteman Weapon System. No anomalies have been found that might indicate a personnel and/or weapon system hazard. Due to changing requirements that require unique testing methods (EMP, in-flight testing, etc.) The Boeing Company is actively involved in refining existing methods of HERO testing and in advancing the state-of-the-art where required.

ACKNOWLEDGEMENT

The author wishes to thank the Boeing "Systems Instrumentation and Telemetry Group" and in particular Mr. Glen E. Miller and Mr. Max Levine for their assistance in designing and building the pneumatic power generator. The author would also like to thank Mr. Richard F. Holtman and Mr. Lee W. Olson of The Boeing Company for their developmental work in the area of micro-electronic thermal sensors.

Special thanks are in order to Dr. Jack G. Hewitt, Jr. of Denver Research Institute whose continuing guidance and assistance helped make this paper possible.

REFERENCES

1. Paul F. Mohrbach, Robert F. Wood, The Franklin Institute, Technical Report F-B2198-1, "RF Susceptibility Evaluation of Minuteman Ordnance Systems," June 1966.
2. Paul F. Mohrbach, Ramie H. Thompson, The Franklin Institute, Technical Report F-C2191-1, "Evaluation of Radio Frequency Susceptibility of Minuteman III Ordnance Systems," October 1968.
3. Sandia Corporation, Final Report P.O. 73-5753, "Improvement of Instrumentation Used in RF Hazard Testing," September 30, 1965.
4. Jack G. Hewitt, Jr., "Instrumentation for Making Broadband Measurements on Electroexplosive Devices," The Franklin Institute, Proceedings of the Sixth Symposium on Electroexplosive Devices, July 8-10, 1969.
5. National Aeronautics and Space Administration, Technical Memorandum 33-280, Proceedings of the Workshop on Voltage Breakdown in Electronic Equipment at Low Air Pressures held at Jet Propulsion Laboratory, August 18-20, 1965.
6. Richard F. Holtman, Lee W. Olson, "The Investigation of Microelectronic Thermal Sensors for Circuit Effects Measurements," Rome Air Development Center, Technical Report No. RADC-TR-67-273, July 1967.

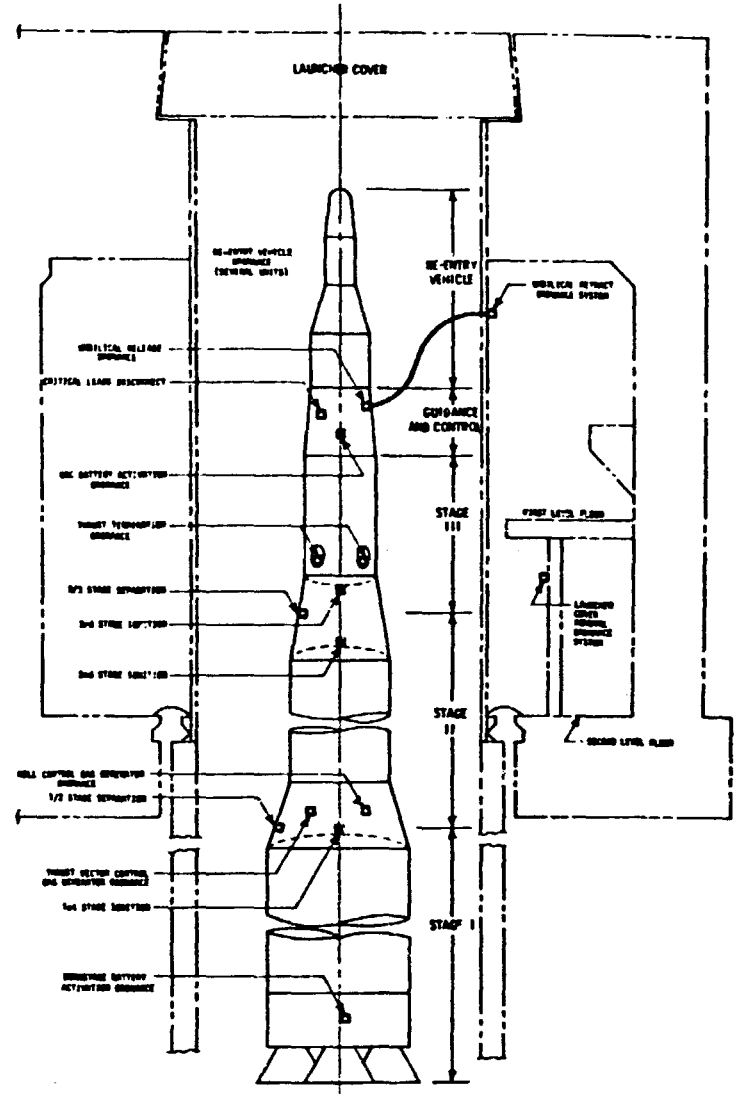

FIGURE 1
LOCATION OF TYPICAL MINUTEMAN EED'S (MINUTEMAN II)

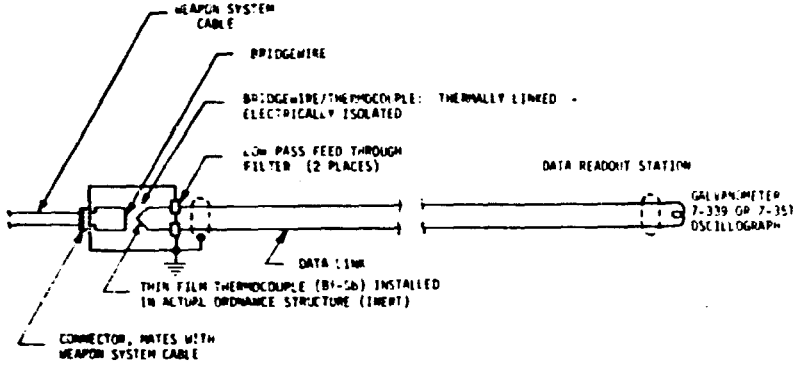

FIGURE 2

ORDNANCE MONITORING INSTRUMENTATION

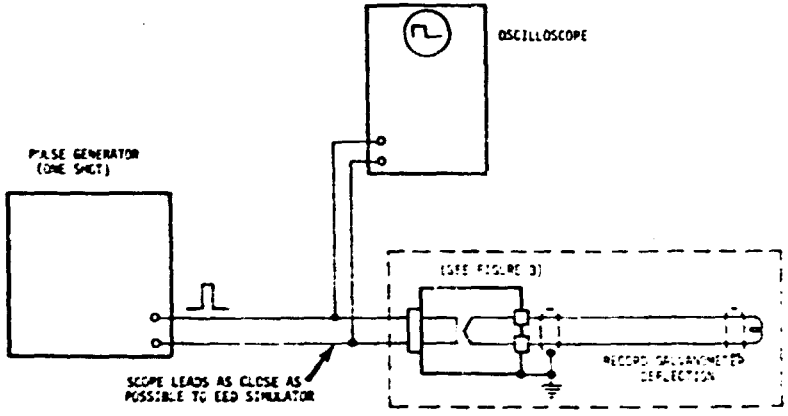

FIGURE 3
PULSED ENERGY CALIBRATIONS

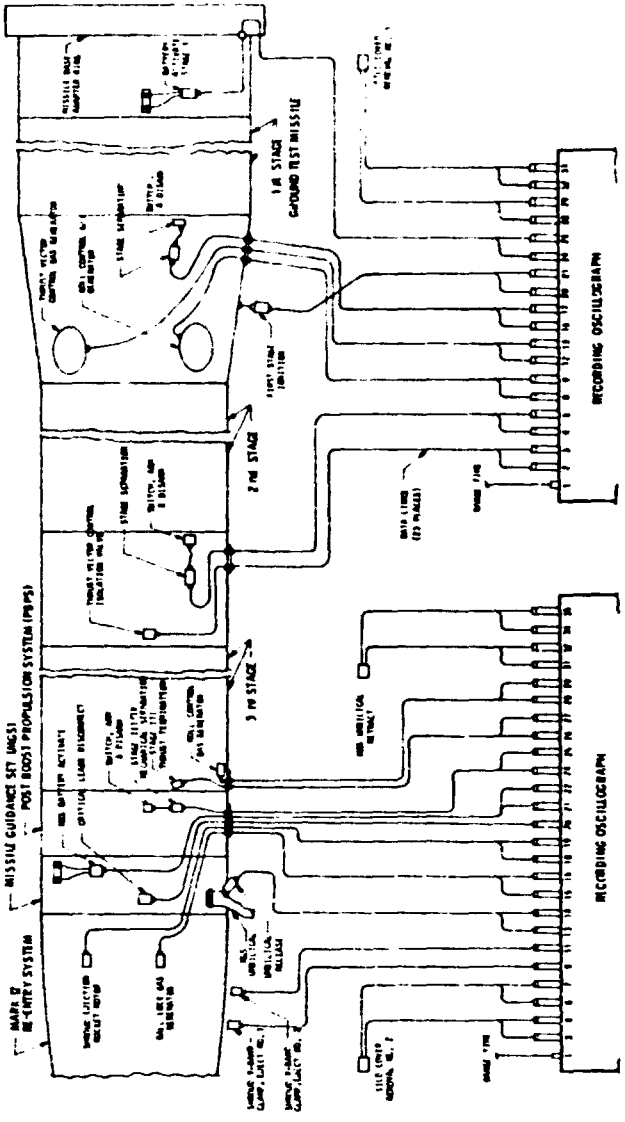

FIGURE 4
ORDNANCE MONITORING INSTRUMENTATION INSTALLATION (MINUTEMAN III)

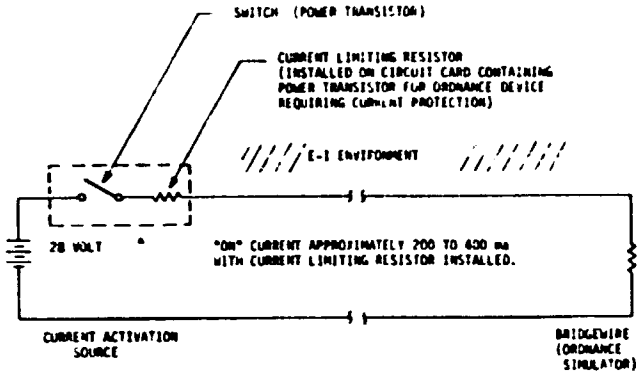

FIGURE 5
CURRENT LIMITING PROTECTION

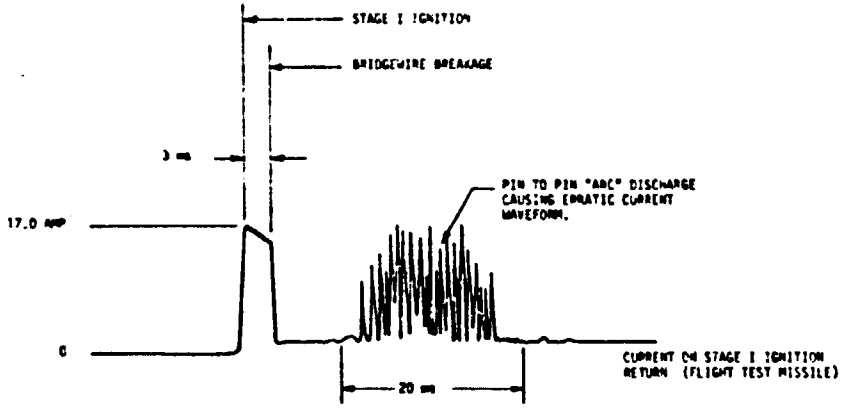

FIGURE 6
FIRING CIRCUIT CURRENT WAVEFORM

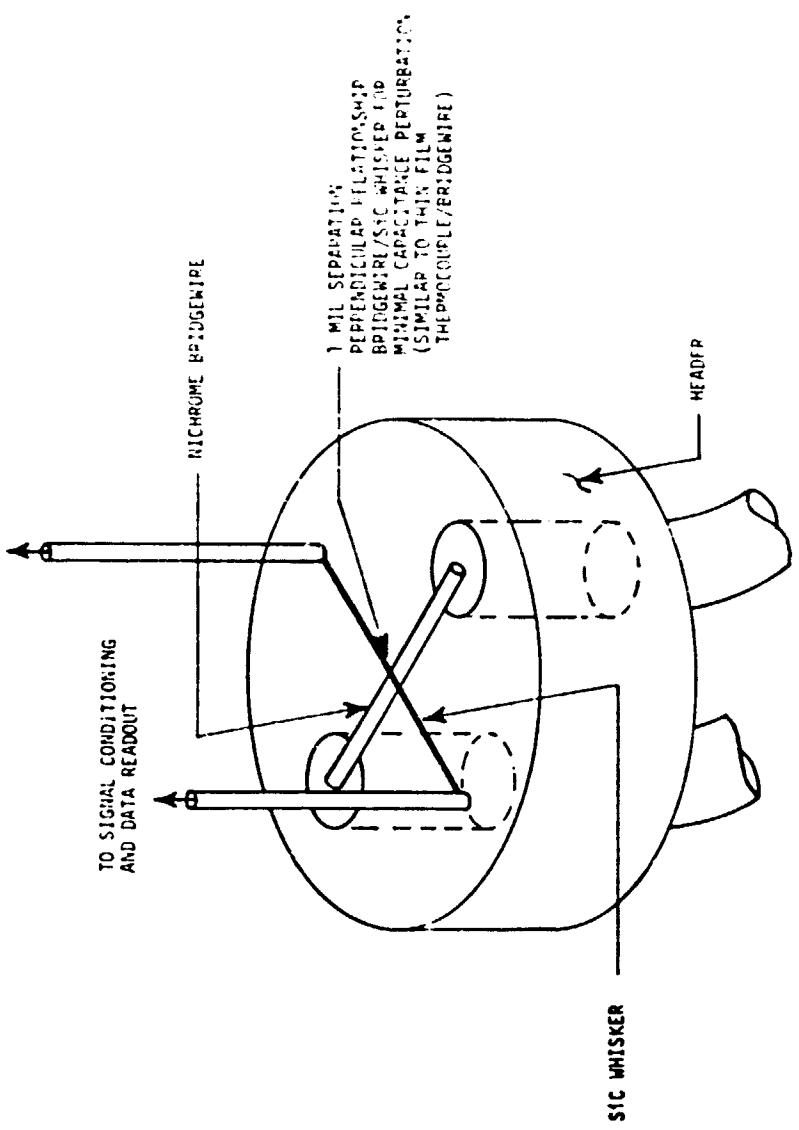

FIGURE 7
SILICON CARBIDE WHISKER THERMISTOR

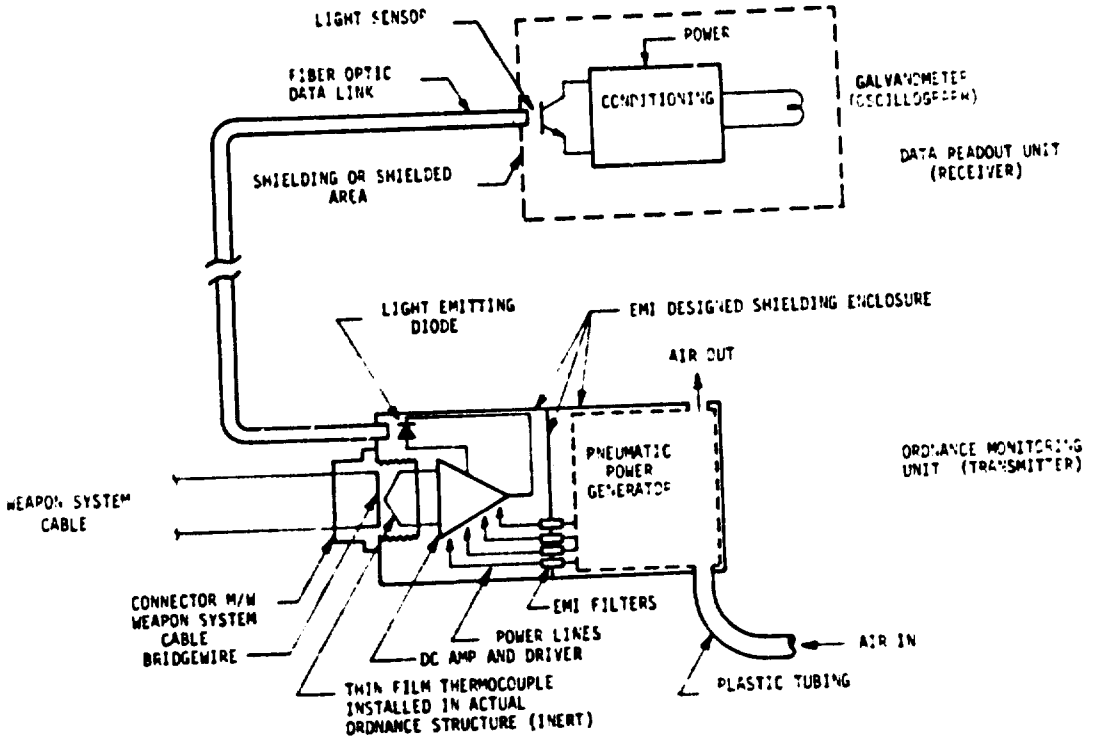

FIGURE 8
PNEUMATICALLY POWERED OPTICALLY LINKED
ORDNANCE MONITORING SYSTEM

II-9. The Colt's RotAct and PyrAcc

C. R. Olsen

Colt's Inc, Military Arms Division, Hartford, Connecticut

Colt's has developed a pyrotechnic Rotary Actuator, the RotAct, which may be used directly with a self contained pyrotechnic or may be operated from hydraulic fluid which can be supplied by a pyrotechnic powered accumulator, the PyrAcc.

The RotAct, illustrated in Fig. 1, is a longitudinally fluted twisted tube which expands and untwists when pressurized by a pyrotechnic charge or fluid pressure. The RotAct is a sealed pressure vessel and is non-contaminating in operation.

A typical small RotAct, shown in Fig. 1, is formed with a 180° initial twist and is fitted with a hexagon cap on the back end to provide a holding key. The fluted section of the tip engages a matching splined socket to transfer the output torque.

Fig. 2 shows the RotAct in its loaded configuration with the initially twisted flute, and in its fired configuration where the flutes have expanded and untwisted providing an output torque and rotation.

Fig. 3 illustrates the effect of inertial load on output rotation. Flywheels of varying weights made from aluminum, steel or tungsten were coupled to a small RotAct (180° initial twist) and test fired to determine rotation of the flywheel. Output rotation drops from 90° with a 3/4 Oz. load to approximately 32° with the 9 Oz. tungsten flywheel. The output torque of the RotAct is a function of tube geometry and internal pressure. Fig. 3 illustrates the relationship between output torque and internal (hydraulic) pressure for a large 3 1/8" ID x .093" wall RotAct.

Torque rises as a function of pressure from 400 to 800 psi, and remains relatively constant from 800 to 1800 psi. Above 1800 psi (with this size RotAct) torque increases with an accompanying steepening of the helix angle at one end until a leak occurs.

Choice of the proper amount of twist for the RotAct is related to the diameter of the tube and the working length of twist. For a given geometry and material there is a critical or optimum helix angle which provides a maximum rotational output. Fig. 4a shows the relationship of helix angle to output rotation for one type of RotAct. The apparent best helix angle in this configuration is 180° of initial twist. Fig. 4b is a photograph of RotActs with the various helix angles used in this test.

Fig. 5 is the same data as Fig. 4a showing initial twist in degrees instead of helix angle.

The torque required to perform the initial twist in these small RotActs is shown in Fig.6. Varying the geometry and material of the fluted tube will shift the curve. The samples used in this test were of the same lot as those used in the previous tests of output rotation vs. twist wherein 180° of initial twist was found to be best in this length.

The effect of temperature on the RotAct is primarily one of the effect of storage or operating temperature on the pyrotechnic or pressurizing fluid, whether gas or liquid. The behavior of the twisted element is relatively constant over the range of temperatures which do not adversely effect the metallurgical properties of the tube material. Fig. 7 shows the effect of hot, cold and ambient firing as well as temperature cycling on output rotation under a constant inertial load, for one lot of RotActs.

The functioning time of these pyrotechnic RotActs is very short. The small units have transferred their energy in approximately two milliseconds while the large units have completed their work in less than ten milliseconds.

This rapid operation characteristic makes the RotAct particularly suitable for the arming of fuzes and operation of switches. This form of self-contained pyrotechnic RotAct is less suitable for operation of high inertial loads such as closing a heavy door at a slow controlled rate. The basic RotAct principle can be used for slow speed high inertia application when powered by hydraulic fluid at a controlled rate of flow.

The pressure torque relationship shown in Fig. 3 represents the average of curves taken with a hand hydraulic pump with a time to reach peak pressure of many minutes. The torque remains essentially constant if the pressure is kept constant. Tests were normally terminated after ½ hour at peak pressure.

The PyrAcc, a Pyrotechnic Powered Accumulator, is shown in Figs. 8 and 9. This device is a sealed one shot, non-contaminating source of fluid pressure. It consists of a longitudinally fluted metal liner sealed in a tubular pressure vessel.

The liner contains a conventional pyrotechnic charge and is surrounded by fluid. The outer vessel is sealed confining the fluid. No ullage is required as the inner fluted liner will deflect to accomodate the thermal expansion of the fluid during temperature cycling.

In Fig. 8 the liner is shown in the fluted state and is surrounded by fluid. Fig. 9 shows the fired condition with the fluted liner expanded and the hydraulic fluid expelled. The pyrotechnic products remain sealed in the expanded liner.

When the RotAct and PyrAcc are coupled together the rate of actuation of the RotAct is determined by the rate of flow from the PyrAcc to the RotAct. This rate can readily be controlled with an orifice to extend RotAct actuation over a period of many seconds.

Maximum operating time is limited only by the pyrotechnic characteristics used in the PyrAcc.

The PyrAcc can be used as a power source for one or more RotActs or can be used alone as a one shot hydraulic power source or fluid dispenser. Its simplicity and low cost make it an excellent candidate for replacing conventional piston or bladder accumulators powered by pyrotechnics or stored gas in missile applications.

Both the RotAct and the PyrAcc can be hermitic sealed, are non-fragmenting and non-contaminating. Storage life is limited primarily by the pyrotechnic and method of sealing selected.

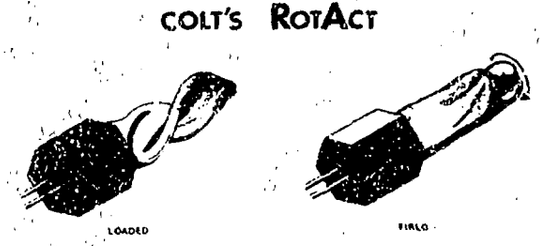

Patent No. 3,376,783

Figure 1.

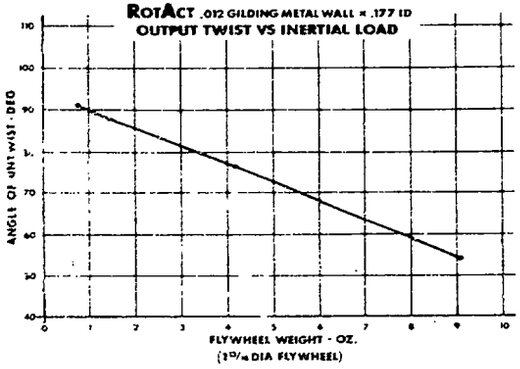

Figure II

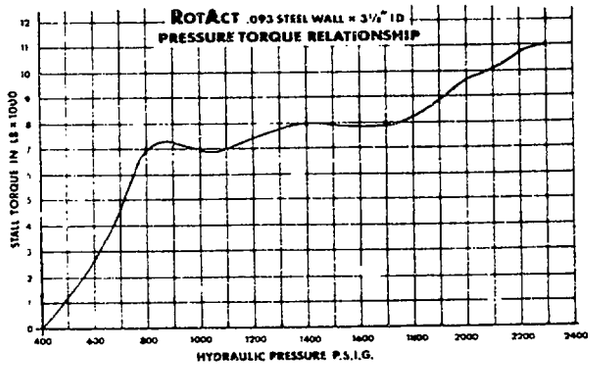

Figure III

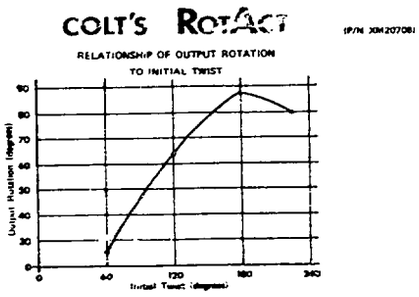

Patent No. 3,376,783

Figure IVa

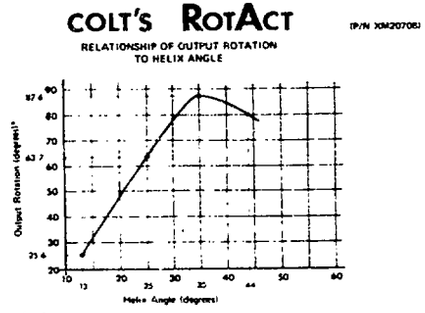

Patent No. 3,376,783

Figure V

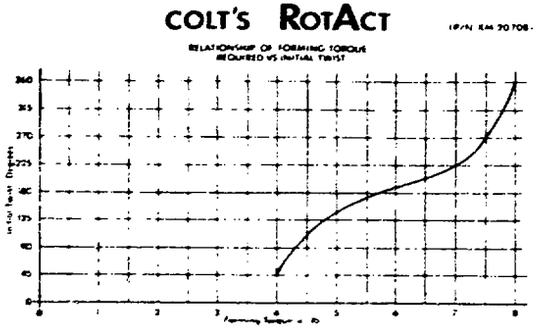

Patent No. 3,376,783

Figure VI

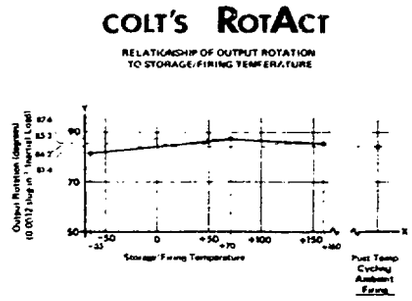

Patent No. 3,376,783

Figure VII

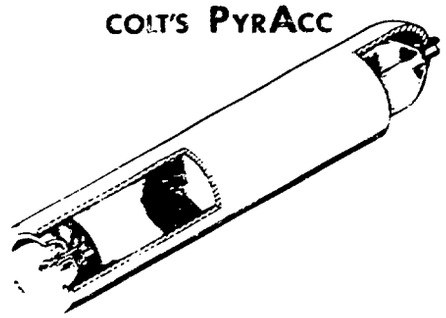

Patent No. 3,483,695

Figure VIII

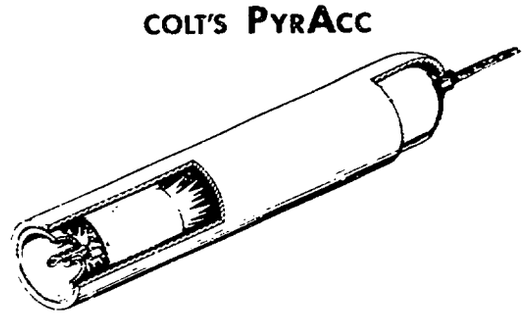

Patent No. 3,483,695

Figure IX

II-10. PYROTECHNIC HAZARD CLASSIFICATION

Joseph H. McLain
W. Alton Jones Prof. of Chemistry
Washington College
Chestertown, Maryland

There are two fundamental analyses that must be performed:

1. What are the chances of having an accidental ignition or initiation leading to a fire or explosion?

2. What amount of damage to personnel and facilities will result from this accident?

Number 1 above is obviously dependent upon the mode of treatment during handling and the sensitivity of the material. Number 2 is dependent upon the type, amount, and rate of energy output.

Sensitivity data tells us how we must treat a material to try and avoid an accident whereas output data tells us what can happen in the event that we do.

Ordnance plants should adopt the philosophy that sooner or later an accident will happen and so design to prevent injuries to personnel and, within a reasonable cost factor, damage to facilities. To do this, output data is required. What is the nature of protection that must be given to personnel? Should it protect against shock wave, over pressure and sympathetic detonation between buildings as in the case of a detonable material or should it protect against fragmentations, radiant heat, smoke inhalation and or suffocation as is the case with most pyrotechnics?

J. E. Settles [1] has made an analysis of ten years of accidents in the propellant and explosives industry. There were 9, accidents and 78 fatalities.

None of the fatalities were due to blast over pressure associated with detonation reactions even when detonation forces were present. Fragments and radiant heat accounted for 77 out of 78 fatalities. These findings, when applied to pyrotechnic operational accidents, hold true even more so.

Settles also makes a very valid criticism of the present practice of accepting a 'fire hazard only' label on reactions of such violence and destructive energy as medium velocity detonations, low velocity detonations, high-rate explosions, medium-rate explosions, and even reactions that do not explode, but still people by burning them to death.'

Pyrotechnic Hazard Classification

A movement is underway to make certain pyrotechnic mixes Class 7. There are two serious objections to this procedure. Firstly, practically none of these mixes meet the criteria for Class 7, namely the Card Gap Test, spelled out in TB 700-2.

A recent report from tests done in the pyrotechnic hazards classification and evaluation program conducted by the General Electric Corporation at the NASA Mississippi test facility [2] lists 18 pyrotechnic mixes from the product line of Pine Bluff Arsenal. None of these (p 3-27) showed evidence of detonation with the Card Gap Test, yet 6 of them are classified as Class 7 hazards, and the output of all of them is no more than 10-20% TNT values.

This same report stresses (p 3-36) that the Card Gap Test is of little value in estimation of pyrotechnic hazards.

Secondly, it is unrealistic and unsafe to try to protect personnel from damaging effects of pyrotechnic accidents (radiant heat and fragmentation) in the same way as one should protect against a true Class 7 detonable solid. The detonable solid's shock wave travels in a straight line and can be barricaded against so that over pressure and sympathetic detonation can be decreased or eliminated.

A medium to high rate explosion which can occur from a pyrotechnic mix kills and damages with fire ball and fragments. Barricades unless of proper height and design only serve to increase the distance of throw of fragments and burning debris.

Thus to classify a pyrotechnic mix as Class 7 denies the definition and sense of the quantity - distance philosophy.

The common sense approach to the problem demands the scientific characterization of those materials whose lethal potential is related to factors other than shock waves traveling at supersonic velocities, and not an indiscriminate shuffling to highest hazard category of H.E.

(1) J. E. Settles, "Deficiences in the Testing and Classification of Dangerous Materials," N.Y. Academy of Sciences Annals, Volume 152, Art. 1, pp 199-205.

(2) Phase III, Segments 1-4, "Investigation of Sensitivity Test Methods and Procedures for Pyrotechnic Hazards Evaluation and Classification," April 19, 1971, Part A, GE-MTSD-R-059, pp 3-23 et seq.

So far I have spoken about the bad parts of the present system and now I would like to make some suggestions for ameliorating these conditions.

Explosives and propellants have been categorized and classified for years. These classifications have been based upon experiment and experience and have served well to establish better and safer procedures for handling, storage, use, manufacture and transport. Attempts to include pyrotechnics, civil and military, have not worked well in the past and are not working well now as has been discussed briefly above.

I would like to propose that pyrotechnics be given a position of their own, separate and distinct from explosives. The classification of pyrotechnics, just as the classification of explosives and propellants must be based upon definitive testing and experience, and just as there are class A, B and C explosives there should be some similar classification for pyrotechnics.

There is or will be shortly a precedent for this step. The National Fire Protection Association, who recently completed and published a code [3] for explosives and blasting agents. They are now working on a separate code for fireworks and pyrotechnics, thus recognizing important differences in safety procedures between the two areas.

I would like to quote from the General Statement of the proposed code on fireworks.

(3) NFPA No. 495, Manufacture, Transportation, Storage, and Use of Explosives and Blasting Agents 1970

"It should be recognized that the problems of safety in manufacture, transportation, handling and storage of fireworks are in many ways very much different from those of explosives and propellants.

In general, the sensitivity of fireworks to shock and impact is considerably less than that of explosives and more to spark and flame.

The problems of protection, if and when an accident occurs are also significantly different. For example, concrete or earthen barricades which are quite effective in preventing sympathetic detonations between detonable materials, can in some cases worsen the problem with fireworks, by increasing the fragment throw distance and even the severity and rate of the explosion.

Degree of containement of deflagrators whether in packaging, building or barricade is of paramount importance, whereas a detonable explosive will go high order when shock initiated even in a loose powder configuration."

Another precedent also exists. It is my understanding that this same need for

Pyrotechnic Hazard Classification

a separate treatment has been recognized by the composite propellant industry and a specific technical bulletin has been written which classifies and categorizes various propellant formulations and packages.

Some of the details that went into the above general statement are discussed below.

Explosives particularly military are generally chemical compounds and/or relatively simple mixtures of aluminum and waxes with the explosive. Their explosive properties are primarily determined by the explosive ingredient.

Pyrotechnics however are highly complex mixtures whose explosive properties are quite variable depending upon the particle size of the ingredients, the oxidant/reductant ratio, porosity of mix (pressed vs. unpressed), degree of confinement and others.

The output of an explosive particularly of a detonable solid is primarily shock wave, over pressure and fragmentation, whereas the output of pyrotechnic mixes primarily fire ball and fragmentation. Death from pyrotechnic accidents generally arise from burns, fragment impact and lung damage.

Even in methods of stimulus the two are quite different. High explosives are shock sensitive but pyrotechnics are flame and spark sensitive. Tests using a blasting cap on a pyrotechnic mix many times do nothing but blow the mix away, however use of a squib can and often does result in a relatively high rate of explosion.

In summary then, explosives and pyrotechnics differ widely in methods of protection, characteristics of output and initiation. Industry and Government must realize these basic differences and take action to make a more realistic code for the protection of life and property.

Before concluding I wish to make one more suggestion. The quantity distance tables of today are largely an outgrowth of studies and tests for storage and transportation of fairly large quantities of explosives. Manufacturing and processing safety procedures may or may not be well served in some instances. This is an important area for the reasons that there is considerably more exposure of the explosive or pyrotechnic to stimulus, larger quantities exist during mixing and much exposure of personnel.

On the basis of the above I recommend very strongly that a joint industry-government committee be formed under the aegis of the Armed Forces Explosives Safety Board or similar to make a scientific study of pyrotechnics and devise a separate, sound and safe, procedure for the manufacture, storage, transportation and handling of civil and military pyrotechnics.

II-11. DOPING EXPLOSIVE MATERIALS FOR NEUTRON RADIOGRAPHIC ENHANCEMENT*

By

K. G. Golliher

Atomics International
A Division of North American Rockwell Corporation
Canoga Park, California

INTRODUCTION

Neutron radiography is similar in principle to X-radiography, but has among its unique capabilities the ability to distinguish and determine hydrogen bearing materials within metallic structures. It is this feature that makes neutron radiography the best nondestructive testing technique for ordnance devices containing organic explosive material.

Atomics International has neutron radiographed more than 10,000 ordnance devices.[1] The devices were neutron radiographed for anomalies in the organic explosive material. Rejections, which amounted to about 10%, were due to (1) void in the explosive material, (2) cracking, (3) explosive interface gap, (4) explosive charge density variance, (5) misalignment, and (6) foreign material. These discrepancies were seen in organic explosives such as RDX (cyclotrimethylene trinitramine), PETN (pentaerythrite tetranitrate) and nitrocellulose compounds, and also in inorganic compounds containing boron. The first three produced good images because of the hydrogen (a neutron scatterer). The boron material images well because of the high neutron-absorbing properties of the element boron.

Most ordnance materials that are inorganic mixtures neutron radiograph poorly, or not at all, particularly if contained within a thick metallic structure. The inability to neutron radiograph inorganics is due, in general, to their low neutron scattering and/or absorbing properties. Typical non-imageable inorganic mixtures are lead oxide, zirconium and molybdenum coupounds, aluminum and sodium nitrate mixtures, potassium chlorate, and barium styphnate.

The ability to neutron radiograph inorganics containing small concentrations of neutron absorbing/scattering elements such as hydrogen in titanium hydride and boron fibers in boron-aluminum composites, suggested the idea of adding small quantities of high neutron absorbing/scattering material to the non-imageable inorganics for image improvement. The process of adding small concentrations of neutron attenuating material(s) to the ordnance mixture is referred to as doping for neutron radiographic enhancement, and is the subject of this paper.

Investigations were made relative to selecting a material(s) with high neutron absorbing property that when added to the explosive mixture enhanced the imaging of the material, and the quantity of the additive such as not to interfere with the proper reaction of the chemical mixture. Because of the inherent problems of working with explosives, their analogs were used as a substitute. This provided flexibility in that the analog allowed working with materials that were readily available and nonhazardous. With these goals established materials were selected and neutron radiography tests were made. The results are herein reported.

Doping of organic and inorganic explosive analogs to improve neutron radiographic imaging has been successfully demonstrated. Samples doped with concentrations ranging from 0.001% to 10% were neutron radiographed with thermal neutrons using the activation transfer and the direct neutron detection techniques.

The inorganic ordnance material was simulated by using Devardas metal (a mixture of aluminum and copper). The organic ordnance material was simulated with lucite, similar to the explosive materials RDX and PETN. To show the sensitivity of doping, a simulated organic explosive linear-shaped charge of 50 grains per lineal foot was doped with a 0.1% rare-earth oxide material-gadolinium oxide (Gd_2O_3). This type of charge, which is sometimes difficult to detect, was then discernible, but to increase the imaging for practical viewing, 3% doping was required. The inorganic material which showed no imaging, by itself, was detectable with the addition of only 0.001%. A 0.3% addition was good for practical viewing. Practical viewing is defined to be visual with standard illuminators.

*Work supported by the National Aeronautics and Space Administration, using the Atomic Energy Commission Shield Test and Irradiation Reactor
NASA SATURN Contract, NAS-7-7200

Charge devices were aluminum tubes 0.0625, 0.1875, and 0.3125-in. ID which, in the inorganic tests, represents 40, 240 and 650 grains per lineal foot, respectively. The same size containers were also used for the organic studies. The 0.0625 cross section of material represents the minimal cross section of an ordnance material submitted for neutron radiography at Atomics International. Devices (detonators, pressure cartridges, etc.) of larger cross sections will be more readily seen because of the effective increase in thickness the material represents.

Gadolinium oxide appears to be one of the best candidates for doping because it has several favorable properties: very high neutron absorption cross section, minimal residual radioactivity, chemically inert, good temperature stability, and good mixing characteristics.

It is proposed that gadolinium oxide, or other rare-earth compounds and boron, can be added to explosive materials by chemical combination or physical mixing in quantities which will enhance the neutron radiographs and yet, have no deleterious effects with the explosive material.

An interesting application of doping explosive materials could be in the study of explosive mixing; for example, doping one of the compounds and subsequently mixing it with other compounds. The homogeneity and density levels could be examined with neutron radiography.

APPLIED NEUTRON RADIOGRAPHY DISCUSSED

Neutron radiography has been successfully used in many situations where conventional radiography or other nondestructive methods cannot be applied. It, therefore, complements conventional radiography in that it makes possible the radiography of a broader range of materials and parts.

Figure 1 illustrates a comparison between X-ray and thermal N-ray for the mass attenuation coefficients vs atomic number. As shown, elements of similar atomic mass which have essentially the same mass attenuation coefficient for X-ray, such as B and C, quite often have good separation in thermal neutron mass attenuation coefficients. The figure also illustrates the advantage of using neutron radiography for some of the light elements with high scattering coefficients (e.g., hydrogen), and the rare earth elements with high absorption coefficients.

Most of the inorganic materials have low thermal neutron cross sections. With the addition of small amounts of gadolinium oxide, having orders of magnitude higher cross section, the inorganic mixture has an effective increase in neutron absorption.

The discussion to this point has concentrated on thermal neutron radiography. Thermal neutrons are those that have been slowed down from the high-energy (~1 Mev) neutron born in the fissioning process. The thermal neutron has an energy of 0.025 ev, which is about 2200 m/sec. The discussion is now directed to epithermal neutron radiography.

Earlier it was stated that the neutron reaction cross section was a function of the neutron's energy. Neutrons with energies greater than 0.3 ev to about 100 kev are classed as epithermal or intermediate neutrons. In the intermediate neutron range, a phenomenon called resonance occurs with some nuclides: the neutron exhibits a very high interaction probability with nuclei at specific kinetic energies of the neutron. Cross sections for neutron capture and scattering, for example, exhibit peaks at these so-called resonance energies and have low values between peaks (see Figure 2). The peak microscopic neutron cross sections at 0.025 and about 25.0 ev for tungsten are 2.3×10^{-24} cm^2, and $14{,}000 \times 10^{-24}$ cm^2, respectively, a noteworthy change of about 6000 times. With the ability to adjust the reactor leakage neutron spectrum from the fast to an intermediate or to a thermal energy, a particular neutron energy group can be selected for its material-penetrating ability, and to correspondingly match image-converting material of high neutron reaction cross section. This technique, for example, was used to highly enhance tungsten weld rod in steel,[2] which can be related to N-radiographing tungsten pyrotechnics in steel. Tungsten is used as an explosive material in slow delay trains.[3]

METHOD

The neutron radiographic technique used was to bombard the specimen with neutrons and image the transmitted neutrons with a detector. The neutrons were of a sufficient energy to penetrate the specimen and the detector was a material highly sensitive to the transmitted neutrons.

The neutrons used for these tests were either thermal or epithermal (defined in the previous section). The intensity of either neutron beam was such that exposures of less than 15 min were needed.

Detectors sensitive to neutrons in the thermal and epithermal energy range were used. Gadolinium detectors with Kodak single coated R film were used for the major part of this work. Dysprosium detectors were used with T film for comparison. Gadolinium is a direct transfer in that the film is placed with the gadolinium to capture the prompt radiation emission from the neutron capture. Dysprosium on the other hand is activated in the neutron beam without the film. The dysprosium, after being activated, was placed in a vacuum cassette overnight with Kodak T photographic film. The overnight autoradiograph takes advantage of the 2.3-hr half life of Dy^{165}. The exposed film was then processed by standard X-ray film processing procedures.

The neutron radiographic parameters for the thermal neutron radiography are shown in the following table. The radiation values are based upon maximum reactor power.

Aperture Size	2 x 2 in.
Aperture to Object	16 ft
*L/D	~100
Cadmium Ratio	205
Gamma Rate	26 r/hr
Neutron to Gamma Ratio	4.7×10^5 n/cm^2/mr
Neutron Flux at 16 ft	3.4×10^6 n/cm^2/sec

*Aperture to object distance divided by the diameter of aperture.

DISCUSSION OF PYROTECHNICS NEUTRON RADIOGRAPHED

Figures 8 through 11 represent typical aerospace delay columns. Some have X-rays for comparison with the N-rays. In each case, the output charge is clearly seen in the N-radiograph, as it should be since it contains hydrogen bearing material. The delay columns are to some degree imaged, but the detail in the delay column is brought out in the areas where the material has boron in its makeup (see N-ray, Figures 8 and 10). By addition of gadolinium oxide in the inorganic material (not being imaged by boron), the delay column would be imaged sufficiently, and would show contrast similar to that seen in the boron section.

A modified spent reefing line cutter (no output charge), Figure 11, was used for doping tests. An X-ray and N-ray of a standard cutter were made for comparison. Devarda's metal doped with 0.1, 1.0 and 10.0% gadolinium oxide were charged into the delay column. The three levels of doping are seen in the N-ray. The doped reefing line cutter represents practical application of doping inorganic pyrotechnic mixtures to improve its neutron radiographic imaging.

DISCUSSION OF RESULTS

Tests show the neutron radiographs of the organic explosive analogs with 50 grains/lineal foot of charge doped with 0.1% gadolinium oxide, and inorganic analogs doped with 0.01% gadolinium oxide produce enhanced radio-images. Doping with 0.1% gadolinium oxide or less can provide image differential with samples under laboratory conditions, but does not lend itself to many actual conditions, such as an explosive train contained within a thick metal housing.

Figures 3, 4 and 5 show the effects of gadolinium oxide doping in Devarda's metal (50% Cu, 45% Al, and 50% Zn). These three figures show test data from neutron radiographs with several varying parameters: (1) direct and indirect neutron radiography, (2) different neutron converters, different films, and different neutron exposures. Comparing the optical density, at 0.3% gadolinium oxide addition, to the optical density with no gadolinium oxide, for the 0.063 in. ID tubes, the change in density is 0.30 to 0.43. This shows that any of the neutron

radiographic processes herein used give about the same results. The most significant change is the improved contrast with the dysprosium – R film (Figure 5). This can be explained by pointing out that a higher film density was obtained, and with the absence of gamma radiation (indirect technique) which produces film fogging, a better contrast was obtained.

Figures 6 and 7 show the doping of the organic explosive analog, lucite. Figure 6 shows doping of about 2% would be necessary to double the imaging capabilities for organics with the smaller charges of 50 grains/lineal foot of charge. With the larger charges (Figure 7), 240 grains/lineal foot of charge (0.1875 ID tubes) the mass of the organic materials is readily imaged, therefore precluding any additives.

The following table summarizes the gadolinium oxide doping in the inorganic and organic analogs with charges of 50 grains/lineal foot of charge.

TEST SUMMARY FOR 0.0625 ID TUBES,
REPRESENTING ~50 GRAINS/LINEAL FOOT OF CHARGE

Converter/ Film	Reference Figure	Negative Background Density	Negative Density With Gd_2O_3 Addition (%)			
			0	0.3	1	3
Copper-Aluminum Mixture						
Dy/M	3	1.88	1.82	1.46	1.03	0.68
Gd/M	4	2.22	2.20	1.90	1.68	1.45
Gd/Rsc	-	1.74	1.72	1.58	1.37	1.20
Gd/Rsc	4	3.11	3.04	2.60	2.20	1.75
Gd/Rsc	-	2.82	2.78	2.53	2.10	1.68
Dy/Rsc	5	3.68	3.55	3.25	2.50	1.25
Lucite						
Dy/AA	-	1.58	1.33	1.31	1.31	1.13
Dy/T	6	1.42	1.18	1.10	1.05	0.86
Dy/M	-	1.82	1.55	1.45	1.41	1.12
Gd/R	-	3.07	2.35	2.20	2.10	1.90

Under present standards, it appears that doping of small organic explosive charges may be undesirable. The impurity level suggested for organic explosive material is 0.3%,[4] and it takes at least 1% gadolinium oxide to enhance the radiograph. Therefore, doping organics with gadolinium oxide above the accepted impurity level would have to be evaluated by the ordnance engineer.

Doping inorganics appears to be most feasible since only 0.1% gadolinium oxide enhances the image. It is common to add up to 15% diluent material (inert, dry admixed powder for pyrochemical mixtures) such as diatomaceous earth to explosive mixtures.[3] Therefore, gadolinium oxide additions of 0.1% to 10% seem feasible; particularly, since gadolinium oxide (Gd_2O_3) and diatomaceous earth (SiO_2) have similar physical and chemical properties.

Subject matter beyond the discussion scope of this paper, but observed and reported herein to stimulate interest are (1) the use of gadolinium oxide as an additive in the study of mixing and material density, (2) gadolinium oxide as an explosive material itself, or at least its compatibility with other explosives (its compatibility was somewhat discussed above), and (3) epithermal neutron radiography for inorganic pyrochemical mixtures containing elements (e.g., tungsten) with high neutron cross section in the epithermal energy region.

An example of determining the homogeneity of a mixture would be to dope one of the compounds and then examine the resultant mixture with neutron radiography. Poor mixing, stratification or density variance of pressed material could then be determined.

The rare earths make up a fascinating family of elements which, until recently, were something of a scientific mystery because: (1) they have nearly identical chemical properties; and (2) most of the physical properties of the rare earths, such as the atomic volume, melting point, hardness, thermal expansion, specific heat, and compressibility vary slightly and systematically from one element to the next. The most important property of gadolinium is that it has the highest thermal neutron capture cross section of any known element (49,000 barns). Although no reference could be found to gadolinium oxide as an explosive material, information was found of other rare earths.[5] Oxides of erbium, thulium, and yttrium have been used as pyrotechnic material.

The results of those studies show that gadolinium oxide is an excellent material for doping explosive materials to enhance the neutron radiographic image. The acceptance of this state-of-the-art improvement will further broaden the nondestructive examination of explosives and pyrotechnics.

REFERENCES

1. K. G. Golliher, L. E. Hanna, Materials Evaluation, Vol XXIX, No. 8, p 165 (1971)
2. K. G. Golliher, "Neutron Radiography Feasibility Studies for Steel Examination for the Liquid Metal Fast Breeder Reactor Program," LMEC-71-2 (1971)
3. R. Zimmer-Galler, "The Combustion Propagation of Tungsten Delay Powders," paper presented to the Sixth Symposium on Electroexplosive Devices, San Francisco, California, July 8-10, 1969
4. C. S. Greenough, Space Division, North American Rockwell Corporation, Downey, California, private communication (1971)
5. Herbert Elbern, Military and Civilian Pyrotechnics, Chemical Publishing Co., Inc., New York, p 92 (1969)

FIGURE 1

MASS ATTENUATION COEFFICIENT vs ATOMIC NUMBER

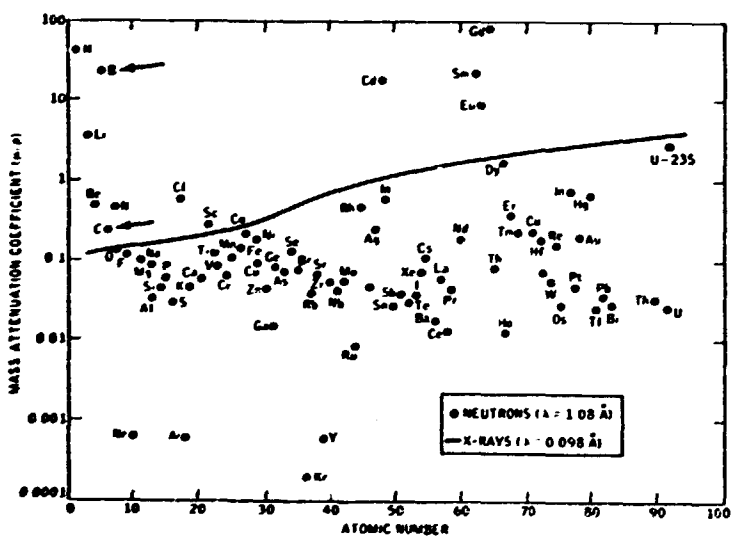

FIGURE 2

TOTAL NEUTRON CROSS SECTION vs ENERGY FOR VARIOUS MATERIALS

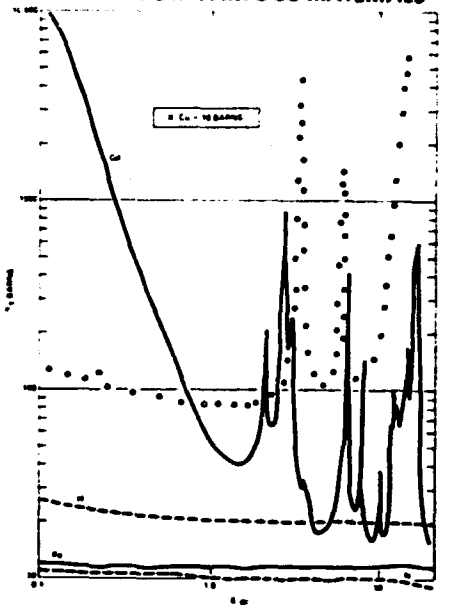

FIGURE 3

DEVARDA-Gd_2O_3 Dy-M FILM (0.063 in. ID TUBE)

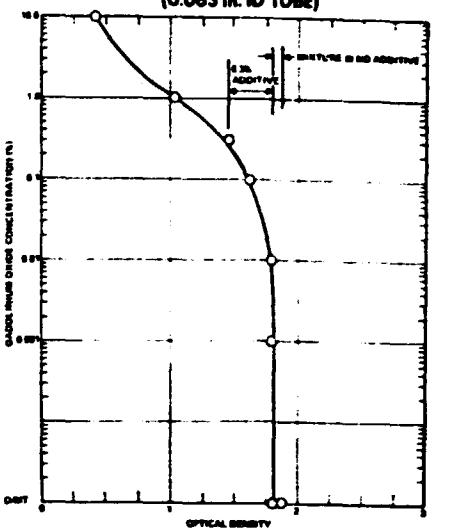

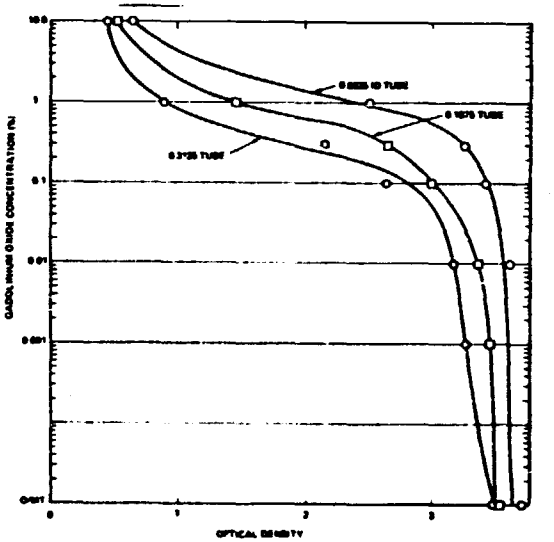

FIGURE 5

DEVARDAS ALLOY DYSPROSIUM-R FILM

GADOLINIUM OXIDE
DOPING IN DEVARDA'S METAL

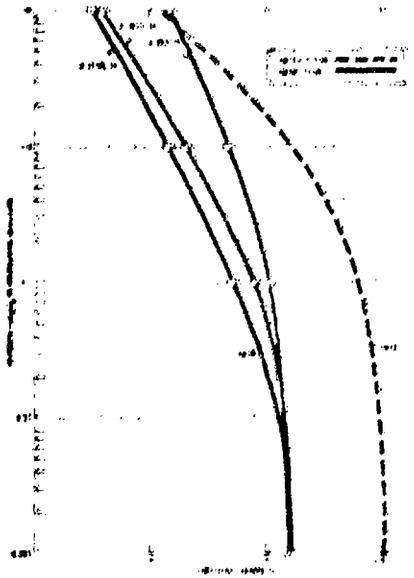

LUCITE, Dy-T FILM
(0.063 TUBE)

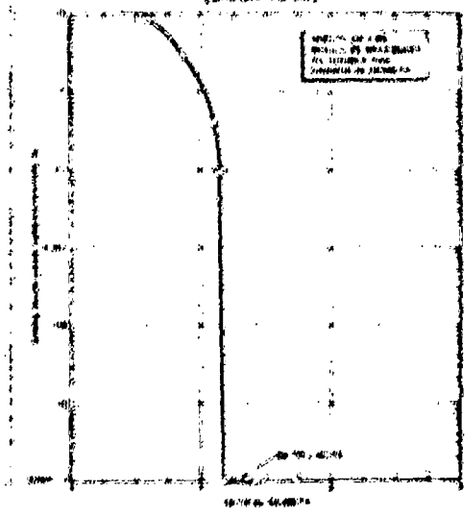

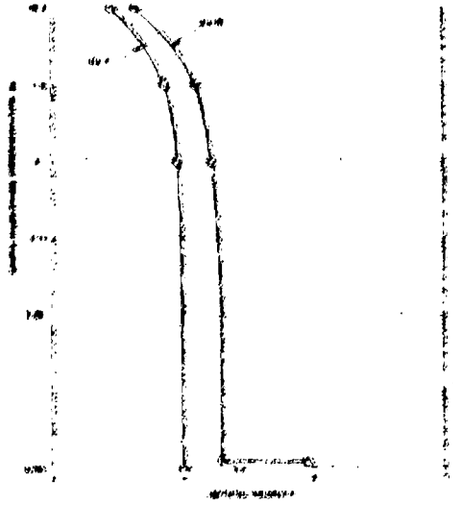

LUCITE
DY-T FILM/DY-M FILM
(0.1875 I.D. TUBE)

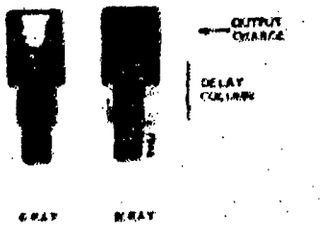

Figure 8
Aerospace Delay
No. 1

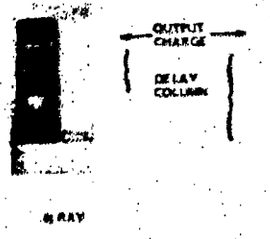

Figure 9
Aerospace Delay
No. 2

Figure 10
Aerospace Delay
No. 3

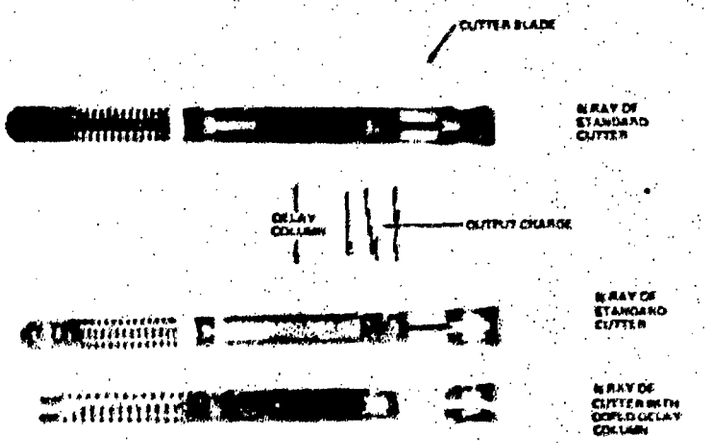

Figure 11
Apollo Reefing Line Cutter

II-12. CONFUSION CONCERNING LEAD AND BOOSTER EXPLOSIVES

R. H. Stresau
R. Stresau Laboratory, Inc.[a]
A Subsidiary of Technical Ordnance

For the last 20 years or so, an effort has been in progress to replace tetryl as the "standard" explosive for leads and boosters. RDX, which is produced in very large quantities for use in main-charge explosive mixtures, is cheaper, more powerful, and has superior thermal stability. On the other hand, RDX is more sensitive by some criteria, and has relatively poor pelleting properties.

Efforts to develop RDX based explosives in which one or both of these disadvantages is alleviated have resulted in the development of RDX, Class C,[1] CH-6,[2] "RDX Pellets,"[3] Composition A4,[4] Composition A5,[5] and various other RDX/binder-desensitizer-lubricant mixtures.[6,7]

The results of these efforts were the beginning of a proliferation of booster explosives which still continues. This proliferation has also been fed by the synthesis of new compounds and the invention of new mixtures to meet special needs (such as resistance to very high temperature) and their infrequent use in applications where the special needs do not appl,.

[a] Address: Star Route, Spooner, Wisc. 54801

Meanwhile, relatively recently, documents, relating to safety,[6,7,8,9] have been issued which limit the choice of explosives for use in such applications to a small fraction of those which had been developed for such use.

Efforts in both areas; the development of new explosives, and the preparation of documents establishing safety criteria, were intended to assist those (such as designers of fuzes and explosive components, and production engineers concerned with such hardware) whose duties include the selection of explosives for such applications. However, in combination and because of their sequence, they have tended to increase the problems of those in such positions.

As the new explosives became available, designers and others were urged to use them to take advantage of the improved properties for which they had been developed or pursuant to the general effort to replace tetryl.

It quickly became apparent that none of the new explosives is an exact duplicate of tetryl[10] with respect to those characteristics which are of interest to a designer or a fabricator of components. The design and production practices and "rules of thumb" which had developed over the years when tetryl was "standard" had to be modified. However, these modifications were somewhat divisive. Typically, a designer or fabricator was influenced to use one or another of a small group of explosives favored by

the agency or branch of the service with which he or his project were associated. He and his associates developed practices and "rules of thumb" which apply to the explosives with which they work.

To the extent that explosives in use were eliminated by the new standard, another cycle of learning and development of practices and "rules of thumb" will be needed for some. Also, there are several fuzes at reasonably advanced stages of development, to which, by its language, the most recent such standard[6] applies, in which explosives are used in locations from which they are proscribed.

MIL-STD 1316A,[6] "Design Criteria for Fuze Explosive Safety," which is "mandatory for use by all Departments and Agencies of the Department of Defense" states that "the following explosives are the only ones permitted in a position leading to the initiation of the main charge without interruption when the fuze is in the safe condition:"

Explosive	Specification
Tetryl	MIL-T-339
RDX Comp CH-6	MIL-R-21723
Tetryl, Pellets	MIL-P-46464
DIPAM	WS 466
HNS Type 1 or Type 2 Gr A	WS 5003

For many (probably most) fuze explosive train applications, the obvious choice of an explosive for leads and boosters is CH-6 (since it is desired to eliminate tetryl, and the other two explosives which are acceptable according to the current standard[6] are almost probitively expensive). However, CH-6 does not perform reliably in all explosive trains. In the event that the reliability of a fuze explosive train is less than required with CH-6 loaded leads or boosters, the following courses of action are available:

(1) Revert to the use of tetryl. Although this runs counter to the objective of replacing tetryl, it is the preferred alternative of many fuze experts with confidence in tetryl based on long experience.

(2) Use HNS of the type (IA or IIA) most appropriate for the application. HNS is acceptable for such use in accordance with MIL-STD 1316A[6] and there are data[10,11,12] which indicate that it will perform reliably in systems where CH-6 fails. However, it is some hundreds of times more costly and HNS IA, which is most susceptible to initiation by small sources, is among the least adaptable to production loading of explosive materials.

(3) Specify a material not listed in MIL-STD 1316A and apply for "written approval . . . from the cognizant technical authority," as provided in the standard,[6] for the use of the alternate material. It is understood that for Navy (and probably Air Force) applications, reasonable confidence can be entertained that such approval will be given leads and boosters of PBXN-5 (which will perform reliably under some circumstances where CH-6 will fail). At the time of this writing, the writer has been unable to contact anyone who would admit to knowing what alternate materials would be accepted for such use in Army applications. One conversation on the subject yielded a list including HMX, Compositions A3, A4, and A5, and six varieties of PBX, which have been proposed for such approval.

Each of these courses of action will meet objections, the first by those who are striving to "phase out" tetryl, the second on the basis of economic and production considerations, and the third by project engineers and managers who must make definite rather than tentative decisions and meet scheduled completion dates.

Since February 1965, a Military Standard[13] has been in preparation on "Qualification Criteria for Booster Explosives." It was originally intended, in MIL-STD 1316 (Navy),[9] to refer to this as a comparison document and to require all explosives for such use to have been qualified in accordance with the comparison document. The list of explosives of MIL-STD 1316[9] was included because the comparison document[13] was not ready for release at that time, as it still isn't.

The document[13] on "Qualification Criteria for Booster Explosives" was not issued in 1965 because some of the tests which were specified had never been performed as specified. The necessary experimental effort progressed rather slowly because of the low level of available funds but by 1969 a draft was prepared in which all tests described had been performed as specified. Since then, procedures have been added and quantitative criteria changed so that some tests again have never been performed as specified. Sufficient funds for the laboratory work which should be completed before release of the document are apparently still unavailable (although some work is in progress at China Lake and the document may be released without laboratory verification of all procedures).

The choice of explosives for leads and boosters could be made more rational by:

(1) Release of the Military Standard[13] on "Qualification Criteria for Booster Explosives," preferably as a DoD document.

(2) Performance of all tests prescribed therein on all seriously proposed booster explosives.

(3) Amendment of MIL-STD 1316A[6] to include, in the list of explosives which may be used "in a position leading to initiation of the main charge without interruption when the fuze is in the safe condition" all explosives which qualify in the tests per Item 2 above and such other criteria which may be applied.

(4) Acquisition of data relating susceptibility to initiation to source size for all qualified booster explosives.

(5) Quantitative comparison of qualified explosives with respect to flow and pelleting characteristics (tests similar to some specified for CH-6 will yield such data).

(6) Compilation of above data, along with cost data, including current prices as quoted by active suppliers and estimates of future costs based on assumed expanded production, in a single document.

(7) Issuance of an advisory instruction, based on the compilation of Item 6 above, and other applicable considerations, giving orders of preference for various applications of lead and booster explosives. This document should be updated at frequent intervals.

The foregoing would substantially increase the probability that each explosive selected for a lead or booster would approach the optimum for the particular application. It is, however, believed that the program outlined would confirm the deficiencies, for one application or another, of each explosive currently available for lead and booster applications and the need for a continuing effort to develop a more generally applicable explosive for such uses.

REFERENCES

1. Military Specification, RDX, MIL-R-398C, 30 October 1963.

2. Military Specification, RDX Composition CH-6, MIL-R-21723 (Nord), dated 23 April 1958.

3. Military Specification, RDX Pellets, MIL-P-45486, 5 Oct 1967.

4. Military Specification, RDX Composition A, MIL-C-440A.

5. Military Specification, Explosive Composition A5, MIL-E-14970 (MU), dated 6 September 1970.

6. MIL-STD 1316A "Military Standard, Fuze, Design Safety, Criteria for," dated 17 September 1970.

7. Fuze Safety Criteria, U. S. Air Force, dated November 1968 (for future publication in AFSC Design Handbook).

8. MIL-STD 332 (MU), "Military Standard Fuze, Army, Design Safety Criteria for," dated 14 May 1969.

9. MIL-STD 1316 (Navy), "Military Standard, Fuzes, Navy, Design Safety Criteria for," dated 16 June 1967.

10. Chamberlain, D. H. and R. H. Stresau, "Micro Scale Gap Test for Explosive Sensitivity," NWCCL TP 841, Naval Weapons Center, Corona Laboratories, March 1969.

11. Stresau, R. H., "A Miniaturized Gap Test," RSLR No. 69-6-1 for the Sandia Corporation, Albuquerque, New Mexico.

12. Stresau, R. H., "A Study of Some Aspects of the Behavior of Hexanitrostilbene (HNS) in Small Charges," RSLR No. 70-3-1 for the Sandia Corporation, Albuquerque, New Mexico.

13. Military Standard "Booster, Explosives, Navy Qualification Criteria for," Department of the Navy, draft of 6 August 1970.

ABSTRACTS - SESSION III RECENT DEVELOPMENTS

III-1 Progress in Explosives and Pyrotechnics — Gunther Cohn

A broad-brush review of explosives and pyrotechnics shows significant progress since Greek fire. Explosives have played a key role not only in warfare but also in industry. Commerce and transportation are absolutely dependent on them. Three sample items:

- Ben Franklin invents electric initiation
- Memoirs of a dynamite salesman
- *explosives and pyrotechnics* newsleter is established

III-2 Direct Laser Initiation of Insensitive Explosives — Vincent J. Menichelli, Lien C. Yang

It has been observed that a shock results when a focussed Q-switched ruby laser pulse (6943Å) interacts with a thin metal film. The shock formed has high potential to immediately detonate explosives such as PETN, RDX, and tetryl. Application of thin metal films to laser initiate explosives is discussed. Results of tests utilizing a special test fixture and smear camera technique are given. Dependance of various parameters such as film material and thickness, loading pressure, and confinement are discussed.

III-3 The Performance Characteristics of Aluminum/Sodium Nitrate Flares in Various Oxygen-Nitrogen Atmospheres — P.L. Farnell, A.J. Beardell, F.R. Taylor

The intensity of light production and burning rate in binary mixtures of aluminum and sodium nitrate have been studied as a function of reactant composition and gaseous atmosphere and the effect of loading pressure was examined. For all systems, the flare burned with low light production when oxygen was excluded from the gaseous atmosphere but was highest in argon and decreased in the same order as the thermal conductivity of the gases increase. As the oxygen content of the gaseous atmosphere was increased the intensity of light production increased steadily and the burning rate was unaffected. It was concluded from these measurements that heat and radiation feedback from the flame have only a minor influence on the burning rate, which is essentially controlled by the exothermic processes at or very near the burning surface. In addition, much of the potential light production that can be achieved using aluminum flares is lost via unreacted aluminum.

III-4 Development of Water-Ignitable Pyrotechnic Compositions — Allen J. Tulis, James L. Austing, Charles K. Hersh

The pyrotechnic formulation consists of a mixture of boron and silver difluoride with a powdered molecular sieve additive. The water-ignitability is attributed to the strong tendency of high valence metal fluorides, such as silver difluoride, to undergo exothermic hydrolysis. The molecular sieve additive allows ignition of the formulation under any method of contact with water, whether the tiniest drop of water is added to the formulation or whether the formulation is dropped into water. Ignition can be achieved under all practical conditions of temperature and pressure; ignition times are in the range of 100 to 150 msec. Typical burning rates are 3 cm/sec, although much higher rates are possible.

III-5 Properties and Performance of Aluminum-Plated Pyrotechnics for Electroexplosive Device Applications — James L. Austing, Robert F. Remaly

Three systems were evaluated, viz., aluminum-plated tungstic oxide, aluminum-plated vanadium pentoxide, and aluminum-plated potassium perchlorate. All of these pyrotechnics are insensitive to pin-to-case electrostatic discharges of the magnitude produced by the human body, and can withstand repeated pulses at potentials of 25 Kv; by way of contrast, the same pyrotechnics formulated from spherical aluminum are extremely sensitive to such discharges. EED's loaded with plated pyrotechnics can be designed to provide a 5-amp, 5-watt no-fire capability. The ignition of the plated pyrotechnics by a hot 5-mil diameter bridgewire at all-fire currents of 15, 20, and 25 amp is shown to be more reliable than ignition of two-powder pyrotechnics under the same conditions.

III-6 Safety Certification of New Pyrotechnic Devices — T.J. Sullivan, Mrs. J.A. McDevitt

The safety evaluation tasks to be performed to certify a new pyrotechnic device for service use in the Navy are presented in this paper. Since the safety evaluation parallels the major life stages of the device, tasks are delineated for concept formulation and contract definition; design and development; evaluation, release for service use and acquisition; and usage and effectiveness determination. A checklist specified requirements for a comprehensive review of the systems design, safety plan, testing, results documentation, and service life. Implementation of various system safety analysis techniques to more effectively assess, describe, and document the safety of the pyrotechnic device is recommended.

III-7 Pyrogen Jet Squib — Dav'd A. Colpitts, Kenneth R. Foote

An experimental electric squib with a jet flame has been developed. The device, containing no primary explosives is initiated within 5 to 10 milleseconds by an electric pulse through a bridgewire coated with a magnesium fluorocarbon mix. A configured tube of the same type of material is used as the main charge. The charge is enclosed in a MARK 1 squib cup and the cup is crimped to a plastic header-plug containing the coated bridgewire. Upon initiation the squib produces a gaseous, coruscative, blow-torch type flame 6-inches long and persists for the 1-1/2 to 2 seconds. The pyrogen squib performs across the temperature range -300°F to +300°F. The squib was developed to initiate difficult-to-ignite propellants and flare compositions.

III-8 Development of a Fully Redundant and Hermetically Sealed Cable Cutter — J.P. Yribarren

This paper presents the mechanical, electrical and pyrotechnical characteristics of an electroexplosive cable cutter. The cutter is designed to cut stainless steel stranded cable or piano wire up to 1.8 mm in diameter. The cable is placed between two movable knives. Both knives and capsules are enclosed in the same body to give a compact device (45 mm x 43 mm x 15 mm). Each cartridge has a single bridgewire and the electrical output can either be flying wires or a 4-pin Bendix type plug. The malleable capsules ensure hermetic sealing during and after firing. The redundancy is complete as the functioning of only one cartridge is sufficient to cut the cable.

III-9 Precision 295 Microsecond Delay Device — R.R. Weinmaster, R.D. Blackshire

A delay device was required which would accomplish a high voltage electrical switch closure at 295±5 microseconds after the input of an EBW firing pulse. A device was designed, built and tested utilizing an EBW detonator, an MDF delay element and an explosively actuated solid dielectric switch. A timing accuracy of 295±2 microseconds was achieved over the extreme temperature range. All detonation products were contained.

III-10 Small Caliber Tracer Ammunition - A Survey Paper — Thomas A. Doris, Jr., Gerald B. Franklin

Micro caliber projectiles have necessitated the development of new techniques for pyrotechnic blending, extrusions and projectile charging. Tracer mixtures with high light output have been developed using zirconium and potassium perchlorate with vinylalcohol acetate resin (VAAR) as a binder. To facilitate charging of these projectiles, a method of extruding pyrotechnic mixtures in a lead sheath of appropriate diameter has been developed. Application of this process has also been accomplished with larger diameters up to 1/4 inch. Pyrotechnic mixtures have been specifically designed to have sustained burning yet emit radiation which is predominantly in the infrared region.

III-11 Potassium Chlorate/Red Phosphorus Mixtures — R.R. Rollins, G.B. Clark

A mixture of $KClO_3/P_4$/Quso/MgO/inert in the proportions 34/14/4/2/46 was tested to determine the variables that affect its sensitivity to initiation by electrostatic discharge, heating, and impact. Modifications of this standard mix, including additives such as Al, Mg, Silica gel, Pyrex, and Cab-o-sil were also investigated. The average 50/50 point energy values determined by the electrostatic, large and small ball drop tests were 0.0145, 0.044, and 0.0018 joules respectively, indicating some effects of interaction and amount of energy required by the different sensitivity tests. The 5 second explosion temperature was 330°C and an activation energy of 16 kcal/mole up to this temperature was calculated. An IR study showed trace amounts of P_4O_{10}, $KClO_4$, KH_2PO_4, and ClO_2 under various environmental treatments.

III-12 Le Decoupage Inter-Etage par Cordeaux Detonant — Pierre Claude

For number of space programs it is often necessary to separate two or several parts of a structure from each other. Explosive devices are quite convenient in such an operation, in order to obtain rapidity, required conditions of simultaneousness, and reliability. It is possible to determine rationally all parameters of an explosive device design by taking into account some elementary principles. In this paper, we present first a schedule of all such parameters, then a definition of a complete explosive device, finally an example of a very simple application. (Paper in French.)

III-1. PROGRESS IN EXPLOSIVES AND PYROTECHNICS

by Gunther Cohn

The Franklin Institute Research Laboratories, Philadelphia, Pa.

To obtain the correct perspective of progress, we should start at the beginning and measure from there. Figure 1 shows the advances of weapons over the years.[1] Without quibbling over what constitutes a whole-order advance, I believe the trend is clear: a typical exponential increase in science and technology. (Note that the artist changed scales at year zero but the distortion matters little.) Two thousand years ago, the phalanx was invincible. How could you overpower a square of men with their shields facing out? But look at the formidable growth since that time.

• 672 Battle of Cyzicus	Greek fire	2-200*
• 1242 Roger Bacon	black powder	3-8
• 1313 Berthold Schwartz	powder weapon	3-10
• 1346 Battle of Crécy	powder weapon used	2-332
• 1578 Bourne	powder tester	3-19
• 1627 Schemnitz, Hungary	powder in mining	3-11
• 1675 Mildon, Mass.	first US powder mill	3-32
• 1701 Charles XII, Sweden	burned damp straw	4-2

From this overview, let us focus in to the year 672 and the introduction of a major new weapon: Greek fire. Decisive and history making, this mixture of sulfur, naphtha, and quicklime was introduced to warfare by the Byzantines during the first Moslem siege of Constantinople. Greek fire burst into flames when wetted. The deadly effect of this weapon upon ships and soldiers can well be imagined. It retained the Byzantine maritime supremacy against a strong Moslem challenge and also helped to keep the walls of Constantinople inviolate.

While black powder was probably known earlier, the composition was specified by Roger Bacon in his defense against the accusation of witchcraft. For the next 600 years, this mixture of saltpeter, charcoal, and sulfur was king. The English are credited with the first use of gunpowder weapons. By our standards, the early weapons were crude, consisting of pot-shaped vessels that propelled arrow-like bolts inaccurately (see Figure 2).

We enter now the age of improvements. They came so fast that I dare not stop at each milestone. To describe just one example, note Bourne's improved output tester (Figure 3). It made use of a small metal cylinder (G) in which the powder is ignited by the hammer (F). The angle turned by the lid attached to the ratchet wheel (H) against the spring (I) is the measure of powder strength. Incidentally, the illustration is from the Diderot encyclopedia. (Diderot, a brilliant thinker, gathered a large team of experts to document all of science. The publication, from the first volume in 1751 to volume 28 (plate 4000) in 1772, was sporadic. Forces in both church and state sought to suppress what they considered dangerous thinking.)

The other examples show that it took almost 400 years for the first commercial application of black powder, that the US started manufacturing in 1675, and that the King of Sweden laid the first smoke screen.

• 1750 Ben Franklin	electric initiation	5-116
• 1800 Edward Howard	mercury fulminate	3-732
• 1814 Francis Scott Key	inspired by rockets	-
• 1831 William Bickford	safety fuse	3-722

It is not generally known but Ben Franklin invented electric initiation (Figure 4). He writes, in a letter to Peter Collinson, "I have not heard that any of your European electricians have ever been able to fire gunpowder by the electric flame. We do it here in this manner. A small cartridge is filled with dry powder, hard rammed, so as to bruise some of the grains; two pointed wires are then thrust in, one at each end, the points approaching each other in the middle of the cartridge till within the distance of half an inch; then, the cartridge being placed in the circuit, when the four jars are discharged, the electric flame leaping from the point of one wire to the point of the other, within the cartridge against the powder, fires it, and the explosion of the powder is at the same instant with the crack of the discharge."

*Means Reference 2, page 200.

Howard's discovery of mercury fulminate introduced the first practical primary high explosive. Francis Scott Key's experience at Ft. McHenry requires no elaboration; however, Bickford's safety fuse does. In the early days, powder was ignited by crude fuses - fine trains of powder prepared by the miners or gunners themselves. Naturally, they were quite uncertain and caused many accidents. Bickford's uniform fuse, encased in jute threads is credited in reducing the number of killed and wounded from blasting accidents by fully 90 percent (see Figure 5).

That explosives played a key role in industry is well known. Commerce and transportation are absolutely dependent on them. The expansion of the West and the building of the Panama Canal could not have been achieved without them. And we need not look that far for examples. For instance, there was no railroad to Pittsburgh in the 1840's. If one wished to travel from Philadelphia he took a boat from there down the Delaware River and into the Chesapeake Bay to the mouth of the Susquehanna River; thence by smaller craft on this river he reached Harrisburg, and from there he traveled by canal to the foot of the mountains. He was then transported over the mountains on an incline railroad operated by cable. His journey was finally completed by canal boat.

• 1861 Alfred Nobel	nitro-glycerin	3-320
• 1867 Alfred Nobel	dynamite & cap	3-322
• 1871 Moses Farmer	blasting machine	3-749
• 1880 Picatinny Arsenal	founded	6-4

This then by way of introduction to the modern period ushered in by true high explosives. Dynamite, like other new fangled ideas, was tough to sell. Miners feared the new, powerful explosive would cut down the number of jobs. Listen to the experiences of Fred Julian, salesman for the Atlantic Giant Powder Co.:

"You will wonder, perhaps, how I convinced these men and hundreds, perhaps thousands, of men afterwards that dynamite was not dangerous. Well, I simply took a cartridge, which I carried with me in a valise, and placed it on a plank; then I would take a sledge hammer and pound it, light a match and set fire to it while holding the cartridge in my hand, let it burn a little while, knock off the fire, and put the remainder in my valise for future use. This I did thousands of times in the next ten years.

"I used to go to the sewers clad in overalls and working boots, get friendly with the men and strike the drill for this man and then that man. At noon and again in the evening I would take the fellows to a saloon. When I felt the time was ripe I would tell them what I wanted. Then I would go to the foreman, and later to the contractor, and if all were willing I would demonstrate. Sometimes I would get an order for fifty or a hundred pounds, often nothing, and so it went along. My salesmen were doing next to nothing in the way of getting orders. They were well dressed, were not experts, and were afraid to soil their clothes. Finally I discharged most of them and hired nine good rock miners, most of whom could not even write, and sent them on the road with instructions to drill holes and demonstrate anywhere and everywhere they could, and if they could not sell dynamite, to give it away, for we simply had to get business, cost what it might.

"In July I went to Southeastern Missouri, to the town of Granby. I had taken, no matter how, about six hundred pounds of dynamite to St. Louis. The railroads would not carry it, if they knew. I had left about 525 pounds in a leading hotel while I went out to Granby. On arriving, while going up the street, I met a miner whom I had known at Hell Gate. When I told him my business, he at once circulated the report among the miners that if they used dynamite they would be severely poisoned. The result was that I was there three weeks before I could get a single man to permit me to make a demonstration in his workings. Finally Harry Tamblyn, who kept a saloon there and was afterwards to become my agent, said: 'Julian, you will never get in a shot unless you set them up for the men.' I at once said: 'Let her go for a hundred dollars.' The next day a man named Chester told me I could put a shot in his workings. So Tamblyn and I went there, drilled our holes, and fired the shot with wonderful success. I then sold 375 lb of dynamite for $1.00 a pound and ordered 2,000 lb more from New York."

After noting the first practical blasting machine, we return to the military. Picatinny had several problems in its early days, none the least of which was Washington. In documenting the depot's brush-clearing operation, an 1887 report

noted the use of "eight public animals - three horses, three mules and a yoke of oxen." Offical Washington took issue with the CO's communique: "Your table of organization and equipment does not show oxen. Where did you get them? Answer by endorsement." One way or another, the chain of commanding officers managed - despite Washington intervention on small matters - to put together an organization that was to continue in a key role for another century (see Figure 6).

• 1916 Battle of Jutland	chemical smoke screen	4-2
• 1916 von Hindenburg	collects saltpeter	Append
• 1927 Ordnance Corps	spelling of fuze	Append
• 1967 Gunther Cohn	e & p newsletter	-

I mention the battle of Jutland in the contemporary period to let you know that we have improved over the King of Sweden. The stories of von Hindenburg and the Ordnance Corps are appended. And, of course, everyone recognizes the commercial for the *explosives and pyrotechnics* newsletter (see Figure 7).

All I have attempted to do in these very broad strokes is to whet your appetite for some of the romance in our business. We have seen the rise and fall of black powder and, more recently, of dynamite.[7] We owe much to the military who have consistently funded innovation. By touching all endeavors of mankind, the history of explosives makes for delightful reading. Try some; you'll enjoy it.

References

1. Gunther Cohn, "Harnessing Technical Information," Current Engineering Practice (Bombay, India), Vol. 13, No. 2, April-May-June 1970, pp. 27-33.
2. R. E. Dupuy and T. N. Dupuy, *Encyclopedia of Military History*, Harper & Row, New York, 1970.
3. A. P. Van Gelder and H. Schlatter, *History of the Explosives Industry in America*, Columbia University Press, New York, 1927.
4. *Military Pyrotechnics, Part I, Theory and Application*, Army Materiel Command, Engineering Design Handbook AMCP 706-185, April 1967.
5. Charles E. Munroe, "Benjamin Franklin's Unheralded Achievement," The Explosives Engineer, Vol. III, April 1925, pp. 115-118.
6. *The Floating Story*, Picatinny Arsenal, Dover, N. J. (no date).
7. "Dynamite Industry Is Quietly Fading Away; Fertilizer Product Gains Most of Market," Wall Street Journal, May 18, 1971, p. 40.

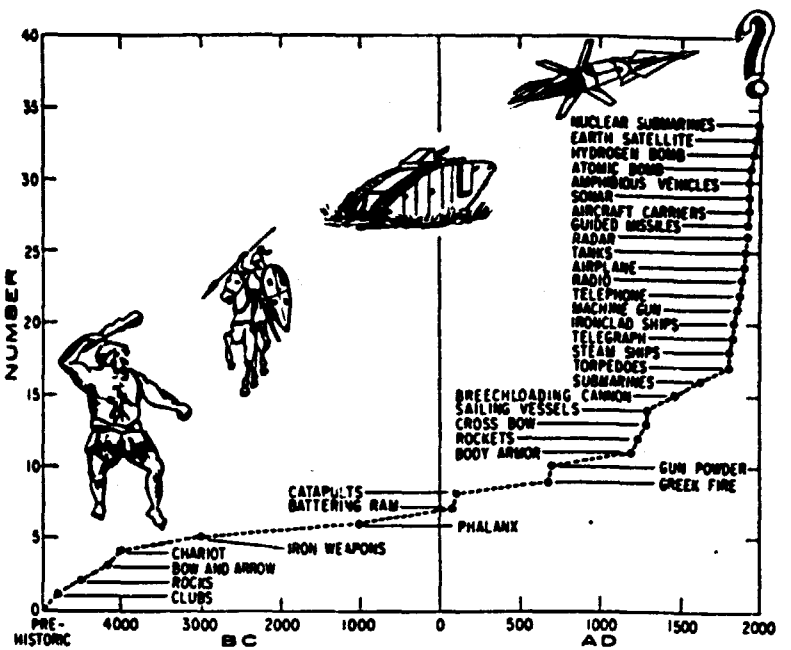

Fig. 1. Changes of Whole Order in Warfare

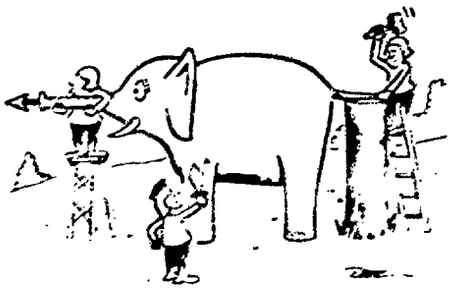

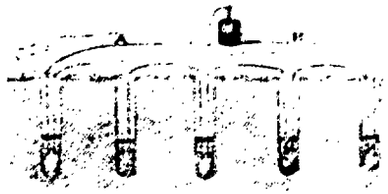

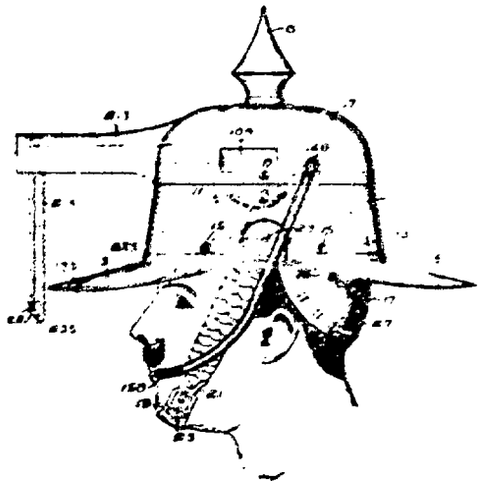

APPENDIX

EXCERPT OF MINUTES OF THE ORDNANCE COMMITTEE MEETING

Meeting No. 13 held Thursday, March 31, 1927
Item 6136: Spelling of the Word 'Fuze' in Printed Publications

"1. This office has been informed that the printing, by the Government Printing Office, of publications containing the word 'fuze' has been held up due to the fact that the Style Manual prescribes the spelling 'fuse'. In view of the fact that the matter is of much greater importance than might at first appear, it is desired to set forth the facts in the case from the standpoint of this office.

"2. The Ordnance Department, soon after the Spanish-American War, adopted the practice of designating by the spelling 'fuze' these items of ordnance materiel which may be defined as follows: 'A mechanical device, with or without explosive elements, used to explode a shell, bomb or other type of projectile.' . . .

"5. To adopt the spelling 'fuse' and change all drawings, specifications, orders, records, etc., and to re-mark all the war reserve of fuzes would involve a prohibitive expenditure of funds and would require years to complete. . . It is conservatively estimated that the remarking of the twenty-seven million fuzes in storage alone would cost at least Two Hundred and Fifty Thousand Dollars; while the cost of the other changes required, though difficult to estimate, would be heavy. The possibility of obtaining the necessary funds from Congress is extremely remote. It is apparent that this course is impracticable.

"6. To use the spelling 'fuse' in the future without asking any changes in existing publications, orders, records, war reserve stocks, etc., would lead to endless confusion, involving two especially important aspects, viz: accidents and complication of supply . . .

"7. To continue the present practice will apparently involve changing the Style Manual, at least to the extent of permitting the printing of either 'fuse' or 'fuze' according to the manuscript submitted. Just what disadvantages this would involve from the standpoint of the Public Printer, this office is of course not in a position to judge. It is, however, ugently recommended that any such disadvantages be carefully weighed against the serious disadvantages of the other two alternatives as indicated above . . .

"The Permanent Board on the Revision of the Style Manual reports that the wishes of the War Department can be met in this instance. Your request is therefore approved and the word 'fuze' will be adopted by this office to indicate a mechanical device used for purpose of explosion. . ."

AN INCIDENT OF THE GREAT WAR

At the beginning of the second year of WWI, Germany had found herself short of saltpetre, one of the most important ingredients in the manufacture of gunpowder. It gave opportunity to demonstrate the wonderful resourcefulness of the German nation as is proved in the fact that the following appeared in the Berlin papers as an official adver isement:

NOTICE

The women of Germany are commanded to preserve their chamber lye, as it is very needful to the cause of the Fatherland in the manufacture of gunpowder. Wagons with barrels and tanks will be sent through the city daily to collect and remove the same.
(Signed) VON HINDENBURG, Commanding

A German soldier in the trenches, even with the fear of Les Majestes in his heart, on seeing the advertisement, perpetrated the following:

Von Hindenburg, Von Hindenburg, you are a funny creature;
You've given to this cruel war a new and funny feature.
You'd have us think, while every man is bound to be a fighter,
The women - bl ss their darling hearts! - should save their "P" for nitre.

Von Hindenburg, Von Hindenburg, where did you get the notion
Of sending barrels 'round the town to gather up the lotion?
We thought a women's duty was at keeping house and diddling,
But now you've put the dears to patrictic piddling.

Von Hindenburg, Von Hindenburg, do pray invent a neater
And somewhat less immodest way of making your saltpetre.
For Fraulein fair, with golden hair, with whom we all are smitten,
Must join the line, and jerk their brine, to kill the bloomin' Briton.

A copy of the poetic effort found its way into a British trench, and an English soldier wrote the following addenda, which was sent back to the German defenses:

Von Hindenburg, Von Hindenburg, we read in song and story,
How many tears, in all the years, have sprinkled fields of glory,
But ne'er before have women helped their braves in deeds of slaughter
Till German beauties dried their tears and went to making water.

No wonder, Von, your boys are brave! Who would not be a fighter
If every time he shot his gun he used his sweetheart's nitre?
And vice versa, what would make an Allied soldier sadder
Than dodging bullets from a pretty women's bladder?

We've heard it said a subtle smell still lingers in the powder,
And as the smoke grows thicker and the din of battle louder,
That there is found to this compound a serious objection -
A soldier cannot take a sniff without having an erection.

'Tis clear now why desertion is so common in your ranks;
An Arctic nature 's needed to withstand Dame Nature's pranks.
A German cannot stand the strain; when, once he's had a smell,
He's got to have a piece or bust - the Fatherland to Hell!

III-2. DIRECT LASER INITIATION OF INSENSITIVE EXPLOSIVES*

Vincent J. Menichelli
L. C. Yang

California Institute of Technology
Jet Propulsion Laboratory
Pasadena, California 91103

ABSTRACT

Instantaneous longitudinal detonations have been observed in confined columns of PETN, RDX, and tetryl when pulsed with light energy from a focused Q-switch ruby laser. The laser energy ranged from 0.5 to 4.2 joules with a pulse width of 25 nanoseconds. Enhancement of the ignition mechanism is hypothesized when a 1000 Å thick aluminum film is vacuum deposited on the explosive side of the window. Upon irradiation from the laser a shock is generated at the aluminum-explosive interface. Steady state detonations can be reached in less than 0.5 microsecond with less than 10 percent variation in detonation velocity for PETN and RDX.

INTRODUCTION

Immediate detonation of secondary high explosives require a strong shock input. The threshold magnitude of the shock being dependent upon such parameters as explosive density, particle size, and confinement. Conventional means of achieving detonation in secondary high explosives is by the use of the explosive train. These trains, in general, are initiated by mechanical firing pins (stab or percussion) or electrically (hot bridgewire). The first component in the train is usually a primary high explosive sensitive to heat, friction, impact, and static electricity, and also having poor simultaniety characteristics. The train then proceeds with increments of less sensitive, more energetic explosives. Eventually, in a short distance, the burning reactions develop into a detonation. These systems require very little energy to initiate (0.1 joule or less) and are quite vulnerable to inadvertent initiation. To ward against accidental initiation of the main charge a Safe and Arming mechanism (S and A) is usually employed. Work has been carried out to develop insensitive explosive trains, using only secondary high explosives which will initiate from a unique energy source e.g., strong light, or exploding wire. The advantages are many fold i.e., the elimination of primary high explosives, elimination of complicated S and A's, and an improvement in simultaniety and functioning time. Bowden, et al studied the sensitivity of explosives to strong light sources (ref. 1). Leopold was able to detonate PETN with exploding bridgewires (EBW) (ref. 2). Detonation of PETN by EBW was very dependent upon parameters such as loading density, particle size and shape, purity, bridgewire size and material, and discharge circuitry.

In order to reach immediate detonation in secondary high explosives such as PETN, RDX, and tetryl threshold external shock strengths ranging from 7 to 15K bars are needed (ref. 3). In recent years pulsed laser radiation as an energy source to initiate explosives has been studied. Space Ordnance Systems, Inc. investigated the sensitivity of pyrotechnics and propellants to laser energy under a JPL contract (ref. 4). During this

*This paper presents the results of one phase of research carried out at the Jet Propulsion Laboratory, California Institute of Technology, under Contract No. NAS 7-100, sponsored by the National Aeronautics and Space Administration.

study no unconfined secondary high explosives could be initiated from a focused ruby or neodymium pulsed laser in the free running mode (up to energy 15 joules). Barbarisi, et al at Picatinny Arsenal, N. J. studied the reaction of PETN to a pulsed ruby laser (focused) in the free running and Q-switched modes (ref. 5). Ignition was obtained in both modes but direct detonations were not confirmed. The Russians have reported similiar work and successfully detonated PETN (density 1.0 g/cm^3) from a pulsed ruby laser (0.5j) in the Q-switched mode (ref. 6). Experiments have been carried out at JPL to detonate secondary high explosives with a focused ruby laser in the Q-Switched mode. Figure 1 shows a cross section of the test vehicle used. Some detonations were achieved with PETN and RDX as witnessed from a dent obtained on a steel witness block and expansion of the steel test vehicle. The time to detonation was not known and it appeared that uncertainties such as explosive surface conditions, trapped air, impurities, and crystal imperfections were playing an important role in the initiation mechanism.

LASER GENERATED SHOCKS

The interaction of Q-Switched laser pulses with a solid target was known to result in rapid expanding plasmas (ref. 7). The process, when observed with a streak camera in air at JPL was not clear, possibly due to ionization of the air by the laser. Figure 2 shows the results of experiments conducted with metal targets in a vacuum (1 mm Hg). The resulting plasma propagation is more defined. An approximation of the shock is measured by the propagation of the luminous plasma boundry. From these results, application of the shock (in the order of several cm/μsec) to detonate secondary high explosives seemed appropriate. The mechanism is similar to EBW or exploding foil. However, the laser shock is physically different in that the shock velocity is an order of magnitude higher and the duration shorter (a few hundred nanoseconds compared to about 2 microseconds).

Selection of target material and thickness for application to laser initiation of explosives was based on some preliminary experiments and considerations. In general, the absorption of light in a solid is completed within 200-1000Å of light path which is close to the light skin depth of the material with the execption of high absorptive materials like carbon black. Carbon black is difficult to prepare and hard to handle as a thin film. Vacuum deposition of thin metal films are quite easy to obtain but are highly reflective at low light energy levels. However, at high light energy levels a plasma is formed which increases the absorptivity by orders of magnitudes. Aluminum was selected because it has a low melting point and is easy to vacuum deposit on a glass substrate. Other metals may be more efficient but a study to optimize the target material was not made. The optimum thickness was found to be about 1000Å. Films thicker than 1000Å caused the average dynamic transmission of the Q-Switched laser light to be less than 1.0 percent and the amount of post irradiated film remaining became significant (Fig. 3). There would be no advantage to increase the thickness because the additional mass would result in a lower temperature and pressure in the plasma during the laser absorbtion period. Films thinner than 1000Å were completely vaporized before absorbtion of all the laser energy. Various thickness aluminum targets were irradiated with 1.67 joules of focused laser energy and the shocks generated are shown in figure 4.

TEST APPARATUS

A Korad K-1Q laser system with a KDP* Pockel cell was capable of producing 4.5 joules of energy in a pulse width of 25 nanoseconds. The laser head utilized a ruby rod 1.43 cm in diameter and 7.6 cm long. The laser beam was focused with a double convex lens 30 cm in focal length. An extra 6-plate Brewster stack polarizer was used to completely eliminate preiasing at high pumping levels. A schematic of the experimental configuration is shown in Figure 5. A Beckman-Whitley Model 200 Simultaneous Streak and Framing Camera was used to record the event. The steel mirror was operated at 1000 RPS which corresponds to a writing speed of 2.76 mm/microsecond or at a time resolution of 50 nanoseconds. The laser power supply was triggered by a synchronous sequence when the rotating mirror reached a preset position and speed. Figure 6 shows the laboratory arrangement for conducting the experiments. The explosive sample is placed in a safety chamber and aligned with the laser. The laser pulse enters the chamber through a portal containing the focusing lens. The streak camera is aligned perpendicular to the axis of the explosive column. Several different explosive test vehicles were used which contained viewing optics so that the light from the reaction could be recorded. Figure 7 shows a test vehicle in which a plastic rod serves as the viewing port. The glass window with the metal film facing the explosive column is held in the cavity provided with an end plate to contain it. The explosive under test is then loaded against the window. A cold rolled steel witness block completes the test vehicle assembly. A second test vehicle is shown in Figure 8. The explosive is loaded into a glass tube and then assembled into a brass fixture in much the same manner as the previous assembly. The components are interference fitted because good confinement is critical in the initial phase of ignition.

TEST RESULTS

Approximately 90 firings were made involving five different explosives; PETN, RDX, Tetryl, HNS, and Dipam. The different parameters studied were density, particle size, explosive diameter, laser energy, and plain or aluminized windows. Dipam and HNS did not detorate under any of the conditions tested although in two cases HNS completely burned at maximum energy input. Table 1 summarizes the results. As expected PETN was the most sensitive to laser energy of the explosives tested. The minimum energy required was below 1.0 joule at 5K psi loading pressure. Detonations were observed with 2 joules of laser energy at loading pressures up to 25K psi. The PETN particle size did not appear to be critical to laser detonation. Table 2 summarizes the PETN data. RDX was tested at loading pressures ranging from 1K to 50K psi. Ignitions were observed up to 50K psi but immediate detonation occurred only up to 5K psi. Particle size apparently influenced the detonability of RDX since no detonations were observed with coarse material. This agrees with Stresau's results (ref. 8). Most detonations occurred using an aluminized window. The RDX results are summarized in Table 3. Only seven tests have been completed with tetryl. Two detonations were observed with milled tetryl at 1K psi loading pressure and aluminized windows. Under the same conditions, except for a plain window, detonation did not occur. The results from these tests are summarized in Table 4.

The streak camera records of most of the items which detonated were analyzed for total reaction time (time from laser pulse to the end of the reaction), transient time (time from laser pulse to start of steady state detonation), and steady state detonation velocity. Several items which detonated are omitted because of the poor quality of the streak record. Table 5 summarizes the data and compares the measured detonation velocities with ideal detonation velocities. The measured detonation velocities are close to the ideal detonation velocities. Steel dent values are also listed and the depth values are directly ordered with the detonation velocity. Figures 9, 10, and 11 show some of the smear records obtained of the items in Table 5. In the case of PETN were coarse power was used the transient time is quite long (microseconds) when compared to the tenths of microseconds for milled PETN. One RDX test had a zero transient time. Tetryl had a relatively long transient time of 1.45 microseconds. It is noted that the laser energy listed is the energy measured at the laser head. The lens, lucite entrance window, and glass window each transmit about 92 percent of light energy.

DISCUSSION

In some instances in the tables, a burn to detonation is recorded rather than a detonation or complete burn. The streak camera results for these cases showed burning during the writing time of the camera. Later the reaction went to detonation which was verified by a dent in the steel witness block. All the streak camera records showed light streaks at the fixture surface/air interface and along the length of the explosive column. This light was emitted when the margin of the laser focal spot interacted with the metal surface. The laser light was also scattered diffusively through the glass tubing or lucite rod.

It is apparent that for PETN and RDX instantaneous detonations were achieved. In some cases, the transient times were less than 0.5 microsecond and variations in detonation velocity less than 10 percent. PETN did not exhibit an increase in sensitivity when the aluminized window was substituted for the plain window. The initiation mechanism for PETN may be very complicated so that the effects of the aluminized window are over shadowed by other mechanisms. RDX appears to be more sensitive to detonation when the aluminized window is used. Tetryl definitely demonstrated that the aluminized window is necessary to achieve detonation. In all cases, the fine particle size (less than 40 microns) and loading pressures below 5K psi increased the explosive sensitivity.

Comparison of the laser detonation results with EBW studies show that laser induced detonations are not as sensitive to loading density as in EBW. This may be due to the much higher shock velocity generated by the laser. Probably for this same reason explosives less sensitive than PETN were directly detonated. Small deviations from 1.0 g/cc in EBW applications makes a considerable difference in sensitivity. Because explosives loaded at densities greater than 1.0 g/cc can be laser detonated a corresponding higher detonation velocity can be achieved. The detonation velocities obtained by laser initiation are closer to the ideal detonation velocity than those reported by EBW initiation.

REFERENCES

1. Bowden, F.P. and Yoffe, A.D., "Fast Reactions in Solids", Butterworths Scientific Publications, 1958
2. Leopold, H.S., "Initiation of Explosives by Exploding Wires III", NOLTR 64-2, U.S. Naval Ordnance Laboratory, White Oak, Maryland, 17 March 1964
3. Scott, C.L., "Effect of Particle Size on Shock Initiation of PETN, RDX, and Tetryl", the Fifth Symposium on Detonation, Pasadena, California, August 1970, pp 148
4. Menichelli, V. J., and Yang, L. C., "Sensitivity of Explosives to Laser Energy", Technical Report 32-1474, Jet Propulsion Laboratory, Pasadena, California, 30 April 1970
5. Barbarisi, M.J. and Kessler, E.G., "Initiation of Secondary Explosives by Means of Laser Radiation", Technical Report 3861, Picatinny Arsenal, Dover, New Jersey, May 1969
6. Brish, A.A. et al, "Initiation of Detonations in Condensed Explosives with a Laser", Combustion and Explosive Physics, No. 3, 1966 pp 132-133, AD676263
7. Basov, N.G. et al, JETP Letter 6, 168, 15 Sept. 1967
8. Stresau, R.H.F. et al, "Confinement Effects in Exploding Bridgewire Initiation of Detonation", Fourth Symposium on Detonation, U.S. Naval Ordnance Laboratory, White Oak, Maryland Oct 1965

TABLE I. CONDITIONS AND RESULTS FOR LASER TESTING OF HNS AND DIPAM

	EXPLOSIVE	CRYSTAL SIZE	LOADING PRESSURE (KPSI)	LASER ENERGY (JOULES)	CHARGE DIA. (CM)	CHARGE LENGTH (CM)	CONFINEMENT	WINDOW	RESULTS
1	HNS	M	1	6.0	0.3	2.54	GLASS	P	FAILED TO IGNITE
2	HNS	M	1	6.0	0.3	2.54	GLASS	Al	FAILED TO IGNITE
3	HNS	C	1	6.2	0.24	2.54	STEEL	Al	FAILED TO IGNITE
4	HNS	C	5	6.2	0.24	2.54	STEEL	Al	BURNED COMPLETELY
5	HNS	C	10	6.2	0.24	2.54	STEEL	Al	BURNED COMPLETELY
6	HNS	C	10	3.0	0.3	2.54	GLASS	Al	FAILED TO IGNITE
7	HNS	C	10	3.0	0.3	2.03	GLASS	Al	FAILED TO IGNITE
8	HNS	C	10	3.0	0.3	2.03	GLASS	Al	FAILED TO IGNITE
9	HNS	C	50	6.2	0.24	2.54	STEEL	Al	FAILED TO IGNITE
10	DIPAM	M	1	3.0	0.27	2.03	STEEL	Al	FAILED TO IGNITE
11	DIPAM	M	1	3.0	0.27	2.03	STEEL	P	FAILED TO IGNITE
12	DIPAM	C	10	3.0	0.3	2.54	GLASS	Al	FAILED TO IGNITE

M = MILLED FOR 16 HOURS IN CHLOROFORM
C = COARSE (AS RECEIVED)
P = PLAIN GLASS WINDOW
Al = 1000 Å ALUMINIZED GLASS WINDOW IN CONTACT WITH EXPLOSIVE

TABLE II CONDITIONS AND RESULTS FOR LASER TESTING PETN

	CRYSTAL SIZE	LOADING PRESSURE (KPSI)	LASER ENERGY (JOULES)	CHARGE DIA. (CM)	CHARGE LENGTH (CM)	CONFINEMENT	WINDOW	RESULTS
1	M	5	0.8	0.38	2.06	STEEL	P	DETONATED
2	M	5	0.5	0.38	2.06	STEEL	Al	BURN TO DETONATION
3	M	5	0.8	0.38	2.79	STEEL	Al	DETONATED
4	C	10	4.0	0.3	2.03	GLASS	Al	BURNED
5	C	10	4.0	0.3	2.03	GLASS	Al	DETONATED
6	C	10	3.0	0.3	2.03	GLASS	Al	DETONATED
7	C	10	3.0	0.3	2.54	GLASS	Al	FAILED TO IGNITE
8	C	10	3.0	0.3	2.54	GLASS	Al	DETONATED
9	C	10	3.0	0.38	2.79	STEEL	P	DETONATED
10	M	19	1.0	0.38	2.06	STEEL	P	DETONATED
11	M	19	1.0	0.38	2.06	STEEL	Al	DETONATED
12	M	25	0.8	0.38	2.06	STEEL	P	BURNED
13	M	25	0.8	0.38	2.06	STEEL	Al	BURNED
14	M	25	2.0	0.38	2.06	STEEL	P	DETONATED
15	M	25	2.0	0.32	2.06	STEEL	Al	BURNED
16	M	25	3.4	0.3	2.54	GLASS	Al	FAILED TO IGNITE

M = MILLED FOR 16 HOURS IN CHLOROFORM
C = COARSE (AS RECEIVED)
P = PLAIN GLASS WINDOW
Al = 1000 Å ALUMINIZED GLASS WINDOW IN CONTACT WITH EXPLOSIVE

TABLE III. CONDITIONS AND RESULTS FOR LASER TESTING RDX

	CRYSTAL SIZE	LOADING PRESSURE (KPSI)	LASER ENERGY (JOULES)	CHARGE DIA. (CM)	CHARGE LENGTH (CM)	CONFINEMENT	WINDOW	RESULTS
1	M	1K	1.0	0.3	2.54	GLASS	P	DETONATED
2	M	1K	1.0	0.3	2.54	GLASS	Al	DETONATED
3	M	1L	1.5	0.1	2.54	GLASS	Al	DETONATED
4	M	1K	3.5	0.27	2.06	STEEL	Al	BURN TO DETONATION
5	M	1K	3.5	0.1	2.54	GLASS	Al	DETONATED
6	M	1K	3.8	0.27	2.06	STEEL	Al	DETONATED
7	M	1K	3.8	0.27	2.06	STEEL	P	BURN TO DETONATION
8	C	1K	3.5	0.38	2.79	STEEL	Al	COMPLETE BURN
9	M	1K	4.0	0.1	1.78	STEEL	Al	DETONATED
10	C	1K	4.2	0.38	1.01	STEEL	Al	FAILED TO IGNITE
11	M	5K	1.0	0.3	2.54	GLASS	Al	FAILED TO IGNITE
12	M	5K	1.0	0.3	2.54	GLASS	P	FAILED TO IGNITE
13	M	5K	2.85	0.3	2.54	GLASS	P	FAILED TO IGNITE
14	M	5K	3.13	0.3	2.54	GLASS	Al	DETONATED
15	M	5K	3.5	0.1	2.54	GLASS	Al	DETONATED
16	M	5K	3.5	0.27	2.06	STEEL	Al	FAILED TO IGNITE
17	M	5K	3.8	0.27	2.06	STEEL	Al	DETONATED
18	M	5K	3.9	0.27	2.06	STEEL	P	DETONATED
19	M	5K	4.0	0.1	1.78	STEEL	Al	DETONATED
20	C	5K	4.2	0.38	1.01	STEEL	Al	COMPLETE BURN
21	C	10K	4.0	0.38	2.79	STEEL	Al	FAILED TO IGNITE
22	M	10K	2.1	0.3	2.54	GLASS	P	FAILED TO IGNITE
23	M	20K	2.1	0.3	2.54	GLASS	Al	FAILED TO IGNITE
24	C	10K	3.0	0.3	2.03	GLASS	Al	COMPLETE BURN
25	C	10K	3.0	0.3	2.54	GLASS	P	FAILED TO IGNITE
26	C	10K	3.0	0.3	2.54	GLASS	P	FAILED TO IGNITE
27	C	10K	3.0	0.3	2.54	GLASS	P	FAILED TO IGNITE
28	C	10K	3.0	0.51	0.76	STEEL	Al	COMPLETE BURN
29	C	10K	3.0	0.38	2.79	STEEL	Al	COMPLETE BURN
30	C	10K	3.0	0.38	2.79	STEEL	P	COMPLETE BURN
31	C	10K	3.0	0.38	2.79	STEEL	P	FAILED TO IGNITE
32	C	20K	3.0	0.24	2.54	STEEL	Al	BURN TO DETONATION
33	C	10K	3.5	0.24	2.54	STEEL	Al	COMPLETE BURN
34	C	10K	3.5	0.24	2.54	STEEL	A	COMPLETE BURN
35	M	10K	3.8	0.3	2.54	GLASS	P	FAILED TO IGNITE
36	C	10K	4.0	0.38	2.79	STEEL	A	COMPLETE BURN
37	C	10K	4.0	0.38	2.79	STEEL	A	COMPLETE BURN
38	M	10K	4.0	0.1	1.78	STEEL	Al	FAILED TO IGNITE
39	M	10K	4.0	0.27	2.06	STEEL	Al	COMPLETE BURN
40	M	15K	4.0	0.3	2.54	GLASS	Al	FAILED TO IGNITE
41	C	15K	4.2	0.38	2.79	STEEL	Al	COMPLETE BURN
42	C	10K	4.3	0.24	2.54	STEEL	Al	COMPLETE BURN
43	C	10K	4.3	0.27	2.06	STEEL	Al	COMPLETE BURN
44	C	15K	4.2	0.38	1.01	STEEL	Al	COMPLETE BURN
45	C	10K	4.2	0.27	2.06	STEEL	Al	COMPLETE BURN
46	M	20K	4.4	0.3	2.54	GLASS	Al	FAILED TO IGNITE
47	M	15K	4.6	0.3	2.54	GLASS	P	FAILED TO IGNITE
48	C	30K	4.0	0.38	2.79	STEEL	P	COMPLETE BURN
49	C	30K	4.0	0.38	2.79	STEEL	Al	FAILED TO IGNITE
50	C	35K	4.0	0.23	2.79	STEEL	Al	COMPLETE BURN
51	C	50K	4.2	0.38	1.01	STEEL	Al	FAILED TO IGNITE
52	C	50K	4.2	0.38	1.01	STEEL	Al	COMPLETE BURN

M - MILLED FOR 16 HOURS IN CHLOROFORM
C - COARSE AS RECEIVED
P - PLAIN GLASS WINDOW
Al - 1000 Å ALUMINIZED GLASS WINDOW IN CONTACT WITH EXPLOSIVES

TABLE IV. CONDITIONS AND RESULTS FOR LASER INITIATION OF TETRYL

	CRYSTAL SIZE	LOADING PRESSURE (KPSI)	LASER ENERGY (JOULES)	CHARGE DIA. (CM)	CHARGE LENGTH (CM)	CONFINEMENT	WINDOW	RESULTS
1	M	1	3.8	0.27	2.06	STEEL	Al	BURN TO DETONATION
2	M	1	3.8	0.38	2.06	STEEL	P	COMPLETE BURN
3	M	1	4.0	0.3	2.54	GLASS	P	FAIL TO INITIATE
4	M	1	4.0	0.3	2.54	GLASS	Al	DETONATED
5	C	10	3.0	0.3	2.03	GLASS	Al	FAIL TO INITIATE
6	C	10	3.0	0.38	2.54	STEEL	Al	FAIL TO INITIATE
7	C	20	3.0	0.51	0.76	STEEL	Al	COMPLETE BURN

M - MILLED FOR 16 HOURS IN CHLOROFORM
C - COARSE AS RECEIVED
P - PLAIN GLASS WINDOW
Al - 1000 Å ALUMINIZED GLASS WINDOW IN CONTACT WITH EXPLOSIVE

TABLE V. CONDITIONS AND RESULTS OF SELECTED LASER DETONATED ITEMS

	EXPLOSIVE	CRYSTAL SIZE	DENSITY G CM^{-3}	LASER ENERGY JOULES	CHARGE DIA CM	CHARGE COLUMN LENGTH CM	CONFINEMENT	WINDOW	TOTAL TIME μSEC	TRANSIENT TIME μSEC	MEASURED DETONATION VELOCITY KM/SEC	DIAL DEFLECTION	STEEL DENT DEPTH mm
1	PETN	M	1.58	0.8	0.38	2.06	STEEL	P	3.11	0.54	7.01	1.661	0.64
2	PETN	M	1.58	0.8	0.38	2.79	STEEL	Al	4.82	0.72	7.726	1.661	0.59
3	PETN	M	1.64	1.0	0.38	2.06	STEEL	P	2.97	0.86	7.620	1.678	0.76
4	PETN	M	1.64	1.0	0.38	2.06	STEEL	Al	2.90	0.43	7.248	1.678	0.61
5	PETN	C	1.64	3.0	0.30	2.06	GLASS	Al	4.05	1.98	7.366	1.678	0.53
6	PETN	C	1.64	3.0	0.30	2.54	GLASS	Al	6.95	3.96	5.651	1.678	0.22
7	PETN	C	1.64	3.0	0.38	2.79	STEEL	P	6.48	2.90	6.836	1.678	0.61
8	PETN	C	1.64	4.0	0.30	2.03	GLASS	Al	9.42	6.66	5.664	1.679	0.18
9	PETN	M	1.72	2.0	0.38	2.06	STEEL	P	2.86	0.38	7.379	1.714	1.78
10	RDX	M	1.18	1.0	0.3	2.54	GLASS	P	5.43	1.66	6.69	1.729	0.46
11	RDX	M	1.18	1.0	0.3	2.54	GLASS	Al	3.98	0.90	6.378	1.729	0.36
12	RDX	M	1.18	1.5	0.3	2.54	GLASS	Al	3.17	2.13	5.618	1.729	0.70
13	RDX	M	1.18	3.5	0.3	2.54	GLASS	Al	5.00	0.80	5.393	1.729	0.13
14	RDX	M	1.19	3.8	0.27	2.06	STEEL	Al	4.16	0.60	5.756	1.729	0.46
15	RDX	M	1.52	2.85	0.30	2.54	GLASS	Al	4.17	0.76	6.741	1.946	0.53
16	RDX	M	1.52	3.5	0.3	2.54	GLASS	Al	5.30	0.40	5.608	1.946	1.28
17	RDX	M	1.52	3.8	0.27	2.06	STEEL	Al	3.62	0.72	6.741	1.946	0.53
18	RDX	M	1.52	3.8	0.27	2.06	STEEL	P	3.73	0.54	5.992	1.946	1.36
19	TETRYL	M	1.08	4.0	0.30	2.54	GLASS	Al	5.43	1.49	5.609	1.858	0.23

M - MILLED FOR 16 HOURS IN CHLOROFORM
C - COARSE AS RECEIVED
P - PLAIN GLASS WINDOW
Al - 1000 Å ALUMINIZED GLASS WINDOW IN CONTACT WITH EXPLOSIVE

*M.A. COOK, THE SCIENCE OF HIGH EXPLOSIVES, REINHOLD PUBLISHING CORP., N.Y., 1958

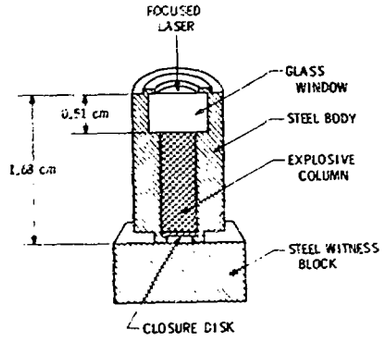

Figure 1. Test Vehicle for Laser Initiation Study

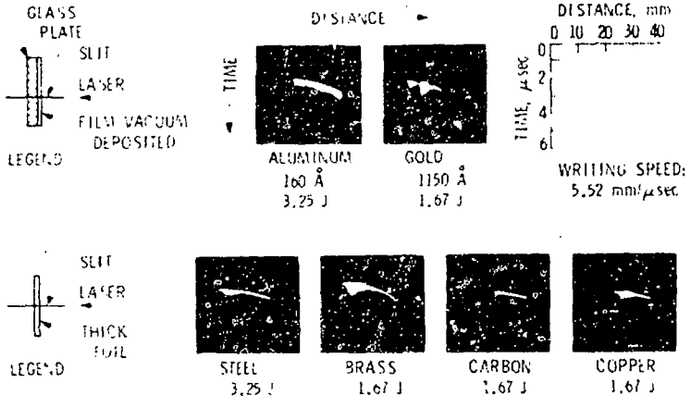

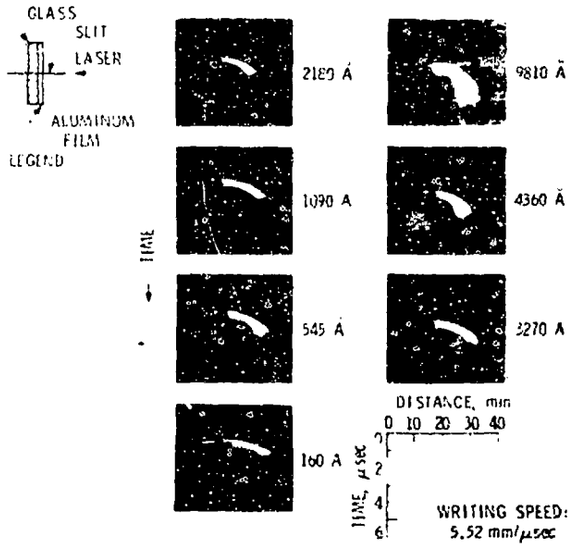

Figure 4. Streak Camera Records of the Plasma Generated in Vacuum for Various Thicknesses of Aluminum Films from a Focused Q-Switched Ruby Laser

ALUMINUM FILMS VACUUM DEPOSITED ON A GLASS SUBSTRATE
MAGNIFICATION - x 14.5
LASER ENERGY - 2.5 J
FOCAL LENGTH OF LENS - 30 cm

Figure 3. Post Irradiation Damage to Thin Aluminum Films by a Focused Q-Switched Ruby Laser

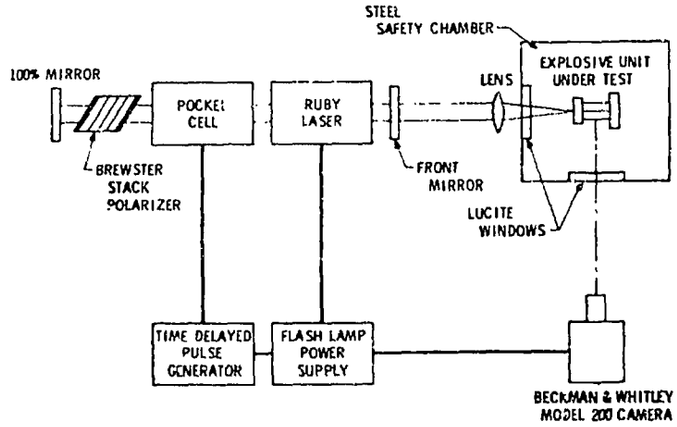

Figure 5. Block Diagram of Experimental Configuration

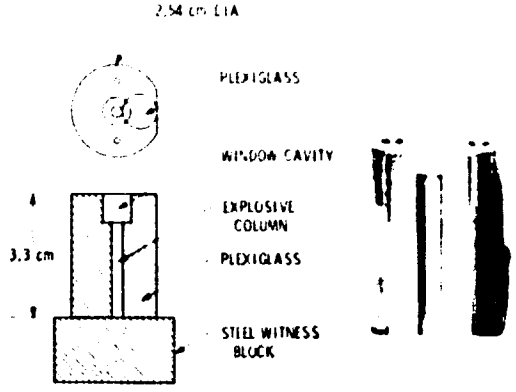
2.54 cm DIA
PLEXIGLASS
WINDOW CAVITY
EXPLOSIVE COLUMN
PLEXIGLASS
STEEL WITNESS BLOCK
3.3 cm

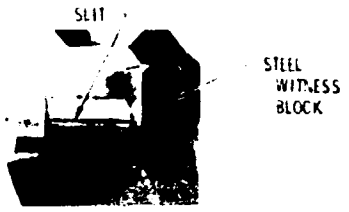
SLIT
STEEL WITNESS BLOCK

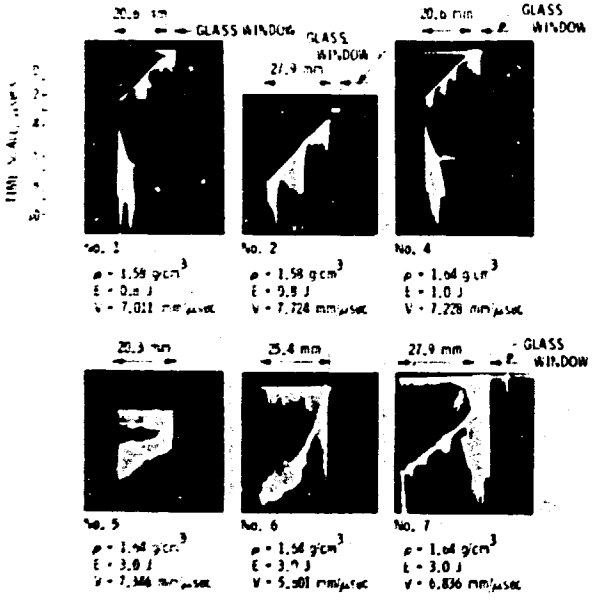
GLASS WINDOW
No. 1
No. 2
No. 4
No. 5
No. 6
No. 7

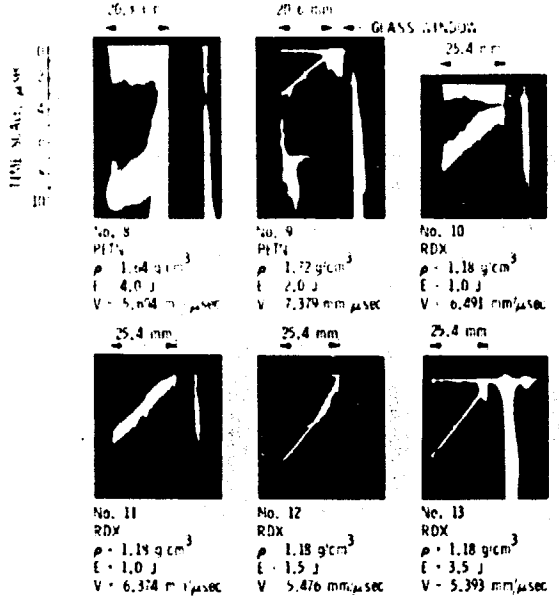
GLASS WINDOW
No. 8
PETN
No. 9
PETN
No. 10
RDX
No. 11
RDX
No. 12
RDX
No. 13
RDX

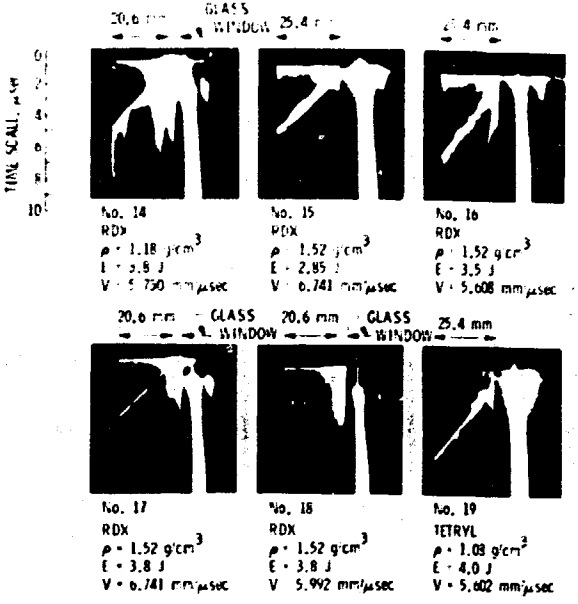
GLASS WINDOW
No. 14
RDX
No. 15
RDX
No. 16
RDX
No. 17
RDX
No. 18
RDX
No. 19
TETRYL

III-3. THE PERFORMANCE CHARACTERISTICS OF ALUMINUM-SODIUM NITRATE FLARES IN VARIOUS OXYGEN-NITROGEN ATMOSPHERES

By

Patricia L. Farnell
Anthony J. Beardell
Francis R. Taylor

PYROTECHNICS LABORATORY
FELTMAN RESEARCH LABORATORIES
DOVER, NEW JERSEY

INTRODUCTION

The luminosity of pyrotechnic flare flames can be considered to be produced by a two-stage process. In the first stage, metal particles are either melted or oxidized by the decomposition products of the oxidizer at or very near the flare surface. In addition, the hot gases produced by this reaction heat the unreacted metal particles and eject them into the atmosphere. The second stage process then consists of the combustion of these metal particles with atmospheric oxygen, and with gases produced by the decomposition of the oxidizer.

It is the objective of the study described here to investigate the second stage process, that is, the increased luminosity that occurs because of the atmospheric combustion of the metal particles. To our knowledge, this type of investigation has not been conducted before; however, it is believed that the extensive investigations of single particle combustion in gases of controlled temperatures and compositions[1,2,3] are directly related to these studies. In addition, previous work by this Laboratory[4] found that powdered Al reacted vigorously with oxidizing gases well below its melting point, and that additives which produced these gases from $NaNO_3$ at low temperature would cause a large increase in the luminosity when the composition was burned. This indicated that experiments should be conducted in which metal-oxidant compositions were burned in atmospheres containing differing amounts of oxygen with various diluents such as nitrogen, argon, or helium. This report presents the results obtained in an investigation conducted by this Laboratory into the effect of atmospheric composition on the performance characteristics of burning Al-$NaNO_3$ pyrotechnic compositions.

EXPERIMENTAL PROCEDURE

Samples consisted of 300 to 400 mg of the composition capped with 100 to 200 mg of non-illuminating igniter composition. This was pressed in a 1/4 inch die at pressures of either 10,000 or 33,000 PSI, resulting in a pellet which was about 1/4 inch long. The samples were then wrapped with two layers of Kraft paper tape to form a case which is necessary to prevent side burning.

These pellets were placed in the center of an upright cylindrical chamber 25 cm in diameter by 23 cm in height, with a total volume of 11.5 liters. There was a removable quartz window in the center of the wall for observing the burning pellet. The chamber was evacuated, then filled with the proper gas mixture to a total pressure of 760 Torr. The pellets were ignited by a hot wire and the resulting light emerging from the window was measured by a calibrated RCA 926 vacuum phototube (having corrective filters to give response essentially equivalent to the human eye) located 85 cm from the flame. The voltage developed by the phototube current flowing through a standard resistor was recorded by a fast-response oscillograph. The duration of burning was measured in seconds, the burning rate (BR) in inches/min., the average luminous output (LO) in candles/in^2, and the luminous efficiency (LE) in candle-sec/gm.

At least six pellets were burned at each atmosphere. Where results were very far from the average in at least two of the three measured parameters, the values were discarded and several more pellets burned. The average deviation for each average value was $\pm$ 10 to 15%, and all points were within 1.96 standard deviation.

Determinations of the amounts of aluminum actually burned in Al-$NaNO_3$ flares were made on the residues from pellets burned in a Bomb calorimeter.

All of the combustion products were washed with water to remove water-soluble components, then filtered, dried, and weighed. The residues were reacted with concentrated NaOH to dissolve the aluminum (which was the only product soluble in NaOH); the precipitates were then filtered, dried, and weighed again. Any loss in weight in the samples was due to unreacted aluminum, and from this the amount of aluminum consumed by each of the burning flares was determined. This was reported as percent ± 5%.

MATERIALS USED

Aluminum powder, atomized, average particle size 6 μ, Alcan Co.
Sodium nitrate powder, average particle size 22 μ, Davies Nitrate Co.
Sodium hydroxide electrolytic pellets, certified ACS grade, Fisher Scientific Co.
Nitrogen gas, 99.9% purity, Linde Corp.
Oxygen gas, 99.6% purity, Linde Corp.
Argon gas, 99.995% purity, Linde Corp.
Helium gas, 99.995% purity, U. S. Government.

RESULTS AND DISCUSSION

Compositions of Al-$NaNO_3$ pressed at 10,000 PSI and mixed in proportions of 50-50, 45-55, 40-60, and 35-65 weight percentages were burned in N_2-O_2 atmospheres of 0, 20, 40, 60, 80, and 100 volume percent O_2. The 50% Al composition was also burned in atmospheres containing argon or helium instead of nitrogen. The effect of loading pressure was investigated by using the 50% Al composition pressed at 33,000 PSI.

Figure 1 shows that the BR's of the compositions pressed at 10K PSI increased sharply with increasing Al content. This effect is attributable to increasing energy feedback into the composition due to increasing thermal conductivity. However, the BR's of these systems remained unchanged as O_2 content was changed, indicating the lack of radiation feedback from flame zone to composition. In regard to the radiation outputs of the compositions, the LO and LE increased as O_2 content of the atmosphere was increased as shown in Figures 2 and 3. The output and efficiency values for the 40 and 45% Al compositions reached a plateau at about 40% O_2 and did not increase as more O_2 was added, while those for the 50% Al composition continued to increase. One would expect a leveling off for compositions containing smaller amounts of Al, for with increasing O_2 concentrations in the atmosphere the compositions cannot supply sufficient metal to the flame zone to effect increasing LO's. In this series of experiments the metal deficient 35% Al composition did not plateau as expected, but this composition burns so inefficiently that any increase in O_2 content is beneficial. The trend continued when the Al content was lowered to 34%. In that case, the pellet burned completely in N_2 but propagation became increasingly difficult as the O_2 content of the atmosphere increased and it failed to ignite in pure O_2. The same phenomenon also occurred using compositions containing 33 and 32% Al. This detrimental effect of O_2 on the combustion of low Al content compositions was corroborated by bomb calorimetry studies by others in which difficulty was encountered in burning Al in pure O_2[5].

The figures also point out that 45 and 50% Al, the LO and LE rose rapidly from 0 to 20% O_2 but the rise became less steep beyond this point, while both parameters increased linearly in this region for 35 and 40% Al. For the reaction

$$4\,Al + 2NaNO_3 \longrightarrow 2Al_2O_3 + 2Na + N_2$$

the stoichiometric amount of aluminum is 39%. Therefore, as Figure 2 shows, those compositions containing aluminum in excess of this amount require an atmosphere containing at least 20% O_2 to produce their maximum rate of oxidation whereas compositions having the stoichiometric quantity or less of Al are able to achieve the maximum rate of oxidation at lower concentrations of O_2. Once this rate has been reached, the LO and LE increase in proportion to the ambient O_2.

As one would expect, the LO increased as the amount of Al in the composition increased due to the greater quantity of Al oxidized either as ejected particulate, liquid or vapor. Figure 2 shows that the slopes of the various curves increase as the Al content increases -- apparently approaching a maximum as the metal content increases beyond 45%. This is undoubtedly due to the fact that as the composition becomes increasingly metal rich, the excess metal begins to act as a strong heat-sink causing a reduction in the reaction rates of the processes occurring in the condensed phase leading to eventual reduction in LO.

Table I presents the results of analyses conducted to determine the amount of unburned Al present in the combustion products of Al-$NaNO_3$ flares. It is seen that approximately 90% of the metal in the 40 and 50% Al compositions was consumed when burned in pure O_2 atmospheres, but a large amount of Al remained in the residues produced by the 35 and 50% Al compositions burned in 20% O_2 atmospheres. This again shows that the radiation output is strongly dependent on the concentration of O_2 in the atmosphere. Furthermore as more Al is pumped into the atmosphere the reaction rates of the processes occurring in the reaction zone of the gaseous phase increase exponentially as the flame temperature rises -- accounting for the large candlepower outputs of the metal rich composition as

TABLE I

Amount of Aluminum Consumed by Al-$NaNO_3$ Flares

Composition by Weight Percentages	% O_2 in Atmosphere	% Al Consumed
50 Al - 50 $NaNO_3$	20	54
35 Al - 65 $NaNO_3$	20	30
50 Al - 50 $NaNO_3$	100	90
40 Al - 60 $NaNO_3$	100	91

TABLE II

Burning Rate of 50-50 Al-$NaNO_3$, N_2-O_2, He-O_2 and Ar-O_2 Atmospheres

O_2	N_2	He	Ar
0	7.25	7.07	7.13
20	7.31	7.44	6.66
40	7.18	7.08	6.32
60	6.74	7.25	6.69
80	7.10	7.28	6.31
100	7.06	7.06	7.06

compared to the metal deficient Al compositions. For example, in a 100% O_2 atmosphere, the 35 and 50% Al compositions generated 20.5 and 67.1 kilocandles, respectively.

Actually the above data indicate a correlation between the amount of Al consumed and the light produced by the burning flare. The luminous efficiency data in Figure 3 are based on the light produced per unit weight of Al, rather than unit weight of composition. This method of representing the data makes it possible to compare directly the relative efficiencies of flares of varying Al compositions. Thus, the 50% Al composition produces the highest luminous efficiency when burned in 100% O_2. This mixture was used as a standard on the assumption that its luminous efficiency represents the maximum value that can be produced by an Al-$NaNO_3$ flare, (see Figure 3). On this basis the ratio of the LE for a given composition to that of the 50% Al-$NaNO_3$ composition burned in 100% O_2 should be a rough measure of the amount of aluminum consumed. When this was done, such a correlation was found. For example this ratio was 0.45 for a 50% Al-$NaNO_3$ composition burned in 20% O_2 whereas the amount of aluminum actually consumed was 54% and for a 40% Al composition burned in 100% O_2 the ratio was 0.92 and the amount of Al consumed was 91%.

Factors which may also influence the performance of the Al flare are the possibility of reaction of N_2 in the high temperature flame and heat loss (or gain) by conductive heat transfer to the flame zone by the ambient atmosphere. To study these effects, ambient atmospheres containing He or Ar instead of N_2 were used. The O_2 content was again varied between 0 and 100%. The burning rate data shown in Table II are essentially constant, irrespective of the inert gas used or its O_2 content. This indicates that the ambient gas has no effect on the burning surface, i.e., conductive heat transfer between the ambient atmosphere and the burning surface is negligible. Similarly, the substitution of the Ar for N_2 in O_2 containing atmospheres had very little effect on LO, as shown in Figure 4, indicating that N_2 does not enter into the reaction in the flame zone to any significant extent and the diffusion of O_2 in the flame zone is the major influence.

The major difference observed was the difference in the LO between a pellet burned in pure He relative to pure N_2 or Ar. In that case a very low value of LO was observed for the pure helium atmosphere, which has a thermal conductivity about 10-fold higher than N_2[6]. It therefore seems likely that where O_2 is not present to react exothermically with the Al, thermal heat transfer from the flame zone to the ambient gas can occur.

The effect of loading pressure on LO is dramatically shown in Figure 5. Here is plotted data obtained by burning 50% Al compositions consolidated at 19K and 33K PSI. The compositions pressed at the lower pressure displayed a minimal change of burning rate of 6.7 to 7.5 in/min with increasing O_2 content, and yielded LO and LE values which rapidly increased, as with most systems, with increasing O_2 content. For the compositions consolidated at 33K PSI, however, the burning rate decreased from 5.9 to 4.8 in/min as the atmospheric O_2 concentration increased. When burned in pure N_2, the composition loaded at the higher pressure produced the highest LO using inert atmospheres. Furthermore, as shown in Figure 6, the LO generated by the latter composition only increased 11% upon going from pure N_2 to pure O_2. In addition, the compositions consolidated at 33K PSI and burned in 20 and 100 O_2 atmospheres showed that 20 and 5%, respectively, of the Al remained as a molten mass. Therefore the expansion of Al fuel is apparently strongly affected by the heat from the flame, which is in turn dependent on the amount of O_2 in the atmosphere. This is due to a reduction in the gaseous permeability caused by the high loading pressure which prevents hot gases from permeating the composition to heat Al below the surface. The vaporization rate is therefore decreased, allowing molten metal to flow from the surface. In the hotter flame achieved in high O_2 atmospheres, more of the Al is vaporized, resulting in an apparently lower burning rate with increasing O_2. However, coalescence is so strongly favored by the close packing of the metal in this composition that much of the Al still escapes from the flame unburned, and consequently the light output remains low.

CONCLUSIONS

The burning process for the compositions studied fall into two parts: a condensed phase and a vapor phase. In the condensed phase, the nitrate melts and decomposes, and the Al melts and agglomerates. For the compositions pressed at the lower loading pressure, this process occurs at a rate which is unaffected by the atmospheric composition, evidenced by the constant BR for each composition, and therefore heat and radiation feedback from the flame play a negligible role in this phase.

The decomposition of excess $NaNO_3$ will remove heat from the compositions with low Al content, resulting in a lower BR and LO due to slower vaporization and a cooler flame. This cooler flame would be very inefficient in burning Al; indeed, this could cause non-propagation when the rate of oxidation exceeds the rate of vaporization, as it would in high O_2 atmospheres. The rate of vaporization would be lower in N_2, however, and thus propagation would be possible in this atmosphere even for low metal compositions.

Unlike the condensed phase, the vapor phase of the burning is greatly affected by the atmosphere. Whereas the Al is vaporizing at a constant rate, the fraction of it which is actually burned is determined by the amount of atmospheric O_2, with nearly all being consumed in pure O_2 but with a great deal remaining unburned in 20% O_2. There are two factors involved here which work against each other. The first is the coalescence of molten metal into a large droplet encased in a protective oxide shell. This shell inhibits the burning and may enable the droplet to pass from the flame zone unburned. The second factor is fragmentation of the droplets followed by complete burning of the fragments. This effect is enhanced by high fractions of both O_2 and Al[7], while the detrimental coalescence is enhanced by high metal content but is affected very little by the atmosphere. We would then have coalescence predominating in low O_2 atmospheres, leaving much Al unburned, with increasing fragmentation to negate this effect as O_2 is increased. Coalescence is more pronounced for 50% than for 45% Al compositions, and therefore 45% Al produces the highest efficiency of all. Fragmentation becomes less and less prevalent as the Al content is reduced further, until finally, for 35% Al, only 20% of the Al burns even in pure O_2.

When the loading pressure is increased, the two phases above are no longer independent of one another. The vaporization now is strongly affected by the heat from the flame, which is in turn dependent on the amount of O_2 in the atmosphere. This is due to a reduction in the gaseous permeability caused by the high loading pressure which prevents hot gases from permeating the composition to heat Al below the surface. The vaporization rate is therefore decreased, allowing molten metal to flow from the surface. In the hotter flame achieved in high O_2 atmospheres, more of the Al is vaporized, resulting in an apparently lower burning rate with increasing O_2. However, coalescence is so strongly favored by the close packing of the metal in this composition that much of the Al still escapes from the flame unburned, and consequently the light output remains low.

REFERENCES

1. Christensen, H. C., Knipe, R. H., and A. S. Gordon, Pyrodynamics 3, 99-119 (1965).

2. Brzustowski, T. A., and I. Glassman, Heterogeneous Combustion, Academic Press, New York, N. Y. (1964) 75, 117.

3. Cassel, H. M., and I. Liebman, Combustion and Flame 3, p. 467 (1959)

4. Leader, P. J., Westerlahl, R. P., and Taylor, F. R., "The Effects of Some Transition Metal Compounds on the Performance Characteristics of Aluminum/Sodium Nitrate Compositions", Picatinny Arsenal Technical Report 3846, May 1969.

5. Weingarten, G. (private communication).

6. Handbook of Chemistry and Physics, 48th Ed., The Chemical Rubber Co., Cleveland, Ohio (1967) p. E2.

7. Brzustowski and Glassman, loc. cit., p. 41.

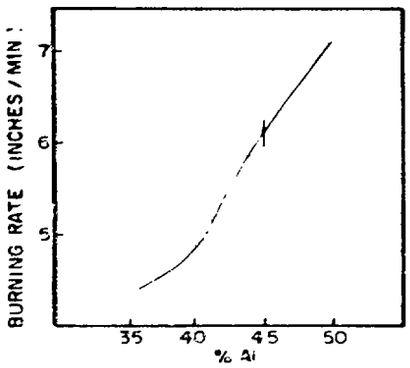

FIG 1. EFFECT OF ALUMINUM CONTENT ON BURNING RATE OF AL-$NaNO_3$ FLARES (LOADING PRESSURE = 10,000 PSI)

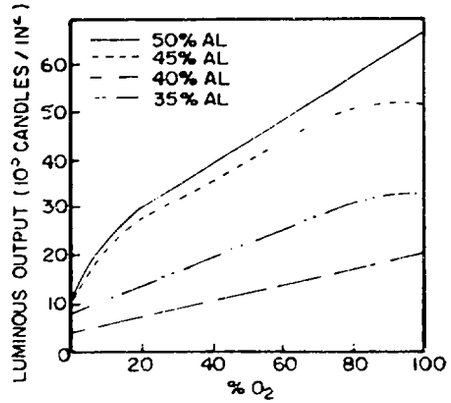

FIG 2. EFFECT OF ALUMINUM CONTENT ON OXYGEN CONTENT OF ATMOSPHERE AND LUMINOUS OUTPUT (LOADING PRESSURE = 10,000 PSI)

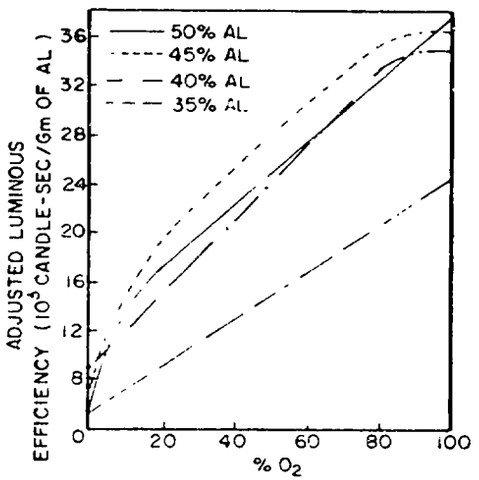

FIG 3 EFFECT OF ALUMINUM CONTENT ON ADJUSTED LUMINOUS EFFICIENCY BASED ON GRAMS OF ALUMINUM (LOADING PRESSURE = 10,000 PSI)

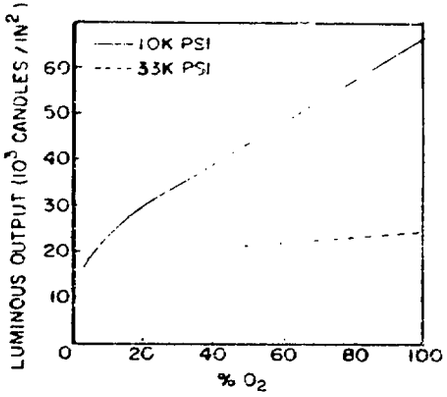

FIG. 5 EFFECT OF LOADING PRESSURE ON LUMINOUS OUTPUT OF AL-$NaNO_3$ FLARE BURNING IN VARIOUS N_2-O_2 ATMOSPHERES

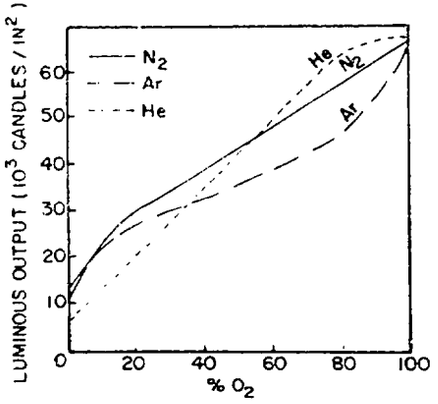

FIG 4 EFFECT OF VARIOUS INERT GASES ON LUMINOUS OUTPUT OF AL-$NaNO_3$ FLARE (LOADING PRESSURE = 10,000 PSI)

III-4. DEVELOPMENT OF WATER-IGNITABLE PYROTECHNIC COMPOSITIONS*

By Allen J. Tulis, James L. Austing and Charles K. Hersh
IIT Research Institute, Chicago, Illinois 60616

INTRODUCTION

A number of applications requiring the water-ignition of the ordnance or hydrospace item such as a detonator, thruster, or photoflash unit can be envisioned. Metal-metal fluoride pyrotechnics formulated from higher valence fluorides such as silver difluoride (AgF_2) or lead tetrafluoride (PbF_4) provide the means to accomplish this goal. The reactions of these compounds with boron (B) are identical to the classical thermite reaction; viz.:

$$2B + 3AgF_2 \longrightarrow 2BF_3 + 3Ag \qquad (1)$$

$$4B + 3PbF_4 \longrightarrow 4BF_3 + 3Pb \qquad (2)$$

The calculated adiabatic reaction temperatures for these reactions are both in excess of 3000°K. Hence these reactions should provide good heat sources for igniting other pyrotechnics or explosives.

The water-ignitability of these mixtures is attributed to the strong tendency of higher valance fluorides to readily undergo highly exothermic hydrolysis. Typical reactions for lead tetrafluoride (Ref. 1) and silver difluoride are given in Equations 3 and 4:

$$PbF_4 + 2H_2O \longrightarrow 4HF + PbO + 1/2\ O_2 \qquad (3)$$

$$AgF_2 + H_2O \longrightarrow 2HF + Ag + 1/2\ O_2 \qquad (4)$$

Approximately 10 kcal/mol are evolved from these hydrolyses. The calculated adiabatic reaction temperature for the hydrolysis of AgF_2, Equation 4, is about 700°K. This represents sufficient thermal energy to initiate the B-AgF_2 reaction, Equation 1.

The initial work was aimed at establishing the feasibility of water-ignition of the pyrotechnic. Approximately 0.5 gram of the B-AgF_2 mixture was placed on a flat surface, and immediately a drop of water from a standard medicine dropper was added. Initially, the mixture gave off white fumes, and then a second or so later the mixture flared vigorously. This experiment was repeated several times, and each time the result was the same -- a drop of water ignited B-AgF_2. However, a limitation presented itself in the early phases of the effort, viz., successful ignition was not achieved if the B-AgF_2 was flooded with excess water or dropped into water. Evidently excess water vaporized and precluded accumulation of sufficient thermal energy to initiate the main reaction between B-AgF_2. This problem was ultimately solved by inclusion of a molecular sieve additive in the formulation.

The work presented in this paper describes the development of the water-ignitable formulation to characterize its performance as a function of temperature, pressure, composition, and type of boron. The utilization of the highly exothermic reaction of

*Work supported by the U.S. Atomic Energy Commission under Contract No. AT(11-1)-578.

$B\text{-}AgF_2$ to initiate lead azide was demonstrated, through the design and evaluation of a special water-activated detonator. In addition, the results of experiments with other pyrotechnics and liquids are presented; it is shown that a water-methanol mixture can ignite $B\text{-}AgF_2$, and that an aluminum-silver difluoride reaction can be ignited with water.

FORMULATION OF BORON-SILVER DIFLUORIDE PYROTECHNICS

Appropriate mixtures of boron and silver difluoride will ignite upon the addition of several drops of water. However, water is also very effective in quenching fires. We quickly encountered difficulty of ignition with too much water, such as dropping the pyrotechnic into excess water. This problem was successfully solved with the inclusion of 5 to 10% molecular sieve powder (Ref. 2) in the igniter formulation. The use of molecular sieves (MS) as an additive is unique in that all of the effects are favorable. For example, the MS (1) dry and maintain system dryness, (2) adsorb excess water to deter flooding of the system, (3) liberate thermal energy when adsorbing water, (4) reduce heat dissipation substantially because of resistance to thermal conduction, and (5) add oxygen to the system, if needed.

The type of boron is also pertinent. It was determined that amorphous boron with a high degree of magnesium impurity was sufficient to allow fast and reliable ignitions. This will be discussed further in the section on the evaluation of type of boron.

The $B\text{-}AgF_2\text{-}MS$ pyrotechnic is formulated as follows:

1. Boron -- The use of an amorphous boron powder is necessary, with a particle size of about one micron or less. A very high purity boron is not necessary nor is desired, as a 92%-boron with high (8.3%) magnesium content has been shown to be extremely beneficial for achieving reliable ignition. However, one extremely important feature of the boron is that it has to be free of moisture.

2. Silver Difluoride -- The silver difluoride must be reduced in particle size by grinding. This operation has to be conducted in a dry atmosphere, as the AgF_2 becomes tremendously hygroscopic as the particle size is reduced. In addition, the AgF_2 is not compatible with many materials, including glass.

3. Molecular Sieves -- The use of either pulverized MS pellets or MS powder is effective.

The MS powder can be added to the silver difluoride either before or after grinding. In the case of MS pellets, pulverizing the pellets together with the silver difluoride is most effective. The use of MS also improves the flow and subsequent mixing properties of the silver difluoride. It is imperative that the boron be dry before it is admixed to the $AgF_2\text{-}MS$. If the boron is not dry, or if the mixing process is conducted in a wet atmosphere, the mixture will increase in temperature and eventually ignite spontaneously. Rapid mixing, such as is achieved on a roller mill, allows fast dissipation of small amounts of heat generated from the trace amounts of water present. Once the system is mixed and all heat is dissipated, the mixture is stable, and exposure to the atmosphere can be tolerated to some extent. However, caution is necessary to prevent a fresh portion of the

mixture from accidentally contacting another portion that has been unduly degraded with moisture. In this case the undegraded portion can remove sufficient water from the degraded portion to cause ignition.

If the boron is sufficiently wet, the silver difluoride will fume (HF liberation) upon contacting the boron, and this can cause spontaneous ignition. Thus, all boron used was dried over phosphorous pentoxide under high vacuum, and in some cases was heated under vacuum to about 150°C. In addition, all molecular sieves were tested prior to use to establish their activity.

Near-stoichiometric mixtures of boron and silver difluoride have exploded. However, the system that has been developed contains 8% boron, 82% AgF_2, and 10% MS, on a weight basis, which corresponds to about 100% excess boron above stoichiometric as based on Equation 1. No explosions were encountered with fuel-rich systems such as this, and in addition the 10% MS is believed to preclude explosion. However, the reaction is still so rapid and vigorous that care must be exercised.

EXPERIMENTAL ARRANGEMENT AND INSTRUMENTATION

The experimental arrangement for studying the hypergolic ignition of B-AgF_2 with water or other liquids is depicted schematically in Figure 1. The experimental procedure was as follows: A small tube containing B-AgF_2 was placed upon a glass plate, which in turn was placed directly on the surface of a Kistler type 910 quartz load cell.* The glass plate merely protected the load cell from the reaction, since force was transmitted directly through the plate. A Texas Instruments type LS-400** phototransistor light detector was aimed at the system. The test was then conducted by removing the beaker that intercepted water from a pipette preset to allow drops to fall into the tube at some nominal rate.*** The impulse of the falling drops hitting the surface of the B-AgF_2 resulted in a pulse output from the load cell. This signal, appropriately amplified with a Kistler model 504 charge amplifier, triggered the sweep circuit of a Tektronix type 551 dual-beam oscilloscope. Any further impulse upon the load cell and the light from ignition observed by the light detector yielded signals monitored on separate channels of the oscilloscope. When appropriate oscillographs were obtained by using an attached Polaroid Land Camera. Thus the time delay to ignition was determined as the time from triggering to the first evidence of light. Burning rate information was obtained from the duration and type of light output in conjunction with the height of the sample in the tube.

---

*Kistler Instrument Co., Clarence, New York.

**Texas Instruments, Inc. Semiconductor-Components Division, Dallas Texas.

***A variation of this arrangement allowed the B-AgF_2 sample to be lowered into a beaker of water, which rested on the glass plate and load cell. This permitted evaluation of the condition whereby the sample was dropped into water.

The traces in Figure 2 illustrate some load-cell responses of AgF_2 to water and various other liquids. The resultant traces in these tests, triggered by the impact of the falling drop, are attributed to the thrust energy resulting from explosive gas liberation and flash vaporization due to hydrolysis. These oscillographs confirmed the visual observation that the higher the alcohol content in water-methanol systems, the greater the violence when in contact with AgF_2. However it appears that the alcohol requires more time to attain peak reactiveness. Note the near-instantaneous and violent response for reaction with about 30% hydrogen peroxide. This is a highly desirable feature in the design of a hypergolic ignition system.

The traces in Figure 3 illustrate typical ignitions of B-AgF_2 with water and methanol alone and with an approximate 1:1 water-methanol mixture. The experimental set-up allowed no control over the size of the drop that formed. The drop of methanol that caused ignition in test 7-C was especially small and steady-state burning did not result. In other tests with larger drops of methanol, burning was always achieved.

PARAMETRIC EVALUATION OF WATER-IGNITABLE PYROTECHNICS

Parametric evaluation of the B-AgF_2 was conducted on a trial-and-error basis initially, by attempting to ignore the less important variables so that the effects of the more important parameters could be established. Unfortunately, several of the assumed lesser variables turned out to be major parameters: the type of boron, for instance, was a prime example.

Boron Evaluation

Amorphous boron is generally manufactured by the methods originally described by Moissan in 1892. Anhydrous boric acid (B_2O_3) is reduced with magnesium, and the resultant mass is leached with acid, water washed, and dried. Amorphous boron of 85 to 92% purity can be produced in this manner. Further purification results in amorphous boron of high purity -- 95 to 98%. The particle size is very uniform -- 0.5 to 2.0 microns. Under some conditions of production, the amorphous boron shows some degree of crystallinity by x-ray diffraction. Crystalline boron can be produced by the reduction of boron halides with hydrogen and subsequent deposition on heated filaments. The chief impurities in all amorphous borons are magnesium and oxygen.

The initial parametric evaluation of the B-AgF_2-MS pyrotechnic was severely impeded with nonreproducible results. The problem was traced to variation in two lot types of boron, designated type (A) and type (B). Both are fine powders, except that upon closer comparative examination it was observed that (A) was much darker than (B), and (B) appeared dustier than (A). With regard to water ignitability of B-AgF_2, (A) was most

effective with instantaneous ignitions, while (B) required several seconds before ignition was achieved, and on some occasions the mixture did not ignite at all.

Table 1 presents the analyses of the various types of boron evaluated. The reasons for the selection of these types are as follows:

Type (A) -- This boron was used in all of our original work with metal-metal fluoride systems, and was found to be highly effective. This boron is no longer available.

Type (B) -- This boron was supplied upon reorder of amorphous boron, and led to nonreproducible results. It is about the same purity and particle size as type (A), but did not contain the magnesium impurity.

Type (C) -- This boron had the highest magnesium impurity of the amorphous borons available (except for a magnesium reactive grade, which was not available). The particle size was about the same as both types (A) and (B).

Type (D) -- This boron was selected because its analysis corresponded most closely to type (A) boron. Its particle size was also about the same as types (A), (B), and (C).

Type (E) --This was a high purity amorphous boron. It was procured at a cost of approximately $600.00 per pound. It is a 99%-purity boron of extremely small particle size, with 99% of the particles in the range of 125 to 500 Angstroms and a median particle size of 300 Angstroms. The bulk volume of this boron is at least ten times as great as each of the other types evaluated. It was important to evaluate this boron, whether it was prohibitive in price or not, to establish the effect of boron particle size.

Type (F) -- This was a high purity (99.56%), crystalline boron powder that was available in our laboratory. The particle size was much larger -- approximately 44 microns (325 mesh).

Table 1

ANALYSES OF THE VARIOUS AMORPHOUS BORONS EVALUATED

Designation Type	Net B, %	Mg, %	H_2O, %	Average Particle Size, microns
A	91.6	3.9	-	0.5 to 2.0
B	90.1	-	1.5	0.5 to 2.0
C	84	8.3	0.5	1.0
D	91.5	4.0	0.18	0.9
E	99+	-	-	0.03
F	99.56	-	-	<44

Both boron types (A) and (B) are amorphous borons of about 90 to 92% purity. Neither of these borons is truly amorphous, because they have considerable crystalline structure. Results of x-ray diffraction analyses indicate that type (A) is more crystalline and in a less-oxidized state than type (B). Type (B) has evidence of a B_2O component, for instance. X-ray diffraction analyses on types (C) and (D) boron confirm that these are similar to type (A). Types (A), (C), and (D) are all distinctly different from type (B).

Samples of these igniter powders were pressed into 0.794-cm diameter by 1.27-cm long configurations and tested in the evaluation apparatus (see Fig. 1) at four different water temperatures The results are presented in Table 2. None of the samples with type (B) boron ignited. Samples with type (A) boron all

ignited. However, samples with types both (C) and (D) boron ignited even more rapidly. As a matter of fact, it appears that the ignition characteristics are directly related to the magnesium impurity.

Table 2

EFFECT OF TYPE OF BORON
ON WATER IGNITABILITY CHARACTERISTICS
AT VARIOUS WATER TEMPERATURES

Type of Boron	Time Delay to Ignition, msec 13°C	24°C	57°C	99°C
A	550	700	850	1000
B	∞	∞	∞	∞
C	210	150	540	450
D	260	240	250	200
E	270	230	170	100
F	∞	∞	∞	∞

Test Conditions: (1) 10% type 4A powder MS
(2) B/AgF_2 ratio of 2:1
(3) 0.794-cm dia. by 1.27- cm long test units
(4) all boron dried over P_2O_5 under vacuum.

The most responsive ignition was obtained for samples with the very fine type (E) boron. Thus, the particle size is as important as the magnesium content. This formulation is exceedingly sensitive, and can be readily ignited by running a metal rod across the loose powder on a flat surface. On the other hand, samples with the course type (F) crystalline boron did not ignite at all under these test conditions. Thus, high purity, high crystallinity, and large particle size are not desired; low boron purity with an associated magnesium impurity and small particle size are necessary for optimum ignition with water.

Silver Difluoride Effectiveness

The silver difluoride was procured from Harshaw Chemical Company, Cleveland, Ohio, in the following lots: (1) March 22, 1967, and (2) November 14, 1967. The Harshaw code for both is 423-004-06. It is an industrial grade of high purity with a typical analysis of 73.7% Ag and 26.1% F; this compares to 73.95% Ag and 26.05% F for pure AgF_2. The silver difluoride is a black-brown powder with about 50% in the form of large chunks, some larger than golf balls. The silver difluoride used for the B-AgF_2-MS evaluation purposes was pulverized with the use of a mortar and pestle in a drybox under a dry-nitrogen atmosphere. Before this finely-divided silver difluoride could be added to either boron or MS, both had to be dry. Silver difluoride will remove water from molecular sieves that have absorbed a large quantity of moisture. Moisture, of course, will render the silver difluoride less effective or ineffective.

Parametric Evaluation Results

Results of the parametric evaluation are reported in tabular from in Tables 3 through 8. The tables are self-explanatory as far as test conditions are concerned; although the results suggest quantitative interpretation, they are meant for qualitative consideration only since the more devious parameters, such as moisture adsorption, compatability, storage or "aging" effects, and so forth have not been sufficiently determined. The B/AgF ratio reported in the tables is based on Equation 1, such that a ratio 1:1 is defined as stoichiometric.

Table 3 indicates the advantages of having the MS additive and excess fuel (boron) in the formulation. Increasing MS additive and increasing the B/AgF_2 ratio improve ignition characteristics; however, data not being presented here show that both degrade the burning rate and consistency of burning at B/AgF_2 ratios above 4:1 and MS levels in excess of 10% to 15%.

Table 4 illustrates two points; (1) that at low MS concentrations type (B) boron is not effective, and (2) that sufficient MS additive can make even type (B) boron effective.

Table 5 indicates the improved ignition of a smaller test unit when MS are added. This pyrotechnic, without MS additive, required 1500 msec for ignition in the larger (0.794-cm diameter) test unit, as indicated previously in Table 3. However, Table 6 indicates that ignition was independent of diameter with MS additive of 10%. Thus, it appears that the performance of $B-AgF_2$ without MS is very dependent on size and geometry and is made

Table 3

EFFECT OF MOLECULAR SIEVE ADDITIVE ON WATER IGNITABILITY CHARACTERISTICS AT VARIOUS TYPE (A) BORON TO SILVER DIFLUORIDE RATIOS

B/AgF_2 Ratio	Time Delay to Ignition, msec			
	0% MS	5% MS	10% MS	20% MS
4:1	1500	360	220	240
3:1	∞	550	440	350
2:1	∞	650	420	200
1:1	∞	-	2500	2800

Test Conditions: (1) pulverized type 5A MS pellets
(2) 0.794-cm dia. by 1.27-cm long test units
(3) boron dried over P_2O_5 under vacuum.

Table 4

EFFECT OF MOLECULAR SIEVE ADDITIVE ON WATER IGNITABILITY CHARACTERISTICS AT VARIOUS TYPE (B) BORON TO SILVER DIFLUORIDE RATIOS

B/AgF_2 Ratio	Time Delay to Ignition, msec		
	0% MS	5% MS	10% MS
4:1	∞	7900	1900
3:1	∞	∞	1800
2:1	∞	∞	1000

Test Conditions: (1) pulverized type 5A MS pellets
(2) 0.794-cm dia. by 1.27-cm long test units
(3) boron dried over P_2O_5 under vacuum.

Table 5

EFFECT OF MOLECULAR SIEVE ADDITIVE
ON WATER IGNITABILITY CHARACTERISTICS
USING A SMALLER TEST UNIT

MS Additive, %	Time Delay to Ignition, msec	Burning Rate, cm/sec
0	650	1.27
10	220	1.27

Test Conditions:
(1) pulverized type 5A MS pellets
(2) 0.476-cm dia. by 1.27-cm long test units
(3) type (A) boron, dried over P_2O_5 under vacuum.

Table 6

EFFECT OF IGNITER DIAMETER
ON WATER IGNITABILITY CHARACTERISTICS

Igniter Diameter, cm	Time Delay to Ignition, msec	Burning Rate, cm/sec
0.794	220	1.14
0.635	220	1.02
0.476	200	1.27
0.318	200	1.27

Test Conditions:
(1) B/AgF_2 ratio of 4:1
(2) 10% pulverized type 5A MS pellets
(3) type (A) boron, dried over P_2O_5 under vacuum.

Table 7

EFFECT OF B/AgF_2 RATIO
ON WATER IGNITABILITY CHARACTERISTICS

B/AgF_2 Ratio	Time Delay to Ignition, msec	Burning Rate, cm/sec
4:1	220	1.14
3:1	440	1.02
2:1	420	1.40
1:1	2500	-

Test Conditions:
(1) 10% pulverized type 5A MS pellets
(2) 0.794-cm dia. by 1.27-cm long test units
(3) type (A) boron, dried over P_2O_5 under vacuum.

Table 8

EFFECT OF SHORT STORAGE OF PYROTECHNIC
ON WATER IGNITABILITY CHARACTERISTICS

Time after Preparation, hours	Time delay to Ignition, msec	Burning Rate, cm/sec
0	220	1.14
24	200	0.88

Test Conditions:
(1) 10% pulverized type 5A MS pellets
(2) 0.794-cm dia. by 1.27-cm long test units
(3) type (A) boron, dried over P_2O_5 under vacuum

independent of these with MS additive. Also, the 10% MS additive apparently does not degrade the burning characteristics of the B-AgF_2 to any appreciable extent.

Table 7 illustrates the effect of B/AgF_2 ratio on the water-ignitability characteristics.

Table 8 indicates the negligible effect of short-time storage upon the pyrotechnic. In other tests, storage for up to a week did not degrade the formulation. Any degradation that was observed is attributed to moisture contamination and incompatability of the silver difluoride with glass or quartz. Neither the silver difluoride nor the B-AgF_2 formulation can be stored in or allowed extended exposure to glass. Silver difluoride stored in a glass vessel overnight or longer will be degraded to AgF or Ag_2F; the powder turns uniformly yellow, and a white scale forms upon the glass surface. This reaction is triggered and runs to completion by moisture, which reacts with the AgF_2 to form HF, which in turn reacts with the glass to form SiF_4. The latter reacts in complex fashion to re-deposit SiO_2 (as alpha quartz) and compounds involving magnesium, sodium, silicon, and fluorine; water is regenerated to continue the process as long as unreacted AgF_2 is present. After mixing of the pyrotechnic formulation, it was transferred to paraffin-coated glass containers or polyethylene containers that in turn were placed in closed, desiccated glass containers.* It should be possible to store B-AgF_2 in steel containers for an unlimited time.

Studies have been conducted to determine the effect of formulation technique and MS form on the ignitability characteristics. Although all types of MS additive and methods of admixing the MS to the B/AgF_2 proved effective, it was established that grinding the silver difluoride together with MS pellets and then mixing with the boron was the most effective. The use of MS powder, admixed to pulverized silver difluoride on a roller mill, is nearly as effective.

Tests have been conducted with both test unit and pyrotechnic cooled to liquid nitrogen temperature. Excellent ignition was obtained when the cooled system was dropped into salt water at a temperature less than 0°C.

Effect of Hydrostatic Pressure

The vessel in which the effect of hydrostatic pressure on the water-ignitability of the boron-silver difluoride-molecular sieve mixture was studied is depicted schematically in Figure 4. The unit was designed to withstand a steady internal pressure of 10,000 psi, but would accept a momentary surge to about double this value. The drawing shows the orientation of the vessel in the ready state prior to the test. The operation is as follows. The vessel is pressurized to the desired pressure with compressed helium. The entire assembly is then inverted, such that the water contacts the probe to trigger the oscilloscope and the

*A charge stored in this manner for nearly a year was tested and proved to be nearly as effective as when formulated.

sample to cause ignition and burning of the sample. The response of the sample is monitored by the previously-described photo-cell through a polished Lucite "light pipe" that makes use of the principle of total internal reflection.

The entire pressure vessel was machined from stainless steel to minimize corrosion problems. "O"-rings were used to seal the threaded assemblies and the end plates. The trigger probe was a two-prong threaded stainless steel-Inconel-glass header that was connected to a condenser-discharge circuit. The water was saturated salt water, which when in contact with the probe permitted the condenser to discharge its voltage through the water and a resistor in series with the condenser. The voltage drop across this resistor then was used to trigger the oscilloscopes.

Table 9 illustrates the results obtained from the hydrostatic pressure evaluation tests. Tests were conducted at 0, 250, 500, 750, 1,000, and 2,000 psig using helium for pressurization. All charges were pre-pressed to 9,000 psi prior to testing. There was some variation in time delay to ignition, but this was attributed to moisture degradation of the silver difluoride, as the partial pressure of water and time exposure of the charge to saturation moisture level increased with increasing pressures. The burning rates were relatively constant at about 14 cm/sec. A maximum transient differential pressure increase of 500 psi was observed upon ignition of the pyrotechnic in the enclosed pressure vessel. Although it was not experimentally confirmed, extension of pressure to 9,000 psi is unlikely to have effect other than to cause some variation in time delay. In an actual application this effect could be precluded for the most part by sealing the charge prior to water contact.

Table 9

EFFECT OF HYDROSTATIC PRESSURE
ON WATER IGNITABILITY CHARACTERISTICS

Pressure on Igniter, psig	Time Delay to Ignition msec	Burning Rate, cm/sec
0	300	6.4
250	200	15.2
500	150	15.2
750	250	12.7
1000	850	15.2
2000	1700	12.7

Test Conditions:
(1) 10% pulverized type 5A MS pellets
(2) B/AgF_2 ratio of 2:1
(3) 0.794-cm dia. by 1.27-cm long test units
(4) type (A) boron, dried over P_2O_5 under vacuum
(5) all charges pressed to 9000 psi.

WATER-ACTUATED DETONATOR

The design and construction of a prototype water-actuated detonator is depicted in Figure 5. The operation is as follows.

A small amount of water, generally two or three drops, was placed upon the polyvinyl alcohol seal remotely. The water penetrated the seal and started to hydrolize the silver difluoride. Within a second, the thermal energy acquired from the hydrolysis reaction was sufficient to initiate the B-AgF_2 reaction. This highly exothermic reaction in turn ignited the aluminum-tungstic oxide pyrotechnic (Ref. 3) which then initiated the lead azide. This in turn caused the PETN base charge to detonate. Evidence of detonation was obtained from the depth of dent produced in a steel witness block on which the detonator was placed. An auxiliary electric detonator was placed next to this detonator so that a malfunctioning system could be safely destructed.

The Al-WO_3 pyrotechnic was utilized as a safety precaution, to avoid a possible compatibility problem between the B-AgF_2 and the lead azide. As more is known about B-AgF_2, it is possible that the Al-WO_3 layer could be omitted.

The depths of dents in the steel witness blocks on which the detonators were sitting were approximately 0.81 mm. This result is in excellent agreement with the measurements of Slie and Strasau (Ref. 4) for detonating explosive charge columns.

WATER IGNITION OF THE ALUMINUM-SILVER DIFLUORIDE SYSTEM

The B-AgF_2 reaction yields BF_3 gas, and is an effective gas generator. Since gas generation is not necesary and can be a hindrance for some applications, the Al-AgF_2 system was also considered. The assumed reaction here is:

$$2Al + 3AgF_2 \longrightarrow 2AlF_3 + 3Ag \qquad (5)$$

The product AlF_3, although possibly a gas in the reaction, has a sublimation point of 1272°C. In addition, this reaction has a greater heat of reaction than the B-AgF_2 system (0.68 kcal/g for Al-AgF_2 and 0.60 kcal/g for B-AgF_2). Type H-3* aluminum powder, containing spherical particles of 3-micron average size, was used.

Preliminary tests were conducted with Al-AgF_2 at approximately 8 4. 2, and 1:1 Al/AgF_2 ratios, on a basis similar to that described for the B-AgF_2 system; e.g., at 2:1 a 100% excess of aluminum was present for the reaction as assumed. In these tests several drops of water were required for ignition. The first drop or two caused a quick sizzling reaction and generally spattered Al-AgF_2 out of the test tube. Additional drops eventually caused ignition. At Al/AgF_2 ratios greater than stoichiometric, violent and blinding-bright burning resulted. At Al/AgF_2 ratios nearer stoichiometric, including the 1:1 ratio, explosion resulted. The glass test tube and plate were completely shattered; portions actually disintegrated. Burning rates are believed to be 100 cm/sec or greater.

*Valley Metallurgical Company, Essex, Connecticut.

The aluminum-silver difluoride formulations have provided an intense light output even underwater. These results suggest an approach for designing a water-actuated photoflash system.

CONCLUSIONS

The major accomplishment of this work was the development of the water-ignitable B-AgF_2-MS pyrotechnic. With the molecular sieve additive the resultant system is reliable and stable, and performance is independent of temperature, pressure, and amount of water. The pyrotechnic can be utilized to design reliable underwater ignition systems for ordnance and hardware applications.

REFERENCES

1. von Wartenburg, H., Z. Anorg. u Allgem. Chem. 244, 337. 1940.
2. Hersh, Charles K., Molecular Sieves, Reinhold Publishing Corporation, New York, 1961.
3. J. L. Austing and J. P. Weber, "Constant Current Ignition Studies of Metal-Metal Oxide Mixtures," Proceedings, 5th Symposium on Electroexplosive Devices, The Franklin Institute, Philadelphia, June 1967.
4. W. M. Slie and R. H. F. Stresau, "Small Scale Plate Dent Test for Confined Charges," NAVORD Report 2422, April 23, 1952.

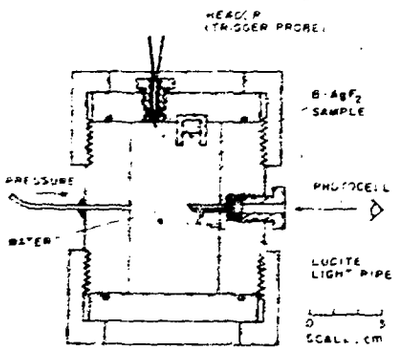

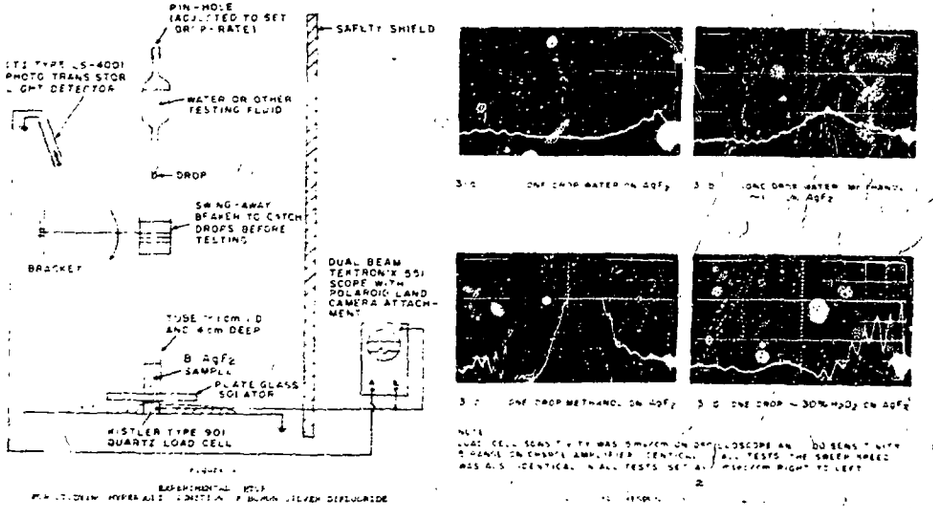

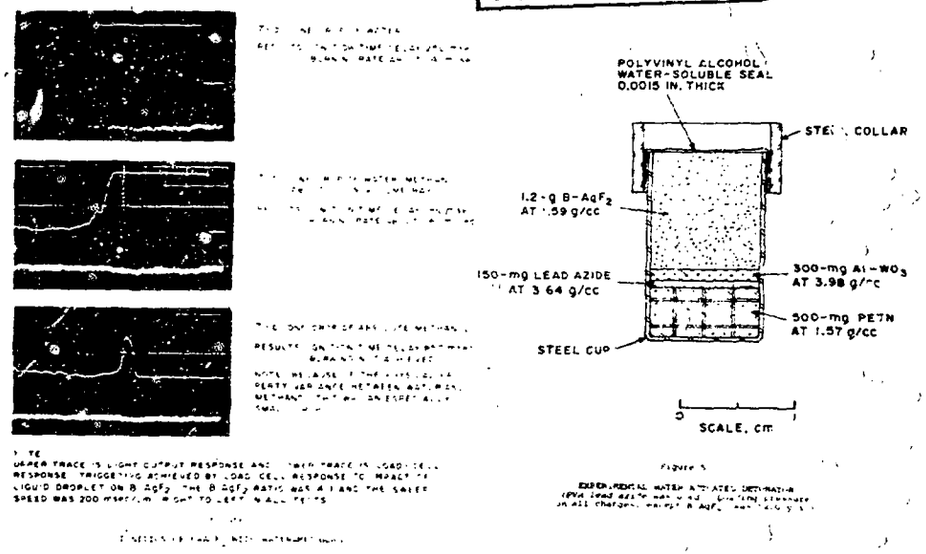

III-5. PROPERTIES AND PERFORMANCE OF ALUMINUM-PLATED PYROTECHNICS FOR ELECTROEXPLOSIVE DEVICE APPLICATIONS*

James L. Austing
Robert F. Remaly
IIT Research Institute
Chicago, Illinois 60616

INTRODUCTION

The work presented in this paper is a continuation of the work discussed by Austing Kennedy, and Weber at the Fifth Symposium on Electroexplosive Devices (Ref. 1) and the First Pyrotechnics Seminar (Ref. 2). The goal of those efforts was to develop electroexplosive devices (EED's) of improved safety, particularly with respect to achievement of specified no-fire levels and insensitivity to electrostatic discharge. The approach taken to meet this goal was to evaluate metal-metal oxidant flash charges formulated from metal and oxidant powders. Several of these mixtures possessed desirable hot-wire ignition characteristics and were able to dissipate a 5-amp, 5-watt no-fire pulse for a period of 15 minutes without being initiated. However, only moderate success was achieved with respect to pin-to-case electrostatic sensitivity; a more recent investigation (Ref. 3) has shown that pyrotechnic mixtures of aluminum and cupric oxide or aluminum and potassium perchlorate formulated from a spherical grade aluminum are very sensitive to electrostatic energies and potentials in the range generated by the human body. Insensitivity to electrostatic discharge could be achieved by utilizing flaked aluminum in the formulations, but then the resulting mixtures did not compact well under pressure and were difficult to ignite from a hot wire.

The present investigation was undertaken to determine whether aluminum-plated pyrotechnics would satisfy all of the requisites of flash charges for EED's. In the present work the plated pyrotechnic is prepared by thermally decomposing a metal alkyl such as triisobutylaluminum in the presence of the oxidant powder: the end product consists of a continuous metal film in intimate contact with the oxidant particles. It was of paramount importance for EED applications that the plated pyrotechnics be insensitive to electrostatic discharge and be capable of reliable ignition from a thermal source such as a hot wire; emphasis was also placed on the ability of EED's loaded with the plated pyrotechnics to dissipate a constant no-fire current of 5 amp for 15 minutes. Three systems were studied extensively, viz., aluminum-plated tungstic oxide, aluminum-plated vanadium pentoxid and aluminum-plated potassium perchlorate. These systems were specifically selected in order that their performance could be compared with that of identical two-powder systems with which we have had extensive experience.

PREPARATION OF ALUMINUM-PLATED PYROTECHNICS

Process

The process for preparing plated pyrotechnics is based on the thermal decomposition of a metal alkyl in the presence of the oxidant powder. The apparatus is depicted schematically in Figure 1. The procedure is as follows. The required quantity

of oxidant powder is slurried in paraffin oil under constant agitation from the stirrer. Initially, the complete system is evacuated and filled with dry nitrogen several times, and then a continuous purge with dry nitrogen is maintained for the remainder of the process. The purge with nitrogen is necessary to preclude air from the system, because triisobutylaluminum as well as other aluminum alkyls are pyrophoric with air. The oxidant-paraffin oil slurry is then heated to approximately 150°C to dry the system. After it has cooled to room temperature, the required amount of triisobutylaluminum is measured in the graduated funnel and allowed to drain into the slurry. The graduated funnel is rinsed with a quantity of the paraffin oil in the reservoir at the top of the apparatus. The entire paraffin oil slurry containing the oxidant and the triisobutylaluminum is then heated to about 250°C and then triisobutylaluminum decomposes according to the following reactions (Ref. 4):

$$(C_4H_9)_3Al \xrightarrow{150°C} (C_4H_9)_2HAl + CH_2=C(CH_3)_2$$

$$(C_4H_9)_2HAl \xrightarrow{250°C} Al + 2CH_2=C(CH_3)_2 + 3/2\ H_2$$

The aluminum that is left behind plates itself mostly onto the oxidant particles. The condenser cools the waste gases, and the isobutylene is trapped in the paraffin oil bubbler.

Up to this point in the process, the plated aluminum from the decomposition of the triisobutylaluminum is in an unoxidized nascent state, because the reaction has been carried cut in a nitrogen atmosphere. Hence, after the slurry has cooled to room temperature the nitrogen purge is discontinued, and in its place a purge with air is conducted overnight with full stirrer agitation The purpose of the air purge is to give the aluminum a chance to oxidize before the product is removed for final wash. It was believed that this step lessens the chances for accidental explosion when the product is finally handled in normal atmosphere.

The final wash is accomplished by puring the slurry into a beaker and adding a large quantity of petroleum ether, and by filtering the product in a Buechner funnel containing a fritted glass disk of pore size 4-15 microns. The aluminum-plated pyrotechnic product is rewashed several more times with petroleum ether, and then finally washed with hexane. The product is then "dried" under vacuum in a vacuum desiccator for 8-16 hours.

Yield and Stoichiometry

Yeilds of product in the above process are essentially quantitative, minus a loss of 1-3% when quantities of approximately 0.25 kilogram of plated pyrotechnic are prepared; this loss is due to the fact that some of the aluminum plates itself onto the sitrrer hardware and the walls of the reaction flask. The proportional loss would be smaller as larger qantities of pyrotechnic are prepared, because the surface to volume ratio of the flask would get smaller as the size of the required flask would increase.

Stoichiometric systems are defined by the following reactions:

$$2\ Al + WO_3 \longrightarrow Al_2O_3 + W$$

$$10/3\ Al + V_2O_5 \longrightarrow 5/3\ Al_2O_3 + 2V$$

$$8/3\ Al + KClO_4 \longrightarrow 4/3\ Al_2O_3 + KCl$$

The aluminum content of each system prepared as described in the preceding section was analyzed by wet chemical techniques. The analyses showed that the aluminum content of each system was follows:

Al-WO_3 system:	83.0% of stoichiometric
Al-V_2O_5 system:	98.1% of stoichiometric
Al-$KClO_4$ system:	48.4% of stoichiometric

PHYSICAL PROPERTIES OF ALUMINUM-PLATED PYROTECHNICS

Particle Size Distribution

A limited amount of work was performed to determine the particle size distribution of the aluminum-plated pyrotechnics. Figure 2 shows such data for either unplated or plated oxidant powders, and the mean particle diameter is indicated for each system. The potassium perchlorate system is shown both before and after plating: the potassium perchlorate* required for the process was ball-milled for 6 hours. It is seen that the aluminum film makes very little difference in the particle size distribution of this product, which indicates that the thickness of the film is small compared to the particle diameter. Calculations show that the thickness of aluminum around a 2-micron diameter oxidant particle is about 0.07 micron, assuming that the particle is a perfect sphere and that the oxidant and aluminum are at crystal density. If these calculations have any meaning at all, the particle size should not be affected by the plating process. Indeed this is what is observed experimentally.

The aluminum-plated tungstic oxide was prepared from the TO-2 grade tungstic oxide,* which as shown in Figure 2 has an average particle size of 1.8 microns. For the aluminum-plated vanadium pentoxide a purified grade of vanadium pentoxide** was utilized; this powder as-received is highly agglomerated, and so its particle size was reduced by ball-milling the powder in paraffin oil for 1.5 hours prior to plating. Figure 2 shows that the average particle size of the aluminum-plated vanadium pentoxide was 11.4 microns.

Density as Function of Loading Pressure

The density of the plated pyrotechnic was recorded for each EED that was loaded for subsequent evaluation; this EED is

*Hummel Chemical Company, Newark, New Jersey.

*Sylvania Electric Products Corporation, Towanda, Pennsylvania.

**Vanadium Corporation of America, Cambridge, Ohio.

depicted in Figure 3, and when bridged with a 5-mil wire has a 5-amp, 5-watt no-fire capability. The loading procedure was as follows. A weighed quantity of pyrotechnic, 200 to 400 mg, was pressed into each EED at a loading pressure of 4,800, 10,300, or 20,000 psi. The ram utilized for pressing was a drill blank of such a diameter as to have a slip fit inside the EED. The height of the column of pressed powder was calculated by subtracting the depth of the EED after loading from the depth prior to loading, both measurements having been made with a depth micrometer.

The density variation for each system is summarized in Table 1 as a function of loading pressure. Comparison of these data with those in Table 2 of Reference 2 shows that the plated pyrotechnic does not press as reproducibly as the pyrotechnic which is a mechanical mixture of two powders, i.e., the standard deviation of the density for the plated pyrotechnic at a given loading pressure is higher. This behavior indicates that the aluminum coating on the oxidant particles is not at crystal density, but perhaps is somewhat porous and slightly spongy. It should be emphasized, however, that the aluminum-plated pyrotechnics did compact well under pressure; thus the loaded EED could be handled normally without fear that the pyrotechnic pressing would become dislodged or break apart.

Table 1

DENSITY VARIATION OF PRESSED ALUMINUM-PLATED PYROTECHNICS

System	Loading Pressure, psi	Density, g/cc Average	Density, g/cc Standard Deviation
Al-Plated WO_3	4,800	2.87	0.20
	10,300	3.08	.11
	20,000	3.32	.09
Al-Plated V_2O_5	4,800	1.68	.08
	10,300	1.76	.04
	20,000	1.87	.05
Al-Plated $KClO_4$	4,800	1.70	.09
	10,300	1.84	.07
	20,000	2.04	0.04

SENSITIVITY TO ELECTROSTATIC DISCHARGE

The ability of an electroexplosive device to withstand electrostatic discharges such as those produced by the human body is an important safety consideration. An extensive evaluation of the pin-to-case electrostatic sensitivity of EED's loaded with the aluminum-plated pyrotechnics was conducted. The procedure was identical to that described in Reference 3, and is briefly summarized here. The EED previously shown in Figure 3 was loaded with one of the aluminum-plated pyrotechnics in the manner described earlier. The pins of this EED were then straightened and fitted with a tight-fitting Teflon sleeve, which was secured to the header and case with an epoxy resin.

The test was conducted by discharging a 500-pf capacitor at a maximum of 25 Kv through the EED connected to the output terminals of the circuit with one terminal connected to the case and the other to the pins. The purpose of the sleeve and epoxy was to prevent external arcing so that the entire discharge occurred inside the EED and traveled through the pressed pyrotechnic; this allowed a valid test of the pin-to-case electrostatic sensitivity of the flash charge without weakening of the spark due to external arcing.

The electrostatic discharge circuit also provides the option of utilizing or omitting a 500-ohm series resistance in the output. This resistance simulates the average resistance of the human body under discharge conditions. Reference 3 shows that the omission of the resistor causes the spark to be more intense and highly oscillatory.

Figure 4 summarizes the results of the electrostatic sensitivity evaluations that were conducted on EED's loaded with the plated pyrotechnics and on EED's loaded with pyrotechnics that were formulated from spherical grade aluminum powder. The bar graph shows the approximate threshold pin-to-case potential that was required to initiate the pyrotechnic. It is seen that all three aluminum-plated pyrotechnics exhibited superior resistance to electrostatic initiation; most of the charges withstood as many as 20 pulses at the highest obtainable potential of 25 Kv.* By way of contrast, the spherical aluminum formulations were very static sensitive, and typically were initiated on the first pulse at potentials in the range 2.5-6.3 Kv. A possible explanation for the improved ability of the plated pyrotechnics to withstand electrostatic discharge is that in a pressed system the aluminum coating provides a continuous conductive path from pin-to-case, such that no gaps exist to permit a spark to occur; the stored energy in the circuit capacitor dissipates itself as ohmic heating in the flash charge, and because the stored energy is small the flash charge is not heated to a very high temperature. We believe that this same reasoning could be applied to most other aluminum-plated metal oxidants; hence, aluminum-plated cupric oxide, which has not been prepared and which is indicated with a question mark in Figure 4, would also be insensitive to electrostatic energies of the magnitude generated by the human body.

CONSTANT CURRENT IGNITION STUDIES

The constant current ignition studies were conducted on EED's loaded with the three plated pyrotechnics; the EED has

*In one test, an aluminum-plated tungstic oxide charge pressed at 4,800 psi and tested with 0 ohms series resistance was initiated at 25 kv; however, none of the plated pyrotechnics pressed at 10,300 or 20,000 psi were initiated in 20 pulses regardless of whether the 500 ohms series resistance was utilized or not.

been previously shown in Figure 3, and the loading procedure has been described earlier. The objective of these studies were three-fold: (1) to ascertain the performance of the plated pyrotechnics at the all-fire currents of 15, 20, and 25 amp; (2) to determine whether the EED's that had passed the electrostatic evaluations could be ignited at an all-fire current of 15 amp; and (3) to determine whether the plated pyrotechnics could pass a 5-amp, 5-watt no-fire test. The construction, operation, and utilization of the constant current firing circuit required for these evaluations is fully described in another paper at this symposium (Ref. 5).

Evaluation of Plated Pyrotechnics at the All-Fire Currents of 15, 20, and 25 amp

The general observation that can be made from the firing of almost 100 EED's is that the performance of the plated pyrotechnics as flash charges is superior; not a single misfire occurred. The performance was strongly influenced by the pyrotechnic loading density, particularly at the firing current of 15 amp.

Least squares equations of the ignition time and unit burning time as functions of loading density were calculated on a Hewlett-Packard model 9100B desk calculator. The following symbols are defined:

ρ_o = loading density

t_i = ignition time

t_{ub} = unit burning time (reciprocal of burning rate)

r = correlation coefficient

The correlation coefficient is an indication of the goodness of the fit of a least squares straight line, and is defined as follows:

$$r = \frac{\sum_1^n (x_i - \bar{x})\ (y_i - \bar{y})}{\left[\sum_1^n (x_i - \bar{x})^2 \sum_1^n (y_i - \bar{y})^2\right]^{1/2}} \qquad (1)$$

where $-1 \leq r \leq +1$; if $r = \pm 1$, the fit is perfect, and if $r = 0$, no correlation exists.

The performance of aluminum-plated tungstic oxide is plotted in Figures 5 and 6. The equations for ignition time at each current are:

At 25 amp, $t_i = 1.03 + 0.275\ \rho_o$ (2)

$r = 0.161$

At 20 amp, $t_i = -1.27 + 1.398\ \rho_o$ (3)

$r = 0.861$

At 15 amp, $t_i = -5.08 + 3.69\ \rho_o$ (4)

$r = 0.815$

The unit burning time is given by:

At 25 amp, $t_{ub} = 210.4 - 139.5\ \rho_o + 24.8\ \rho_o^2$ (5)

At 15 and 20 amp, $t_{ub} = 170.6 - 99.9\ \rho_o + 16.5\ \rho_o^2$ (6)

Equation 6 predicts a minimum in unit burning time at a density of 3.02 g/cc; this minimum does not necesrarily occur physically, but is caused by the mathematics of the least squares fit.

The upper graphs in Figures 5 and 6 show the performance of a mixture of spherical aluminum and tungstic oxide powders from Reference 1. This mixture, which was stoichiometric, was very difficult to ignite at 15 amp, and this fact accounts for the fewness of points. On the other hand, no such difficulty was encountered at all for the aluminum-plated system. Notice in particular how much more quickly the plated system was ignited and how much more rapidly it burned, as compared to the two-powder system.

Figure 6 indicates that the 25-amp firing current overdrove the reaction, in as much as unit burning times at the lower densities were somewhat lower. Figure 7 shows the results of a series of experiments in which the burning time was recorded as a function of the column height of the pyrotechnic. It is seen that the effect is transient, and that in a sufficiently long column the unit burning time would increase to the steady state value predicted by Equation 6.

Figures 8 and 9 show the performance of the aluminum-plated vanadium pentoxide. The ignition time is given by the following equations:

$$\text{At 25 amp,} \quad t_i = -1.62 + 1.85\,\rho_o \qquad (7)$$
$$r = 0.804$$

$$\text{At 20 amp,} \quad t_i = -2.49 + 2.78\,\rho_o \qquad (8)$$
$$r = 0.568$$

$$\text{At 15 amp,} \quad t_i = -10.86 + 8.57\,\rho_o \qquad (9)$$
$$r = 0.882$$

The unit burning time appears to be independent of firing current, and is given by

$$t_{ub} = -19.9 + 12.99\,\rho_o \qquad (10)$$
$$r = 0.83$$

Previously unpublished data (Ref. 6) showed that a formulation of spherical aluminum and vanadium pentoxide powders was very difficult to ignite at 15 amp; as shown the upper parts of Figures 8 and 9, the ignitions that were obtained required a longer time and the resultant burning was considerably slower than for the plated pyrotechnic.

The ignition time of aluminum-plated potassium perchlorate is shown in Figure 10. Because the burning rate of aluminum-potassium perchlorate is in the neighborhood of 0.05 in./μsec (Refs. 7 and 8), the difference between ignition time and overall function time in our EED's would be only about 4 μsec. Such a short time was not resolvable on the oscilloscope, which was swept in the milliseconds-per-centimeter range. Hence the ordinate in Figure 10 is also labeled overall function time, to convey the idea that the burning time is very short. The

equations for the ignition time of aluminum-plated potassium perchlorate are as follows:

At 25 amp, $t_i = 4.31 - 1.48\ \rho_o$ (11)
$r = -0.504$

At 20 amp, $t_i = 8.81 - 3.27\ \rho_o$ (12)
$r = -0.612$

At 15 amp, $t_i = 7.73 - 1.90\ \rho_o$ (13)
$r = -0.230$

Unlike the equations for the other two systems, Equations 11 through 13 have negative slopes. Note also that the scatter in the points in Figure 10 is severe, especially for the 15-amp curve; this scatter is attributed to the very low aluminum content of the plated potassium perchlorate system, which as reported earlier was only 48.4% of stoichiometric. It is believed that at higher aluminum contents the system would be ignited more reproducibly.

Equations 2 through 13 represent design equations for electroexplosive devices in which the flash charge is one of the plated pyrotechnics. The goal, of course, is to predict the overall function time at a given firing current. The overall function time is related to the ignition time and unit burning time by the expression

$$t_{of} = t_i + h\ t_{ub} \quad (14)$$

where h is the height of the pressed flash charge column.

Ignition of EED's after Electrostatic Sensitivity Evaluations

It was shown earlier that the aluminum-plated pyrotechnics had exhibited superior insensitivity to electrostatic discharges. Since the EED's had been pulsed as many as 20 times at 25 Kv, the question was posed whether the hot wire ignition characteristics of the pyrotechnics had been degraded. Each EED was therefore fired at 15 amp, and the ignition time and unit burning time were recorded as a function of pyrotechnic loading density. The data for each system is plotted as squares and dashed curves in Figures 10 through 15 ; the previous all-fire data at 15 amp from Figures 5, 6, and 8 through 10 has been superimposed as circles and solid curves. For all three systems, the data for the ignition following the electrostatic evaluations agree very well with the previous all-fire data.

The least squares equations of the dashed curves in Figures 11 through 15 are as follows, for a firing current of 15 amp:

For aluminum-plated tungstic oxide,

$$t_i = 47.74 - 32.32\ \rho_o + 6.12\ \rho_o^2 \quad (15)$$

$$t_{ub} = -7.23 + 8.20\ \rho_o \quad (16)$$
$$r = 0.829$$

For aluminum-plated vanadium pentoxide,

$$t_i = 35.98 - 43.58\ \rho_o + 14.44\ \rho_o^2 \quad (17)$$

$$t_{ub} = 8.94 - 22.27\ \rho_o + 10.91\ \rho_o^2 \quad (18)$$

For aluminum-plated potassium perchlorate,

$$t_1 = 6.39 - 1.19\ \rho_o \quad (19)$$

$$r = -0.203$$

Notice in all of the figures that scatter in the points is about the same for both sets of data. The conclusion that can be drawn is that the electrostatic pulses did not degrade the pyrotechnic flash charges.

5-amp, 5-watt No-Fire Experiments

Table 2 summarizes the experiments to determine whether the EED's loaded with aluminum-plated pyrotechnic flash charges would dissipate a constant 5-amp, 5-watt pulse maintained for 15 minutes. The EED's become very hot, especially when suspended in free air. Under this condition, however, the aluminum-plated tungstic oxide and potassium perchlorate flash charges survived the test and did not cook-off in the 15 minute period; on the other hand, the aluminum-plated vanadium pentoxide survived for only 4 to 8.5 minutes. Two additional experiments were run in which the EED's were snugly fitted into a steel block, which provided a heat sink; the table shows that under this condition the aluminum-plated vanadium pentoxide flash charges did not cook-off. (In actual application, EED's are generally mounted in other metal hardware that would serve as a heat sink.)

After cooling to room temperature, those EED's that had survived the no-fire test were evaluated at an all-fire current of 15 or 25 amp. This performance is summarized in columns 5 through 7 of Table 2. Notice that (1) the ignition times are considerably longer than those previously measured, and (2) all but one of the aluminum-plated potassium perchlorate flash charges misfired. These problems are attributed to thermal expansion, which during the no-fire test altered the physical contact between the bridgewire and the pressed flash charge. It should be pointed out, however, that many specifications do not require that the EED be firable after a 5-amp, 5-watt no-fire test, and so the above difficulties are of no major concern. The important requirement is that the EED not function during the no-fire test, and this ability has been demonstrated for the three aluminum-plated pyrotechnics.

SUMMARY

The data presented in this paper show the applicability of aluminum-plated pyrotechnics as flash charges for electroexplosive devices. There are, however, numerous other potential applications; these include the utilization of plated pyrotechnics as photoflash composition, flare materials, and delay column ingredients. Another obvious characteristic that would offer an advantage in some applications is that the plated pyrotechnic is not susceptible to segregation of the components in handling and vibration environments.

The oxidants that were plated in the work discussed in this paper were all temperature stable compounds. If it is desired to plate a less stable compound, an aluminum alkyl that decomposes at a temperature less than 250°C could be utilized. The process could easily be extended to plate metals other than aluminum; other metal alkyls with desirable decomposition temperatures are either available commercially or could be synthesized (Ref. 9). In addition, binary alloys could also be plated, by using two alkyls with nearly the same decomposition temperature or by using one alkyl with the two metals in the same molecule.

ACKNOWLEDGEMENTS

The authors are indebted to Dr. Morton J. Klein and Mr. Charles K. Hersh, whose cooperation and direction made this work possible. Dr E. L Grove supervised the aluminum wet chemical analyses. The conscientious efforts of Mr. Douglas E. Baker, who conducted the electrostatic sensitivity studies and assisted in the constant current ignition studies, are deeply appreciated. The authors also acknowledge the interest of Mr. John P. Weber of Sandia Laboratories, Albuquerque, New Mexico, who supported the preparation of the aluminum-plated potassium perchlorate.

REFERENCES

1. J. L. Austing and J. P. Weber, "Constant Current Ignition of Metal-Metal Oxide Mixtures," Paper No. 3-3, Proceedings Fifth Symposium on Electroexplosive Devices, The Franklin Institute, Philadelphia, June 1967.

2. J. L. Austing, J. E. Kennedy, and J. P. Weber, "Ignition and Output Characteristics of Pyrotechnics for EED Applications," Proceedings, First Pyrotechnics Seminar, USNAD RDTR No. 131, October 1, 1968, Crane, Indiana.

3. J. L. Austing and R. Gortowski, "Circuit for Studying the Electrostatic Sensitivity of Electroexplosive Devices," Manuscript to be published in Explosivstoffe.

4. K. Ziegler et al., Angew. Chem. 67, 424-425, 1955.

5. J. L. Austing and A. L. Usher, "Fast-Rise, High-Current, Constant Current Firing Circuit for Electroexplosive Devices," Paper No. II-3, This Symposium.

6. J. L. Austing and J. E. Kennedy, Previously unpublished data.

7. J. Hershkowitz, F. Schwartz, and J. V. R. Kaufman, "Combustion in Loose Granular Mixtures of Potassium Perchlorate and Aluminum," Eighth Symposium (International) on Combustion, The Williams and Wilkins Company, Baltimore, 1962, p. 720.

8. L. D. Pitts, "Electrical Probe Technique for Measurement of Detonation and Deflagration Velocities," Proceedings Fourth Symposium (International) on Detonation, ONR Report No. ACR-126, October 1965.

9. U. A. Lehikoinen, Ethyl Corporation, Ferndale, Michigan, Personal communication, August 16, 1968.

Table 2

SUMMARY OF 5-AMP, 5-WATT, 15-MIN NO-FIRE EXPERIMENTS*

System	Density, g/cc	5-amp Test: Cook-off Time, minutes	5-amp Test: Heat Sink ?	After Cooling: Ignition Current, amp	After Cooling: Ignition Time, msec.	After Cooling: Unit Burning Time, msec/inch
Al-Plated WO_3	3.02	>15	No	14.6	18.5	14.9
	3.03	>15	No	14.6	18.7	22.1
	3.06	>15	No	15.0	19.3	20.4
	3.09	>15	No	14.8	17.9	16.2
	3.06	>15	No	14.8	19.1	17.1
Al-Plated V_2O_5	1.77	4	No	-	-	-
	1.77	8.5	No	-	-	-
	1.74	7.5	No	-	-	-
	1.77	>15	Yes	15.0	6.0	3.0
	1.78	>15	Yes	14.8	6.3	3.6
Al-Plated $KClO_4$	1.87	>15	No	15.0**	No go	-
	1.77	>15	No	14.8**	No go	-
	1.78	>15	No	14.9**	No go	-
	1.86	>15	No	25.8**	No go	-
	1.86	>15	No	25.9**	No go	-
	1.89	>15	No	14.6**	No go	-
	2.01	>15	No	15.0**	No go	-
	1.89	>15	No	26.1	2.8	~0

*EED is depicted in Figure 3.

**One-minute current duration.

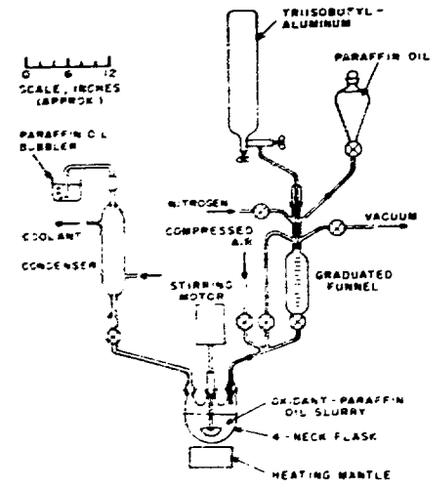

Figure

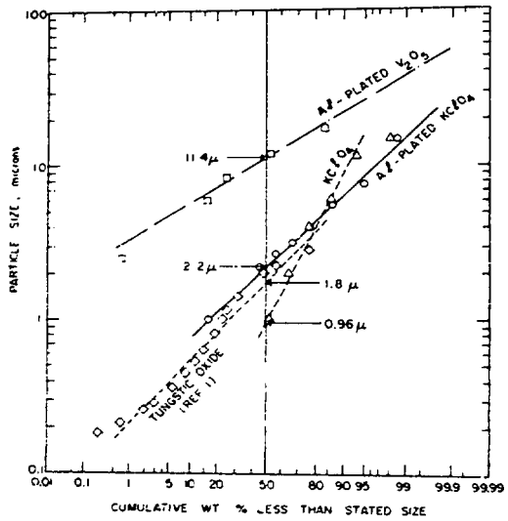

Figure 2

PARTICLE SIZE DISTRIBUTION OF PLATED PYROTECHNICS AND OXIDANTS

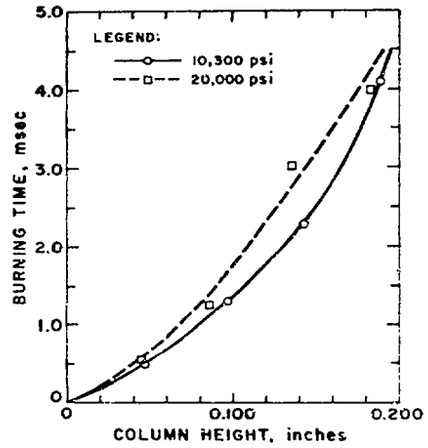

Figure 7

VARIATION OF BURNING TIME WITH COLUMN HEIGHT FOR ALUMINUM-PLATED TUNGSTIC OXIDE AT FIRING CURRENT OF 25 AMP

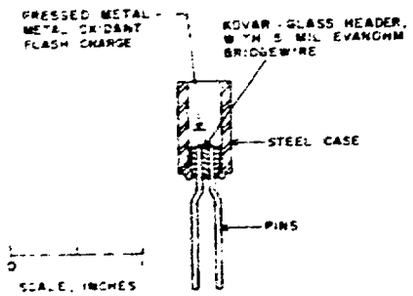

Figure

ELECTROEXPLOSIVE DEVICE

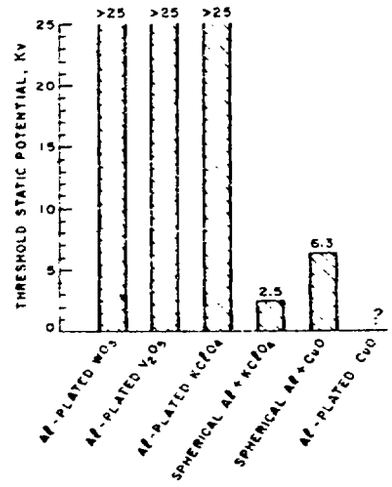

Figure 4

PIN TYPE GLASS ELECTROSTATIC SENSITIVITY OF VARIOUS PYROTECHNICS

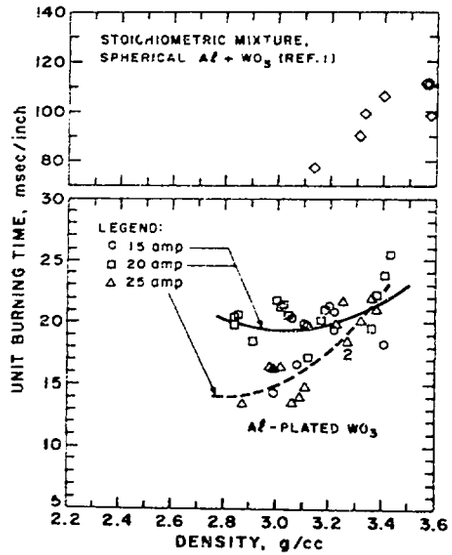

Figure 6

COMPARISON OF UNIT BURNING TIMES OF ALUMINUM-TUNGSTIC OXIDE SYSTEMS

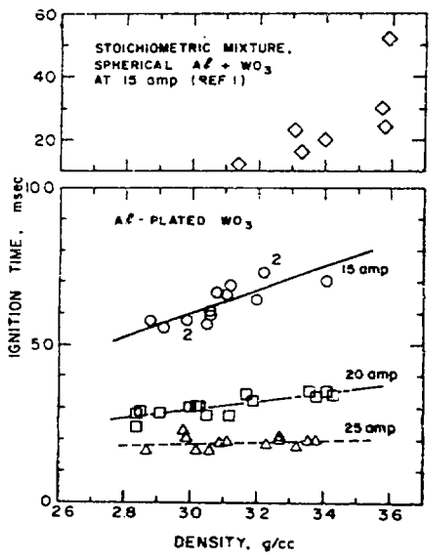

Figure 5

COMPARISON OF IGNITION TIMES OF ALUMINUM-TUNGSTIC OXIDE SYSTEMS

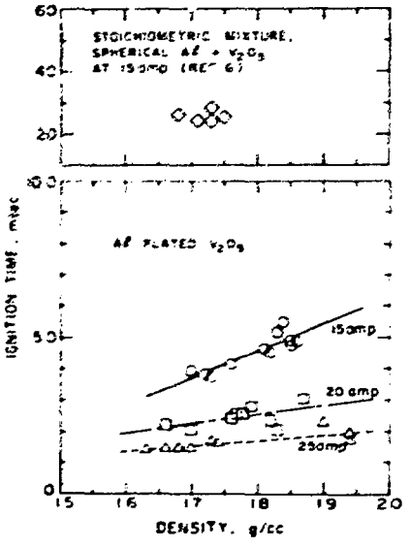
STOICHIOMETRIC MIXTURE,
SPHERICAL Aℓ + V_2O_5
AT 15 amp (REF. 6)
Aℓ PLATED V_2O_5
15 amp
20 amp
25 amp
IGNITION TIME, msec
DENSITY, g/cc

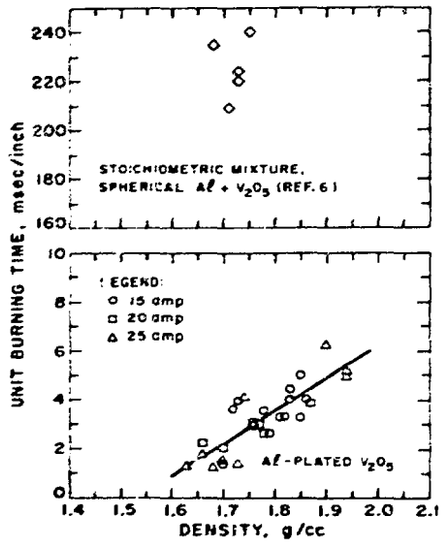
STOICHIOMETRIC MIXTURE,
SPHERICAL Aℓ + V_2O_5 (REF. 6)
LEGEND:
15 amp
20 amp
25 amp
Aℓ-PLATED V_2O_5
UNIT BURNING TIME, msec/inch
DENSITY, g/cc

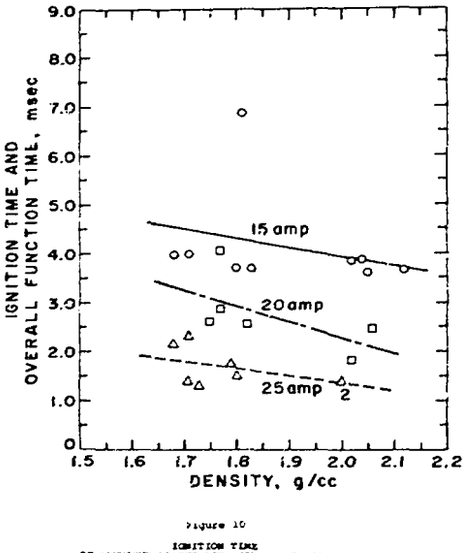
15 amp
20 amp
25 amp
IGNITION TIME AND
OVERALL FUNCTION TIME, msec
DENSITY, g/cc

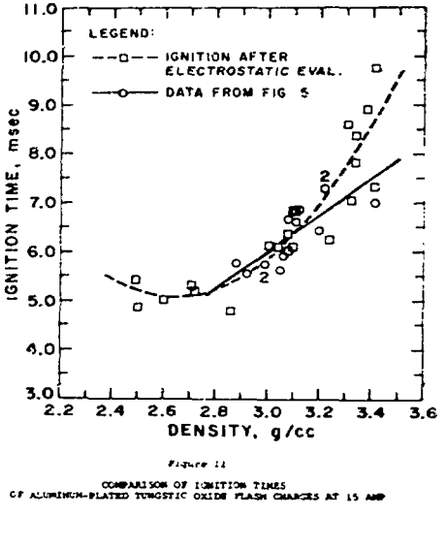
LEGEND:
IGNITION AFTER
ELECTROSTATIC EVAL.
DATA FROM FIG 5
IGNITION TIME, msec
DENSITY, g/cc

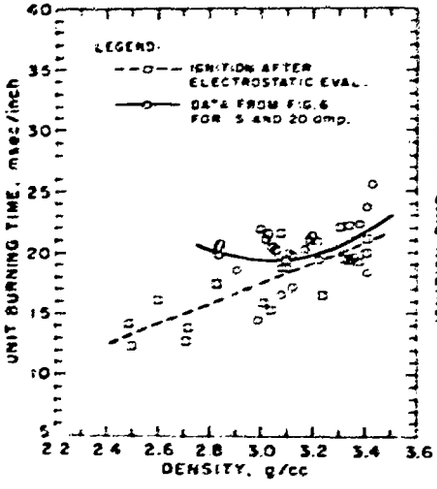
LEGEND:
IGNITION AFTER
ELECTROSTATIC EVAL.
DATA FROM FIG. 6
FOR 5 AND 20 amp.
UNIT BURNING TIME, msec/inch
DENSITY, g/cc

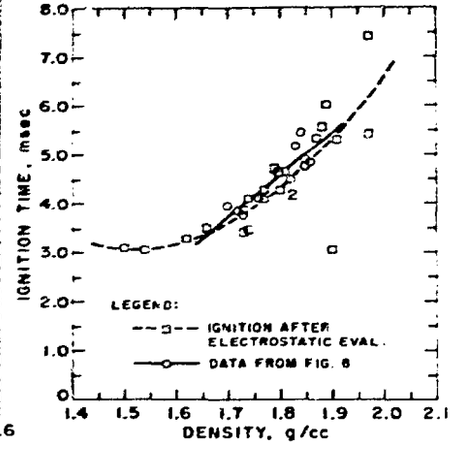
LEGEND:
IGNITION AFTER
ELECTROSTATIC EVAL.
DATA FROM FIG. 8
IGNITION TIME, msec
DENSITY, g/cc

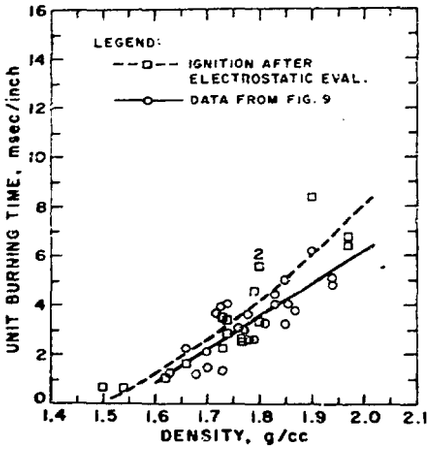
LEGEND:
IGNITION AFTER
ELECTROSTATIC EVAL.
DATA FROM FIG. 9
UNIT BURNING TIME, msec/inch
DENSITY, g/cc

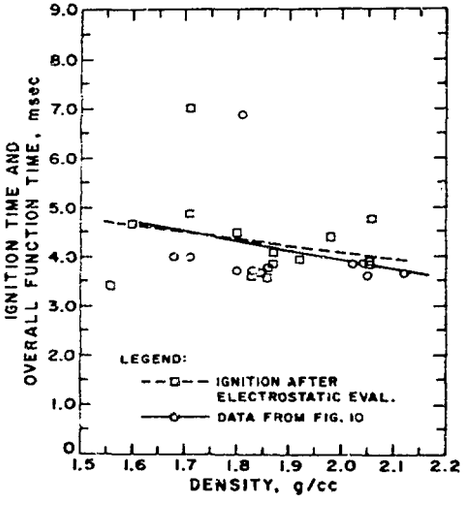
LEGEND:
IGNITION AFTER
ELECTROSTATIC EVAL.
DATA FROM FIG. 10
IGNITION TIME AND
OVERALL FUNCTION TIME, msec
DENSITY, g/cc

III-6. SAFETY CERTIFICATION OF NEW PYROTECHNIC DEVICES

by T. J. Sullivan and Mrs. J. A. McDevitt
Naval Ordnance Station, Indian Head, Md.

INTRODUCTION

Every weapon system and every item of explosive ordnance for the Navy must be reviewed, tested, and an explosive safety certification obtained before a system shall be permitted to advance to the next stage of development and before units can be introduced to the fleet. The responsibility for safety certification is vested in the Naval Ordnance Systems Command through the Weapon System Explosives Safety Review Board (WSESRB). The life stages covered by the WSESRB include Research and Development, Testing, Production, Rework, Loading, Handling, Shipment, Storage, Maintenance, Usage, and Disposal. The end items, or weapons, are categorized into the following groups: Air and Surface Launched Weapon and Target Systems, Underwater Weapon Systems, Security Destruct Devices, Pyrotechnics, and Cartridge-Actuated Devices. This paper presents the safety evaluation tasks which are performed for the WSESRB by the Naval Ordnance Station, Indian Head, Maryland to assess the safety of a pyrotechnic device during its entire life cycle.

APPROACH

The safety evaluation parallels the major life stages in the development of a new pyrotechnic device (shown in Figure 1). A series of evaluations are conducted beginning with the concept formulation stage and continuing through development and into final release to service use. These evaluations include a review of the design, safety plan, test results, operational plan, and safety documentation, and implementation of system safety analytical techniques. At each life stage, the decision is made either to advance the sequence, or to hold it at its present stage for further consideration.

The specific safety certification tasks associated with each life stage are described in the checklist shown in Table I.

Concept Formulation

Concept Formulation for a new pyrotechnic may arise as a result of operational need, an improvement of an existing device, or new technology making it possible to produce an advanced device. Most of the safety work at this stage is that of comparing the idea with present technology and resolving functions, designs, and materials. A Preliminary Hazards Analysis should be initiated to identify the inherent hazards associated with each design or modification and to verify the safety of the design concept.

Project Definition

During Project Definition, the contractor submits a proposal or Technical Development Plan (TDP) which describes the step-by-step procedure for arriving at the end item. Safety requirements in the preliminary specification must be reviewed for compliance with existing pyrotechnic and general

safety specifications. Additional specifications may be called for to verify the safety design features and operating safety characteristics. The major effort at this stage is to ascertain that safety has been included in the TDP and that the safety studies, analyses and tests to be accomplished during engineering development will ensure the highest degree of safety consistent with performance requirements.

Design and Development

Design and Development is the first stage where conjecture may be replaced by factual evidence. The test program is reviewed to ensure that tests and data generated verify the safety of the design. In particular, failure analyses and investigations are reviewed to identify additional hazards or problems which might degrade safety. The design must be safety certified upon completion of design feasibility testing and prior to manufacturing prototype units. When the design is in doubt, the unit is generally released to limited production with the stipulation that additional safety testing be conducted.

An independent assessment of the safety of the design using subsystem/system hazards analysis techniques should be performed to determine that all hazardous failure modes have been considered before the design is frozen. A Failure Mode and Effects Analysis may be conducted to analyze the hazards associated with components which must function for the pyrotechnic to operate. The Fault Tree Analysis is concerned with all components including interfacing hardware whose performance degradation or functional failure could result in a hazardous condition. These analyses provide a critical examination of all conveivable failures which could occur with the pyrotechnic device and an evaluation of the effects of each failure. For each end effect determined to be critical or catastrophic, a Fault Tree Analysis would be performed to analyze all logical combinations of functional fault events which would have to occur.

Evaluation, Release for Service Use, Acquisition

Evaluation of a prototype unit normally is made by a customer by determining the conformance of test results to developed specifications. Performance is of concern to the safety evaluation only when a hazard is involved. Unreliability must be examined to determine the effects of the failure on safety; a unit may fail safe. A hazardous incident must be analyzed to determine the failure mode and the possibility of recurrence with other units. The probability that a pyrotechnic can enter a hazardous failure mode may be reduced by redesigning for higher reliability.

Additional testing using pilot lot and preproduction units is necessary to verify the results obtained with prototype units. Production tooling and operating personnel generally are not used for prototypes, and when the transition is made from highly skilled engineers, designers, and technicians to production personnel, faults may appear which were not evident before. The basic documentation written

for design development and production of a few prototype units is reviewed during pilot production. The production techniques, assembly procedures, facilities, testing, and inspections critical to the safety of the pyrotechnic device must be evaluated for their effect on safety. Units shall be manufactured for preproduction tests in accordance with the production specifications. No changes to the unit after approval of the preproduction test sample shall be made without prior written approval of the customer. Upon successful completion of the preproduction test, subsequent production shall utilize the same equipment, processes, materials, propellant, and ignition elements and the same design including dimensions and tolerances as the approved qualification design.

Operational Evaluation is conducted by the user to prove the effectiveness of the pyrotechnic in an operational environment. This evaluation is conducted with pilot or preproduction units manufactured by production specifications. Modifications in operating procedures and proposed operational manuals may be expected at this stage. The total system's safety must be assessed and all documentation including test reports, specifications, pilot production records, safety and handling manuals, and manufacturing drawings and procedures is presented for review. An Operating Hazard Analysis should be conducted to assess the operational safety level of the pyrotechnic considering the personnel, procedures, and ground equipment required for the various operations during its intended use. The safety evaluation team would review previous recommendations concerning safety to assure they had been complied with and submit other reservations or recommendations to the WSESRB.

Release for Service Use is made by the project manager based upon recommendations made by the WSESRB. A presentation by the developer and customer to the WSESRB is made of the design, development summaries, qualification test results, manufacturing process, and other pertinent data which might effect the release of the unit for service use. Production Release is given by the project manager but naturally is contingent on the need for the pyrotechnic. Ideally, a release for service use and the need for procurement of the item would coincide.

Usage

The safety of a pyrotechnic device during its entire service life from manufacture to use or disposal should have been determined, reviewed, and certified in earlier life stages. Maintenance and rework safety, although presumably resolved concurrent with approval for manufacture of the original item, cannot be evaluated fully until the unit has some sustained production and storage life. Maintenance procedures generally are minor in nature and do not present any additional hazard. Rework or retrofitting of items in use to reflect the latest design configuration may present

new hazards because of the age and consequent deterioration of the item or its components.

Surveillance programs are conducted to predict the safe and useful life of the pyrotechnic device. Units are subjected to conditions which simulate the operational environment during storage and to accelerated aging tests. Based on the surveillance data, procedures are written for maintenance, rework overhaul, or removal from service use. These documents are reviewed for safety with special emphasis on the fact that the item is aged.

Explosive Ordnance Disposal (EOD) procedures are required to dispose of an unusable item. The safety review would ascertain that disposal procedures have been considered by EOD personnel as early in the life cycle as possible.

During service use, accident/incident reporting utilizes a feedback system between engineering and operating personnel for all malfunctions, personnel injuries, and results of special safety tests. These reports are reviewed by the Safety Office in the Navy and appropriate action is taken. Incidents at manufacturing plants, in shipment, and in service must be handled expeditiously and acted upon to prevent recurrence, keep serviceable items in the inventory, and assure safety at all life stages.

SUMMARY

The safety evaluation tasks which were performed to certify a new pyrotechnic device for service use in the Navy have been described. System safety analytical techniques were implemented to identify the hazards associated with components, equipment, procedures, and personnel during all phases of the pyrotechnic life cycle. The hazards analyses incorporated during each life stage are shown in Figure 2. Implementation of these techniques provides for a comprehensive safety review and assessment of the safety of the pyrotechnic device. This checklist provides guidelines for safety evaluation during each stage of procurement applicable to all new ordnance for the Navy.

TABLE I

SAFETY CERTIFICATION CHECKLIST FOR PYROTECHNICS

A. Concept Formulation

1. Review technical approaches of safety design features for gross incompatibilities, technical risks, or problems in design considering the state-of-the-art technology.

2. Perform a comparative safety evaluation to determine that the new system or subsystem would not degrade safety inherent in present mode or similar items.

3. Perform a preliminary hazards analysis to determine qualitatively the hazards of the end item in its intended operating environment.

B. Project Definition

1. Review trade-off studies and assure that the highest degree of safety consistent with requirements is maintained. Refines results in preliminary hazards analysis.

2. Approve the safety design criteria, objectives, and goals.

3. Review new and/or existing specifications and standards for meaningful acceptance and/or failure criteria of the safety design requirements.

4. Review safety studies, analyses, test plans, and data required in engineering development for adequacy in demonstrating the operating safety characteristics of the system.

5. Review the system safety plan in the contractor data requirements list.

C. Design and Development

1. Review preliminary drawings to evaluate safety features of the new design prior to fabrication of prototype items.

2. Approve safety guides for manufacturing considering ingredients handling, processing, assembly, equipment, and facilities.

3. Conduct subsystem/system hazards analyses to identify all components and equipment whose performance degradation and function failure would result in a hazardous condition. Update the analyses as results of tests become available.

4. Review laboratory test results which establish the sensitivity and stability characteristics of the explosive materials. Laboratory tests for consideration include:

Heat stability
Vacuum stability
Hygroscopicity
Self-heating
Impact sensitivity
Friction sensitivity
Ignitability
Electrostatic discharge
Compatibility

5. Review tests results for establishing the explosive hazard classification (storage compatibility, quantity-distance, DOT classification and markings) for storage and shipment. Review classification when testing of the end item has been exempted by establishing an analogy with existing classified items. Tests for classification of bulk pyrotechnic material include:

Blasting cap
Ignition and unconfined burning
Thermal stability
Impact sensitivity
Card gap test

Tests of the packaged and stored configuration include:

Detonation-propagation within and between containers, five tests each
External heat-one test using one to six containers

6. Review design feasibility test summaries with emphasis on failure analyses, investigations, and problems which might degrade safety.

7. Review safety tests conducted on prototype items to determine potential problems and verify corrective action required. Tests may include:

40-foot drop
Malassembly

8. Review results of special safety investigations conducted to define and minimize or eliminate the hazard associated with item use. Analyses may include:

Toxicity - Contact Naval Ordnance Environmental Health Center
HERO
Electrostatic discharge
Lightning
Physiological effects
Eye hazards

9. Construct a fault tree to analyze all the logical combinations of functional fault events which can cause a critical or catastrophic hazard (determined by fault hazards analysis).

10. Apply other analytical techniques for example: aging, situational, use-life, physiological human factors, and accident feedback analyses which have been proposed by the certification team to assure a comprehensive system safety analysis.

11. Approve the systems design upon completion of design feasibility demonstration.

12. Approve the safety and technical evaluation test plan. Standard tests which should be considered in developing the safety evaluation plan include:

Jolt
Jumble
40-foot drop
Safety function
Fast cook-off
Slow cook-off (autoignition)
Bullet impact

Standard tests which should be considered in developing the technical evaluation plan include:

Control
Low temperature function

Ambient function
High temperature function

Handling
5-foot drop
Temperature and humidity
Rough handling (packaged)

Transportation
Vibration
Catapult and arrested landing

Storage
Surveillance - ambient aging

Series
First sequence to simulate the environment of actual service usa
Subsequent series to be conducted in a random order

Specific Environment
Storage: Extreme temperature conditioning
Shipboard: Immersion
Tropical: Salt spray
Fungus resistance
Water-proofness
Vacuum-steam-pressure
Desert: Sand and dust
Aircraft: Altitude

Inspection - Pre- and post-testing
Visual
X-ray
Disassembly

Design Verification
Operational effectiveness tests as related to safety

Special Hazard Classification
HERO and static electricity
Toxicity

13. Approve release to limited production

D. Evaluation, Release for Service Use, Acquisition

1. Review safety evaluation test results and test procedures.

2. Review of techeval results with emphasis on failure analyses, investigations, and problems which might degrade safety.

3. Review redesign or changes required to meet design criteria.

4. Conduct an operating hazards analysis.

5. Review warnings, cautions, special precautions required for safe operation and maintenance.

6. Review special procedures for servicing, handling, storage, and transportation of the item in its intended environment.

7. Review engineering documentation drawing package, classification of defects, ordnance pamphlets, technical manuals to assure safe operation and maintenance.

8. Review training and certification programs for service personnel.

9. Update subsystem/system hazards.

10. Approve final design.

11. Approve release for service use.

12. Review purchase specifications, SOP's, process quality control, lot inspection and acceptance test procedures to assure that safety can be maintained during production.

13. Approve release for production.

E. Usage

1. Review operational safety tests and procedural checklists in the fleet to determine if the design and the operating and maintenance procedures are adequate.

2. Review ordnance alterations.

3. Review of recertification programs of service personnel.

4. Assure that explosive ordnance disposal procedures have been established.

5. Analyze accidents, incidents, and failures to identify major or critical characteristics of safety significant items which deteriorate with age and environment.

6. Review change orders to technical manuals and operational procedures, and modifications to equipment to assure that inherent safety is not degraded.

7. Verify adherence to safety regulations by periodic inspection.

8. Check adherence to ammunition reclassification (unserviceable, suspended, and limited use) as to the proper use and disposition of items affected.

- CONCEPT FORMULATION
- PROJECT DEFINITION
- DESIGN AND DEVELOPMENT
- EVALUATION, ACQUISITION
- USAGE, DISPOSAL

FIGURE 1. PYROTECHNIC LIFE CYCLE

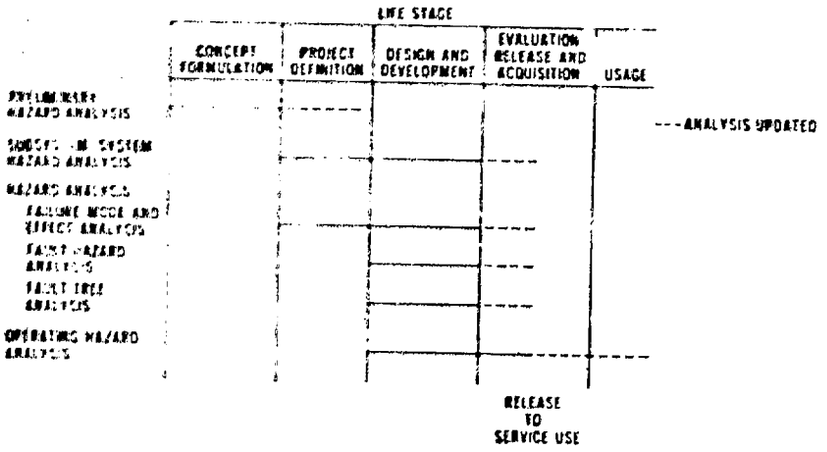

FIGURE 2. SYSTEM HAZARD ANALYSIS

III-7. Pyrogen Jet Squib

by
David A. Colpitts and Kenneth R. Foote
Propulsion Development Department
Naval Weapons Center
China Lake, California

ABSTRACT: An experimental electric squib-igniter, with a jet flame, has been developed. The squib was developed to ignite difficult-to-ignite propellant and flare materials. The squib does not contain primary explosives and is initiated within 5 to 10 milliseconds by an electric pulse through a bridgewire coated with a magnesium-fluorocarbon mixture. A configured pellet of the same type of material is used as the main charge. The subassembly is enclosed in a Mk 1 or Mk 2 gilding metal cup. The cup is crimped onto the plastic header-plug containing the coated bridgewire and the main charge. Upon initiation, the squib produces a gaseous, coruscative, blow-torch type flame about 6-inches long and persists for 1-1/2 to 2 seconds. This type of squib can perform properly at -300°F to +300°F.

INTRODUCTION: Several years ago the writers collaborated to develop a squib which would produce a hot, coruscative flame for a longer duration than conventional squibs. Concurrently, the basic approach was to use the pyrogen technique, using a family of magnesium-fluorocarbon propellants being developed. These magnesium-fluorocarbon pyro-propellants have several unique characteristics which aided in the development of the pyrogen jet squib. The Magnesium-Teflon pyro-propellant system is a metal-oxidant system with a stoichiometric ratio of 38-62. However, this sytem contains no oxygen. For this system fluorine performs a similar function as oxygen. Stoichiometric burning yields magnesium fluoride and carbon. In general, the formulations used in the research studies and resultant development are fuel rich and contain an energetic binder, Viton A, which makes the propellant extrudable.

Design Configuration

Probably a good deal of the state-of-the-art of squib manufacture was established during the development and production of the Mk 1 and Mk 2 squibs. Between 30 to 50 million have been fabricated and used in a variety of military applications. No known failures have been reported when proper electric energy was applied to the squib. The basic Mk 1 and Mk 2 squib components were selected for the jet squib because of the low cost of already proven, manufacturable and available parts. The functionality of the pyrogen squib igniter lends itself to further development of more exotic headers bridgewire configuration and main charge combinations.

The design of the jet squib is shown in Figure 1. The device, for this paper uses the Mk 2 header and bridgewire system. A comparison of the Mk 2 squib and the pyrogen jet squib is shown in Table 1. The jet squib contains no primary explosives. The bead mix and the main charge for the jet squib are essentially identical in chemical formulation. The basic difference is the finer granulation particle size of magnesium for the bead mix. Viton A is dissolved in acetone to form a lacquer, then magnesium powder is added to the lacquer to form a slurry. During development bridged headers were dipped in the slurry several times with a drying cycle between each dip. A preferrable technique is the application of the slurry to the suspended bridgewire with a small brush until 3 to 5 milligrams have been attached to the bridgewire. After drying, a good bond is achieved between the wire, the plastic header and the fluorocarbon (Viton A).

The main charge is also magnesium powder, Viton A and Teflon. The material is compounded by the "shock" or "quench" technique, which provides for a coating of Viton A on individual particles of magnesium and Teflon. The protective coating provides hydroscopic protection to the magnesium. This pyrotechnic

mixture is extruded in spaghetti form. The extruded strand is then guillotine-cut to proper length and the resulting cylindrical shaped grains are reconsolidated at 12,000 psi pressure into a finished grain shape. This finished grain is the main squib charge. The grains are then slip-fit onto the header and the cup slipped over the grain and forced onto the header and crimped in place.

Performance

The jet squib cup bottom, on initiation, bursts open from the functioning of the bridge bead combustion. Simultaneously the interior surfaces of the main charge grain are initiated and burn. The resulting flame from the main charge produce a jet shaped flame 2 to 6 inches long and persists for 1-1/2 to 2 seconds duration. This jet action appears to be more vigorous at increasingly depressed temperatures, as witnessed from comparison of the high speed motion pictures. The device performs effectively across the temperature range -300°F to +300°F. Successful tests have been performed at temperatures of -320°F to +500°F.

Using the standard squib styrofoam pocket forming test procedure, the Mk 2 squib burns a cavity in the styrofoam which holds 3-15 milli-liters water. The pyrogen jet squib produces a pocket which holds 100-140 ml. water. These tests, shown in Figure 2, picture the relative comparison of the output of the two squibs fired into a styrofoam block.

Currently, this squib is being evaluated as the ignition element for a weather modification flare containing silver iodate in pyrotechnic composition. The resulting composite is difficult to ignite by normal ignition standards. The jet squib has no difficulty in initiating the flare. The ignition element is being used to ignite a tracking flare without use of first fire mix. The jet squib has also ignited thermite-type and eutectic mixtures of metal oxidents.

Conclusions

An electric squib has been developed having the following advantageous characteristics:

1. Performs for extended periods of time (2,000 ms vs 30 millisec. for the standard squib).

2. Performs from -300°F to +300°F.

3. The device contains no primary explosives (as generally considered).

4. The device is a one-component pyrotechnic propellant system. No compatibility problems are foreseen.

5. The device utilizes the basic components of well-proven squib systems (Mk 1 and Mk 2).

6. The squib is considered to be mass producible and would cost comparable less than with the Mk 1 and Mk 2 squib. (Comparable to 25¢ each in large quantities.)

7. The single system pryotechnic system is adaptable to a variety of bridgewire systems and squib configurations. This includes exploding bridgewire techniques, since N-35 propellant has been shown to ignite to its burning phase from a detonating shock wave.

8. The pyrotechnic propellant lends itself to handling and processing as a slurry form, granular powder, pellet or grain preparation by either pressing or extrusion techniques.

9. The heat energy released from the squib is advantageous for igniting or initiating difficult-to-ignite materials.

10. The pyrotechnic propellant is relatively unaffected by moisture, since each particle of the agglomerate is Viton coated. This coating also diminishes the possibility of magnesium oxidation.

11. The Pyrogen jet squib is officially designated SQUIB, ELECTRIC, BBU-29(XCL-1)/C and qualification tests are nearing completion.

Characteristic	Mk 2 Elec. Squib			Electric Squib BBU-29(XCL-1)/C		
Physical						
Size	0.283 dia. x .425			Same		
Cup	Gilding Metal			Same		
Plug	Phenolic Resin			Same		
Bridge	.0025 dia. Plat. 80/RHOD 15, RUTH 5			Same		
Lead Wires	No. 24 Solid Copper; Celanese Cotton			Same		
Chemical						
Bridge Bead	N. Lead Styphnate, Zirc & PbO_2			Magnesium-Teflon-159 Mix		
Booster	Black Powder, 50/100 40 mg			None		
Main Charge	Black Powder, 50/100 50 mg.			Magnesium-Teflon-N-35 240 mg.		
Energy Output	718 cal/gm.			> 3000 cal/gm-Flame 4000°F		
Electrical						
Resistance	0.14 to 0.20 ohms			Same		
No-Fire	1.0 amps (28 volts)			Same		
50% Fire	2.0 amps			Same		
All-Fire	5.0 amps			Same		
Dielectric	> 50 megohms-case to lead			Same		
Firing Time	@ 3.0 amps - 11 millisec. delay			@ 3.0 amps - 5-10 millisec. delay		
Performance						
Flame Duration	20-30 Millisec.			1500-2500 Millisec.		
Temp. Range	-65°F to +165°F			-300°F to +300°F		
Flame Temp.	3880°F			4000°F		
Altitude Function	4mm Hg (115,000 ft.)			87mm Hg (70,000 ft.)		
Hydroscopicity	Black Powder Absorbs			Unaffected by Water		
Styrofoam	Pocket holds 3-15 ml water			Pocket holds 100-140 ml water		
Sensitivity	Black Powder	Lead Styphnate	$ZrPbO_2$	159 Mix		N-35 Propellant
				Wet	Dry	
Friction ZIL	Snaps	N.A.	18 lb.[1]	513 lb.	1000 lb. NF	750 lbs.
Impact (2.5k)	32 cm	17cm	NF*	NF*	30 cm	NF*
Static		2000-4000 ergs	7000-9000 ergs	2,500,000	20,000 ergs	NF*
Formulation - classified				Bead		Main Charge
Ingredients	Black Powder			Magnesium Powder Viton A		Magnesium Powder Teflon Viton A

*NF = No fire.
[1]50% Pt. with pendulum at 45°.

TABLE 1. Comparing Mk 2 and Pyrogen Jet Squib.

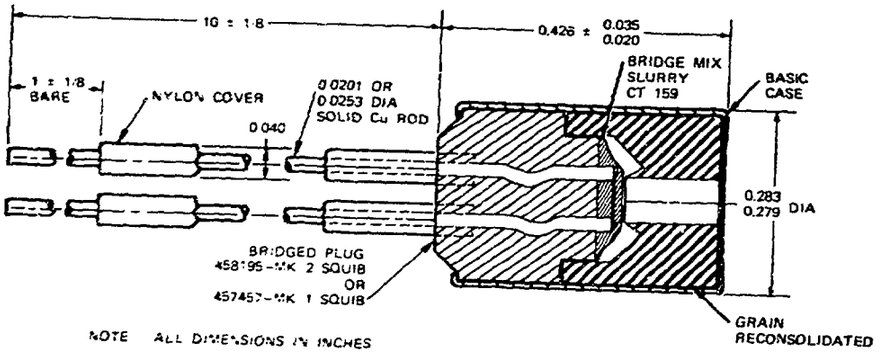

(U) Fig. 1 Pyrogen Jet Squib

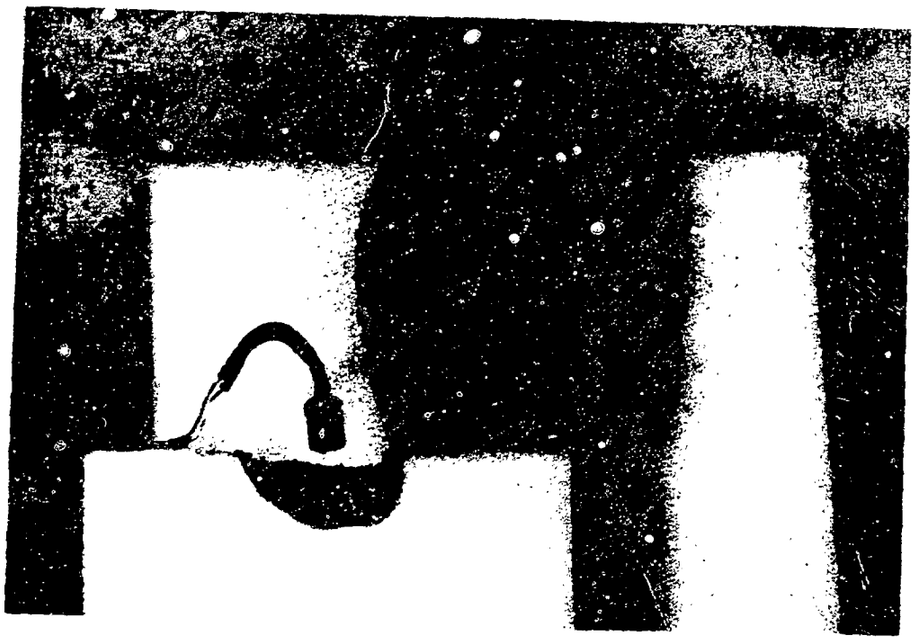

FIGURE 2. Comparing Output Performance of Mk 2 and Pyrogen Jet Squib in Styrofoam.

III-8. DEVELOPMENT OF A FULLY REDUNDANT AND HERMETICALLY SEALED CABLE CUTTER

J.P. Yribarren
European Space Research and Technology Center
Noordwijk, Holland

INTRODUCTION

This paper presents a cable cutter especially developed for space applications.

The increased sophistication of requirements for electro-explosive devices in space has led to the development of a high quality cable cutter for small cable diameter.

Its main characteristics are hermetic sealing and complete redundancy.

Development was performed by the pyrotechnical department of the Avions Marcel Dassault Company in France for the European Space Research Organisation (ESRO).

ESRO has subsequently space qualified this particular cutter.

The first use of the cutter will be on the ESRO satellite TD, which will be launched at the beginning of 1972.

Many problems arose out of the development, and the final design has led to a complex unit compared to a normal guillotine. However, the result has been quite satisfactory and one can foresee other devices based on the same technique.

1. REQUIREMENTS

1.1 Functional

This cable cutter was designed to cut stainless steel stranded cable or piano wire up to 1.6 mm (1/16 inch in diameter).
Characteristics of the nominal standard cable:

composition. 7 strands of 7 wires

ultimate load: 2200 N

Characteristics of the piano wire:

stainless steel or berylium copper

maximum permissible tension stress for the wire: 1.4×10^4 bars

The same knife should be able to cut both stranded cable and piano wire.

1.2 Sealing

In general guillotines are sealed by "O" rings but this solution is far from satisfactory for many applications.

The cleanliness on some scientific satellites is such that one must prevent any pollution from the electro-explosive devices after firing, including the gas contamination. For this reason we were led to find a compatible design with our requirements for cleanliness.

1.3 Contamination

Leaks are not the only source of contamination. Outgassing from all materials in this unit had to be reduced as much as possible. Fragments, produced when the unit functions, must be prevented.

1.4 Redundancy

The cable cutter had to be fully redundant, i.e. electrically, pyrotechnically and mechanically redundant.

The method of using two guillotines side by side, connected with two separate power sources but cutting the same cable, is not fully redundant. One of the guillotines, when it functions badly, could damp one part of the cable.

Present designs very often use two bridgewires in the same cartridge, however, in this case only electrical redundancy is achieved.

1.5 Magnetism

All materials have to be non-magnetic, if possible.

1.6 Environmental

From the start the design had to take the severe space environmental conditions into consideration, which could be encountered in a large number of missions.

Some of the main environmental conditions are presented below:

- Electrostatic discharge
- Thermal range
- Life time
- Vibration
- Shock
- Thermal shock

2. DEVELOPMENT

2.1 Initial Design

Two main considerations were at the base of the design:

a. To achieve a hermetic seal, using a cartridge sealed inside an expandible capsule. The expansion of this capsule, when pressurised, gives sufficient motion to the knife to cut the cable that is placed underneath.

b. In order to achieve full redundancy, two different capsules, one acting on the knife, the other acting on the anvil, were used. If only one capsule functions, this is sufficient to cut the cable.

In order to reduce the overall sizes of the unit, the two cylindrical capsules were placed parallel such that the expansion of two opposite sides is achieved. Knife and anvil are located between them and are shown in Figure 1.

For the capsule a suitable material had to be chosen in order to allow the expansion without cracking or shearing around the back of the knife. Nickel was adopted for its strength and high elongation co-efficient.

The thickness of the deformable part of the capsule had to be defined with the pyrotechnical charge during preliminary tests. The capsule's header was designed to withstand shockwave and high static pressure. The shock wave is absorbed using a damping system, whereas the static pressure is maintained by a glass to metal seal.

The knife had to be made of hard steel, at least harder than the material to cut ($> 1.5 \times 10^4$ bars)

The body of the cutter was optimised between its mass and its resistance to loads produced by the capsule when functioning. The body is made of an aluminium alloy, machined as shown in Fig. 2

On the electrical part a common fusehead with very well-known characteristics and a high degree of reliability was adopted. It has a single bridgewire of 1.5 Ω resistance. The fusehead functioning time versus current is plotted in Figure 3.

2.2 Preliminary tests and modifications

Preliminary tests showed that to cut a cable in this design, a very high load had to be applied on the knife during a short period. The release of such energy led to the use of a detonator charged with lead azide. The functioning process of this cutter is quite different from other common guillotines. The shock wave generated by the detonator produces a very fast deformation on the capsule. This deformation applies a high acceleration to the knife, which is transformed into kinetic energy, which in turn cuts the cable. Tests have confirmed this process because the expansion on the deformable part of the capsule after firing is smaller than the travel of the knife. Figure 4 shows a capsule before functioning and a capsule after functioning. The indentation made by the back of the knife is quite visible on the capsule after functioning.

During those tests the best results were obtained with 1 mm thick capsules charged with 200 mg of lead azide. A cable with a 1.4 mm diameter was cut in order to allow for a safety margin in nominal use. Some difficulty was experienced in making the holes in the body, in which the anvil and cutter slide. At first they were drilled through and then the outer unwanted holes plugged. However, the plug did not withstand the shock load produced by the capsule. Finally the two holes were made by using the spark erosion process with excellent results.

During tests many modifications were made on the knife. It appeared that to cut piano wire as well as stranded cable, two knives were better than one knife and an anvil.

To prevent overlapping when functioning, a special shape was given to the knives to provide stops.

Knives had to withstand the shock when functioning without the cable between them. Since the material of the knives was hard, they were brittle and very often they broke. To prevent this effect the knives were made out of bronze with a tungsten carbide edge brazed on it. They are shown in Figure 5. At this stage the capsule was working satisfactorily. Only the header had to be reinforced because of the very high pressure against it.

2.3 Improvements of the capsule

To improve magnetic cleanliness, a capsule made out of nickel was not fully satisfactory. To replace the nickel capsule a choice was made between several non magnetic alloys having similar properties: Inconel, Monel and Arcap. Finally the material Inconel was chosen, which has about the same mechanical properties as Nickel: it is also non-magnetic in a large range of temperatures.

After a large number of tests in this new configuration, defects were observed on some of the fired capsules (Fig. 6). Precise inspection of those failures showed that sometimes cracks appeared at the external surface, some of them extending through the thickness and creating a leak. One of them appears on the photomicrograph (Fig. 7). After investigation these non systematic cracks were found to be caused by impurities in the Inconel. Rapid loading and plastic deformation of the metal during the detonation caused the section containing the voids to fracture. After expansion the capsule was not filling all the room available, so the shock wave crossing the capsule wall rebounded on the external unsupported surface. The surface defects can be explained by the high stresses thus produced.

High purity alloys are not easy to obtain on the market so we came back to pure nickel. Not only the expanding end of the capsule is made out of nickel and brazed into a stainless steel collar to form the threaded fastening. The other modification was to reduce the size of the free space in the body.

3. QUALIFICATIONS

3.1 Aim

Qualification specifications were established to be compatible with some satellites in process of design. These conditions were less severe than the development tests conducted by AMD. After the large number of firings done during development, the reliability of the device was proven and only 30 units were used for qualification program. Bruceton tests had been done beforehand on the detonator.

3.2 Preliminary tests

- Visual, dimensional and mass inspection
- Radiographic inspection
- Magnetic inspection
- Bridgewire resistance test
- Insulation resistance test. It must be greater than 50 MΩ at 500 V
- Static discharge sensitivity. From a 500 pf capacitor charged to 7500 V.

3.3 Environmental tests

- Temperature humidity test. 95% humidity at 50°C during 203 hours.
- Sinusoidal vibration. 5 mm from 10-75 Hz (peak to peak) 60 g from 75-600 Hz.
- Random vibration. 0.5 g^2/Hz between 50 and 300 Hz.
  0.155 g^2/Hz between 300 and 2000 Hz.
- Shock test. 100 g during 5 ms. ½ sine wave.
- Acceleration test. 60 g during 1 minute.
- Thermal shock test. 10 cycles as following:
  -60°C for 6 hours. +50°C for 6 hours.
- Thermal vacuum. 10^{-8}Torr in the following conditions:
  -60°C for 48 hours and +50°C for 48 hours.

3.4 Functional test

Nominal functioning tests were done with both capsules ignited by a 1 amp. current. The cable being cut is 1.6 mm in diameter. Marginal functioning tests were done with one capsule ignited and a cable of 1.8 mm diameter.

All firings were done under 10^{-6}Torr at a temperature of -60°C or +50°C.

Leak detection was done by pressure measurement and by mass spectrometer analysis. At each test burn-out time and functioning time were recorded. These times are simultaneous. Between 1.5 and 2 ms at +50°C and between 2.5 and 3 ms at -60°C. At the end of the program all units were successfully fired without any misfire.

Figure 9 shows a record of time measurement at +50°C. The upper trace gives burn-out time of the bridgewire and the lower trace shows the time for the cable to be cut.

4. NEW DEVELOPMENTS

An improvement of this cable cutter is actually in process of design. It is the replacement of the fuzehead by a "1 Amp, 1 Watt, No Fire" matchhead. This match head has been designed by Avions Marcel Dassault Co. and a predevelopment program showed that the design is sound. Actually this match head is able to withstand 1 amp during 5 minutes in the temperature range

-195°C to +120°C. Its functioning time versus current is plotted in Figure 10.

The match head is not affected by the repetition of a great number of 1 amp pulses.

A special arrangement of the design is provided to withstand, between pin and body, electrostatic discharges from a 500 pF capacitor charged at 25,000 V. One can expect that the modification of the fuzehead by the new match head should not cause many problems, so in a short time this versatile cable cutter will be achieved.

Another small modification is to replace the flying wires' output by a standard Bendix type plug. But now a new field of investigation is open to determine what the possibilities are of this functioning process.

The use of an explosive in a sealed configuration can be the principle of small space devices able to deliver a high power in a short time.

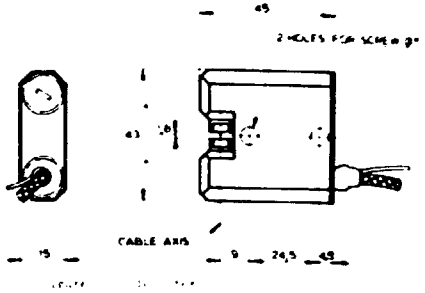

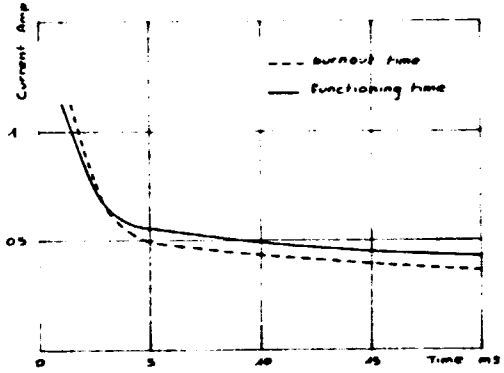

Figure 3 Firing current vs functioning time

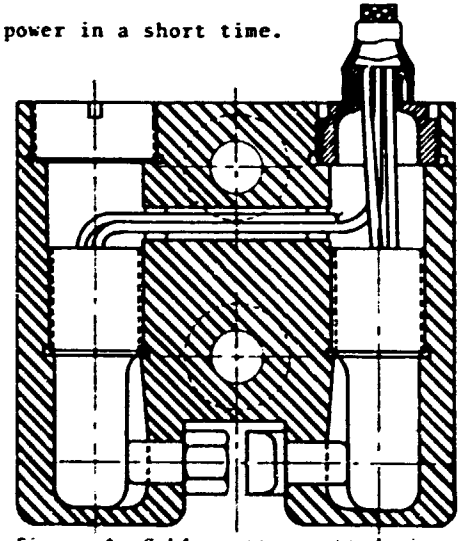

Figure 1 Cable cutter cutted view

Figure 9 Functioning time measurement. 1 ms/division.

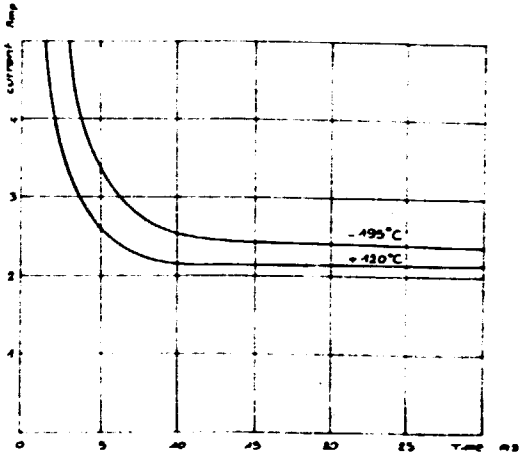

Figure 10 Firing current vs functioning time

Figure 5 Knives

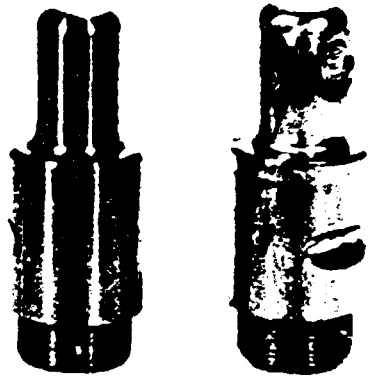

Figure 4 Capsules before and after firing

Figure 6 Crack on a capsule

Figure 7 Photomicrograph of a crack

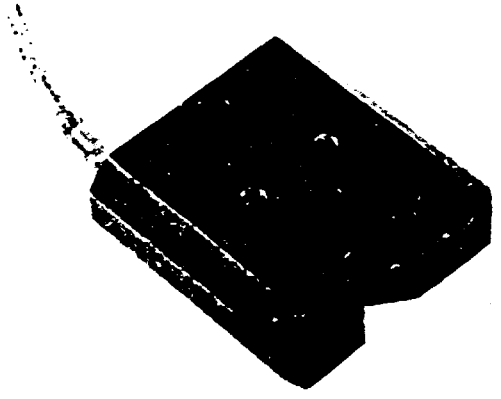

Figure 8 Final design of the cable cutter

III-A. PRECISION 20 MICROSECOND DELAY DEVICE

By R. K. Weinmaster, Sandia Laboratories
and F. D. DiNebile, Unidynamics/Phoenix, Inc.

ABSTRACT

A delay device was required which would accomplish a high voltage electrical switch closure at 20 ± ½ microseconds after the input of an EBW firing pulse. A device was designed, built, and tested utilizing an EBW detonator, an MDF delay element, and an explosively actuated solid dielectric switch. A timing accuracy of 20 ± ½ microseconds was achieved over the extreme temperature range. All detonation products were contained.

INTRODUCTION

A delay device was required which would accomplish a 5.5 kilovolt electrical switch closure at 20 ± ½ microseconds after initiation. An additional requirement was that all detonation products and shrapnel must be completely contained. The approach taken was to design around the known technology of MDF delay elements and solid dielectric switches to meet the timing accuracy and electrical requirements.

DESIGN CONSIDERATIONS

The overall design concept is illustrated in Figure 1. The delay device consists of an electrical detonator, an MDF delay element, a booster, a track plate containing an explosive to provide switching energy, a switch, and a body to contain shrapnel and other products of explosion.

Detonator. An EBW detonator was used in this application to achieve the required controlled precision in initiation timing. An EBW Detonator was selected on the basis of its demonstrated capability of initiating the MDF delay element and its radial output characteristics.

Delay Element. Precision timing was, of course, the paramount technical consideration in the selection of a delay element, along with the practical requirement of availability. The material settled on for this design is aluminum sheathed HNAB MDF, loaded to a density of two grains per foot, which has well documented precision timing characteristics. Before it is incorporated in the delay unit, this MDF is isostatically pressed in an oil bath at 60,000 pounds per square inch to yield a highly uniform core density and precise detonation velocity.

In application, two parallel MDF elements are provided to further reduce timing variations and increase reliability of function. These elements are approximately eight feet long and are wound into close fitting helical grooves in a mandrel two inches in diameter. A one-eighth inch spacing between the MDF strands is adequate to prevent cross-talk.

Booster. Two booster charges of pressed PETN, measuring 0.070 inch in diameter by 0.150 inch long, transfer detonation from the MDF to the track plate.

This work was supported by the United States Atomic Energy Commission.

Track Plate. The function of the track plate, illustrated in Figure 2, is to provide explosive transfer of energy to the switch and electrical isolation between the switch plate and ground. The plate is fabricated from Lexan, and contains an extruded plastic explosive (silicone bonded PETN).

Switch. A solid dielectric switch, as shown in Figure 3, is used in this design. It consists of a G-10 grade fiberglass-reinforced body containing an 0.032 inch thick aluminum electrode disk, an 0.003 inch thick Mylar dielectric disk, and two No. 0-80 stainless steel socket head cap screw contacts connected in parallel. Silicone sealant is used to prevent electrical breakdown around the dielectric disk.

Switching occurs when the explosive in the track plate drives the aluminum electrode disk against the cap screw heads and shears the Mylar around the edges of the screw heads and socket. Oscillographs of the electrical discharge through the switch, Figure 4, show no evidence of contact chatter or bounce during the seven microseconds of capacitor discharge or the following interval of circuit ringing, approximately 20 microseconds in duration.

Containment. The structural materials comprising the body of the delay unit are 6061-T6 aluminum alloy and G-10 grade fiberglass reinforced epoxy. Vinyl tape is wrapped around the mandrel to absorb the detonation shock of the MDF. All tested units of the final design configuration completely contained detonation products and produced no shrapnel.

TEST EVALUATION

Three lots of timers have been fabricated for development testing. Two of these lots have been tested to date.

The first lot was manufactured to yield a nominal delay time of 315 microseconds. As shown by the test data presented in Figure 5, these units exhibited very satisfactory timing and switching characteristics. However, they failed to contain the detonation adequately. As indicated in Figure 5 three of the units were tested at a separate test site with different instrumentation and personnel.

Two switch subassemblies were electrically tested separately from the timer assemblies. These switches were subjected to 10,000 applications of 5.5 kilovolts of one minute duration with an off time of 30 seconds. No evidence of deterioration was detected.

The second lot, fabricated to produce a nominal time delay of 284 microseconds, was strengthened to meet the containment requirement. These units met all design requirements. Test data is shown in Figure 6.

The third lot was essentially like the second except that the time delay was changed to the final 295 $\pm$ 5 microsecond value. At this time these units are awaiting tests in next assembly hardware.

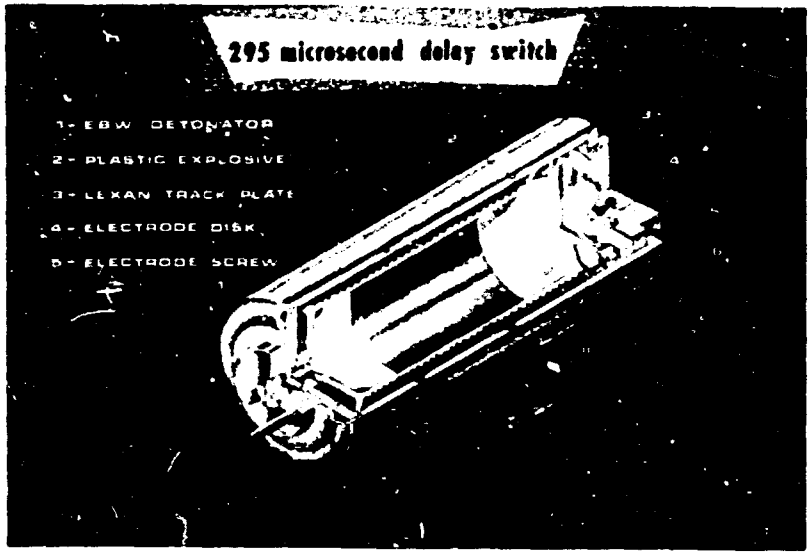

FIGURE 1

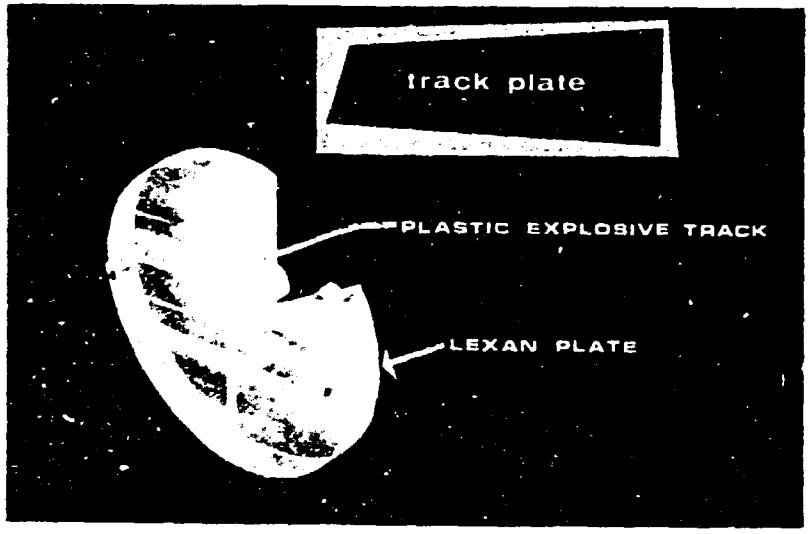

FIGURE 2

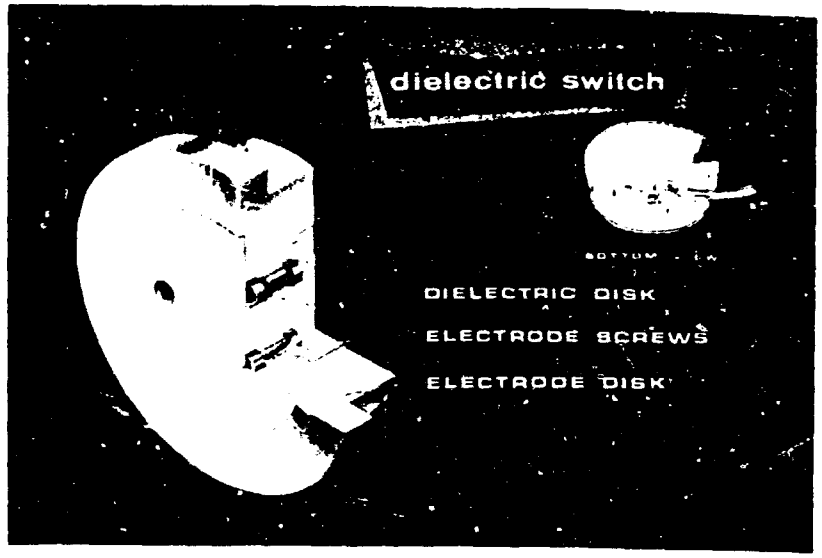

FIGURE 3

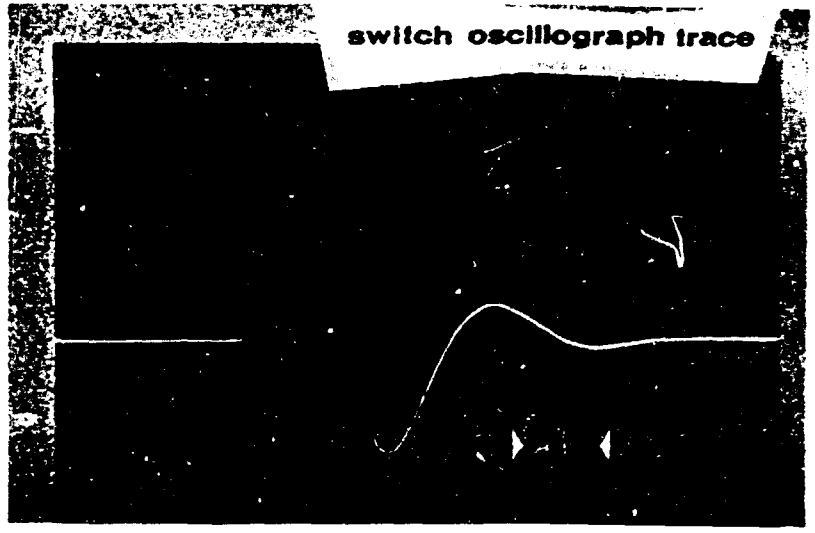

FIGURE 4

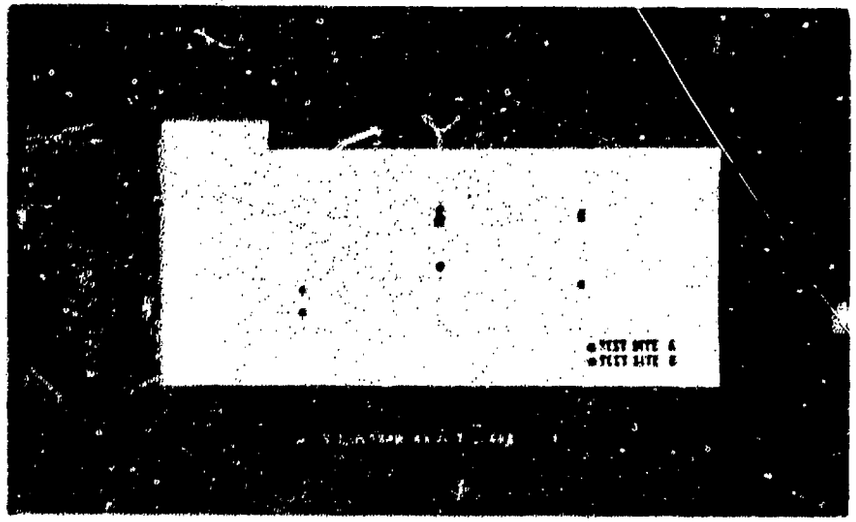

FIGURE 5

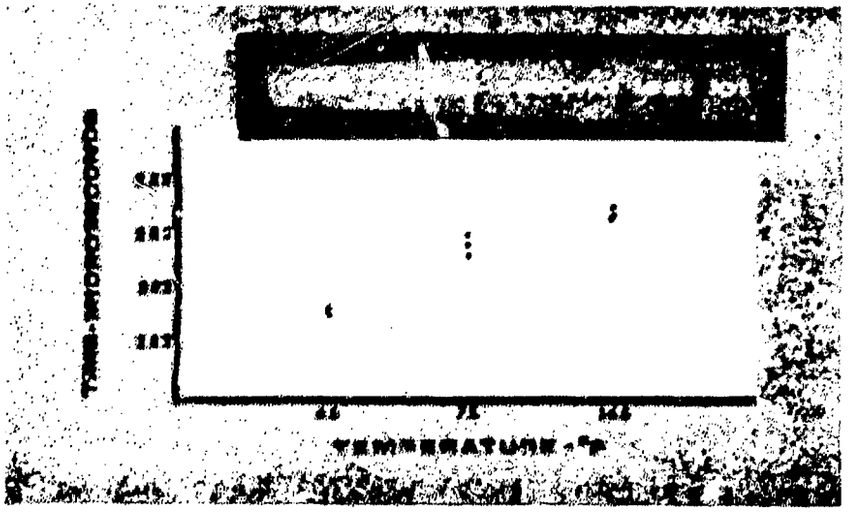

FIGURE 6

III-10. SMALL CALIBER TRACER AMMUNITION - A SURVEY PAPER

THOMAS A. DORIS, JR.
GERALD B. FRANKLIN

FRANKFORD ARSENAL

In this survey paper we are going to discuss some of the recent work done on small caliber tracer ammunition. The topics will be limited to the 7.62mm or cal. .30 and smaller sizes of projectiles, and to several novel approaches of charging small diameter projectiles.

One of the newer developments to see combat use is the XM-276 Dim Trace round. This is a round that is compatible with night vision devices which operate in both the visible and infra-red portions of the spectrum. The light output is so low that it is invisible to the naked eye, subsequently aiding in night covert activity. The pyrotechnic formulation used in this round is composed of calcium resinate, barium and strontium peroxides, and magnesium carbonate[1].

Another development increased the visible range of 7.62mm tracer projectiles from approximately 850 meters to 1500 meters. Intended for helicopter use, this increased visible range was accomplished by not only increasing the length of the tracer cavity in the projectile but by adding parlon to the standard NATO tracer mixture which consists of magnesium, strontium nitrate, and polyvinyl chloride. The tracer round was used in combination with M118 match ball ammunition where good trajectory match was obtained[2].

There is a general trend toward employing smaller caliber ammunition because the weight reduction would give the infantryman the ability to carry a greater supply of ammunition resulting in increased firepower. The 5.56mm round is the smallest ammunition that has been standardized for Army use and it uses the same tracer mixture as the 7.62mm tracer. A major problem encountered in the development of the tracer round was maintaining integrity of the bullet jacket upon firing. At high ambient temperatures, the jacket would split, producing erratic flight and failure to trace. Adoption of a gilding metal clad steel jacket overcame this problem.

Caliber .17 tracer projectiles are still under investigation. The feasibility of providing a tracer display was demonstrated in 1967.[3] It was found that, as with the 5.56mm tracer, the bullet jacket had to be thick enough to withstand the high spin rates imparted to the projectile by the barrel of the gun. For example, with 0.014 inch thick jackets, erratic flight and tracer characteristics were observed. However, with the thickness increased to 0.017 inch, these malfunctions were eliminated. The pyrotechnic formulation used in this round is again similar to the previously mentioned 7.62mm and 5.56mm tracers.

We shall now discuss tracer projectiles having cavities of .060 inch and .090 inch diameters. These dart-like finned projectiles are similar in geometry. The XM-216 (Figure 1) is the smaller of the two and has a tracer cavity of .060 inch in diameter with a depth of 5/8 inch. The requirement for the tracer is that it be visible, in daylight, for 500 meters. Development of the

[1] T.A. Doris, Jr., and P.B. Taylor, "Development of Cartridge, 7.62mm, Dim Tracer - XM-276", Frankford Arsenal Report R-1988, December 1970.

[2] F. W. Dietsch, "7.62mm Extended Range Ammunition for Helicopters", Fort Rucker Briefing - unpublished.

[3] A. F. Schlack, J. J. Lucianetti, "Feasibility of Providing Tracer Display with the use of a Microcaliber (Cal. .17) Projectile", Frankford Arsenal MR Report M68-22-1.

tracer mixture for these projectiles was described in an Ordnance magazine article entitled Smaller, Faster, Brighter.[4] It is composed of 69% zirconium (23μ particle size), 30% potassium perchlorate, and 1% vinyl alcohol acetate resin (VAAR). The binder is added to the fuel and oxidizer in a solution of ethyl acetate, which upon evaporation leaves all the particles of mixture coated with VAAR, providing for integrity of the column during the high G-forces of launch. The same pyrotechnic mixture is used in both projectiles with the firing tests showing the larger projectile having more reliable tracer functioning.

Charging of such a high ratio length to diameter cavity would normally be done in a series of increments which is a time consuming process that does not lend itself to high volume production. This charging problem was overcome by the development of visacore.[5,6] Pyrotechnic mixture is placed in a lead tube which is then extruded to the desired diameter. The final wall thickness of the lead sheath is approximately 0.004 + 0.001 inch. Charging of the projectile is accomplished by inserting the visacore into the tracer cavity and cutting off the excess. The column is then consolidated at 110,000 psi. The small amount of compaction is then compensated for by the addition of powdered tracer mixture which acts as the igniter. Dimensions of the consolidating punch have been found to be critical. To effect reliable ignition, the punch must have an .035 inch diameter protrusion. Performance increased from 60% using a flat faced punch to over 90% with the step punch[7].

The next figure (Figure 2) presents the same projectile in another candidate cartridge case (XM-645). In this case, the primer action plays a part in automatic gun cycling. On initiation, it is blown back, retracting the firing pin to the sear position, while the gas-operated extraction and chambering steps occur. It can readily be seen that the distance between the primer and the tracer igniter is approximately 5/8 inch. Firing tests have shown that the intervening propellant grains interfered with the output of the primer with a resulting decrease in ignition reliability. For example, in the XM-216 case, where this distance is 1/8 inch, the reliability was 90%. The same tracer projectile, when charged into the XM-645 case, had a trace reliability of about 50%.

To investigate a means of obtaining a more reliable ignition level, a booster igniter was designed (Figure 3). This device couples the energy from the primer to the tracer igniter by means of a short length of lead azide in an extruded lead sheath (azacore). This booster consists of 2 grains of lead azide per foot. To position this length of azacore, it is inserted in a piece of molded propellant. Levels of performance using this igniter approach are 90 - 95% ignition with a trace range in excess of 500 meters. Although providing excellent tracer ignition, this igniter device does not lend itself to mass production and has deleterious effects on the internal ballistics.

Another approach for providing a trace to the projectile has been to cement pyrotechnic mixture on the base and between the fins of the projectile.

---

[4] W. W. Cavell, W. E. Perkins, and J. J. Caven, Smaller, Faster, Brighter, Ordnance, July-August 1967.

[5] U.S. Patent No. 3,401,630, Clad Pyrotechnics, T. Q. Ciccone et al, 17 September 1968.

[6] Contract No. AMC-2412, Development and Manufacture of Visacore, Ensign-Bickford Company.

[7] W. E. Perkins, T. A. Doris, Jr., Development of Tracer for SPIW System, XM-216 Cartridge, Frankford Arsenal Report - being published.

This method basically uses the same pyrotechnic formulation of zirconium and potassium perchlorate, with the addition of lead dioxide to aid combustion in the presence of the cement, which is 17% of the total composition. Reliable ignition has been obtained with this design, although daylight trace visibility has been marginal. At present, a combination of the two techniques offers promise of providing good ignition characteristics and high tracer visibility in the projectile with the .060 inch tracer cavity.

Charging techniques of standard tracer projectiles such as 5.56mm and larger, have remained unchanged for years. The procedure is to volumetrically place powder into the tracer cavity and consolidate it. With high speed production machinery, this method is not satisfactory. A current approach in charging tracer projectiles is to preform pellets immediately prior to insertion into the tracer cavity. In this way, handling difficulties are substantially reduced, thus minimizing breakage and dusting of the pellet. The visacore technique of charging was also considered for 5.56mm ammunition, but several problems were encountered. The wall thickness of the metal sheath was excessive, giving rise to short burn time. Furthermore, one result of the low length to diameter ratio of the pyrotechnic column was poor mechanical strength, with dusting and breakup of the composition occurring.

Several new concepts involving novel pyrotechnic materials that may have application to tracer ammunition will now be discussed.

Hypergolics

Aluminum alkyls are an interesting family of compounds due to their pyrophoric nature. Although they have been used in various flame weapons, very little work has been conducted on their application to small arms tracer ammunition. By combining the aluminum alkyl with a metal and an inorganic oxidizer, it can be seen (Figure 4) that mixtures can be formulated which have appreciable light output. Applications to other types of ammunition are also possible with these compounds. In conjunction with various complexing agents, aluminum alkyl compounds have potential merit for application in spotter ammunition and infrared radiation emittence for use with night vision devices.

It was proposed that triethylaluminum (TEA) and trimethylaluminum (TMA) be used to alleviate ignition problems, enhance flame characteristics, and to serve as potential tracer materials themselves. Initial work consisted of conducting compatibility tests between these materials and twenty-four inorganic oxidizers (Table 1) under nitrogen atmosphere. Those systems deemed compatible were then exposed to air in a laboratory test to observe their burning characteristics (Table 2). The best of these were then augmented with a metal or metal hydride in order to increase their brightness (Table 3). When compared to the standard NATO tracer mixture, ideally, a tracer formulation should have a short ignition delay, fast burning rate, and considerable flaring. On this basis, the $NaClO_3$-Mg-TEA system was superior in the static test, with the rest being inferior. All of the combinations tested gave a yellow colored light. In an attempt to obtain a red flame, three systems were prepared which contained strontium as an oxidizing agent. Two of the three formulation - [SrO_2 / Mg / TEA] and [$Sr(NO_3)_2$ / Mg / TEA] - did not self-ignite when exposed to atmospheric oxygen, but did yield a bright red flare-like fire when ignited by a match. The third spontaneously ignited to yield a fast burning, bright red, flare-like fire.

Due to the great reactivity of these organo-metallic compounds with air and moisture, it is mandatory that the tracer cavity be well sealed to prevent chemical reactions from occurring. Presently, work is being conducted to design various closure systems for the 5.56mm tracer projectile in order to evaluat

these mixtures as to light output under conditions of actual firings. The following sketch shows an insert which is placed into the 5.56mm jacket and crimped.

5.56MM JACKET WITH INSERT

Adequate sealant materials are presently being investigated. Further work is being conducted on a second generation of formulations having improved flame and ignition characteristics. In addition to magnesium, zirconium metal powder is also being tested in combination with the aluminum alkyls.

Intermetallic Reactions

When certain combinations of powdered metals and/or metal-like elements are intimately mixed, they yield, on ignition, sufficient energy to melt or vaporize the mixture, leading to a highly luminous source[8].

These intermetallic combinations undergo condensed phase reactions, whereas standard pyrotechnic compositions undergo gas phase reactions. The reaction rate of these combinations can be varied to some extent by controlling the particle size and thermal conductivities of the constituents. Their use as a tracer composition appears to have several possible advantages such as the ability to ignite from the propellant flame, and absence of oxidizers which could lead to improved reliability and long term stability.

Future Goals

Future tracer composition work will be aimed at developing new mixtures and modifying standard mixtures with additives to provide burning rate controls, combined with desired spectral emittence and luminosity as required by users in the field.

Novel compositions will include intermetallics (binary and tertiary); single or binary component compositions to reduce processing complexities; and compositions having dim, infra-red, ultraviolet or narrow frequency, visible light outputs for compatibility with new generation night-vision devices.

Novel tracer ammunition designs could incorporate other than chemical effects such as thermo- or chemiluminescece displays; "blinking" trace performance; extrudable compositions having metal sheathed or castable forms; vents and dispersion ports for optimizing afterburning to enhance tracer display.

Human Engineering studies will (a) relate target/lethality aspects to tracer ammunition frequency; (b) study the relative roles of physiology and psycology (from the standpoint of both the gunner and the enemy) in the overall effectiveness of tracer ammunition; and (c) match, correlate, and contrast current electro-optical instrumentation with the human eye.

TABLE 1

Compatibility of Triethylaluminum with Inorganic Oxidizers*

Compatible	Not Compatible
$NaNO_3$, $NaClO_3$, $NaIO_3$	KIO_4, $FeCl_3$, $KClO_3$
$NaCrO_4$, Na_2O_2, NaF, KNO	$KBrO_3$, NH_4ClO_4
K_2CrO_4, $K_2Cr_2O_7$, $KMnO_4$, SrO_2	Bi_2O_5
$Sr(NO_3)_2$, $Sr(ClO_4)_2$, BaO_2, $Ba(NO_3)_2$	
CuO, MnO_2, B_2O_3	

* Under nitrogen atmosphere

[8] A. P. Hardt, Study of Tracer Munitions Using Intermetallic Reactions, Lockheed Missile and Space Company, Technical Proposal - D081722, 15 March 1971.

TABLE 2*

Burning Characteristics of Systems Containing TEA and an Oxidizing Agent

Agents	Ignition Delay	Burning Rate	Flaring
$NaNO_3$	average	average	none
$NaClO_3$	short	fast	a lot
$NaIO_3$	short	fast	none
Na_2CrO_4	long	average	none
Na_2O_2	short	fast	a lot
NaF	did not ignite	-------	-----
KNO_3	did not ignite	-------	-----
K_2CrO_4	long	average	none
$K_2Cr_2O_7$	short	fast	some
$KMnO_4$	long	fast	some
SrO_2	long	average	some
$Sr(NO_3)_2$	average	average	none
BaO_2	short	short	some
$Ba(NO_3)_2$	did not ignite	-------	----
CuO	short	fast	none
MnO_2	short	fast	none
B_2N_3	short	average	none

* The terms used are qualitative and are used in comparison to the standard NATO tracer mixture.

TABLE 3*

Burning Characteristics of Systems Containing TEA, an Oxidizing Agent, and Metal or Metal Hydride

Agents	Ignition Delay	Burning Rate	Flaring
$NaClO_3$-ZrH_2	long	fast	bright
$NaClO_3$-Al	long	fast	bright
$NaClO_3$-Al	short	very fast	very bright
$NaClO_3$-B	short	fast	bright
$NaClO_3$-$LiAlH_4$	average	fast	bright
Na_2O_2-ZrH_2	average	fast	bright
Na_2O_2-Al	average	fast	bright
Na_2O_2-Mg	average	fast	bright
Na_2O_2-B	average	fast	bright
Na_2O-$LiAlH_4$	average	slow	fair

* The terms used are qualitative and are used in comparison to the standard NATO tracer mixture.

FIGURE 1. [illegible]

FIGURE 3. IGNITION BOOSTER

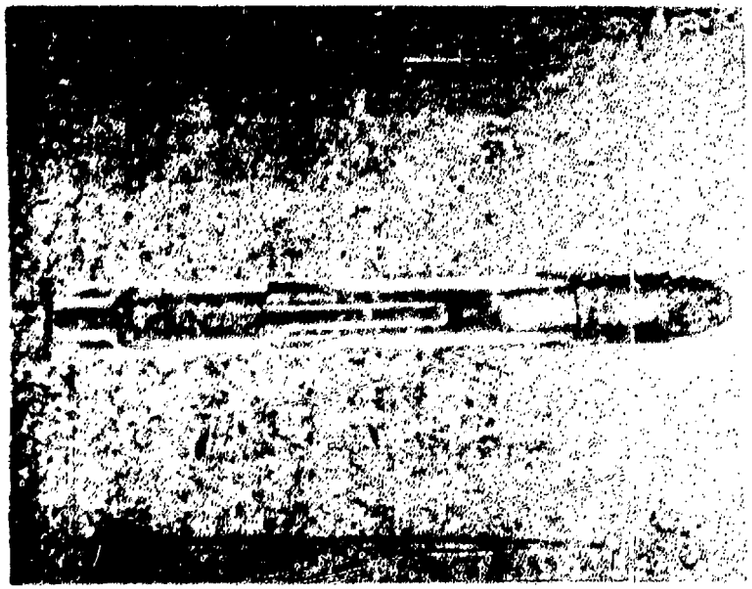

FIGURE 2. [illegible]

FIGURE 4. BURNING CHARACTERISTICS OF HYPERGOLIC MIXTURE $Sr(ClO_4)_2$/Mg/TEA

III-11. POTASSIUM CHLORATE/RED PHOSPHORUS MIXTURES[1]

Ronald R. Rollins
Professor of Mining Engineering
Rock Mechanics and Explosives Research Center
University of Missouri-Rolla
Rolla, Missouri

INTRODUCTION

The major portion of this research was performed on a standard mix consisting of $KClO_3/P_4$/Quso/MgO/inert, in the ratio of 34/14/4/2/46 and modifications of this mix including silica gel, pyrex glass, aluminum, magnesium, and Cab-o-sil. Potential users of these mixtures are interested in the variables affecting the stability and tendency to spontaneously explode, in order to make use of these highly reactive materials safely.

Values as low as 0.0014 joules of impact energy have initiated explosive reactions in test specimens. Under normal conditions, a human being can generate an electrostatic charge of 0.015 joules on his body, which exceeds that required for initiation by a factor of 10. The standard mix, in a dry state, must always be handled carefully because of its extreme sensitivity. For experimental purposes, quantities were limited to 1 gram in any one container and to a total of 5 grams for any one batch.

[1]Research performed on Contract No. DAAA-21-67-C-0682 for Picatinny Arsenal, Dover, New Jersey 07801. The assistance of George B. Clark, Director of the Center, and the following students who worked on the project is acknowledged; S. Beard, V. Crane, C. Delong, W. Hall, J. Meuser, J. Rue, L. Schoeneck, and F. Taylor.

SPECTROPHOTOMETRY

A Beckmann IR 12 Spectrophotometer and a Beckman Microspec were employed to examine the standard mix, its components and the effects of various environmental conditions upon the presence and formation of reactive intermediates, reaction products, and the possible mechanisms involved. Reactive intermediates are undesirable since they cause conditions of instability leading to spontaneous initiation. Localized regions of such substances can be as small as 10^{-3} to 10^{-5} centimeters in diameter.

The heats of formation of the molecules of interest in this study (Table I) were used to calculate heats of reaction of chemical reactions involved in the decomposition kinetics of the standard mix (Table II).

TABLE I

Heats of formation of selected molecules (1)

Molecule	ΔH_f(kcal/mole)
P(red)	- 4.4
ClO_2	24.7
Cl_2O_7	63.4
HPO_3	-234.9
H_3PO_4	-306.2
H_3PO_3	-232.2
H_3PO_2	-145.5
P_4O_6	-526.0
P_4O_{10}	-709.4
PH_3	2.21
$KClO_3$	- 93.5
$KClO_4$	-103.6
KH_2PO_4	-372.05
KH_2PO_2	-211.35
$HClO_3$	- 23.50
$HClO_4$	- 31.41
HCl	- 40.02
H_2O	- 68.32
KCl	-104.18

The negative sign indicates an exothermic reaction

TABLE II

Calculated heats of reaction

Reaction	ΔH(kcal/mole)
1. $P_4 + 3O_2 \longrightarrow P_4O_6$	-521.6
2. $P_4O_6 + 6H_2O \longrightarrow 4H_3PO_3$	7.12
3. $4H_3PO_3 + H_2O + \text{heat} \longrightarrow 3H_3PO_4 + PH_3 + H_2O$	12.41
4. $2H_3PO_4 + 3KClO_3 \longrightarrow KClO_4 + 2KH_2PO_4 + 2ClO_2 + H_2O$	26.28
5. $2ClO_2 + UV \longrightarrow Cl_2 + 2O_2$	- 49.4
6. $P_4O_6 + 2O_2 \longrightarrow P_4O_{10}$	-183.4
7. $P_4 + 5O_2 \longrightarrow P_4O_{10}$	-705.0
8. $H_3PO_4 + KClO_3 \longrightarrow HClO_3 + KH_2PO_4$	4.15
9. $4HClO_3 \longrightarrow 3HClO_4 + HCl$	- 40.25
10. $4HClO_4 + P_4O_{10} \longrightarrow 2Cl_2O_7 + 4HPO_3$	22.24
11. $HPO_3 + H_2O \longrightarrow H_3PO_4$	- 2.98
12. $P_4O_{10} + 6H_2O \longrightarrow 4H_3PO_4$	-105.48

Chlorine peroxide (ClO_2) is highly explosive and light sensitive. Chloric acid ($HClO_3$) is highly reactive and unstable and chlorine heptoxide (Cl_2O_7) is also highly explosive.

The large negative values of the oxides indicates the importance of these reactions in chemical initiation mechanisms.

The transient theory of thermal self-ignition includes functions characterizing the reaction rate, the spatial distribution of temperature in the reaction volume, and the change in concentration of a reacting substance throughout the reaction time. In the system under investigation the exothermic chemical reactions that lead to a spontaneous initiation are those having a negative ΔH and a reaction rate rapid enough to liberate heat in a sufficiently large volume to initiate a deflagration process. Heat is lost in warming the reacting mass, by conduction, and by convection to the surroundings. The low heat conductivity of this system is conducive to the buildup of localized temperatures. Better heat dissipation and inhibition of the exothermic reactions decrease the probability of self-ignition. However, once a reaction has begun it accelerates, being autocatalytic. The presence of any reactive products is important since it indicates the others are or were present.

Single components (Table I) and various mixtures of them were prepared and examined in an as-received condition, and after being subjected to various treatments, i.e., alcohol wash, exposure to moisture, heated, ultra violet irradiation, and combinations of these.

The UV irradiated samples appeared to be the most sensitive since several exploded even with careful handling. Wide absorption bands were observed in these specimens at 1000 cm^{-1}, corresponding to the H_3PO_4 spectrum. The spectra from treated specimens also indicated trace amounts of P_2O_5, $KClO_4$, KH_2PO_4 and ClO_2. Water treated samples containing P_4 and $KClO_3$ showed the presence of H_3PO_2 and H_3PO_4. Little or no product formation was observed when the P_4 or the $KClO_3$ were treated separately, supporting the hypothesis that the formation of the reactive intermediates is at least a two-step process. The first step involves the formation of acid, as follows:

$$P_4(\text{red}) + 6H_2O \xrightarrow{\text{air}} PH_3(g) + 3H_3PO_2$$

$$P_4(\text{red}) + 3O_2 \longrightarrow P_4O_6 \xrightarrow{H_2O} 4H_3PO_3$$

$$4H_3PO_3 \xrightarrow[\text{heat}]{H_2O} 3H_3PO_4 + PH_3(g)$$

The acid then reacts with the oxidizer:

$$2H_3PO_2 + 3KClO_3 \longrightarrow 2ClO_2 + KCl + 2KH_2PO_4 + H_2O$$

$$2H_3PO_4 + 3KClO_3 \longrightarrow 2ClO_2 + KClO_4 + 2KH_2PO_4 + H_2O$$

Chlorine peroxide (ClO_2) in concentrated form is unstable and provides one mechanism for spontaneous initiation by its exothermic decomposition.

$$2ClO_2 \xrightarrow{UV} Cl_2 + 2O_2 \qquad -49.4 \text{ kcal/mole}$$

Silica gel, ZnO or MgO inhibit the formation and accumulation of undesirable reactive intermediates. Silica gel removes the H_2O, while ZnO or MgO neutralizes the acid.

$$3\,MgO + 2H_3PO_4 \longrightarrow Mg_3(PO_4)_2 \cdot 3H_2O$$

The specimens treated to produce observable quantities of phosphoric acid were too sensitive to handle and exploded during preparation. Some spontaneous initiations were observed after 6 to 8 days in the $P_4 + KClO_3 + H_2O$ treated systems. Samples of P_4 exposed to various humidity and temperature conditions were analyzed, and showed trace amounts of acid but no noticeable effects due to the presence of acid. This is a good indication of the lack of reactivity of stabilized red phosphorus.

Little or no product formation was observed in separately treated reactants. The presence of $KClO_3$ appears to enhance or catalyze the oxidation of P_4. Traces of ClO_2, KH_2PO_4, and $KClO_4$ were observed in the spectra of $P_4 + KClO_3$ samples. The postulated mechanism is as follows:

$$P_4(red) + 6H_2O \xrightarrow{air} PH_3(g) + 3H_3PO_2 \qquad -3.77 \text{ kcal/mole}$$

$$2H_3PO_2 + 3KClO_3 \longrightarrow 2ClO_2 + KCl + 2KH_2PO_4 + H_2O \qquad -296.7 \text{ kcal/mole}$$

Based on the experimental evidence this two-step process is presented as a sensitizing mechanism accounting for spontaneous activity of the mixture. The first reaction can be controlled by elimination of water and air, and can be monitored by detecting the evolution of PH_3 gas.

ELECTROSTATIC DISCHARGE

An electrostatic discharge sensitivity test was used to determine the 50/50 point energy level of intiation of the standard mix and as a sensitive test to determine small variations in the 50/50 point for modified specimens. The parameters investigated were: 1.) type of confinement, 2.) effect of series resistance on the 50/50 point, 3.) effect of humidity, 4.) gap length, 5.) density, 6.) electrode conditions, and 7.) effect of residual voltage on energy dissipated.

Confinement method 4 (Fig. 1) gave reproducible results and was used in most of the testing. Results from methods 1 and 2 were erratic and not reproducible. Method 3 approached method 4 in reproducibility but the loading density could not be controlled.

A number of experiments were made to determine the effect of varing the series resistance upon the 50/50 point (Test No. 13, 14, 15, 18, 19, 20 and 21) (Table III). The resistance values vary from 10 to 10^7 ohms in powers of 10 (Table IV). The relationship between the 50/50 point capacitance and energy versus the series resistance (Fig. 2) indicates that between 10 and 10^5 ohms the energy is essentially linear and slowly increasing. Above 10^5 ohms it increases rapidly and approaches a limiting value at 10^7 ohms, beyond which the discharge energy would be insufficient to initiate a reaction in the materia

TABLE IV
Capacitance and 50/50 point energy vs. resistance

Capacitance (pf)	50/50 point energy (joules)	Series Resistance (ohms)
353	0.0100	10
428	0.0120	10^2
433	0.0122	10^3
512	0.0144	10^4
565	0.0159	10^5
750	0.0211	10^6
2550	0.0717	10^7

As the series resistance was increased the time duration of the spark was increased and for a constant capacitance the average energy per unit time was decreased. Also, more energy was dissipated in the resistor. Consequently, a larger value of capacitance was needed for a larger resistor. The addition of a series resistance changed the oscillatory discharge to an unidirectional one, while with zero value the discharge was oscillatory from initiation to completion. Upon the addition of 10 to 100 ohms the discharge became unidirectional for the last 80% of the discharge. The addition of more resistance, from 10^2 to 10^6 ohms, affected the 50/50 point energy but did not change the voltage and length of the discharge. When the series resistance was increased to 10^7 ohms the discharge became discontinuous.

The temperature range was varied from 68 to 77°F and no effect on the 50/50 point was observed within this small range. Relative humidity variations from 23 to 50% had no noticeable effect on the test results. Values above 50% gave questionable or meaningless results.

Electrical properties of the electrode gap containing the sample were varied with all other parameters in the series circuit held constant. To minimize changes in the discharge due to variable properties of the gap, the gap length was minimized to 0.025 inches and held constant. This value was large enough to prevent a contact spark (greater than 0.005 inches) and small enough that the breakdown voltage (about 4000 volts) was easily achieved. Confined, tamped specimens gave the best results as compared to confined, non-tamped samples and was therefore used but the extent of the tamping effect was not determined.

The effect of residual voltage on the discharge energy is calculated from the formula:

$$E = 1/2\ CV^2$$

where:

E = energy in joules

C = capacitance (farads)

V = voltage (volts)

Test No. 24 (Table III) was made at eight capacitance levels for a total of 160 shots. Unconfined experiments (Test No. 2-6) gave uniform energy values, 0.0253 to 0.0267 joules, with the exception of Test No. 5, 0.0171 joules. This sample was allowed to stand at ambient conditions for four hours prior to testing. Normally the prepared material was removed from the drying oven and used immediately. Some of the samples showed a tendency to become more sensitive with elapsed time. Test No. 5 confirmed this hypothesis exhibiting a value about half-way between the confined and unconfined values. This type of sensitization is believed to be due to moisture pickup and caking. The confined values were the lowest (Test No. 7, 10, and 11) ranging from 0.0073 to 0.0090 joules.

Test No. 23 was made to determine the difference between subjecting the sample to fewer electrons falling through a higher potential in less time as compared to a higher number of electrons possessing less energy for a longer time. A capacitance value (428 pf) and resistance (10^6 ohms) were selected to require a high voltage. The voltages ranged from 9,180 to 11,300 volts with a calculated mean value of 10,076 volts corresponding to a 50/50 point energy of 0.0214 joules. This energy value corresponds to that of test 13, namely 0.0211 joules, indicating a total energy initiating effect with the time of application constant.

In Test No. 24, 20 specimens were tested at eight capacitance levels for a total of 160 shots (Table V).

TABLE V

Probability of initiation for the standard mix from the electrostatic discharge test

Capacitance (pf)	Number of Trials	Fires (go's)	No Fires (no go's)
350	20	0	20
400	20	1	19
450	20	3	17
500	20	8	12
550	20	11	9
600	20	17	3
650	20	19	1
700	20	20	0

The 50% probability point (Fig. 3) corresponds to 525 pf or a 50/50 point initiation of 0.0143 joules. To confirm this value a separate run was made (Test No. 22) under identical conditions giving values of 516 pf, 0.0145 joules, which is an excellent correlation. This value is also in agreement with Test No. 18. Copper chlorotetrazole was also tested (Test No. 17) giving a 50/50 point energy value of 0.0185 joules.

THERMAL INITIATION

Ten No. 8 booster shell casings were loaded with 10 mg of standard mix for each series of thermal experiments (Table VI). Each point on the experimental curves (Fig. 4 and 5) is an average of 10 tests. With the exception of Tests 2 and 9 all of the 5 second reaction temperatures fall within a very narrow range. Test 2 was the only one stored at ambient conditions during testing, while all other specimens were kept in desiccators prior to testing. Test 9 is an extrapolated value from 6.5 to 5 seconds, the 6.5 second value being 328°C.

The values for copper chlorotetrazole are about 25°C higher than the published value of 305°C (2). This is believed to be a result of long time storage under a 50/50 ethanol/water solution. This material was obtained from Picatinny Arsenal to be used as a comparison standard and for test evaluation purposes. It was not known until later that it was surplus material that had been stored for an undetermined length of time. The different treatments on tests 5, 6 and 7 were performed to make sure the material was thoroughly dried and the higher values were not due to the presence of moisture.

Test 8 was made at a constant temperature of 315°C and the ignition time in seconds is plotted versus the sample weight in milligrams (Fig. 4). The decrease in ignition time with an increase in weight (or volume) is a contact surface area effect. As the total surface area in contact with the sample holder increases, the reaction time decreases. For reproducibility and comparative purposes the sample size was held constant.

Tests 9, 10, 11, and 12 were conducted under constant experimental conditions to check reproducibility, and to calculate the activation energy of the standard mix. From the effect of temperature on the induction period

and application of the relation ln t = E/RT + constant, where t is the induction period, and E is the activation energy, values of E of 16 kcal/mole at temperatures below 330°C and 83 kcal/mole at higher temperatures for the standard mix were calculated. The higher value at temperatures above 330°C indicates desensitization due to partial decomposition. The melting point of $KClO_3$ is 356°C and as this temperature is approached the decomposition reaction will become more important.

Activation energies are not normally determined for mixtures, and the values of E presented here are not a measure of the true activation energy for the reaction leading to an explosion, since they are dependent upon physical characteristics of the system. This is even more the case if self-heating occurs and plays an important part in the initiation of an explosive reaction. If there is a reaction during the induction period that either sensitizes or desensitizes the material that is different from a reaction that occurs later and culminates in an explosive reaction, the values of E for the initial and final periods of the induction time will be different. This appears to be the case for the standard mix.

Potassium chlorate can undergo an exothermic, spontaneous decomposition reaction:

$$2\,KClO_3 \longrightarrow 2KCl + 3O_2 \qquad \Delta H = -21 \text{ kcal/mole}$$

Compounds containing such oxidizers are particularly sensitive to mechanical disturbances and possess explosive properties. Perchlorates are less reactive because of their lower heat of reaction.

$$2KClO_4 \longrightarrow 2KCl + 4O_2 \qquad \Delta H = -1 \text{ kcal/mole}$$

Physical changes that take place in a compound during storage are usually due to absorption of moisture. The oxidation of Mg or Al by water, for example, advances rapidly if $KClO_3$ or any other high energy oxidizer is present. Since these reactions are strongly exothermic they can cause spontaneous combustion. The oxidation rate of red phosphorus increases with temperature but is inhibited when stabilized or coated with a protective film.

IMPACT (LARGE BALL)

This test was developed to evaluate larger, less sensitive specimens than those used in the small ball drop test. Samples of 200 mg each were used. The results were recorded as a go (fire, explosion) or a no go (no fire, no reaction) and the 50/50 point energy was calculated (Table VII).

Tests 1 through 5 were performed on only 4 to 8 samples each, which is an insufficient number to render a statistical analysis. The approximate value of 580 g-cm is higher than the 440 g-cm average from the experiments where there were 15 or 10 specimens per test. Varying the ball weight indicated a tendency toward lower kinetic energy values for lighter weights dropped from greater heights (Fig. 6). This observation was confirmed by additional experiments with the small ball drop test.

The specimens tested with freon (Table VII) contained an excess of the freon and were dried to the 30% value as determined directly by weighing. This was a more accurate procedure than attempting to add the exact amount desired by a mini-pet and also ensured a more uniform blending of the freon with the mix.

IMPACT (SMALL BALL)

A lower input energy method was developed as a more sensitive version of the test just described (Fig. 7). The sample weight was 20 mg and the ball weight was approximately 7 g (Table VIII). Also included in this phase of the investigation were tests to determine the effect of 1.) varying the stoichiometry of the standard mix, 2.) adding various grit particles, 3.) the optimum test energy, 4.) sample size, and 5.) measuring the per-

formance characteristics of the impact tester. Rebound studies were performed to allow correlation with other similar testers.

The two unconfined tests (No. 5 & 6) had 50/50 point energies about one-half of the confined values (Table VIII). Tests 10 and 11 were made on material that had been stored at ambient conditions for long periods of about a week, to compare with freshly prepared specimens. The higher values indicate some desensitization on storage. Hypothesis tests were made on tests 7, 8 and 9, with the sample weight varied from 4.5 to 15 mg. The energy levels (g-cm) were analyzed to compare 9 with 7 and 8 with 7. For a 95 confidence interval, the analysis showed that tests 9 and 7 were significantly different while 8 and 7 were approximately the same. Small sample sizes were excluded for this type of testing as a result of this analysis. Test 12 was made with a 30 mg sample size and the higher 50/50 point energy indicates a cushioning, energy absorbing effect of the larger sample sizes when the lighter drop weights are used.

The value for the stoichiometric mix (38.0 g-cm) was about double that of the fuel rich mix. The effect of the additives (Al, Mg, and silica gel) was to decrease the sensitivity by a factor of 2 or 3. This provides a method of obtaining a range of sensitivity values for the standard mix. Tests 21 and 22 show that as the relative humidity increased from about 30 to 35%, to 40%, to 45%, and to 50%, the energy level increased from about 24 to 35 g-cm, to about 60 g-cm. It is thus important to perform experiments under known, controlled environmental conditions.

Statistical calculations have been made on the results from the small impact test. Combined results from similar tests, 150 specimens, gave a calculated mean of 18.6 ± 5.5 g-cm, a median or 50/50 point, based on a log normal distribution of 17.8 ± 4.8 g-cm, and a median based on a log normal distribution of 16.5 ± 5.0 g-cm. All results combined, 290 tests, gave a mean of 17.6 ± 4.8 g-cm, a normal median of 16.2 ± 4.6 g-cm, and a log normal median of 15.3 ± 4.7 g-cm. In general the mean is about 16 ± 5 g-cm for the standard mix as determined by the small ball drop (impact) test.

The go-no go test results of the standard mix are log normally distributed, although within the test range they are also normally distributed. Chi square tests have indicated that the distribution may be either log normal or normally distributed within the 50% range.

The rebound versus drop height relationship has been determined for the test conditions (Fig. 8). Each point is a average of 20 determinations. The coefficient of resitution (e^2) is defined as the ratio of the rebound height to the drop height. The values are presented on the graph. Ideally, the deviation from the theoretical value should be a straight line. Also, the greater the deviation, the lower the efficiency of the apparatus. The impact tests on the standard mix, using the same ball weight (6.87 g), have been on the lower portion of this curve, up to 4.5 to 5.0 cm, where the efficiency or coefficient of resitution is higher.

The 50/50 point energy level versus drop height and ball weight relationships for the standard mix and copper chlorotetrazole have been determined (Figs. 9 and 10). The points represent the 50/50 values for a large number of tests. Two valves obtained by Anzalone for CCT (2) are included. These figures demonstrate the significance of momentum in the initiation process. For comparative purposes it would be better to test at or near the crossover point. Figure 9 shows scatter around a point, variations within a small test range, as compared to the trends from the large impact test (Fig. 6).

CONCLUSIONS

A mixture of $KClO_3/P_4$/ Quso/MgO/inert in the proportions 34/14/4/2/46 and modifications of this standard mix, including additives such as Al, Mg, Silica gel, Pyrex, and Cab-o-sil, have been investigated to determine the sensitivity to initiation by electrostatic discharge, heating, and impact.

Confined and tamped specimens gave reproducible results in the electrostatic discharge test. The 50/50 point energy level was 0.0145 joules at a median capacitance of 516 pf and a resistance of 10^4 ohms.

The 5 second explosion temperature for the standard mix was 330°C as determined by the thermal initiation test. An activation energy of 16 kcal/mole was calculated for temperatures from 300 to 330°C.

The large ball drop impact test, 50/50 point energy level, on specimens desensitized by the addition of 30% freon for a 200 mg sample was 848 g-cm. Small ball drop impact test values obtained for the dry, standard mix were about 18 ± 5 g-cm.

An IR study showed trace amounts of P_4O_{10}, $KClO_4$, KH_2PO_4, and ClO_2 under various environmental treatments. A proposed reaction mechanism for spontaneous ignition is:

$$P_4(red) + 6H_2O \xrightarrow{air} PH_3(g) + 3H_3PO_2 \quad -3.77 \text{ kcal/mole}$$

$$2H_3PO_2 + 3KClO_3 \longrightarrow 2ClO_2 + KCl + 2KH_2PO_4 + H_2O \quad -296.7 \text{ kcal/mole}$$

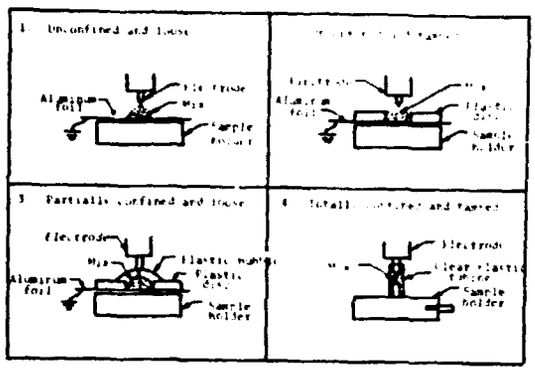

Test Results using Different Mixes

Run No	Confinement Type	Resistance	50/50 Point (approx)	Variation about Mean
4	1	2.1 k	1000 pf	very large
5	1	2.1 k	750 pf	very large
6	1	2.1 k	1000 pf	very large
7	3	2.1 k	300 pf	small
19	3	1.0 k	411 pf	small

Figure 1

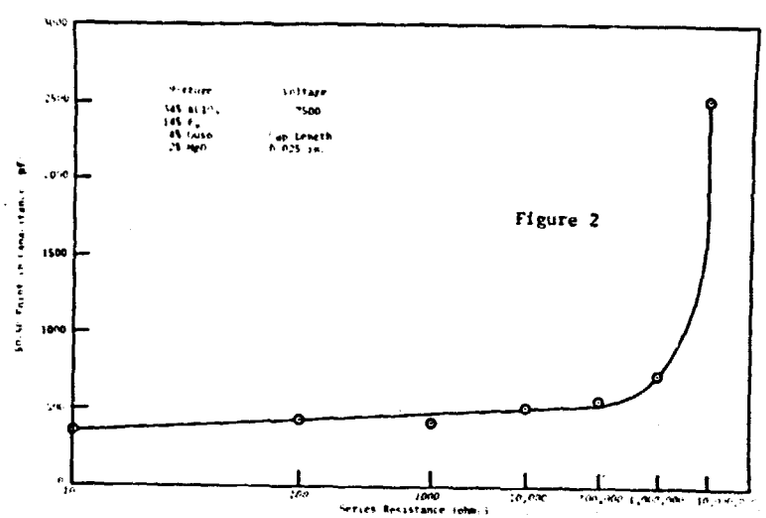

Figure 2

REFERENCES

1. Standard Chemistry Handbooks.
2. Anzalone, Alfred M., et.al., "Characteristics of Explosive Substances for Application in Ammunition," FRL Tech. Rpt. No. 2179, Picatinny Arsenal, May 1955.

TABLE III

Results of the electrostatic discharge testing

Test No.	Median Capacitance (pf)	Resistance (ohms)	50/50 point energy(joules)	Other Comments
2*	943	0	0.0267	cap. interval 25 pf
4*	937	"	0.0265	cap. interval 100 pf
5*	606	"	0.0171	4 hrs. at room T&P before testing
6*	900	"	0.0253	tamped
7	318	"	0.0090	confined, T & R.H. controlled
10	306	2	0.0086	confined & tamped
11	259	2	0.0073	acid free P_4
13	750	10^6	0.0211	resistance varied
14	2550	10^7	0.0717	" "
15	565	10^5	0.0159	" "
17	658	2	0.0185÷	CCT series
18	512	10^4	0.0144	resistance varied
19	433	10^3	0.0122	" "
20	428	10^2	0.0120	" "
21	353	10	0.0100	" "
22	516	10^4	0.0145	repeat of No. 24
23	428(const.)	10^6	0.0214	voltage varied
24	525	10^4	0.0148	see Fig. 3

Note 1: * unconfined (all others confined)

Note 2: test numbers omitted were invalid results due to experimental difficulties

Note 3: ÷ aged material

Note 4: standard mix, 34/14/4/2, $KClO_3/P_4$/Quso/MgO used in all tests except No. 17 which was copper chlorotetrazole.

Note 5: 7500 volts DC used in all tests except No. 23 where it was varied with an average value of 10,076 volts.

Note 6: gap length was 0.035" through test No. 7 and 0.025" for the rest

Note 7: sample size was 50 mg through test No. 7 and 33 mg for the rest

Note 8: ambient conditions, 73 ± 4°F and 40 ± 17% relative humidity

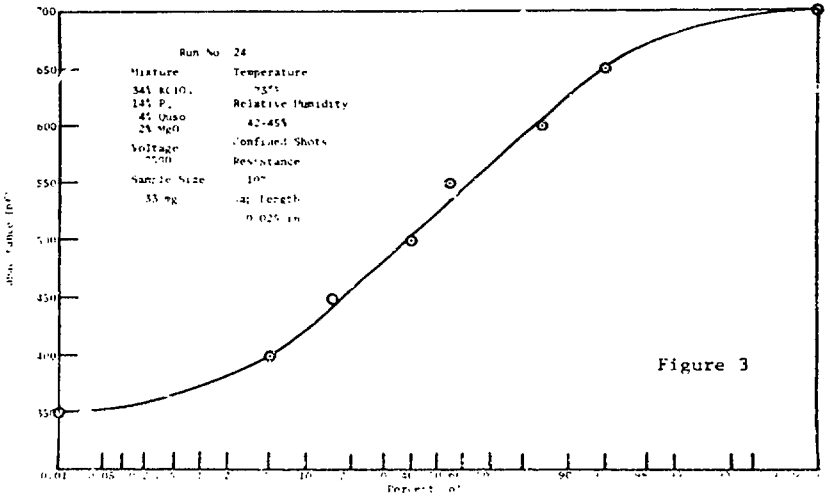

Figure 3

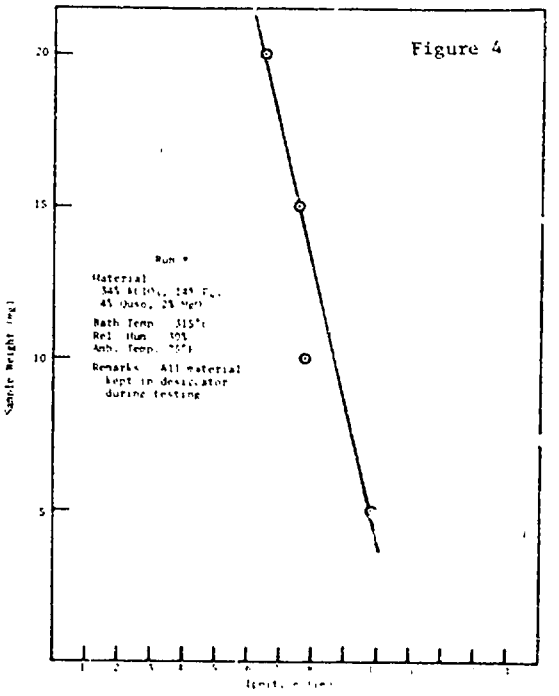

Figure 4

TABLE VI

Results of the thermal initiation testing

Test No.	5 second reaction Temperature (°)	Comments
1	--	lost due to accident
2	341	stored at room T & P during testing
3	328	acid free P mix
4	325	stored in desiccator
5	327†	(CCT) dried 90 hrs at 85°C
6	329†	washed with ethanol, dried 48 hrs. at 110°C
7	330†	dried 24 hrs. at 110°C
8	--	See Fig. 4
9	338*	Test Nos. 9, 10, 11 and 12 were made as nearly identical as possible for an activation energy determination
10	329	
11	329	
12	331	

Note 1: Standard mix - 34% $KClO_3$, 14% P_4, 4% Quso, 2% MgO, balance inert used in all tests except No. 5 which was copper chlorotetrazole.

Note 2: All samples were kept in desiccators prior to testing, except Test No. 2

Note 3: Ambient conditions, 75 ± 7°F, 30 ± 6% relative humidity

Note 4: The sample size was 10 mg for all tests

Note 5: * extrapolated value from 6.5 down to 5 seconds

Note 6: † aged material

TABLE VII

Results of the large ball drop (impact) test

Test No.	Sample Wt. (mg)	Ball Wt. (g)	Specimens in Test	Mean Ht. (cm)	50/50 Point Energy (g-cm)
1	200	44.61	4 to 8	13	580
2	"	"	"	13	580
3	"	"	"	13	580
4	"	"	"	13	580
5*	"	"	"	19	848
6*	"	"	"	19	848
7	"	"	15	10	446
8	230	"	15	9.7	433
9	"	"	20	9.9	442
10	"	35.81	20	11.4	406
11	"	21.65	20	14.6	316
12*	"	44.61	20	19.9	889

Note 1: standard mix - 34/14/4/2, $KClO_3$/P/Quso/MgO used in all tests

Note 2: * denotes standard mix plus 30% freon

Note 3: relative humidity, 28 ± 2%

Note 4: room temperature, 73 ± 3°F

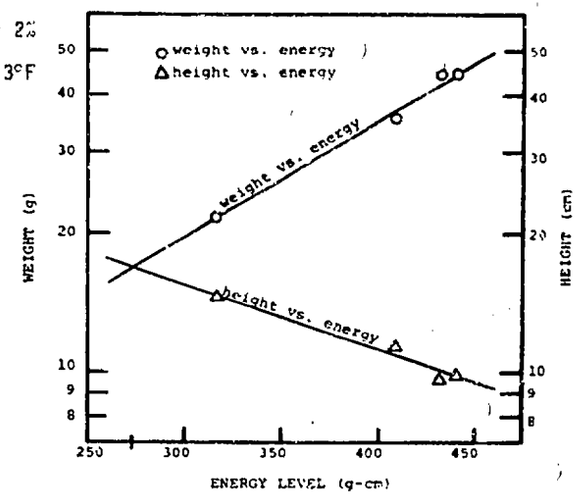

Figure 6

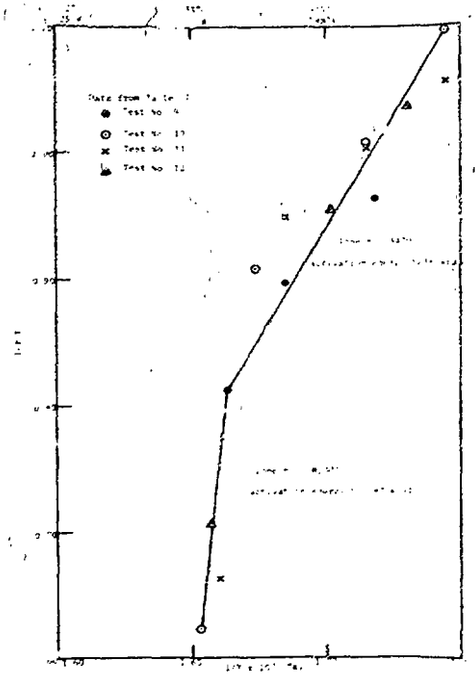

Figure 5

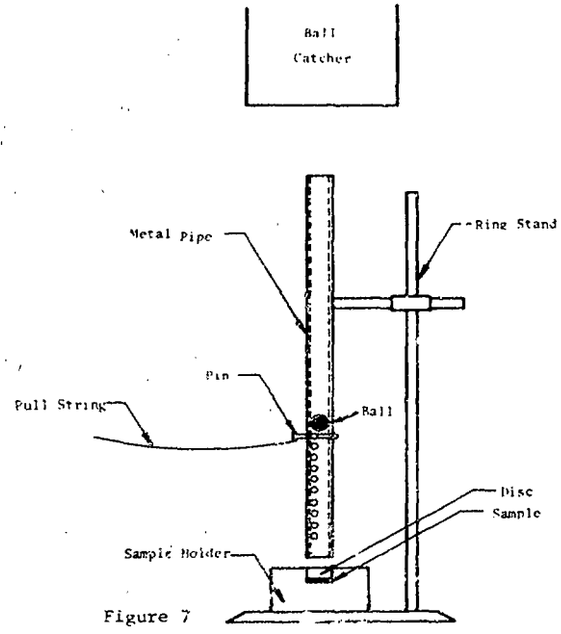

Figure 7

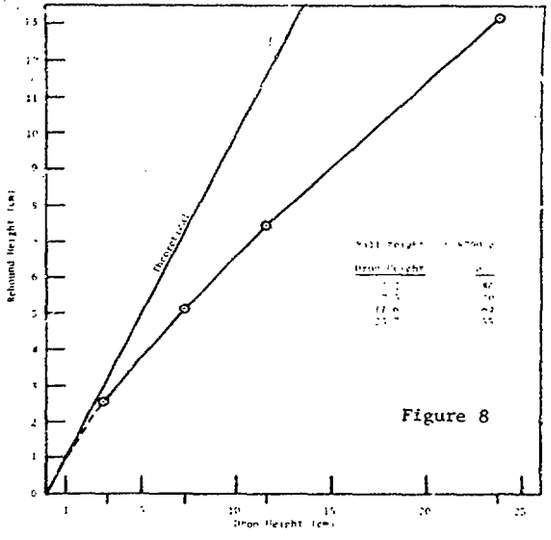

Figure 8

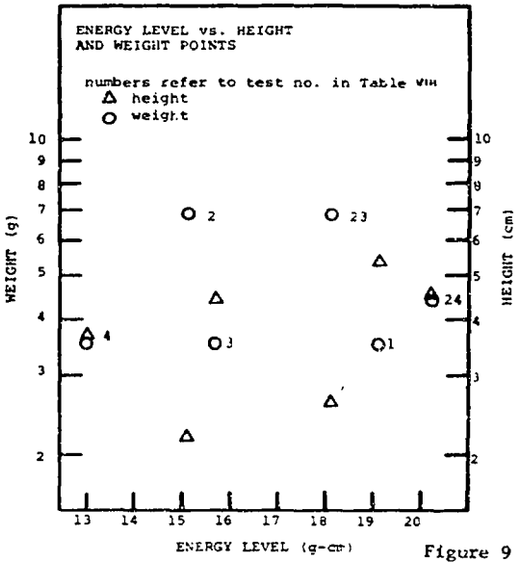

Figure 9

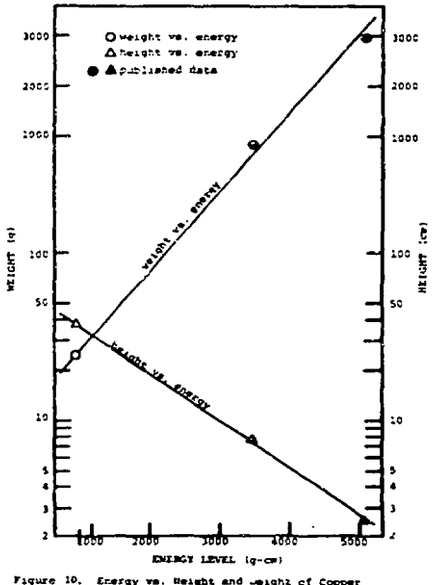

Figure 10. Energy vs. Height and Weight of Copper Chlorotetrazole - Large Impact Test

TABLE VIII

Results of the small ball drop (impact) test

Test No.	Sample	Sample Wt.(mg)	Ball Wt.(g)	Specimens in Test	Mean Ht. (cm)	50/50 point Energy(g-cm)
1a	34/14/1 $KClO_3/P_4$/ Cab-O-Sil	4-5	3.31	20	(practice run)	
2a	" "	"	"	30	4.42	16.8
3a	5/2 $KClO_3/P_4$	16-17	3.53	20	2.85	10.1
4a	" "	10	"	"	3.20	11.3
5a	" "	20	"	"	3.65	12.9
1	34/14/4/2 $KClO_3/P_4$/ Quso/MgO	"	"	"	5.40	19.1
2	" "	"	6.87	"	2.20	15.1
3	" "	"	3.53	"	4.45	15.7
4	" "	25	"	"	3.70	13.0
5*	" "	25	3.47	35	2.26	7.8
6*	" "	25	"	"	1.77	6.1
7	" "	9	6.87	"	2.23	15.3
8	" "	15	"	"	2.36	16.2
9	" "	4.5	"	"	2.04	14.0
10	" (aged 1 week)	15	"	"	3.33	22.9
11	" (aged 1 week)	15	3.47	"	3.03	20.9
12	" "	30	6.87	"	5.14	35.3
13	76.9/23.1 $KClO_3/P_4$ (stoichiometrix mix)	20	"	23	5.54	38.0
14	" plus 5% Al	20	"	21	6.07	41.7
15	34/14/4/2 plus 5% Al	20	"	35	7.89	54.2
16	34/14/4/2 plus 5% Mg	20	6.87	36	8.91	61.2
17	34/14/4/2/46 $KClO_3/P_4$/Quso/MgO/Silica gel)	"	"	35	8.83	60.0

TABLE VIII

Results of the small ball drop (impact) test

Test No.	Sample	Sample Wt.(mg)	Ball Wt.(g)	Specimens in Test	Mean Ht. (cm)	50/50 point Energy(g-cm)
18	34/14/4/2/46 $KClO_3/P_4$/Quso/ MgO/Silica gel	20	6.87	34	8.34	57.3
19	34/14 $KClO_3/P_4$	"	"	16	8.19	56.2
20	34/14/4/2 + 46 Pyrex glass	"	"	10	10.30	70.7
21	34/14/4/2	24	"	36	6.79	46.6
22	"	24	"	48	4.28	29.4
23	"	24	"	75	2.64	18.1
24	"	"	4.47	75	4.51	20.2
25	" (20 shots at 6 levels)	"	6.87	120	--	--
26	" (aged for 30 days)	"	"	75	3.38	23.2
27	Copper chlorotetrazole	11	24.76	26	38.0	940†
28	Copper chlorotetrazole	11	"	25	"	940†

Note 1: * All tests confined except No. 5 and 6

Note 2: relative humidity 37 ± 13%, temperature 76 ± 6°F

Note 3: † Aged material

Combined 50/50 point energy of 290 tests performed on the standard mix = 17.6 g-cm ≈ 0.0018 joules

III-12. LE DECOUPAGE INTER-ETAGE PAR CORDEAUX DETONANT

Pierre CLAUDE

Etablissement d'Etudes et de Fabrications d'Armement de BOURGES (FRANCE)

1 - INTRODUCTION -

Dans les utilisations spatiales, il est souvent nécessaire de découper une structure. La découpe peut concerner un intéretage (séparation d'étages) ou un propulseur (opération de destruction).

Les qualités que l'on demande à découpage sont bien sûr très nombreuses ; on peut noter parmi les principales, la rapidité et la simultanéité, la sûreté de fonctionnement quel que soit l'environnement. On demande aussi au système d'être léger de façon à embarquer un poids sont minimal.

Le découpage par cordeau détonant répond bien à l'ensemble de ces conditions.

Le but de cette communication est de montrer que la détermination d'une chaîne de découpage peut se faire de façon très rationnelle en tenant compte de quelques principes élémentaires. On décrira au passage les éléments pyrotechniques intervenant dans cette réalisation : éléments constitués essentiellement d'explosif sous différentes formes : amorces, relais, et d'abord cordeaux.

2 - LES CORDEAUX DETONANTS -

Deux grandes catégories de cordeau sont fabriqués : les cordeaux de découpage et les cordeaux de transmission.

2.1. LES CORDEAUX DECOUPEURS

a) Définition et principe

Le cordeau découpeur est constitué d'une gaine métallique dont l'âme est remplie d'explosif. Celui qui est fabriqué par la Direction des Poudres, comporte de l'hexogène sous gaine de plomb antimonié. La section droite du cordeau a la forme d'un V. Elle est inscriptible dans un carré ou dans un rectangle. Il existe des cordeaux de dimensions très différentes, par exemple les 3 x 3,5 mm, les 4 x 4 mm .... jusqu'au 10 x 10 mm (Figure 1, Planche I).

Amorcé en un point, il est parcouru par une onde de détonation qui se propage perpendiculairement au plan de la section droite. L'interaction de cette onde de détonation avec la gaine du cordeau provoque un jet de particules métalliques, convergent vers l'élément à découper.

Ce jet de très grande énergie attaque la plaque à découper, et suivant le grosseur et le type du cordeau, découpe cette plaque partiellement ou complètement (C.f. Figure 2, Planche I : Forme du jet).

Puisque l'on recherche des effets dirigés, il faudra que le cordeau présente une homogénéité de chargement et une régularité de forme aussi parfaite que possible. Cette régularité de forme sera obtenue plus facilement dans le cas d'un cordeau présentant un plan de symétrie. Le jet se propagera alors dans ce plan et lorsque le cordeau sera posé bien à plat sur une plaque, la découpe sera perpendiculaire à cette plaque.

Si le cordeau n'est pas symétrique, la découpe se fera de travers, l'épaisseur à découper sera plus forte et le cordeau devra être de dimensions supérieures.

Or, dans bien des cas, les utilisateurs demandent des cordeaux bien adaptés, c'est-à-dire, capables de découper une structure donnée avec le minimum d'effets destructeurs, et par conséquent, on a tout intérêt à choisir un cordeau symétrique (Figure 3, Planche II : Effet d'une dissymétrie).

b) Types de cordeau

Dans la famille des cordeaux découpeurs, il existe deux types : le cordeau dit à charge réduite (noté CR) et le cordeau dit à charge normale (noté CN) (Figure 4, Planche II : Section droite des deux types de cordeau).

Ces deux types ont le même aspect et les mêmes dimensions extérieure. Ils ne diffèrent que par les dimensions et la forme de l'âme ; il en résulte donc une différence dans la charge linéaire qui est la masse d'explosif par unité de longueur. A titre d'exemple, le cordeau de dimensions extérieures 5 x 5 mm possède une charge moyenne de 8,1 g/m dans la version normale et seulement 3,4 g/m dans la version réduite.

On constate expérimentalement que les découpes effectuées avec le cordeau à charge réduite sont au moins aussi profondes que celles réalisées avec le cordeau à charge normale. En plus, les découpes sont plus nettes, cela pouvant s'expliquer par le fait que le cordeau produit un jet beaucoup plus étroit donc mieux dirigé.

Un autre avantage du cordeau à charge réduite provient des faibles effets arrières constatés ce qui a une très grosse importance lorsque le cordeau doit passer à proximité d'organes vitaux comme les tuyères, les blocs électroniques .....

Par contre, les principaux inconvénients de ce type de cordeau viennent d'une plus grande difficulté d'amorçage et surtout d'une faible aptitude à initier d'autres brins de cordeau.

2.2. [illegible]

Le cordeau détonant de transmission est formé d'une gaine de section circulaire et d'une âme explosive. Comme le cordeau de découpage, celui de transmission fabriqué par la Direction des Poudres est constitué d'hexogène dans une gaine de plomb.

Il existe deux différents diamètres, à partir de 2 mm (Figure 5, Planche III : Section droite du cordeau).

Associé en ligne, il détone avec une très bonne régularité de vitesse qui est de l'ordre de 7 500 m/s.

On l'emploi le pour transmettre la détonation dans les explosifs pyrotechniques. Dans le cas qui nous intéresse, il va assurer la liaison entre l'amorce électrique placée en bout de mèche et le cordeau découpeur qui en assurera l'amorçage définitif. Grâce à la souplesse de sa gaine, il pourra suivre les sinuosités des montages.

Le retard pyrotechnique le plus important de ce cordeau est le pouvoir d'amorçage, c'est-à-dire, la nature de l'explosif, primaire ou secondaire, qu'il est capable d'initier.

Par exemple, il faut un cordeau de diamètre au moins égal à 5 mm, soit une charge linéaire de 1,5 g/m pour initier de l'explosif secondaire, pentrite ou hexogène.

Le cordeau de transmission pouvant être en contact direct avec les spectateurs, il est nécessaire de limiter au maximum les effets arrières. On arrive particulièrement à ce résultat en enrobant le cordeau dans une gaine thermoplastique (silicone de polyvinyle ou polyéthylène). Cet enrobage offre en plus une protection contre les impacts extérieurs et une plus grande facilité dans les manipulations.

3 - [illegible] -

Le choix du cordeau ne peut se faire qu'en considérant l'ensemble de trois critères :

- nature et épaisseur du matériau à découper
- importance des effets arrières tolérés
- pouvoir d'amorçage du cordeau

Ces trois critères s'interpénétrant, le choix définitif ne pourra être qu'un compromis.

3.1. [illegible]

Pour la réalisation de la destruction d'un engin balistique, l'utilisateur désire découper une certaine épaisseur d'un certain matériau. Ne sachant pas à l'avance quel cordeau lui convient, il en choisira sur une fiche commerciale deux ou trois types et il pourra rapidement déterminer le cordeau adapté à son besoin grâce à la méthode simple et rapide du coin et à sa vérification.

Le principe de la méthode du coin consiste à placer un cordeau sur une tôle dont l'épaisseur varie linéairement en fonction de l'abscisse (Figure 6, Planche IV).

Le cordeau étant amorcé du côté où le coin est le plus épais afin de diminuer les effets d'arrachement, on constatera que le coin est découpé à partir d'une certaine épaisseur caractéristique du cordeau utilisé et du matériau.

On pourra alors déterminer une zone où l'épaisseur est découpée correctement, une zone où la découpe est incertaine et une zone non découpée.

Si l'épaisseur dont on veut obtenir la découpe est comprise dans la zone correctement découpée sur le coin, on passera ensuite à des essais sur le matériau à découper réellement de façon à déduire un taux de sûreté de fonctionnement. Les essais devront être réalisés dans une configuration simplifiée, mais qui soit tout de même très proche de la réalité. En particulier, si le cordeau est destiné à découper un intédigo, on pourra effectuer les essais sur des montages maintenus en l'air, par exemple, par des aimants (Figure 7, Planche IV).

Si le taux de sûreté n'est pas jugé suffisant, c'est-à-dire, si l'on a constaté un ou plusieurs ratés, les essais devront être recommencés avec un cordeau de dimensions plus importantes.

Dans l'hypothèse où l'on n'a pas constaté de raté, le taux de sûreté dépendra bien sûr du nombre d'essais. Par exemple, si l'on a effectué 100 essais satisfaisants, le taux sera de 0,97 avec un intervalle de confiance à 95 %. Si l'on veut porter ce taux à 0,997, il faudra 1 000 essais.

Ainsi, par approches successives, l'utilisateur pourra déterminer le cordeau de dimensions minimales répondant à son problème. A titre d'exemple, avec le cordeau de découpe 5 x 5 à charge réduite, et après avoir effectué 100 tirs sur des coins en acier AC 10 F de dimensions 200 x 50 mm et de pente 2 °, on a obtenu la courbe d'efficacité de découpage n° 1 (Figure 8, Planche V). Ensuite, 4 différentes épaisseurs choisies à partir de cette courbe, on a fait une série de 100 tirs sur tôles planes et on en a déduit la courbe n° 2 (Figure 8, Planche V).

Le décalage que l'on constate entre les fonctionnements est dû au phénomène d'arrondissement qui se produit avec le coin et qui réduit de l'épaisseur évolutive. C'est là l'inconvénient majeur de la méthode du coin, mais il ne faut pas oublier que ce n'est qu'une méthode d'approche.

3.2. CHOIX EN FONCTION DES EFFETS ARRIERE

Par effets arrières, on entend les effets en général non recherchés du cordeau qui peuvent causer des dégâts sur des organes vitaux de l'engin.

Ces effets sont dus à l'onde de choc créé par la détonation du cordeau et à la projection à grande vitesse de particules de plomb.

En ce qui concerne la surpression due à l'onde de choc, il semble qu'elle soit très faible tout au moins pour les cordeaux à charge linéaire peu élevée. L'effet principal est donc dû à l'impact des éclats de plomb.

Ces effets arrières sont difficiles à évaluer. On a cherché à employer une méthode comparative qui consistait à mesurer la déformation subie par une tôle cible placée au-dessus du cordeau (Figure 9, Planche VI). Cette méthode s'est heurtée à des difficultés d'étalonnage et l'on envisage une méthode conduisant à des résultats beaucoup plus absolus. On peut simplement dire à ce jour que les effets dépendent principalement de la charge linéaire et non de la masse de plomb ce qui montre le grand intérêt en ce domaine du cordeau à charge réduite.

3.3. CHOIX EN FONCTION DU POUVOIR D'AMORCAGE

Pour les montages sur engins balistiques de dimensions importantes, on est obligé de prévoir plusieurs brins de cordeau qui viendront bout à bout (Figure 10, Planche VI).

Malheureusement, du fait de sa faible charge, le cordeau est peu apte à transmettre la détonation à un cordeau voisin. Les distances maximales permettant d'amorcer le cordeau receveur peuvent être définies à la suite d'essais systématiques.

A titre d'exemple, un cordeau 4 x 4 à charge réduite (charge linéaire 2 g/m) est capable de transmettre la détonation à un cordeau identique placé à 0,5 mm tandis qu'un cordeau 4 x 4 à charge normale (5 g/m) peut le faire à 2 mm.

Comme on le voit, la comparaison est ici en faveur du cordeau à forte charge, mais il ne faut pas oublier que cet avantage ne peut être acquis qu'au détriment des effets arrières.

3.4. CHOIX DEFINITIF

On vient de considérer les critères pouvant commander au choix définitif du cordeau.

Les essais sur matériau à découper ont permis de déterminer une dimension de cordeau capable de la découpe dans de bonnes conditions. Le cordeau retenu ne pourra donc être inférieur, mais deux cas seront alors à considérer suivant l'importance des effets arrières tolérés.

Si ces effets ne sont pas craints, on aura tout intérêt à choisir un cordeau à charge normale de dimensions importantes. Ce sera le cas de la destruction d'étages où l'on pourra même rechercher une surpuissance.

Si les effets sont craints, on choisira un cordeau à charge réduite de dimensions minimales et, éventuellement, on étudiera avec soin la transmission de cordeau à cordeau pour pallier l'infériorité du cordeau à faible charge en ce domaine. Ce sera le cas de la séparation d'étages sur des engins balistiques où l'on veut éviter au maximum les dégâts sur les organes importants contenus dans l'intéretage.

4 - DEFINITION DE LA CHAINE PYROTECHNIQUE -

Le cordeau étant choisi, il faudra ensuite déterminer la chaîne pyrotechnique. Dans le cas général, il faudra prévoir l'initiation de la détonation, sa transmission au cordeau de découpe, l'amorçage de ce cordeau de découpe ainsi que la transmission d'un brin de cordeau à un autre.

4.1. INITIATION

On ne peut retenir actuellement que des amorces électriques. Les avantages en sont bien connus. On peut citer le temps de fonctionnement très court, la très faible consommation d'énergie, des petites dimensions, et bien sûr, une très grande facilité de synchronisation à l'intérieur d'une séquence quelconque.

Selon la sensibilité de l'amorce choisie, il sera nécessaire ou non d'interposer une interruption de chaîne pyrotechnique. En règle générale, il faudra éviter que des éléments contenant de l'explosif primaire puissent se trouver au-delà de cette interruption de chaîne bien que ce point puisse être soumis à discussion.

4.2. [illegible] L'INITIATION DE LA DETONATION

L'amorce provoquant l'initiation peut être assez éloignée du cordeau de découpe à amorcer. Il faut donc prévoir une transmission au moyen de cordeau qui, grâce à sa souplesse pourra épouser des formes à peu près quelconques.

Le choix du cordeau de transmission sera moins délicat que celui du cordeau de découpe, mais il y aura tout de même lieu de tenir compte des effets arrières et du pouvoir d'amorçage.

En ce qui concerne les effets arrières, un simple amorçage plastique comme il a été dit précédemment permet déjà de réduire les dépôts dans un rapport 2. Un gainage supplémentaire destiné peut-être à supporter le cordeau, pourra absorber la plus grande partie de l'énergie restante.

Pour le pouvoir d'amorçage, il faudra réaliser des essais systématiques. Toutefois, comme on l'a dit, il faut au minimum un cordeau de diamètre 3 mm soit 1,8 g/m de charge linéaire pour pouvoir amorcer de l'explosif secondaire sans l'intermédiaire d'explosif primaire. Encore faut-il noter qu'avec ce cordeau l'amorçage ne peut être obtenu que si le contact avec l'explosif est parfait. Si l'on désire se garder la possibilité d'un léger jeu, il faudra obligatoirement choisir un cordeau de charge nettement plus forte.

L'importance du contact entre cordeau et explosif oblige aussi à étudier avec soin le montage du relais sur le cordeau. Ce montage qui peut être obtenu par collage ou par sertissage devra être contrôlé par radiographie si l'on désire une très bonne sûreté de fonctionnement.

4.3. AMORÇAGE DU CORDEAU DE DECOUPE

Par l'intermédiaire du relais monté sur le cordeau de transmission, la détonation arrive au cordeau de découpe. Quelle configuration doit-on alors adopter pour obtenir l'amorçage de ce cordeau ? Trois géométries sont possibles : en bout axialement, en bout perpendiculairement, sur le dessus perpendiculairement.

a) En bout axialement (Figure 11, Planche VII)

C'est une solution très satisfaisante du point de vue pyrotechnique. Le relais serti sur le cordeau de transmission est capable de provoquer l'amorçage même dans des conditions de montage très mauvaises. Avec un relais chargé à 150 mg de pentrite, on a obtenu de bons résultats jusqu'à 7 mm de distance entre cordeau et relais.

Malheureusement, cette solution peut être [illegible] en pratique tout au moins en [illegible] type. En effet, elle [illegible] page sur toute la circonférence [illegible] centrer dans le cas de la [illegible] destructeur est placé le long d'une [illegible]

b) En bout perpendiculairement (Figure 12, Planche VII)

C'est aussi une solution satisfaisante du point de vue pyrotechnique. Le relais découpe parfaitement son emplacement ce qui permet cette fois d'avoir une continuité de découpage.

D'autre part, les distances d'amorçage cordeau relais et cordeau sont encore importantes. On obtient de bons fonctionnements avec 5 mm entre un relais chargé à 150 mg de pentrite et un cordeau de découpage 4 x 4 à charge réduite.

Ce type de montage peut être particulièrement intéressant pour l'amorçage des explosifs en cartouches. En effet, sans aucune difficulté de montage, il est parfaitement possible d'initier simultanément 4 brins de cordeau (figure 13, Planche VIII).

c) Perpendiculairement sur le dessus (Figure 14, Planche VIII)

C'est cette fois une solution assez peu satisfaisante du point de vue pyrotechnique. En effet, on initie une très faible quantité d'explosif peu sensible (hexogène) à travers un écran de plomb d'épaisseur relativement importante.

Il s'agit pourtant de la solution la plus employée car elle simplifie considérablement le montage et permet bien entendu d'obtenir une découpe circulaire.

Des essais sont nécessaires pour déterminer la charge du relais. Celle-ci doit être assez importante en raison de l'écran de plomb, ce qui renforce les effets destructeurs au niveau de l'initiation.

4.4. TRANSMISSION DE CORDEAU A CORDEAU

On a déjà vu que du fait de sa faible charge, le cordeau de découpe était peu apte à transmettre la détonation. La transmission directe sans interposition de relais n'est donc possible qu'avec des cordeaux de gros calibres dimensions, c'est-à-dire, dans des cas bien particuliers et assez rares.

Dans tous les autres cas, il va falloir intercaler des relais. Les critères à considérer pour la réalisation de ces relais sont les suivants :

- [illegible]
[illegible] obtenir un "effet [illegible]".

- [illegible]

- [illegible]

[illegible]

[illegible]

[illegible]

[illegible] (figure 17, planche [illegible]).

La sûreté de fonctionnement [illegible] peut être très grande. A titre d'exemple, sur des renforçateurs [illegible], on n'a jamais obtenu de raté sur environ [illegible] essais ce qui correspond à une probabilité de fonctionnement de l'ordre de [illegible].

5 - [illegible] -

On va [illegible], à titre d'exemple, le système de découpage de l'ogive d'un petit engin balistique. Le découpage se fait selon le schéma de la figure 18, planche [illegible].

A partir d'un relais placé en haut de l'ogive, on [illegible] deux [illegible] de cordeau de découpage disposés longitudinalement. Les deux [illegible] entourent la jonction [illegible]. Après découpage, on obtient donc deux [illegible] qui sont éjectés à grande vitesse.

Les remarques suivantes peuvent être formulées :

a) La transmission de la détonation est effectuée directement par le cordeau de découpage [illegible]

b) [illegible] (figure 18, planche [illegible]).

On peut [illegible] le temps nécessaire à la découpe dans le cas d'un fonctionnement normal, [illegible], lorsque les deux cordeaux longitudinaux ont bien été amorcés simultanément.

Le temps peut se subdiviser en :

- fonctionnement du relais d'amorçage = 5 μs

- transmission de la détonation par les renforçateurs d'un brin de cordeau à un autre = 2 μs x 4 = 8 μs

- durée de la découpe : [illegible] à parcourir à = 7 000 m/s donc 140 μs.

On voit donc que l'on arrive à un total de 150 μs environ ce qui apparaît tout à fait négligeable dans la séquence de vol.

6 - CONCLUSION -

L'exposé qui vient d'être fait ne prétend en aucune façon avoir épuisé le sujet du découpage par cordeau détonant. On s'est seulement attaché à mettre en évidence les différents points qui doivent être pris en considération lors d'un projet de découpage.

On espère avoir bien montré que le choix du cordeau de découpe peut se faire de façon très systématique en tenant compte de la facilité de découpage, des effets arrière et du pouvoir d'amorçage. Le choix effectué, on ne voit pas [illegible] d'ennuis sur ce point. En effet, la technique actuelle de fabrication permet de proposer des cordeaux parfaitement reproductibles et possédant une grande sûreté de fonctionnement.

Le cordeau étant choisi, la chaîne pyrotechnique d'initiation ne pose pas de problèmes sérieux. Toutefois, étant donné l'ambiance très sévère à laquelle les différents éléments doivent être soumis, on ne peut se permettre d'utiliser que des composants parfaitement qualifiés et convenablement contrôlés. A ce sujet, il faut noter que l'importance des contrôles doit être considérée comme primordiale. Ce n'est qu'à ce prix que l'on pourra obtenir le taux de sûreté de fonctionnement très élevé que l'on est en droit d'attendre.

Fig 1 Section droite d'un cordeau de découpe

Fig 4 Les deux types de cordeau de découpe

Fig 6 Méthode du coin

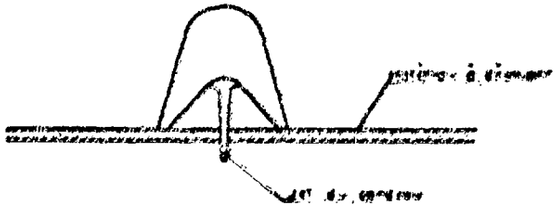

Fig 2 Forme du jet du cordeau

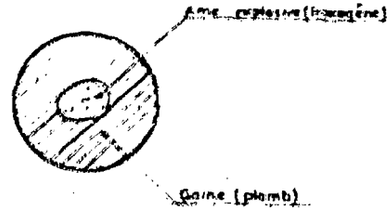

Fig 5 Section droite du cordeau de transmission.

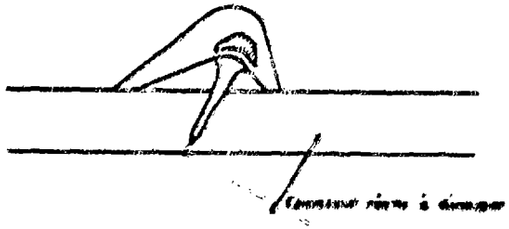

Fig 3 Effet d'une dissymétrie

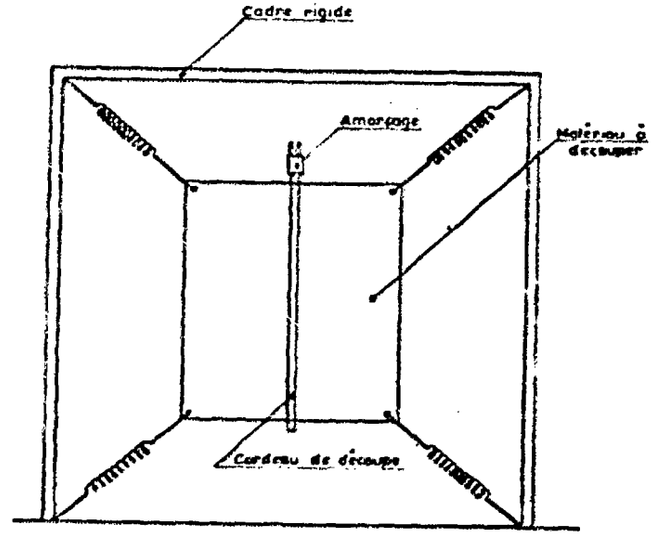

Fig 7 Essais de découpe sur matériau réel

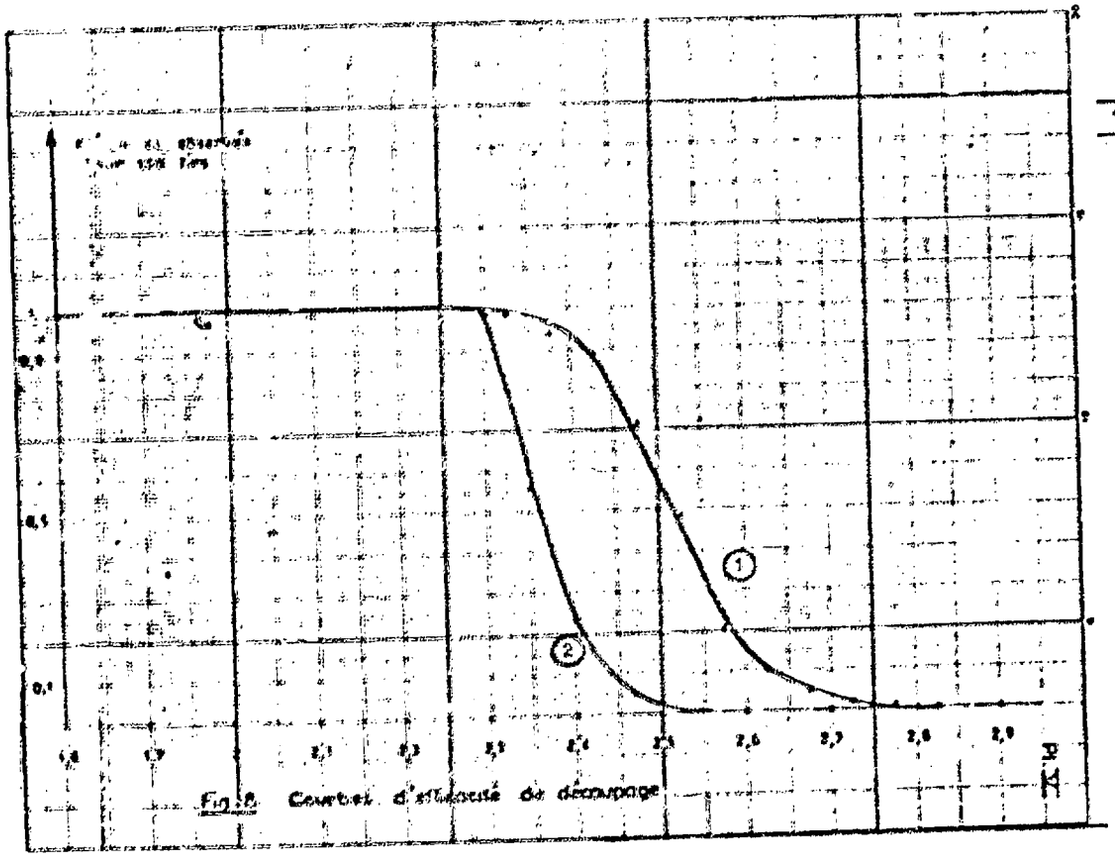

Fig. 8 Courbes d'efficacité de découpage

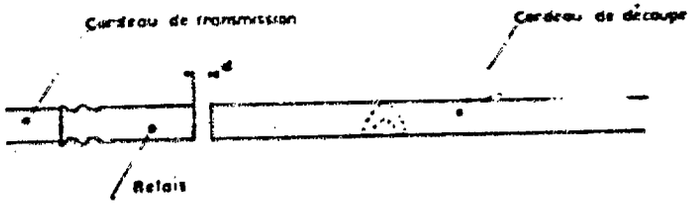

Fig. 11 Amorçage en bout axialement.

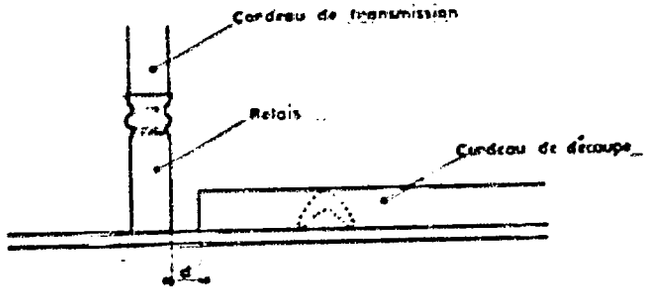

Fig. 12 Amorçage en bout perpendiculairement

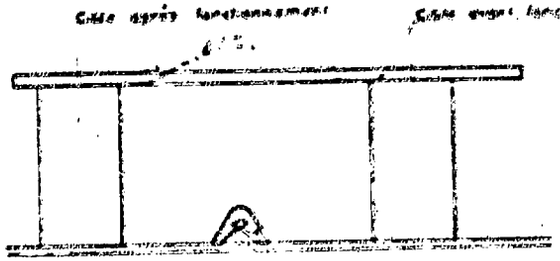

Fig. 9 Montage pour évaluation des effets arrières

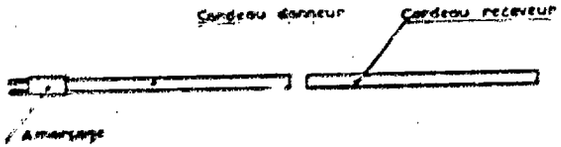

Fig. 10 Cordeaux bout à bout

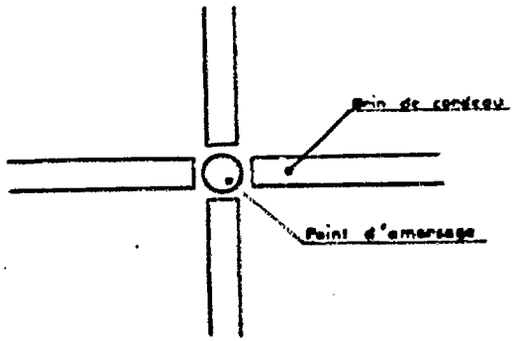

Fig. 13 Initiation d'un croisement de cordeau

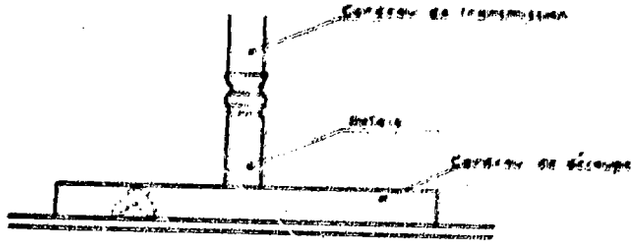

Fig. 14 Amorçage perpendiculaire sur le cordeau de découpe

Fig. 15 Renforçateur pour cordeau de découpe

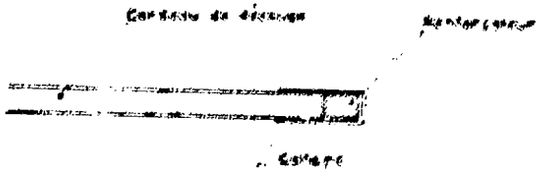

Fig. 16 Montage des renforçateurs sur le cordeau de découpe

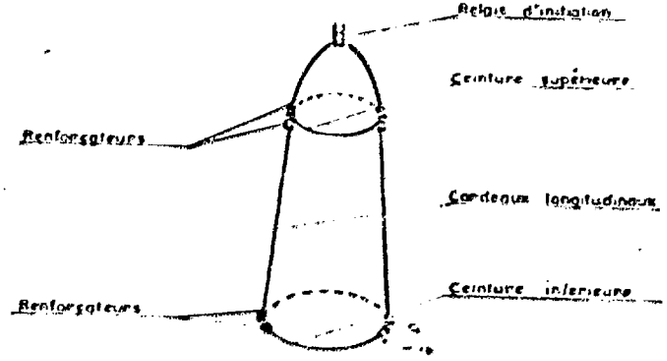

Fig. 18 Système de découpage de l'ogive

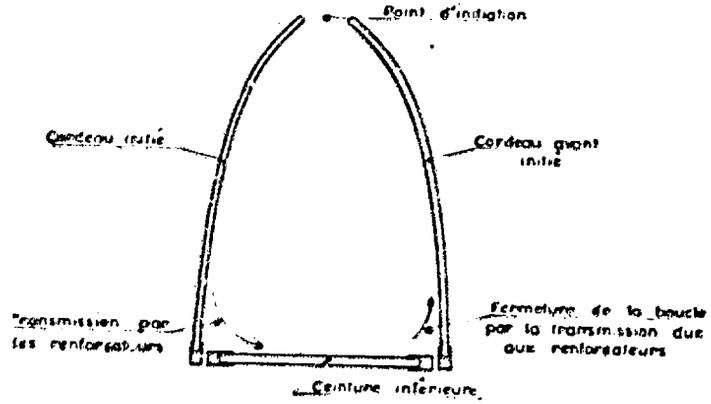

Fig. 19 Redondance obtenue par les renforçateurs de la ceinture inférieure.

ABSTRACTS - SESSION IV PRODUCTION TECHNIQUES

IV-1 The Laser Welding of Miniature Explosive Detonators — Joseph A. Barrett, C.R. Hargreaves

The hermetic sealing of miniature explosive devices, especially detonators, has been extremely difficult to achieve on a mass production basis. The term "miniature" refers to devices whose external dimensions are approximately 0.125 diameter by 0.250" long, or even smaller. The article describes the normal processes used to produce truly hermetic seals - soldering, overlapping spot welding, percussive welding, electron beam welding - and presents the engineering problems which are associated with each process when related to sealing miniature devices. Discussed in particular are a detonator 0.100" diameter x 0.250 long, extremely efficient in output, with the potential for high rates of production. Its size ordinarily would preclude any of the forementioned processes in sealing. The laser weld accomplishes the seal very reliably (test data is included).

IV-2 Welding of Aluminum With Linear Ribbon Explosives — Laurence J. Bement

Explosive welding of aluminum alloys, 1100, 6061, 2024, 2024-Alclad, and any combination has been accomplished with lead-sheathed RDX linear ribbon explosive. The amount of explosive used to accomplish welding, 25 grains/foot or less, is much smaller than any other explosive welding technique, comparing the amount of explosive required per thickness of metal to be welded. An experimental program was conducted to evaluate the effects of variables, such as explosive quantity, metal thicknesses, standoff, surface finish, etc. Highly successful bonding has been achieved in aluminum thicknesses from 0.02 to 0.10 inch, producing strengths approaching that of the parent metal.

IV-3 Modernization of Detonator Manufacture — Stanley M. Adelman

The processing of primary explosives and their incorporation into detonators is currently based on techniques and equipment which date back thirty or more years. Due to inherent resistance to change and the sensitive nature of the explosive materials, none of the high-volume, automated techniques common in other industries have been extensively utilized in the detonator industry. Picatinny Arsenal is currently engaged in a program to modernize techniques, processes and equipment so that detonator manufacture can be performed at high rates with uniform products and minimum exposure of personnel to hazardous materials and operations. Various approaches toward this end are presented and a possible facility of the future is described.

IV-4 Injection Molding of Explosives — Ron R. Vigneault, Jack Sherman

A process and explosive for injecting a material of booster sensitivity into very small diameter columns and grooves has been developed and is being used in some Navy fuzing systems. After loading of explosives, the columns have been initiated and propagated through their entire lengths. The explosive has been injected into stainless steel, aluminum, plastic and rubber heavy-wall tubes. These tubes had an inside diameter ranging from 0.030 to 0.060. Pressures required to perform this was 750 PSI to 20,000 PSI. In the 0.060 inside diameter tube, the explosive has been injected for a length of 24 inches; in the 0.030 inside diameter tube for a length of 21 inches. The explosive has also been successfully injected into open grooves, giving a printed circuit type of geometry. It has also been possible to get this explosive to detonate in very thin columns unconfined.

IV-5 Design of Manifolds for Explosive Transmission Lines — Paul B. Tweed

This paper discusses the successful design of low-cost, lightweight, rugged explosive and non-explosive manifolds for explosive transmission lines. Designs of manifolds with single and multiple outputs for a variety of transmission line characteristics are discussed. Pitfalls that should be avoided during the design, performance and safety-testing phases are described. Novel procedures for testing the gap which the transmission line booster will jump are given. Results of severe environmental testing of manifolds are also given.

IV-6 A Simplified Approach to Parachute Mortar Design — J.W. Drexelius, M.L. Schirmel

A design technique is described for avoiding the complicated ballistics and lengthy testing normally associated with high-low propellant systems. The method, based on use of ignition granules as the energy source, is illustrated by means of McDonnell Aircraft Company programs requiring parachute ejection. Design, operation and ballistic comparisons are made between the two approaches to parachute mortar development.

IV-7 Replacement of SR 4990 by Barium Styphnate in the MK 24 Actuator — S. Urman

This paper describes the experimental work involved in finding a replacement for duPont SR 4990, a single-base propellant used in Navy explosive actuators. Due to difficulties in the manufacturing processes, this powder is no longer produced. Candidate materials were first screened using a pressure bomb apparatus, and then tried in the Mk 24 Actuator. Test results showed that, of the materials tested, barium styphnate is the best substitute for use in the Mk 24 Actuator.

IV-8 Smoke Generation from Castable Pyrotechnic Compositions

H. Joseph Zilcosky

A pour castable or extrudable, polymer fueled composition has been developed for disseminating chlorobenzalmolonitrile. Expanded design versatility, simplified processing, increased safety, and excellent dissemination efficiencies are accomplished with this composition. Caseless munitions have been developed using this composition. They function without flaming or surface inhibitors. The process of deflagration appears to occur without a gas phase flame. The combustion process is discussed and thermocouple traces are shown.

IV-1-(46) "THE LASER WELDING OF MINIATURE EXPLOSIVE DETONATORS"

Co-Authors:

Joseph A. Barrett
Atlas Chemical Ind., Inc.
Tamaqua, Pa.

Charles R. Hargreaves
Government & Aeronautical
Products Division
Honeywell Inc.
Hopkins, Minn.

Enrique Bernal G. and John F. Ready
Corporate Research Center
Honeywell Inc., Hopkins, Minn.

A. Introduction

The hermetic sealing of miniature explosive devices such as detonators, small igniters, actuators, etc., has been extremely difficult to achieve on a mass production basis with a high degree of reliability and simplicity.

The term "miniature" here refers to explosive devices whose external dimensions are approximately 0.125" diameter by 0.250" length or smaller.

The normal processes used to produce truly hermetic seals - i.e. - seals whose leak rates are less than 1×10^{-8} cc/sec of tracer gas at one atmosphere differential - present engineering problems that are very difficult to overcome or control in mass production. The term mass production is stressed because under lab controlled conditions, it is sometimes possible to achieve reliable seals which are not reproducible in high volume. The advent of the laser has given pyrotechnic designers a tool which has produced a breakthrough in achieving a hermetic seal combining integrity, strength and ease of manufacture. This is especially true in regard to miniature detonator design and manufacture.

To appreciate the engineering and production problems in manufacturing very small explosive devices, we shall discuss the conventional processes briefly, pointing out their advantages and disadvantages.

We shall then describe the physical processes by which high power laser radiation interacts with metallic surfaces and produces a fusion zone which propagates into the material. We shall point out the advantages of the laser for making seals on miniature devices and show how it overcomes the problems with competing techniques, at no sacrifice in quality and reliability.

We shall then describe the choice of laser and discuss its properties. Finally, the properties of the laser-welded devices will be presented.

B. Conventional Sealing

Soldering

Soldering has been used for years to produce hermetic seals which are both reliable and mass producible. The ordnance industry has designed countless devices in which the hermetic seal is made by soldering a glass-to-metal sealed header to a suitable can containing explosive. See Figure 1. Typical dimensions for devices for which soldering is practical are a diameter D of 0.3" and height of 0.5". There is a distance Z around 0.25" from the joint to the explosive.

Usually the solder joint is made in a high frequency induction coil with thickness around 0.125", using solder preforms and a non-corrosive resin flux. A properly fixtured process can yield 1000 to 10000 devices per shift. For miniature devices, soldering has several disadvantages.

1) Even though the induction heating technique can be controlled within localized areas for minimum heat transfer, the process eventually becomes mass limiting, i.e. a point is reached where the entire mass of the device being soldered heats to some dangerous level, regardless of the local control on heating or optimum conduction away from the heat zone. When the dimension Z becomes smaller than the thickness of the induction coil, it is difficult to make this joint without firing the explosive.
2) Under normal conditions, soldering requires that the materials being sealed are truly solderable metals such as tin, copper, brass or other copper alloys. In lieu of this, base metals must be plated with a suitable alloying material such as tin, nickel or gold.

Electron Beam Welding

Electron beam welding has been used for production of ordnance products for approximately ten years. Structural welds providing hermetic seals can be made, with the beam focused to provide very high energy density in small localized weld zones. Thus, heat transfer can be minimized. Seam welds can be made around the periphery of a typical detonator designed as shown in Figure 2 with a diameter of 0.3".

The disadvantages of EB welding for miniature ordnance devices are:

1) The necessity of welding in a vacuum lengthens weld cycle rates and makes fixturing difficult. Some work has been done on welding out of vacuum but this involves an increase in beam diameter and decrease of power density.
2) In the dual phase process of continuous electron beam welding, some of the material being welded is first vaporized and escapes the weld zone. Re-solidification of the melted portion occurs in the hole created by vaporization and is generally not 100% complete. In fact, it can be uneven, porous and raised above the pre-welded surface levels. A time-consuming practice is to make a second pass with a defocused beam to smooth over the first weld area.
3) A third and major reason why EB welding cannot be successfully employed on devices of the size under discussion here lies in the geometrical shape of the weld - a cone - and its depth. To make a localized seam weld, the weld beam must follow a seam gap of perhaps .001-.003" thickness. To insure proper overlap to cover this gap the EB weld must penetrate to a depth of approximately 0.010". A typical profile of an electron beam weld is shown in the inset of Figure 2. At this depth, the thermal energy imparted to a small device, however localized, is quite high and sufficient to auto-ignite most common explosives.

Overlapping Spot & Ultrasonic Welding

These are two other well-recognized and reliable means of hermetic joining. In order to make either type of weld, it is necessary to apply a force to the weld zone. See Figure 3. For a miniature device with a typical case wall thickness of 0.010", the small area on which the force can be applied presents a very tricky positioning problem for a ring weld. In addition, applying a force axially parallel to the wall of the case would tend to collapse this thin wall. In order to roll a seam weld on the side of the case and header with either process, the surfaces must be relatively co-planar. If they differ by 0.001-0.003", the weld can be uneven and non-hermetic.

Adhesive Sealing

Sealing with adhesives such as epoxies, polyurethanes or silicone rubber has been used for ordnance products.

For the present application, a match of the coefficients of thermal expansion is preferred; both the header and can should expand and/or contract at the same rate. When this is achieved a hermetic seal can also be achieved. However, our experience has shown that those adhesives which produce good stable hermetic seals generally are chemically incompatible with the initiation mix. There is some debate as to whether this is in itself a valid objection to adhesives, since it is possible to isolate the adhesive from the explosive cavity. Nonetheless, it is exceedingly difficult to predict adhesive long term storage effects - especially when in contact with other elements in an assembly which can volatize reactive gases over long periods.

C. Laser Welding

The laser can deliver extremely high power densities to localized areas of a workpiece. The radiation can be collected efficiently by a simple lens system and focused to an area with a diameter around 0.010". Small focal areas can be obtained under laboratory conditions, but in a production environment, it becomes difficult to obtain reproducible focal diameters much less than 0.010". The peak power available from common pulsed commercial lasers ranges upward from 10^5 watts. This means that power densities in excess of 10^9 watt/in^2 can be obtained easily.

The laser can thus deliver much higher levels of power density than any other technique. Only the electron beam is comparable in this respect.

The incident light is absorbed near the surface of the metallic workpiece, and is converted into thermal energy. The diffusion of the thermal energy into the metal is governed by conventional heat conduction. The high power density delivered by the laser beam quickly heats the metallic surface to its melting point. At easily attainable laser power densities, it may take less than one microsecond for the surface to begin melting. Thereafter, a fusion front propagates into the metal. The velocity of the fusion front depends on the thermal properties of the material. The scale depth D for penetration of heat into a metal of thermal diffusivity k is approximately:

$$D = (4\ k\ t)^{1/2}$$

where t is the time scale of interest. For a thermal diffusivity of 0.007 in^2/sec, a typical value for stainless steels, and a time duration of 10^{-4} seconds, a typical value for laser pulses, one obtains D = 0.002". Thus, the depth of penetration of heat into stainless steel is limited. For metals of higher thermal conductivity, D will be somewhat larger, but still may be of the order of 0.010". Thus, the depth of the weld nugget produced by the laser beam is limited by the ability of the heat energy to be conducted into the workpiece. Typical laser welds tend to be shallow, 50 mils or less for a laser emitting a few hundred watts.

One might expect to increase weld depth by increasing power. However, one desires maximum melting under conditions where surface vaporization does not occur. Melting without vaporization is produced only within a narrow range of laser parameters. If the laser power density is too high, the surface begins to vaporize before a significant depth of molten material is produced. This means that there is a maximum power density suitable for welding applications.

D. Advantages of Laser Welding

The laser offers a non-contact process with extremely localized heat deposition. As previously mentioned, the fusion zone is small compared to other methods of welding, and the heat-affected zone surrounding the weld nugget is extremely narrow. This means that laser welds can be made on miniature devices without degradation or detonation of the explosive. The dimension Z in Figure 1 can be made smaller than for the other welding methods.

Laser welding does not exhibit the difficulties presented by solder joining. Proper optical techniques can focus a laser beam to a spot as small as 0.010" in diameter with no difficulty. Thus, the weld heat zone is very localized and little mass heating occurs. In the device shown in Figure 2, the weld zone is only 0.020-0.030" away from the explosive, but no auto-ignition occurs. In addition, the wide selection of laser pulse durations, wavelengths, and beam energies allows most common metals to be joined with no plating needed. Welding occurs easily in most ferrous metals, especially in stainless steels. Good weld joints can also be made with facility in aluminum and in a number of aluminum alloys.

The electron beam technique is the one most directly comparable to laser welding. Both are energy beam techniques, in which the energy is delivered at high power density to a localized area, without direct contact of the welder to the workpiece. Both methods can make seam welds very readily. Note the shape of the welds as shown in Figure 2. An EB weld is cone-shaped. Its depth is roughly equal to its width, normally about 0.010" for explosive devices. The laser weld zone is crescent shaped. The depth of penetration can be as little as 0.002-0.003", and the width can be 0.005-0.015". Thermal effects outside the weld zone are very minimal. The laser weld is not structurally equal to the EB weld but it has adequate strength for detonators.

Because a pulsed type laser can produce high peak powers at short pulse lengths, it is possible to prevent deep vaporization. The weld zone first melts with minor surface vaporization, then quickly resolidifies so that no metal is lost in the process. The penetration is minimized and, consequently, thermal input is kept low outside the weld zone.

There is no need to weld in a vacuum with the laser; a stream of inert gas passes over the weld zone. Laser welding can thus be done at extremely high rates, both for continuous welding in inches/second and in relation to work cycles or operations produced per second. A typical cylindrical weld, for example, on a part 0.100" in diameter will take approximately 1.0 second to complete with either an electron beam or laser. The major difference is that with the proper feed mechanisms, of a very simple, unsophisticated nature, parts can be laser welded at rates of 10,000 to 15,000 parts in a normal eight hour shift, while the same part welded by electron beam may only approach 1,000 to 2,000 per shift, primarily because of the idle time pulling a high vacuum in the welding chamber and problems in feeding the welder because of vacuum chamber restrictions.

Table I compares the capabilities of laser welding of miniature detonators with the other sealing methods described in Section B.

TABLE I Comparison of Sealing Method for Miniature Devices

	Laser Weld	Solder Joint	Electron Beam Weld	Overlapping Spot and Ultrasonic	Adhesive Sealing
Production of stable hermetic seal	Good	Good	Good	Good	Poor*
Localization of heat	Best	Poor	Good	Good	----
Preservation of explosives from degradation during sealing	Best	Poor	Not Completely	Fair	Fair
Operation in atmosphere	Inert gas	Air	Vacuum	Air	Air
Ability to seal many metals	Good	Poor	Good	Poor	Fair
Applicability to high volume production	Good	Good	Fair	Fair	Fair
Applicability to miniature devices	Good	Poor	Poor	Fair	Fair
Method requires no contact nor forces applied	Yes	No	Yes	No	No
Relative cost	Low	Moderate	Very high	Moderate	Moderate
Initial investment	Relatively high	Moderate	Very high	Moderate	Nil

* Sealant - explosive compatibility problem.

E. Choice of Laser

There are only four types of laser which have developed sufficiently to be considered for metalworking applications. They are: (a) The ruby laser operating at a wavelength of 0.6943 microns in the red portion of the visible spectrum. (b) The neodymium--glass laser, operating in the near infrared at 1.06 microns. (c) The neodymium--YAG laser (yttrium aluminum garnet doped with the rare earth element, neodymium) also operating at 1.06 microns. (d) The CO_2 laser (really a CO_2-N_2-He laser) operating at 10.6 microns, fairly far in the infrared.

The ruby and neodymium--glass lasers both have good capability for making spot welds, and many welding studies using these lasers have been performed. Seams can be made by overlapping spots, but the speed is much too low for the present application.

Both the neodymium--YAG and the CO_2 laser can be operated at average power levels of 100 watts or more. These levels are capable of producing seam welds at reasonably high rates. Seam welding has in fact been demonstrated in thin metallic samples with both the CO_2 laser and the neodymium--YAG laser. For example, seam welding at a rate of 300 inches/minute is possible in 0.010" thick stainless steel. For welding applications, a CO_2 laser and a neodymium--YAG laser operating at comparable levels of output power will probably have about equal capabilities.

For our work, we have used the CO_2 laser. At the present time, the CO_2 laser appears to offer better economy, both in initial cost and in operating expense, as compared to a neodymium--YAG laser of equal welding capability. In addition, safety for the operator is easier to provide with a CO_2 laser. The entire work station may be enclosed in Lucite, which is opaque at 10.6 microns. This allows the operator to view the operation, but does not allow the laser light to escape.

There are two types of CO_2 lasers capable of seam welding; the continuous CO_2 laser operating at output levels up to a few hundred watts; and the repetitively pulsed CO_2 laser, operating at an average power level around 100 watts. In

our judgment, the repetitively pulsed CO_2 laser can weld at higher speeds than a continuous CO_2 laser of comparable average power level. This occurs because the high peak power pulse can break down the surface reflectivity of the metal, which is originally high at 10.6 microns, so that the energy is absorbed more effectively in the workpiece.

Accordingly, for this work, we employed a repetitively pulsed CO_2 laser, with the capability of emitting an average power of 75 watts.

F. Laser Welding of 1DT154 Detonator

Atlas Chemical Industries in cooporation with Honeywell Inc. has designed a detonator (the 1DT154 miniature detonator) with an envelope size of 0.100" diameter by 0.250" long. The size of this small detonator ordinarily would preclude the use of conventional sealing processes. The hermetic sealing was accomplished by using a CO_2 laser to weld a glass-to-metal-sealed header to a can containing the high explosive. The can and header typically were 302 stainless steel, but use of other metals is possible. This design was made possible because the laser beam making the weld could be precisely positioned and the welding spot diameter controlled to as little as 0.005" diameter and 0.003" depth. These latter features localized the heat generated by the weld to a tightly controlled area. The weld itself is produced by operation of a CO_2 laser in the repetitively pulsed mode. The pulse energies fell in the 0.1 to 0.3 joule/pulse range and duration was approximately forty (40) microseconds. The beam produces individual, overlapping spots of metal melt which resolidify to form a homogenous weld area. A seam weld made by such a laser is shown in Figure 4. In this photograph, the header is at the top and the seam lies around the periphery of the can, just below the header, and the can containing the explosive is at the bottom. The width of this seam is approximately 0.015". The marks made by the overlapping of pulses are visible.

The welds are truly hermetic and have enabled the device to withstand such adverse environments as a 28 day T&H cycling per MIL-STD-331, 13,000 g shock in any direction, thermal shock alternating continuously between -65°F and +160°F and a number of other tests which are summarized in Table II.

The detonator was designed under an Air Force contract for Honeywell, Incorporated. It has undergone formal qualification testing for this system and has successfully performed on all qualification requirements. Some of its features are as follows:

1) All fire - 1.6 volts from a 100 microfarad capacitor (approximately 1300 ergs).
2) Output -
   a. Will produce a 0.007" minimum dent in steel of R/b 85-90 at a standoff of 0.150".
   b. Will initiate a HMX booster (lead) over an airgap of 0.150" min. This gap can be as much as 0.225, although the reliability at this level has not been demonstrated.
3) Functioning Time - Approximately 150 microseconds at the all fire level.
4) Hermetic seal - 1×10^{-8} cc/sec at one atm differential.

TABLE II
1DT154 Qualification Testing

Test Req'd.	No. Test	Failures	Results
All-Fire	530	0	All functioned
Steel Dent Output	290	0	$\bar{X}$=.0286 High - .038 Low - .015
Booster Initiation	240	1*	$\bar{X}$=.0874 High - .097 Low - .082
28 Day T&H (MIL-STD-331, Test 105) -65°F to 160°F	140	0	Steel Dent $\bar{X}$=.092 High - .038 Low - .020 Booster Initiation $\bar{X}$=.0878 High - .097 Low - .082
56 Day Temp. Storage (MIL-STD-331, Test 112) -65°F to 160°F	100	0	Steel Dent $\bar{X}$=.0876 High - .034 Low - .015 Booster Initiation $\bar{X}$=.0876 High - .095 Low - .083
Thermal Shock (MIL-STD-331, Test 113) -65°F to 160°F	50	0	Steel Dent $\bar{X}$=.0281 High - .038 Low - .020
Leak Test (MIL-STD-202, Method 112A) Max. Leak Rate - 1×10^{-8} atm cc/sec	260	0	

*Failure attributed to low priming charge.

A cross section of the laser weld is shown in Figure 4, at 370 X magnification (1). The weld was etched in equal parts potassium cyanide (10%) and ammonium persulfate (10%), followed by diluted Marble's reagent. The weld nugget has dimensions of 0.010" by 0.003". The appearance of the weld nugget indicates the rapidity of the process. The material appears to have been turbulently intermixed. The grain size in the weld nugget is very small. The weld cross section does not appear so neat as those of welds made by other techniques. However, the strength of the weld joint is high, and the required hermetic seal is provided.

The laser used in the development and initial production of these detonators was a 75 watt, Model 130 Superpulsed CO_2 Laser, supplied by Photon Sources, Incorporated, of Plymouth, Michigan. It was supplied to Atlas by Honeywell and since this program it has been relocated in Honeywell's Metallurgical Laboratory at Hopkins, Minnesota. This equipment was selected because of its ability to be used on a multi-shift per day production basis without significant downtime. It can perform the required welds with a minimum of unwanted thermal input.

The laser is manufactured to JIC electrical/electronic specifications so that a plant electrician was qualified to perform routine maintenance. Additional operating economics were achieved because the Model 130 Laser used individual cylinders of helium, nitrogen and carbon-dioxide in place of more expensive pre-mixed gas. Installation costs were minimized because the equipment was used in the same environment as any conventional machine tool.

5. Conclusion

Laser welding offers significant advantages over conventional techniques for hermetic sealing of miniature detonators. A repetitively pulsed CO_2 laser has been employed in this work and has produced devices which meet the required standards. The laser weld is made within 0.030" of a temperature-sensitive primary explosive. With proper fixturing, automated production at high volume rates is possible. Safety can be provided for the operator and the CO_2 laser either by remote operation or by shielding.

Reference: (1) Industrial Applications of Lasers, by J.F. Ready, Paper 3.5, presented at the 1971 IEEE/OSA Conference on Laser Engineering and Applications, Washington D.C., June 2-4, 1971.

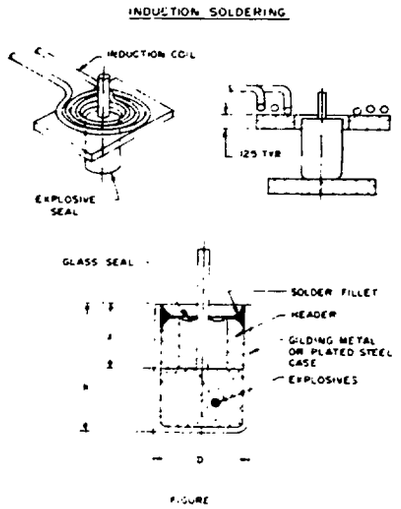

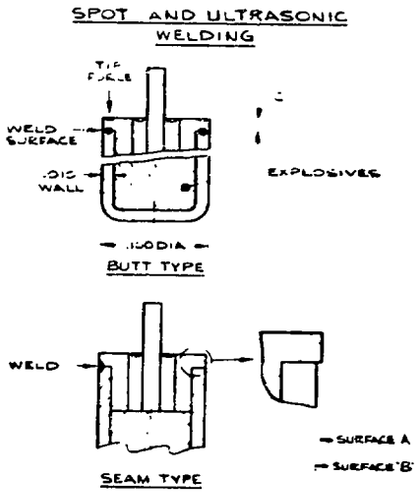

FIGURE 3

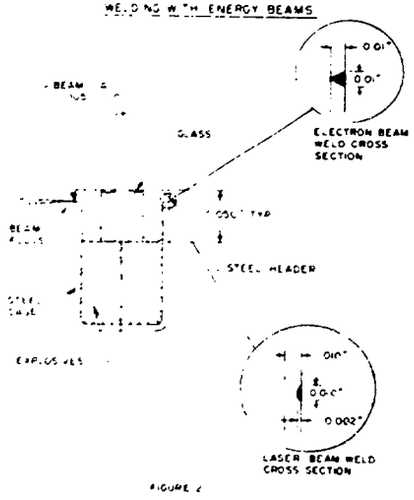

Figure 4. A sample from Photon Source's qualification test consisting of 370 samples. Etchant: Equal parts Potassium cyanide (10%) and Ammonium persulfate (10%) followed by diluted Marble's Reagent. Magnification 370X

Figure 5. DF364 Detonator

IV-2. WELDING OF ALUMINUM WITH LINEAR RIBBON EXPLOSIVES

By Laurence J. Bement
NASA - Langley

INTRODUCTION

Explosive welding was introduced in the 1950's as the "ultimate fabrication technique," since it provided a method of joining dissimilar metals that were difficult if not impossible to join with conventional welding techniques. This was later shown to be a gross overstatement, due primarily to the dynamics of the explosive-driver process. However, the advantages of joining dissimilar metals, maintaining the material properties, and lack of expense of materials and apparatus have maintained the interest and support for this fabrication technique. With the advent of highly complex aerospace structural and fabrication requirements the use of explosive welding is a highly promising tool to complement existing fabrication techniques.

The actual explosive welding process, as described in Reference 1, is a complex, high-pressure oblique angle collision of two metal plates which causes a jetting action. The basic mechanism of the metallurgical bonding jetting process have not been exactly determined. To quote from the generally accepted theory, Reference 1, "A jetting collision is defined as an oblique collision in which the plate velocity, pressure, collision angle and collision point velocity are controlled such that a jet or spray of metal is formed at the apex of the collision and is forced outward from between the colliding plates at very high velocities. A jet is pictured in the oblique collision shown in Figure 1." The explosive welding process strips off both surfaces due to the collision of the plates, and the high pressures produced by the impact forces the now clean surfaces into intimate contact to achieve metallurgical, inter-atomic bonding.

Explosive welding applications have been generally oriented toward the bonding of areas; the largest being several hundred square feet. The explosives used in this application are commonly termed "bulk" explosives, and are generally measured in weight per unit area. These bulk explosives, such as TNT (trinitrotoluene), nitroguanidine pentolite, composition 4, and a series of dynamites, are generally packed by hand onto the area to be welded. Their detonation velocities have a range from 4,000 to 12,000 feet/second. A second type of commonly-used explosive with a detonation velocity over 20,000 feet/second is Dupont's Detasheet which is PETN (pentaerythritoltetranitrate) in a rubber binder. An example of the explosive welding of 0.25 inch aluminum is given in Reference 2. Two loads of Detasheet were used to accomplish a 1 x 24 inch weld; a 6 x 24 inch quantity of 0.5 grams/square inch (7.7 grains/square inch), and a 1 x 24 inch area of 2.5 grams/square inch, (28.5 grains/square inch) on the centerline of the weld area.

Present success in the field of explosive welding has been empirical, and attempts to analytically predict success and describe the characteristic wavy interface of explosive welding have met with little success. Difficulty has been experienced in making long, continuous welds in small area bonds, such as below one-half inch in width. The problems encountered are in minimizing the explosive quantity; in the workability of the explosive to prevent damage, or breakage, in these minimum quantities, and in maintaining detonation propagation. Also, many existing welding techniques rely on bending the metal driven by the explosive to preset angles to establish the jetting collision. This report describes a unique, simplified technique

of welding aluminum alloys up to 0.125 inch thick using linear ribbon RDX explosives in quantities from 7 to 25 grains per running foot.

PROCEDURES

The concept of explosive welding generated at Langley Research Center is a simplified technique of lap welding aluminum alloys, utilizing the explosive output of very small quantities of ribbon explosives. The ribbon explosive is lead-sheathed RDX (cyclotrimethylenetrinitramine), rolled to very thin dimensions. The dimensions of the explosives, which includes the lead sheath, for the various core loadings in grains per running foot are shown in Table 1. The velocity of propagation of this material averages 26,000 feet per second. The step by step procedure in its simplest approach developed for this welding process follows: See Figure 2.

1. Chemically clean all surfaces (except for commercially pure aluminums) to remove oxides.
2. Provide a 0.010 inch standoff to separate the plates. Two layers of masking tape separated by one-inch were used for this demonstration.
3. Place the plate to be welded across the masking tape, paralleling the base plate.
4. Place the ribbon explosive in the center of the gap formed by the tape, and tape into position. Longer lengths of explosive than that shown in the sketch are necessary to prevent damage to the weld area by the blasting cap used to initiate the explosive.
5. Initiate the explosive.

The actual mechanism of the colliding plates which produces the jetting action is shown in Figure 3. This process produces a jet that is ± 60 to 75° from the direction of the detonation propagation which can be explained as follows:

1. Since the linear explosive detonation velocity is higher than the sonic velocity of the aluminum (approximately, 17,000 feet/second) neither jetting nor welding will occur in the direction of detonation (See Reference 1). The metal is simply driven down and impacts the base plate.
2. The high pressure (several million psi) of the explosion continues to drive down the plate, and the jet-producing impact angle and velocities are established to the side.

A photograph of the jet streaks and a one-inch weld in 0.040 inch 2024-0 aluminum is shown in Figure 4. The area that was bonded has a shiny appearance. Since the jet is to the side, a localized event, the length of the weld in the direction of detonation is unlimited.

The weld strengths were evaluated in this study by pulling them in shear as shown in Figure 2b. All welds were conducted under laboratory atmosphere, except for a series conducted on the Alclads at a vacuum of 2×10^{-5} torr.

The widths of the parallel bond areas of the explosive weld, as well as the ultimate weld strengths are influenced by the following major variables:

1. Standoff - (separation between plates)
2. Plate thickness
3. Explosive quantity

4. Plate surface cleanliness and smoothness
5. Supporting structures (anvils)
6. Buffer materials between the explosive and plates to minimize indentations.

Experiments were conducted on each of these variables to determine their optimum values.

The possible length limitation of this explosive welding technique was investigated by welding a twelve foot length of 0.063 inch 2024-T3 Alclad to 0.250 inch 2024-T3 Alclad with a 20 grain/foot ribbon explosive. The total explosive quantity used for this weld was 240 grains, or 0.55 ounces, less than two tablespoonsful of explosive. Five one-inch wide samples were taken at six intervals down the length of the weld.

As a rough indication of the pressure integrity of these welds, three 0.040 inch and one 0.063 inch 2024-T3 Alclad plates were welded to 0.5 x 3 x 3 inch 6061-0 blocks that contained a threaded port as shown in Figure 5. The interface created between the plates was pressurized with dry nitrogen to pressure failure.

To demonstrate the fabrication feasibility of this welding technique, an eighteen inch diameter model of a space station-type structure was constructed of 0.040 inch 2024-T3 Alclad sheet, four 0.125 x 0.75 inch 6061-0 angles and three 25 x 0.50 inch, eighteen inch diameter 6061-0 rings. Two portholes were constructed by welding sheets of 0.03 inch plexiglass between the skin and a 0.125 inch plate. Seven grains/foot linear explosive was used in this construction.

RESULTS

The weld strengths measured to date for a range of alloys in this continuing study are shown in Table 2. Coupon thicknesses from 0.033 to 0.125 inch were welded to 0.250 inch base plates. Welding success was achieved using any combination of the following alloys: 2024-T3 Alclad, 2024-0, 6061-0, 7075-0 and 1100, as well as 6061-T6 to 6061-T6, and 7075-T6 to 6061-T6. The one-inch coupons are listed in the thicknesses tested, followed by the average ultimate tensile strength of the coupon, the quantity of explosive used in the welding process, and the maximums, averages and minimums with their standard deviations appearing above the averages. The average weld strengths were as high as 90% of the coupon tensile strengths for one group. The largest standard deviation for any group was 25% of its average value. The weld series having the highest strength in this study was the 7075-T6 to 6061-T6 combination which had an average value of 2685 pounds/linear inch. There was no appreciable effect of vacuum on welding performance.

In the analysis of the variables, the following results were obtained:

1. Standoff - the 0.010 inch fixed standoff appeared to be optimum, since no higher strengths could be obtained and larger standoffs produced larger plate bending and distortion.
2. Plate thicknesses - difficulty was experienced in welding when the base plate was not at least twice the thickness of the plate to be welded.
3. Explosive quantity - the objective was to use the explosive quantity to maximize the bond area, but minimize the indentation caused by the explosive pressure. Table 1 shows the explosive determined optimim for each thickness and alloy.

4. Surface cleanliness and smoothness - the aluminum alloys were chemically cleaned to remove oxide layers which exhibit considerably different physical properties of hardness and ductility than the parent alloys. However, little change in weld strength was observed in welding metals that had been aged several days. The pure aluminums, including the Alclads, were merely wiped clean with alcohol. In general, the smoother surfaces yielded the strongest welds. The jetting process would skip over scratches as little as 0.002 inch deep.

5. Supporting structures (anvils) - the indentations in the base plate caused by the explosive pressure were minimized through the use of 0.5 and 1.0-inch 2024-T4 anvils. Successful welds could be made on base plates that were suspended with tape. However, the base plate was bent to approximately a 15° angle. The weld strengths were improved through the use of anvils, by the absorption of internal damaging shock waves. (See Reference 1) For example, the weld strength of 0.063 inch 2024-T3 Alclad to 0.250 inch 2024-T3 Alclad was improved by 5% by using a one-inch 2024-T4 anvil. All the welds shown in Table 2 were made on a one-inch 2024-T4 anvil.

6. Buffer materials - several buffers were attempted, such as masking tape, aluminum foil, and steel sheet stock. The masking tape proved to be the most efficient; a 0.020-inch layer increased the average weld strength of 0.063-inch 6061-0 coupons from 1095 to 1239 pounds, a factor of 13%.

The twelve foot weld exhibited excellent uniformity in shear strength down the entire length. The six groups had average shear strengths of 2725, 2515, 2810, 2715, and 2455 pounds. An average for all thirty samples was 2663 pounds with a standard deviation of 322.

The pressure tests of the .040 inch 2024-T3 Alclad plates welded to 0.5 x 3 inch 6061 blocks produced brusts through the middle of the welds at 1300, 1350 and 1525 psi. One of these three was held at 1000 psi for several minutes with no appreciable leakage. The 0.063 inch 2024-T3 Alclad plate was pressurized to 1950 psi without any indication of leakage or burst.

The space station-type model fabrication was successful, as shown in Figure 6. The estimated average weld strengths are greater than 1000 pounds per linear inch.

CONCLUSIONS

This report describes a small-scale simplified, parallel plate process of welding aluminum with very small quantities of lead sheathed linear ribbon RDX explosive. The largest explosive quantity utilized in this study was 25 grains/foot in the welding of 0.125 inch aluminum. The explosive welding setup in its simplest configuration requires only masking tape to establish the standoff separation between plates, to act as a buffer to prevent explosive damage to the plates, and to hold the components in position. The welding process is somewhat different from conventional processes in that the "jetting" caused by the high velocity impacting of the two metals to be welded are at ± 60 to 75° from the direction of detonation propagation.

The results of the welding of five different alloys 2024-T3 Alclad, 2024, 6061, 7075 and 1100 in thicknesses from 0.033 to 0.125 inch in any combination have shown that weld strengths were obtained that were up to

90% of the parent metal tensile strength. The largest standard deviation for any group of this series was 25% of its average. The strongest weld series, 0.063 inch 7075-T6 to 0.25 6061-T6 had an average shear strength of 2685 pounds/linear inch. The effect of vacuum in the welding process is negligible. The major variables of explosive welding were evaluated and optimized for this process, such as: standoff, plate thickness, explosive quantity, plate surface effects, supporting structures, and buffer materials.

The welds produced by this technique were demonstrated to have good pressure tight integrity. The fabrication feasibility of this technique was demonstrated by the construction of an eighteen inch diameter model of a space station-type structure utilizing light aluminum sheet stock, angle and rings.

The advantages of this technique are:

1. The simplicity of the parallel plate weld setup.
2. The placing of welds in small, localized, predictable areas.
3. The efficient use of very small amounts of linear explosive.
4. The flexibility and workability of the linear ribbon explosive.
5. The welding technique is apparently not length limited.

TABLE .

Cross-sectional Dimensions of Linear Ribbon PDX Explosive

Explosive Load grains/foot	Thickness inch	Width inch
7	.12	0.220
10	.12	0.300
15	.125	0.315
20	.13	.365
25	.135	0.370

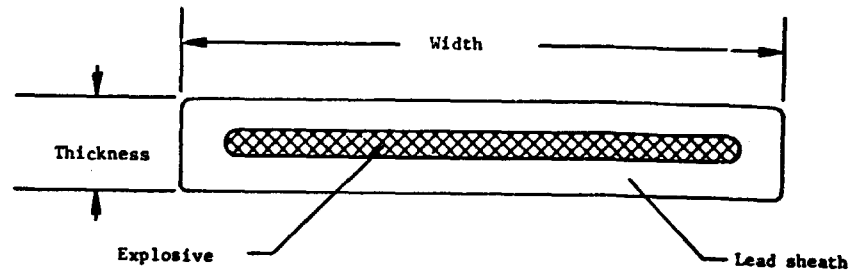

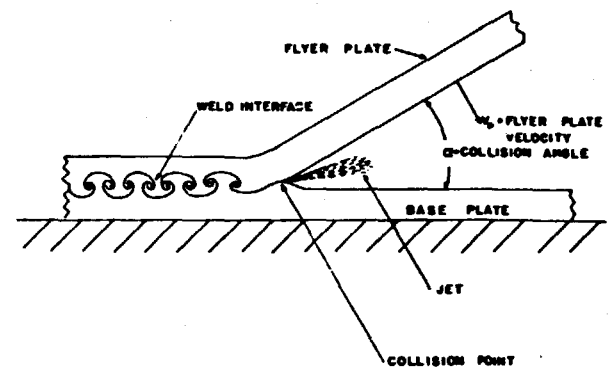

Figure . Schematic of an Oblique Collision of Metal Plates Like That Obtained in an Explosive Welding Operation

REFERENCES

1. Carpenter, S. H.; and Wittman, R. H.: "The Theory and Application of Explosive Welding" The University of Denver
2. Lindbergh, C.; and Currin, D.: "Maintenance and Repair of Expeditionary and Theater Operation Air Field Landing Mat Using Explosive Impulse Welding" AFWL-TR-70-160

TABLE 2.

EXPLOSIVE WELDING PERFORMANCE

Coupon Material Thickness, Inches	Explosive Weight per Square Foot, Pounds	Coupon Tensile Strength, Pounds	One-Inch Explosive Weld Strength in Pounds, Standard Deviation, Maximum/Average/Minimum — 0.25 Inch Thick Base Plate Material: 2024-T3 Alclad	2024-0	6061-0	7075-0	6061-T6
2024-T3 Alclad							
0.040	10	2325	283 2025/1655/1240				
0.063	20	4370	209 2475/2180/1430	503 3000/1950/1125	413 3100/2183/1500	345 2503/1819/1350	395 3021/2520/1650 125 gr/ft²
0.090	25	6000+	158 1600/1403/1130				
2024-0							
0.063	9	703		40 710/629/590			
0.090	10	1987		131 1510/1332/1060			
0.125	15	2585	199 1950/1654/1220	132 1530/1369/1110	169 2000/1788/1450	164 1650/1485/1240	
0.190	20	3483		244 2060/1652/1240			
6061-0							
0.190	9	730			167 750/607/500		
0.063	10	1800	43 1170/1090/1000	48 1140/1062/1000	73 1180/1095/980	53 1130/1063/925	

TABLE 2. - cont'd

EXPLOSIVE WELDING PERFORMANCE

Coupon Material Thickness, Inches	Explosive Weight per Square Foot, Pounds	Coupon Tensile Strength, Pounds	One-Inch Explosive Weld Strength in Pounds, Standard Deviation, Maximum/Average/Minimum — 0.25 Inch Thick Base Plate Material: 2024-T3 Alclad	2024-0	6061-0	7075-0	6061-T6
6061-0							
0.090	15	1980			130 1650/1430/1330		
0.125	25	3700			274 2775/2400/2025		
6061-T6							
0.063	20	4050	130 2500/2367/2150		218 3000/2693/2350	288 2300/1906/1525	165 2700/2508/2150
7075-0							
0.063	9	1120				59 1030/936/840	
0.090	10	2225	152 1793/1534/1300	110 2100/1921/1800	112 2100/1927/1775	187 2125/1838/1590	
0.125	15	2825				313 2560/2015/1400	
7075-T6							
0.063	20	5500	263 2325/1968/1600				396 3150/2685/2040 125 gr/ft²

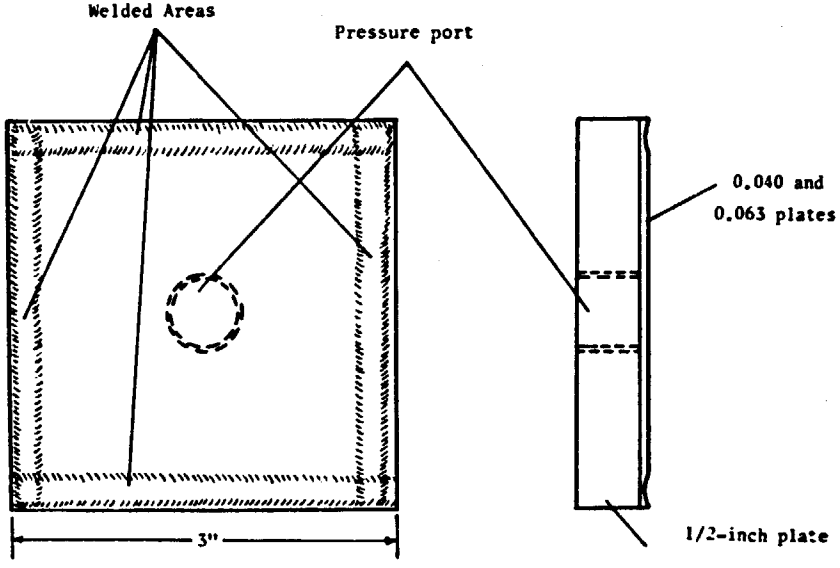

Figure 5. - Setup for pressure integrity tests

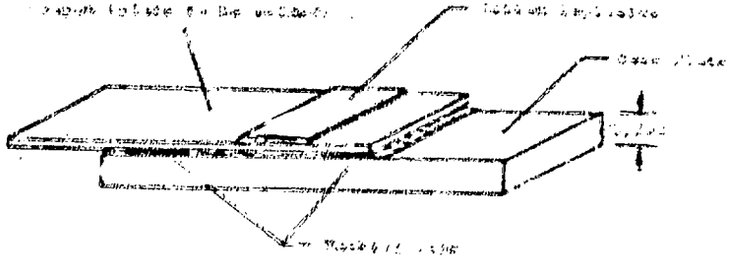

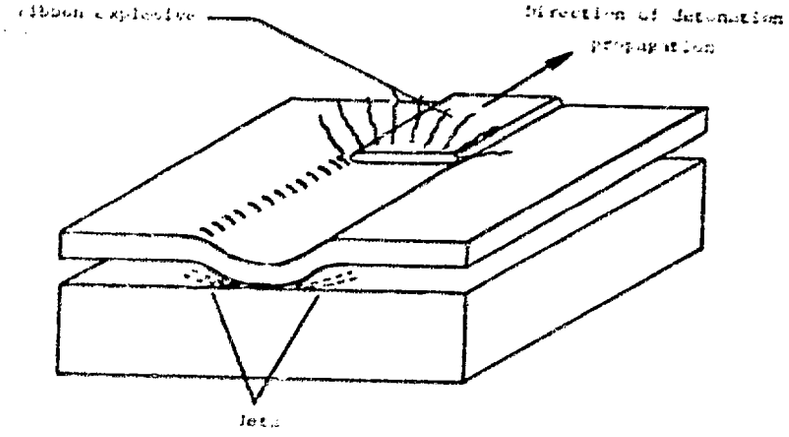

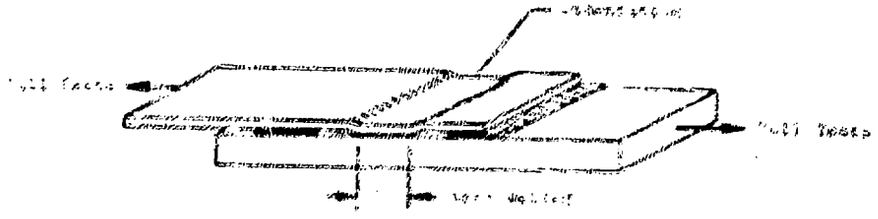

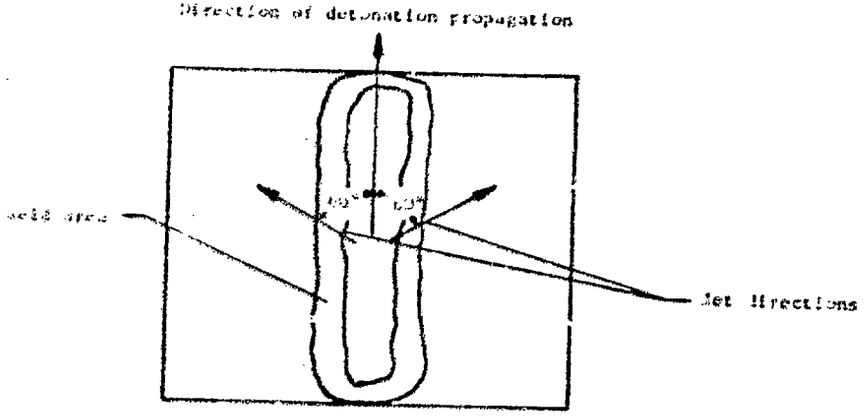

Figure 3.- Mechanism of NASA-LRC - developed explosive welding.

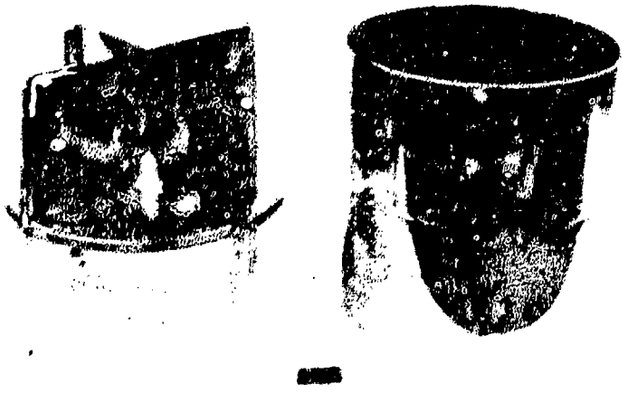

IV-3. MODERNIZATION OF DETONATOR MANUFACTURE

AUTHOR: STANLEY M. ADELMAN, ADVANCED TECHNOLOGY LABORATORY

PICATINNY ARSENAL

Current practice and facilities for processing primary explosives have not kept pace with the modernization which has taken place in other industries. We have advanced far beyond the point where the process worker would be perched on a one-legged stool to keep him properly alert, as in the 19th century; but there is still much room for improvement.

Continuous loading automatic machines such as the Jones Loader certainly constitute an advance over the manual procedures of yesteryear; but production rates are not particularly high, a disproportionate number of personnel is required and the machines lack versatility. The technology of 1970 utilized in other industries has not been applied to these operations.

The very sensitive nature of the explosive materials of course mitigates against rapid changes in technology or equipment. Safety is of paramount importance and we cannot blame the producer for reluctance to adopt new techniques when the old have resulted in few accidents. Nevertheless, projected future requirements demand that we realize the benefits to be derived from modern, automated production systems.

The goals are:

1. Vastly increased production rates and capacities
2. Quick reaction
3. Minimum downtime
4. Elimination of personnel exposure to hazardous materials and operations
5. Reduction of cost
6. Improvement of quality and uniformity of product

In an effort to attain these objectives, we have instituted a program to [illegible]nize processes and equipment and to perform all operations in one in[illegible]ated plant complex which will combine all processing of primary explosives; loading, assembly, and packout of detonators; and storage of materials and product as required. Figure 1 outlines the process flow for the Detonator Production Facility. In Figure 2 we see the site plan for this facility. A minimum of 20 acres will be required for the eight structures and linking conveyor system for the facility. Separation distances and construction features are in accordance with the latest safety requirements developed for explosive storage and handling. The only personnel required will be housed in the Control Building which will also contain a computer, automatic warehousing, controls, instrumentation and information displays. Note that the paved road is confined to the approximate periphery of the installation so that if movement on these roads should be required while the plant is in operation, a maximum of

protection is afforded pedestrian or vehicular traffic. All processes will be performed automatically under the direction of the computerized monitoring and control system with closed circuit TV surveillance of all operations. Programming will be built into the computer to permit rapid changes in process parameters, rates, choice of equipment, and test limits. Delivery of all materials to magazines and reception points will be performed on an off-shift basis. Internal movement will be by means of conveyors travelling on inclosed ramps. All buildings will be environmentally controlled.

Figure 3 shows the Back Line Building which will process as-received, desensitized primary explosive and convert it into dried, screened material suitable for loading operations. The building is divided into ten cells each designed to process 2.5 lbs. of dry material per hour. Each cell is so constructed that an interior explosion will cause only superficial damage to adjoining cells. It is possible to repair a damaged cell while operations are continued in seven cells. Desensitized explosive in its shipping container is placed on the roller conveyor which circulates the container around a protective blast wall. This blast wall will prevent the propagation of an explosion on the operating side to the explosive on the storage side and will also provide complete protection to any personnel on the storage side. A robot unloader, perhaps the one in Figure 4, moving on rails will remove the bags containing explosive from the shipping container and will measure out the required amount into reception tanks at each cell. Additional fluid will be added at this point and the resultant slurry pumped into the processing cell by means of a peristaltic pump. A rotary liquid extractor such as that in Figure 5 will remove excess fluid and dry the primary explosive. If further processing is required, an internal conveyor will pass the material through the equipment required. Several programs are currently under way to develop equipment for automatic processing. At the end of the process cycle the dry material will pass through a blast lock and will be placed onto the main conveyor.

The conveyor will link the Back Line Building with both the Blender Building and the Intermediate Storage Building. The Blender Building (shown in Figure 6) will consist of two cells so constructed that an explosion in one cell will leave the other intact. The process under investigation for installation in this building is the continuous pneumatic mixing of reactive ingredients developed at the Naval Ordnance Station, Indian Head, Maryland. This process (diagrammed in Figure 7) mixes ingredients as they flow at high velocity while dispersed in an inert gas. As a result of the gas dilution very small amounts of explosive material are in process at a given time. There are no mechanical moving parts, production rates are high, design is simple and product homogenity is very good. We are attempting to adopt this technique to the blending of primer mixes. If this should not be possible, alternatives are being explored for the improvement of conventional type blenders and mixers.

Processed primary explosives and blended primer mix will be stored in the Intermediate Storage Building until required for loading operations. This building (shown in Figure 8) will contain ten storage cells with a 100 pound explosive capacity per cell. Each cell will be subdivided by

stacking frames for conveyor cars containing conductive rubber powder buckets. The cars, stacking frames, internal conveyor and external conveyor will all be a part of the automatic, computer-controlled warehousing system. This system will identify, call out and route the appropriate cars to the required destinations for plant operations. If production schedules should so demand, the conveyor cars may pass directly through the building from the Back Line or Blender Buildings directly to the loading building. Each cell in the Intermediate Storage Building will be individually environmentally controlled.

The planned detonator loading, assembling, and packing building layout is shown in Figure 9. This layout is one of seven such modules which would make up the complete LAP, or Front Line, Building. All material enters by conveyor and is automatically injected into the line at the appropriate points. Operations will be completely automatic, remotely controlled and monitored. The line will be composed of plug-in units to provide maximum flexibility and to permit by-pass of malfunctioning stations and insertion of replacement stations. Each module as shown in the figure will be composed of a reception and feed area; five stations each with a high-speed, continuous motion loading machine for actually inserting, metering, and consolidating the explosive charges; an automatic sealing and crimping station; and automatic packout station and a holding area for the completed product. Inspection will be an in-line process. We plan to develop an in-line, automatic firing station to be integrated with the line to perform random selection of items and subsequent functioning tests.

The loading machines which will perform the actual explosive metering and pressing operations will be of the high speed type similar to those in current use in the pharmaceutical industry. Such machines are in successful operation at a number of loading plants manufacturing RDX and tetryl leads. Modification of these machines or the use of additives to the primary explosive will probably be necessary to ensure safe handling of very sensitive materials. The basic principle (see Figure 10) is a dial consisting of many punches which rotates over a fixed cam which imparts the pressing motion to each punch as it passes over the cam. This is similar to the principle of the Gatling Gun.

After loading, the proper sample will be automatically extracted from the line and test fired with the results automatically recorded. The computer will monitor test results and will be capable of signalling the loading stations for necessary adjustments if test results do not meet specifications. Marking, non-destructive testing, and inspection of loaded detonators will be performed automatically on the loading line. Loaded and assembled detonators will be delivered by conveyor to automatic packout stations where they will be properly oriented, deposited in shipping containers, and overpacked.

We are investigating a number of concepts for the LAP area, some of them rather unconventional. These include the floating pallet system; vacuum pickup and dispensing systems; tooling which combines powder pickup, dispensation, metering and consolidation in a single unit; and automatic sealing using locallized RF heating. We are also studying the production and use of primary explosives in sheet form, in extrudable form,

and, in combination with a volatile solvent, the use of an explosive ink for silk screen processing. Figure 11 outlines the manner in which sheets of explosive corresponding to the several increments required might be aligned, registered, and the complete charge cored out and inserted into detonator cups. These methods require basic changes in the explosive formulation but extremely high production rates could be realized through their use.

In addition to these approaches, we are looking into a technique developed by Naval Ordnance Laboratory, Silver Spring and proved out on a laboratory basis. This method electroplates explosive pellets with an aluminum casing thus eliminating cup manufacture, sealing and crimping operations.

Completed detonators will exit from the Hold Area and will be transported by conveyor to a Storage Magazine. There will be three such magazines; one for as received desensitized primary explosive, one for RDX and tetryl, and one for packed detonators awaiting off-plant shipment. Figure 12 shows the construction of such a magazine.

A conveyor system will be utilized to transport all materials within the complex. Not including the in-building portions, approximately 1500 feet of conveyor will be required. There will be interior conveyor ramps and completely enclosed weatherproof ramps for exterior runs. Small cars will ride the conveyor and will be automatically switched in or out of the system as required. Loading and unloading will be automatic. Items will be automatically stored, retrieved and delivered to any required area. Two systems have been designed and built and are now being subjected to [illegible]. One such system consists of a short [illegible] loop with prototypes of the turn-on transfer and diversion change units which would be required for the full system. This is similar to the [illegible] system. Another system which was designed and built to meet an existing need has been installed and is undergoing test.

Figure 13 shows the layout for the Control Building and is included primarily for the purpose of emphasizing that no personnel will be anywhere in the Detonator Production Facility [illegible] operation of this [illegible]. The [illegible] will be computer [illegible] monitors, information displays, [illegible] and those amenities required to make it livable for humans. Upon the completion of this facility, we will have moved the process technician from his one-legged stool and will have placed him in a comfortable chair in front of a display of lights, TV screens, dials and gages. Thus have we progressed.

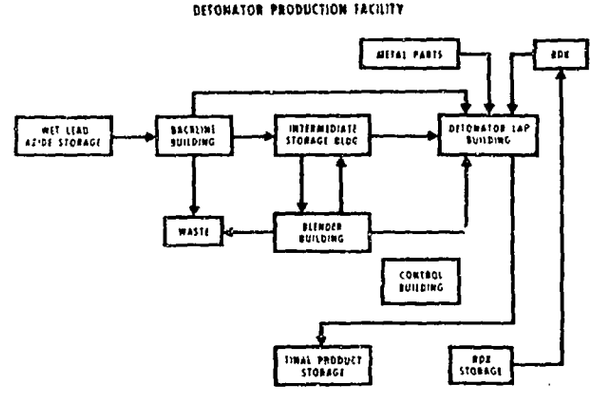

Figure 1

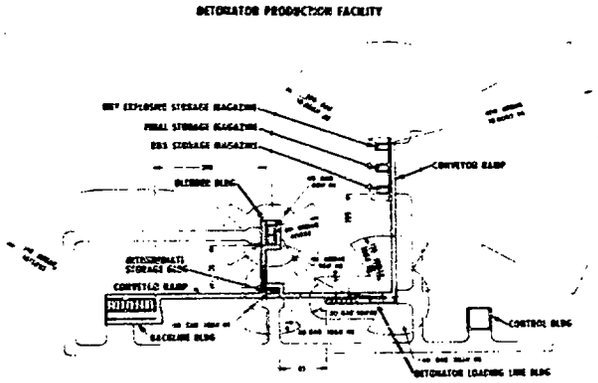

Figure 2

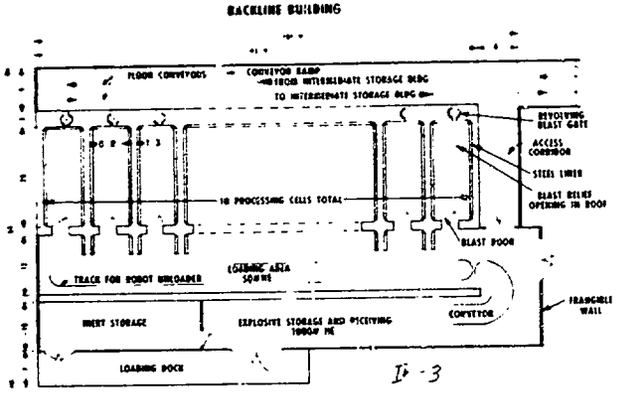

Figure 3

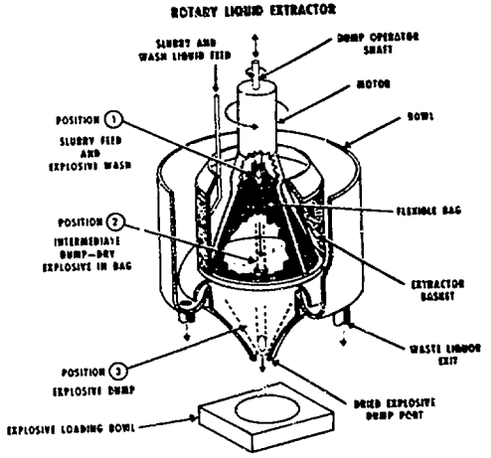

Figure 5

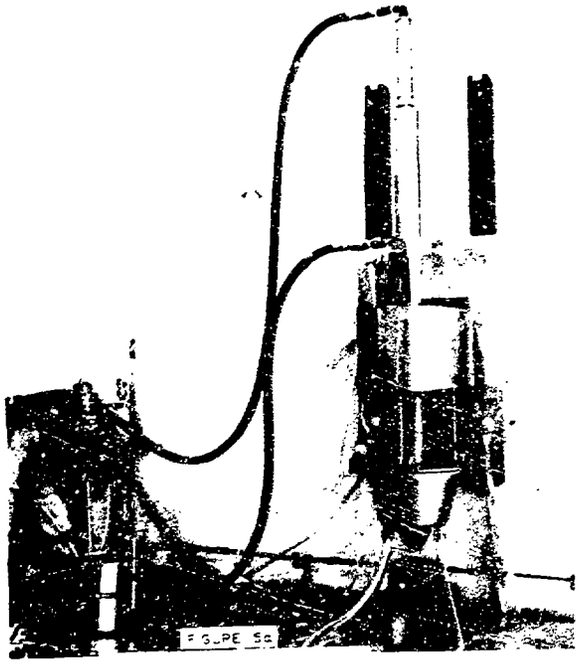

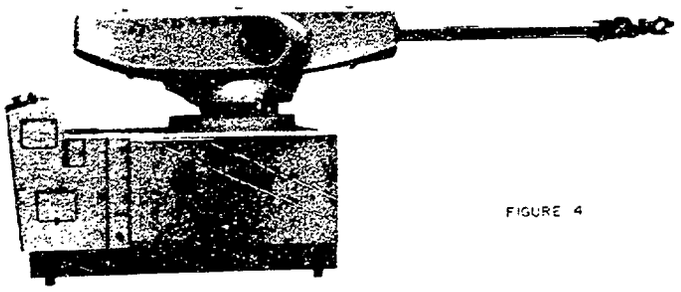

FIGURE 4

ROBOT - HYDRAULICALLY POWERED ARM,
PNEUMATICALLY OPERATED FINGERS

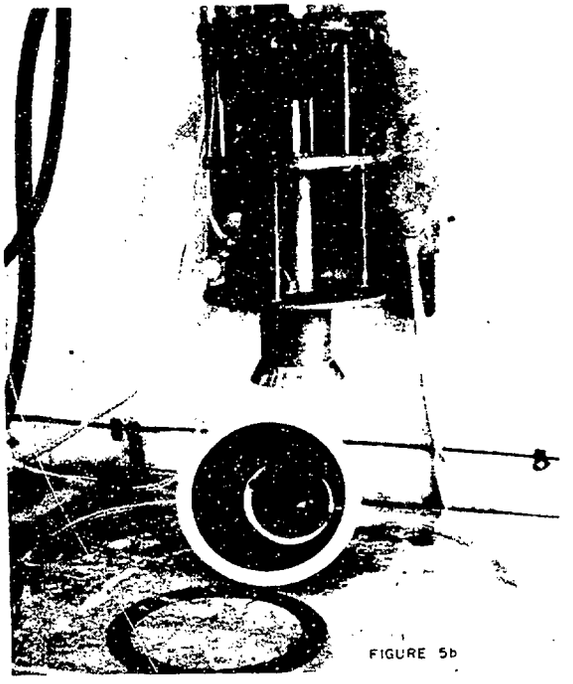

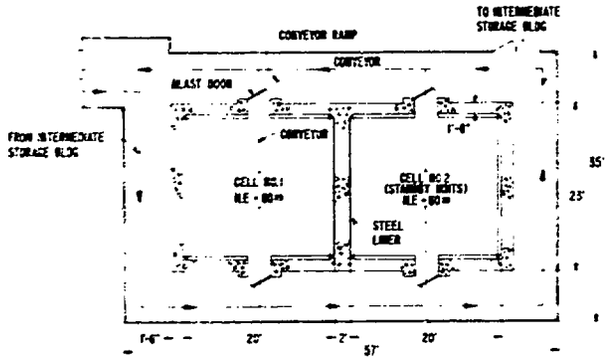

Figure 6 BLENDER BUILDING

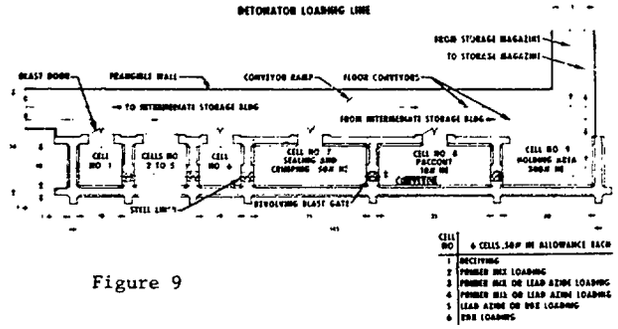

Figure 9

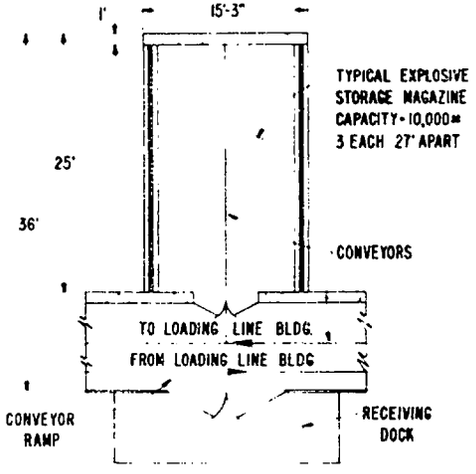

STORAGE MAGAZINE
Figure 12

PNEUMATIC BLENDING PROCESS

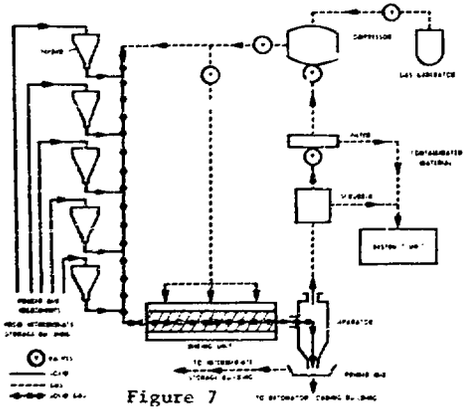

Figure 7

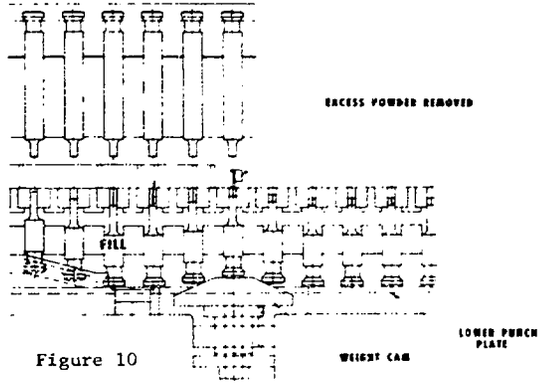

Figure 10

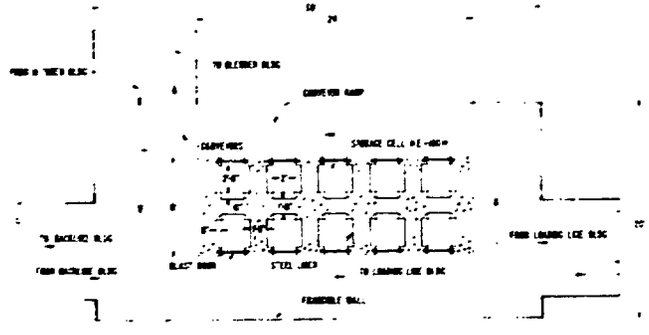

Figure 8 INTERMEDIATE STORAGE BUILDING

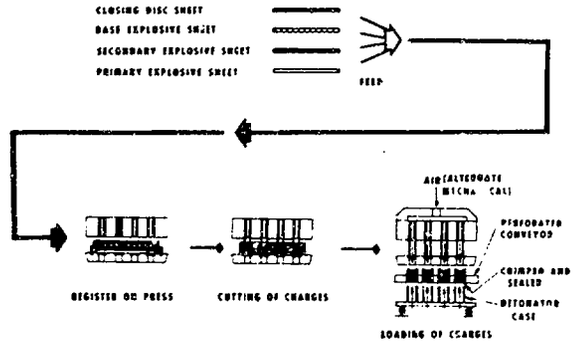

SHEET EXPLOSIVE LOADING SYSTEM
Figure 11

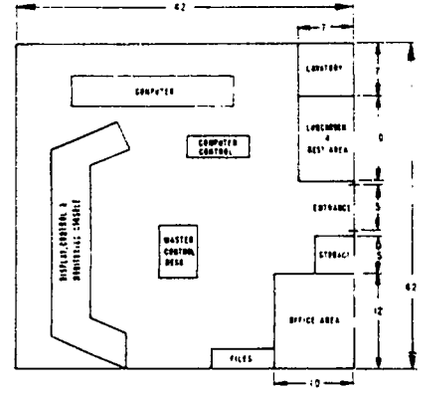

CONTROL BUILDING
Figure 13

IV-4. Injection Molding of Explosives

by
Jack Sherman & Ronald R. Vigneault
Propulsion Development Department
Naval Weapons Center
China Lake, California

ABSTRACT: A process and explosive for injecting a material of booster sensitivity into very small diameter columns and grooves has been developed and is being evaluated in some Navy Fuze Transfer Systems. Studies have been performed on the injection of the explosive into stainless steel, aluminum, plastic and rubber tubes with inside diameters ranging from .030 to .200 and lengths up to 3 feet. The material can be detonated in very thin unconfined columns.

INTRODUCTION: Military explosives used in warheads and fuzes are processed by many different methods. They may be molten and cast, they may be in the form of a cold-slurry, they may be pressed or extruded as dry powders. Recently, a new technique that is being studied has shown interesting possibilities for use in fuze trains and small warheads.

This technique is designated injection molding and it involves movement of explosive into a cavity from a reservoir. This is accomplished by means of pressure being applied to the material in the reservoir. The material flows into the cavity, the item is removed, and the material eventually "cures" as a rubbery solid. The high loading content allows the ability for this material to be initiated and propogate detonation in very small sizes.

Explosive Material

The ability to use this kind of process for filling small grooves and cavities is dependent to a large extent on the material being used. A material is under development that has these properties. The explosive is designated PBXC-303 and is an adaption of an explosive developed at the Los Alamos Scientific Laboratory (designated XTX8003). The material has a composition of 80% pentaerythritol tetranitrate (PETN) and 20% silicone rubber. The important characteristics of this material are the extremely small particle size of the PETN and the "curable" features of the silicone rubber that allow homogenizing to a very uniform putty-like consistency. Table 1 gives properties of PBXC-303. This putty-like material can be "injected" into very small orifices (0.030) diameters and grooves and eventually cures with a rubbery characteristic.

Injection Molding Techniques

Figure 1 is a schematic diagram illustrating the injection technique.

Because of the unique properties of this injectionable explosive, studies of behavior are in progress to obtain design data for use in fuze trains, detonation transfer train mechanisms and small warheads. Some preliminary data on studies of injecting this material into tubes are shown in Table 2.

The sensitivity characteristics of PBXC-303 may allow it to be placed in the category of booster-type explosives and would allow its use on the warhead side of the fuze.

Some examples of the use of PBXC-303 in a Naval weapon fuze transfer trains are as follows: single, multipoint, line initiator and spiral. These

are shown in Figures 2, 3, 4 and 5.

Experimental injection tooling are shown in Figures 6, 7 and 8.

The utility of these techniques in applying the "printed circuit" concept to explosives is also being studied. They have potential advantages in design flexibility and mass production methods.

It is also possible to extend these techniques to include pyrotechnic materials such as delays, flares, and ignition devices.

It is expected that PBXC-303 will be released for military use in the near future.

TABLE 1. Properties of PBXC-303

Composition, %	PETN/Sylgard 182 80/20
Melting Point °C, Lowest melting constituent	140
VTS at 100°C, in ml/g/48 hrs.	0.12
Autoignition Temperature, °C	179
DTA 1st Exotherm, °C	160
Sensitivity Type of Test Performed	**Test Result[a]**
Impact 2-1/2 Kg Wt. 50% Pt. Cm	18
Friction ABL Sliding Pounds Force	10/10 NF @ 794
Electrostatic 50% Pt. Joules	10/10 NF @ 0.25
Small scale gap sensitivity Density, g/cc 50% Pt. in decibangs	- 1.40 5.37
Impact Vulnerability 1/8" Plate vel in ft/sec vs. go's/attempt	1800-0/3, 1950-3/12 2100-9/9, 2250-1/1

[a]Cured a minimum of 2 hours at 60°C.

Tube No.	Column Dia.	Length of Travel	Pressure Used For Injection Psi	Dwell Time (Minutes)
1	0.080	8 inches	2000	2
2	0.060	6.75 inches	2000	3
3	0.060	17.38 inches	6000	3
4	0.060	24.00 inches	8000	2
5	0.040	24.00 inches	8000	5
6	0.040	24.00 inches	8000	4
7	0.040	24.00 inches	8000	2
8	0.090	11.00 inches	4000	10
9	0.090	15.25 inches	15,000	10

TABLE 2. Pressure vs Time vs Travel.

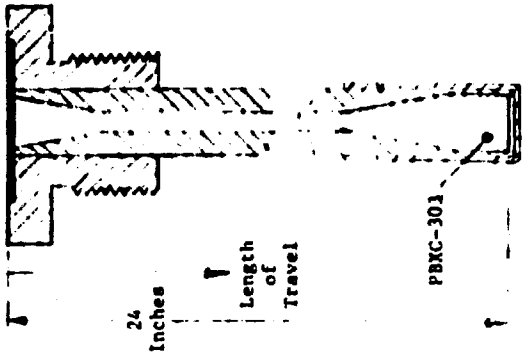

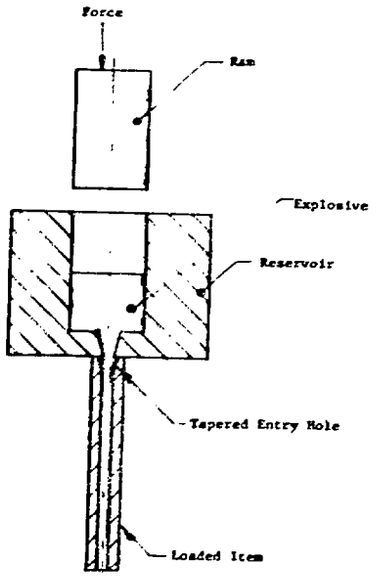

FIGURE 1. Loading Technique.

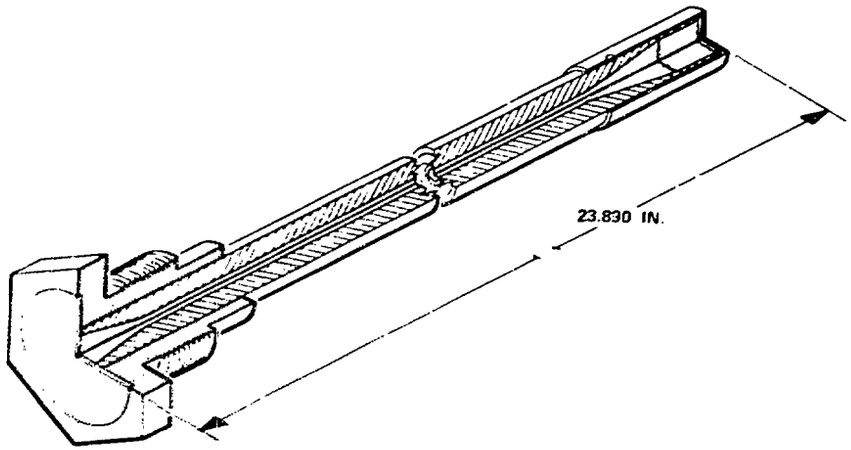

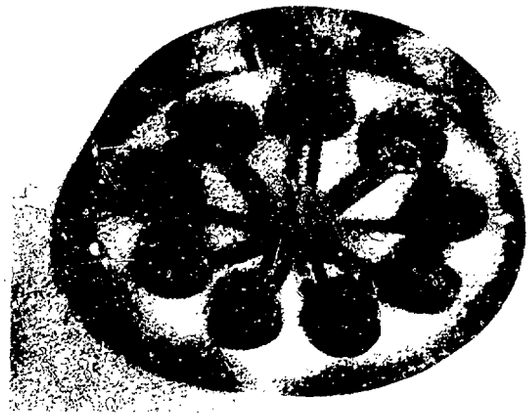

FIGURE 3

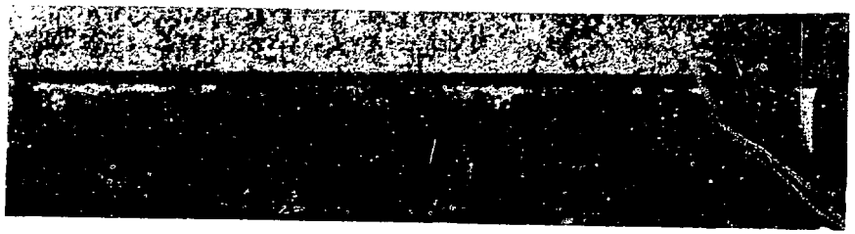

FIGURE 4

FIGURE 5

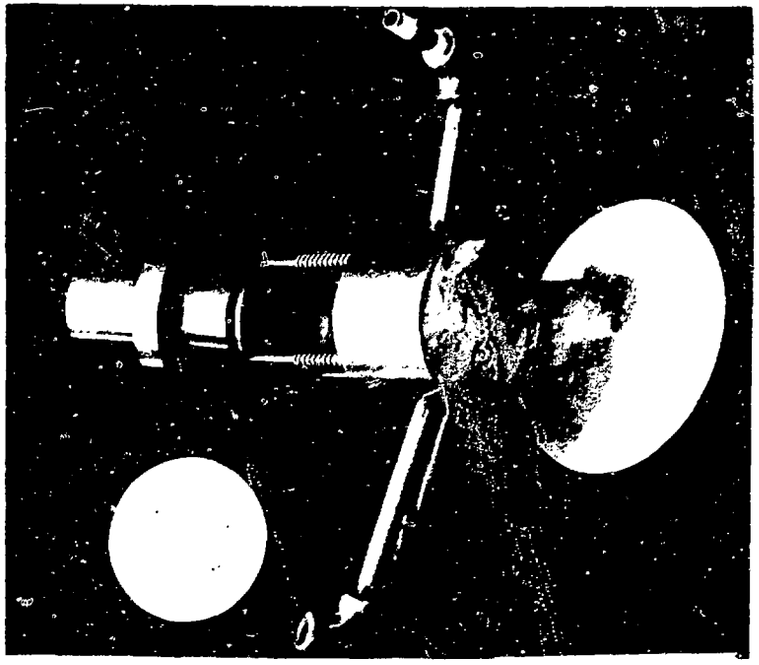

FIGURE 7

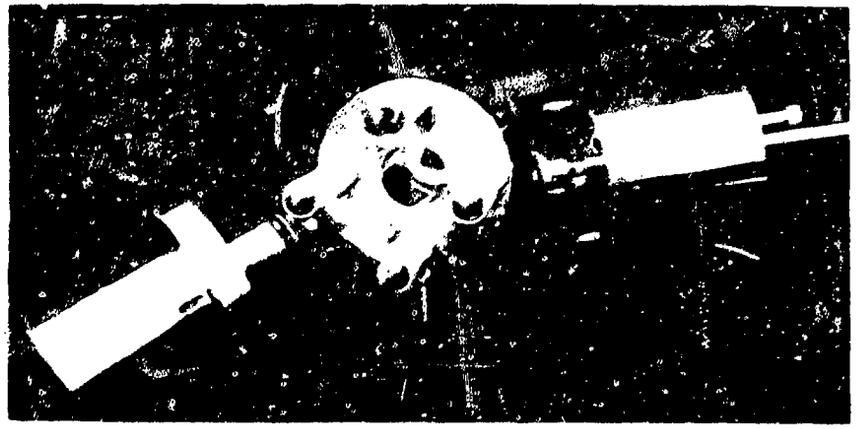

FIGURE 6

FIGURE 8

IV-5. Design of Manifolds for Explosive Transmission Lines

Paul B. Tweed
Martin Marietta Corporation
Orlando, Florida

Introduction

Manifolds are used in ordnance design to provide junction or transfer points for explosive functions. An example of a simple manifold is the one-way device shown in Figure 1, which positions the 250 mg RDX booster of a 10-grain-per-foot reinforced detonating fuse (RDF) line within 90 mils of 50-grain-per-foot flexible linear-shaped charge (FLSC). A more complex manifold, shown in Figure 2, has two inputs and six outputs close to a central 20-grain-per-foot mild detonating fuse (MDF) line. An expansion chamber parallel to the MDF line relieves pressure caused by the detonation of the MDF and boosters so that the manifold will not fragment. There are also deflagrating explosive trains which require manifolds, but these will not be addressed in this presentation.

Manifolds of small size and weight became feasible when explosive transmission lines, 10-grains-per-foot and less, were developed. Small boosters for the transmission lines were also required, as well as a means to propagate detonation reliably from the small coreloading to the booster. Information on MDF and its boosters has been discussed many times in previous Explosives and Pyrotechnics Symposia. This presentation is primarily concerned with transferring detonation from one booster to another inside a manifold.

Typical Design Problems

Many missile systems need lightweight manifolds which will withstand severe environments and allow the reliable transfer of detonation from input to output explosive transmission lines. Design of these manifolds is assumed to be relatively straightforward. Due to lack of quantitative design data, hardware failures caused by well-known general conditions but not so well documented specific problem areas have been experienced by many organizations. Some of these problem areas are discussed in the following paragraphs.

Fragmentation - Most manifolds have stringent requirements concerning the allowable fragments. Manifold housings should have adequate strength to resist internal blast and shock without fracture. An inadvertent change from bar stock to rolled stock of the manifold shown in Figure 2 resulted in fragmentation of the aluminum when the MDF detonated. Even when material strength is not a problem, the fragmentation characteristics of a redundant-type manifold with explosive transfer lines and an explosive booster may vary depending on the direction of propagation of the detonation. (See Figure 3.) During the functioning of such a manifold, one input can be expected to detonate the booster and the second input detonates afterwards due to non-simultaneity of input signals; this produces a smaller force per unit of time at the input location than is produced at the output location because the outputs detonate essentially simultaneously. Thus the damage at the input end can be appreciably smaller than that at the output end. Furthermore, if the construction of the manifold is such that the input end is more rugged than the output end, the variation in fragmentation may be more pronounced, requiring that the direction of detonation be fixed by design.

Confinement - Confinement of the explosive elements inside a manifold greatly affects propagation distances. Lack of backup behind a tetryl receptor pellet prevented its initiation at a 50-mil gap from a tetryl booster in an MDF line; with backup, the system functioned reliably at 125 mils.

Tolerances - Dimensional tolerances of boosters and their locations in manifolds need to be carefully checked to avoid interference or excessive gaps during assembly. An RDX lead in an elbow-type manifold lost its closure disk and some explosive after exposure to severe mechanical environments. Damage was caused by interference between the lead and its confining surfaces.

Directionality - The donor and receptor should be coaxial for maximum energy transfer (see Figure 4). A 250 mg booster 30 mils away from an identical booster did not transfer detonation when the angle was 60°; detonation was propagated at 180° when the gap was over 500 mils.

Rough Handling - Severe mechanical environments may loosen or reconsolidate explosive charges, thus changing their sensitivity to initiation.

Desensitization - Additives or impurities may partially desensitize explosives. This condition is usually aggravated by exposure to temperature extremes with associated decomposition and exudation problems.

Moisture - Moisture originally in the explosive or absorbed during humidity exposure due to poor hermetic seals can cause unwanted reactions or desensitization.

Quick Redesign

All of you are familiar with instances where project direction requires very rapid changes in explosive ordnance configuration, with very few hardware samples for test. When manifolds must be modified under such constraints, we perform gap tests far beyond design limits rather than use the Bruceton technique for determining the mean and adding on the required number of standard deviations. In this way we get a quick answer on our design gaps which can later be verified by system and preflight certification tests. Such a procedure was used when we changed from a 3-way to a 6-way and finally to a 4-way manifold in a missile destruct system. That part of the destruct system, which is located near the second stage motor dome, is shown in Figure 5. In the total destruct system, fragmentation was permitted, provided the locations of the explosive components were such that the fragments would not interfere with the detonation functions.

During the initial development of the destruct system, two 3-way manifolds were needed to transfer the detonations in each of two RDF lines coming from the warhead section to two RDF lines leading to an FLSC destruct as well as two RDF lines leading to a second stage motor detonation device. Figure 6 shows the design of the 3-way manifold, which houses three 10-grain-per-foot RDF lines, each with a 250 mg RDX booster. When one of the angled ports was used to hold an input booster (A), the horizontal booster (B) and the other angled port booster (C), detonated; the measured distance between (B) and (A) or (C) was 30 to 40 mils. When the distance between (B) and (A) or (C) was increased to

60 or 70 mils, both outputs also detonated.

Due to non-simultaneity in the redundant signals coming from the warhead section, a 6-way manifold with two input and four output signals was investigated (Figure 4). Using number 1 port of the hexagonal manifold as an input, detonation was initiated in two of five RDF boosters at ports number 2 and 4. When a 600 mg RDX booster was introduced at right angles to the six RDF boosters, all five outputs detonated. Moving the RDF boosters from a nominal 30 mils, 20 or 40 mils further away from the central booster, did not prevent detonation of all five outputs.

In order to improve the redundancy of the missile destruct system, two 4-way manifolds replaced the single 6-way manifold. Figure 3 shows the 4-way manifold, which includes a 1.6 gram RDX lead between the two sets of ports. During the design of the 4-way manifold, the gap jumping ability of the unconfined RDF booster was investigated. It was found that one booster would detonate another 288 or 328 mils away when the axes of the boosters made an angle of 160° with each other. The 288 mil condition represents the maximum design gap in the 4-way manifold; the latter represents a condition of improper assembly. Thus it could be postulated that, inside the manifold, an RDF booster will propagate across the gap created by the absence of the RDX lead. During development tests of the manifold, it was found that one RDF booster would initiate the other three boosters when the gap between the boosters and RDX lead was as much as 40 mils above the design value of 30 mils. In a modified system test, the RDF output lines from the redundant 4-way manifolds yielded satisfactory dents in steel blocks even when the RDX lead was omitted from one of the two manifolds. In a complete system test, all components functioned satisfactorily. In preflight certification tests, the 4-way manifolds with their RDF lines functioned properly after being subjected to temperature shock from -40° to 160°F, pressure as low as 0.1 psia, random vibration from 50 to 3000 Hz with a maximum power spectral density of 2.04 G^2/Hz and a total of 57.7 G rms, acceleration of 110 percent of the missile breakup value, and mechanical shock from 300 to 10,000 Hz with a maximum value of 7000 G. The destruct system functioned properly in a static missile test as well as in all flight tests.

Summary

In summary, we have a technique for designing various manifolds employing 10-grain-per-foot RDF lines with 250 mg RDX boosters for transferring detonation in missile destruct systems. Boosters inside the manifolds are often necessary if the inputs and outputs are not coaxial. The manifolds with their associated RDF lines will withstand severe mechanical environments and possess a high reliability for the transfer of detonation. The designs are relatively simple and inexpensive. The same design principles should be applicable to smaller coreloadings, MDF with smaller boosters, and explosive trains with explosives other than RDX.

ONE WAY MANIFOLD

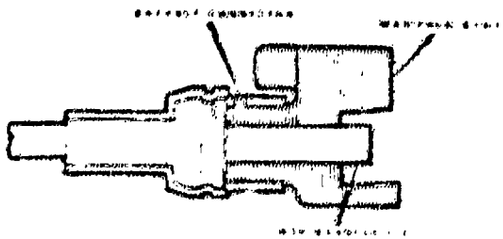

MANIFOLD WITH EIGHT PORTS

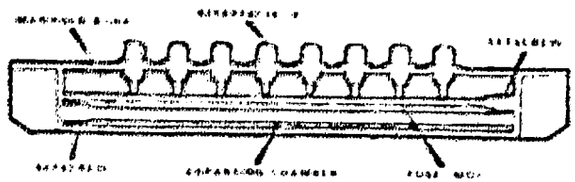

DESTRUCT SYSTEM - SECOND STAGE PORTION

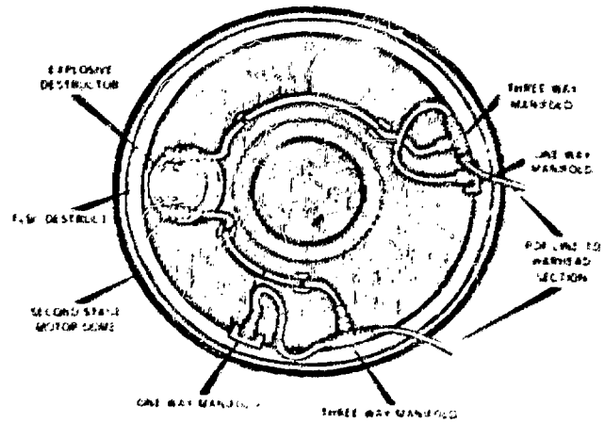

FOUR WAY MANIFOLD

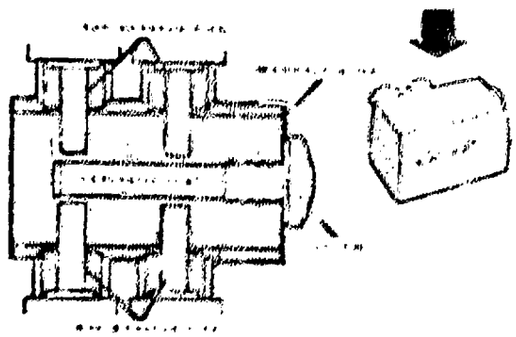

SIX WAY MANIFOLD

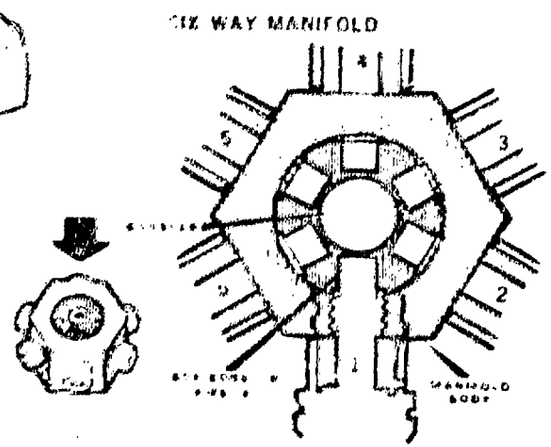

THREE WAY MANIFOLD

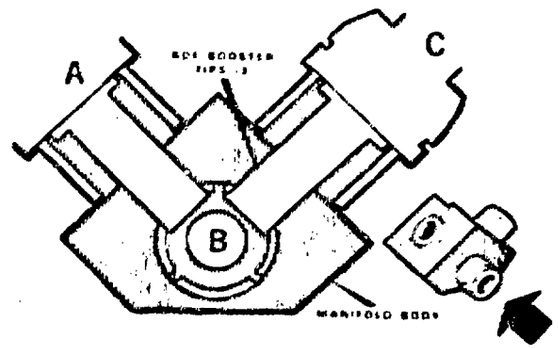

IV-6. A SIMPLIFIED APPROACH TO PARACHUTE MORTAR DESIGN

V. W. Drexelius and M. L. Schimmel

McDonnell Aircraft Company

St. Louis, Missouri

INTRODUCTION

Propellant actuated devices such as parachute mortars are required for many aircraft and spacecraft applications. Often, a basic problem arises because gas pressure required for parachute ejection is substantially lower than that at which popular double-base propellants can be burned in an efficient and controlled manner. The conventional solution has been to utilize a high-low system in which the propellant is burned at relatively high pressure in a fixed-volume chamber and is then ported through orifices to the working chamber where it expands and acts against the payload at a much reduced pressure. The ballistics involved in the design of a high-low system are quite complicated. At the last E.E.D. Symposium, Heiney[1] used 21 equations to define such a system, and a computer program to aid in their solution.

An alternate approach to this problem has been utilized on two McDonnell Aircraft Company programs requiring parachute deployment. In both applications, boron potassium nitrate granules were used as the propellant energy source. Although this material was developed as a rocket igniter, its use as the propelling charge in parachute mortars has resulted in several important advantages. The major benefit is elimination of the need for a high-low system, with resulting simplified ballistics and substantially reduced development testing. Other benefits include tolerance to operating temperatures higher than that achievable with conventional propellants, and relatively uniform performance over a wide range of ambient temperatures. These advantages should be applicable to many propellant actuated devices.

Historically the use of boron/potassium nitrate as a main propellant in cartridge actuated devices has been minimal, mainly as a result of its lower impetus value. Because of its "forgiving" qualities as stated above, its impetus level can be offset by increasing the charge weight.

The two different approaches to development of parachute mortars will be compared from the standpoint of design, operation and ballistics.

HIGH-LOW PROPELLANT MORTARS

The Gemini spacecraft drogue mortar, shown in Figure 1, is a typical example of a high-low system using double base propellant. Dual electrical cartridges are simultaneously initiated. The ignited propellant burns and releases combustion gases in the breech. Propellant burning rate is a function of pressure, and the propellant must be burned at higher pressure than would occur if combustion gases were released directly into the mortar tube. Orifices are therefore provided between the breech and mortar tube, and a frangible bolt holds the gas in the breech until a predetermined pressure level is reached. When the bolt breaks, high breech pressure is maintained by the orifices which control gas flow into the mortar tube where a substantially lower working pressure acts against a sabot and ejects the parachute. Apollo mortars, shown in Figure 2, operate in essentially the same manner [2] The ballistics of these high-low systems are so complicated that a rigorous mathematical definition of performance characteristics was shown by Heiney[1] to require 21 equations. A more common method of development usually involves a cut-and-try approach. The major parameters which can be varied include: type and grain configuration of propellant, ignition material, volume of breech, orifice size, and piston area. For either the rigorous or the cut-and-try approach, development is made difficult by the tendency of orifices to clog or erode, as well as the marked dependence of propellant burning rate on both pressure and temperature.

BORON POTASSIUM NITRATE PARACHUTE MORTARS

McDonnell Aircraft Company has developed two parachute mortars which eliminated the requirement for a high-low system by use of boron/potassium nitrate (B/KNO_3) as the energy source. This material was originally developed for ignition of rocket propellants and is widely used for this purpose. As such, it burns satisfactorily at low pressure. In the first application as found on the F-111 Crew Module, it is used to deploy a chute which provides stabilization and deceleration when the module is ejected from the aircraft. B/KNO_3 was selected because available conventional propellants would not meet the high temperature requirement of 100 hours at 275°F. An important additional benefit was that development of the mortar proved considerably simpler than normally experienced with conventional propellants as shown by reduced testing and insensitivity to minor geometry changes. As a result, B/KNO_3 was also used for a second parachute mortar application in which an F-4 flight test airplane was fitted with a parachute for recovery assistance from flat spins. The mortar deploys a pilot chute which pulls out the recovery chute. Here again, use of B/KNO_3 as the energy source resulted in a brief, simple development program. Each of these mortars will be described from the standpoints of design, development and performance.

F-111 CREW MODULE PARACHUTE MORTAR

The F-111 mortar requirement was to deploy a 36-lb drag chute at a velocity of 105 ft/sec.

Design - Figure 3 illustrates design of the F-111 Crew Module mortar. It is unconventional in that installation constraints made it necessary to pack the parachute outside the mortar. Initiation is accomplished by redundant shielded mild detonating cord (SMDC) inputs which deflect a deformable firing pin to fire a #49-type percussion primer. The primer fires an ignition mixture

of zirconium, barium chromate, which in turn ignites the output charge of B/KNO_3. When combustion pressure is sufficient, the two shear pins holding the pressure plug to the inner barrel are severed. The plug, outer barrel, end fitting and parachute pack are then propelled forward, while the inner barrel remains stationary. The outer barrel also engages a blast shield which protects the parachute pack from combustion products when the barrels separate. Although a large free volume is provided in the inner barrel to reduce the initial pressure, the excellent ignition characteristics and relative insensitivity of B/KNO_3 to pressure eliminated the need for a high-low system. Design details are presented in Figure 4.

Development - In order to obtain the needed impetus and burning time data for B/KNO_3, initial tests were run on cartridges containing 20g of granules which were fired into a closed bomb with a volume equal to that of the unfired mortar. The curves of Figure 5 show how the burning time of B/KNO_3 is affected by granule size. Thus the same weight of powder resulted in the same peak pressure; however, the finer granules (Type I) reached peak pressure in less than 10 msec, while the coarser material (Type II) required over 25 msec. Data obtained from these closed bomb tests were used to select the cartridge load to be used in the mortar. Figure 6 shows typical pressure-time curves obtained during instrumented firings. One of the advantages of B/KNO_3 for this type of application is that its rapid burning is relatively unaffected by the temperature extremes shown. Because the pressure varies from about 3700 to 1100 psi during powered stroke, the piezometric efficiency is certainly lower than could be achieved by an optimized system using conventional propellants.[3] From a practical standpoint, however, this impulsive type loading resulted in no weight penalty since the wall thickness of the aluminum barrels (less than 0.10 in.) was determined by column loading rather than breech pressure.

Performance - The mortar successfully passed qualification testing which consisted of 60 tests, divided between +270°F, -65°F and ambient temperature firings, after exposure to the standard military environments.

F-4 SPIN CHUTE MORTAR

The second application, an F-4 mortar, was required to deploy an 8.5 lb pilot chute at a velocity of 100 ft/sec.

Design - The F-4 mortar illustrated in Figure 7, is of conventional configuration in that the parachute is packed within the device. Dual electrical cartridges ignite the output charge of B/KNO_3. Combustion gases act against a polyurethane sabot. The shear rivets holding the end closure to the mortar barrel are severed, and the chute is propelled from the barrel. Details of the design are tabulated in Figure 8.

Development and performance - Using previous experience on the F-111 mortar as a guide reduced the amount of ballistic development on the F-4 program to simply adjusting the quantity of powder to obtain the desired ejection velocity. The main development task consisted of preventing sabot leakage. This was accomplished by using O-rings and a filler block between the sabot and chute. Only 13 static development tests were required before the mortar was considered ready for flight testing. One of the low temperature tests is shown in Figure 9. After aircraft installation, six successful air deployments were made prior to delivery to the Air Force.

BALLISTIC COMPARISON

A tabulation of ballistic parameters for the F-111 and F-4 mortars is given in Figure 10. The major difference is that the B/KNO_3 delivered impetus for the F-4 mortar was significantly more than that for the F-111 application. This difference in efficiency is caused by system geometry. Examination of Figure 6 shows that at F-111 end of stroke, pressure is 1200 psi; while Figure 9 shows that for F-4, end of stroke breech pressure is essentially ambient. Thus, in the latter application substantially more propellant energy is converted to kinetic energy.

CONCLUSIONS

1) Use of boron, potassium nitrate as an energy source in parachute mortars eliminates the need for a high-low system. For the two applications described, ballistics were considerably simplified, with resulting reduction in development cost and time.

2) While the piezometric efficiency of B/KNO_3 mortars is relatively low, this factor did not significantly affect device weight. These mortars have been successfully qualification tested to military environments, including exposure to 270° for 100 hours.

3) The impetus delivered by B/KNO_3 is a function of system geometry. For the F-111 and F-4 applications, the values were 70,000 and 120,000 ft-lb/lb respectively.

REFERENCES

1) Heiney, O. K., "Interior Ballistics of High-Low Propulsion Systems," Sixth Symposium on Electroexplosive Devices, July 1969.

2) "Apollo Spacecraft Pyrotechnics," NASA Technical Memo TMX-58032, October 1969.

3) Drexelius, W. W. and Schimmel, M. L., "Pressure-Controlled Propellant - Actuated Devices," Sixth Symposium on Electroexplosive Devices, July 1969.

CATAPULT		
	Length	29.5 in.
	Outside Diameter	1.5 in.
	Outer Barrel Area	1.45 in.^{2}
	Stroke	24 in.
CARTRIDGE		
	Primer	249 (G-11)
	Ignition Material	0.4 g Zirconium, Barium chromate mix
	Propellant	40.6 g F-NO-2C boron potassium nitrate ignition granules (Type II)
PARACHUTE		
	Weight	36 lb
	Ejection Velocity	100 ± 15 ft/sec

Figure 4 - Parachute Mortar Design Details

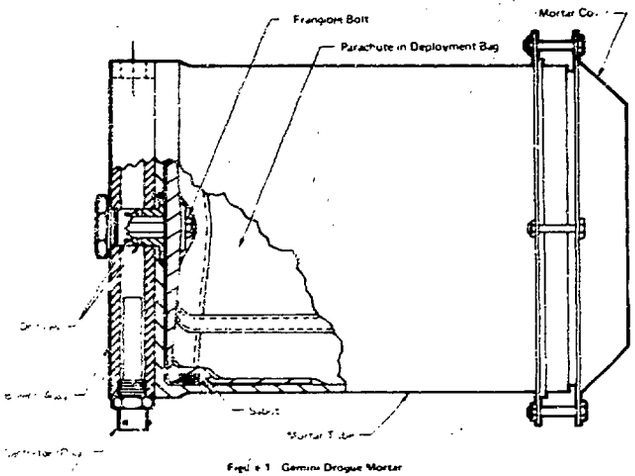

Figure 1 Gemini Drogue Mortar

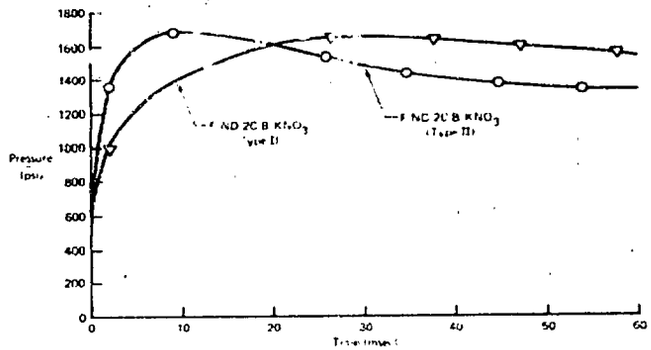

Figure 5 Closed Bomb Tests

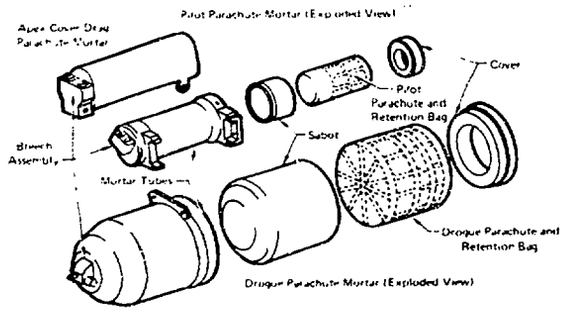

Figure 2 Apollo Mortar Assemblies

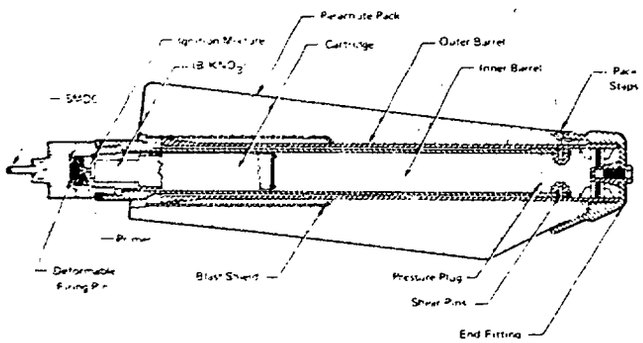

Figure 3 F 111 Parachute Mortar

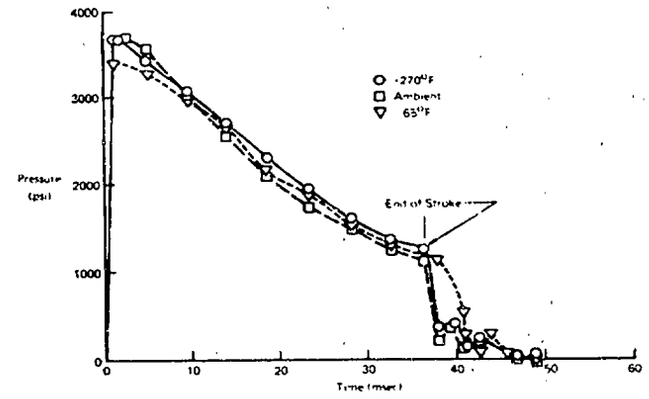

Figure 6 - Pressure vs Time for F 111 Mortar

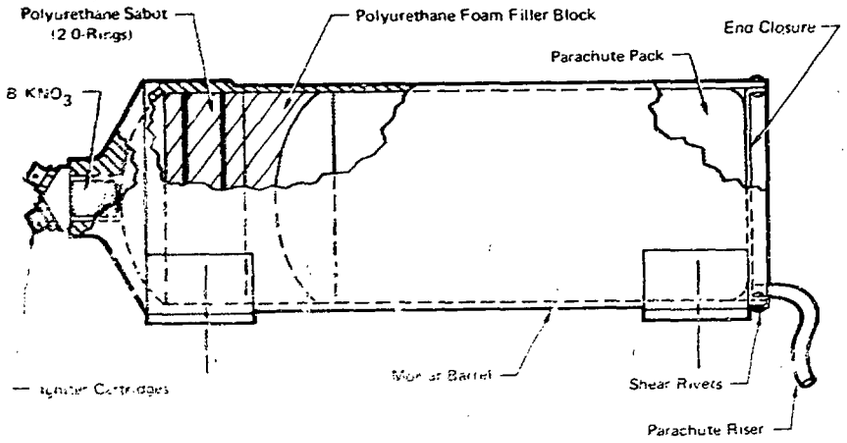

Figure 7 - F-4 Spin Test Mortar

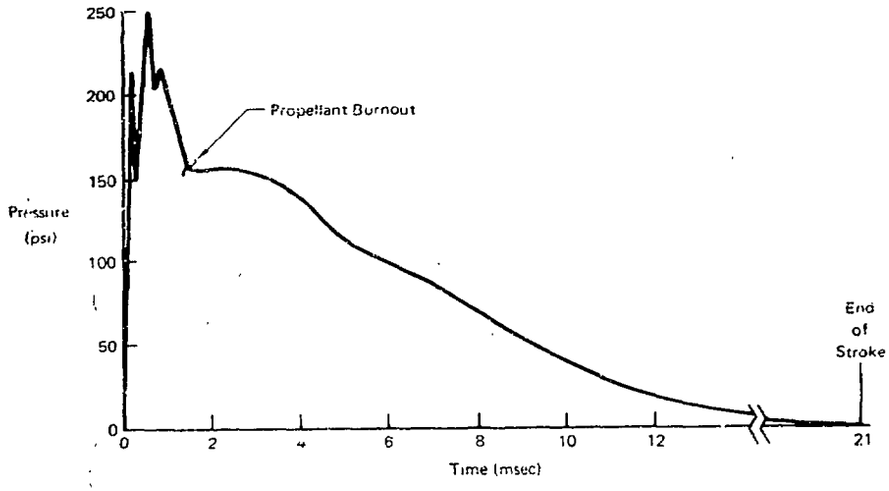

Figure 9 - F-4 Spin Chute Mortar Parachute Ejection Test at –65°F

MORTAR	
Length	20.4 in
Outside Diameter	6.6 in
Inside Diameter	6.0 in
Stroke	16 in
CARTRIDGE	
Ignitor Cartridges (2)	Holex 3300
Propellant	5.0 g FNH-2C boron/potassium nitrate ignition granules (Type II)
PARACHUTE	
Weight	8.5 lb
Ejection Velocity	105 ± 15 ft/sec

Figure 8 - F-4 Spin Chute Mortar Design Details

	F-111	F-4
Ejected Weight (lb)	36	8.5
Ejection Velocity (ft/sec)	105	100
Energy Output (ft-lb)	6150	1320
Weight of Propellant (lb)	0.088	0.011
B/KNO_3 Impetus (ft-lb/lb)	70,000	120,000

Figure 10 - Ballistic Comparison of F-111 and F-4 Mortars

IV-7. REPLACEMENT OF SR-4990 BY BARIUM STYPHNATE IN THE MK 24 ACTUATOR

S. Urman
Naval Ordnance Laboratory
White Oak, Silver Spring, Maryland

INTRODUCTION

1. The Mk 24 Mod 0 Actuator, used in the Mk 20 Cable Cutter, contains SR-4990 as the propellant base charge. SR-4990 is a single base smokeless powder manufactured by DuPont and has been used as the propellant material in Navy actuators because it produces a very desirable rapid pressure rise. However, DuPont has ceased production of SR-4990, making it necessary for the Navy to find a suitable replacement material for use in the Mk 24 Mod 0 Actuator.

2. Besides a rapid pressure rise, the replacement material should have: (a) high pressure output, (b) good loading properties, (c) safe handling properties, (d) storage stability, and (e) bulk density sufficiently high to assure that an adequate quantity of base charge can be loaded within the present volume of the actuator. In addition to possessing these qualities, it is desirable that the replacement be non-proprietary and covered by a military specification.

3. Various available materials were considered as possible replacements for SR-4990. Two proprietary samples supplied by DuPont and said to have pressure-time responses similar to that of SR-4990, were included in initial testing in case non-proprietary substitutes were not successful. They were SR-8044 and "Hi-Skor" 700-x (DuPont Powders). Lead mononitroresorcinate is used in various dimple and bellows motors and was thought to have possible application. A literature search revealed that barium styphnate had a pressure-time response which suggested its possible applicability.

4. The experimental work was divided into two phases. A basic survey was first made of the possible substitutes by testing in a pressure bomb to determine how closely the substitute materials matched the pressure-time curves produced by SR-4990. Materials found satisfactory in the pressure bomb test were then tested in the Mk 24 Actuator.

EXPERIMENTAL APPARATUS

5. A small pressure bomb was used to compare the pressure time profiles of the test materials with that of SR-4990. This pressure bomb, Fig. 1, has been successfully used by E. E. Kilmer[1] to evaluate different propellant materials for actuators.

6. A Norwood strain gage pressure transducer, with a range up to 10,000 psi, was used in conjunction with a Model 5AC Pressure Monitor. The pressure monitor provides a source of power and completes the bridge and calibrating circuits. This arrangement was monitored by a Tekronix oscilloscope, Model 545, and the resultant curves were recorded by a Polaroid Land camera. A block diagram of the experimental arrangement is shown in Fig. 2.

7. The Norwood bonded strain gage pressure transducer has been used in static and dynamic pressure measurements over the years. The gage's catenary diaphragm is designed to minimize temperature effects and volume changes. An increased pressure on the diaphragm produces a minute dimensional change in the strain tube. This change is reflected by an equivalent resistance change in the strain gages bonded to the tube. Past experience with propellant powders has shown this transducer to be unaffected by corrosive gases, that it has the desired electrical characteristics, and it facilitates the cleaning of the pressure bomb.

8. For convenience of testing, the Mk 15 Actuator, Fig. 3, was used as the test vehicle to compare the different candidate powders. The Mk 15 Actuator has 25 mg of propellant base charge compared with 1 gram of propellant base charge in the Mk 24 Actuator. Thus, the pressure generated from the Mk 15 Actuator is much less than that of the Mk 24 Actuator and therefore more adaptable to the pressure bomb arrangement described above. In addition, smaller amounts of substitute material can be used for testing purposes. Also, the Mk 15 Actuator is relatively simple in design and easier to fabricate than the Mk 24 Actuator.

EXPERIMENTAL RESULTS

Pressure-Bomb Work

9. Initial exploratory experiments were performed using one Mk 15 Actuator with 25 mg of SR-4990. A typical response is shown in Fig. 4. A peak pressure of approximately 1900 psi is generated in the pressure bomb in 2-3 milliseconds. To isolate the pressure-time effect of SR-4990 from the ignition charge of lead styphnate, various charge weights of lead styphnate were tried. See Fig. 5. When these results are compared with the normal Mk 15 profile, (Fig. 4), a marked difference in the pressure build up was noticed. This effect of pressure on burning rate demonstrated that the 25 mg tests might not scale too well with larger amounts of material in the final Mk 24 Actuator design. Actuators with 15 mg of lead styphnate gave the closest duplication of the pressure-time response of the normal Mk 15. It was concluded that a five milligram charge of lead styphnate would be sufficient to isolate the response of the propellant. To ensure adequate ignition of the propellant, five milligrams of FA 678 Igniter Mix* were pressed at the same loading pressure as the lead styphnate in the charge holder on top of the increment of lead styphnate. This igniter mix is used to ignite the propellant charge in the Mk 24 Actuator and is very effective when used in this operation. As shown in Fig. 6, the response of these actuators was as good as the original design containing 20 mg of lead styphnate.

10. "Hi-SKOR" 700-x and SR-8044. These are two DuPont powders which were recommended by DuPont as possible substitutes for SR-4990. The same weight (25 mg) as SR-4990 was employed. Figure 7 shows these powders to be promising, giving pressures in the 1500-2000 psi range within 2-4 milliseconds. It was decided to keep them in reserve for further study if necessary in case the non-proprietary materials were not satisfactory.

11. Barium Styphnate (Barium Trinitroresorcinate). Twenty-five mg of barium styphnate, loaded loose (the same conditions as SR-4990) resulted in a low pressure and extremely quick response time. See Fig. 8a. (The charge holder in this test was not filled completely due to the higher density of barium styphnate compared with SR-4990.) Filling the charge holder (55 mg) with loose barium styphnate increased the pressure correspondingly, and the fast rise time was maintained. See Fig. 8b. To determine whether we could achieve a slower burning rate with a suitable peak pressure tests were run with actuators containing ninety mg barium styphnate but pressed in the charge holders at different loading pressures. Figure 9 shows typical oscillograms illustrating the results obtained at 5000 psi, 10,000 psi, and 15,000 psi. The charge holder was filled completely at 5000 psi loading pressure. The pressure rise times and magnitude of the peak pressures for the various loading methods are summarized in Table 1. Figure 10 shows the P-T profiles

* 40% zirconium, 20 barium nitrate, 20% lead peroxide, and 20% PETN.

of actuators loaded with barium styphnate compared with those loaded with SR-4990. By using 5000 psi as the loading pressure, the desired response could be produced in the same volume as SR-4990.

12. Lead Mononitroresorcinate. Lead Mononitroresorcinate (LMNR) when used by itself generated a pressure which was too low. Its rate of burning was also too low. See Fig. 11. This is due to the "oxygen deficiency" of LMNR. For LMNR, the oxygen balance was determined to be -48% to CO_2 and -15% to CO. However, when used with an oxidizer added for complete combustion, the pressure build up can be enhanced. The oxidizer used here was $KClO_4$ and the different ratios by weight tried were 85% LMNR - 15% $KClO_4$, 80% LMNR - 20% $KClO_4$, 75% LMNR - 25% $KClO_4$, and 60% LMNR - 40% $KClO_4$. See Fig. 12. The actuators loaded with a 75/25% mixture pressed at 5000 psi gave pressure-time profiles most similar to those of actuators with SR-4990. The different responses from varying loading conditions and mixtures are summarized in Table 2. In Fig. 13, the P-T profile of LMNR-$KClO_4$ (75/25%) as obtained from the pressure bomb is plotted and compared with SR-4990.

Mk 24 Actuator Work

13. The next phase of the program consisted of replacing the base charge in the Mk 24 Actuator with barium styphnate and LMNR/$KClO_4$ (75/25%) and comparing their performance with the standard Mk 24 Actuator. Work on the proprietary powders was discontinued at this time pending the results of the subsequent experimentation. The Mk 24 Actuator, Fig. 14, is a hermetically sealed, stab initiated device which contains 135 mg of NOL 130 primer mix, 150 mg of FA 878 igniter mix, and one gram of SR-4990 as the base charge.

14. The SR-4990 explosive load was replaced with 4.4 grams of barium styphnate pressed at 5000 psi and 5.6 grams of LMNR/$KClO_4$ at 5000 psi. During the fabrication of the actuators with LMNR/$KClO_4$, difficulty was encountered during the soldering process. When heat was applied to melt the solder, a few actuators accidentally ignited during the process. No accidental ignitions were obtained when the barium styphnate loaded actuators were sealed.

15. The actuators loaded with the two candidates were tested for output using the Mk 24 Actuator output fixture. In this device, the actuator drives a piston which is required to shear a 0.172-in. steel rod. All of the samples tested (10 each) passed the test at room temperature and at -65°F. In fact, rods up to 0.218-in. diameter could be successfully sheared at room temperature. (The upper bound on the output from SR-4990 loaded Mk 24 Actuators is 0.197 in.) Actuators with the two candidates were tried in the Mk 20 cable cutter and successfully sheared the 1-in. diameter cable.

16. The actuators were then subjected to rough handling and surveillance tests. (See Table 3.) Two out of fifteen acutators with LMNR/$KClO_4$ fired on impact in the 40-ft. guided drop test. This is not too uncommon for stab initiated items, as they occasionally will fire on this test. All actuators with barium styphnate successfully passed the safety tests. The samples remaining from the safety tests were tested in an output fixture by the impact of a two-ounce steel ball from four inches on a standard firing pin. The 0.172-in. diameter steel drill rod was sheared successfully each time by actuators containing barium styphnate. One out of fifteen actuators loaded with LMNR/$KClO_4$ failed to shear the rod after being subjected to the 40-ft. guided drop test. One out of fifteen failed after being stored at 160°F and two out of fifteen failed after a sequential transportation, high

frequency vibration test. The reasons for the failures are not known. As a result of these tests, barium styphnate was judged to be more consistent and reliable than lead mononitroresorcinate when used in the Mk 24 Actuator.

DISCUSSION

17. The results of impact sensitivity tests of the candidate materials are shown in Table 4. Although both candidates are more impact sensitive than SR-4990, barium styphnate is considerably less impact sensitive than LMNR/$KClO_4$. Although barium styphnate is regarded as a primary explosive, it is safer to manufacture and use than most other primaries.[2] It is also relatively unsusceptible to accidental ignition from electrostatic sources.[2]

18. A cost analysis revealed no significant difference between the current price of LMNR (price of $KClO_4$ can be neglected when compared with LMNR) and barium styphnate. However, the extra step of mixing LMNR and $KClO_4$ must be considered. Efforts have to be made to insure uniform blending of the two ingredients. Otherwise, inconsistent burning times with varying pressure outputs will result. To facilitate the blending, it is necessary to use potassium perchlorate crystals which are of very small size. Also, because of the sensitivity of these materials, adequate safety precautions must be taken during the mixing process.

19. The difficulty of soldering actuators with LMNR/$KClO_4$ was previously mentioned. The soldering is done with the use of a high frequency induction heater equipped with a reset timing device. The amount of heat delivered and its duration can be varied depending on the particular item to be soldered. The settings are very crucial to insure proper melting of the solder without any accidents. Hence, extra time and efforts were necessary to solder a complete batch of actuators with LMNR/$KClO_4$. Due to the small difference between the melting point of the solder and the ignition temperature of LMNR/$KClO_4$, a lower melting point solder (tin-indium) would have to be used. If not successful, an alternate method for hermetically sealing the actuator would have to be found. There were no difficulties encountered in soldering actuators loaded with barium styphnate.

20. Barium styphnate, has been found to be relatively stable to heating and to storage in vacuum and humid conditions.[2] It is also compatible with the metals and other materials likely to be in contact with it in explosive stores. A photomicrograph of barium styphnate is provided in Fig. 15. The particle size ranges from 10 to 500 microns. As is shown in the pressure-time profiles in Fig 9, it is possible, by varying the loading pressure of barium styphnate in the actuator, to closely approximate the burning response of SR-4990.

CONCLUSIONS

21. Two possible non-proprietary candidates for replacement of SR-4990 have been found. Work with the Mk 24 Actuator has shown barium styphnate to be more reliable than a lead mononitroresorcinate/$KClO_4$ mixture. Superior chemical and physical properties have also demonstrated the advantage of using barium styphnate over the LMNR/$KClO_4$ mixture.

22. Barium styphnate is recommended as the substitute for SR-4990 in the Mk 24 Actuator.

REFERENCES

1. Kilmer, E. E., "The Actuator, Explosive WDX-231, An Actuator to Replace Actuator Mk 3 Mod 0 in the Explosive Switch Mk 46 Mod 0", NAVORD Rept. 6701, May 1960.

2. Taylor, G. W. C., Thomas, A. T. and Holloway, K. J., "The Manufacture of Barium Styphnate RD 1340" (U), Ministry of Supply, Explosive Research and Development Establishment, Rept. No. 28/R/55, Feb. 1956, conf.

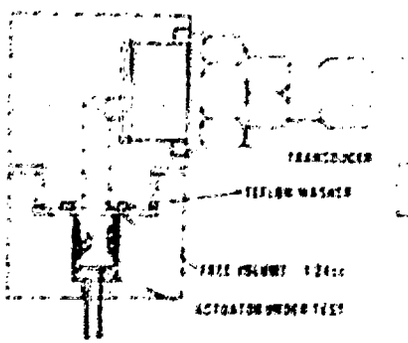

FIG. 1 ASSEMBLY FOR PRESSURE BOMB TESTING

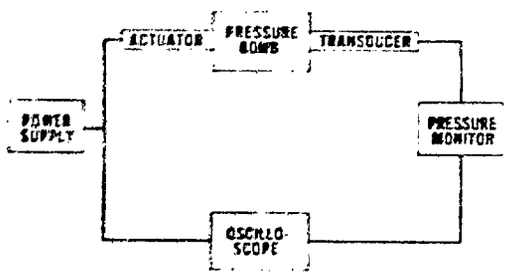

FIG. 2 TEST ARRANGEMENT

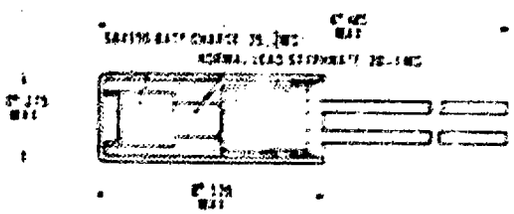

FIG. 3 MK 15 ACTUATOR

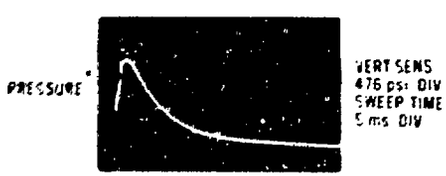

FIG. 4 PRESSURE - TIME PROFILE OF THE MK 15 ACTUATOR

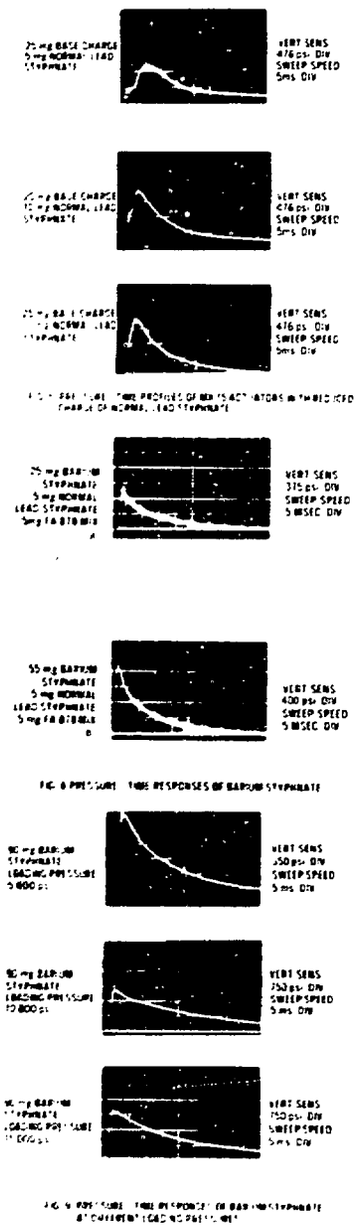

25mg BASE CHARGE
5 mg NORMAL LEAD STYPHNATE
5mg FA 876 MIX

VERTICAL SENSITIVITY 485 psi DIV

SWEEP SPEED: 5 MSEC DIV

FIG 6 PRESSURE - TIME PROFILE OF MK 15 ACTUATOR WITH REDUCED IGNITION CHARGE

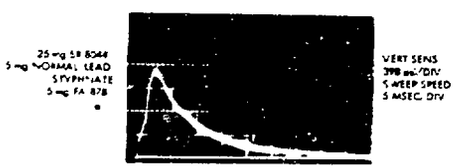

FIG. 7 PRESSURE-TIME RESPONSES OF DUPONT POWDERS

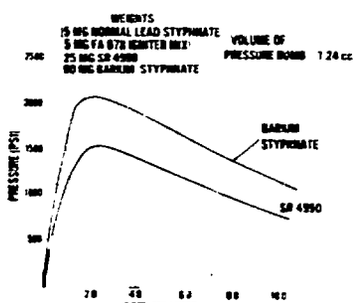

FIG 10 PRESSURE - TIME RESPONSES OF SR4990 AND BARIUM STYPHNATE

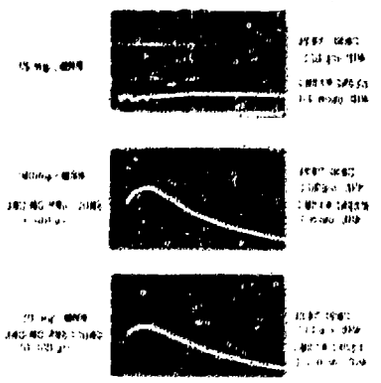

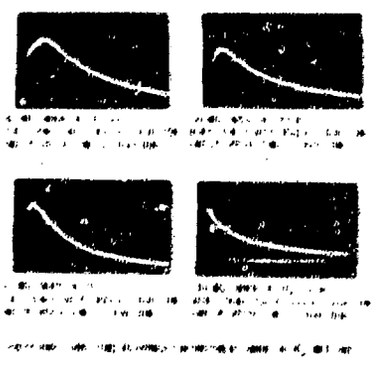

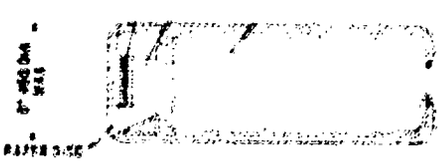

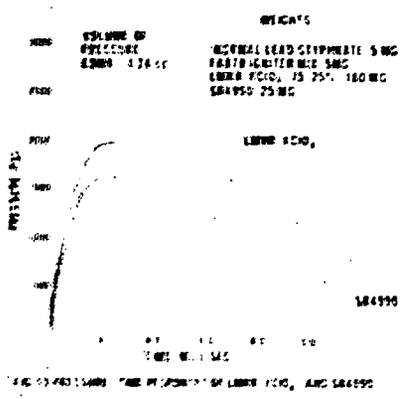

TABLE 1 PRESSURE - TIME RESPONSES OF BARIUM STYPHNATE

• • 0.1 mm

REMARKS NOTE THE WELL-FORMED CRYSTALS CONTAINING OCCLUDED MATERIALS. PROBABLY MOTHER LIQUOR THE DARK CRYSTALS OCCUR BECAUSE OF THEIR ORIENTATION ON THE POLARIZING MICROSCOPE PARTICLE SIZE RANGE IS FROM 10 TO 500 MICRONS

FIG 15 U PHOTOMICROGRAPH OF BARIUM STYPHNATE

TABLE 2 PRESSURE-TIME RESPONSES OF LMNR AND LMNR/$KClO_4$

POWDER	POWDER WEIGHT	LOADING PRESSURE	PRESSURE RISE TIME (MILLISEC	PEAK PRESSURE
LMNR	15 mg	0	—	250
LMNR	120 mg	10,000	5.0	560
LMNR	180 mg	5,000	6.0	875
LMNR-$KClO_4$ 85/15	180 mg	5,000	6.0	2,320
LMNR-$KClO_4$ 80/20	180 mg	5,000	3.0	1,750
LMNR-$KClO_4$ 75/25	180 mg	5,000	2.0	2,320
LMNR-$KClO_4$ 60/40	180 mg	5000	—	1900

TABLE 3 ROUGH HANDLING SURVEILLANCE TEST RESULTS

	ACTION DURING TEST		OUTPUT RESULTS		
	LMNR $KClO_4$	BARIUM STYPHNATE	LMNR $KClO_4$	BARIUM STYPHNATE	
T&H CYCLING TEST 105			\	\	
DROP TEST 101	NO FIRES	NO FIRES	\	\	
TUMBLE TEST 102	NO FIRES	NO FIRES	\	\	\ PASS 0 FAIL
40" GUIDED DROP	2 15	NO FIRES	0 1 15	\	ACCIDENTAL IGNITION
160 F STORAGE 28 DAYS			0 1 15	\	
TRANSPORTATION VIBRATION TEST 104	NO FIRES	NO FIRES	0 2 15	\	

NOTE TEST NUMBERS REFER TO MIL STD 331

TABLE 4 IMPACT SENSITIVITY TESTS

SAMPLE	50% HEIGHT (CM)	STANDARD DEVIATION (LOG UNITS)
BARIUM STYPHNATE (BARETOOLS)	19	0.07
BARIUM STYPHNATE (SANDPAPER	19	0.03
LMNR $KClO_4$ 75% 25% (BARETOOLS	7	0.06
LMNR $KClO_4$ 75% 25% (SANDPAPER	12	0.10
SR 4990 (BARETOOLS)	37	0.19
SR 4990 (SANDPAPER)	45	0.06

IV-8. SMOKE GENERATION FROM CASTABLE PYROTECHNIC COMPOSITIONS

by H. Joseph Zilcosky
Edgewood Arsenal, Edgewood Area, Aberdeen Proving Ground, Maryland

INTRODUCTION

Pyrotechnic compositions whose purpose is to generate smoke are used for screening, signaling and active agent dissemination. Generally, widely different compositions are used for each purpose. A new composition has been developed that is capable of performing in all of the above situations. It is the purpose of this paper to describe the physical properties and combustion characteristics of this composition and to discuss its uses in some new devices.

DISCUSSION

A new castable composition in which a variety of active ingredients and fillers are dispersed has been developed in our laboratories. The same basic composition has been used with only slight modification to disseminate CS, silver iodate, pyrethrum, and the organic dyes commonly used in colored smoke formulations. CS dissemination has been found to occur with efficiencies of approximately 70%. Studies are in progress on silver iodate and insecticide efficiencies.

The combustion of these compositions has some very interesting characteristics. As the mix burns, emitting copious quantities of smoke, a porous ash rises from the surface in a manner similar to the action of a pyrotechnic snake. The entire process seems to occur without evidence of a luminous gas phase flame. Accordingly, we have referred to its action as "Flameless Combustion." The "flameless" nature of the combustion and the castability of the mix permit the fabrication of caseless pyrotechnics; i.e., a completely combustible solid charge. No case or surface inhibition is necessary probably because of the flameless nature of the combustion. The flameless feature also suggests a low combustion temperature which might contribute to improved efficiencies in the dissemination of organic materials of limited thermal stability. The combustion process was investigated more fully with thermocouples and high speed photography because of the "Flameless" aspect and the probability of a low combustion temperature.

Fine iron-constantan and chromel-alumel wires were imbedded in samples of cast composition. The wires were 3 mil diameter with a 1 to 3 mil junction. The wires were welded in a Heliarc welder using an argon atmosphere. The thermocouple was imbedded in the sample by loading composition into both halves of a split cylinder and then placing the thermocouple between the two halves and clamping them together. The nominal sample size was 1" in diameter and 1" long. Temperature profiles are recorded as the sample is burned in cigarette fashion at room temperature and atmospheric pressure. Recordings were made on a Model 1508 Visicorder.

For data reduction, plots of log temperature vs. time were made and the criterion for positioning the surface temperature was the first significant deviation from linear behavior and the ash temperature or flame temperature was the plateau portion of the trace. (See figures 1 and 2.)

Surface temperatures were determined according to a method described by Sabadell, Wenograd, and Summerfield.[1] Measurement of temperature profiles during combustion indicate an average surface temperature of 500 ± 30°C and an average temperature above the surface (normally called flame temperature, but in this case it is actually the ash temperature) of 700 ± 30°C.

Although there is no visible flame during combustion, high speed close up photography shows some interesting phenomena. The combustion process was photographed at 2x magnification and 18, 64, 400 and 2,000 fps with a Hycam 16mm high speed motion picture camera. When shown on a screen at about 40x magnification, there is evidence of a small luminous zone just above the surface that is believed to be a reaction between the products and diffused oxygen from the air. This luminous zone is confined within the porous structure of the ash which is probably why it goes undetected by the observer.

When cast or extruded in a one-inch cross section, the pyrotechnic mass is flexible and does not shatter upon impact. The impact sensitivity is greater than 100 cm on a U. S. Bureau of Mines Impact Tester with a 2 kg weight.

Another interesting property is the failure of the burning composition to ignite shredded paper and dry grass. This property is probably due to the absence of flame.

The nominal burn rate of the solid composition at atmospheric pressure is 0.06 in./sec. and by utilizing designs similar to those of solid rocket propellants a wide range of mass consumption rates (or smoke generation rates) is possible. For example, an 80 gram cylinder of the same composition can be consumed in 10 seconds or 90 seconds, depending on the surface area available for combustion.

The composition of the smoke cloud is believed to consist mainly of ammonium chloride and zinc chloride. The pungent odor due to the zinc chloride in the HC type smoke is absent and it seems probable that the predominant particulate matter is hydrolyzed ammonium chloride. Although the formula contains zinc oxide, the reaction is not considered to be the HC type because of its relatively low combustion temperature.

Presently, the composition is used in two general types of devices: cords and caseless pyrotechnics.

The first is called Smoke Cord, or Smoke Rope. (See Figure 3.) It produces smoke plus CS or insecticide or silver iodide. It is a continuous elongated cord consisting of a central igniter stem surrounded by a main smoke charge (agents contained in smoke charge) which is covered with textiles or plastic. The cord has a burn rate range of 5 feet/minute to 30 feet/second, depending on the burn rate of the central igniter. In the 0.375" diameter cord the smoke composition burns for about 6 seconds after

ignition from the central igniter. Using a fast burning central igniter a wall of smoke 50 feet long by 20 feet high by 20 feet thick can be generated in about 8 seconds.

The second item is a Caseless Grenade. (See Figure 4.) It is a cylinder 4.0" long and 1.0" in diameter. Its burning characteristics are those of the unconfined pyrotechnic masses discussed earlier. It can disseminate CS, silver iodide, insecticide, and most organic dyes used for colored smoke. The agents can be intimately mixed with the composition during processing or placed in columns surrounded by the smoke generating mixture. The Caseless Grenade burns in approximately 15 seconds. However, grenades of any practical size or configuration can be produced.

REFERENCES:

1. Sabadell, A. J., Wenograd, J., and Summerfield, M. "Measurement of Temperature Profiles through Solid-Propellant Flames Using Fine Wire Thermocouples.", AIAA Journal Vol.3, No. 9, pp. 1580-1584, September 1965.

BASIC FORMULA	TECHNICAL DATA SHEET
MATERIAL	PERCENT RANGE
AMMONIUM PERCHLORATE	15 - 35
AMMONIUM CHLORIDE	5 - 15
ZINC OXIDE	15 - 40
BINDER	20 - 40
BURN RATE RANGE	003 TO 026 INCHES PER SECOND
AVERAGE FLAME TEMPERATURE	700 ± 50° C
AVERAGE SURFACE TEMPERATURE	500 ± 50° C
DENSITY	15 GRAMS PER CUBIC CENTIMETER
SMOKE COLOR	WHITE

FIGURE NO 5

WHITE SMOKE COMPOSITION (CASTABLE) STANDARD FORMULA - VISICORDER
MOD. 1503 (TRACE TRANSPOSED - SCALE 1:1)
CHART SPEED 4"/SEC. - SENSITIVITY 1 MV./1" - ROOM TEMP. 25.6 °C
THERMOCOUPLE - .003 IRON CONSTANTAN

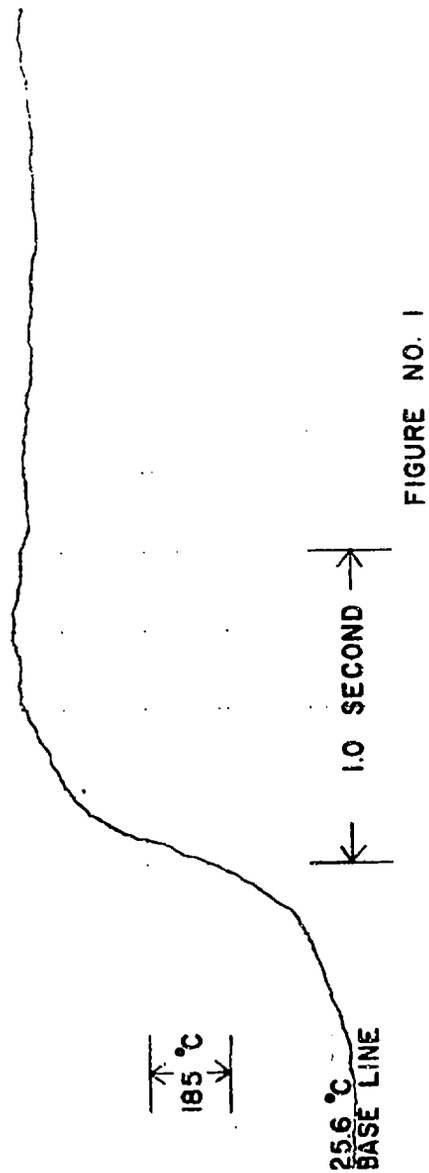

FIGURE NO. 1

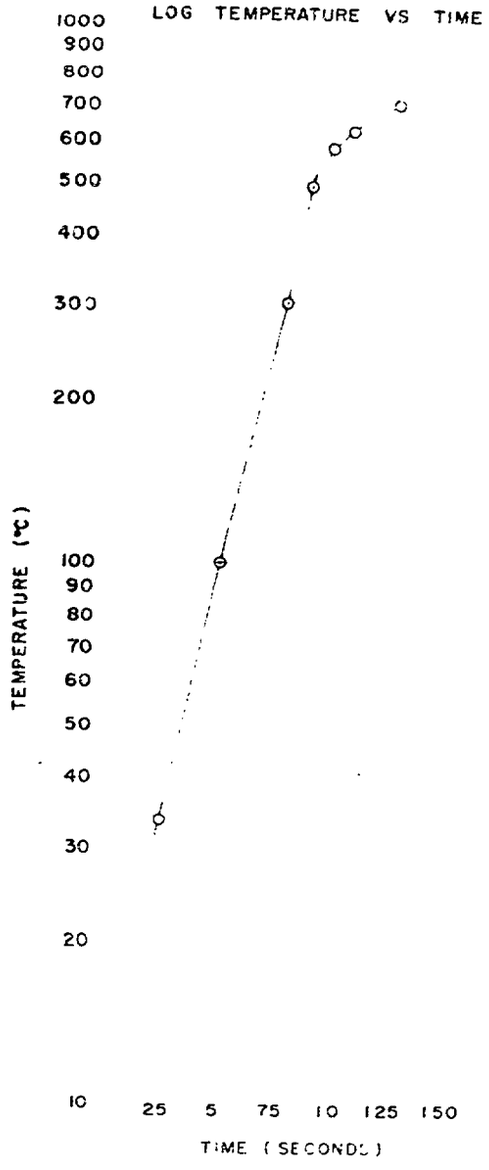

FIGURE NO 2

SMOKE CORD

CORD DIAMETER	0.375" (3/8 INCHES)
SMOKE CHARGE LOAD	100 GRAMS PER FOOT (1.1 OZ
TOTAL WEIGHT	167 GRAMS PER FOOT (1.92 OZ
SMOKE CHARGE IGNITION RATE	30 FEET PER SECOND
METHOD OF IGNITION	M 60 FUSE IGNITER
CORD COLOR	CLEAR
SHELF LIFE	3 YEARS
TENSILE STRENGTH	64 POUNDS
SMOKE COLOR	WHITE

NOTE - FIFTY FEET OF CORD CAN GENERATE A WALL OF SMOKE 50 FEET LONG X 10 FEET HIGH X 10 FEET THICK IN APPROXIMATELY 80 SECONDS

SMOKE CORD - CS

CORD DIAMETER	0.375 INCHES
CS LOAD	2.3 GRAMS PER FOOT (.08 OZ)
SMOKE CHARGE LOAD	4.9 GRAMS PER FOOT (.17 OZ)
TOTAL WEIGHT	7.2 GRAMS PER FOOT (.2 OZ)
SMOKE CHARGE IGNITION RATE	30 FEET PER SECOND
METHOD OF CORD IGNITION	M 60 FUSE IGNITER
CORD COLOR	OLIVE GREEN
SHELF LIFE	3 YEARS
TENSILE STRENGTH	64 POUNDS
SMOKE COLOR	WHITE

NOTE - FIFTY FEET OF CORD CAN GENERATE A WALL OF SMOKE 50 FOOT LONG X 10 FOOT HIGH X 10 FOOT THICK IN APPROXIMATELY 80 SECONDS

FIGURE 3

CASELESS SMOKE GRENADE

LENGTH	4.0 INCHES
DIAMETER	1.0 INCHES
SMOKE CHARGE	80 GRAMS
TOTAL WEIGHT	110 GRAMS
BURN TIME	150 SECONDS
CASE MATERIAL	NONE
SHELF LIFE	3 YEARS
SMOKE COLOR	WHITE, OTHERS AVAILABLE ON REQUEST

CASELESS SMOKE GRENADE - CS

LENGTH	4.0 INCHES
DIAMETER	1.0 INCHES
SMOKE CHARGE LOAD	70.0 GRAMS (2.5 OZ)
CS LOAD	13.0 GRAMS (0.5 OZ)
TOTAL WEIGHT	83.0 GRAMS (3.0 OZ)
BURN TIME	150 SECONDS
CASE MATERIAL	NONE
SHELF LIFE	3 YEARS
SMOKE COLOR	WHITE

NOTE - THE SMOKE CHARGE LOAD IS A CASTABLE PYROTECHNIC AND IT REQUIRES NO CASE

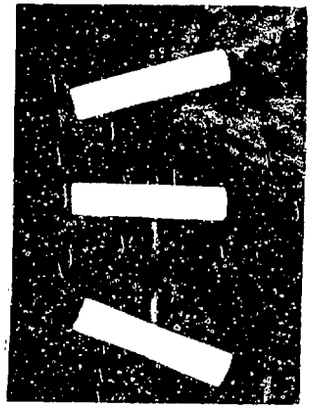

FIGURE 4

ATTENDANCE

Adelman, Stanley M.	Picatinny Arsenal
Ainslie, Robert E.	Naval Air Devel. Center
Allen R. C.	Teledyne McCormick Selph
Andreasen, W. D.	North American Rockwell
Austing, James L.	IIT Research Institute
Avrami, Louis	Picatinny Arsenal
Babcock, Melvin	Monsanto Research Corp.
Barrett, Joseph A.	Atlas Chemical Industries, Inc.
Bartolucci, Richard L.	Sandia Laboratories
Bastyr, Richard	Research, Inc.
Beardell, A. J.	Picatinny Arsenal
Beeman, Donald R.	Holex, Inc.
Bement, Laurence J.	NASA/Langley Research Center
Benedict, A. G.	ARC Associates/Automate Assoc.
Benson, John R.	Penguin Industries, Inc.
Bernstein, Charles N.	Small Arms Systems Agency
Betts, Robert E.	Redstone Arsenal
Blackshire, R. D.	Unidynamics/Phoenix, Inc.
Blake, T. G.	Hanley Industries, Inc.
Boggs, Brian	Ensign Bickford Co.
Bordman, Isaac	Government of Israel
Bowman, Arthur F.	Atlas Chemical Industries, Inc.
Bratton, Francis H.	Aprand, Inc.
Brucker, Stephen	TRW Systems
Buchanan, J. D.	Land Warfare Lab.
Bunting, Wade H.	Frankford Arsenal
Burkdoll, Frank	Explosive Technology Inc.
Claude, Pierre	E.F.A.B. France
Cohn, Gunther	The Franklin Institute
Colpitts, David A.	Naval Weapons Center
Conner, Allan L.	Los Alamos Scientific Lab.
Cosman, Montford	Harry Diamond Labs.
Cote, William I.	Hercules, Inc.
Dansby, H. Bishop	Martin Marietta Corp.
Davey, Charles T.	The Franklin Institute
Davis, Leland E.	Thiokol Chemical Corp.
Demberg, Edmond	Picatinny Arsenal
Devine, Michael	Frankford Arsenal
Doellner, Leonard	The Boeing Co.
Doris, T.	Frankford Arsenal
Dougherty, E.	Picatinny Arsenal
Drexelius, Victor W.	McDonnell Douglas Corp.
Driscoll, Hiram E.	Hercules, Inc.
Earnest, John	Jet Propulsion Laboratory
Ellington, Donal G.	Picatinny Arsenal
Engel, William F.	Jet Research Center
Evans, John H.	Atlas Chemical Industries, Inc.
Evans, Robert W.	Atlantic Research
Everett, Leo A.	Defense Contracts Admin. Svs.
Farmer, R. R.	Monsanto Research Corp.
Farnell, P. L.	Picatinny Arsenal
Fenn, Charles S.	Sandia Laboratories
Ferguson, Robert M.	Canadian Arsenals Ltd.
Ferrell, Robert B.	Los Alamos Scientific Lab.
Ferrett, Charles S., Jr.	Small Arms Systems Agency
Fitzgerald, W. J.	Aerospace Corp.
Fitzhugh, Robert S.	Los Alamos Scientific Lab.
Frank, B. V.	Picatinny Arsenal
Franklin, Gerald B.	Frankford Arsenal
Gaither, Donald	Naval Ammunition Depot, Crane
Garton, W. P.	North American Rockwell
Gehrig, Robert G.	Eaton Corporation
Gin, Winston	Jet Propulsion Laboratory
Gleyre, H. Ron	New Mexico State Univ.
Glover, E. J.	Trojan Powder Co.
Golliher, Kenneth G.	Atomics International
Gorzynski, Carl S.	Martin Marietta Corp.
Hackenberry, Lester S.	Los Alamos Scientific Lab.
Hall, W. S.	British Embassy
Haluza, Dennis, J.	United Technology Center
Hardt, A. P.	Lockheed Corp.
Hargreaves, Charles R.	Honeywell Inc.
Hawley, John	Ensign Bickford Co.
Heaston, Robert J.	Office, Chief of R&D
Hoffman, Norman H.	Technical Ordnance, Inc.
Ingham, R. W.	Teledyne McCormick Selph
Irish, C. G.	Olin Corporation
Jablovskis, J.	Naval Weapons Laboratory
Johnson, Charles H.	Radford Army Ammo. Plant
Johnson, Theodore B.	Remington Arms Co.
Joppa, Richard M.	Los Alamos Scientific Lab.
Kelly, Michael G.	The Franklin Institute
Kennedy, J. E.	Sandia Laboratories
Kent, R. R.	2nd Bat. Fort Bragg
Kirshenbaum, A. D.	Picatinny Arsenal
Koeller, T. L.	Monsanto Research Corp.
Lamphere, Frank J.	General Electric Co.,IPO
Leopold, H. S.	Naval Ordnance Laboratory
Lerman, Russell	Picatinny Arsenal
Locklin, H. W.	General Electric Co./ASD
Lorey, R. A.	Naval Weapons Laboratory
Luth, Perry A.	Hi-Shear Corp.
MacAnispie, Thomas	Land Warfare Lab.
Male, Edwin K. Jr.	Goodyear Aerospace
Marchese, Vincent P.	The Singer Company
McClay, R. E.	Naval Ordnance Station
McLain, Joseph H.	Washington College
McLellan, Quinton A.	Harry Diamond Laboratories
McLaughlin, Clinton D.	Navtoysta Keyport
Menichelli, Vincent	Jet Propulsion Laboratory
Miller, Paul H.	Atlas Chemical Industries, Inc.
Mohrbach, Paul F.	The Franklin Institute
Montesi, Louis J.	Naval Ordnance Laboratory
Moses, S. A.	McDonnell Douglas Corp.
Murphy, Phillip	Ensign Bickford Co.
Nesbitt, Scranton	Naval Ordnance Laboratory
Noblett, Michael G.	TRW Systems
Olson, R. C.	Colt Industries
Osterkamp, A.	Space Ordnance Systems, Inc.
Petrick, John T.	Naval Weapons Laboratory
Pierron, Lucien	Avions Marcel Dassault, France
Poulard, Serge	Com. l'Energy Atom., France
Radke, Harold H.	The Aerospace Corp.
Reed, David W.	Del Mar Engineering
Richardson, Neil R.	Technical Ordnance, Inc.
Richardson, W. G.	Canadian Industries, Ltd.
Riley, John F.	Lockheed Missiles & Space Co.
Roberts, A. L.	Roberts Research Lab.
Rollins, Garland N.	NASA/Langley Research Center
Rollins, Ronald R.	University of Missouri
Rose, James E.	Naval Ordnance Station
Rosenthal, Louis A.	Consultant, JPI
Roulstone, John	Space Ordnance Systems
Rubin, Uziel	Israel Aircraft Industries
Rufenacht, Jack	Battelle Geneve
Russell, John H.	Los Alamos Scientific Lab.
Schimmel, M. L.	McDonnell Douglas Corp.
Schneider, Norman A.	Lawrence Livermore Lab.
Schwarz, A. C.	Sandia Corporation
Schwerdtfeger, Lee H.	Johns Hopkins University
Scott, Calvin L.	Naval Ordnance Laboratory
Seard, Elliott H.	AMC Ammunition School
Seddon, K. C.	Embassy of Australia
Seeger, Donald E.	Picatinny Arsenal
Shani, B.	Government of Israel
Sharockman, John M.	Naval Ordnance Systems Command
Shira, Glenn L.	Land Warfare Laboratory
Sinclair, James E.	Naval Postgraduate School
Slykhouse, Thomas E.	Dow Co./Larkin Lab.
Smith, R. D.	Unidynamics/Phoenix, Inc.
Smith, William	Ensign Bickford Co.
Spratt, J.	Reynolds Industries
Stecker, Ernest J.	Holex, Inc.
Sterling, Walter L.	TRW Systems
Stevens, F. E.	Pyrofuze Corp.
Stresau, Richard H.	R. Stresau Lab. Inc.
Sullivan, T. J.	Naval Ordnance Station
Tepper, Frederick	Catalyst Research Corp.
Thomas, W. R.	Hercules, Inc.
Thompson, Ramie H.	The Franklin Institute
Towell, Gordon	Canadian Industries Ltd.
Tucker, T. J.	Sandia Laboratories
Tweed, Paul B.	Martin Marietta Corp.
Urman, S. C.	Naval Ordnance Laboratory
Vaselich, R. A.	Naval Weapons Laboratory
Voreck, W. E.	Picatinny Arsenal
Wagner, Robert L.	Picatinny Arsenal
Warner, R. K.	Harry Diamond Laboratories
Warren, C. E.	Lunsy Technical Center
Warrick, John D.	Atlas Chemical Industries, Inc
Weber, John F.	Sandia Corporation
Weinmaster, Reuben R.	Sandia Corporation
Wisely, G. T.	Olin Corp.
Worwag, William	Martin Marietta Corp.
Yang, L. C.	Jet Propulsion Laboratory
Young, Galen R.	Holex, Inc.
Yribarren, J. P.	Estec Esro Holland
Zilcosky, Joseph	Ensign Bickford Co.